ACCESSORY MINERAL GROWTH HISTORIES : IMPLICATIONS FOR GRANITOID PETROGENESIS

Bruce Andrew Paterson

A Thesis Submitted for the Degree of PhD
at the
University of St Andrews

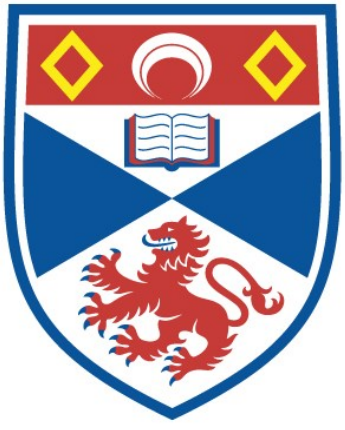

1990

L

ACCESSORY MINERAL GROWTH HISTORIES: IMPLICATIONS FOR GRANITOID PETROGENESIS

Bruce Andrew Paterson

Thesis presented in partial fulfilment of the
Degree of Doctor of Philosophy,
April 1990.

DECLARATION.

I, Bruce Andrew Paterson, hereby certify that this thesis has been composed by myself, that it is a record of my own work, and that it has not been accepted in partial or complete fulfilment of any other degree or professional qualification.

Signed  Date 26 April 1990

I was admitted to the Faculty of Science of the University of St. Andrews under Ordinance General No. 12 on 1st October 1986 and as a candidate for the Degree of Ph.D. on the 1st October 1987.

Signed  Date 26 April 1990

I hereby certify that the candidate has fulfilled the conditions of the Resolution and Regulations appropriate to the Degree of Ph.D.

Signed  Date 26 April 1990

COPYRIGHT.

In submitting this thesis to the University of St. Andrews I understand that I am giving permission for it to be made available for use in accordance with the regulations of the University Library for the time being in force, subject to any copyright vested in the work not being affected thereby. I also understand that the title and abstract will be published, and a copy of the work will be made available to any *bona fide* library or research worker.

ACKNOWLEDGEMENTS.

First I wish to thank Ed Stephens for giving me the opportunity to do this project and for his guidance, enthusiasm and support, even if he could be very elusive at times! Much of the work presented in this thesis would not have been possible without the electron microprobe operating abilities of 'lager tops' drinker, thrill seeker and Glasgow Celtic supporter Donald Herd. Invaluable technical support and sound advice was also given by Andy Mackie, Angus Calder, Richard Batchelor, Jim Allan and Judy Kinnaird. Work carried out at the SURRC, East Kilbride was carried out under the supervision of Graeme Rogers, Brian Davidson, Tim Dempster and John Whitley. In addition I would like to thank Ian Williams of the Australian National University who was kind enough to donate a zircon grain separate which was to prove so invaluable during the course of this study. Financial support in the form of a research studentship from the Natural Environment Research Council is gratefully acknowledged.

Many thanks are also due to Mark Errington, Dave Lowry, Ricky Yarr, Mike MacDonald, Justin Dix, Charles Morrison and many others too numerable to mention with whom I have had many fruitful and fruitless discussions and shared many enjoyable times during the last few years. I particularly wish to thank Richard "Offbeat" Curry and Martin "I eat very slowly" Gillespie for providing a very pleasant and relaxed atmosphere in which to escape from the rigours (?) of work and I would ask them both to continue the 6 Dempster Court tradition of preparing that chameleon of delicacies the 'Baked Bean Surprise'.

Finally I would like to thank my parents for supporting me financially and morally during my time at university, this they did in the mistaken belief that in the future I will be able to keep them in the manner to which they are accustomed.

ABSTRACT.

Accessory minerals in granitoids are major repositories of several geochemically-important trace elements and isotopes and in order to quantify the influence that they have over granitoid petrogenesis it is necessary to characterize fully their behaviour. In particular it is necessary to understand accessory mineral/melt partitioning of trace elements and within grain elemental diffusivities, the latter is of relevance when assessing the state of isotopic equilibration between a refractory accessory phase and a contacting melt.

In this study the backscattered electron (BSE) imaging technique, coupled with quantitative electron microprobe analysis indicate that granitoid zircons and titanites (mainly taken from Caledonian intrusive complexes) are commonly compositionally zoned. The zoning textures observed in these minerals, namely crystal face-parallel zoning, non-planar compositional zoning (included here are subhedral and anhedral core structures) and compositional sector zoning, indicate that the kinetic factors of crystal growth, *ie.* within magma elemental diffusion rates, crystal growth rates, interface kinetics and dissolution kinetics, are largely responsible for the patterns of compositional zoning that have been observed. This finding is in marked contrast to other studies which have assumed that kinetics are not important in crystallizing plutonic granitoid magmas.

Accessory mineral growth histories have been studied in a few well constrained samples from the Caledonian-age Strontian Complex of NW Scotland. The zircons from the central intrusion of this composite pluton have abundant inherited cores. The cores contain a variety of zoning structures and have a wide range of composition, which are taken to indicate that the cores had a wide variety of ultimate sources. Titanites from both the outer and inner intrusions have compositional sector zoning and the range of composition shown by the titanites is largely due to this fact. In this pluton magma composition appears to have little influence on titanite chemistry. The REE abundances in both parts to the intrusion are largely controlled by the accessory phases and each of these phases have very different rock-normalised REE distribution patterns. These abundance patterns are dependent on the relative partition coefficients that each phase has for the REE, the accessory mineral assemblage present and the crystallization order of that assemblage.

The zircons from the central acid member of the Strontian Complex, which are known to have substantial U-Pb inheritance were extracted and analysed for their Sm-Nd isotopic composition. The results apparently indicate that refractory zircons can also preserve their Sm-Nd isotopic composition, a phenomenon not previously reported. That is diffusion of Sm and Nd (and presumably the other REE) within refractory zircon at elevated temperatures appears to be sufficiently slow that complete isotopic equilibration between a zircon and a contacting melt may not always occur. Such disequilibrium potentially enables granitoid magma provenance to be studied with much greater resolution than hitherto possible.

CONTENTS.

Frontispiece. Z-contrast backscattered electron image of a zoned zircon from the Glen Sanda Granodiorite of the Caledonian Strontian Complex. This particular grain has had a complex history involving repeated periods of dissolution and/or mechanical abrasion, cracking and new zircon growth.

15 401 0467 0100.00

Chapter 1
Introduction.

"The sides of the gallery assumed a crystallized tint, with sombre hue, white mica began to commingle more freely with feldspar and quartz, to form what may be called the true rock, - the stone which is hard above all, that supports, without being crushed, the four stories of the earth's soil. We were walled by an immense prison of granite!"

Jules Verne, *A Journey to the Centre of the Earth*

1.1) BACKGROUND AND OBJECTIVES.

It has only recently been appreciated that while granitoid accessory phases have low modal abundances they are capable of controlling the behaviour of many trace elements and geochemically-important isotopes during processes of granitoid magma production and crystallization (*eg.* Gromet & Silver, 1983). Watson & Harrison (1984) stated that the influence and effectiveness of accessory minerals in controlling the behaviour of trace elements during granitoid processes could be gauged through knowledge of the three so-called "fundamental accessory-phase parameters".

1) The solubility and stability of accessory phases in crustal melts. Stability information can be used to assess the likelihood of accessory phases being residual during processes of partial melting and thus having the potential to be entrained in the extracted melt.

2) The equilibrium mineral/liquid partition coefficients for trace elements and isotopes of interest. Partitioning information is essential to the quantitative modelling of crystal/liquid fractionation processes during both melting and crystallization.

3) The within mineral diffusivities that govern the rates at which equilibrium between an insoluble mineral and a contacting melt will be approached.

A number of workers have applied the experimental quantification of these parameters to the study of granitoid melt production and crystallization, the following are examples.

1) From the presence of intra-grain variations in the REE concentrations of titanites (detected using centre/edge electron microprobe analyses) Sawka *et al.* (1984) inferred changes in titanite/melt REE partitioning behaviour during progressive crystallization of a zoned granodiorite pluton from the Sierra Nevada Batholith.

2) Barbey *et al.* (1989) used accessory phase solubility and partitioning information to model the production of some Algerian migmatites by partial melting.

3) Using zircon solubility information Harrison *et al.* (1987) explained the contrasting patterns and magnitude of zircon inheritance in two otherwise similar peraluminous granitoids from New Hampshire.

Many studies of granitoid accessory minerals tacitly assume that the kinetics (*ie.* time dependent phenomena) of crystal growth processes within a magma, *eg.* nucleation rate, crystal growth rate, elemental diffusion and crystal interface kinetics, do not greatly influence the chemistry of accessory minerals growing in a plutonic granitoid magma, and that partitioning of elements into a growing mineral is a process that occurs under conditions in which there is equilibrium between the mineral interface and the bulk magma. It is interesting to note that most studies also tacitly assume that the kinetics of *within* grain equilibration processes *are* important in preventing compositional zoning (assumed to have been caused by progressive changes in conditions during crystallization) from being destroyed. However, Sawka (1988) did acknowledge the potential influence of crystal growth kinetics in determining the effective partition coefficients of accessory phases, although he did not explore further the zoning structures that might be produced if crystal growth kinetics were important or the extent to which effective partition coefficients might deviate from equilibrium

partition coefficients. Gromet & Silver (1983) identified zoning in accessory allanite and titanite from a plutonic granodiorite, but rejected the idea that crystal growth kinetics were the cause on the basis that such a magma would have crystallized "quite slowly" and that processes of elemental diffusion would have been more rapid that crystal growth rates.

A major finding of the research presented here is that crystal growth kinetics *are*, at least in part, responsible for the zoning commonly found within accessory minerals from plutonic granitoid environments and as such the minerals were not in chemical equilibrium with the *bulk* magma at the time of growth. As a consequence the aims of this thesis are to document the range of internal zonation textures that have been observed in two of the most common granitoid minerals, namely titanite and zircon, and to explore the possible origins and implications of compositional zoning in these phases. Titanite was chosen because several studies (*eg.* Gromet & Silver, 1983 and Sawka *et al.*, 1984) have shown that it is commonly zoned and that it is frequently the dominant phase controlling the distribution of the REE in granitoids. Zircon was chosen because of its importance in U-Pb geochronological studies and its common occurrence as inherited grains in many granitoid zircon populations.

1.2) METHODOLOGY.

To establish how common compositional zoning of zircons and titanites is examples were taken from a variety of Scottish Caledonian calc-alkaline basic to acid igneous rocks, although some from other localities, notably the Bega Batholith of SE Australia, were also studied. The compositional zoning of these phases was explored using a combination of backscattered electron (BSE) imaging, which allows the relative variations in the internal composition of a given mineral grain to be studied, and quantitative electron microprobe analysis. In addition to studying samples from a variety of rock types and localities, a few well constrained samples from one Scottish Caledonian plutonic complex, Strontian, were also studied; this was for three main reasons.

1) To study the influence of magma chemistry on the textural and chemical variations of titanite across a compositionally zoned granodiorite pluton given that crystal growth kinetics strongly influence the partitioning of trace elements into titanite.

2) To apply the ability to determine accessory mineral growth histories to assessing the likelihood that accessory phases were refractory during the magmatic event that resulted in the Strontian Complex (the usage of the term refractory is defined in Section 1.4).

3) To study the Sm-Nd isotope systematics of the accessory phases given that some show textural evidence and/or have documented U-Pb isotope evidence of having been refractory.

1.3) THE ORGANISATION OF THE THESIS.

Since the use and exploitation of the backscattered electron (BSE) imaging technique has been of central importance to the findings of this research Chapter 2 describes the controls on BSE emission and the optimisation of machine conditions necessary to observe the internal compositional variations of minerals and in particular accessory minerals. In addition Chapter 2 also documents the electron microprobe analysis methods used for analysing titanites, zircons and apatites.

In Chapters 3, 4, and 5 the various zoning textures that have been observed to occur in zircons and titanites are documented and their origin discussed. For reasons of simplicity and clarity it was decided not to tackle the description of the textures on the basis of locality, since this would have resulted in considerable overlap in the description of the textures, but to describe each texture separately with illustrative examples being taken from suitable localities. An additional benefit of this approach is that it helps to reinforce the assertion that such zoning textures are extremely common and that similar textures almost certainly exist in zircons and titanites in many other granitoid plutons.

An extensive base of published work exists for the Caledonian Strontian Complex pluton, much of which is summarised in Chapter 6. In Chapter 7 the whole rock and major mineral chemistry, for which there is a lack of published data, is documented. The textural and compositional aspects of the accessory phases of the Strontian Complex, including their Sm-Nd isotope systematics, are described and discussed in Chapters 8 and 9. While in Chapter 10 the main findings and conclusions of this research are summarised and suggestions for future work included.

1.4) A NOTE ON DESCRIPTIVE TERMINOLOGY AND DEFINITIONS.

The use of *descriptive* terminology in this thesis is intended, as far as it is possible, to be non-genetic. Chapter 3, which describes zircon zoning textures, contains definitions of the compositional zoning textures, the same definitions are employed in the description of zoning textures in other minerals. Where the commonly-used descriptive terms are poorly defined or considered to have genetic connotations, suitable alternatives have been sought or the existing terms have been redefined.

Many of the mineral zoning textures presented in this study are interpreted as representing crystals that have remained undissolved or unmelted for the duration of the magmatic event (*ie.* initial melting through to final crystallization), in such cases the crystal is described as having been **refractory**. Chappell *et al.* (1987) discussed the role of refractory material, which they termed **restite** (residual source material), entrained in a granitoid magma in determining the composition and compositional variations of granitoid plutons. However, it is considered that restite implies that the refractory material originated from the deepest magma source, *ie.* the use of the term restite has restrictive genetic connotations. In practice it may be difficult to distinguish unambiguously between refractory material entrained from the

deepest source from refractory material incorporated into a magma at a higher level through partial assimilation processes.

Where a refractory mineral retains a signature (probably an isotopic signature although it could conceivably be chemical) of its source then such a mineral should be described as **inherited**. This is consistent with the current usage of the term to describe the preservation of U-Pb isotope systematics in refractory zircon. This usage of the term inherited to describe a refractory mineral is not meant to imply anything about its original source, *ie.* it could have been entrained from the original (deepest) magmatic source, or have been included into the magma by partial wall rock assimilation during ascent or through magma mixing.

Chapter 2
Electron microprobe methods.

2.1) INTRODUCTION.

It is only recently that high quality backscattered electron (BSE) images have been used to tackle geological problems. It is only through optimisation of the factors that influence BSE images that has, for instance, allowed sector zoning in titanites to be described for the first time (Paterson *et al.*, 1989). In this chapter the factors that influence the final BSE image are described, in particular the machine specific factors; scan rates, signal amplification and processing and final recording. It is important to understand the influence of each of these factors over the final image before deciding on the conditions necessary to achieve a particular aim. This last point should not be forgotten, the BSE technique is capable of being applied to a wide variety of problems but for each problem the optimised conditions will be different.

This chapter also describes the electron microprobe analysis technique used for the accessory phases. In particular it details the X-ray lines used, background positions, limits of detection and the errors due to counting statistics. Knowledge of the reliability of the technique is necessary to allow critical appraisal of the information contained in accessory phase electron microprobe analyses.

2.2) THE BACKSCATTERED ELECTRON (BSE) TECHNIQUE.

2.2.1) BSE emission.

In both the scanning electron microscope (SEM) and the electron probe microanalyser (EPMA) a finely focussed beam of electrons (from now on referred to as the beam) irradiates a target specimen; the interaction of the primary beam with the solid specimen is complex and results in a wide variety of emission signals; these include backscattered electrons, secondary electrons, Auger electrons and X-rays characteristic of the specimen. For a comprehensive review of the different emission signals the reader is referred to Goldstein *et al.* (1981). The signals emitted can be used to obtain qualitative and quantitative information about the specimen composition, surface topography and to some extent its internal structure.

Backscattered electrons are primary beam electrons that undergo a number of elastic scattering events within the specimen that result in changes of trajectory, such that they re-emerge at the specimen surface. The degree of backscattering is described by the dimensionless backscattered electron coefficient (η) which is defined by the following equation (Goldstein *et al.*, 1981):

$$\eta = \frac{n_b}{n_i} \qquad \text{(Eqn. 2.1)}$$

where n_b is the number of backscattered electrons and n_i is the number of incident beam electrons. BSE can emerge some distance from the original impact point of the beam. For a flat specimen with 0° tilt, the frequency and energy distribution of the BSE is peaked and

symmetrical about the point of impact. The area of probable BSE emergence determines the spatial resolution.

2.2.2) Sample related controls on BSE emission.

Atomic number dependence.

The number of backscattering events increases with increasing atomic number (Z), or in the case of compounds the mean atomic number ($\overline{z}$). $\overline{z}$ is defined by the following equation (Lloyd, 1987):

$$\overline{z} = \frac{\Sigma(NAZ)}{\Sigma(NA)} \qquad \text{(Eqn. 2.2)}$$

where N is the number of atoms of each element of atomic weight A and atomic number Z. For a given compound the η can be calculated using the following equation (Heinrich, 1966):

$$\eta_c = \sum_{i=1}^{n} C_i \, \eta_i \qquad \text{(Eqn. 2.3)}$$

where η_c is the calculated BSE coefficient, C_i is the concentration by weight of each element in the compound, η_i is the elemental BSE coefficient and n is the number of elements. The relationship between Z (or $\overline{z}$) and η is shown graphically in Figure 2.1.

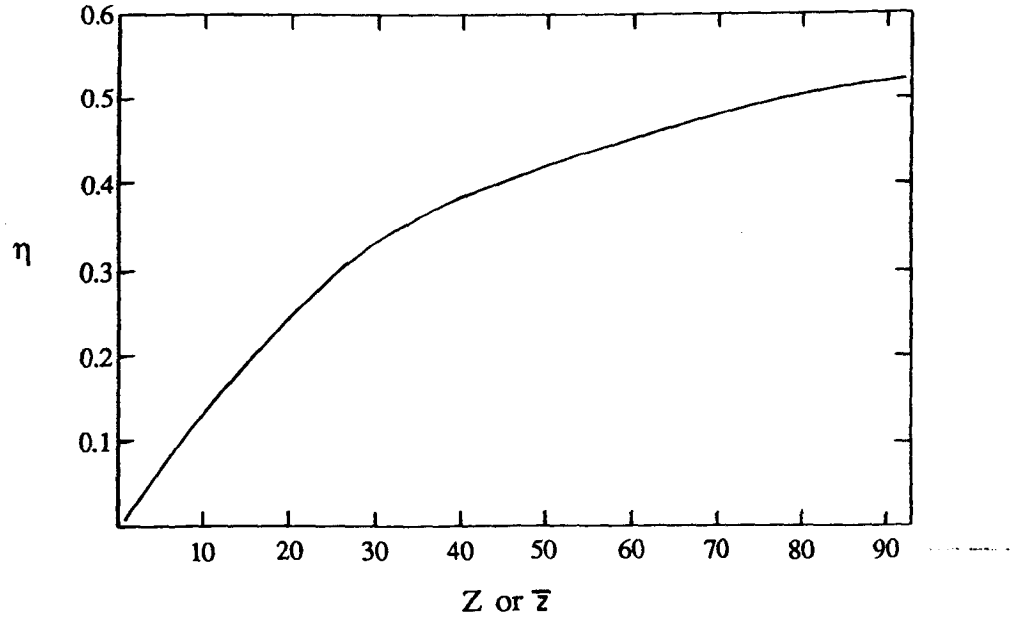

Fig. 2.1. The relationship between Z (atomic number) (or $\overline{z}$ (mean atomic number)) and η (BSE coefficient), after Oatley (1972).

The $\overline{z}$ of a specimen also affects the volume in which the scattering events occurs and hence the area from which the BSE apparently originate, with a specimen of high $\overline{z}$ the area over which BSE emerge is smaller than for a specimen of low $\overline{z}$ (Murata, 1973).

Tilt dependence.

Tilt is defined as the angle between the beam and a line normal to the specimen. A perfectly flat specimen at right angles to the beam has 0° of tilt. Tilt influences the signal on the scale of the diameter of the incident beam, so that a specimen with a poor polish *locally* has high degrees of tilt. As the tilt angle increases the η also increases and the BSE become more directional, so a rough specimen will give a highly variable η signal (Goldstein *et al.*, 1981).

Electron channelling.

In crystalline material the η is also influenced by the orientation and arrangement of atoms within the structure of the crystal, the electrons of the beam can be channelled by the planes of atoms deeper into the sample than would be expected for a given $\overline{z}$. Electron channelling does not occur where conventional, mechanical polishing is used in preparation, as this introduces surface damage on an atomic scale sufficient to destroy observable electron channelling effects (Goldstein *et al.*, 1981).

2.2.3) Electron beam related controls on BSE emission.

The accelerating voltage (beam energy) and the beam current (the density of electrons) exert very little influence on η, but the beam conditions can greatly affect the volume of the specimen affected and also the diameter of the incident beam. The beam current determines the minimum beam diameter, increasing beam current results in a wider primary beam and therefore a greater volume of the specimen is affected. High accelerating voltages result in a greater volume of interaction because higher energy electrons are able to penetrate further. These are important factors to bear in mind when assessing the spatial resolution of the BSE technique.

2.2.4) The types of images possible with BSE.

By rastering the primary beam a number of different images that give quantitative information about a target specimen can result:

1) Z-contrast images (ZCI, Paterson *et al.* (1989)) that give information about the variations in $\overline{z}$ of the specimen, be it a rock with a number of different phases or a zoned mineral. Variations are normally displayed as different grey-levels, the brighter areas having high values of $\overline{z}$. This is the type of image that has been extensively used in this study and only very recently become widely used in mineralogy and petrology.

2) Images that give information about the surface of the specimen due to the dependence of η on the angle of tilt. In the case of the EPMA used in this study the tilt effect is separated electronically from the raw signal, this is described below in Section 2.2.5.

3) Crystallographic contrast images which result from electron channelling effects (see Lloyd (1987) for a review of this application). This type of image has not been used in this study.

2.2.5) Machine practice for Z-contrast images (ZCI).

This section deals with the detection, processing, display and recording of the BSE signal, concentrating on the practice necessary for the EPMA used in this study, the JEOL JCXA 733 Superprobe in the Department of Geology, University of St. Andrews. A brief mention is made of alternatives that are available but no comment can be made on the relative merits of other systems.

BSE signal detection.

During the detection process BSE can be distinguished from other electron signals on the basis of energy, BSE have the highest energies since they do not undergo significant energy loss during the backscattering process. There are two basic types of BSE detector; the scintillator-photomultiplier detector (often called a Robinson detector after Dr. V.N.E. Robinson (Robinson, 1975)), and solid-state semiconductor detectors. The relative merits of the two types are discussed by Robinson & Nickel (1983) and Hall & Lloyd (1983). The solid-state type, a semiconductor silicon P-N junction type of divided annulus, effectively two detectors, was used in this study. The divided annulus is arranged in a horizontal plane ~5 mm above the surface of the specimen, with the primary beam passing through a hole in the centre of the detector.

BSE signal processing and adjustment.

The detected BSE signal is processed in a number of ways before it is displayed on the cathode ray tube (CRT), Figure 2.2 shows a flow diagram of the BSE processing and display system of the JEOL 733 EPMA, a detailed description is given below.

1) The **Pre-Amplifier** takes the raw signals from the two halves (A and B) of the annular detector and amplifies them both independently without altering the signal to noise ratio.

2) A usable signal is created from the A and B signals by the **Operational Amplifier**. The two halves of the detector "see" the specimen from slightly different angles, any topographic tilt results in the two parts of the signal being of different intensity, although the part of the signal due to variations in $\overline{z}$ is the same for both detectors. If the signals are then mixed by addition or subtraction, two different signals result; addition generates a BSE signal that is due only to $\overline{z}$ variations (a ZCI), and subtraction generates a signal due to tilt variations on the surface of the specimen (designated TOPOgraphic Image by JEOL) (Fig. 2.3).

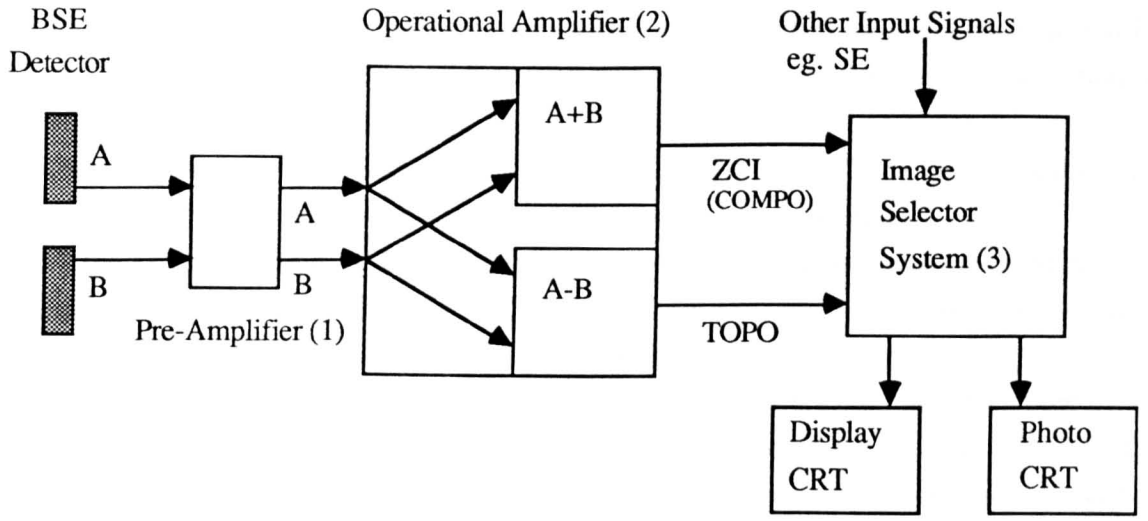

Fig. 2.2. A flow diagram showing the constituent parts of the BSE detector, amplifier and display system. The two halves of the BSE detector are denoted A and B. The numbers on this diagram correspond to numbers in the text below.

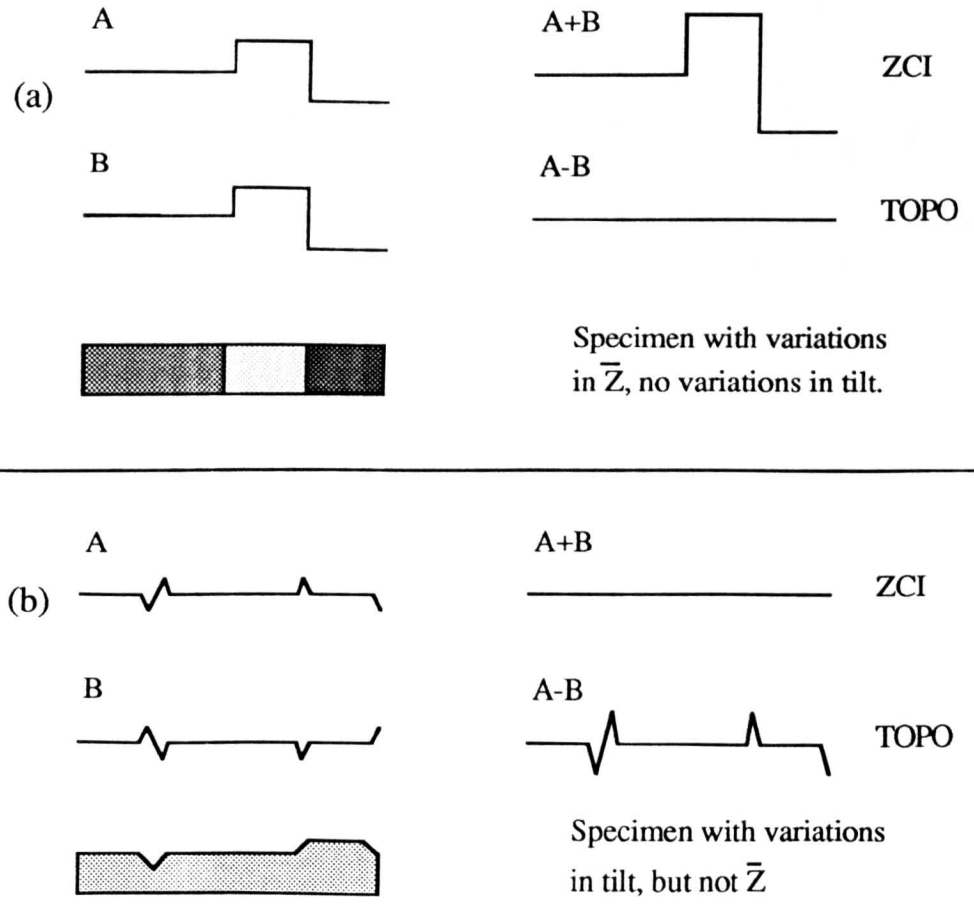

Fig 2.3. The effect of $\overline{z}$ variations (a) and tilt variations (b) on A and B signals and how mixing the signals produces the ZCI (COMPO) and TOPO images.

Where extreme tilt variations are present the signal processing is not completely effective and a tilt contribution may be seen in the ZCI.

3) The **Image Selector System** allows the selection between different possible images, both those resulting from BSE as well as those from other detectors, the selection is displayed on both CRT displays.

The image on the CRT display, and therefore the Photo CRT, can be adjusted to the desired contrast and brightness by changing various amplifier parameters:

1) The **Gain** adjusts the AC component of the signal, but at the same time it varies the strength of the total signal (Fig. 2.4(a)). High gain settings give increased contrast and a greater overall signal, and are often required to pick out mineral zoning.

2) **DC Suppression** adjusts the DC part of the signal, increasing the DC suppression lowers the overall signal, but also increases the range (contrast) of the AC part (Fig. 2.4(b)). DC suppression thus performs two functions; it increases the contrast of the signal and by lowering the signal it protects against saturation of the amplifier electronics.

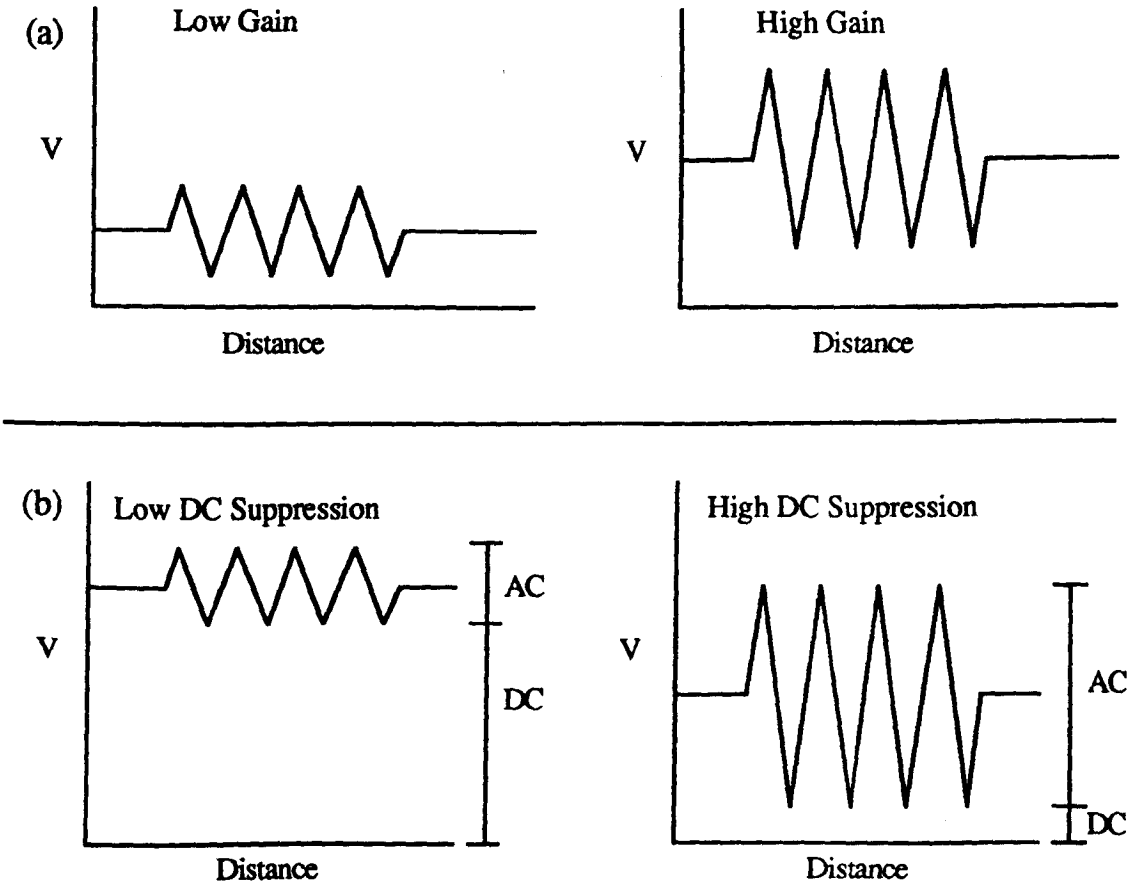

Fig. 2.4. The effect of (a) gain and (b) DC suppression on the range (contrast) and total strength of the signal. V is the signal voltage.

3) If DC suppression cannot prevent amplifier saturation, the input signal to the operational amplifier can be reduced in a series of steps by using the **Attenuator**.

4) The **Brightness** control linearly amplifies the signal prior to display and is used to fine tune the brightness of the final image.

The signal can be processed in a number of other ways including differentiation of the signal, none of these techniques have been used here and are not described.

The JEOL 733 EPMA has exposure and contrast meters to help determine the correct exposure settings, these devices have been of little or no use in obtaining the images presented here. However, the BSE signal can be displayed as a waveform against a background of horizontal scale bars, the optimum position relative to the bars being determined by trial and error. Once calibrated for the commonly used conditions, reliable images are easily obtained. The Photo CRT display has brightness and contrast controls which affect the exposure of the film, the settings recommended in the instructions of the manufacturer have been used.

The effect of other machine parameters on the BSE images.

The rate of rastering of the beam, both horizontally and vertically, has a profound effect on the final image. On a slow horizontal scan rate the BSE signal is greater, and has higher contrast, than a signal from a faster scan rate. However, if slower horizontal scan speeds are used this results in fewer scan lines on the photograph, such that, in extreme cases, they become visible on the film. Thus it is important to match the horizontal and vertical scanning rates such that the individual scanning lines cannot be seen on the final photograph. The horizontal scanning speeds, for photographic purposes, on the JEOL 733 EPMA are variable between 2 and 500 ms $line^{-1}$ in nine steps. The vertical scanning speeds are variable between 0.5 and 600 s $frame^{-1}$ (see below).

Machine conditions used for ZCI.

The main machine variables are the beam conditions and the scanning rates. As explained in Section 2.2.3 high accelerating voltages and currents are best avoided, most images presented have been obtained using an accelerating voltage of 15 kV and a current of 20 nA, this results in a beam diameter of about 0.2 μm. Because these conditions are also generally used for routine silicate analysis, time consuming adjustment of the beam geometry is avoided, bar adjustments to focus and monitoring of astigmatism. On the JEOL 733 EPMA the scanning rates of the beam are set via a numbered cam wheel, the settings used are given in Table 2.1.

Table 2.1. The horizontal and vertical scanning rates used in this study and the resultant number of scanning lines.

Horizontal Scanning Rate (ms line^{-1})	Vertical Scanning Rate (s frame^{-1})	Number of Scanning Lines (lines frame^{-1})
40 (6)	100 (7)	2500
100 (7)	100 (7)	1000

The numbers in brackets refer to the cam wheel settings and the two combinations given are the ones used in this study; (6,7) (horizontal/vertical) and (7,7).

2.2.6) The interpretation of Z-contrast images.

The signal is displayed on the screen as different grey-levels representing variations in $\bar{z}$, bright areas represent higher $\bar{z}$ than darker areas (Plate 2.1). The samples are prepared to reduce the tilt contribution to a minimum, however topographic contributions still exist in most polished sections in the form of scratches (marked A in Plate 2.1). The processing of the signal tends to display cracks as black areas on the final images.

Although the amplifiers are adjusted to prevent electronic saturation occurring, a grain that has a high $\bar{z}$ relative to its surroundings can cause local saturation. This manifests itself on the final image as a dark trail in the scan direction of the beam (marked B in Plate 2.1). As the amplifiers recover the trail fades away. The same effect occurs where a part of the image has a very low $\bar{z}$ relative to its surroundings, except the resulting trail is bright. Careful selection of the scan direction can avoid the trails falling across areas of a grain that are of interest. The length of the trail can be reduced by using a slower scan rate. Even by taking these precautions in many cases the problem cannot be totally eradicated. In the case of accessory minerals (which in general have high $\bar{z}$ compared to major silicate minerals), a ZCI will often consist of the mineral of interest in a black background, this is especially true of minerals mounted in epoxy. The inherently high Z-contrast in such cases means that the problem of amplifier saturation becomes more acute and results in one edge of the mineral being anomalously bright (marked A in Plate 2.2), amplifier saturation should not be confused with genuine variations in $\bar{z}$.

Quantitative electron microprobe analysis allows assessment of which elements are responsible for the variations in grey-levels observed on a given ZCI. However, this process is compromised by the fact that even when an element is below detection limits it is still capable of controlling the observed variations in η. This is particularly true of minerals in which the principal substitutions involve trace quantities of a given element or elements, *eg.* the accessory minerals. However, this helps to illustrate the potential of the BSE technique, particularly when considering substitution of trace quantities of an element in a given mineral. Given the correct circumstances the BSE technique is more sensitive to variations in composition than quantitative analysis by electron microprobe.

Plate 2.1. ZCI of a titanite crystal from a thin section showing how variations in $\bar{z}$ are reproduced as different grey levels, with the bright areas having higher $\bar{z}$ than dark areas. The effect of scratches on the resulting ZCI are also shown (A). The area marked B shows the visible manifestation of amplifier saturation, in this case dark trails after a area of high η. Amplifier saturation is explained in the text.
15 kV, 20 nA, (6,7), scale bar 100μm.

Plate 2.2. ZCI of a separated zircon crystal mounted in epoxy. In this case the extreme contrast in the η of the epoxy and the zircon causes amplifier saturation. This results in the edge of the grain (marked A) which faces the direction from which the scan originates being anomalously bright. The apparent high η is not real and is a machine artifact. All the ZCI's of zircons mounted in epoxy show this effect and is the most extreme manifestation of amplifier saturation that can be seen on the photomicrographs presented.
15 kV, 20 nA, (7,7), scale bar 100μm.


A
A


A
B

The information given in the figure captions.

The figure caption of the each ZCI will note; 1) if the ZCI is from a polished section or a grain mount, 2) where the signal has been due to sample related factors and machine related artifacts, 3) the accelerating voltage and current of the primary beam and 4) the horizontal and vertical beam scanning rates (see Table 2.1). Figure 2.5 shows the information presented on the photograph data panel.

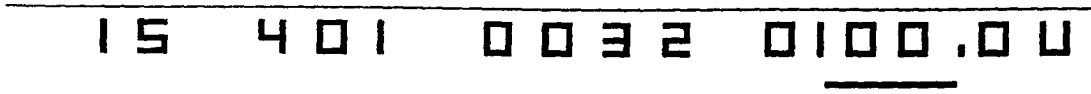

kV	Magnification	Photograph No.	Scale Bar
15	40 x 10^1	32	100.0 μm

Fig. 2.5. The layout and information given on the data panel of the ZCI photographs.

2.2.7) Sample preparation.

Minerals in standard polished thin sections and mineral separates mounted in epoxy were used. The latter overcomes the problem of the low probability of finding accessory minerals in thin sections. Diamond polishing was employed and is preferred to Ce or Sn oxide which can become trapped in cracks, and as high $\bar{z}$ materials adversely affect the BSE signal. A good polish is essential to reduce to a minimum any tilt contribution. Some specimens prepared for other studies were originally polished with Sn oxide, for this work they were repolished with diamond.

After polishing all specimens were cleaned in an ultrasonic bath and carbon coated in the standard way. Keeping the surface of a polished thin section clean is of the utmost importance in ZCI studies, *any* dust will degrade the image.

2.3) QUANTITATIVE ELECTRON MICROPROBE ANALYSIS OF ACCESSORY MINERALS.

Background information.

The fine scale and complexity of the compositional zoning that has been observed in granitoid accessory phases during the course of this research requires an *in situ* analysis technique with a very high spatial resolution. The only commonly available method that has the necessary spatial resolution is wavelength dispersive spectrometry (WDS) of electron microprobe-induced X-ray emissions. This generally gives detection limits in the order of a few hundred parts per million (ppm). Ion microprobe analysis, for instance, allows lower detection limits, in the order of a few ppm or less, but the spatial resolution is poor, the diameter of the primary ion beam is usually in the order of 20-30 μm.

There are three main problems associated with electron microprobe analysis methods for investigating the composition of trace element-rich accessory minerals (Exley, 1980).

1) Low count rates, and hence poor counting statistics leading to poor precision (although accuracy should be good).

2) Line interferences in the complicated REE L-series X-ray spectra.

3) The lack of well characterised, suitable standards.

To alleviate partially the problem of poor counting statistics most studies use long count times, high probe currents and high accelerating voltages; the latter allowing more efficient excitation of X-ray emissions from the REE and better peak to background ratios. Interferences in the REE L-series X-ray spectra are generally overcome by using one of two methods; choosing lines that show minimum interferences (*eg.* Exley, 1980) or using correction factors for peak overlap (*eg.* Åmli & Griffin, 1975 and Roeder, 1985).

The most commonly used standards for the REE (and Y) are those of Drake & Weill (1972) which are a set of four synthetic glasses which between them contain 14 REE and Y. In most cases natural minerals do not contain sufficiently high concentrations of the trace elements of interest to be of any use in the calibration of the electron microprobe, although independently analysed compositionally homogeneous trace element-rich accessory minerals would be useful to analyse as unknown calibration checks. BSE studies indicate that finding sufficiently large homogeneous specimens may prevent this ideal becoming a reality. Pure elements or single element oxides are generally used as standards for other elements.

The purpose of this section is to define the specific methods used in this study, documenting the electron beam conditions, the chosen X-ray lines, the positioning of the spectrometers for background determinations, calibrating standards used and the data processing procedures. This is done here as all other published studies which have similar analytical objectives have failed to define *fully* the conditions used for analysis. Given the problems highlighted above this is a serious omission and considerable research effort was put into finding the best conditions for analysis in this project. Also included here are tables of typical detection limits and analytical uncertainties due to counting statistics for ranges of typical concentrations. Due to the low concentrations many of the results presented for trace elements have high analytical uncertainties, it is important to understand this before considering the data presented in this thesis.

2.3.1) Analytical procedure.

The analytical procedure follows the general philosophy and method of Exley (1980); for example he observed that the accurate analysis of Eu was not possible because of interferences from the $L\beta_2$ peaks of Pr and Sm. Some of the initial titanite analyses were restricted to 14 elements due to computer hardware and software limitations, later analyses (some of the titanite analyses and all of the zircon and apatite analyses) were carried out using a new hardware and software developed in-house in order to allow the analysis of a greater number of elements.

Machine operating conditions and procedures.

All analyses were performed using the same machine used to obtain the ZCI images - a JEOL JCXA 733 Superprobe. This was operated at an accelerating voltage of 20 kV and a probe current of 50 nA. For zircon and titanite analyses a focussed beam was used, while in the case of apatites a focussed beam caused specimen degradation due excessive heating and thus for apatites the beam was rastered over an area of approximately 10 μm by 15 μm. For the counting of some of the standards, *eg.* the REE-doped glass standards of Drake and Weill (1972), it was also necessary to use a defocussed or rastered beam.

For most of the analyses count times of 100 s were used for both peak and background positions on standards and unknowns, the 14 element titanite analyses were obtained using 60 s count times. Computer controlled peak seeking was employed when counting all standards, but in the case of unknowns was only used for elements present in large concentrations; Si and Zr for zircons, Al, Si, Ca, Ti and Fe for titanites and Ca and P for apatites. Regular recounting of standards reduced any systematic errors associated with the determination of elements for which peak seeking was not employed.

X-Ray lines, background positions and standards.

The choice of background positions within the X-ray spectrum for a given X-ray peak is as important as the choice of peak itself and assumes an even greater importance when measuring low concentrations. The background positions must be free of interferences and yet must be suitably close to the peak to be representative of the background at the peak position. In some cases it is necessary to choose background positions that are some distance from the peak. This can introduce systematic errors into the measurement of unknowns, particularly if the nature of the background changes drastically between a standard and an unknown or if the background is curved in any way. Curvature of the background (convex or concave) is a possible source of large systematic errors in the determination of elements present in low concentrations. As far as possible such effects were minimised by careful choice of the background positions used and by the selection of suitable standards.

For each of the three accessory minerals analysed, zircon, titanite and apatite, the peak interference problems for some elements are different, thus the background positions employed for some of the elements differs depending on the mineral being analysed. Full listings of the analysing crystals, the X-ray lines, the background positions and the standards used for the zircon, titanite and apatite analyses are given in Table 2.2. Due to low REE abundances in some minerals, and in an effort to keep total analysing times to a minimum, not all the REE that it is possible to measure were analysed for in the three phases under study. The initial titanite analyses only included the following elements; Mg, Al, Si, Ca, Ti, Mn, Fe, Y, La, Ce, Pr, Nd, Sm, and Yb, but otherwise analysis conditions were the same.

Within the limits imposed by the counting statistics (see below) the variations in the composition of the unknowns that are reported are considered to be real and not artifacts of the analysing method. In most cases the measured variations in the composition can be qualitatively related to variations in the grey-levels of Z-contrast images.

Table 2.2. The analysing crystals, X-ray lines, background positions and standards used for the electron microprobe analysis of zircon, titanite and apatite. n = 1.

Zircon

Element	Analysing Crystal	X-ray Line	Peak Pos. (nλ)	Background Positions (nλ)	(nλ)	Standard
Mg	TAP	$K\alpha_1$	9.89000	9.61394	10.16560	Periclase
Al	TAP	$K\alpha_1$	8.33934	7.78800	8.58540	Corundum
Si	TAP	$K\alpha_1$	7.12542	6.52772	7.40110	Zircon
Y	TAP	$L\alpha_1$	6.44880	6.35590	6.54039	REE - 3
Hf	TAP	$M\alpha_1$	7.53900	7.40110	7.67697	Zircon
Mn	LiF	$K\alpha_1$	2.10182	2.07204	2.15354	Mn metal
Fe	LiF	$K\alpha_1$	1.93604	1.86410	2.01500	Fe metal
La	LiF	$L\alpha_1$	2.66570	2.63700	2.69404	REE - 3
Ce	LiF	$L\alpha_1$	2.56150	2.53276	2.59050	REE - 3
Pr	LiF	$L\beta_1$	2.25880	2.23710	2.28042	REE - 3
Nd	LiF	$L\beta_1$	2.16690	2.15397	2.18160	REE - 2
Sm	LiF	$L\beta_1$	1.99806	1.86854	2.01687	REE - 2
Dy	LiF	$L\beta_1$	1.71062	1.69868	1.83141	REE - 4
Er	LiF	$L\alpha_1$	1.78425	1.69868	1.83141	REE - 4
Yb	LiF	$L\alpha_1$	1.67189	1.63560	1.69868	REE - 2
P	PET	$K\alpha_1$	6.15700	6.12630	6.21925	Apatite
Ca	PET	$K\alpha_1$	3.35839	3.29565	3.42124	Wollastonite
Zr	PET	$L\alpha_1$	6.07050	6.00720	6.13280	Zircon
Th	PET	$M\alpha_1$	4.13810	4.07592	4.20049	ThO_2
U	PET	$M\alpha_1$	3.91000	3.84870	4.00248	UO_2

Titanite

Element	Analysing Crystal	X-ray Line	Peak Pos. (nλ)	Background Positions (nλ)	(nλ)	Standard
Na	TAP	$K\alpha_1$	11.91010	11.63225	12.18600	Albite
Mg	TAP	$K\alpha_1$	9.89000	9.61394	10.25816	Periclase
Al	TAP	$K\alpha_1$	8.33934	7.78800	8.58540	Corundum
Si	TAP	$K\alpha_1$	7.12542	6.52772	7.40110	Wollastonite
Y	TAP	$L\alpha_1$	6.44880	6.35590	6.54039	REE - 3
V	LiF	$L\beta_1$	2.28440	2.25569	2.31243	V metal
Mn	LiF	$K\alpha_1$	2.10182	2.07204	2.15354	Mn metal
Fe	LiF	$K\alpha_1$	1.93604	1.86410	2.01500	Fe metal
La	LiF	$L\alpha_1$	2.66570	2.63700	2.69404	REE - 3
Ce	LiF	$L\alpha_1$	2.56150	2.53276	2.59050	REE - 3
Pr	LiF	$L\beta_1$	2.25880	2.23710	2.28042	REE - 3
Nd	LiF	$L\beta_1$	2.16690	2.15397	2.18160	REE - 2
Sm	LiF	$L\beta_1$	1.99806	1.86854	2.01687	REE - 2
Gd	LiF	$L\beta_1$	1.84680	1.81820	1.87555	REE - 1
Dy	LiF	$L\beta_1$	1.71062	1.69868	1.83141	REE - 4
Yb	LiF	$L\alpha_1$	1.67189	1.63560	1.69868	REE - 2
Ta	LiF	$L\alpha_1$	1.52197	1.42128	1.56584	Tantalum
K	PET	$K\alpha_1$	3.74140	3.67900	3.80340	Orthoclase
Ca	PET	$K\alpha_1$	3.35839	3.29565	3.42124	Wollastonite
Ti	PET	$K\alpha_1$	2.74851	2.68800	2.81364	Rutile
Nb	PET	$L\alpha_1$	5.72430	5.63130	5.84895	Nb metal
Th	PET	$M\alpha_1$	4.13810	4.07592	4.20049	ThO_2
U	PET	$M\alpha_1$	3.91000	3.84870	3.97296	UO_2

Table 2.2. Continued.

Apatite

Element	Analysing Crystal	X-ray Line	Peak Pos. (nλ)	Background Positions (nλ)	(nλ)	Standard
F	TAP	$K\alpha_1$	18.32000	18.13500	18.49780	MgF_2
Na	TAP	$K\alpha_1$	11.91010	11.63225	12.18600	Albite
Mg	TAP	$K\alpha_1$	9.89000	9.61394	10.25816	Periclase
Al	TAP	$K\alpha_1$	8.33934	7.78800	8.58540	Corundum
Si	TAP	$K\alpha_1$	7.12542	6.89598 (1)	7.58471	Wollastonite
Fe	LiF	$K\alpha_1$	1.93604	1.86410	2.01500	Fe metal
La	LiF	$L\alpha_1$	2.66570	2.63700	2.69404	REE - 3
Ce	LiF	$L\alpha_1$	2.56150	2.53276	2.59050	REE - 3
Pr	LiF	$L\beta_1$	2.25880	2.23710	2.28042	REE - 3
Nd	LiF	$L\beta_1$	2.16690	2.15397	2.18160	REE - 2
Sm	LiF	$L\beta_1$	1.99806	1.86854	2.01687	REE - 2
Gd	LiF	$L\beta_1$	1.84680	1.81820	1.87555	REE - 1
Dy	LiF	$L\beta_1$	1.71062	1.69868	1.83141	REE - 4
Er	LiF	$L\alpha_1$	1.78425	1.69868	1.83141	REE - 4
Yb	LiF	$L\alpha_1$	1.67189	1.63560	1.69868	REE - 2
P	PET	$K\alpha_1$	6.15700	6.09421 (2)	6.21925	Apatite
S	PET	$K\alpha_1$	5.37216	5.31000	5.43456	Pyrite
K	PET	$K\alpha_1$	3.74140	3.67900	3.80340	Orthoclase
Ca	PET	$K\alpha_1$	3.35839	3.29565	3.42124	Apatite
Sr	PET	$L\alpha_1$	6.86280	6.80040	6.92840	Celestine
Ba	PET	$L\alpha_1$	2.77595	2.71302	2.83925	Barite
Th	PET	$M\alpha_1$	4.13810	4.07592	4.20049	ThO_2
U	PET	$M\alpha_1$	3.91000	3.84870	3.97296	UO_2

(1) - background position for Si in apatite analyses differs from that used in zircon and titanites analyses because of interferences from $CaK\alpha_1$. (2) - background position for P in apatite analyses differs from that used in zircon and titanites analyses because of interference from $CaK\beta_1$.

Data processing procedures.

Most of the accessory mineral analyses (some of the titanite and all of the zircon and apatite analyses) were obtained during development of the new computer hardware and software package for the JEOL JCXA 733 at St. Andrews University, this meant that the apparent concentrations of some of the analyses were subject to later offline ZAF correction rather than correction at the time of analysis (online). The following ZAF method was used (see Goldstein *et al.* (1981) for a full description).

Z: calculated using the Duncumb & Reed (1968) formulation.

A: calculated using the Philibert (1963) simplified model which employs a new and more accurate formulation for mass absorption coefficients (Heinrich, pers. comm. to W.E. Stephens, 1989) and Heinrich (1969) formulations for σ and h.

F: calculated using the Reed (1965) formulation for fluorescence due to characteristic X-ray lines. No continuum fluorescence correction was applied.

The method used for the earlier 14 element titanite analyses and the major mineral analyses of Chapter 7 used the same general method except that the mass absorption coefficients were taken from Heinrich (1969).

2.3.2) Detectable limits and analytical uncertainties.

The ability to detect a given element by electron microprobe analysis is determined by whether the count rate in the peak position is significantly greater than statistical fluctuations in background. It can be shown that a given peak is significant (to 99 % confidence limits) if the count on the peak position is three standard standard deviations above the background level. The minimum detectable limit (C_{MDL}) for a particular element can be calculated from the peak and background counts obtained on the relevant standard using the following equation (Scott & Love, 1983):

$$C_{MDL} = (3/\sqrt{(I_{P-B}t)})(\sqrt{(I_B/I_{P-B})})(1/C_S) \qquad \text{(Eqn. 2.4)}$$

where I_{P-B} is the net peak intensity in counts per second, t is the counting time, I_B is the background intensity in counts per second and C_S is the concentration of the element in the standard expressed as a fraction of one. However, the background intensity is a strong function of atomic number and the actual detection limits will be higher when analysing a light element in a heavy matrix and lower for a heavy element in a light matrix, thus the C_{MDL} values obtained using Equation 2.4 should only be used as *guide* to the expected detection limits when analysing an unknown. The minimum detectable concentrations calculated from typical calibration analyses of the standards under the conditions and procedures outlined above are given in Table 2.3.

Table 2.3. Minimum detectable concentrations (C_{MDL}) calculated using Equation 2.4 from calibration counts obtained using an accelerating voltage of 20 kV, probe current of 50 nA and count times of 100 s on peak and each of two backgrounds. The X-ray lines used for analysis are given in Table 2.2. The C_{MDL} values shown are typical values obtained during routine calibration.

Element	C_{MDL} (wt%)	Standard	Element	C_{MDL} (wt%)	Standard
F	0.080	MgF_2	Zr	0.042	Zircon
Na	0.007	Albite	Nb	0.031	Nb metal
Mg	0.004	Periclase	Ba	0.020	Barite
Al	0.002	Corundum	La	0.033	REE - 3
Si	0.007	Wollastonite(1)	Ce	0.026	REE - 3
Si	0.004	Zircon(2)	Pr	0.039	REE - 3
P	0.014	Apatite	Nd	0.037	REE - 2
S	0.009	Pyrite	Sm	0.036	REE - 2
K	0.004	Orthoclase	Gd	0.043	REE - 1
Ca	0.005	Wollastonite(3)	Dy	0.039	REE - 4
Ca	0.005	Apatite(4)	Er	0.021	REE - 4
Ti	0.006	Rutile	Yb	0.021	REE - 2
V	0.064	V metal	Hf	0.015	Zircon
Mn	0.009	Mn metal	Ta	0.095	Ta metal
Fe	0.008	Fe metal	Th	0.038	ThO_2
Sr	0.042	Celestine	U	0.035	UO_2
Y	0.018	REE - 3			

(1) - calibration of Si for titanite and apatite analyses. (2) - calibration of Si for zircon analyses. (3) - calibration of Ca for zircon and titanite analyses. (4) - calibration of Ca for apatite analyses.

Apart from knowledge of detection limits, which are of obvious importance when determining the concentration of elements present in trace quantities, it is also important to know the analytical uncertainties associated with the measurement of particular elements when assessing the quality of unknown determinations. The standard error of a given unknown determination for a particular element is a combination of the standard error determined on the unknown and on the relevant standard. The standard error of a given net peak count rate (ε_{P-B}) is given by the following equation (Scott & Love, 1983):

$$\varepsilon_{P-B} = (\sqrt{((N_P/t_P^2) + (N_B/t_B^2))})/((N_P/t_P) - (N_B/t_P)) \qquad \text{(Eqn. 2.5)}$$

where N_P is the number of peak counts (not count rate), N_B is the number of background counts, t_P is the peak counting time and t_B is the background counting time. The resultant standard error of the unknown specimen and element standard peak errors (ε_{SPEC} and ε_{STND}), the intensity ratio (ε_k), is given by the following equation (Scott & Love, 1983):

$$\varepsilon_k^2 = (\varepsilon_{SPEC})^2 + (\varepsilon_{STND})^2. \qquad \text{(Eqn. 2.6)}$$

Tables 2.4 and 2.5 show the typical standard errors obtained during routine analysis of accessory phases.

Table 2.4. Approximate standard errors based on counting statistics of electron microprobe analyses of the major element constituents of accessory minerals. Values calculated using Equations 2.5 and 2.6 from counts obtained on standards and typical unknowns. Standard errors are shown as absolute values (wt%) rather than as relative values.

Mineral	Element	Analytical Uncertainty wt% oxide (2σ).
Zircon	Si	0.06
Zircon	Zr	0.49
Titanite	Si	0.05
Titanite	Ca	0.07
Titanite	Ti	0.07
Apatite	P	0.26
Apatite	Ca	0.12

Table 2.5. Standard errors of electron microprobe analyses of accessory minerals at various absolute elemental concentrations. Values calculated using Equations 2.5 and 2.6 from counts obtained on standards and typical unknowns at the conditions outlined above. Standard errors are expressed as relative errors (2σ). A dash denotes where elements have not been found in those concentrations.

Element	0.1 wt% oxide level % error (2σ).	0.5 wt% oxide level % error (2σ).	1 wt% oxide level % error (2σ).
F	-	9.4	-
Na	22	-	-
Mg	-	-	-
Al	-	5.1	1.4
Si	11	-	-
P	18	-	-
S	5.2	-	-
K	11.5	-	-
Ca	6.2	2.2	-
V	67	-	-
Mn	10	-	-
Fe	7.3	3.7	2.0
Sr	23	-	-
Nb	24	7.3	-
Ba	-	-	-
Y	29	9.8	3.1
La	34	9.6	-
Ce	27	7.8	5.1
Pr	46	-	-
Nd	39	9.8	5.7
Sm	38	-	-
Gd	47	-	-
Dy	47	-	-
Er	22	-	-
Yb	21	-	-
Hf	-	-	3.7
Ta	24	-	-
Th	20	5.6	2.9
U	21	6.0	-

Chapter 3
Compositional zoning in granitoid zircons.

3.1) INTRODUCTION.

The purpose of this chapter is two-fold: 1) to describe the range of zircon zoning textures that have been observed during the course of this research; and 2) to document the variations in composition that are responsible for the zonation patterns. The rocks from which the examples are taken come from a variety of localities, although all are taken from intrusive calc-alkaline granitoid environments either from the Caledonian or Lachlan (SE Australia) fold belts. Many of the zircons contain subhedral and anhedral core structures (the term core is defined in Section 3.5), these cores *may* have originally crystallized in other environments about which little or nothing is known, hence no attempt is made in this chapter to describe the zoning textures of the cores themselves. However, it is important to note that the zircon cores often do have internal zoning textures, the possible implications of this are discussed in Chapters 8 and 9.

The different textural types have been arbitrarily divided into three non-genetic categories: 1) crystal face-parallel continuous and discontinuous zoning; 2) non-planar continuous and discontinuous zoning; and 3) compositional sector zoning (Hollister, 1970). At the beginning of each section the principal textural types are defined, the same terms with the same definitions are used in again Chapter 4 when describing the zoning textures in titanites. Although in this chapter the textures are described separately it is important to stress that the different types commonly occur together within the same grains.

Background information.

The widespread occurrence of zircon in a variety of igneous rock types makes it a potentially useful petrogenetic indicator mineral, although its main use has been in U-Pb geochronological studies. The ^{207}Pb and ^{206}Pb isotopes (generally referred to as radiogenic Pb or Pb*) produced by the radioactive decay of ^{235}U and ^{238}U, respectively, are retained in the structure of zircon to temperatures far above those normally encountered during crustal processes, notably granitoid production. This means that a U-Pb age recorded by a zircon is a crystallization age and should not reflect post-crystallization cooling. Ambiguities and inaccuracies in the interpretation of U-Pb zircon data can be introduced by two processes: 1) at low temperatures some of the Pb* can be lost, this is usually thought to occur at the surface of crystals or along cracks (Krogh, 1982b); and 2) more than one age of zircon may be present within a rock or within single crystals. Both processes result in discordant ages and to interpret such ages it is necessary to have independent evidence, or to make assumptions, about the timing of Pb* loss and the number of different ages of zircon that are present. Since analyses that plot on concordia require no such assumptions it has been the aim of recently developed techniques to try and reduce or eradicate the discordance problem. For example, many workers now employ the abrasion methods of Krogh (1982b), which attempt to remove the effects of surface-correlated Pb* loss by abrading the outermost surface of crack-free grains.

Granitoids often contain zircon populations which have more than one age, material that grew at the time of emplacement (cogenetic zircon) and an refractory inherited component (*eg.* Gulson & Krogh, 1973 and Pidgeon & Aftalion, 1978). The occurrence of inherited zircon in granites is testament to the retentiveness that undissolved zircon has for Pb* at the elevated temperatures of crustal melts. Early studies extrapolated the discordia line, generated by the presence of zircon inheritance, back to intercept the concordia in an attempt to infer an age of the inherited zircon and that of the source. In all such cases a tacit assumption is that the inheritance within the zircon population has a single age, but it is increasingly being realised that such an assumption is, in many cases, unfounded. Recent studies, notably those involving single grain analyses of zircons found in sediments (*eg.* Schärer & Allègre, 1982; Krogh, 1986) and the *in situ* analyses of selected parts of zircons from both high grade metamorphic and igneous environments using ion microprobe techniques (primarily by a group based at the Australian National University (ANU) using the 'SHRIMP' instrument), have shown that potential granite source regions and granites themselves commonly contain zircon populations with *more* than one age (*eg.* Harrison *et al.*, 1987, Williams *et al.*, 1988 and Compston & Kröner, 1988). Granites containing inherited zircon populations with more than one age are described as having mixed inheritance (Miller *et al.*, 1988). The reverse discordia generated by a zircon population with mixed inheritance will have an upper intercept which is an *average* age of the inherited component and does not necessarily have any geological meaning.

The experimental studies of E.B. Watson and T.M. Harrison (Watson, 1979, Harrison & Watson, 1983 and Watson & Harrison, 1983) on the solubility of Zr in granitic magmas have largely explained why zircon often remains partially undissolved during crustal melting episodes. They observed that Zr solubility in crustal melts is controlled by melt composition, more specifically the cation ratio (Na+K+2Ca)/(Al·Si), and temperature; in peralkaline melts Zr solubility is high, whilst in peraluminous melts the solubility is low. If the Zr concentration in the source is high then Zr saturation of a granitic peraluminous melt may be reached before complete zircon dissolution occurs and thus the potential exists for the melt to entrain an inherited zircon component.

In summary, the available data, both isotopic and experimental, suggests that granitoid zircon grains have often had complex and protracted histories.

3.2) ZIRCON CHEMISTRY AND CONTROLS ON OBSERVED ZCI GREY-LEVEL VARIATIONS.

3.2.1) Zircon chemistry.

Naturally occurring zircon, $ZrSiO_4$, is a tetragonal crystal and the principal structural unit is a chain of alternating, edge sharing $[SiO_4]$ tetrahedra and $[ZrO_8]$ triangular dodecahedra extending parallel to the c-axis (Robinson *et al.*, 1971). Other elements substitute into the structure in either the eight-coordinated Zr site (A) or the four-coordinated Si site (B). Up to

50 elements have been reported in zircon analyses, although the following list represent some of the more common: in the A-site - Hf, Y, U, Th, REE, Pb, Ca, Fe^{2+}, Fe^{3+}, Na, K, Ti, Nb, and Ta; in the B-site - Al, P and S (Speer, 1982). Zircon is isostructural with several other minerals; including hafnon ($HfSiO_4$) and xenotime (YPO_4), these give an indication of the important substitutions in naturally occurring zircons. Hf, U and Th substitute directly for Zr, Y and the REE substitute for Zr through the linked substitution of P for Si, although Caruba *et al.* (1975) noted that substitution of the REE and Y into the A-site during initial crystallization may also be achieved by a coupled substitution involving $(OH)^-$ in the B-site. Radiation damage of the zircon structure caused by the radioactive decay of U and Th to form so called metamict material may also allow water to enter the structure, this water is thought to be absorbed onto the metamict material in the form of H_2O or $(OH)^-$ (Speer, 1982).

There is a general tendency for zircons in magmas to concentrate the HREE and Y, that is the HREE have higher zircon/liquid partition coefficients than do the LREE (Nagasawa, 1970). Watson (1980), using zircons experimentally grown in felsic peralkaline liquids, confirmed the general REE distribution pattern of Nagasawa (1970), but showed that the HREE end of the pattern is concave downwards. The actual concentrations of REE in zircons will obviously reflect not only the relative partition coefficients of the different REE, but also the absolute REE composition of the medium from which the grain was grown.

3.2.2) Compositional controls on ZCI grey-level variations in zircons.

In general the most important substitutions in the zircon analyses presented here are due to incorporation into the structure of Hf, Y, the HREE, U and Th (the other elements listed above have only been detected occasionally). Substitution of any of these elements into zircon results in an *increase* in the $\bar{z}$ over that of an ideal zircon ($ZrSiO_4$). A given grey-level cannot be uniquely related to a particular composition due to the complexity of the zircon substitution scheme in terms of numbers of elements that are commonly involved.

3.3) THE SAMPLES USED TO STUDY ZIRCON ZONING TEXTURES.

All the examples of zircon zoning textures were taken from the following granitoid intrusions; Ratagain and Strontian, both Scottish Caledonian plutons to be found NW of the Great Glen Fault (see Brown (1983) or Stephens (1988) for a review of the province) and Kameruka, a pluton from the Bega Batholith of the Lachlan Fold Belt of SE Australia (see Chappell & White, 1976). Further details of the sample localities are given in Appendix 1. The U-Pb zircon systematics of these intrusions have been documented, at least in part.

Pidgeon & Aftalion (1978) found that the monzonitic facies of the Ratagain intrusion contains inherited zircon, which they attributed to the observed presence of rounded and irregular cores in many grains. Subsequent work on a pyroxene-mica diorite sample from Ratagain by Rogers & Dunning (1990, in press) also found a substantial inherited zircon component, but the analysed grains contained no optically visible rounded or irregular cores.

The outer, earlier intrusion of the Strontian Complex, the Loch Sunart Granodiorite of this work, contains a very small amount of zircon inheritance (Rogers & Dunning, 1990, in press); and the inner, later part of the intrusion, the Glen Sanda Granodiorite, contains a substantial amount of inheritance (Halliday *et al.* (1979)). The inherited zircon systematics of the Strontian Complex are described in more detail in Chapter 6 (Section 6.2.4 and Tables 6.2 and 6.3), Chapter 8 (Section 8.2) and Chapter 9.

Using 'SHRIMP' ion microprobe dating of zircon separates it has been shown that zircons from the Kameruka Granodiorite of the Bega Batholith do contain inheritance. The complete findings of this research into the protoliths of the Bega Batholith Granites have yet to be published, although the initial findings for the batholith as a whole have been published in abstract form (Williams *et al.* (1988)) and been made available through a personal communication with Dr. I.S. Williams. The zircons from the Kameruka Granodiorite used in this study are the same zircons used in the 'SHRIMP' ion microprobe study.

The examples of zircon zoning textures were either taken from thin section (Ratagain) or from separated grains mounted in epoxy, cut and polished (Strontian and Kameruka).

3.4) CRYSTAL-FACE PARALLEL CONTINUOUS AND DISCONTINUOUS COMPOSITIONAL ZONING.

Definitions: crystal face-parallel continuous and discontinuous zoning.

All apparently linear compositional interfaces (they are assumed to be planar structures) which cannot be assigned to another zoning category and appear to be, or have been, parallel to crystal faces, are described as **crystal face-parallel. The terms continuous** and **discontinuous** indicate, respectively, a gradual or an abrupt change in composition and are not related to continuous and discontinuous reaction of crystals with melt (MacKenzie *et al.*, 1982). Multiple zoning occurs where a crystal has repeated discontinuous zones and if such zones show a regular pattern of repetition it is described as being oscillatory (MacKenzie *et al.*, 1982). The multiple zones of many of the zircons do not circumscribe the crystal, such that different sectors have different patterns of multiple zoning, this is considered to be a form of compositional sector zoning and is described in Section 3.6.

Minerals that are part of a solid solution, such as plagioclase feldspars, are often described has having normal zoning, that is they are zoned from centre to edge from a high to a low temperature component, the term reverse zoning being used to denote the opposite. These terms have no analogues in the description of zoning in accessory minerals.

Previously reported occurrences of crystal face-parallel zoning in zircons.

Numerous studies have reported the occurrence of crystal face-parallel zoning, often very misleadingly referred to as "growth zoning", in zircons, particularly those found in igneous environments; *eg*. Mackie (1926), Poldervaart (1956) and Silver & Deutsch (1963). In the main the zoning is of the multiple discontinuous type and is usually interpreted as being due to free growth in a melt, as evidenced by its euhedral habit (Speer, 1982).

Due to the presence of U in the structure of zircon both fission track density methods or HF acid etching can be used to assess the spatial distribution of U. Yeliseyeva (1977), using fission track density, and Krogh (1982b), using HF acid etching, both noted the common parallelism of U-rich zones with the faces of crystals. Speer (1982) summarised much of the compositional data on zoning in general by stating that the elements which substitute for Zr and Si (*ie.* Y, REE, Ca, Al, Fe, Th, U and P) usually increase together, although there is often a negative correlation between Y and Hf, *eg.* Romans *et al.* (1975). The changes in composition of the multiple zones are usually taken to reflect changes in chemical and physical conditions as crystallization proceeded (Speer, 1982).

3.4.1) Examples of crystal face-parallel zoning in zircons.

This section describes the occurrence of continuous and discontinuous crystal face-parallel zoning in zircons using a number of different examples,. All the granitoid zircons studied during the course of this study contain crystal face-parallel zoning and most contain numerous continuous and discontinuous interfaces and thus it is impractical to determine the composition of every zone. Full details of the microprobe analyses from the individual examples are in Appendix 3. All three examples are mounted in epoxy, the c-axis of each of them is in the plane of the section and orientated east-west relative to the page.

Example 1 (Plate 3.1).

This grain contains many crystal face-parallel zones, however these are not sufficiently regular to be described as oscillatory but are best described as multiple. The boundaries are on the whole discontinuous. To investigate the composition of the crystal face-parallel zones a traverse of nine electron microprobe analyses within a single sector was carried out. The positions of electron microprobe analyses are marked with numbers on Plate 3.1.

The analyses detected the presence of Hf in all the zones and a few of the HREE (the other REE were all below detection limits), Y, U and Th within at least some of the zones. From centre to edge there is very little variation in the concentration of Hf and the same is true between light and dark zones, particularly when the typical analytical uncertainty of the Hf determinations (approximately ±0.05 wt% Hf, 2σ) is considered. However, the distributions of the HREE, Y, U, and Th appear to be linked, the zones which contain appreciable contents of the HREE also contain Y, U and Th in significant quantities. The grey-levels appear approximately to contour the distribution of the HREE, Y, U and Th, the brighter zones contain higher concentrations of these elements than the darker zones. For instance, Figure 3.1 shows the variation of Y between the nine analysis points, Y varies from between 0.18 wt% in some of the bright zones to below detection limits in the darker zones. Y was used as it is present in higher concentrations than the HREE, U and Th and thus the measured concentrations are subject to lower analytical uncertainties.

Plate 3.1. ZCI of separated zircon from the Loch Sunart Granodiorite (BPSRT1) of the Strontian Complex. The numbered points are the electron microprobe analysis points (see Appendix 3). A description of the zoning is given in the text. The black areas within the grain are mainly apatite inclusions, the cracking was mainly caused by polishing and the bright left hand edge is due to amplifier saturation.
15kV, 20nA, (7,7), scale bar 100μm.

Plate 3.2. ZCI of separated zircon from the Loch Sunart Granodiorite (BPSRT1) of the Strontian Complex. The numbered points are the electron microprobe analysis points (see Appendix 3). A description of the zoning is given in the text. Contains many small apatite inclusions, the cracking is mainly an artifact of polishing and the effects of amplifier saturation can be seen along the left hand side of the grain and to the right of inclusions.
15kV, 20nA, (7,7), scale bar 100μm.

no'ooio 6hho 18h 5i
1
2
3
4
5
6
7
8
9

no'ooio 5hho 1hh 5i
1
2
3
4
5
6
7
8
9
10
11
12
13
14
15
16
17

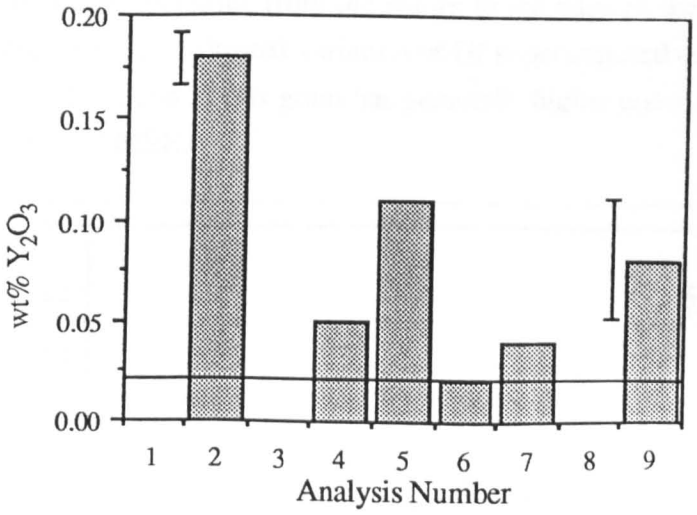

Fig. 3.1. Histogram showing Y_2O_3 concentrations of the analyses of the zircon in Plate 3.1. The line at 0.02 wt% is the approximate limit of detection. Error bars are shown for analyses 2 and 9. The analysis numbers correspond to those shown on the Plate 3.1.

Example 2 (Plate 3.2).

The fact that the crystal face-parallel zoning is off-centre is real and not an artifact of the orientation or cut of the crystal. The grain contains many crystal face-parallel zones and it is also compositionally sector zoned (see Section 3.6). Three of the electron microprobe analyses (15, 16 and 17) were carried out on the low η area to the top right of the grain, these are relevant to Section 3.5.3 and are not discussed here.

Like Example 1 the variations in the concentrations of the HREE, Y, U and Th in this example appear to be linked, in addition the grey-levels of the crystal face-parallel zones appear approximately to contour the variations in the concentrations of these elements. However, unlike Example 1, the concentration of Hf does vary slightly (from 1.41 to 1.71 wt%) between the different crystal face-parallel zones analysed.

Example 3 (Plate 3.3).

This grain apparently shows a greater range of grey-levels than the first two examples, this in part is due to differential polishing rates between the zones and is thus indirectly due to compositional differences. The relief on the surface of the crystal means that locally there can be a substantial tilt contribution to the original BSE signal and this has not been completely eradicated by the processing of the signal (see Section 2.2.5). Only areas of the surface free from substantial variations in tilt have been analysed.

Like the first two examples this grain is compositionally sector zoned, however the crystal face-parallel zoning of this example is on a much finer scale than that of the first two examples, this combined with the fact that X-rays emerge from a greater excitation volume than backscattered electrons (this is because X-rays have higher energies) means that the

quantitative analyses represent averages of two or three very narrow zones. Although compositionally this grain is very similar to Example 2 it differs slightly in two respects: 1) the Hf concentration increases from the centre to the edge of the crystal (see Fig. 3.2), *ie.* there is continuous compositional variation of Hf superimposed on discontinuous zoning of Y, HREE, U and Th; and 2) this grain has *generally* higher concentrations of U and Th and to lesser extent the HREE.

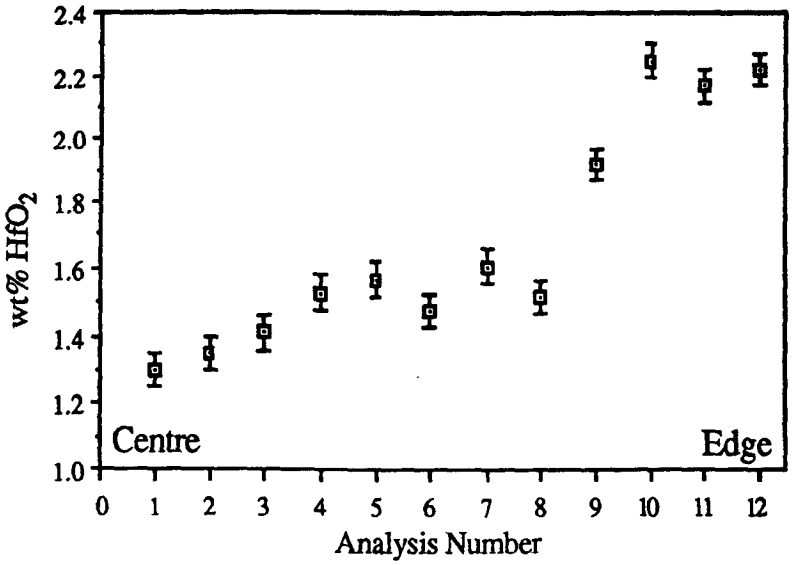

Fig. 3.2. Diagram showing how HfO_2 concentration increases from the centre to the edge of the zircon grain shown in Plate 3.3. Some of the HfO_2 variation is due to small scale discontinuous changes of concentration. There is no horizontal scale, the actual spacing between the analyses is shown on Plate 3.3. The error bars represent ±0.05 wt% HfO_2 (2σ).

It should be noted that P was not detected in any of the three examples given above, the detection limit for P being approximately 0.02 wt%, thus the coupled substitution $Zr^{4+} + Si^{4+} \Leftrightarrow Y^{3+} + P^{5+}$ cannot be invoked to explain the substitution of the REE and Y. As explained above in Section 3.2.1 Caruba *et al.* (1975) noted that substitution of the REE and Y into the A-site could be achieved through a coupled substitution involving $(OH)^-$ into the B-site.

3.5) NON-PLANAR CONTINUOUS AND DISCONTINUOUS COMPOSITIONAL ZONING.

Definitions: non-planar continuous and discontinuous compositional zoning.

Such zoning is defined as **continuous** or **discontinuous** changes in composition that occur across a **non-planar** boundary. The terms multiple and oscillatory, as defined in Section 3.3, can also be employed where appropriate. It is important to note that compositional sector zoning can give rise to non-planar compositional boundaries, such features are described in Section 3.6.

Plate 3.3. ZCI of separated zircon from the Glen Sanda Granodiorite (BPSRG1) of the Strontian Complex. The numbered points are the analysis spots (see Appendix 3). A description of the zoning is given in the text. There is a significant tilt contribution to the BSE signal due to differential polishing of the cut surface. Most of the cracking is an original feature and was not induced during sample preparation. As with the grain in Plate 3.2 there is some amplifier saturation effects.
15kV, 20nA, (7,7), scale bar 10μm.

Plate 3.4. ZCI of separated zircon from the Glen Sanda Granodiorite (BPSRG1) of the Strontian Complex. Low η subhedral core with high η euhedral rim, there is some faint zoning within the core. The rim shows marked differential polishing. The photomicrograph was exposed to allow the zoning of the core to be seen, thus the detail in the rim is mainly lost.
15kV, 20nA, (7,7), scale bar 10μm.

10
8
9
7
6
5
4
3
2
1
11
12

The terms core and rim are often used in the literature to denote the approximate position of *in situ* analyses (usually electron microprobe analyses) across a particular crystal. However, it is felt that these terms imply the existence of distinct parts to a crystal. Thus it is proposed that terms such as centre and edge should be used to describe relative position within a crystal, with the terms core and rim being reserved for parts of a crystal that are distinct in terms of composition or zoning texture and have a generally concentric relationship. The shape of a core should be qualified by the terms euhedral, subhedral or anhedral accordingly. This definition of the core/rim terminology is intended to allow for the occurrence of several generally concentric core/rim structures within a single crystal.

Previously reported occurrences of non-planar interfaces in zircons.

The previously reported occurrences are mainly restricted to granitoid zircons that contain subhedral or anhedral centrally positioned cores in otherwise euhedral grains, these have usually been interpreted as representing older inherited material which has been the site of new zircon growth during cooling and crystallization of the host granitoid. Where U-Pb isotopic studies have identified the presence of old zircon material it is usually assumed to be present as anhedral cores with euhedral magmatic rims. There are many examples where this assumption has been made, but Pidgeon & Aftalion (1978) and Harrison *et al.* (1987) give corroborative textural evidence in the form of transmitted and reflected light photomicrographs.

In addition to these granitoid occurrences, non-planar compositional interfaces have been observed in zircons found in metamorphic environments. Several U-Pb isotopic studies using ion microprobe techniques have demonstrated that new zircon growth and in particular partial recrystallization of pre-existing zircon may take place during metamorphic events. Studies using the 'SHRIMP' ion microprobe have also presented textural observations made using conventional optical methods (reflected and transmitted light) of the internal structures of the zircons dated. Black *et al.* (1986) described internal zircon structures from a granulite-grade orthogneiss finding zircons with crystal-face parallel multiple zones deeply embayed and mantled by apparently homogeneous zircon. These authors interpreted these textures as resulting from recrystallization rather than new zircon growth over an irregular core. Similar interpretations have been made by Williams & Claesson (1987) on zircons from high grade paragneisses and by Compston & Kröner (1988) on zircons from a tonalitic gneiss.

3.5.1) Subhedral and anhedral core and core related structures.

This section has two aims; 1) to describe the range of subhedral and anhedral core shapes present within many zircon grains, and 2) to describe the nature of the boundaries between cores and rims. For the sake of convenience structures associated with cores are also described here. In the main this section is not concerned with absolute composition, but with the textures of the compositional variations indicated by the different grey-levels on the

Z-contrast images. The definitions of the terms core and rim given above require that there is a significant contrast in the average composition and type of zoning between the core and the rim, not the presence of a non-planar interface, although most do have non-planar interfaces.

Non-planar interfaces which separate areas of *similar* composition and zoning style are described in Section 3.5.2.

Zircon core shapes.

Zircon cores have a variety of possible shapes, in all of the examples described below the boundary between the core and the rim is compositionally discontinuous and the position of the core/rim boundary is well defined.

1) Plate 3.4. This shows a subhedral core totally surrounded by a euhedral rim, the sense of curvature of the core/rim boundary is in all places convex outwards.

2) Plate 3.5. This zircon contains a central, broadly euhedral core with a generally low Z, one section of the outer boundary (marked A) is subhedral and is seen to truncate compositional zoning structures within the core.

3) Plate 3.6. Although the outline to the core of this grain is highly contorted, it has concave outward parts to its length, it is everywhere smooth. The complex outer shape of the core has apparently influenced the morphology of the surrounding rim.

4) Plate 3.7. This grain has a generally rounded core, but locally the outline is ragged on the scale of a few microns.

Highly rounded core shapes with convex outward margins are by far the most common type observed, highly irregular cores are the exception.

The nature of the boundary between cores and rims.

Although many grains do have obvious core/rim relationships the nature of the core/rim boundary can be highly variable, such that the exact position of the dividing line can be difficult to trace. Three broad types of core/rim boundary have been identified.

1) Compositionally discontinuous; the core/rim boundary is sharp within the resolution of the electron beam conditions employed. Plates 3.4, 3.5, 3.6 and 3.7 all have compositionally discontinuous core/rim boundaries.

2) Compositionally continuous; there is a compositional gradient between the core and the rim. The distance over which the compositional change is achieved is greater than the resolution limit of the beam. Plate 3.8 shows a grain with two approximately concentrically arranged cores, the inner most of which has a gradational outer boundary with the second core (marked A).

3) In some grains tracing the exact position of the core/rim boundary is difficult, even although tracing the exact position of the core/rim boundary is difficult. This is usually for one of two reasons: i) the core and the rim, in the region of the interface, may have similar grey-levels and thus the boundary is difficult to distinguish; or ii) the core/rim boundary region may contain other zoning structures which obscure the true nature of the relationship between the core and the rim. For example, Plate 3.9 shows a cored grain which has an area

Plate 3.5. ZCI of separated zircon from the Kameruka Granodiorite (AB 40) from the Bega Batholith. The core to this grain is broadly euhedral, however one section of the outer boundary (A) is concave outwards and it truncates the zoning of the core. Amplifier saturation occurred along the left hand side of the crystal.
15kV, 20nA, (7,7), scale bar 100μm.

Plate 3.6. ZCI of separated zircon from the Glen Sanda Granodiorite (BPSRG1) of the Strontian Complex. The outline of the core is highly contorted, with many sections being concave outward. The effects of amplifier saturation can be seen along the left hand side of the grain.
15kV, 20nA, (7,7), scale bar 100μm.

A

Plate 3.7. ZCI of separated zircon from the Glen Sanda Granodiorite (BPSRG1) of the Strontian Complex. The outline, although generally rounded, is ragged on the the scale of a few microns. The photomicrograph was exposed to allow the zoning of the core to be seen, thus the detail in the rim is mainly lost.
15kV, 20nA, (7,7), scale bar 100μm.

Plate 3.8. ZCI of separated zircon from the Kameruka Granodiorite (AB 40) of the Bega Batholith. The inner most core of this grain has a gradational outer boundary (A) with the second core structure. The bright left hand edge is caused by amplifier saturation.
15kV, 20nA, (7,7), scale bar 10μm.


15 441 0284 0100,0U


A
15 541 0421 0010,0U

Plate 3.9. ZCI of separated zircon from the Glen Sanda Granodiorite (BPSRG1) of the Strontian Complex. The precise position of the core/rim boundary is difficult to identify in this crystal because of the presence of other zoning structures (A). The photomicrograph was exposed to allow the zoning of the core to be seen, thus the detail in the rim is mainly lost. The bright left hand edge is caused by amplifier saturation.
15kV, 20nA, (7,7), scale bar 100μm.

Plate 3.10. ZCI of separated zircon from the Glen Sanda Granodiorite (BPSRG1) of the Strontian Complex. Between the core and the crystal face-parallel zoning of the rim lies a narrow band (A) which varies in width and contains irregular compositionally continuous zoning. Much of the radial cracking in the rim is an original feature and not caused by sample preparation. The effects of amplifier saturation can be seen along the left hand side of the grain and to the right of inclusions.
15kV, 20nA, (7,7), scale bar 10μm.

A

A

(marked A), between the core and the crystal face-parallel zoning of the rim, in which the zoning is sufficiently complex that the position of the core/rim boundary is ambiguous.

Core related structures.

The remainder of this section describes the types of structures that have been commonly observed associated with the core/rim boundary regions of zircon grains and which, although they may occasionally make the core/rim boundary difficult to identify, may potentially yield information about the relationship between cores and rims.

Plate 3.10 shows a grain which has a similar structure to that shown in Plate 3.9, except that the core/rim boundary can be easily identified. Between the core and the crystal face-parallel zoning of the rim lies a narrow area (marked A), which varies in width, with irregular compositionally continuous zoning. This type of area (a volume in three-dimensions) is commonly seen between the subhedral and anhedral cores of zircon grains and the first crystal face-parallel zone of rims. Its size is usually limited such that at least one part of the zoning in the rim is in contact, or nearly so, with the core; Plate 3.11 shows such an area (marked A), in this case it has a relatively low η and no internal structures can be seen. Only where the core shape is highly irregular, say with concave outward sections, does the size of this volume become significant; the area marked A on the zircon in Plate 3.12 is an example. One of the examples referred to earlier, Plate 3.6, also shows this feature.

3.5.2) Non-planar interfaces other than core/rim structures.

Two other types of non-planar interface have been observed in zircons.

1) Plate 3.13 shows a grain with many crystal face-parallel zones, interrupting this simple pattern are several non-planar interfaces that form closed loops. They are broadly concentric with the crystal face-parallel zoning and separate areas of multiple crystal face-parallel zoning which are similar in average composition and character of zoning (*eg.* spacing of zones, range of grey-levels). They are not considered to be a core structures because they do not separate concentrically arranged parts which are distinctly different in terms of overall grey-level and character of zoning. Unlike the interfaces observed in some core/rim structures, the type described here are *always* convex outwards, never markedly curved, they often truncate only the corners of crystal face-parallel zones, and the interfaces are always compositionally discontinuous. Several of the photographs used to illustrate other textures also have this type of non-planar interface, *eg.* Plates 3.1, 3.2 and 3.3.

2) Plate 3.14 shows an example of the second type of non planar interface, the zircon grain has crystal face-parallel zoning which is truncated by areas (volumes in three-dimensions) which internally are not zoned, these are marked A. The boundaries, which in the main are compositionally discontinuous, can be both non-planar (marked B) and planar (marked C). It is important to note that where these interfaces are planar they are parallel to the crystal faces and are always on the side of the internally unzoned area nearest to

Plate 3.11. ZCI of separated zircon from the Loch Sunart Granodiorite (BPSRT1) of the Strontian Complex. In this example the volume between the core and the crystal face-parallel zoning of the rim, which has a relatively low η, is structureless. The extensive cracking around the edge of the grain is due to the sample preparation procedure. The effects of amplifier saturation can be seen along the left hand side of the grain and to the right of inclusions.
15kV, 20nA, (7,7), scale bar 100μm.

Plate 3.12. ZCI of separated zircon from the Kameruka Granodiorite (AB 40) of the Bega Batholith. This is a fragment of a much larger grain. The shape of the core to this grain is highly irregular, such that the volume of material between the core and the crystal face-parallel zoning is significant. The text gives a full description of this type of texture. The bright left hand edge is caused by amplifier saturation.
15kV, 20nA, (7,7), scale bar 100μm.

A

A

Plate 3.13. ZCI of separated zircon from the Kameruka Granodiorite (AB 40) of the Bega Batholith. The relatively simple pattern of crystal face-parallel zoning is interrupted by several non-planar interfaces forming closed loops, however unlike core structures the interface separates areas of similar zoning. The bright left hand edge is caused by amplifier saturation.
15kV, 20nA, (7,7), scale bar 100μm.

Plate 3.14. ZCI of separated zircon from the Loch Sunart Granodiorite (BPSRT1) of the Strontian Complex. Note the areas (A) with which internally are not zoned, the boundaries to these areas can be both non-planar (B) and planar (C). The effects of amplifier saturation can be seen along the left hand side of the grain and to the right of inclusions. The cracking is an artifact of the sample preparation process.
15kV, 20nA, (7,7), scale bar 100μm.

A
A
C
A
B
A

the crystal faces. If there are several of these unzoned areas within a given crystal then they usually have similar grey-levels. It is important to note that they are not commonly associated with cracks. Initially these unzoned areas were thought perhaps to be some artifact of the sample preparation procedure, but subsequent electron microprobe analyses have shown them to be real. Electron microprobe analyses 15, 16, 17 on the grain shown in Plate 3.2 all have concentrations of the REE, Y, Th and U which are below electron microprobe detection limits, although they have similar concentrations of Hf to the other parts of the grain. Several Plates used to illustrate other textures also show this type of structure, *eg.* Plates 3.1 and 3.2.

3.6) COMPOSITIONAL SECTOR ZONING.

Definitions: compositional sector zoning.

The portion of a crystal that is present 'inside' a given face is called a **sector**, and in general most crystals bounded by faces contain several sectors. Where a crystal has sectors of different chemical compositions it is described as having **compositional sector zoning** (Hollister, 1970). The qualifying term 'compositional' is necessary since the sector zoning in, for example, andalusite and chloritoid generally result from variations in the density of inclusions and not compositional differences in the host phase (Deer *et al.*, 1982). Hollister (1970) observed that sectoral variations may also take the form of differences in cation ordering within the crystal structure and suggested that such sectoral variations could be found in combination with compositional sector zoning. It is worth noting that the spatial pattern of the sectors is due to the relative importance of the different crystal faces developed during the growth of a given mineral grain, *ie.* whatever causes compositional sector zoning it is, *by definition*, always associated with the development of crystal faces.

Where other types of zoning are present, *ie.* crystal face-parallel multiple zoning, it is important that the equivalence or otherwise of the zoning between sectors is established in addition to comparing the chemistry of the sectors. Where there is a non-equivalence of the multiple zoning between sectors a crystal is considered to be sector zoned (simple systematic variations in thickness of zones between sectors is not considered to constitute non-equivalence).

Previously reported occurrences of compositional sector zoning in zircon.

Before describing the previous occurrences of compositional sector zoning in zircons it is necessary to document the crystal faces that are found in granitoid zircons, a subject extensively studied by J.-P. Pupin and coworkers. The faces that are commonly present can be divided into two groups (Pupin *et al.*, 1978): pyramidal faces, usually (211), (101) and (301); and prism faces, (110) and (100). In practice it can be difficult to identify the particular crystal faces that are present when dealing with sectioned grains, although it is usually possible to distinguish prism faces from pyramidal faces.

Compositional sector zoning in zircon was produced experimentally by Chase & Osmer (1966), they grew zircon in an environment doped with UO_2 and found that it was

preferentially incorporated into the pyramidal (111) sectors (*ie.* the sectors associated with the (111) face). It should be noted that (111) is a face not commonly developed in granitoid zircons. Similar compositional patterns were noted by Fielding (1970) in a zircon from a pegmatite and by Krogh (1982b) in zircons from an Archaean granodiorite. In both cases U was preferentially incorporated into the pyramidal sectors, although which pyramidal faces were involved was not specified. The zircons that Krogh (1982b) described (and illustrated with optical photomicrographs) have the type of sector zoning described above in the section on definitions, *ie.* the different sectors are not equivalent in terms of their patterns of multiple zoning.

A pattern of compositional sector zoning different from that described by Chase & Osmer (1966) and Fielding (1970) was observed using cathodoluminescence by Hoffman & Long (1984). They described sectoral variations between the prism sectors, (100) and (110), of zircons from the granodioritic Tollie Gneiss of the Lewisian. The (100) sectors were enriched in Y and depleted in Hf and Zr, whilst the (110) sectors were slightly enriched in Hf and depleted in Y. Hoffman & Long (1984) were not able to describe the distribution of U with respect to the different sectors since U was below the electron microprobe detection limits. Using cathodoluminescence Ohnenstetter *et al.* (1989) identified compositional sector zoning in zircons from a Corsican ophiolitic albitite, the sectoral differences in composition were due to variations in the concentration of the REE and Y; they did not give details of how these compositional variations were related to specific sectors. Paterson *et al.* (1989) identified, using the BSE technique, compositional sector zoning in a zircon from the Ratagain intrusion.

In none of the previously reported occurrences was any attempt made to interpret the compositional sector zoning with respect to petrogenesis.

3.6.1) Examples of compositional sector zoning in zircons.

Much of the compositional sector zoning found in granitoid zircons during the course of this research is in the form of sectors which are not equivalent in terms of their crystal face-parallel zoning patterns. Thus the emphasis of the descriptions given below is necessarily on the textural rather than the compositional aspects. As with crystal face-parallel zoning a number of examples are considered in some detail, each was chosen to illustrate the range of textures observed. It should be emphasised that many grains in these and other rocks have similar textures and the examples chosen are by no means unusual. A number of Plates used to illustrate other textures in zircon grains, notably those with crystal face-parallel zoning (*eg.* Plates 3.1, 3.2 and 3.3) also exhibit compositional sector zoning. Full details of the microprobe analyses from the individual examples are in Appendix 3.

Plate 3.15. ZCI of zircon in a thin section from a Ratagain diorite (RAT 13/1). Both the core and rim of this grain contain compositional sector zoning. The numbered points are the electron microprobe analysis points (see Appendix 3). The text gives a description of the compositional variations. The pattern of the cracking suggests that it is not due to sample preparation.
15kV, 20nA, (6,7), scale bar 10μm.

Plate 3.16. ZCI of separated zircon from the Loch Sunart Granodiorite (BPSRT1) of the Strontian Complex. In this the compositional sector zoning due to differences in the patterns of crystal face-parallel zoning between sectors, a full description is given in the text. The effects of amplifier saturation can be seen along the left hand side of the grain and to the right of inclusions. The cracking occurred during sample preparation.
15kV, 20nA, (7,7), scale bar 100μm.

10
9
2
1
4
6
8
3
5
7

1
2
3

Example 1 (Plate 3.15).

This example is taken from a dioritic rock from the Ratagain intrusion of the NW Highlands and originally appeared in Paterson *et al.* (1989). The grain contains an obvious rounded core which internally has compositional sector zoning, the rim is also compositionally sector zoned and it is this that the description below is concerned with. In this example the compositional sector zoning is marked by clear changes in composition across the sector boundaries.

The rim of this grain contains only very faint crystal face-parallel zoning and it appears to be present only within the generally brighter sectors and not in the darker sectors. These darker sectors are, however, continuously zoned, becoming progressively brighter towards the edges of the crystals, a trend also seen in the generally brighter sectors. Whilst this grain has concentrations of the REE, Y, U and Th that are at or below detection limits, Hf shows variations in concentration that are considered significant. Within all the analysed sectors Hf increases in concentration towards the crystal edges, but between sectors the variations are less clear and do not show a straightforward correlation with the observed grey-levels. For instance, Sector 1 has the lowest overall concentration of Hf of any of the analysed sectors, yet has a η which is higher than the adjacent sector (Sector 2) which is more enriched in Hf.

The fact that the observed grey-level variations are not related in a simple way to Hf concentration suggests that another element (or elements) in addition to Hf, is responsible for the variations in the observed grey-level variations within sectors and between sectors. Such an element must either be present in quantities below detection limits, or the element involved was not included in the original analysis. Clearly it is difficult to comment further on the last possibility. The occasional detection of the REE, Y, U and Th in the quantitative analyses of this crystal suggests that they certainly contribute to the overall η and it is entirely possible that their distribution combined with that of Hf could explain the qualitative variations in composition observed on the ZCI.

This example illustrates that in the right circumstances the BSE technique is more sensitive to variations in composition than quantitative analysis by electron microprobe.

Example 2 (Plate 3.16).

This zircon grain is from the Loch Sunart Granodiorite of the Strontian Complex, it is mounted in epoxy with the c-axis lying east-west and parallel to the plane of the section. This example is intended to illustrate the variability of zircon sectors in terms of their crystal face-parallel zoning patterns and how this influences the position and shape of the boundaries between sectors.

The three sectors (Sectors 1, 2 and 3) with which this description is concerned are very different in terms of their patterns of zoning.

1) Sector 1 ((101)) has several wide multiple zones of low η that have no equivalent in the adjacent Sector 2 ((211)).

2) Sector 2 contains a large number of multiple zones many of which have high η, few of these zones have equivalents in Sector 1.

Plate 3.17. ZCI of separated zircon from the Glen Sanda Granodiorite (BPSRT1) of the Strontian Complex. The pyramidal 'faces' (marked A) were eradicated during growth such that they are no longer exist on the outermost faces of this particular crystal. The very dark areas within the rim are the result of differential polishing probably caused by these areas being metamict. The bright left hand edge is caused by amplifier saturation.
15kV, 20nA, (7,7), scale bar 10μm.

Plate 3.18. ZCI of separated zircon from the Loch Sunart Granodiorite (BPSRT1) of the Strontian Complex. A full description of the compositional sector zoning in this example is given in the text. The numbered points are the electron microprobe analysis points (see Appendix 3). The effects of amplifier saturation can be seen along the left hand side of the grain and to the right of inclusions. The cracking occurred during sample preparation.
15kV, 20nA, (7,7), scale bar 10μm.

A
A
A
A

A
B
1
2
3
4
5
6
7
8
9
10
11
12
13
14
15
16
17
18
19
20

3) Sector 3, (100) or (110) (it is difficult, in this section, to determine which), has similarities to Sector 2 in terms of numbers of zones, although there are fewer high η zones.

The fact that so many zones within a given sector do not have equivalents within adjacent sectors means that the boundary between sectors is not smooth but is very angular and 'saw-toothed' in its appearance. This is a common feature of granitoid zircons, although in the example presented here the amplitude of the 'teeth' is large (5-10 μm), in most cases the amplitude is small (often less than 1 μm). Since sector zoning is related to the development of crystal faces then the shapes of sector boundaries record fluctuations in the relative importance of crystal faces during growth. Even in zircon crystals which are not compositionally sector zoned, but contain crystal face-parallel zoning, Z-contrast images permit study of the changes in the relative importance of different crystal faces during progressive growth.

An extreme example of non-growth of faces is shown in Plate 3.17, one of the pyramidal faces (marked A) has been eradicated during growth by virtue of the fact that normal (perpendicular) growth has occurred solely on these faces; or stated another way, there has been lateral only growth of the two adjacent faces to such extent that the face in between has been eradicated, this is illustrated diagrammatically in Figure 3.3. In this particular example there is also a marked change in the grey-level of the zircon at the point during growth at which the pyramidal faces start to be eradicated.

Similar structures due changes in the relative importance of crystal faces during growth have been observed in granitoid titanites, these are described in Chapter 4.

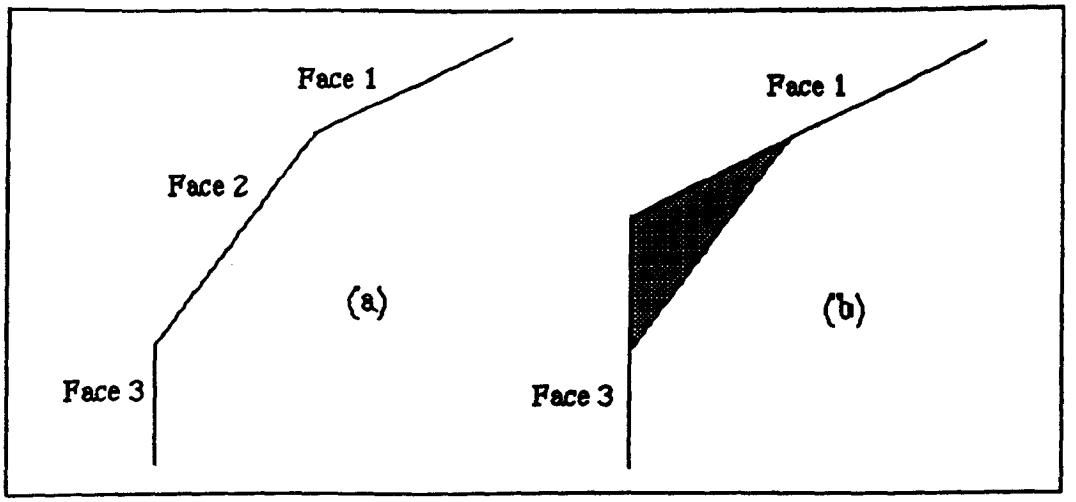

Fig. 3.3 (a) and (b). This diagram shows how by preferential perpendicular growth of Face 2 (shaded material - (b)) and no perpendicular growth on the adjacent faces Face 2 is eradicated. It is important to note that whilst there has been no *perpendicular* growth of Faces 1 and 3 there has been *lateral* growth.

Example 3 (Plate 3.18).

This crystal is from the same rock sample as example 2, the rock being from the Loch Sunart Granodiorite of the Strontian Complex. The c-axis is aligned east-west in the Plate, parallel with the plane of the section, the crystal faces parallel with the c-axis are the prism faces ((100) and (110)), the other faces being the pyramidal faces of the crystal terminations ((101), (301) and (211)). This example combines features of examples 1 and 2. The compositional sector zoning in this example manifests itself in two forms: 1) individual discontinuous multiple zones have different compositions within different sectors and they are separated by distinct compositionally discontinuous boundaries; and 2) differences in the pattern of crystal face-parallel zoning between sectors.

The crystal face-parallel zoning within the sectors of the pyramidal faces contain a large number of bright (high η) zones. Most of these high η zones do not continue into the adjacent prism sectors (marked A on Plate 3.18) or if they can be traced across the boundary into adjacent sectors then they generally show a change in composition across that boundary (marked B on Plate 3.18). Compositionally the high η zones of the pyramidal sectors are marked by higher concentrations of the HREE, Y, U and Th than the darker zones of the same sectors (see Table 3.1). Concentrations of Hf, on the other hand vary only slightly

Table 3.1. Comparison of Y_2O_3, $HREE_2O_3$, ThO_2 and UO_2 concentrations (wt%) of different crystal face-parallel zones of the zircon shown in Plate 3.18, the zones with high η (represented by analyses 5 and 6) generally have higher concentrations than zones with low η (analyses 1 and 7).

	1	5	6	7
Y_2O_3	n.d.	0.17	0.11	n.d.
Er_2O_3	n.d.	0.04	0.04	0.04
Yb_2O_3	n.d.	0.06	0.04	n.d.
ThO_2	n.d.	0.09	n.d.	n.d.
UO_2	0.06	0.16	0.07	0.06

between the light and dark zones of the pyramidal sectors. The zones within the prism sectors contain concentrations of the HREE, Y, U and Th that are *below* detection limits and as with the pyramidal sectors Hf concentration does not vary significantly within the prism sectors. However, between the pyramidal and prism sectors Hf concentration does vary systematically, Hf concentration being approximately 0.15 wt% higher in the prism sectors than the pyramidal sectors, see Table 3.2.

Table 3.2. Comparison of HfO_2 concentrations (wt%) between pyramidal and prism sectors of zircon in Plate 3.18, HfO_2 concentrations are slightly (0.1-0.2 wt%) higher in the prism sectors than in the pyramidal sectors. The analysis numbers are in pairs (1 and 12, 6 and 14, 7 and 19), *ie.* analyses are approximate equivalents of each other within the two sectors.

Pyramidal Sector:		Prism Sector:	
Analysis Number	HfO_2	Analysis Number	HfO_2
1	1.42	12	1.55
6	1.36	14	1.52
7	1.53	19	1.73

This example of compositional sector zoning in zircon is similar to that described by Krogh (1982b) in that U-enriched zones preferentially occur within the pyramidal sectors. Krogh (1982b) did not document the distribution of other elements and thus it is not known if the REE, Y, Th and Hf of his examples have a similar distribution to that of the crystal shown here.

3.7) SUMMARY.

3.7.1) Crystal face-parallel continuous and discontinuous compositional zoning.

This study has observed that crystal face-parallel zoning in granitoid zircons is ubiquitous, at least within material thought to have crystallized from the melt which gave rise to the granitoid, *ie.* not material which may be inherited from other very different environments. The scale of the zoning is very fine, from ~1 μm up to ~5 μm for the width of a single zone. Within the three examples described variations in the concentrations of the HREE, Y, U, Th and Hf are most important in determining variations in the observed grey-levels of the crystal face-parallel zones. The concentrations of the HREE, Y, U and Th appear to be positively correlated with each other, Hf on the other hand appears to be negatively correlated in two of the three examples.

3.7.2) Non-planar continuous and discontinuous compositional zoning.

Non-planar interfaces in zircons can be arbitrarily divided into two types.

1) Subhedral and anhedral core and related structures. Zircon cores with non-planar interfaces can have a variety of shapes from virtually euhedral through highly rounded to complexly irregular. The core/rim boundary can be compositionally discontinuous, continuous or in some cases other structures in the core/rim boundary area can obscure its true nature. The rims to zircon crystals with cores commonly have crystal face-parallel

zoning, between this zoning and the core is an area (volume in three dimensions) which is either structureless or contains irregular compositionally discontinuous zoning. These volumes between the core and the crystal face-parallel zoning of the rims are restricted such that at least part of the zoning in the rim is in contact with the core.

2) Other non-planar interfaces. Two types have been identified, the first occurs in association with crystal face-parallel zoning and is found within the zones and occasionally truncating them. The interface is always convex outward and never markedly curved. It differs from a core structure in that it separates areas of similar zoning style. The second type occurs as irregular areas (volumes) which are internally structureless and truncate crystal face-parallel zoning. In the examples shown they do not contain detectable quantities of the HREE, Y, U and Th, unlike the crystal face-parallel zones that they are seen to truncate.

3.7.3) Compositional sector zoning.

Two variaties of compositional sector zoning have been observed in granitoid zircons.

1) A non-equivalence in the crystal face-parallel zoning between sectors, such that a given zone has no equivalent within an adjacent sector, this is shown diagrammatically in Figure 3.4. The most common manifestation of this is where HREE, Y, U and Th enriched crystal face-parallel zones preferentially occur within the pyramidal sectors. In the examples which show this type of compositional sector zoning there also differences in the Hf concentrations between sectors; the prism sectors usually contain higher concentrations of Hf than the pyramidal sectors.

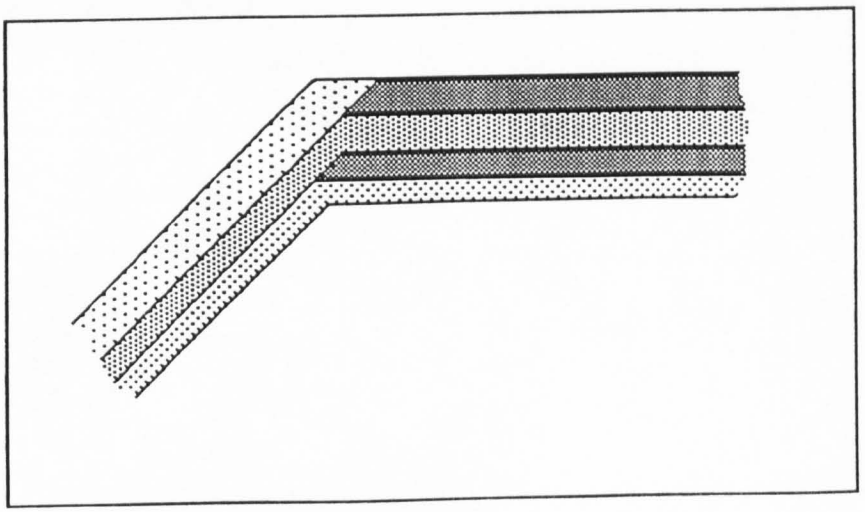

Fig. 3.4. This shows diagrammatically the type of sector zoning in which there is a non-equivalence in the crystal face-parallel zoning between adjacent sectors.

2) Crystal face-parallel zones that can be traced between sectors, but across the boundary the zones show distinct changes in composition (diagrammatically illustrated in Fig. 3.5). This is often due to variations in the concentration of the HREE, Y, U and Th, such that these elements are enriched in the pyramidal sectors. Hf on the other hand is usually preferentially concentrated within the prism sectors, *ie.* there is a negative correlation between the concentrations of HREE, Y, U, Th with that of Hf.

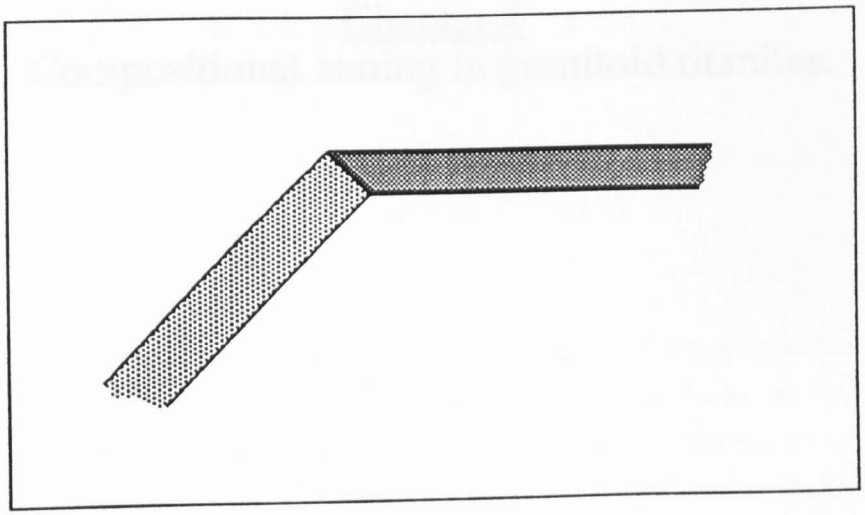

Fig. 3.5. This shows diagrammatically the type of sector zoning in which there is a distinct change in composition across the boundary between the sectors.

Chapter 4
Compositional zoning in granitoid titanites.

4.1) INTRODUCTION.

The main type of zoning texture that has been observed in titanites from calc-alkaline granitoids is compositional sector zoning, although it usually occurs in association with other textures, most notably crystal face-parallel continuous and discontinuous zoning. Thus whilst the *aims* of this chapter are similar to those of Chapter 3, the *organisation* is slightly different; a number of examples of grains with compositional sector zoning are described rather than the textures being described in isolation. The other textures that are present within the examples shown here are described only briefly. The definitions of all the zoning textures are given in Chapter 3.

It is noted that the International Mineralogical Commission requires the name titanite to be used rather than sphene (*Mineralogical Magazine*, **52**, p290).

Background information.

Titanite is a widespread accessory mineral in igneous rocks, being found in intermediate to acid intrusive and extrusive rocks, rocks of the Caledonian 'appinite' suite, nepheline syenites and acid pegmatites amongst many others. In many of these rocks it is often the dominant Ti-bearing phase. The importance of titanite in controlling the behaviour of trace elements, and in particular the REE of calc-alkaline granitoids, has been demonstrated by many studies; for example Gromet & Silver (1983) studied a granodiorite from the Peninsular Ranges batholith of southern California and estimated that the titanite contained approximately 30% of the total whole rock concentration of LREE and up to 90% of the HREE in the rock, the other LREE were mainly contained in allanite. Subsequent studies (*eg.* Sawka (1988) on the McMurry Meadows Pluton of the Sierra Nevada batholith) have confirmed these general findings and showed that such figures are typical in titanite-bearing intermediate to acid plutonic rocks of Cordilleran granites, particularly where allanite is not present.

4.2) TITANITE CHEMISTRY AND CONTROLS ON OBSERVED ZCI GREY-LEVEL VARIATIONS.

4.2.1) Titanite chemistry.

Like zircon, a large number of elements have been reported as being substituents in titanite, $CaTiSiO_5$. The structure of titanite (which is monoclinic) consists of independent Si-O tetrahedra linked by groups of $[CaO_7]$ and $[TiO_6]$ (Deer *et al.*, 1982). In general substitutions involving Si are not important (Ribbe, 1982), substitutions involving Ca, Ti and an underbonded O site dominate. REE, Mn, Sr, Na and Ba can all substitute for Ca, the REE being of particular importance in calc-alkaline rocks. It is known from both experimental studies (Green & Pearson, 1986a) and observations on 'real' systems (*eg.* Sawka *et al.*, 1984) that the MREE have higher titanite/liquid partition coefficients than do the

LREE or the HREE. Ti is most commonly replaced by Al, Fe^{2+}, Fe^{3+}, Mg, Nb, Ta, V and Cr. O in the underbonded site is usually replaced by OH, F and Cl.

The following represent the dominant coupled substitution schemes in natural titanites according to Deer *et al.* (1982) and Ribbe (1982).

1)	$2Ca^{2+} + Ti^{4+} \Leftrightarrow 2REE^{3+} + Fe^{2+}$	(Exley, 1980)
2)	$2Ti^{4+} \Leftrightarrow (Nb, Ta)^{5+} + (Al, Fe)^{3+}$	(Clark, 1974)
3)	$(Al, Fe^{3+}) + (F,OH)^{-} \Leftrightarrow Ti^{4+} + O^{2-}$	(Smith, 1970)

4.2.2) Compositional controls on ZCI grey-level variations in titanite.

As with zircon the most important substitutions in titanite result in the inclusion of elements which generally have higher atomic numbers than either Ca or Ti, this will result in an increase in the $\bar{z}$ (and η) over that of an 'ideal' titanite ($CaTiSiO_5$), this is particularly true of titanites with high concentrations of REE. In some of the examples described below the grey-levels of a ZCI micrograph may be interpreted as *primarily* reflecting the substitution of the REE, although because of the potential complexity of titanite substitution schemes a given η cannot be uniquely related to a particular composition of titanite.

4.3) PREVIOUSLY REPORTED OCCURRENCES OF COMPOSITIONAL ZONING IN IGNEOUS TITANITES.

Unlike zircon, compositional zoning in titanites has generally received little attention, this is mainly due to the fact that compositional variations in titanite have little effect on optical properties, although the colour can vary slightly depending on Fe and REE content (Ribbe, 1982), and thus detection of zoning relies on other, more specialised techniques. Most studies of igneous titanites have used centre/edge or grain traverse electron microprobe analysis strategies in order to detect zoning (*eg.* Exley, 1980; Gromet & Silver, 1983; Sawka *et al.*, 1984), however, to interpret such analyses it is necessary to make assumptions about the texture of the zoning that is present. For instance, Sawka *et al.* (1984) found centre/edge contrasts in the REE content of titanites from a granodiorite pluton and assumed that these contrasts reflected continuous changes in mineral composition brought about by changes in the partitioning behaviour of the REE during growth. All studies which analyse 'blind' are compromised by the need to make unsubstantiated assumptions about the texture of the composition variations and the origin of that texture.

Paterson *et al.* (1989) (work carried out under the auspices of this research) reported compositional zoning in granitoid titanites detected using ZCI, including the first reported occurrence of sector zoning in titanite, and stated that such examples of chemical disequilibrium in granitoid titanites are common. It should be noted that two studies, Franz & Spear (1985) and Bernau & Franz (1987), have also used ZCI to look at the texture of compositional zoning in titanites from *metamorphic* environments.

4.4) COMPOSITIONAL SECTOR ZONING IN TITANITE.

With a few exceptions the zoning patterns seen in cut sections of compositionally sector zoned titanites are not immediately obviously those of sector zoned crystals, this is a function of the crystal habit of titanites and how it can change with progressive growth. Thus the first part of this description (Section 4.4.1) describes the typical crystal habit of the titanite crystals that have been studied and in addition describes the patterns of sector zoning that are possible given this habit. In addition to compositional sector zoning most of the examples described have other types of zoning most notably crystal face-parallel zoning, these features are only briefly described.

The samples used to study titanite zoning textures are taken from a wide variety of rock types from a number of localities: appinites and granodiorites from Strontian (Caledonian, NW Scotland); diorites and monzonites from Ratagain (Caledonian, NW Scotland); and a Precambrian gneiss of granodiorite composition from the Kråkmo area of West Central Norway. Full details of all the localities are given in Appendix 1.

In all the Caledonian granites that have been studied the titanite, if present, has been compositionally sector zoned, these include: Shap (Lake District), Criffel (Southern Uplands), Etive (SW Highlands) and Cluanie (NW Highlands), none of these examples are described here.

4.4.1) Crystal habit of titanite and patterns of compositional sector zoning.

The crystal habit of natural titanites is highly variable, *ie.* there are a variety of crystal forms that can dominate. In the case of most of the examples described here the crystal habit is dominated by the {111} form (see Fig. 4.1(b)), this, combined with the fact that many of the crystals are elongate parallel to the {111} form, leads to the crystals being blade-like. It is important to note that many orientations of section cut through a titanite crystal with such a habit will give a diamond-shaped outline, thus it is difficult to use outline shape as a guide to which faces are present in a given section.

The crystal shown in Figure 4.1(b) is typical of many titanites studied during the course of this research, although not all the faces shown in this drawing are always developed, this latter point is expanded upon below. Figure 4.1(c) is of a titanite with the sectors arising from the {100}, {001}, {102} and {110} forms shown shaded, for the sake of clarity the sectors of the dominant {111} form are left blank. The patterns of compositional sector zoning in two sections of the crystal are illustrated in Figures 4.1(e) (cut parallel to the a and c-axes) and (f) (cut perpendicular to the {111} form). It should be clear that even in a simple case such as Figure 4.1(c), where the relative importance of the different crystal faces remained the same during growth, the internal patterns of compositional sector zoning in titanites can apparently be complex.

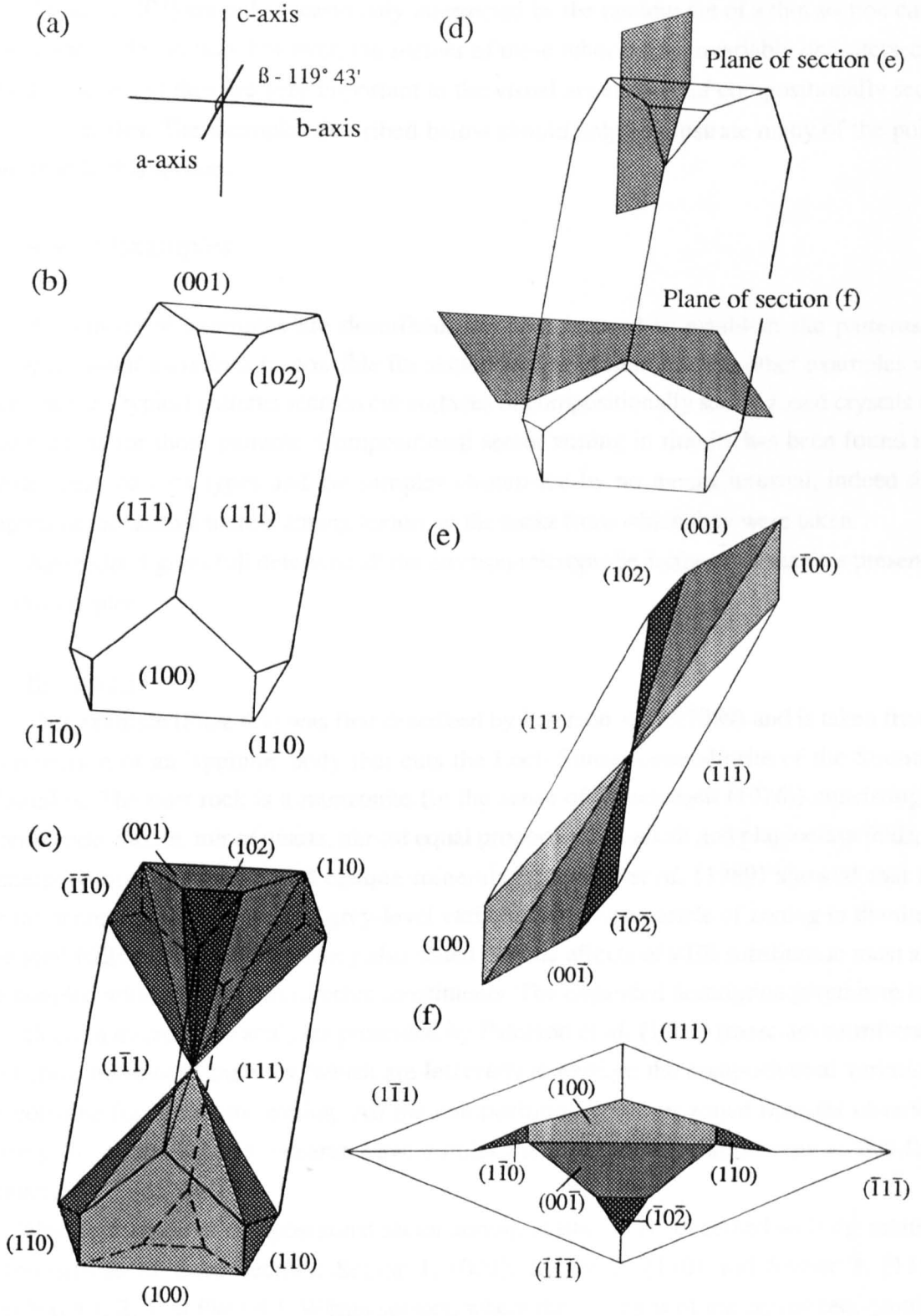

Fig. 4.1(a). Reference crystal axes for diagrams (b), (c) and (d). Titanite is monoclinic, the angle β (a^c) = 119°43'. (b). Orthographic projection of a titanite crystal, morphology is dominated by the {111} form. (c). As (b) but with the sectors arising from the {001}, {100}, {110} and {102} forms shown shaded, the sectors of the {111} form have been left blank. (d). As (b) but showing the orientation of the cross-sections of (e) and (f). (e). Section cut parallel to the a and c axes showing the pattern of compositional sector zoning. (f). Section cut perpendicular to the {111} form showing the pattern of compositional sector zoning. See text for further explanation.

Due to the dominance of the {111} form the faces of the other forms ({001}, {100}, {102} and {110}) are only occasionally intersected by the random cut of a thin section cut by the plane of the section, however, the *sectors* of these other forms invariably *are* intersected by the plane and thus are very important to the visual appearance of compositionally sector zoned titanites. The examples described below should help to illustrate many of the points outlined in this section.

4.4.2) Examples.

A number of examples are described, the first is used to establish the patterns of *compositional* variations responsible for sector zoning in titanites, the other examples will illustrate the typical patterns seen on cut surfaces of compositionally sector zoned crystals and the reasons for those patterns. Compositional sector zoning in titanite has been found in a wide range of rock types and the samples chosen are by no means unusual, indeed they represent the normal titanite zoning texture in the rocks from which they were taken.

Appendix 4 gives full details of all the electron microprobe analyses of titanites presented in this chapter.

Example 1.

This example (Plate 4.1) was first described by Paterson *et al.* (1989) and is taken from a thin section of an 'appinite' body that cuts the Loch Sunart Granodiorite of the Strontian Complex. The host rock is a monzonite (in the sense of Streckeisen (1976)) consisting of hornblende, biotite, minor quartz, almost equal proportions of alkali and plagioclase feldspar, accessory titanite, apatite and opaque minerals. Paterson *et al.* (1989) showed that the primary control on the observed grey-level variations of this example of zoning in titanite is the total REE content, although they also stated that the effects of REE substitution must also be coupled with substitutions of other constituents. The expanded description given here uses the electron microprobe analyses presented by Paterson *et al.* (1989) (these are **numbered**) and some additional analyses (which are **lettered**) to explore the compositional variations responsible for the sector zoning. All the compositionally sector zoned titanites observed during the course of this research have similar *compositional* relationships to this first example.

This description of compositional sector zoning in titanite is concerned with the relative compositions of three sectors; Sector 1, (001), Sector 2, (110) and Sector 3, (111), numbered 1, 2, 3 on Plate 4.1. Within sectors, where the zoning is of the crystal face-parallel continuous type - there being no discontinuities, there are positive correlations between the total REE content and the concentrations of Al and Fe, however between sectors the opposite is true (Paterson *et al.*, 1989) (see Fig. 4.2). For example, analysis 7 in Sector 1 has a total REE_2O_3 content of 4.2 wt% and Al_2O_3 and FeO (Fe was calculated as FeO, the actual oxidation state is not known) concentrations of 1.08 and 1.17 wt% respectively, this contrasts with analysis 23 of Sector 3 which has a total REE_2O_3 content content of 3.3 wt%

Plate 4.1. ZCI of a titanite from an 'appinite' (BPSRA1) from within the Loch Sunart Granodiorite of the Strontian Complex. This grain is compositionally sector zoned. This photograph first appeared in Paterson *et al.* (1989), as did the numbered electron microprobe analysis points. The lettered points are additional analyses that included a larger number of elements, all analyses are given in Appendix 4. The numbering of the sectors and the traverses is explained in the text. 15 kV, 20 nA, (6,7), width of the field of view is approximately 200 μm.

Plate 4.2. ZCI of a titanite from a diorite (RAT 11/1) within the Ratagain intrusion. This grain is compositionally sector zoned, the pattern of compositional variations is consistent with those shown by the grain in Plate 4.1, see Table 4.2 and Figure 4.3.The two black areas within the grain are anhedral apatite inclusions. The bright areas around the cracks is an artefact of local tilt on the sample.
15 kV, 20 nA, (6,7), scale bar 100 μm.

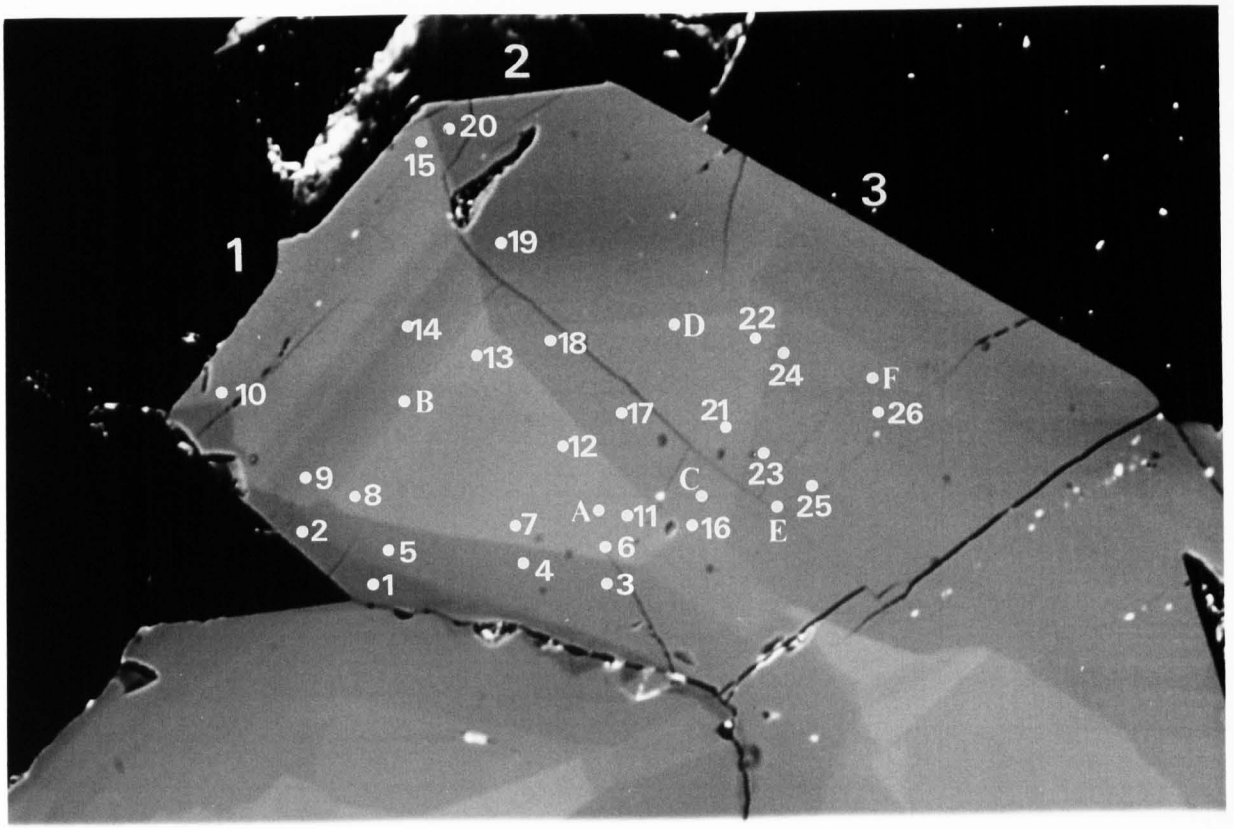
2
3
1
20
15
19
14
D
22
18
13
24
F
10
B
17
21
26
12
9
C
23
8
25
A
11
7
16
E
2
5
6
4
1
3

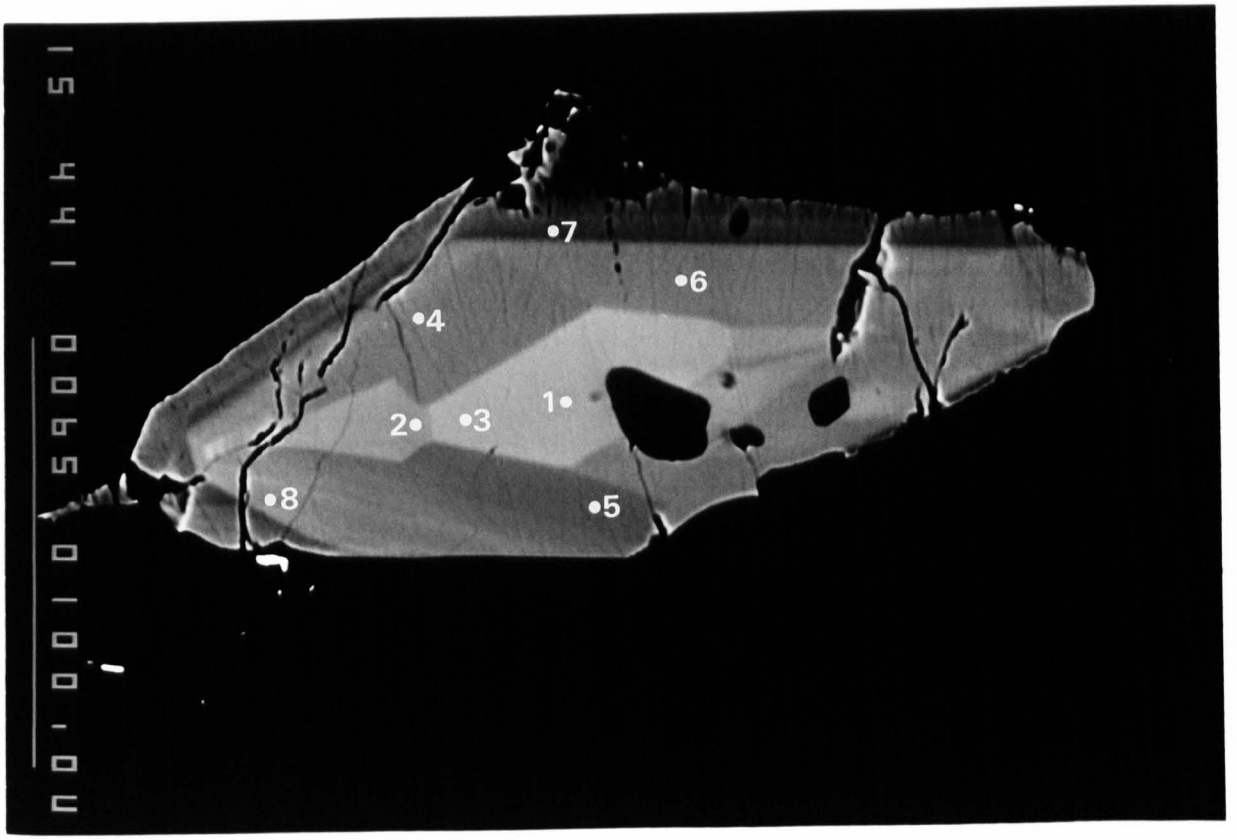
7
6
4
1
2
3
8
5
NO·001059000 1hh 51

and Al_2O_3 and FeO concentrations of 1.34 and 1.25 wt% respectively. The additional (lettered) analyses, over and above those presented by Paterson *et al.* (1989), which included a greater number of elements, show that the relative distribution of Nb within and between sectors is similar to that of the REE (see Table 4.1).

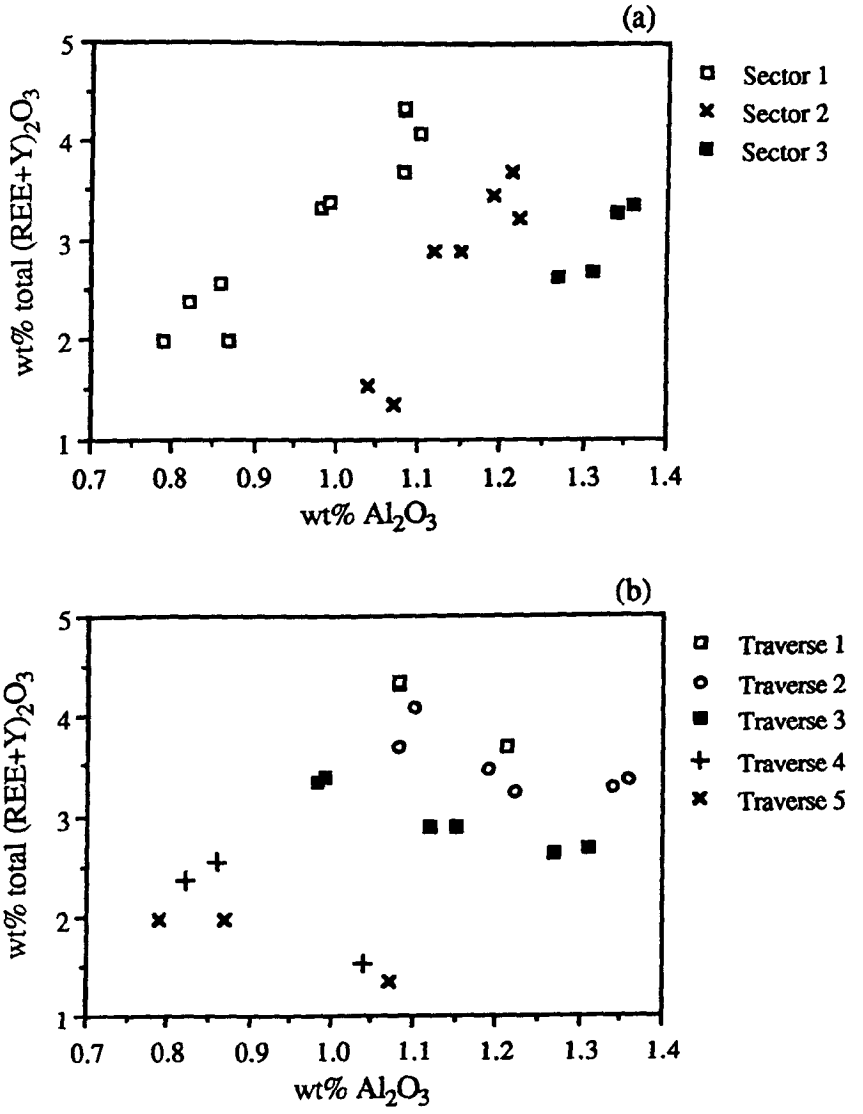

Fig. 4.2. Both of these graphs show Al_2O_3 plotted against total $(REE+Y)_2O_3$. In graph (a) the analyses are divided on the basis of sector, 1, 2 or 3. Within sectors there is a positive correlation between Al_2O_3 and the total $(REE+Y)_2O_3$. In graph (b) the analyses are divided on the basis of traverse, a traverse consisting of analyses which come from equivalent zones within the three sectors. Between sectors there is a negative correlation between Al_2O_3 and the total $(REE+Y)_2O_3$.
Traverse 1 - analyses 6, 11, 16.
Traverse 2 - analyses 7, 12, 17, 21, 23, 25.
Traverse 3 - analyses 8, 13, 18, 22, 24, 26.
Traverse 4 - analyses 9, 14, 19.
Traverse 5 - analyses 10, 15, 20.

Table 4.1. Summary of compositional data for the six lettered analysis points shown on Plate 4.1. Values are given in wt% oxide.

Analysis	Al_2O_3	FeO	Total $(REE+Y)_2O_3$	Nb_2O_5
Sector 1:				
A	1.091	1.284	4.479	0.341
B	0.936	1.102	3.597	0.395
Sector 2:				
C	1.253	1.361	3.908	0.324
D	1.166	1.176	2.982	0.294
Sector 3:				
E	1.349	1.388	3.533	0.223
F	1.275	1.185	2.747	0.168

The results can be related to the equilibrium partition coefficients of the substituting elements and the relative growth rates (measured perpendicular to the crystal face) of the different sectors. Elements with equilibrium partition coefficients (K_o) greater than one, *ie.* the REE and Nb, are preferentially incorporated into the sectors with the highest growth rates, whilst elements with equilibrium partition coefficients less than one, *ie.* Al and Fe, are preferentially incorporated into the sectors with the slowest growth rates (Paterson *et al.*, 1989)).

The following discussion is concerned with the substitution schemes of the three different sectors of the example in Plate 4.1 and in particular analyses C, E and G. It is assumed that the REE and Y substitute into the Ca site by coupled substitution with Fe^{2+} in the Ti site (Exley, 1980), *ie.* substitution scheme 1 of Section 4.2.1. Excess Fe from the substitution of the REE and Y in the Ca site is assumed to be present in the 3+ oxidation state and is used along with Al to charge balance the presence of Nb in the Ti site (Clark, 1974), *ie.* substitution scheme 2. Excess Fe^{3+} and Al from this is thought to be present within the structure by charge balancing with F and OH^- in the underbonded O site (Smith, 1970), *ie.* substitution scheme 3. The positive correlations between the total REE content and the concentrations of Al and Fe within sectors are consistent with the operation of all three of the substitution schemes outlined. However, the negative correlations between the total REE content and the concentrations of Al and Fe between sectors can only be accommodated by *these* schemes if in the sectors with high concentrations of REE the third substitution scheme (*ie.* $(Al, Fe^{3+}) + (F,OH)^- \Leftrightarrow Ti^{4+} + O^{2-}$) is diminished in its importance. It is difficult to prove that this occurs since O and OH^- cannot be determined by electron microprobe. An additional prediction of this work is that there should be differences in the ratio of Fe^{2+} and Fe^{3+} between the different sectors since Fe^{2+} is required to charge balance the presence of the REE and Y in the Ca site; Sector 1, which has relatively high REE concentrations but low Fe concentrations, should have higher Fe^{2+}/Fe^{3+} ratios than Sector 3, which has relatively low REE concentrations and high Fe concentrations.

Example 2.

This example of compositional sector zoning (Plate 4.2) is taken from a diorite of the Ratagain intrusion of NW Scotland. This differs from the first example in one important respect, the pattern of compositional zoning seen on the cut face is more typical of the patterns seen in the majority of crystals that have been studied, this is due to two reasons: firstly, the cut of the first example is quite different from that of example 2; and secondly, the {111} form is relatively more important in this example than in the first example. Although the *apparent* internal compositional zoning pattern is quite different from that of example 1 it is still a manifestation of compositional sector zoning. This is confirmed by the fact that the compositional relationships between the sectors are the same as those of the first example; the analyses are summarised in Table 4.2 and Figure 4.3. The visual pattern of compositional sector zoning in this example is not unlike the pattern shown in Fig. 4.1(f).

It should be noted that the outermost parts of this example also have faint low η continuous crystal face-parallel zoning.

Table 4.2. Summary of compositional data for the numbered analysis points shown on Plate 4.2. The first three analyses are from a sector of the {001} form, they are high in total $(REE+Y)_2O_3$ content, but low in Al_2O_3 and FeO. The rest of the analyses are from sectors of the {111} form and are low total $(REE+Y)_2O_3$ content, but high in Al_2O_3 and FeO. See Figure 4.3. Values are given in wt% oxide.

Analysis	Al_2O_3	FeO	Total $(REE+Y)_2O_3$
{001} form:			
1	1.04	1.86	5.27
2	1.07	1.60	4.79
3	1.09	1.84	5.15
{111} form:			
4	1.17	2.03	3.76
5	1.15	1.91	3.28
6	1.25	2.06	3.81
7	1.04	1.67	2.12
8	1.12	1.93	3.74

Plate 4.3. ZCI of a titanite from the Loch Sunart Granodiorite (BPSRT4) of the Strontian Complex. The internal pattern of compositional sector zoning resembles a stylised 'Christmas tree', this is due to variations in the relative importance of different crystal faces during progressive growth. The text and Figures 4.3 and 4.4 further explain and illustrate the textural effects possible as the result of this process. The very bright area is an inclusion of an opaque mineral, the black inclusions are apatite.
15 kV, 20 nA, (6,7), scale bar 100 μm.

Plate 4.4. ZCI of a titanite from the Loch Sunart Granodiorite (BPSRT4) of the Strontian Complex. In this example the internal patterns resulting from compositional sector zoning are very complex, the text and Figure 4.5 explain how this degree of complexity may arise by variations in the relative importance of the faces of the {001} and {102} forms. Small apatites can be seen around the edge of the larger titanite. The dark areas within the titanite are apatite and feldspar inclusions.
15 kV, 20 nA, (6,7), 100 μm.

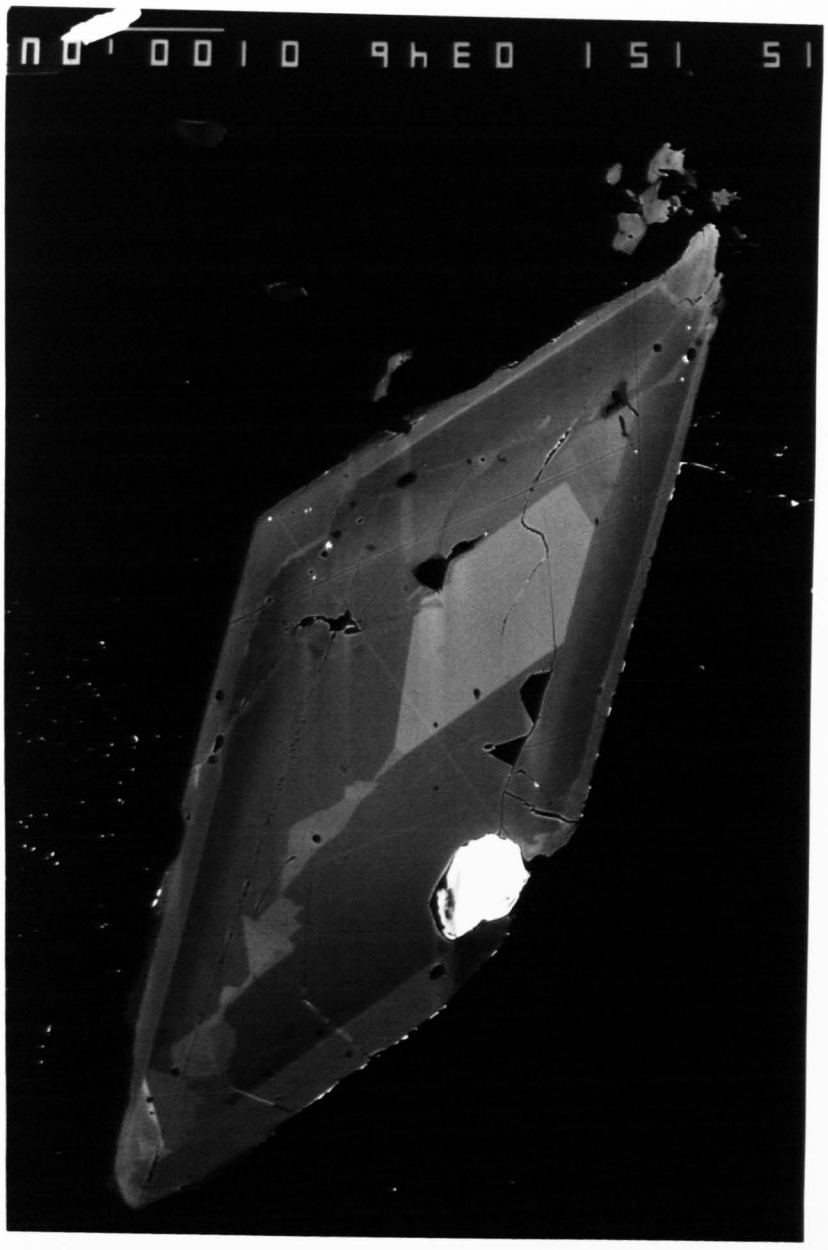

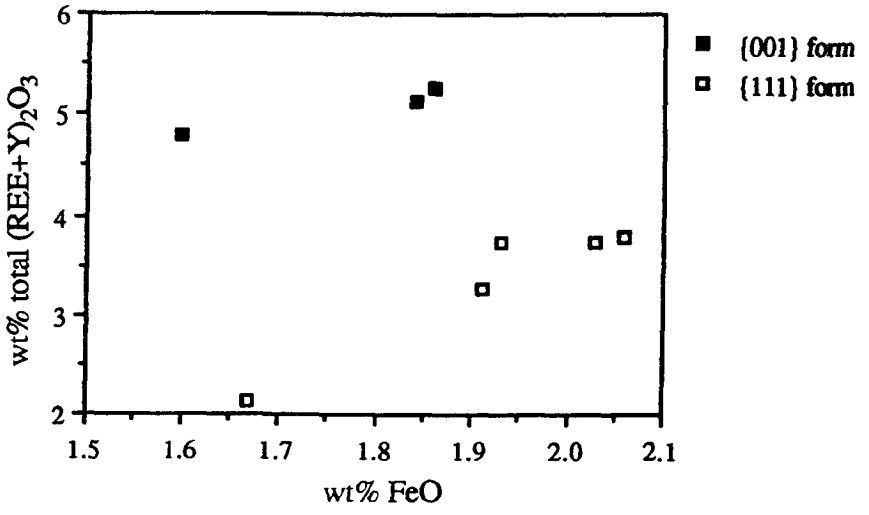

Fig. 4.3. FeO plotted against total $(REE+Y)_2O_3$ for the analysis points given on Plate 4.2 and summarised in Table 4.2. The analyses are grouped depending on the crystal form from which they originate. Analyses from the {001} form have generally higher concentrations of the REE and Y for a given FeO concentration than the analyses from the {111} form. This figure should be compared with Figure 4.2(a) and (b).

Example 3.

In Section 4.4.1 it was noted that the faces of the {100} and {102} forms are usually of minor importance in the titanites observed here, however they are still usually present, or were present at some time during growth of a particular crystal. As explained in Section 4.4.1 the faces themselves are seldom cut by the plane of the section, although their associated sectors invariably are. In addition, these faces fluctuate in their importance during growth creating very complex sector boundaries and hence apparently complex internal compositional variations. The grain in Plate 4.3 (taken from the Loch Sunart Granodiorite of the Strontian Complex) illustrates these effects well, fluctuations in the relative importance of the different crystal faces has given rise to complex 'saw-tooth' shaped sector boundaries. In this case, and many others, the fluctuation in the importance of the face is extreme, such that at times during growth it was not present at all, this phenomenon also occurs in granitoid zircons (see Section 3.6.1, Fig. 3.3). However, unlike zircons the fluctuations in the relative importance of crystal faces are accompanied by only slight within-sector crystal face-parallel compositional variations.

The outermost rim of this example shows a marked compositional discontinuity which can be traced all the way around the crystal, outside this the zoning is dominantly of the discontinuous crystal face-parallel type.

Variations in the importance of different crystal faces during growth and slight within sector variations have an important influence on the visual appearance of all compositionally sector zoned minerals, not only titanite. Figure 4.4 diagrammatically illustrates the effect on the pattern of internal compositional variation of changing the relative importance of a minor crystal face, in titanites small changes in the importance of such a face can give rise to sectors which are shaped rather like stylised Christmas trees. In addition to 'Christmas tree' structures variations in the importance of a minor face can give rise to sectors of a variety of other shapes, some of which are illustrated diagrammatically in Figure 4.5. Such sector shapes have been found to be very common in titanites from calc-alkaline granitoids. The two boundaries of the minor sector usually show some symmetry and unlike the diagrammatic illustrations of Figure 4.5 can be non-planar, although it is interesting to note that planar forms dominate.

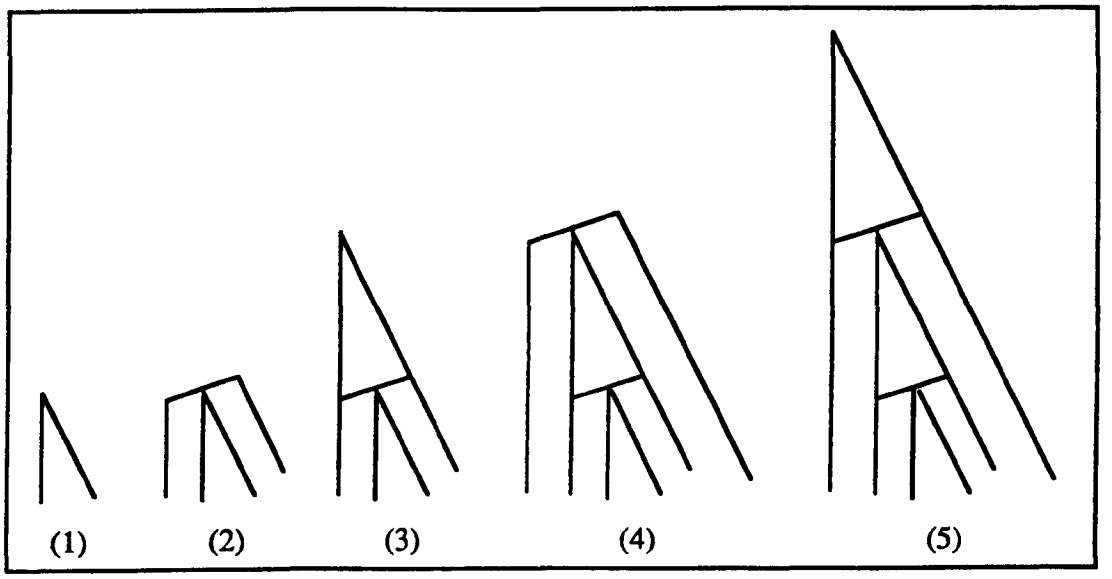

Fig. 4.4. Diagram showing how relative changes in the importance of crystal faces during progressive crystal growth (stages 1 to 5) can give rise to sector zoning structures which resemble stylised Christmas trees. Other possible shapes resulting from the same process are shown below in Figure 4.5.

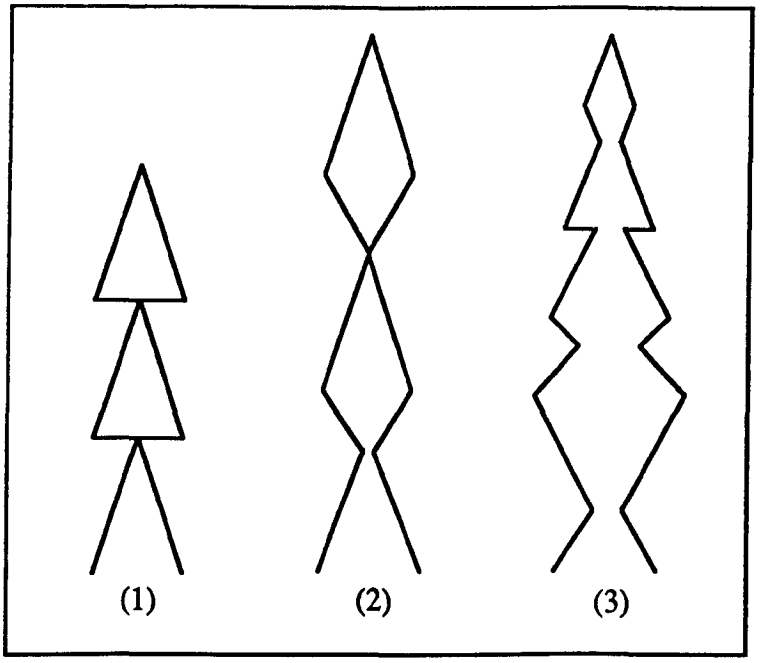

Fig. 4.5. Possible internal patterns of compositional sector zoning resulting from changes in the relative importance of different crystal faces during progressive growth. These shapes should be compared with Plates 4.1 - 4.5 which all show compositionally sector zoned titanites.

In many of the crystals presented here it is the faces of the {001} and {100} forms which gives rise to these complex patterns of compositional sector zoning, although in some examples the sectoral patterns arise from growth and compositional differences between faces of the {001} and {102} forms, example 4 is such a case.

Example 4.

This example, also from the Loch Sunart Granodiorite of the Strontian Complex, demonstrates particularly well many of the principles outlined above and illustrated using examples 1, 2 and 3. In this case (Plate 4.4) both the {001} and {102} faces have been important during the growth of the crystal and it is changes in the relative importance of faces of these two forms and faces of the adjacent form ({111}) that are responsible for the internal pattern of compositional sector zoning. It can be seen that the crude 'Christmas tree' structure running the length of the crystal is zoned internally, some is due to crystal face-parallel zoning and some of which is caused by changes in the relative importance of faces of the {001} and {102} forms. The pattern of zoning within the 'Christmas tree' structure is due to two processes: 1) growth alternating between faces of the {001} and {102} forms, this in combination with the fact the that the interfacial angle of these two faces is small (21°) gives rise to a pattern which in places resembles a series of interlocking wedge shapes; and 2) relatively simple compositional sector zoning in which faces of the {001} and {102} forms grew simultaneously. Both of these features are shown diagrammatically in Figure 4.6, the highly angular pattern of the sector boundaries is typical of the internal patterns of compositional sector zoning in the titanites studied during the course of this research.

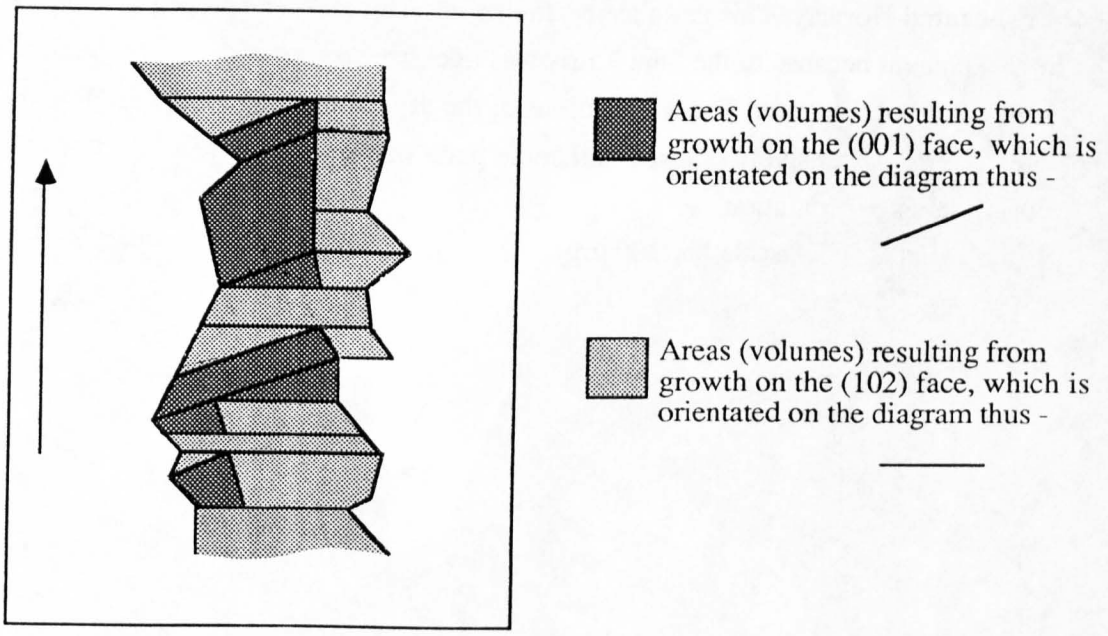

Fig. 4.6. Diagram showing how changes in the relative importance of the (001) and (102) faces during growth can give rise to some of the patterns of compositional sector zoning that have been observed.

The outermost rim of this crystal shows a marked compositional discontinuity which can be traced all the way around the crystal, outside this the zoning is mainly of the discontinuous crystal face-parallel type, although some compositional sector zoning can be seen towards the right hand crystal termination.

The first four examples of compositional sector zoning in titanite were taken from basic, intermediate and acid calc-alkaline igneous rocks; to further demonstrate how common this feature is example 5 is taken from an augen gneiss which is thought to have had an igneous precursor.

Example 5.

The augen gneiss from which this example was taken is granodioritic in composition and from the Kråkmo area of West Central Norway (Robertson, 1988), this Precambrian body had an igneous origin but was subject to later Caledonian deformation and metamorphism (Roberts and Wolff, 1981). Deformation produced a distinct foliation defined by mica-rich layers and quartz ribbons mantling feldspar augen, titanite is present as large generally idioblastic grains (Robertson, 1988). The grain shown in Plate 4.5 shares many of the textural features of the examples described above, *ie.* the grain is compositionally sector zoned and the sectors themselves have angular 'saw-tooth' edges. Although the titanites in this rock generally have good crystal shapes many of them have irregularly-shaped low η (and hence low REE content) areas at crystal edges and in particular at the wedge shaped crystal terminations.

Plate 4.5. ZCI of a titanite from a granitic gneiss from the Kråkmo area of west-central Norway. This grain shows faint compositional sector zoning which is most apparent because of the faint 'Christmas tree' structures that can be seen in the very centre of the grain. The terminations of the crystal have areas of very low η. This grain is extensively cracked and some parts of the grain have been plucked during sample preparation.
15 kV, 20 nA, (6,7), scale bar 100 μm.

NO 10010 6E20 1 2E 51

The existence of compositional sector zoning in titanites from a rock which has undergone metamorphism and deformation suggests that if the texture is originally igneous and not due to growth in metamorphic environment that intra-grain diffusion of the REE within titanites at elevated temperatures is very slow.

4.5) SUMMARY.

Compositional sector zoning in titanites has been found to be a very common feature of a variety of calc-alkaline rock types, ranging from the basic rocks of the appinitic suite, through monzonites, diorites and granodiorites to true granites. In addition compositional sector zoning of titanites has also been found preserved in a granodioritic augen gneiss of originally igneous origin. Studies of typical crystal habits of titanites from calc-alkaline rocks show that the faces of the {111} form dominate, however it is the other morphologically less important forms, {001}, {100}, {102} and {110}, that are largely responsible for the visual patterns of compositional sector zoning that have been observed. The patterns of compositional sector zoning are dominated not only by the number of crystal forms developed in titanites but also by changes in the relative importance of the different crystal faces during progressive growth.

The compositional sector zoning in titanite is due to variations in the concentrations of the REE, Y, Nb, Fe and Al. Elements with equilibrium partition coefficients greater than one (*ie.* the REE, Y and Nb) preferentially occur within the sectors with the highest growth rates (measured perpendicular to the crystal face) and elements with equilibrium partition coefficients less than one (*ie.* Al and Fe) preferentially occur within the sectors with the slowest growth rates.

Chapter 5
Discussion and interpretation of compositional zoning in zircon and titanite.

5.1) INTRODUCTION.

The purpose of this chapter is to discuss the possible origins of the zoning textures of zircons and titanites described in Chapters 3 and 4. Each texture type will be discussed in a general way with proposed models of formation being described; in a separate section the preferred interpretations of these textures are given along with the relevant supporting information. It should be noted that although the textures are considered separately it is possible that they have common causes, that is the different textures represent different responses to the same set of growth conditions.

In Chapters 3 and 4 it was noted that zoning in titanite and zircon is usually due to trace amounts of several elements and it is assumed that the partitioning of these elements obeys Henry's Law, that is partitioning is not affected by the absolute concentration of the trace element in question. Watson (1985) on the basis of existing experimental studies and studies on natural systems discussed the applicability of Henry's Law to trace element partitioning and concluded that the failure of Henry's Law in natural systems due to high or low trace element concentration was probably not of widespread significance.

5.2) CRYSTAL FACE-PARALLEL CONTINUOUS AND DISCONTINUOUS COMPOSITIONAL ZONING.

5.2.1) Discussion.

This discussion is restricted to zoning that is present within material that crystallized along with the host rock, *ie.* it does not cover zoning present within any subhedral or anhedral cores and only includes the zoning present in the outermost rim of such crystals. It is necessary to exclude such core material from the discussion since it may not have grown in the environment in which it is now present (see Section 5.3.2). It is a basic premise that the crystal face-parallel zoning records progressive outward growth by addition of new material on crystal faces.

Changes of composition recorded in the crystal-face parallel zoning could be due to three general mechanisms (it is important to emphasise that these mechanisms are *not* mutually exclusive, they have only been separated to allow clarification of the arguments and it is possible that the same processes within a magma may result in the operation of more than one of the general mechanisms outlined below), namely.

1) Changes in composition due to pervasive changes in the physical or chemical conditions of the whole magma, even on the smallest scale. Equilibrium is maintained between the growing crystal face and the *bulk* magma.

2) Changes in composition due to local changes of physical or chemical conditions within the immediate vicinity of the growing crystal. Equilibrium is maintained only between the growing crystal face and the immediately adjacent magma, not the bulk magma.

3) Changes in composition due to processes occurring across the growing interface or as a result of the nature of the interface, *ie.* interface kinetics. Equilibrium between the crystal and the magma, even the magma immediately adjacent to the crystal, may not be achieved.

Each mechanism will be discussed in turn.

Magma-wide changes in physical or chemical conditions.

Here the discussion is concerned solely with the physical and chemical controls on mineral/liquid trace element partitioning, it is possible that magma-wide changes in some physical or chemical parameter will also have some additional effect, such as allowing convection or changing the crystal growth rate, but for the sake of clarity these processes are not discussed here. It is assumed, for the purposes of discussion, that the physical and chemical changes that may control zircon/liquid partitioning result in an homogeneous liquid, *ie.* there are no compositional heterogeneities developed within the melt.

The dependence of mineral/liquid trace element partition coefficients on various chemical and physical parameters has been demonstrated for many systems. Green & Pearson (1986a) studied the partitioning of REE between titanite and silicate liquid and discovered that the REE increasingly partition towards titanite with increasing SiO_2, increasing pressure and decreasing temperature. For zircon /liquid systems there is only the REE partitioning study of Watson (1980) outlined in Chapter 3 and this work did not explore the effects of varying physical and compositional parameters. Little can be said in either a quantitative or a qualitative way about the controls on partitioning in the zircon/liquid system, however it seems likely that the partitioning behaviour of zircon will depend on the physical and chemical conditions that prevailed within the melt at the time of growth. Even if the trace element partition coefficients for a given accessory phase (or indeed any mineral) were constant during progressive crystallization, the concentration of elements within the mineral would change with time due to progressive changes in the concentrations within the melt brought about by crystallization of the phase of interest and/or other phases (*ie.* model B-3 of Albarède & Bottinga (1972) see Table 5.1).

Table 5.1. Summary of the crystallization models of Albarède & Bottinga (1972).

A. Infinite liquid reservoir:

A-1 The growth rate of the crystalline phase is small enough to allow continuous equilibrium, *ie.* the resultant crystalline phase will be homogeneous.

A-2 Diffusion in the liquid is too slow to maintain a homogeneous liquid phase and consequently to maintain equilibrium between the bulk phases.

B. Finite liquid reservoir:

B-1 Like A-1.

B-2 Diffusion in the crystal is too slow to assure re-equilibration with the varying composition of the liquid phase, the crystal will be zoned.

B-3 Diffusion in the liquid is too slow to maintain a homogeneous liquid phase, the crystal will be zoned but compositionally different from case B-2.

Local changes in physical or chemical conditions adjacent to the interface.

Much as changes in the physical and chemical parameters of the magma as a whole may alter the partitioning of trace elements, local changes may have essentially the same effect, the only difference is the scale and scope of influence of the changes and the range of possible causes. Albarède & Bottinga (1972) predicted, on the basis of crystallization models (their A-2 and B-3 models, Table 5.1), that disequilibrium in terms of trace element partitioning could exist between a crystal and the bulk magma if there was an imbalance between the rate of crystal growth and the rates of elemental diffusion in the magma. The imbalances in diffusion and growth rate would result in the existence of a boundary layer adjacent to the growing crystal. Such a boundary layer could affect the composition of the growing crystal in two ways: 1) it may have a different trace element composition to the bulk magma, but the same partition coefficients may operate; and 2) partition coefficients different from those of the bulk magma may operate within the boundary layer. Clearly both effects could occur in the boundary layer. These local changes of composition brought about by imbalances in the crystal growth rates and trace element diffusion rates could be generated by growth of the phase of interest or by an adjacent crystal. Clearly potentially complex systems could be developed in a magma containing several simultaneously crystallizing phases.

Interface kinetics.

The group of processes that are considered here are those that occur at the growing interface as a result of the processes of growth or due to the nature of the interface. Much is known both experimentally and theoretically about the general processes of crystal growth (Kirkpatrick (1981) reviewed the kinetics of crystallization of igneous rocks). Central to the theoretical models of crystal growth is the rate at which atoms are attached to the interface. The rate of attachment is dependent on the degree of supersaturation of the growing crystal and the mechanism of attachment of atoms to the crystal surface. The mechanisms of attachment of atoms onto the crystal surface can be divided into two types (Kirkpatrick, 1981).

1) *Continuous growth*, in which the atoms become attached wherever they encounter the crystal interface, this type of growth is usually associated with 'rough' non-planar interfaces (Dowty, 1980).

2) *Layer* (or *lateral*) *growth*, in which the crystal interface is atomically smooth and atoms become attached permanently only at the edges of layers or steps where they are effectively bonded to two surfaces (Dowty, 1980).

Many experimental studies have demonstrated the importance of growth rates and growth mechanism (a reflection of interface type) on the effective partition coefficients (as opposed to equilibrium partition coefficients), that operate in a given mineral/liquid system: *eg.* Kouchi *et al.* (1983a) on Ni distribution between olivine and melt; Kouchi *et al.* (1983b) on Al and Ti distribution between clinopyroxene and melt; and Gamble & Taylor (1980) on crystal/liquid partitioning in augite as a function of cooling rate. The variations in composition recorded by crystal face-parallel zones may reflect variations in the mechanisms of growth and/or crystal

growth rate. Interface kinetics in connection compositional sector zoning is further discussed in Section 5.4.

5.2.2) Interpretation of crystal face-parallel continuous and discontinuous zoning in titanites and zircons.

Discontinuous changes in composition.

The rate at which a crystal grows can be controlled by one of three processes (Dowty, 1980): 1) the rate at which material is transferred across the crystal interface and attached to the crystal surface; 2) the rate of material transport through the growth medium to the site of growth; and 3) the rate of removal of the latent heat of crystallization from the interface.

In siliceous melts crystallizing in a plutonic environment heat diffusion is much more rapid than chemical diffusion, thus the transfer of the latent heat of crystallization does not influence the rate of crystal growth (Dowty, 1980). This implies that in the absence of external influences on the absolute temperature of a magma in a plutonic environment that a high degree of thermal stability will be maintained at any point within the magma and throughout significant volumes of the magma. For this reason the effect of the diffusion of the latent heat of crystallization is assumed to be unimportant and is disregarded in the following discussion.

It is considered that repeated fluctuations in the physical and chemical conditions within siliceous plutonic environments are unlikely to occur, such changes are likely to take place progressively and over significant periods of time. If each multiple crystal face-parallel zone within a mineral records a relatively rapid magma-wide change in physical or chemical conditions then the magmas from which the examples of crystal face-parallel zoning in this study were taken must have suffered typically 20-30 such events during growth. This is considered unlikely as there is no other or independent evidence of such events having taken place and no obvious mechanism by which these changes of chemical and physical conditions may be brought about.

The crystallization models of Albarède & Bottinga (1972) predict that under suitable conditions of crystal growth compositional gradients will be established within a magma if rates of elemental diffusion control crystal growth rates, *ie.* elemental diffusion is slower than the interface reaction. The important question in assessing the applicability of these models to growth of zircon and titanite in siliceous melts is whether crystal growth rate is controlled by elemental diffusion in the magma and if so what effect this has on the composition of the growing crystal? Since any compositional gradients established during crystal growth will not be preserved in the finally crystallized granitoid, evidence of their former existence relies on: 1) theoretical models which assume values for the rates of interface reaction and element diffusion; or 2) on the ability to reproduce the necessary conditions in laboratory crystal growth experiments.

As an aside, some workers (*eg.* Bacon, 1989 and Green & Watson, 1982) have explained the existence of mineral inclusions (in particular accessory minerals) in other

phases on processes of local saturation and nucleation owing to the formation of a compositional boundary layer around the growing crystal caused by imbalances in the crystal growth rates and diffusion rates in the magma. However, whilst being consistent with the current understanding of the solubility of accessory minerals, such explanations of the cause of mineral inclusions should not be used as unequivocal evidence for the former existence of crystal growth-induced compositional gradients since there are alternative models for the origin of mineral inclusions.

Experimental studies of accessory mineral growth in siliceous magmas under representative conditions would require unrealistically long experimental durations, thus little is known directly about accessory mineral growth rates or whether compositional gradients are established around growing accessory minerals. Although more is known about diffusion of elements in siliceous melts from both an experimental and theoretical standpoint, the question is whether the diffusion rates of the elements which make up accessory phases, included are the minor elemental constituents, are incompatible with typical accessory mineral growth rates. Two general situations are possible.

1) The accessory mineral growth rates are sufficiently slow that diffusion processes will maintain an homogeneous melt composition (Models A-1 and B-2 of Albarède & Bottinga (1972), Table 5.1). Crystals grown from such a melt will be unzoned if the melt was an infinite reservoir (Model A-1), or continuously zoned if the melt was a finite reservoir (Model B-2).

2) The accessory mineral growth rates are more rapid than diffusion processes within the melt, *ie.* the melt will be compositionally heterogeneous on a small scale (Models A-2 and B-3 of Albarède & Bottinga (1972)) and diffusion will control crystal growth rate. Minerals grown from such a melt will be continuously zoned. It is possible that these compositional gradients are not only self induced but also due to the crystallization of other, adjacent minerals.

If the growth rates of zircon and titanite are controlled by the rates of element diffusion then compositional gradients of some elements will be established within the melt around the growing crystal. The width of a compositional gradient for a particular element will depend on the crystal/liquid partitioning ratio of that element, its diffusivity and the growth rate of the crystal. Zhang *et al.* (1989) demonstrated, using mineral dissolution experiments where crystal dissolution was controlled by diffusion rate, that the compositional gradients of different elements had different widths. Henderson *et al.* (1985) emphasised the role of cation charge on the rate of element diffusion in silicate melts, they observed that, with the exception of monovalent cations, diffusion rate is mainly dependent on cation charge rather than ionic radius, diffusion rate decreasing with increasing cation charge. The observations of Henderson *et al.* (1985) can be used to predict that the REE Y (all 3+), Ti, Zr, U Th (all 4+) and Nb (5+) would all have relatively slow diffusion rates (compared to the major constituents of siliceous melts) and that if compositional gradients are induced around growing zircon and titanite crystals that they will likely involve these elements.

It is considered that relative movement between a crystal and a melt containing compositional gradients would result in multiple crystal face-parallel zoning of the type observed in zircons and titanites. Relative movement of crystals and magmas could be brought about by three processes which are not mutually exclusive: 1) gravity-driven crystal settling; 2) convection induced by heterogeneities in magma density (density heterogeneities will accompany compositional gradients); and 3) an externally induced forced convection brought about by processes of transport, emplacement or deformation of a partially crystallized magma.

Only small scale relative movements (in the order of the size of the diffusion gradients) of a growing crystal and a melt containing compositional gradients would be necessary to have the desired effect of changing the composition of the melt adjacent to the growing crystal interface and thus changing the composition of the growing crystal. Assessing the relative importance of the three processes of movement within a crystallizing magma requires independent evidence as to whether these processes did occur or are likely to have occurred. However, it is likely that all three processes of movement probably contribute to causing the observed crystal face-parallel zoning patterns, although the scales of crystal settling and magma convection within a granitoid magma are probably restricted by high magma yield strengths and viscosities.

If multiple crystal face-parallel zoning in zircons and titanites is due to the processes outlined above then the growth rates of these two phases will not have been constant but will have fluctuated depending on the concentration adjacent to the interface of the elements required for growth. Earlier (see Section 5.2.1 and in particular the section on interface kinetics) it was noted that the crystal growth mechanism, which is dependent on the growth rate and the degree of supersaturation, can directly influence the partitioning of trace elements into growing crystals. Thus, in addition to the effect of relative movement of a crystal and a locally inhomogeneous magma on partitioning, it may be possible that interface kinetics influence the pattern of crystal face-parallel zoning in granitoid zircons and titanites. The possible influence of interface kinetics on the partitioning of trace elements into zircon and titanite during growth are further discussed in Sections 5.3.2 and 5.4.2.

Continuous changes in composition.

Some of the zircon and titanite crystals analysed showed *general* increases or decreases of a particular element or elements towards their edges, such features are thought to reflect gradual bulk-magma changes of composition and/or physical parameters caused by progressive crystallization of the medium of growth, *ie.* Model B-1 of Albarède & Bottinga (1972).

5.3) NON-PLANAR CONTINUOUS AND DISCONTINUOUS COMPOSITIONAL ZONING.

5.3.1) Discussion.

A given non-planar interface within an otherwise euhedral crystal could be formed by one of three processes.

1) It represents a previous exterior surface, the shape of which is due to the crystal having undergone a reduction in size. The crystal subsequently underwent renewed growth.

2) It initially grew with a subhedral or anhedral shape, but subsequently grew with a faceted morphology, *ie.* there was *no* intermediate reduction in crystal size.

3) It underwent some process of *partial* post-growth *solid* state recrystallization or alteration which resulted in non-planar interfaces.

Each possibility will be discussed in turn.

The non-planar interface as a surface that has been reduced in size.

The following discussion is concerned with the processes of crystal size reduction that may take place in a silicate melt, or prior to incorporation in a silicate melt. Only two processes may bring about the reduction in size of a crystal; 1) partial dissolution, and 2) mechanical action.

A given crystal would be subject to dissolution in a silicate melt if: 1) it was incorporated into a melt undersaturated with respect to the major components of the crystal, or 2) it was present within a melt that subsequently underwent a physical or chemical change that resulted in undersaturation with respect to the components of the crystal. Harrison & Watson (1983) investigated the kinetics of zircon dissolution and Zr diffusion in granitic melts of variable water content and found that in the absence of bulk magma flow (*ie.* diffusion is the only transport mechanism) that the dissolution rate of zircon is controlled by the rate of Zr diffusion rather than the interface kinetics. This implies that the undersaturation which is causing dissolution is sufficiently great that the rates of diffusion and interface reaction, and their relative rates, become important. Zhang *et al.* (1989) concluded from the results of silicate dissolution experiments that interface reaction was relatively unimportant in determining dissolution rates of silicate minerals in silicate melts and that in the absence of bulk magma movement diffusion would be the most important control. Where diffusion is the rate controlling step it is expected that a crystal would lose its faceted morphology and become rounded (Donaldson, 1985) since dissolution at the corners and edges will be more rapid than in the middle of faces as there is better bulk melt access.

Under conditions of bulk magma movement, in which a crystal is in continual contact with the bulk melt (*ie.* a diffusion gradient is never established), the rate determining step would be interface reaction. Zhang *et al.* (1989) stated that interface reaction would also become important when dissolution temperatures were close to the liquidus of the dissolving crystal, *ie.* the magma was only slightly undersaturated with respect to the dissolving crystal.

Under these conditions, both bulk magma movement and low degrees of undersaturation, dissolution would be controlled by interface reaction and may result in faceted morphology (Donaldson, 1985). A necessary corollary of this is that the refractory component of a granitoid, say its inherited zircon, may be present as faceted material, however whether suitable conditions of dissolution are commonly met during granitoid melting events is not known. Refractory components could also be present as euhedral crystals if prior to incorporation into the melt they were initially euhedral and did not undergo dissolution once in the melt. If interface reaction is the dissolution rate controlling step it is possible that a crystal which is compositionally zoned, contains many inclusions, or is altered, may undergo differential dissolution due to differential interface reaction rates, such a crystal could have a complex outline.

The initial shape of a crystal incorporated into a melt will depend on the type and crystallization history of the parent rock from which it has been derived. In general zircons from acidic (subalkaline) rocks are euhedral whilst those from more basic or alkaline rocks can be very irregular, usually reflecting their position within the crystallization sequence of their parent rock. There are a variety of factors that control the range of euhedral forms of zircons that can be grown in igneous rocks, Speer (1982) summarises much of the available data. The shapes of zircons in sedimentary rocks reflect the ultimate source and the effect of sedimentary processes (Poldervaart, 1956). Robson (1987) investigated the shapes and surface textures of zircons that have been subject to sedimentary processes and he described the following features.

1) Variable degrees of abrasion from well preserved euhedral grains to highly rounded polished grains.

2) Acicular crystals that have survived largely intact.

3) Grains with pitting due physical impact and/or localised dissolution.

4) Cavities due to the weathering and removal of inclusions.

5) Fractured grains.

6) Secondary (authigenic) outgrowths on the surface of grains.

It is clear that the shapes of zircons that have been subject to sedimentary processes can be highly variable and thus it is not entirely valid to generalise about the morphologies of grains subsequently incorporated into a granitoid magma. In certain cases it may be possible to identify zircons within granites which are *morphologically* similar to the types outlined above.

It can be concluded that a mineral present within a melt undersaturated with respect to the components of that mineral would experience dissolution until saturation was reached and that the resultant shape would be a function of the rate of diffusion, interface reaction rate, bulk magma movement, the degree of undersaturation and the initial shape of the crystal. It should be noted that a crystal incorporated into a melt already saturated in the components of that mineral would not experience dissolution.

The Non-Planar Interface as a Growth Surface.

Holmes (1921) noted that curved faces can arise in some crystals during growth and Donaldson (1985) discussed the possibility that under certain conditions of growth, notably supercooling (or supersaturation), the growth mechanism may result in the faces of some crystals being non-planar. There are no documented cases of such a process occurring during the growth of zircon. It may be of relevance to the growth of zircon under supersaturated conditions that Naslund (1984) observed the occurrence of hopper-shaped zircon crystals (as opposed to rounded) in part of the Skaergaard intrusion grown under conditions of supersaturation.

Partial post-growth solid state recrystallization or alteration.

Very little is known from a theoretical standpoint about the possible processes of recrystallization or alteration that may occur in zircon. Partial recrystallization (no substantial loss and gain of components by the crystal) or alteration (substantial loss and gain of some components) could be brought about by partial re-equilibration of the grain due to changes in the surrounding chemical and physical conditions. Alteration, as defined above, would require an efficient mechanism of transport of the components involved. It might be expected that alteration or recrystallization would armour a given crystal preventing completion of the process and possibly resulting in internal non-planar interfaces. The key to identifying whether recrystallization or alteration took place may lie in the nature of the interface with the pristine material and the internal zoning patterns (if there are any) of the recrystallized or altered material.

5.3.2) Interpretation of non-planar structures in zircons.

This section is divided into three parts; the first considers the interpretation of subhedral and anhedral core structures in zircons, the second considers core-related structures, and the third considers the origin of internally unzoned areas. All three sections are concerned with the actual structures described in Chapter 3 and a general explanation for all such structures within zircons is not intended. The interpretation of some of the structures necessarily involves the use of independent lines of evidence, not only the textural and compositional evidence presented in Chapters 3 and 4.

Subhedral and anhedral core structures in granitoid zircons.

The preferred interpretation of most subhedral and anhedral core structures seen in the granitoid zircons during the course of this research is that they represent refractory material incorporated into the magma. There are several lines of evidence which have led to this conclusion.

1) The crystal face-parallel and sector zoning structures often present within cores are commonly truncated by the core/rim boundary. Crystal face-parallel zoning and compositional sector zoning structures are interpreted as resulting from processes occurring

during growth of faceted crystals (see Sections 5.2.2 and 5.4.2), truncation of these structures implies that the core/rim boundary either represents a previously existing outer surface to the grain and thus the grain must have undergone a process of reduction in size or that the rim material represents recrystallized or altered core material.

2) The shapes of many of the zircon cores are consistent with a process of partial dissolution in a magma controlled by the rate of Zr diffusion or physical abrasion in a clastic sedimentary environment prior to incorporation into the magma.

3) The rim material usually contains crystal face-parallel zoning, a feature which is interpreted as being due to processes occurring during progressive outward growth in a melt by growth of new material on crystal faces (see Section 5.2.2). The pattern and overall shape of the zoning in the rims often reflects the shape of the core and this implies that the core/rim boundary was a surface upon which the rim material was grown.

4) The cores of the majority of zircons have very different internal zoning textures when compared to the zoning textures of the rims, this would be expected if the core and rim grew at different times and possibly in contrasting environments.

5) The interpretation of the subhedral and anhedral cores as being refractory material is consistent with the published U-Pb zircon data for the plutons from which the examples have been taken.

The nature of this latter evidence is circumstantial, the rock samples used in this study are, with one exception, *not* the same as those used in the various published accounts of U-Pb zircon systematics. The exception being the Kameruka Granodiorite from the sample loaned by I.S. Williams, the zircons from this sample were dated by U-Pb using the 'SHRIMP' ion microprobe (the technique is explained by Compston & Kröner, 1988) *and* the same zircons were studied using ZCI.

The age data obtained for the Kameruka zircons by I.S. Williams and his coworkers during the course of their 'SHRIMP' ion microprobe study have yet to be fully processed and published, while the actual ages obtained are available to the author these are not quoted here. Plate 5.1 shows six zircon grains from the Kameruka Granodiorite all of which have subhedral and anhedral core structures and have been dated using the 'SHRIMP' ion microprobe, the pits created by the primary ion beam during analysis can be clearly seen. All the ages obtained for the rims are consistent with their having grown during crystallization of the granitoid (~400 Ma), the cores on the other hand give a spectrum of ages from late Precambrian through to Archaean. One grain which texturally contains two concentric core structures (grain (c) Plate 5.1) gave two distinctly *different* Precambrian ages. In summary: the preferred interpretation of zircon core structures within the Kameruka Granodiorite as being old refractory material is entirely consistent with the U-Pb ages obtained using the *in situ* 'SHRIMP' ion microprobe methods.

It should be noted that texturally identical structures could also be due to processes occurring within the same general magmatic event. For instance, during crystallization of a given grain growth conditions may change sufficiently to allow slight dissolution to occur prior to a period of renewed growth. This may occur on many scales possibly resulting in

Plate 5.1. All the photographs are Z-contrast images of zircon grains from the Kameruka Granodiorite (AB40) from the Bega Batholith. The zircons have been U-Pb dated using the 'SHRIMP' ion microprobe, the round pits created by the primary ion beam during analysis are clearly visible. The cores to these grains yielded a variety of ages Archaean through late Precambrian, the text explains in more detail the significance of these ages.

(a) 15 kV, 20 nA, (7,7), scale bar 10 μm.

(b) 15 kV, 20 nA, (7,7), scale bar 10 μm.

(c) 15 kV, 20 nA, (7,7), scale bar 10 μm.

(d) 15 kV, 20 nA, (7,7), scale bar 100 μm.

(e) 15 kV, 20 nA, (7,7), scale bar 100 μm.

(f) 15 kV, 20 nA, (7,7), scale bar 10 μm.

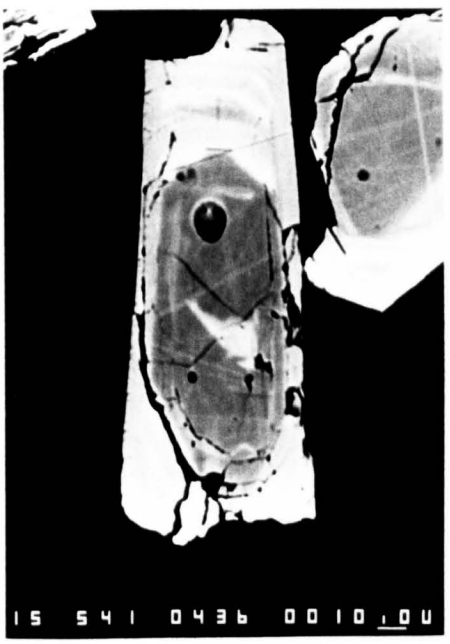
(a)
15 541 0436 0010.00

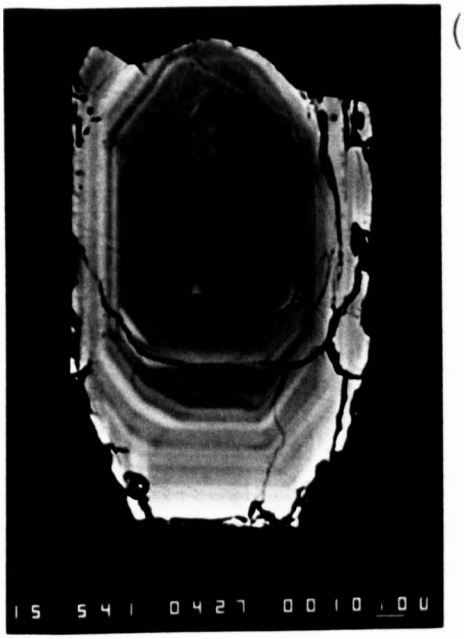
(b)
15 541 0427 0010.00


(c)
15 541 0421 0010.00


(d)
15 361 0419 0100.00

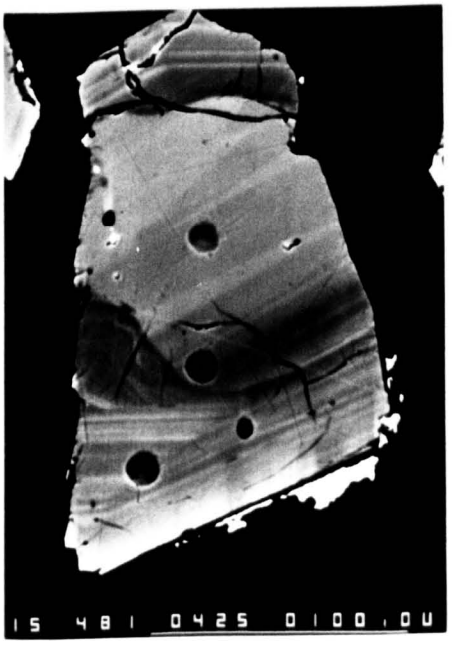
(e)
15 481 0425 0100.00

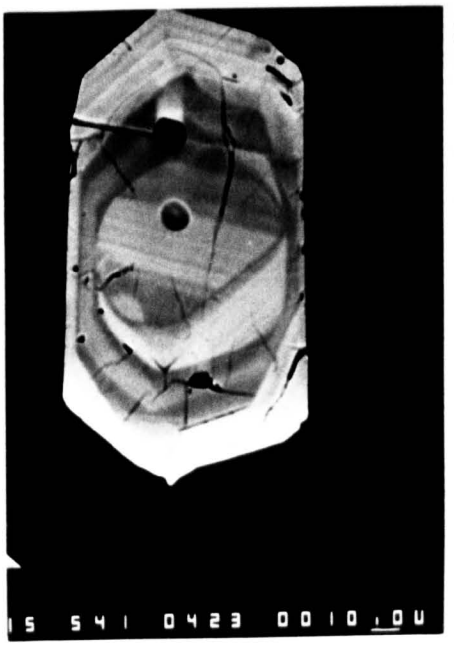
(f)
15 541 0423 0010.00

grains with structures indistinguishable from those resulting from incorporation of refractory grains. Periods of slight dissolution during general growth of a crystal may be consistent with growth in a magma containing local heterogeneities (as envisaged in Section 5.2.1); within such a magma there may be volumes that are oversaturated and volumes that are undersaturated with respect to the components of a growing crystal, movement of that crystal within the magma may result in both periods of growth and periods of dissolution. The slight rounding of crystal face-parallel zoning that was described in Section 3.5.2 may be an example in which such a process operated. The zircon grain used in Section 3.5.2 to illustrate this texture was from the Kameruka sample, a U-Pb 'SHRIMP' ion microprobe measurement obtained on the centre of this grain, within the loop formed by the non-planar interface, gave an age consistent with growth at time of granite crystallization (~400 Ma)

Core related structures in zircons

This section discusses structures to be found between the core and the first crystal face parallel zone of the surrounding rim of zircons. It covers the processes of crystal growth which are relevant to the growth of euhedral rims on irregular zircon cores, this transition to faceted growth was called the "recovery process" by Hosoya & Kitamura (1978). This discussion assumes that core structures represent a previously existing surface which was subsequently the basis for growth of an ultimately euhedral rim.

Initially the surface of growth (the zircon core) would have had a non-faceted morphology and therefore it would have been 'rough' on an atomic scale, (*ie.* there would have been topographic relief on the crystal surface - Kirkpatrick, 1975). A rough interface can be thought as having a very large number of irrational (high index) faces, however during the recovery process the number of high index faces is progressively reduced and the low index (rational) faces become dominant. During the initial stages of the recovery process, growth occurs on a non-faceted (rough) interface and thus will be of the continuous growth type of mechanism (as opposed to the layer growth mechanism), but later on during the recovery process, as planar crystal faces are progressively established, the layer growth mechanism will become dominant (Cahn *et al.*, 1964; Hoysoya & Kitamura, 1978 and Kouchi *et al.*, 1983b).

The recovery process as observed in granitoid zircons appears to involve the minimum addition of new material that is needed to establish a completely faceted morphology, this implies that layer growth is the *stable* mechanism of adding material to zircon growing in a granitoid magma.

Internally unzoned areas.

The origin of these small unzoned areas (see Section 3.5.2) that occur within otherwise strongly zoned zircon grains is not understood. However from the available data the following observations can be made.

1) The low grey-level of the unzoned areas compared to the *average* grey-level of the zoned parts implies that they are not merely patches in which internal diffusion (without loss

or gain of elemental components) has destroyed the crystal face-parallel zoning, rather it implies that there has been, at some stage, loss of elemental components. If the unzoned areas resulted from internal diffusion their grey-levels would be the average of the zoned areas.

2) Since many of the these unzoned areas occur within grains (as opposed to the margins) and do not have an obvious association with cracks, coupled with the fact that the planar structures are parallel to the crystal faces and occur on the side of the internally unzoned area nearest to the crystal faces, implies that the process that is responsible occurred during growth rather than later.

5.4) COMPOSITIONAL SECTOR ZONING.

5.4.1) Discussion.

If a given crystal is sector zoned then it was not in equilibrium with its growth medium during growth, although it is possible that there was local surface equilibrium. Many models exist to interpret the origin of this form of compositional disequilibrium.

1) Difference in the atomic configurations or adsorption layers present on different faces during growth.

2) Difference in normal growth rates (*ie.* growth rates perpendicular to crystal faces) between different faces and the relative elemental diffusion rates within the melt.

3) Differences in partition coefficients between crystal faces due to differences in the lateral growth rates and differences in interface roughness.

Most of the proposed models of compositional sector zoning have been based on examples found in rocks and thus lack detailed knowledge about the parameters of growth that operated, although it is usually implied that 'rapid growth' is the ultimate cause of sector zoning. What is meant by the term 'rapid growth' is rarely defined. Very few experimental studies have been undertaken to elucidate the conditions of growth for given examples of sector zoning, but the following are exceptions; *eg.* Lofgren (1973) for plagioclase feldspar, Long (1978) for alkali feldspar, Kouchi *et al.* (1983a) for olivine and Kouchi *et al.* (1983b) for clinopyroxene. Most of these experimental studies found a close relationship between undercooling (supersaturation), growth rate and the resulting chemical composition of the various sectors.

Each of these general models are described and discussed.

Differences in the atomic configurations and adsorption layers of the crystal faces.

This model has largely been advocated by Nakamura (1973) and Dowty (1976), it is based on the premise that each crystal face will have an adsorption layer of characteristic composition on its face during growth, part of which may be metastably incorporated by the lateral spread of growth steps. The differences in the composition of the adsorbed layers of the crystal faces are due to the differences in the geometry of partially bonded structural sites

(or protosites - Nakamura, 1973) on the different faces. Dowty (1976) proposed rules by which the composition of the adsorbed layer may be predicted; 1) the layer will consist of atoms that have high charge and small size, *ie.* strongly bonded atoms, and 2) in the absence of charge and size limitations the composition of the adsorbed layer will approach the composition of the growth medium more than that expected from the equilibrium partition coefficients, *ie.* the effective partition coefficients will tend to be closer to one than the equilibrium partition coefficients.

Imbalances between the growth rates of crystal faces and the rates of diffusion of elemental species in the melt.

This model assumes that there is local (interface) equilibrium on each of the growth faces, but that imbalances in the growth rates of the different faces and diffusion in the melt results in different compositions of melt immediately adjacent to the growing interface (Downes, 1974). Larsen (1981) discussed an essentially similar model of compositional sector zoning in terms of the crystallization models of Albarède & Bottinga (1972), suggesting that because of the different growth rates of different faces that the compositional boundary layer for each face would be different.

Differences in partition coefficients between crystal faces due to differences in lateral growth rates and differences in interface roughness.

Kouchi *et al.* (1983b) studied the relationship between chemistry and growth rate of clinopyroxenes at various degrees of supercooling during experiments in which they successfully produced compositional sector zoning. They demonstrated a relationship between crystal growth rate and element partitioning; ***within*** sectors elements with $K_o<1$ showed an increase in concentration with increasing ***normal*** growth rate (*ie.* measured perpendicular to the growing crystal face), whilst elements with $K_o>1$ showed a decrease in concentration with increasing normal growth rate. However, between sectors, where differential normal growth rates exist, the opposite was true, the sectors with the high normal growth rates had greater concentrations of elements with $K_o>1$ than the sectors with low normal growth rates. Kouchi *et al.* (1983b) argued that these compositional relationships were related to the relative *lateral* growth rates of crystal faces, *ie.* the rate of advance of growth layers across the crystal surface, since crystal faces with low ***normal*** growth rates have high *lateral* growth rates (in general the lateral growth rates of morphologically important faces are 10^{2-3} times larger than the normal growth rates (Kouchi *et al.*, 1983b)). Sectors associated with faces with high lateral growth rates have effective partition coefficients tending towards one from above ***and*** below. Faces with low lateral growth rates have effective partition coefficients which deviate less from the equilibrium values. It should be stressed that the model of Kouchi *et al.* (1983b) is only applicable where the layer growth mechanism operates as it is assumed that the steps of growth layers provide the principal sites for element incorporation.

Kitamura & Sunagawa (1977) and Kouchi *et al.* (1983a) demonstrated a relationship between crystal face roughness and element partitioning, such that the low index smooth interfaces have K_{eff} which are greater than K_{eff} for high index rough interfaces, this also suggests that the growth mechanism is the controlling factor.

5.4.2) The interpretation of compositional sector zoning in zircon and titanite.

Sector zoning in any mineral, not just zircon and titanite, cannot be explained *solely* by imbalances in the normal growth rates of different faces and in the diffusion rates of elements in the melt. These imbalances in growth and diffusion rates should, from consideration of the crystallization models of Albarède & Bottinga (1972), result in the compositional boundary layer for faces being different. However, such a situation would also result in lateral diffusion (*ie.* not perpendicular to the growing interface) between the different boundary layers associated with each face. Lateral diffusion would mean that there would not be a sharp compositional break between the boundary layers and as a result there would not be compositionally discontinuous boundaries between sectors. The crystallization models of Albarède & Bottinga (1972), although extremely useful in concept, cannot and should not, be applied to explain the origin of compositional sector zoning since their models assume that the growth surface is a simple plane perpendicular to both the direction of normal crystal growth and elemental diffusion.

It is difficult to apply rigorously the protosite model of Nakamura (1973) and Dowty (1976), their model requires the assessment of the size and "degree of bonding" of a partially bonded site and to do this it is necessary to assume where the bonds are cut by a particular face. Thus the coordination of partially completed sites is difficult to assess unambiguously and in turn the selection of elements that will fill these sites is not unique.

The observed compositional sector zoning of zircon and titanite is thought to best fit the relative partition coefficient changes between sectors that Kouchi *et al.* (1983b) described in experimentally grown clinopyroxenes.

Compositional sector zoning in zircons and titanites.

Two types of compositional sector zoning have been identified in zircon and titanites: 1) differences in the patterns of crystal face-parallel zoning between sectors (this is particularly common in zircons, although analogous structures have been observed in titanites); 2) individual discontinuous multiple zones which have different compositions within different sectors and are separated by compositionally discontinuous boundaries, the type usually described in other minerals.

The first type arises simply by the growth of one face whilst at the same time growth does not occur on adjacent faces and as conditions of growth change this process affects different faces. Such a situation implies that different conditions of growth favour particular crystal faces at the expense of others. Various authors, on the basis of both experimental and

petrological studies, have noted that there is a close relationship between crystal habit (*ie.* the relative importance of different faces) of zircon and the physical and chemical conditions of growth. For example: Lipova & Mayeva (1971) noted that the substitution of the REE, U and Th favours the development of pyramidal faces (Chase & Osmer (1966) first noted this pattern with the REE), whilst Hf substitution favours the development of prism faces; and Pupin *et al.* (1978) noted that the temperature and water content of a melt determine which of the prism forms, {110} or {100}, dominate; the {100} form becomes more important with decreasing temperature and decreasing water content. Similar correlations have not been previously identified in titanites but the observations presented in Chapter 4 do suggest that the crystal habit of titanite is, to some extent, dependent on the chemistry of the growth medium. The model favoured for the origin of multiple crystal-face parallel zoning, *ie.* the creation by processes of crystal growth of a compositionally heterogeneous magma and subsequent relative movement of the growing crystal with such a magma, should, from consideration of the work of Chase & Osmer (1966), Lipova & Mayeva (1971) and Pupin *et al.* (1978) on zircon habit outlined above, result in small-scale fluctuations in the relative importance of different faces during growth, this is the pattern that has been observed.

The second type of compositional sector zoning, as observed in zircons and titanites, appears to fit best, with one notable exception, the relative partition coefficient changes between sectors that Kouchi *et al.* (1983b) described in experimentally grown clinopyroxenes. However, it is important to note that it is not possible to compare fully the compositional relationships of sector zoned titanites and zircons (in terms of relative changes of partition coefficients) with those of the experimentally-grown clinopyroxenes of Kouchi *et al.* (1983b). This is for two main reasons: 1) it is only possible to study the effect of the relative growth rates of different sectors on element partitioning, the effect of the absolute growth rate of individual sectors on the effective partition coefficients is not known and is impossible to measure in the natural systems dealt with here; and 2) from the model of Kouchi *et al.* (1983b) it is possible to predict the pattern of sectoral variations shown by particular elements. However because some elements are present in concentrations below detection limits it is not always possible to test these predictions, this is particularly true of compositional sector zoning in zircons.

In the sectors associated with the faces of titanites which have high lateral growth rates (measured relative to other faces) the effective partition coefficients of the elements present in trace quantities are closer to unity than the sectors associated with faces with low lateral growth rates. The model favoured for compositional sector zoning in titanites is one whereby the effective partitioning behaviour is controlled by the lateral growth rates of the different faces, the faster the rate of lateral growth the greater the tendency for the effective partition coefficients to tend towards unity from both above and below. This implies that the steps of the growth layers are the principal sites of element incorporation (Kouchi *et al.*, 1983b) and thus interface kinetics play an essential role in the formation of sector zoning in titanites. The sectoral variations observed in zircons are, with the exception of Hf, consistent with the observed variations in titanites and the model of Kouchi *et al.* (1983b). Even although Hf has

an equilibrium zircon/liquid partition coefficient of greater than unity and should therefore be enriched in the faces with low lateral growth rates it was found to be preferentially incorporated in the prism faces which have high lateral growth rates. This could be due to the often observed tendency for there to be a negative correlation between Hf and the REE (included here is Y), even although the substitution of these elements in zircon is not linked by a coupled substitution scheme.

It is considered that the ultimate driving force causing compositional sector zoning is the nucleation and growth behaviour of the mineral and the relative rates of crystal growth, and elemental diffusion in the magma. In many of the rocks from which the titanite sector zoning examples were taken titanite occurs as a few relatively large crystals, this contrasts with the apatite in the same rocks which usually occurs as many small often unzoned crystals. This implies that there is a marked difference in the nucleation behaviour (nucleation density) and growth rates of titanite and apatite in calc-alkaline granitoid melts. Lofgren (1980) stated that in general nucleation density is related to the nucleation rate and thus it is inferred that the nucleation rate of titanite in calc-alkaline magmas is low, relative to apatite. It has been noted that curves of crystal growth rate as a function of supersaturation have essentially similar shapes to curves of nucleation rate as a function of supersaturation, however the curves are generally displaced relative to one another. A possible arrangement of the growth rate and nucleation rate curves is shown in Figure 5.1; at low degrees of supersaturation, where nucleation rate is low, crystal growth rate is often high (point A). If titanite did grow under such conditions it may help to explain why, from consideration of mineral zoning, crystal growth rate would appear to be limited by rates of elemental diffusion.

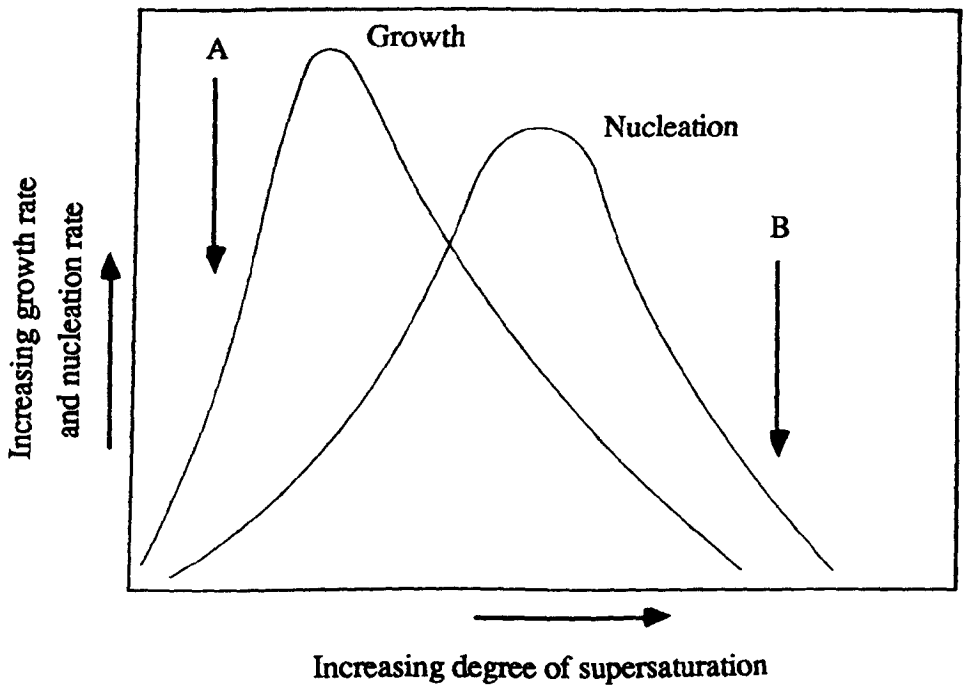

Fig. 5.1. Schematic diagram showing a *typical* relationship between: 1) nucleation rate and degree of supersaturation; and 2) growth rate and degree of supersaturation. The significance of points A and B are explained in the text. The scales on both axes are arbitrary.

It should be noted that there is no independent experimental evidence that crystal growth of titanite in the examples presented occurred under the regime just described and it is possible that even at high degrees of supersaturation (where nucleation and crystal growth rates are low, point B on Fig. 5.1) that elemental diffusion would still be the rate determining step of crystal growth. High degrees of supersaturation could be brought about by delays in nucleating titanite, caused by high magma viscosities or low concentrations of the titanite components. For instance, Lofgren (1980) stated that increasing magma viscosity decreases the potential for nucleation of a given mineral at a given degree of supersaturation, and Donaldson (1979) noted that nucleation of olivine in basaltic magmas could be delayed if the concentration of olivine components in the melt was low. Thus it is possible that titanite nucleation could be delayed until relatively high degrees of supersaturation are attained, particularly if the magma was viscous and/or the concentration of titanite components in the magma was low (as is usually the case).

Only experimental work on the nucleation and growth behaviour of titanite under a variety of conditions would help resolve some of the points raised in this section.

5.5) SUMMARY AND IMPLICATIONS.

5.5.1) Summary.

Crystal face-parallel continuous and discontinuous compositional zoning.

The presence of multiple crystal face-parallel zoning is taken to indicate that the growth rates of the zircon and titanite crystals studied were controlled by elemental diffusion rates and not by the rate of attachment of material to the growing crystal. The fact that elemental diffusion rates appear to control growth rates implies that magmas locally become compositionally heterogeneous. The multiple crystal face-parallel zoning of the zircons and titanites observed during the course of this study is thought to be due to the relative movement of the growing crystals and a compositionally heterogeneous magma. The continuous changes in composition between the centre and edge of a crystal that are often superimposed on the multiple discontinuous zoning patterns probably reflect bulk magma changes in physical and chemical conditions and partition behaviour.

The interpretation of non-planar continuous and discontinuous compositional zoning in zircon.

The preferred interpretation of subhedral and anhedral core structures in zircons is that they in the main represent the textural manifestation of refractory (inherited) zircon. The shapes of zircon core structures are consistent with two possibilities: 1) partial zircon dissolution in a magma where Zr diffusion is the rate controlling step, or 2) incorporation into a magma of zircon material that has already undergone reduction by physical abrasion in a clastic sedimentary environment. However, it is important to note that not all such structures may be due to the presence of refractory material, some may be due to complex

magmatic histories involving relatively short-lived periods of dissolution followed by renewed growth. Such cases may be indicated where the style of zoning within the non-planar interface is essentially the same as the zoning outside.

Isotopic analysis is the only unambiguous method of proving or disproving that subhedral and anhedral zircon cores represent refractory material.

The interpretation of compositional sector zoning in zircon and titanite.

Crystal interface kinetics are thought to play an essential role in the formation of compositional sector zoning in zircon and titanite. With the exception of Hf distribution in zircon, the sectoral distribution of trace elements in both titanite and zircon appears to be consistent with the relative partition coefficient changes between sectors that Kouchi *et al.* (1983b) described in experimentally grown clinopyroxenes. Kouchi *et al.* (1983b) are able to demonstrate that the lateral growth rates of the different faces (assuming that growth occurs by the layer growth mechanism) controls the effective partition coefficients; faces with high lateral growth rates (and hence low relative normal growth rates) cause the partition coefficients to tend towards unity from both above and below, faces with low lateral growth rates (high relative normal growth rates) have more extreme partition coefficients.

5.5.2) Implications.

This section stresses the principal implications of the existence of zoning in zircon and titanite, much of the discussion given below is necessarily based on the author's preferred interpretations of the individual zoning structures.

1) It has been demonstrated that kinetic (time-dependent) phenomena are important to the processes involved in the growth of zircon and titanite in calc-alkaline plutonic environments. These kinetic processes, *eg.* diffusion rates, crystal growth rates and interface kinetics, allow the effective partition coefficients of the minor components of these phases to deviate from the equilibrium partition coefficients, compositional sector zoning represents the epitome of these kinetic processes.

2) All the textures are interpreted as being of magmatic origin, *ie.* grown from a melt, and not significantly altered by subsequent post-crystallization processes, specifically excluded is material thought to have been refractory (the implications of zoning within material interpreted to have been refractory is discussed in Chapters 8 and 9). Identification of textures resulting from post-crystallization processes would allow processes of element mobility to be better understood.

3) Many of the zoning textures of zircon and titanite are thought to be consistent with growth rate being controlled by the diffusion rates within the magma of their major and minor elemental components. Although slow diffusion of the major and minor elemental components of zircon and titanite in silicate melts is in accord with the findings of experimental studies (Henderson *et al.*, 1985 and Zhang *et al.*, 1989), nothing is known about the growth rates of zircon or titanite and thus it is impossible to *prove* that the growth

rates of these minerals are controlled by elemental diffusion. However on the basis of the crystallization models of Albarède & Bottinga (1972) it is argued that if crystal growth rate was not controlled by diffusion that unzoned or continuously zoned crystals would be the result.

4) Both direct ('SHRIMP' ion microprobe) and circumstantial evidence suggests that subhedral and anhedral cores in zircons represent refractory inherited material. Similar textures in other minerals could also be used as evidence of refractory behaviour, although obtaining corroborative evidence may prove difficult since occurrences of inherited U-Pb systematics are almost exclusively restricted to zircon. However, it is worth noting that Copeland *et al.* (1988) claimed to have identified inherited U-Pb systematics in monazite from a leucogranite of the High Himalaya, clearly textural studies similar to those presented here could provide additional evidence to test such a possibility.

Chapter 6
The Strontian complex: a description.

6.1) INTRODUCTION.

In Chapters 3, 4 and 5 compositional variations within accessory minerals from a number of different localities were described and discussed, but it was only possible to discuss in general terms the host rock. To this end a more detailed study was undertaken of the intra- and inter-grain compositional variations of granitoid accessory minerals from a well studied plutonic environment - namely the Caledonian Strontian Complex. Chapters 6, 7, 8, 9 and 10 are devoted to this aim.

The purpose of this chapter is: 1) to describe, using published work, the Strontian Complex; 2) to outline and comment on the interpretations that have been proposed in the literature and; 3) to highlight the problems that still appear to be outstanding.

6.2) THE STRONTIAN PLUTONIC COMPLEX.

6.2.1) Regional setting.

Regional stratigraphic relationships.

The Strontian Complex is a Caledonian-aged granitoid (see Brown, 1983 and Stephens, 1988 for reviews of Caledonian magmatism) which intruded into Moine (Proterozoic-aged) metasedimentary and metaigneous rocks. The Moines have been divided into three units; namely the Morar, Glenfinnan and Loch Eil Divisions (Johnstone *et al.*, 1969), although the nature and position of the boundaries is not clear (see Johnson, 1983 and Roberts & Harris, 1983 for further discussion). The Strontian Complex is in contact with all three Moine Divisions and is transgressive across their boundaries (see Fig. 6.1).

Country rock lithologies and metamorphic grade.

The metasedimentary rocks of all three Moine Divisions are mainly psammitic, semi-pelitic and pelitic, but there are also subordinate quartzites, migmatites of several generations and various deformed igneous bodies, including the Ardgour Gneiss.

The Moines adjacent to the Complex are in the sillimanite zone of a kyanite-sillimanite regional metamorphic sequence (Winchester, 1974). However, Ashworth & Tyler (1983) identified three aureole zones around the northern part of the complex.

1) Muscovite-Sillimanite-K-Feldspar Zone, K-feldspar in.

2) Sillimanite-K-Feldspar Zone, muscovite out.

3) Cordierite-K-Feldspar Zone, andalusite occurs in a few localities within this zone.

The aureole has a strong asymmetry in its outcrop pattern (Fig. 6.2), with the zones being considerably broader in the east than in the west (Ashworth &Tyler, 1983).

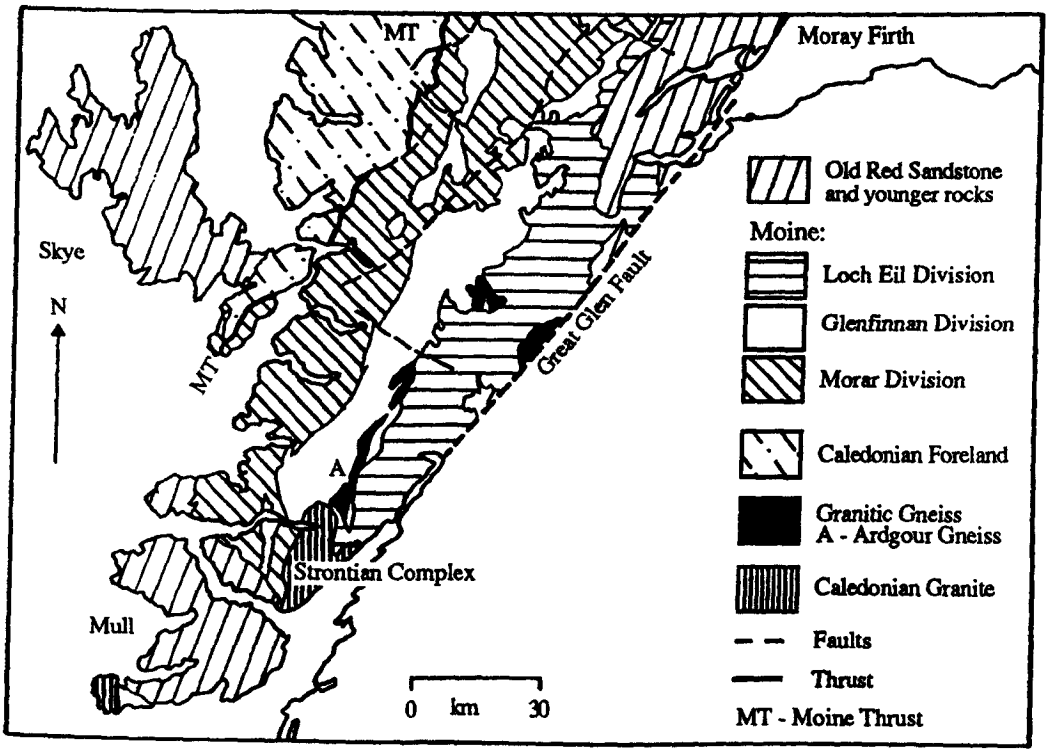

Fig. 6.1. Map of the regional geology of the northwest Highlands showing the relationships of the Strontian Complex to the Moines. After Rathbone & Harris (1979).

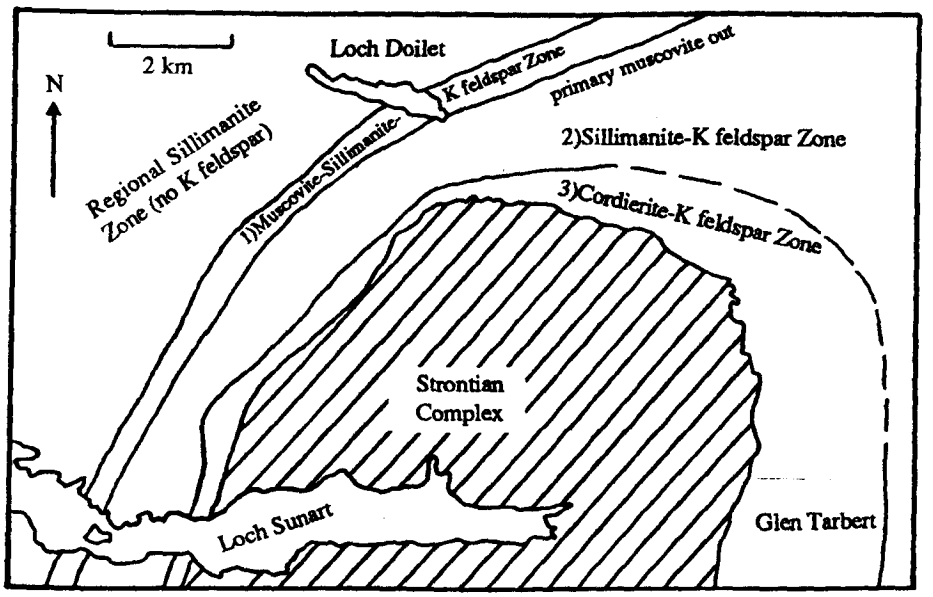

Fig. 6.2. The distribution of metamorphic aureole zones around the northern end of the Strontian Complex. Note the strong asymmetry, the zones being considerably broader in the east. Map from Ashworth & Tyler (1983).

Interpretation of metamorphism adjacent to the Strontian Complex.

Metamorphic zonal patterns around the Complex resulted from the interaction of waning regional metamorphism and a thermal, intrusion-related, effect (Ashworth & Tyler, 1983). An aureole assemblage including cordierite and andalusite indicates that intrusion took place at a lower pressure (0.41±0.04 GPa or 4.1 kbar) than the earlier regional metamorphism and therefore there had been intervening uplift (Tyler & Ashworth, 1982). A temperature of 690°C is indicated for the Cordierite-K-Feldspar isograd. Ashworth & Tyler (1983) interpreted the asymmetry of the aureole as being due to superimposition of thermal metamorphism on a lateral regional temperature gradient of 5°C/km - temperature was highest in the east. They considered that there was no similar pressure gradient and that the apparent lateral temperature gradient was real and not a function of subsequent regional tilting.

Regional structures in the Moines.

The deformational history of the Moines occurred in two main episodes. The age of the first deformation is the subject of much debate; Brook *et al.* (1976), on the basis of a Rb-Sr whole rock age for the Ardgour Gneiss of 1028±45 Ma, argued for the first deformation being Grenvillian, although the subsequently published U-Pb zircon data of Aftalion & van Breemen (1980) is considered to be consistent with a significantly younger age for this body (G. Rogers, pers comm., 1990). The second deformation was Caledonian, this is largely based on a U-Pb zircon age of 456±5 Ma for the Glen Dessary syenite (van Breemen *et al.*, 1979). The regional structure consists of open to tight, major and minor folds, with N-S to NE-SW trending axial traces. The Loch Quoich Line, which is truncated by the Complex, is considered by Roberts & Harris (1983) to represent the eastern limit of intense D_3 (Caledonian) deformation. West of the Quoich Line and the Complex, the Moines consist of large NNW and SSE trending upright folds, but to the east the rocks are less intensely folded and generally flat lying.

6.2.2) Rock units within the Strontian Complex.

A note on terminology.

The terminology previously used for rock units within the Complex and that used in this study is given in Table 6.1. It is proposed that the outer parts of the Complex (the 'tonalite' and 'porphyritic granodiorite' of past usage) should now be termed the **Loch Sunart Granodiorite** (with non-porphyritic and porphyritic facies) and the inner part (the 'biotite granite') should now be called the **Glen Sanda Granodiorite**. Figure 6.3 shows the distribution of rock units within the Complex.

Loch Sunart Granodiorite.

This is a grey medium to coarse grained plagioclase, alkali-feldspar, quartz, hornblende and biotite rock with accessory titanite, apatite, zircon, opaques and rare allanite (See Plates 6.1 and 6.2). The outer non-porphyritic facies and the inner porphyritic facies are

mineralogically very similar, the boundary being gradational over distances ranging from a few metres to 1.5 km (Sabine, 1963; Munro, 1965). The phenocryst phase is alkali-feldspar (often pink); here the term phenocryst is used to mean a large crystal set in a finer grained groundmass and is not intended to have any genetic connotation. There is no fine grained contact zone between the two facies and no veining of one facies in the other (Munro, 1965).

Table 6.1. The terminology previously used for the three main intrusive units of the Strontian Complex and the terminology used in this work.

MacGregor & Kennedy (1932)	Tonalite	Porphyritic granodiorite	Biotite-granite
Sabine (1963) and Munro (1965)	Tonalitic granodiorite ('tonalite')	(Porphyritic) granodiorite	Biotite granite or biotite adamellite
Munro (1973)	Non-porphyritic granodiorite	Porphyritic granodiorite	Adamellite
This Work	**Loch Sunart Granodiorite:** non-porphyritic facies	porphyritic facies	**Glen Sanda Granodiorite**

Both facies contain abundant microdiorite enclaves that on a pluton scale are evenly distributed (Munro, 1965), although locally there are high concentrations (Holden, 1987).

Save for the development of alkali-feldspar phenocrysts in the porphyritic facies the two facies of the Loch Sunart Granodiorite are also texturally similar. Plagioclase, hornblende and biotite are generally euhedral, quartz and alkali-feldspar (with the obvious exception of the porphyritic facies) are interstitial (Sabine, 1963). The phenocrystic alkali-feldspar includes other phases and the edges of these generally euhedral crystals are ragged (Holden, 1987).

Glen Sanda Granodiorite.

This is intrusive into the Loch Sunart Granodiorite and is a pink fine to medium grained plagioclase, quartz, alkali-feldspar and biotite rock (there is occasional hornblende) with accessory apatite, zircon, opaques and rare titanite, allanite and monazite (See Plates 6.3 and 6.4). There are some alkali-feldspar phenocrysts and locally it is coarse grained. In all places the contact between this body and the Loch Sunart Granodiorite is sharp although in the north it is extensively sheeted. Microdiorite enclaves are present, but very uncommon (Munro, 1965). Plagioclase is found as euhedral laths, with quartz, biotite and alkali-feldspar being, in general, interstitial. Alkali-feldspar locally can occur as phenocrysts often enclosing euhedral plagioclase (Holden, 1987).

Minor intrusives.

Several basic igneous bodies of variable composition (generally the term 'appinite' is used in the Caledonian literature) are present within both the Loch Sunart Granodiorite and

Plate 6.1 and 6.2. Transmitted PPL (top) and XPL (bottom) photomicrographs of a thin section of a rock from the porphyritic facies of the Loch Sunart Granodiorite (BPSRT3). Plagioclase and hornblende both generally occur are euhedral grains, however, quartz, biotite and alkali-feldspar are interstitial. In the porphyritic facies of the Loch Sunart Granodiorite alkali-feldspar can also occur as phenocrysts (bottom right hand corner) these although *generally* euhedral commonly include other phases and have ragged edges. From textural considerations Sabine (1963), Munro (1965) and Holden (1987) considered these phenocrysts to have a late replacive origin. In the light of whole rock chemical data the origin of the alkali-feldspar phenocrysts is discussed in more detail in Chapter 7.
Width of the field of view 7.5 mm.

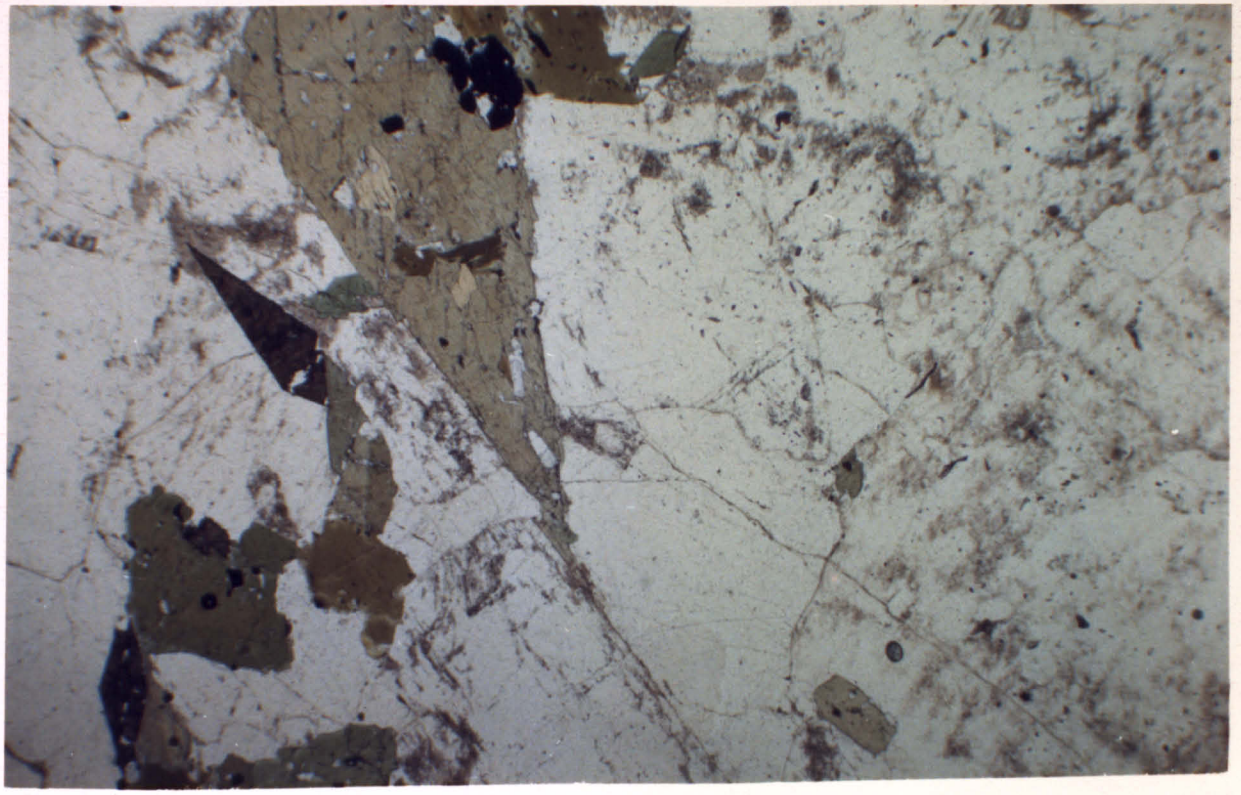

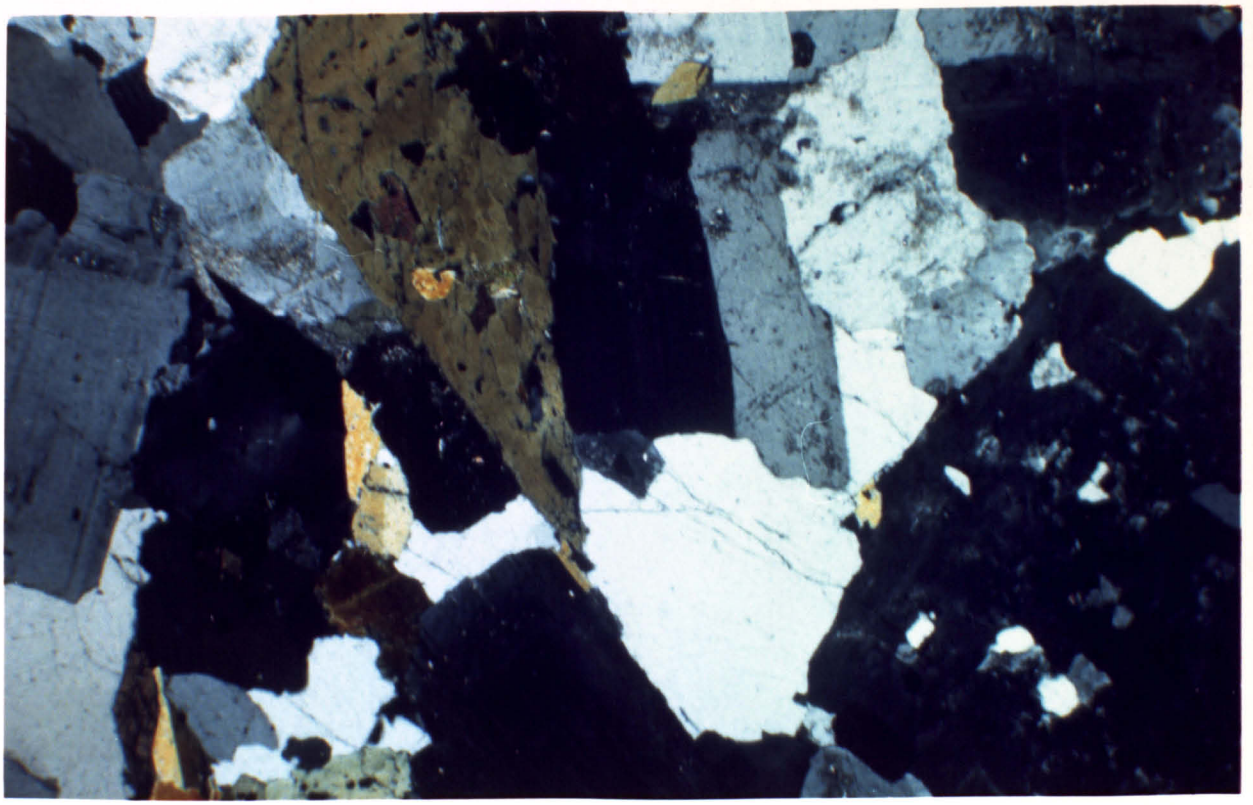

Plate 6.3 and 6.4 Transmitted PPL (top) and XPL (bottom) photomicrographs of a thin section of a rock from the Glen Sanda Granodiorite (BPSRG1). Plagioclase occurs as euhedral laths, quartz, biotite and alkali-feldspar are interstitial. Both feldspars are generally dusty in appearance, this probably indicates limited alteration to secondary clay phases. Biotite is commonly altered to chlorite and an opaque phase (centre bottom).
Width of the field of view 7.5 mm.

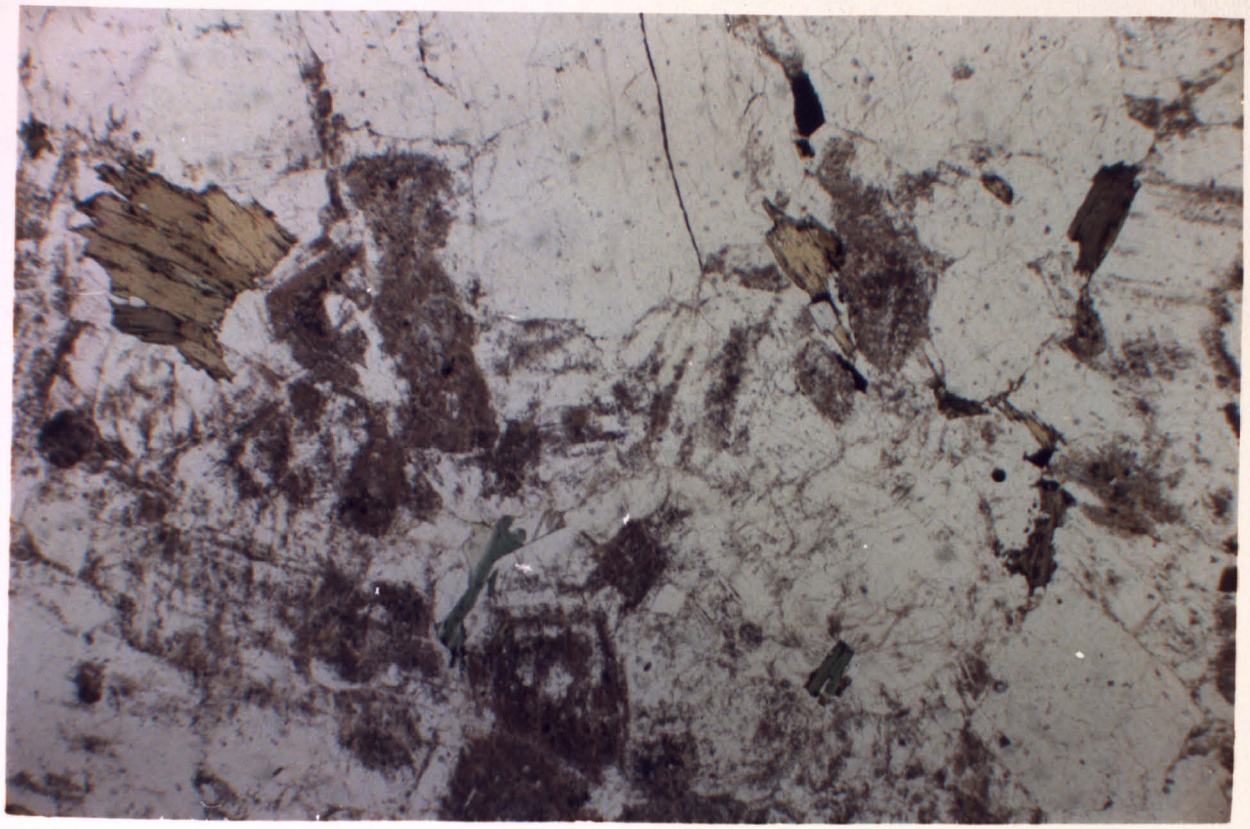

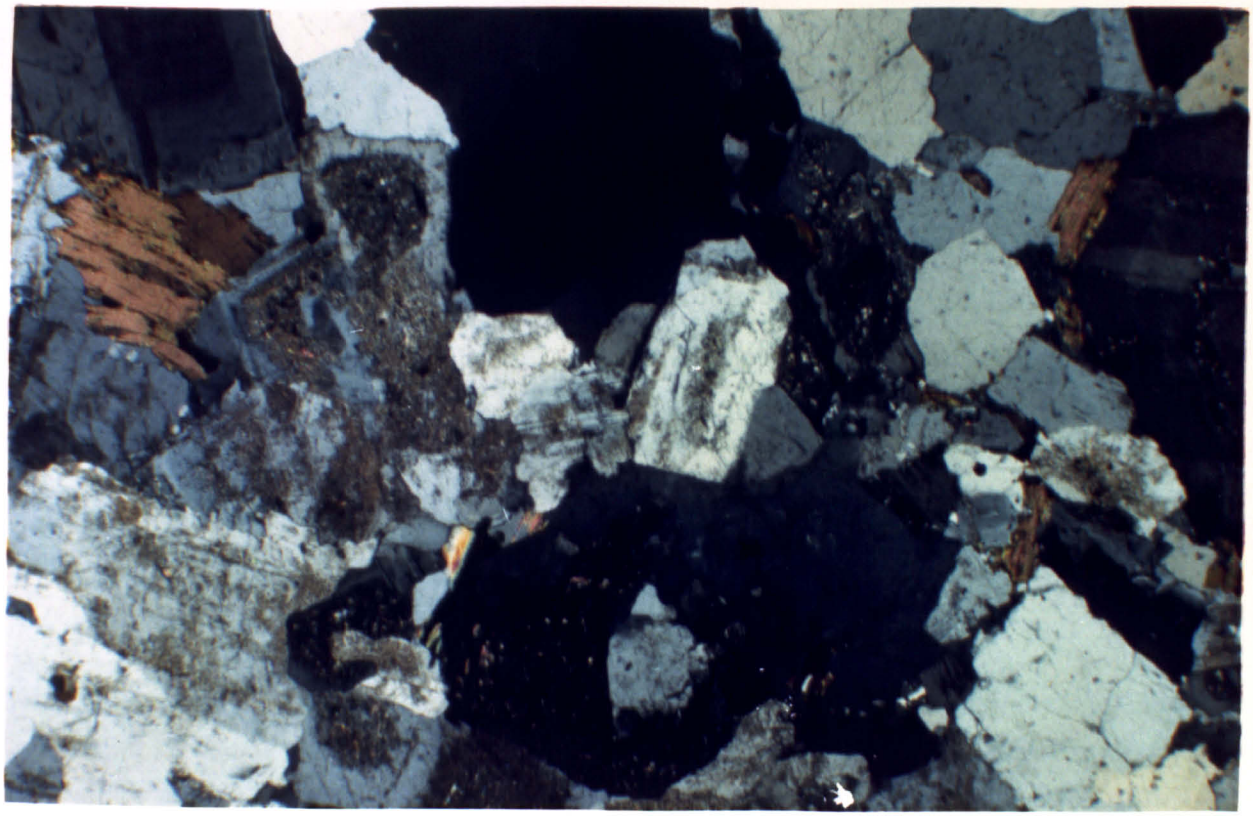

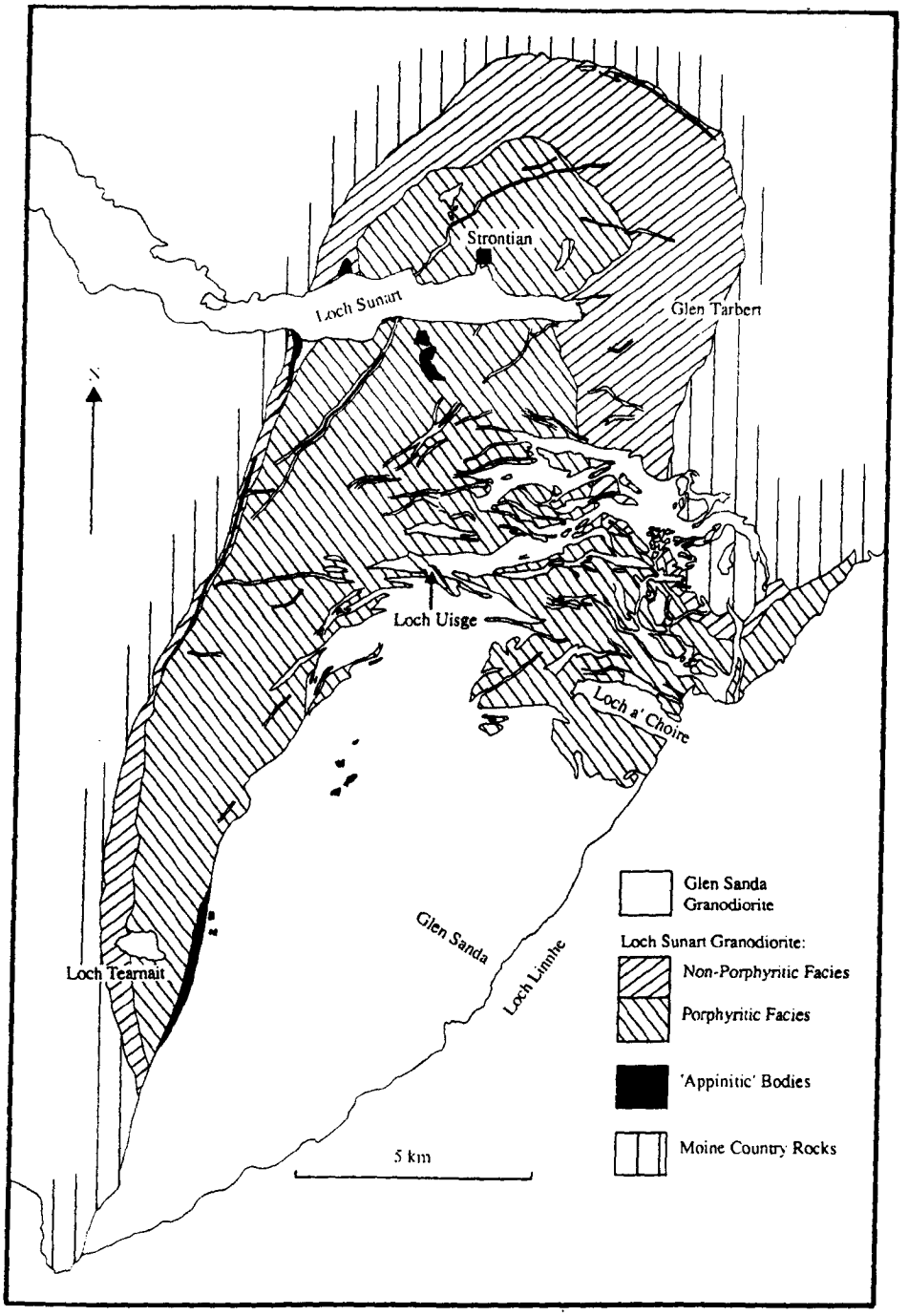

Fig. 6.3. The distribution of rock units in the Complex, also shown are major geographical features. Map compiled from the following sources; IGS (now BGS) Scotland sheets 44, 52 and 53, and Sabine (1963).

the Glen Sanda Granodiorite (see Fig. 6.3). The bodies that are found within the Strontian Complex, although extremely variable, consist mainly of hornblende, biotite, clinopyroxene, alkali-feldspar and subsidiary plagioclase with accessory titanite, apatite and opaques. They are generally small and irregular, but broadly equidimensional (~250-500 m across) and may be pipe-like in three dimensions. The contact with the pluton of at least one of the bodies is

lobate and 'pillowed' (Holden, 1987). A number of dyke-like 'appinitic' bodies have also been mapped.

Lamprophyres, aplites, pegmatites, and porphyritic acid dykes cut both parts of the Complex, some of the porphyritic dykes that cut the Loch Sunart Granodiorite are thought to be related to the later Glen Sanda Granodiorite (Sabine, 1963).

6.2.3) Structural features of the Strontian Complex.

The description given here covers features internal to the Complex, but also external structures that are thought to be due to processes of intrusion.

The structure of the Loch Sunart Granodiorite.

It has long been recognised that regional structures were truncated by the pluton, but also locally deflected (MacGregor & Kennedy, 1932; Sabine, 1963). Observations by Sabine (1963), Munro (1965) and Hutton (1988a and 1988b) indicate that deformation concordant with the pluton margins is restricted to a narrow zone (<1 km wide) around the Complex. Shear directions within this zone are consistently dextral or if flat-lying show a top towards the south sense of movement (Hutton, 1988a).

The contacts between the Loch Sunart Granodiorite and the Moines are inwardly dipping, the western contact being steepest. There is a well developed foliation parallel to the margins defined by alignment of plagioclase, hornblende, and biotite (Fig. 6.4). Alkali-feldspar and quartz are generally unaligned. The minerals, on the whole, do not show internal deformation and the foliation is thought to be a pre-full-crystallization fabric (Hutton, 1988b). However, a crystal plastic strain fabric that overprints the earlier pre-full-crystallization fabric does occur in the south-west between the Moines and the Glen Sanda Granodiorite (Hutton, 1988b).

Hutton (1988b) used the abundant microdiorite enclaves and fabrics in the Loch Sunart Granodiorite to look at the variations in degree and orientation of strain. These measurements indicate the following.

1) The principal axes of the strain ellipsoids lie in the plane of the pre-full-crystallization fabric.

2) The long axis of the strain ellipsoids are orientated approximately N-S.

3) The strain is highest at the contact with the Moines and diminishes towards the centre.

4) The strain in the south-western area of the Loch Sunart Granodiorite between the Moines and the Glen Sanda Granodiorite increases towards both contacts and is also is generally higher than elsewhere.

5) In the this south-western area there are also several N-S dextral shear zones.

Emplacement of the Loch Sunart Granodiorite.

Prior to the work of Hutton (1988a and 1988b), this part of the pluton was thought to fit a "diapir/balloon" model (Hall, 1987). Such a model is inconsistent with the limited, emplacement related, deformation in the Moines and the shape and siting of the pluton is

considered by Hutton (1988a) to be controlled by pre-existing country rock structures. The listric shape, indicated by the structural data, and the sense of movement indicators are consistent with intrusion and synchronous deformation of a partially crystallized magma between an overlying hangingwall and its footwall (Hutton, 1988b). The space for intrusion being largely created by relative movement of the footwall and the hangingwall, rather by extensive country rock deformation.

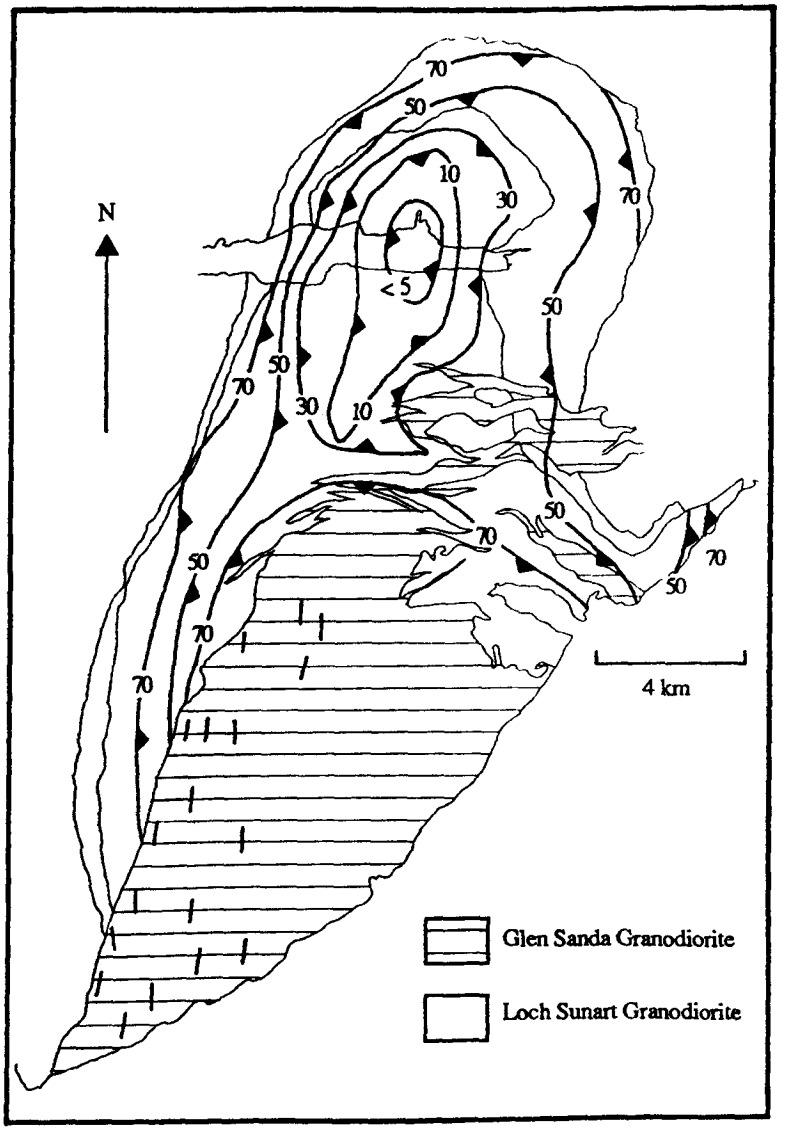

Fig. 6.4. Map showing the basic structure of the Strontian Complex. Solid lines with barbs are generalised foliation trend lines with specified dip ranges in the Loch Sunart Granodiorite. The short unornamented lines are foliations in the Glen Sanda Granodiorite. Map taken from Figure 3 of Hutton (1988b).

The structure of the Glen Sanda Granodiorite.

This is an essentially undeformed body (Sabine, 1963; Munro, 1965) that intruded the earlier Loch Sunart Granodiorite and in places the Moines. In the south-west, adjacent to the contact with the Loch Sunart Granodiorite, Hutton (1988b) found local development of

pre-full-crystallization deformation fabrics and discrete N-S dextral shear zones (Fig. 6.4), parallel to crystal plastic strain fabrics developed in the earlier Loch Sunart Granodiorite. The degree of strain indicated by these fabrics decreases towards the northern sheeted complex.

Emplacement of the Glen Sanda Granodiorite.

Hutton (1988b) considers that the siting of the Glen Sanda Granodiorite was controlled by a dextral shear zone (a splay of the Great Glen Fault related to the Loch Quoich Line) on the western side of the Granodiorite which diminishes northwards in its movement and terminates in an extensional fracture zone (the northern sheeted complex). The overall shape of the intrusion is similar to the Loch Sunart Granodiorite and the space for the intrusion was created by movement of a hangingwall attached to the southern side of the Great Glen Fault (Hutton, 1988b) (Fig. 6.5). The crystal plastic strain fabrics in the Loch Sunart Granodiorite are due to the emplacement of the Glen Sanda Granodiorite.

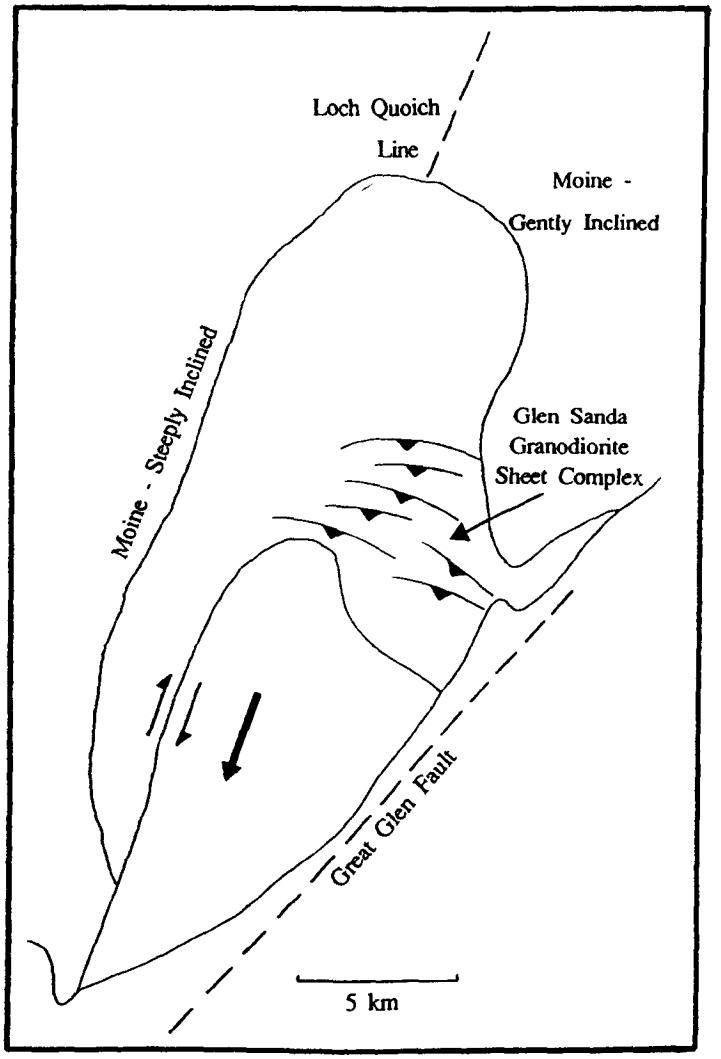

Fig. 6.5. A model explaining the emplacement mechanism of the Glen Sanda Granodiorite in a dextral shear zone termination related to the Great Glen Fault. Taken from Figure 7 of Hutton (1988b).

6.2.4) Radiometric age and U-Pb zircon data.

Loch Sunart Granodiorite.

Radiometric ages have been obtained by various methods and by various workers (Miller & Brown, 1965; Pidgeon & Aftalion, 1978; Rogers & Dunning, 1990, in press) and the U-Pb zircon systematics have also been studied (Pidgeon & Aftalion, 1978; Halliday *et al.*, 1979; Rogers & Dunning, 1990, in press). Table 6.2 summarises the results of all of this work.

Table 6.2. Summary of age and inherited zircon data available for the Loch Sunart Granodiorite of the Strontian Complex.

Age (Ma)	Method	Comments
429 ± 19	K-Ar biotite isotope dilution.	The K-Ar ages have been recalculated using decay constants of Steiger & Jäger (1977).
415 ± 18	K-Ar biotite isotope dilution.	
441 ± 19	K-Ar biotite total volume.	
Miller & Brown (1965). Locality - "2 miles west of Strontian".		
435 ± 10	U-Pb zircon upper intercept.	No indication of inheritance.
Pidgeon & Aftalion (1978). Samples used; RC1258 (non-porphyritic facies) and RC1259 (nearby microdiorite enclave). Locality - NM 850610.		
(~435)	U-Pb zircon, $^{207}Pb/^{206}Pb$ age.	U-Pb intercepts 504 $^{+433}_{-69}$ and 339 $^{+68}_{-383}$ Ma. Inheritance thought unlikely by Halliday *et al.*. (1979) because the $^{207}Pb/^{206}Pb$ age is close to 435 Ma age of Pidgeon & Aftalion (1978). See below - Rogers & Dunning (1990, in press).
Halliday *et al.* (1979). Sample; RC1841 (porphyritic facies). Locality - NM 780560.		
425 ± 3	U-Pb zircon upper intercept of longitudinal cracked prisms which contained no inheritance.	Sample as Halliday *et al.* (1979). Small amount of inheritance in abraded prisms and prism tips, this is in contrast to the findings of Halliday *et al.* (1979). The prism tips gave an upper intercept of 1713 $^{+191}_{-155}$, the prisms 1083 $^{+202}_{-140}$.
Rogers & Dunning (1990, in press).		

Glen Sanda Granodiorite.

Two sets of workers have obtained age data on the Glen Sanda Granodiorite - Miller & Brown (1965) and Halliday *et al.* (1979). The latter also presented work on the U-Pb zircon systematics. All the available data is presented in Table 6.3.

Table 6.3. Summary of age and inherited zircon data available for the Glen Sanda Granodiorite, part of the Strontian Complex.

Age (Ma)	Method	Comments
388 ± 17	K-Ar biotite isotope dilution.	The K-Ar ages have been recalculated using decay constants of Steiger & Jäger (1977).
Miller & Brown (1965). Locality - 'L. Uisge'.		
$381\ ^{+9}_{-10}$	Zircon U-Pb, lower intercept of reverse discordia.	Upper intercept $1462\ ^{+102}_{-96}$ Ma. Marked inherited component.
Halliday *et al.* (1979). Sample RC1840. Locality close to that of Miller & Brown (1965) - NM 809553.		

Discussion of the radiometric age data.

Because of the low blocking temperature of the K-Ar decay scheme in biotites (~300°C, Purdy & Jäger (1976), Turner & Forbes (1976)) the ages obtained from granitoids reflect post-emplacement cooling. Pidgeon & Aftalion (1978) disregarded the K-Ar age of 388 ± 17 Ma for the Glen Sanda Granodiorite obtained by Miller & Brown (1965) because of the low K_2O content (4.74%) obtained from the biotite separate. However, Miller & Brown (1965) attributed the low K_2O content to the presence of other non-potassium containing phases.

The U-Pb zircon studies of Pidgeon & Aftalion (1978), Halliday *et al.* (1979) and Rogers & Dunning (1990, in press) have established that the Loch Sunart Granodiorite has minor inheritance whilst the Glen Sanda Granodiorite has substantial inheritance. The U-Pb zircon lower intercept age of $381\ ^{+9}_{-10}$ Ma obtained by Halliday *et al.* (1979) for the Glen Sanda Granodiorite indicates a substantial time gap between the Loch Sunart Granodiorite and the Glen Sanda Granodiorite. However, this age was not obtained using modern U-Pb zircon techniques (*ie.* careful grain separation and selection procedures and abrasion techniques (Krogh 1982a and 1982b)) and for this reason is not considered to be accurate.

The 425 ± 3 Ma U-Pb zircon age of Rogers & Dunning (1990, in press) for the Loch Sunart Granodiorite was obtained using careful grain selection procedures and abrasion techniques and is considered the only reliable age determination available for any part of the Complex. However, it should be noted that the marked differences in many aspects of the Loch Sunart Granodiorite and the Glen Sanda Granodiorite do not prevent the latter being significantly younger.

The nature of zircon inheritance in the Complex, in the light of ZCI studies, is discussed at some length in Chapter 8.

6.2.5) Chemical and isotopic observations.

Whole rock chemistry.

The chemistry of the Complex has been considered by Sabine (1963), Marston (1970), Pankhurst (1979) and Holden (1987).

Sabine (1963) showed that the chemistry of the porphyritic and non-porphyritic facies of the Loch Sunart Granodiorite is very similar, both parts have similar silica concentrations (~60 to 70 wt%). Sabine (1963), Marston (1970), Pankhurst (1979) and Holden (1987) noted that there are uniform variations of many elements; for example there are increases in K_2O and Al_2O_3 and decreases in Fe_2O_3, CaO, TiO_2, P_2O_5 and Sr, and to a lesser extent the REE and Zr with increasing SiO_2.

The Glen Sanda Granodiorite has a higher, but more restricted range of SiO_2 content, about 70 to 73 wt% (Sabine, 1963; Holden, 1987). It has lower contents of Fe_2O_3, CaO, TiO_2, P_2O_5, Zr, Sr, Ba and the REE than the Loch Sunart Granodiorite (Sabine, 1963; Pankhurst, 1979; Holden, 1979). Pankhurst (1979) described the general decrease of total REE content with increasing evolution, although he considered that the Loch Sunart Granodiorite and the Glen Sanda Granodiorite were related by fractional crystallization. The REE data of the Complex is considered in more detail in Chapter 7 in the light of more detailed knowledge of whole rock chemistry and other constraints.

Holden (1987) showed that the 'appinites' have a broad compositional range from about 46% to 64 wt% SiO_2 (the norm is about 50-55 wt%) and are generally high in Fe_2O_3, CaO, MgO, Ni and Cr.

Isotope chemistry.

Apart from the radiometric age dates and inherited U-Pb zircon data there is a considerable base of Sr, Nd, O, H and S isotope data, this is summarised in Table 6.4.

The following points about the available isotope data should be noted.

1) There is a marked contrast in the $^{87}Sr/^{86}Sr$ initial ratios, the εNd values and the stable isotope ratios of O and S for the Loch Sunart Granodiorite and the Glen Sanda Granodiorite.

2) Enclaves found in the Loch Sunart Granodiorite have $^{87}Sr/^{86}Sr$ initial ratios that are similar to their immediate host, but the εNd values for the enclaves are ~2 units higher.

3) The limited Sr isotope data on enclaves from the Glen Sanda Granodiorite show that they have slightly lower $^{87}Sr/^{86}Sr$ initial ratios than their hosts.

4) There is a large range of $^{87}Sr/^{86}Sr$ initial ratios and εNd values for the appinites, even within single bodies.

Table 6.4. Summary of available Sr, Nd, O, H and S isotope data for the Strontian Complex.

	$^{87}Sr/^{86}Sr$ (425 Ma)	εNd (425 Ma)	$\delta^{18}O$ (‰ SMOW)	δD (‰ SMOW)	$\delta^{34}S$(1) (‰ CDT)
Sources (see below)	1, 2, 5, 6	1, 5, 6	3	4	7
Loch Sunart Granodiorite	0.70530 to 0.70600 (22)	-2.3 to +0.4 (9)	7.1 and 7.3 (2)	-57 and -52 (2)	-1.8 (mean of 6)
Enclaves	0.70505 to 0.70608 (5)	+0.3 to +1.5 (5)	-	-	-
Glen Sanda Granodiorite	0.70682 to 0.70718 (5)	-6.4 (1)	8.5 (1)	-56 (1)	+7.0 (mean of 3)
Enclaves	0.70591 to 0.70657 (3)	-	-	-	-
Appinites(2) T2	0.70599 (1)	-5.7 (1)	-	-	-
PG	0.70595 (1)	-1.5 (1)	-	-	-
BG	0.70569 (1)	-2.2 (1)	-	-	-
Edge to Centre traverse through BG	0.70674 (E) to 0.70574 (C) (6)	- -	- -	- -	- -

Numbers in brackets correspond to the number of determinations. All initial $^{87}Sr/^{86}Sr$ ratios and εNd values have been recalculated to the 425 Ma U-Pb zircon age of Rogers and Dunning (1990, in press). More than one isotope technique has been used on some of the samples, notably those for the enclaves and appinites, the reader is referred to the relevant papers.
(1) - S isotope data obtained from pyrite and pyrrhotite separates.
(2) - naming of individual appinites from Holden (1987): PG and T2 are in the Loch Sunart Granodiorite, BG in the Glen Sanda Granodiorite.
References: 1, Hamilton *et al.* (1980); 2, Halliday *et al.* (1979); 3, Harmon & Halliday (1980); 4, Harmon (1984); 5, Holden (1987); 6, Holden *et al.* (1987); 7, Laouar (1987).

Discussion of the isotope data.

The εNd values of around +1 for the enclaves of the Loch Sunart Granodiorite led Holden *et al.* (1987) to suggest that they represents mantle input into the genesis of the granitoid. Equilibration of Sr isotopes is thought to be the reason there is not a contrast in $^{87}Sr/^{86}Sr$ initial ratios for the enclaves and their host (Holden *et al.*, 1987). They also state that because the enclaves plot at the end of the Sr-Nd array for the Loch Sunart Granodiorite that mantle derived Nd is an important contributor to the overall Nd budget of the Loch Sunart Granodiorite. The limited Pb isotopic memory shown by zircons from the Loch Sunart Granodiorite indicates that there was some crustal contribution.

The εNd values, the $^{87}Sr/^{86}Sr$ initial ratios and the substantial zircon inheritance shown by the Glen Sanda Granodiorite indicate that there was a greater crustal input in its genesis than in the Loch Sunart Granodiorite (Halliday, 1984) and that the two parts of the intrusion cannot be related solely by fractionation processes.

The centre to edge variation of $^{87}Sr/^{86}Sr$ initial ratios of an appinite that cuts the Glen Sanda Granodiorite was interpreted by Holden (1987) as being due to mixing with the host granitoid. The most primitive of these values indicate that the appinites have a mantle origin (Holden, 1987). However the limited data base, the lack of understanding of the petrogenesis of the Caledonian 'appinite' suite and the variability of the Sr and Nd isotope results preclude more extensive comment.

6.3) PROBLEMS OUTSTANDING.

It can be seen that many aspects of the Complex are well understood, although it should be equally clear that there are problems remaining and areas in which the data base is deficient.

The relationship between the Loch Sunart Granodiorite and the Glen Sanda Granodiorite.

The pluton has been considered, without good foundation, to be normally zoned (*ie.* more evolved in the centre). This is probably for two reasons; firstly, the previously used field terminology for the rock units was rather loosely defined and used, and secondly, prior to the existence of isotopic data, the Glen Sanda Granodiorite had been assumed to related to the earlier Loch Sunart Granodiorite by fractionation processes (Pankhurst, 1979). The fact that the Glen Sanda Granodiorite is clearly later and was not centrally emplaced into the Loch Sunart Granodiorite, the Complex is best described as being composite.

Exactly how the Loch Sunart Granodiorite and the Glen Sanda Granodiorite are related to one another is not clear. The different isotopic signatures cannot be explained *solely* by fractionation processes. Although the differences could be due to two, isotopically distinct, sources and/or variable mixing of more than one source. The mantle signatures of the enclaves (Holden *et al.*, 1987) suggest that the latter process did occur, although this should not be taken to indicate that this is necessarily the reason for the isotopic differences between the Loch Sunart Granodiorite and the Glen Sanda Granodiorite. An accurate U-Pb zircon age for the Glen Sanda Granodiorite is clearly needed as a first step in solving this problem.

The relationship and between the porphyritic and non-porphyritic facies of the Loch Sunart Granodiorite.

The structural studies of Hutton (1988a and 1988b) indicate that the emplacement of the two facies should be considered as one event. Furthermore, the chemical and mineralogical similarities of the porphyritic and non-porphyritic facies led Sabine (1963) and Munro (1965) to suggest that the two facies are closely related. An adequate knowledge of the spatial distribution of whole rock variations in the Loch Sunart Granodiorite is required to explore further the relationships between the two facies.

Mineral chemistry and the relationship to whole rock chemistry.

There is simply no published data on the mineral chemistry of either the Loch Sunart Granodiorite or the Glen Sanda Granodiorite. Knowledge of the mineral chemistry would allow a better understanding of the crystallisation history, including fractionation processes and subsolidus changes. Together this information allows critical consideration of the whole rock chemistry.

The origin and role of the 'appinites' in the petrogenesis of the Strontian Complex.

The lobate and 'pillowed' contacts that at least one of the basic 'appinitic' bodies has with the pluton suggests that granitic and basic liquids coexisted (Holden, 1987). Holden (1987) also suggested that the microdiorite enclaves, which are thought to represent input of mantle material, may be closely related to the basic bodies. Further work on the 'appinites' is required before their relationship to the pluton and its enclaves is fully understood.

Chapter 7
The whole rock and major mineral chemistry of the Strontian Complex.

7.1) INTRODUCTION.

This Chapter has three aims: 1) to describe the compositional variations in the Loch Sunart Granodiorite and the Glen Sanda Granodiorite; 2) to describe the geographical distribution of composition in the Loch Sunart Granodiorite; and 3) to document the REE and major mineral chemistry of a small, but representative subset of samples. The same subset of samples is used in the description of the accessory phases which is considered in Chapter 8.

7.2) WHOLE ROCK CHEMISTRY.

The whole rock concentration of major and trace elements was determined by XRF. Full details of the sample localities, methods and analytical results are given in Appendices 1A, 2, and 6 respectively.

7.2.1) General chemistry of the Strontian Complex.

In Figure 7.1 analyses of samples from Loch Sunart Granodiorite (59 samples) and the Glen Sanda Granodiorite (34 samples) are shown on an AFM plot and a total alkalies versus SiO_2 diagram. These demonstrate the calc-alkaline and subalkaline affinities of both parts of the Strontian Complex. Harker-type variation diagrams are shown in Figure 7.2; for most elements there is no clear distinction between the two main parts to the Complex, although there is no extensive overlap either, only for total Fe (Fe determined as Fe_2O_3) is there a 'compositional gap', about 0.5 wt%. The porphyritic and non-porphyritic facies of the Loch Sunart Granodiorite show an almost complete compositional overlap, confirming the

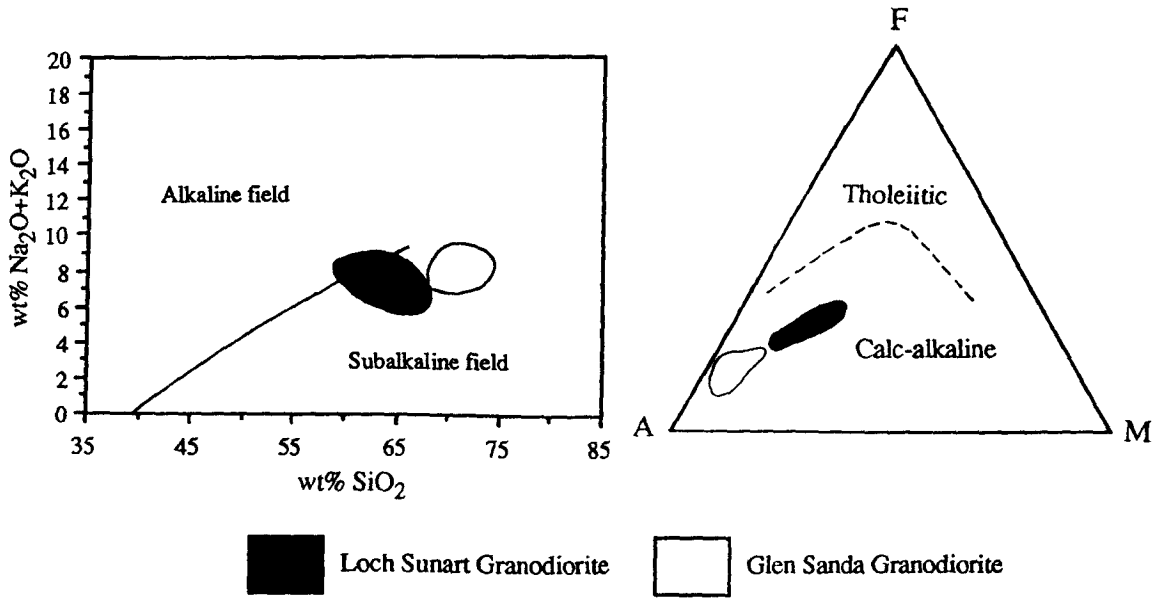

Fig. 7.1. Total alkalies versus SiO_2 diagram (a) and an AFM plot (b) showing the calc-alkaline affinities of both parts of the Strontian Complex. Division lines after Irvine & Baragar (1971).

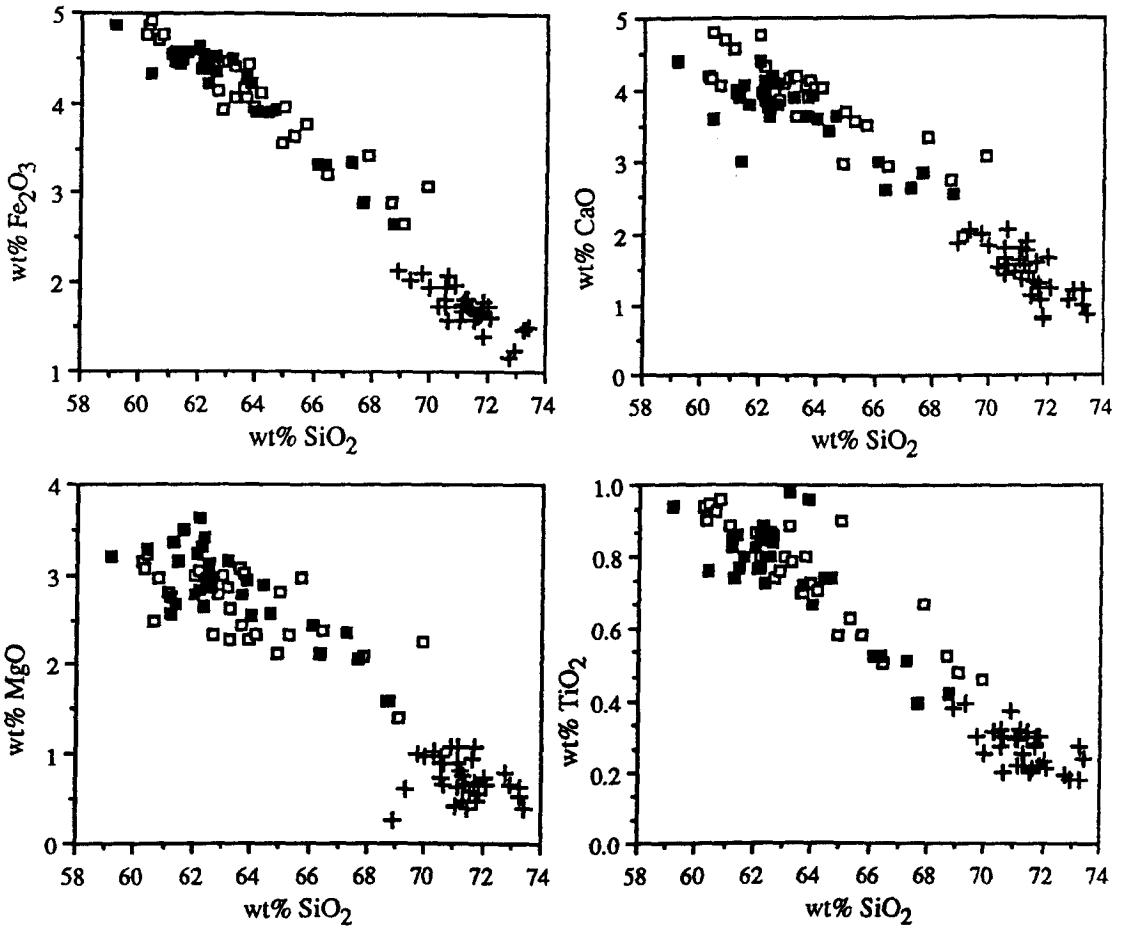

Fig. 7.2. Harker variation diagrams of total Fe (determined as Fe_2O_3), TiO_2, CaO and MgO. Symbols: Loch Sunart Granodiorite - non-porphyritic facies, □; porphyritic facies, ■; Glen Sanda Granodiorite, +.

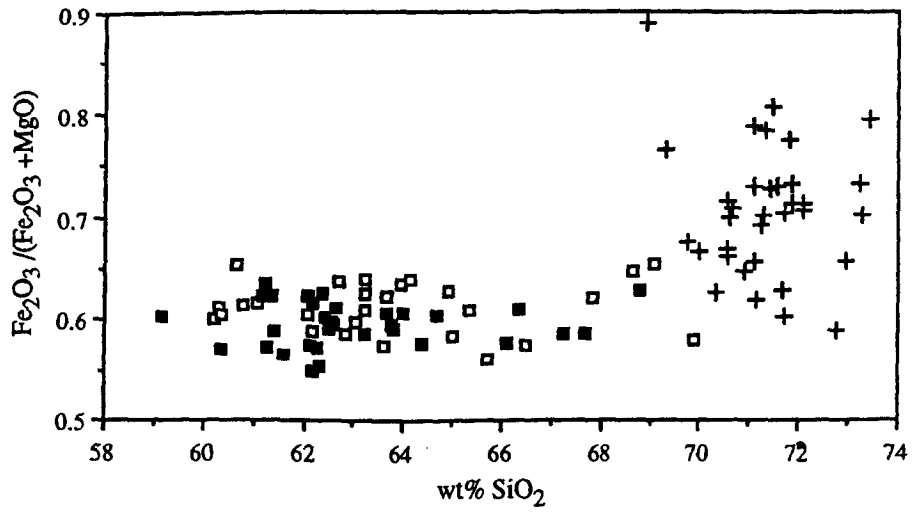

Fig. 7.3. Diagram of SiO_2 versus Fe/(Fe+Mg) for the Strontian Complex. Fe is total Fe expressed as Fe_2O_3. Symbols as in Figure 7.2.

observations of Sabine (1963). The Fe/(Fe+Mg) values for the Loch Sunart Granodiorite do not change systematically through the range of composition, however, there is notable scatter beyond that expected from analytical uncertainty. Most of this scatter is due to variations in the MgO concentration. The pattern in the Glen Sanda Granodiorite is similar although the Fe/(Fe+Mg) values are generally higher (Fig. 7.3).

In both parts to the Complex there are systematic decreases in total Fe (as Fe_2O_3), TiO_2, CaO and to a lesser extent MgO, with increasing SiO_2. Similar plots for Na_2O and K_2O (Fig. 7.4) show a greater degree of scatter, with ill defined trends. However, the K_2O content of the porphyritic facies of the Loch Sunart Granodiorite is generally higher than the otherwise similar non-porphyritic facies.

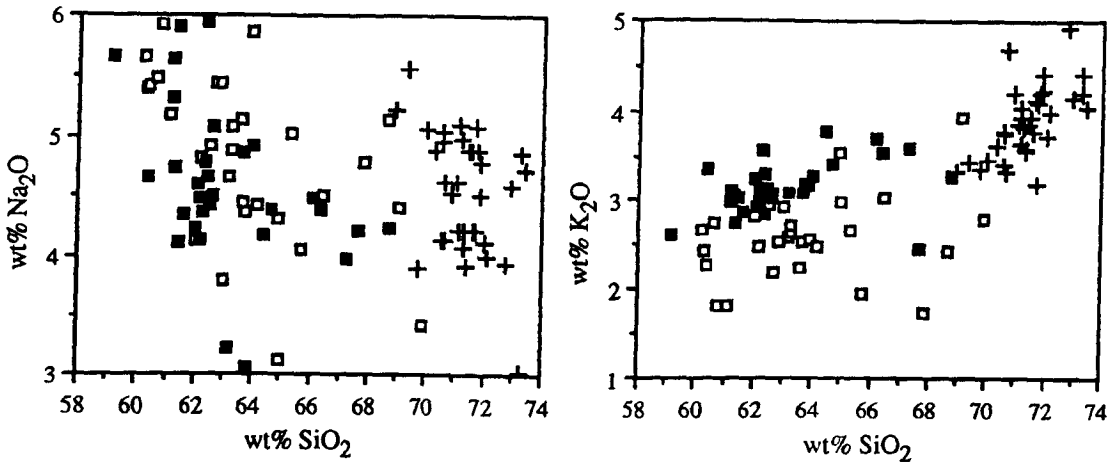

Fig. 7.4. Harker variation diagrams of Na_2O and K_2O for the Strontian Complex. Symbols as in Figure 7.2.

In Figure 7.5 various trace element variation diagrams for the Complex are shown. The plots of V and Sr show most of the characteristics of the Harker variation diagrams of Figure 7.2, there is no compositional gap or extensive overlap between the two main parts and there are coincident trends. For Ba and Zr there is a high degree of scatter, beyond that expected from analytical error. Rb shows very little variation in the Loch Sunart Granodiorite, but it is significantly higher in the Glen Sanda Granodiorite. This difference in the Rb concentrations is shown by the Rb/Sr ratio (Fig. 7.6).

In the description of the Complex given in Chapter 5 it was noted that the REE content is lower in the more siliceous Glen Sanda Granodiorite than in the Loch Sunart Granodiorite (Pankhurst, 1979), a feature seen in other granitoid plutons (*eg.* Mittlefehldt & Miller, 1983). When considered separately the pattern of REE concentrations in the Loch Sunart Granodiorite is not so simple, plots of Ce and Y (as measured by XRF) have a high degree of scatter (Fig. 7.7), greater than the analytical uncertainty. Within this scatter there is a very general trend towards reduced REE concentrations in the more siliceous rocks. Pankhurst (1979) noted that in both parts the relative REE distribution is LREE enriched, there is no Eu anomaly and the patterns for a wide range of compositions are essentially parallel. The latter

observations are consistent with the Ce/Y ratios plotted in Figure 7.7 which show no systematic variation with whole rock evolution.

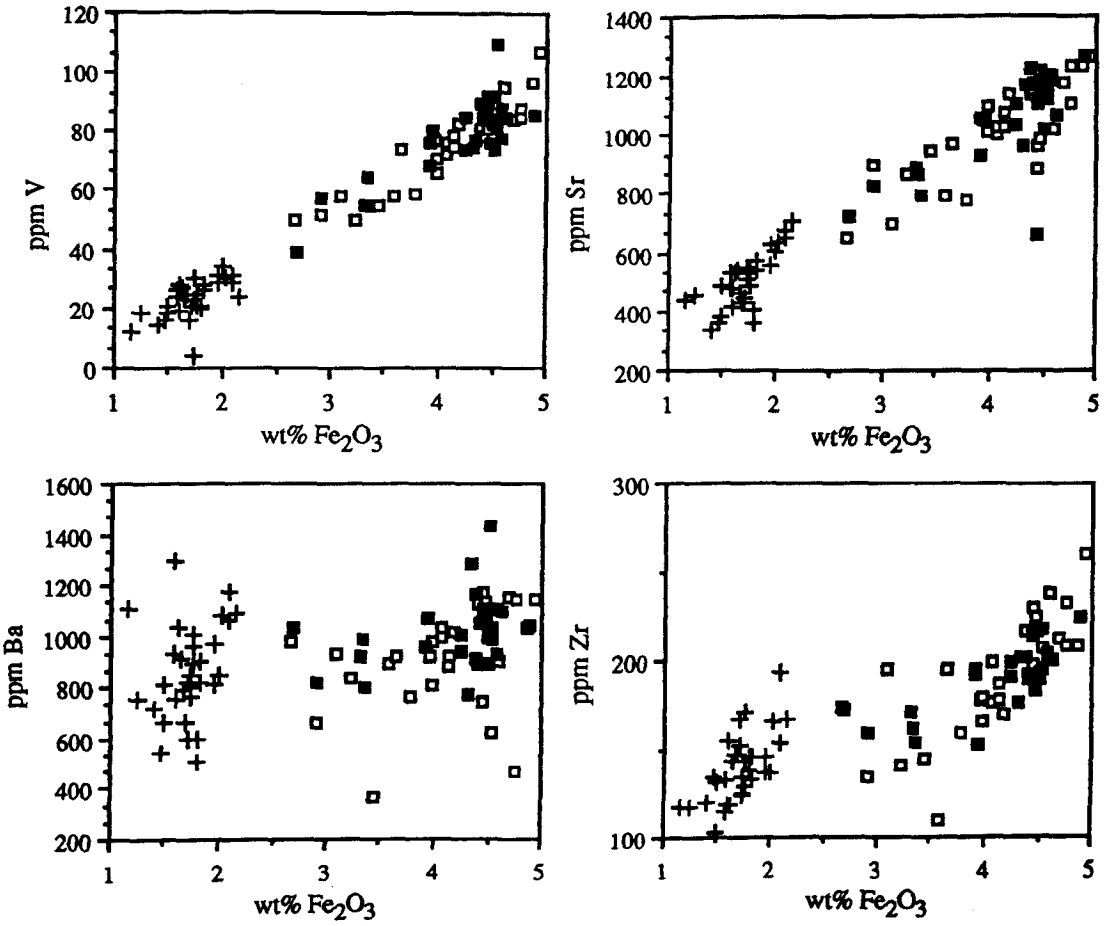

Fig. 7.5. Variation diagrams of total Fe versus V, Sr, Ba and Zr for the Strontian Complex. Symbols as in Figure 7.2.

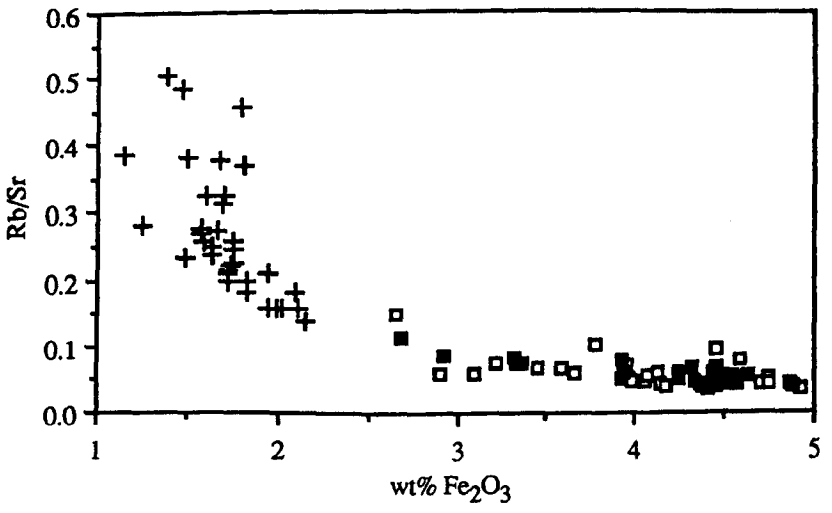

Fig. 7.6. Diagram of total Fe versus Rb/Sr ratio for the Strontian Complex. Symbols as in Figure 7.2.

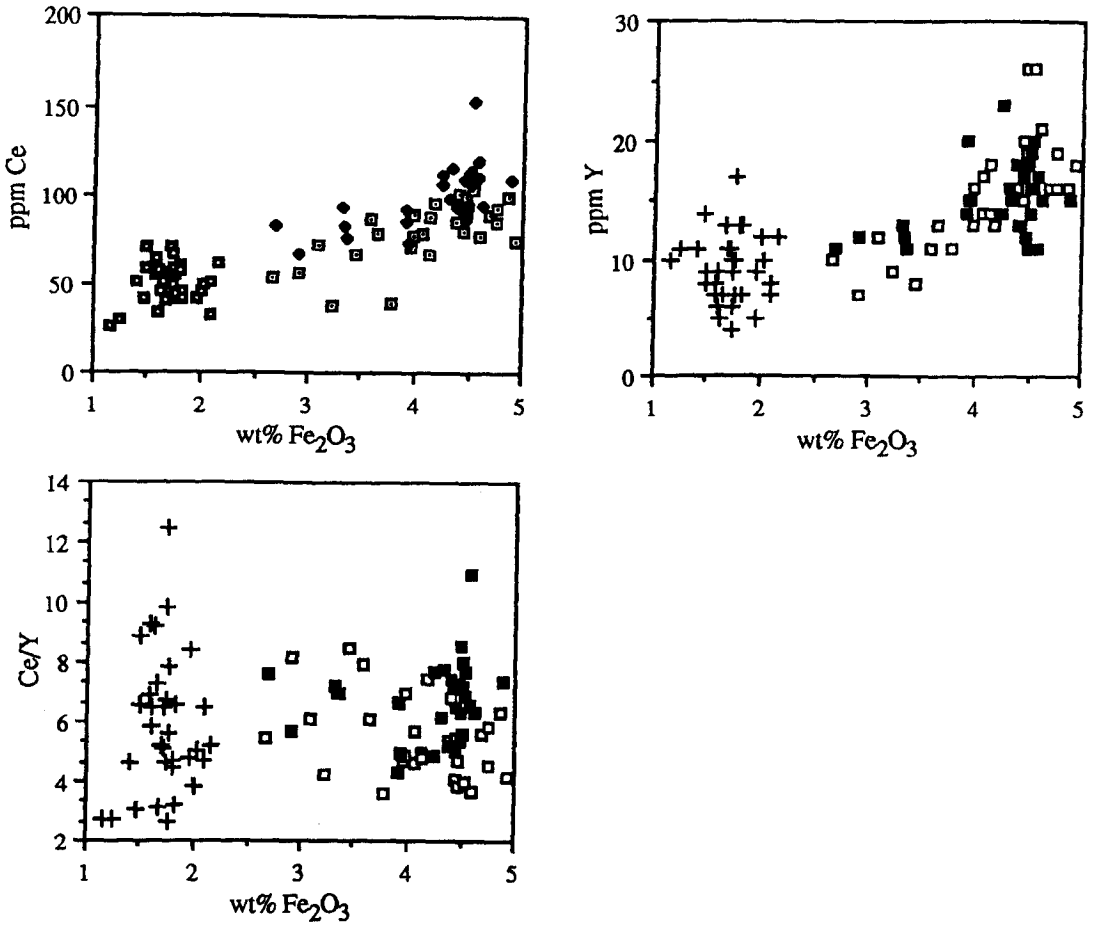

Fig. 7.7. Variation diagrams of total Fe versus Ce, Y and Ce/Y for the Strontian Complex. Symbols as in Figure 7.2.

7.2.2) The spatial distribution of composition in the Strontian Complex.

The contoured composition maps were produced using Surface II, a programme written by R.J. Sampson and published by the Kansas Geological Survey. An outline of the contouring method used by Surface II is given in Appendix 2D. Only contoured composition maps of SiO_2 and total Fe are shown, however, similar patterns result for maps contoured for other elements. Due to the restricted compositional range (~69-73 wt% SiO_2) of the Glen Sanda Granodiorite only the spatial distribution of composition in the Loch Sunart Granodiorite is considered.

Included in the data set are the analyses of Mercy (1963) (9 samples), Sabine (1963) (1 sample) and Holden (1987) (8 samples), making a total of 77 (the sample numbers and grid references of all samples are in Appendix 1A). The spacing of contours was chosen to be greater than the statistical variation of the data, estimated using the multiple analyses of Holden (1987). The distribution of sample localities is shown in Figure 7.8, in some areas the density of sample localities is sparse.

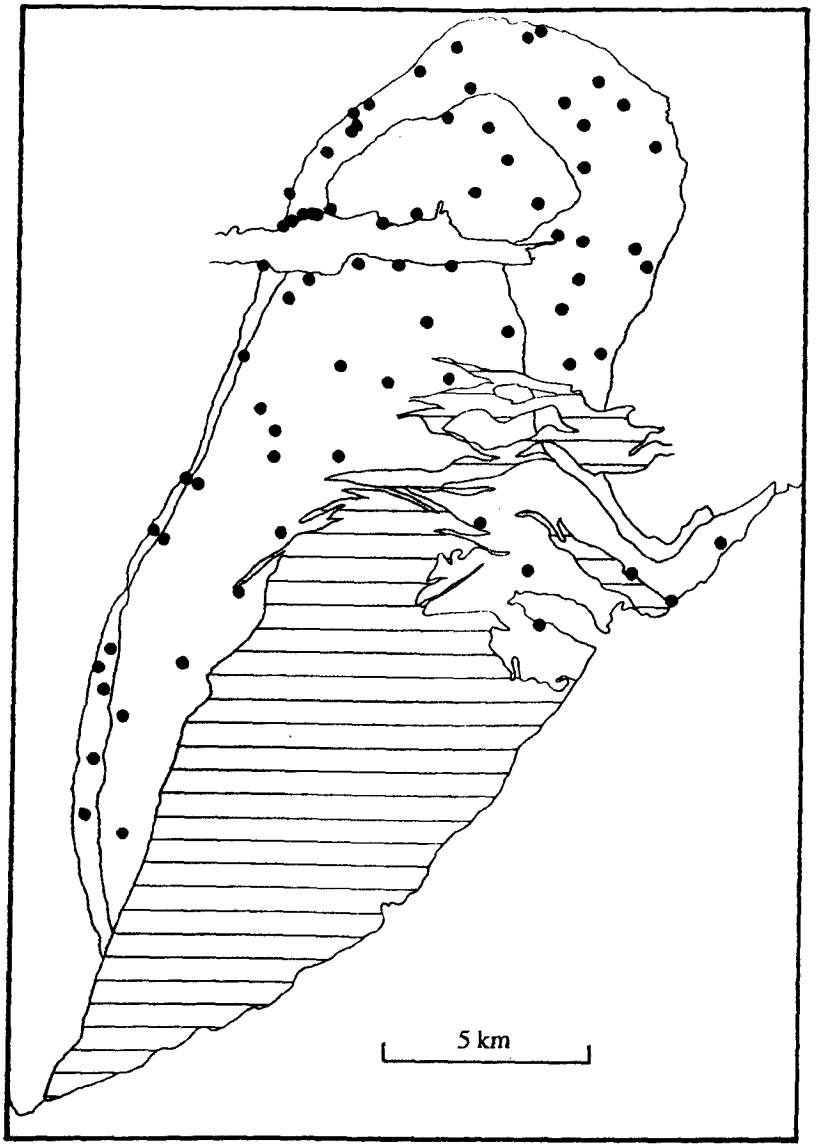

Fig. 7.8. Map showing the distribution of sample localities in the Loch Sunart Granodiorite used in the contouring of compositional data, included are the localities of Mercy (1963), Sabine (1963) and Holden (1987).

The spatial distribution of composition in the Loch Sunart Granodiorite.

Maps showing the spatial distribution of SiO_2, and total Fe are given in Figure 7.9 and 7.10 respectively. The distribution patterns for the two elements, as would be expected, are very similar, there are some areas with smoothly varying composition and others with steep compositional gradients, the latter possibly indicating internal contacts. In Glen Tarbet, for example, the SiO_2 concentration is seen to vary from ~60 to 69 wt% over a distance of ≤600 m (600 m is the distance between two adjacent samples). The distribution pattern for both SiO_2 and total Fe appears to be independent of the mapped porphyritic/non-porphyritic contact, a fact which is consistent with the observations presented in Section 7.2.1.

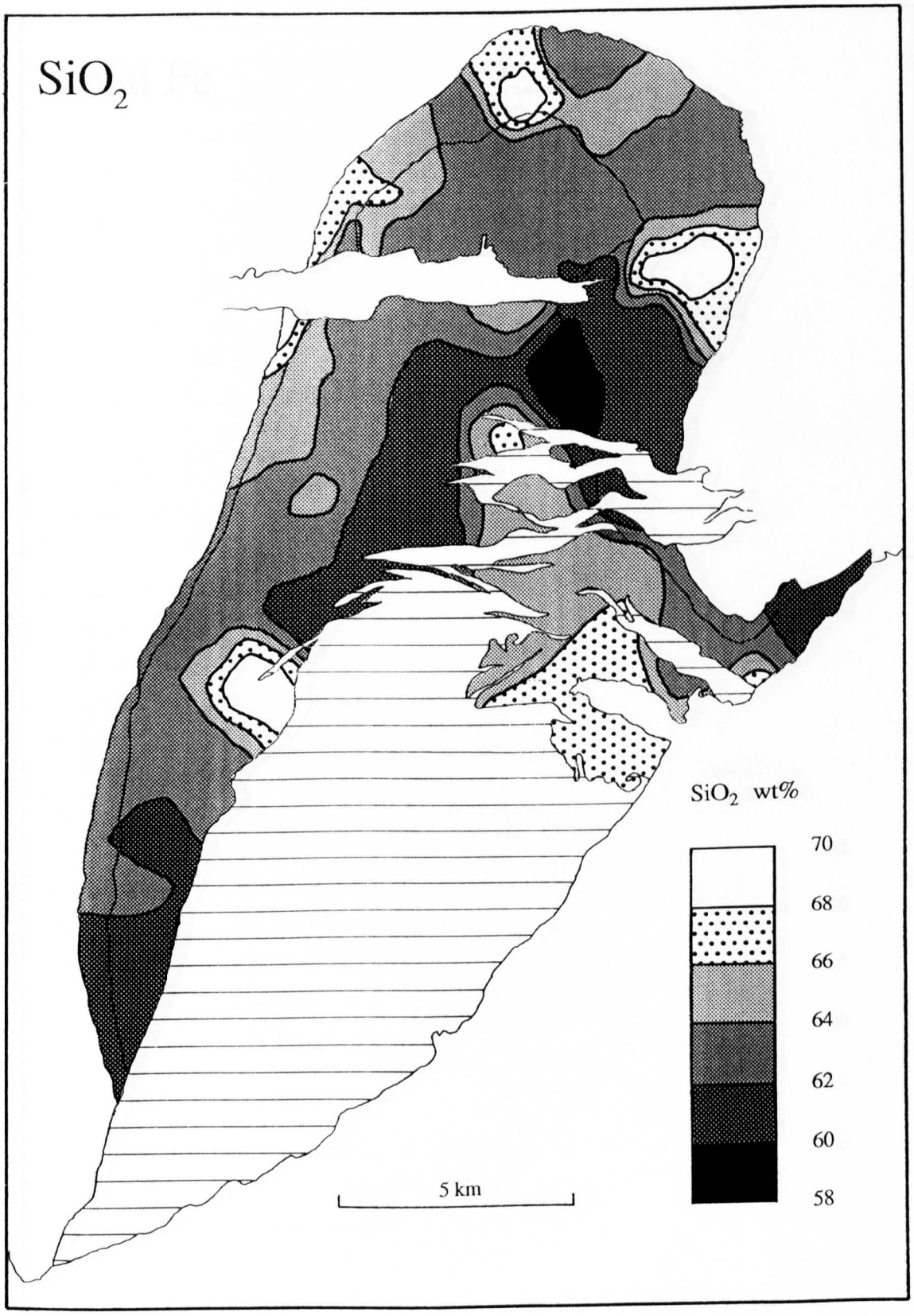

Fig. 7.9. Map of the Loch Sunart Granodiorite showing the spatial distribution of SiO_2 concentration (wt%). The dark areas are the most basic (low in SiO_2), the light areas the most acid (high in SiO_2).

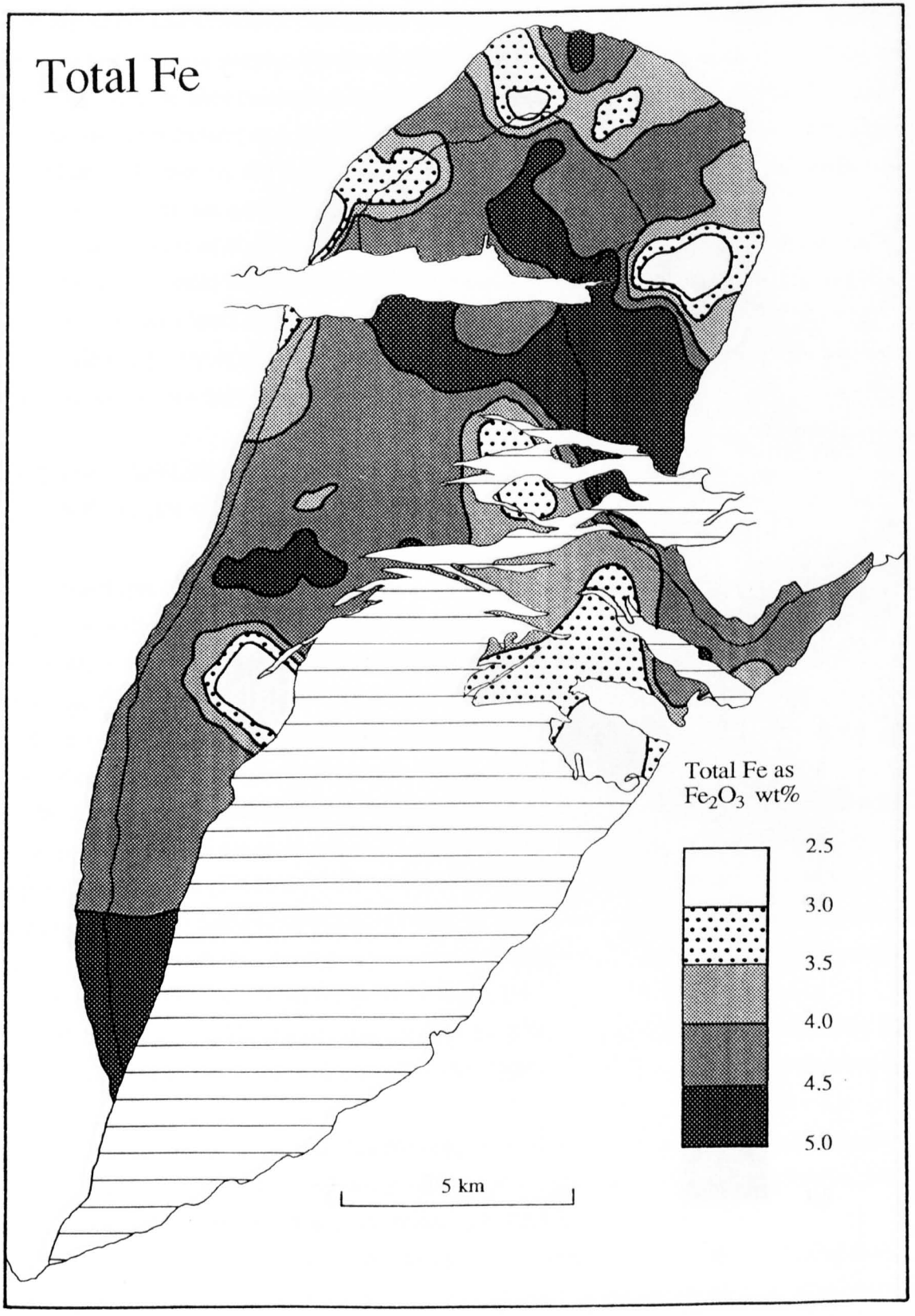

Fig. 7.10. Map of the Loch Sunart Granodiorite showing the spatial distribution of total Fe concentration (FeO wt%). The dark areas are the most basic (high in total Fe), the light areas the most acid (low in total Fe).

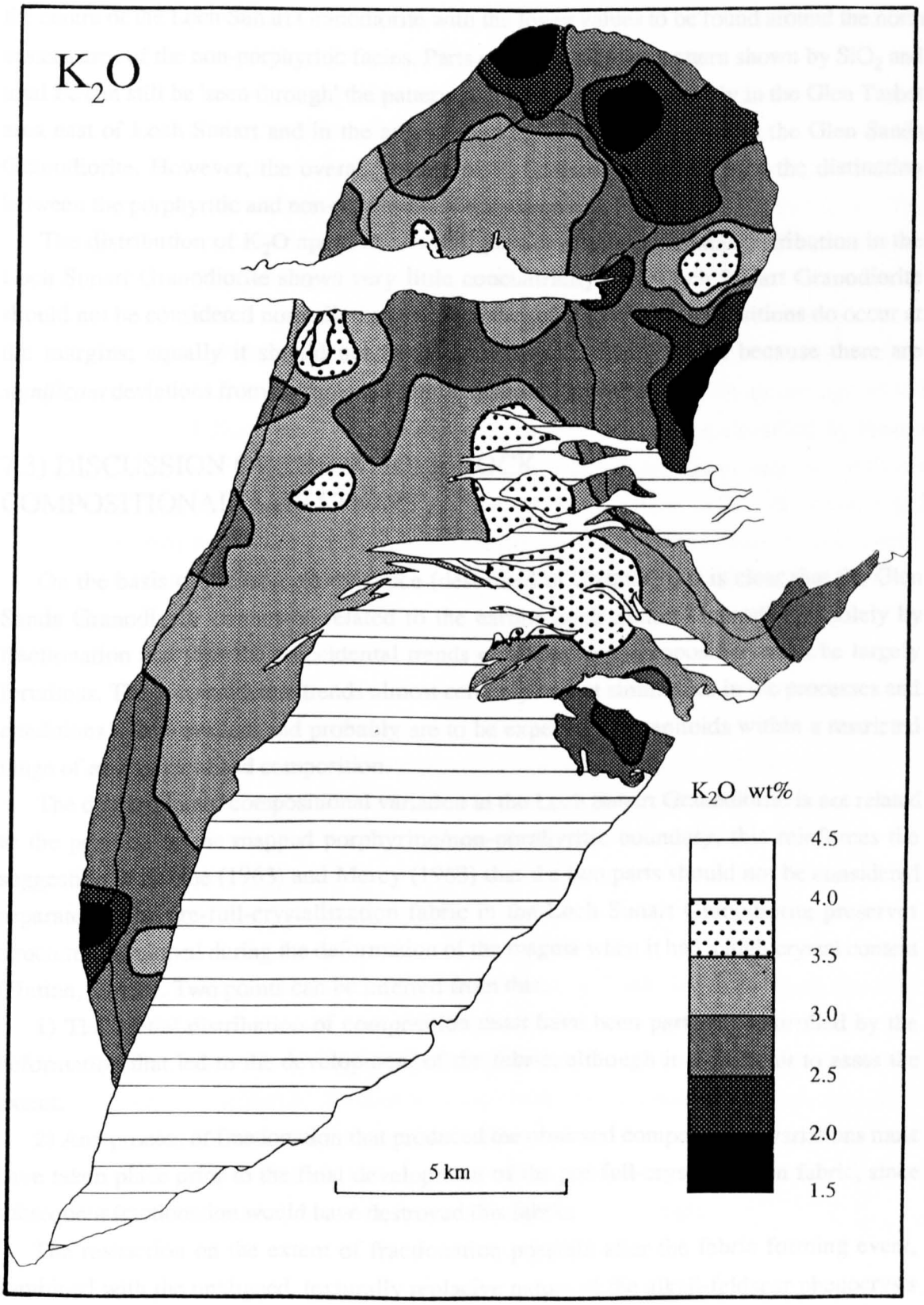

Fig. 7.11. Map of the Loch Sunart Granodiorite showing the spatial distribution of K_2O concentration (wt%). The dark areas are low in K_2O and the light areas are high in K_2O.

However, the position of the porphyritic/non-porphyritic boundary does appear to be relevant for K_2O concentration (Fig. 7.11), the higher K_2O concentrations occurring towards the centre of the Loch Sunart Granodiorite with the lower values to be found around the north eastern area of the non-porphyritic facies. Parts of the distribution pattern shown by SiO_2 and total Fe can still be 'seen through' the pattern of K_2O distribution, notably in the Glen Tarbet area east of Loch Sunart and in the area around the sheeted contact with the Glen Sanda Granodiorite. However, the overall pattern of K_2O distribution confirms the distinction between the porphyritic and non-porphyritic facies shown in Figure 7.4.

The distribution of K_2O apart, the overall pattern of compositional distribution in the Loch Sunart Granodiorite shows very little concentricity. The Loch Sunart Granodiorite should not be considered normally zoned, since the more evolved compositions do occur at the margins; equally it should not be described as reversely zoned because there are *significant* deviations from a simple concentric distribution pattern.

7.3) DISCUSSION OF THE WHOLE ROCK COMPOSITIONAL VARIATIONS.

On the basis of the isotopic evidence (described in Chapter 6) it is clear that the Glen Sanda Granodiorite cannot be related to the earlier Loch Sunart Granodiorite solely by fractionation and thus the coincidental trends of whole rock composition must be largely fortuitous. These coincidental trends almost certainly reflect similarities in the processes and conditions that prevailed, and probably are to be expected of granitoids within a restricted range of environment and composition.

The distribution of compositional variation in the Loch Sunart Granodiorite is not related to the position of the mapped porphyritic/non-porphyritic boundary, this reinforces the suggestion of Sabine (1963) and Mercy (1963) that the two parts should not be considered separately. The pre-full-crystallization fabric in the Loch Sunart Granodiorite preserves structures developed during the deformation of the magma when it had a high crystal content (Hutton, 1988b). Two points can be inferred from this.

1) The spatial distribution of composition must have been partially controlled by the deformation that led to the development of the fabric, although it is difficult to asses the extent.

2) Any process of fractionation that produced the observed compositional variations must have taken place prior to the final development of the pre-full-crystallization fabric, since subsequent fractionation would have destroyed this fabric.

The restriction on the extent of fractionation possible after the fabric forming event, combined with the unaligned, texturally replacive nature of the alkali-feldspar phenocrysts (Sabine, 1963 and Munro, 1963) and the independence of K_2O distribution, suggests that a mobile, fluid phase was in part responsible for the distribution of K_2O. Thus it is proposed that the development of the alkali-feldspar phenocrysts of the porphyritic facies of the Loch Sunart Granodiorite must have been, in part, due to a late, post-emplacement metasomatic

event and not wholly due to primary magmatic crystallization. The central position of the porphyritic facies and the listric shape of the Loch Sunart Granodiorite suggest that if the phenocrysts do have a replacive metasomatic origin that the late fluid phase responsible was concentrated in the roof, although the roof is no longer present due to erosion.

The existence of steep compositional gradients may indicate the presence of internal contacts other than that between the porphyritic and non-porphyritic facies. If there are internal contacts the fact that they have not be identified is probably due to the importance that has been attached to the differences between the non-porphyritic and porphyritic facies. This importance is understandable, since the textural contrasts of the two facies dominates their appearance in the field, although the chemical evidence suggests that it is not warranted.

The internal contacts of the Ardara pluton are marked by sharp changes in the amount of strain measured from deformed microdiorite enclaves (Holder, 1979), with concomitant changes in texture and mineralogy. Similar sharp changes of strain or swings in the orientation of the foliation in the Loch Sunart Granodiorite were not identified by Hutton (1988b). The fact that there is a lack of internal structural discontinuities may be consistent with the essentially passive emplacement of the Loch Sunart Granodiorite that is envisaged by Hutton (1988a and 1988b); the space for intrusion being largely created by the relative lateral movement of a hangingwall and a footwall. It may also be significant that the strain measurement traverses carried out by Hutton (1988a and 1988b) did not approach any of the steep compositional gradients identified in this work.

Both the gradational and sharp changes of composition could be due to episodic emplacement of a magma of changing composition. This would require that the process responsible for the compositional variations to have taken place below the level of emplacement. The exact nature of the steep compositional gradients can only be investigated by further field observations, structural studies and whole rock analyses.

7.4) THE SUBSET OF SAMPLES.

The subset of samples consists of four rocks from the Loch Sunart Granodiorite (two from each of the facies) and two from the Glen Sanda Granodiorite (see locality map, Fig. 7.12). They are representative of the whole rock variations encountered in the two main parts to the Complex. The subset of samples was used in the determination of whole rock REE concentrations (by INAA), modal analysis of major mineral phases (by point counting) and major phase chemistry (by EPMA). The rock numbers of the subset, *eg*. BPSRT1, all share the same stem (BPSR) and thus will be referred to only by the last part.

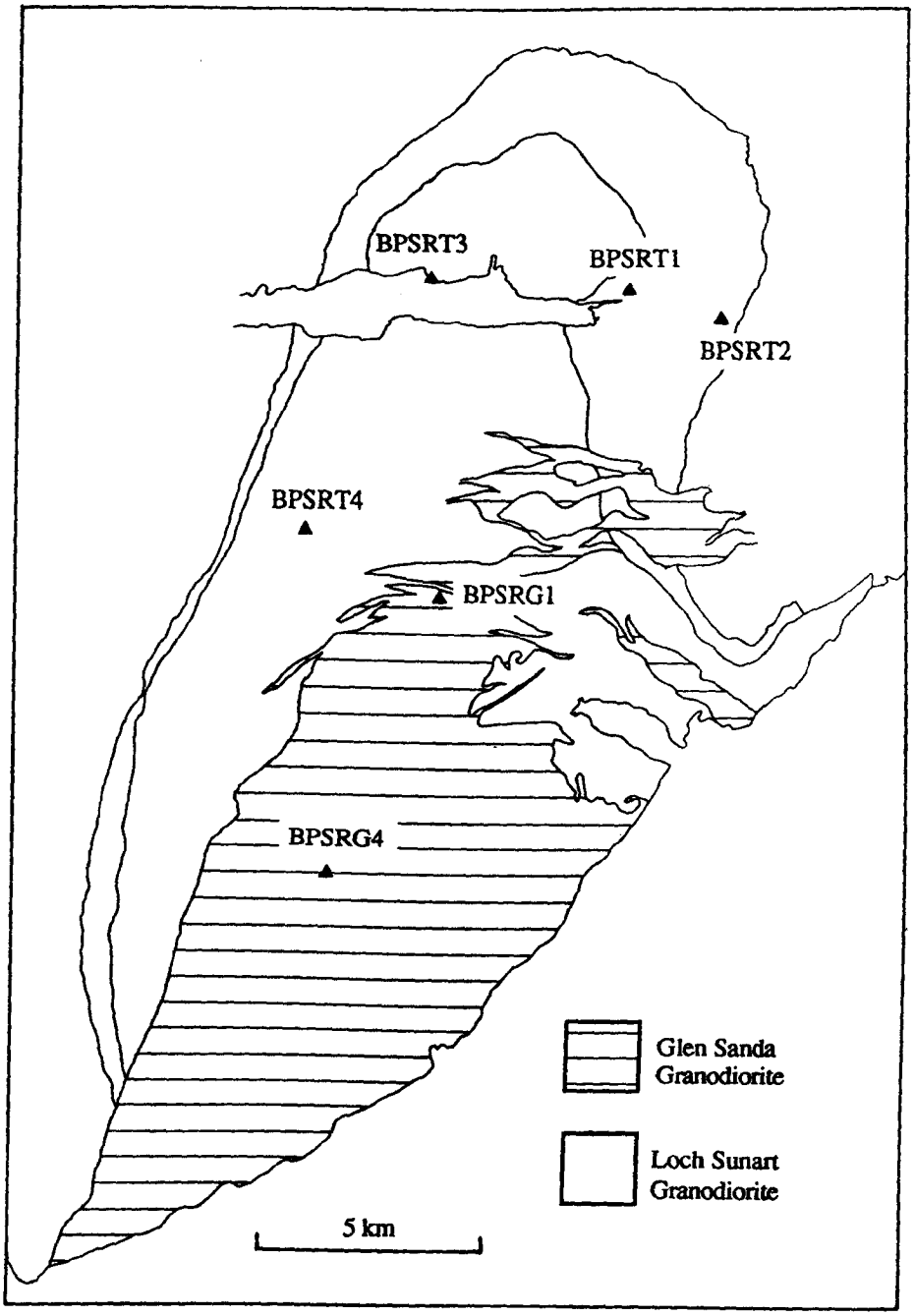

Fig. 7.12. Map of the Strontian Complex showing the location of the subset of samples.

7.4.1) Whole rock chemistry of the subset of samples.

The whole rock XRF and INAA data for the subset of samples is shown in Table 7.1. The methods and results of the INAA are given in Appendices 2E and 7 respectively.

Table 7.1. The whole rock chemistry (by XRF and INAA) of the samples used in the study of mineral chemistry. Major elements (XRF) are expressed as wt% oxide, trace elements (XRF) as ppm, REE (INAA) as ppm. The total includes the trace element concentrations obtained by XRF.

	Loch Sunart Granodiorite: Non-Porphyritic		Porphyritic		Glen Sanda Granodiorite	
Sample	BPSRT1	BPSRT2	BPSRT3	BPSRT4	BPSRG1	BPSRG4
SiO_2	60.34	69.07	62.25	64.37	72.93	71.14
TiO_2	0.95	0.48	0.89	0.74	0.18	0.30
Al_2O_3	17.10	15.32	16.03	15.59	14.75	15.47
Fe_2O_3	4.93	2.66	4.44	3.92	1.25	1.76
MnO	0.08	0.05	0.07	0.07	0.03	0.04
MgO	3.22	1.40	3.30	2.88	0.65	1.08
CaO	4.80	1.97	3.76	3.43	1.20	1.79
Na_2O	5.43	4.41	4.37	4.17	4.58	4.22
K_2O	2.26	3.95	3.56	3.78	4.14	4.04
P_2O_5	0.36	0.17	0.33	0.27	0.08	0.10
Loss	0.80	0.80	0.60	0.60	0.60	0.20
Total	100.59	100.50	99.90	100.08	100.55	100.34
Nb	10	9	14	15	5	6
Zr	260	174	214	196	117	144
Sr	1263	655	1107	931	458	543
Rb	43	100	67	74	130	133
Th	10	14	18	30	13	22
Pb	13	24	18	18	32	32
Zn	71	48	60	42	16	34
Cu	8	20	19	18	13	16
Ni	50	15	49	43	9	10
Cr	71	19	61	58	3	9
V	107	50	92	68	18	25
Ba	1150	981	1111	964	753	964
Hf	7	5	6	6	4	4
La	37	33	57	45	14	22
Ce	75	54	90	86	30	45
Y	18	10	18	20	11	17
La	49.7	43.9	66.6	59.1	19.0	24.7
Ce	97.3	70.1	122.6	109.3	42.7	43.7
Nd	36.4	20.5	41.6	36.7	16.0	16.1
Sm	5.82	4.30	6.21	5.89	2.14	3.15
Eu	1.58	1.06	1.39	1.38	0.66	0.81
Yb	1.42	1.08	1.53	1.80	0.65	1.18
Lu	0.22	0.18	0.23	0.25	0.13	0.16

The REE data is shown on a chondrite normalised plot (Fig. 7.13). The REE distribution patterns are LREE enriched, generally parallel and have no Eu anomaly (all features first noted by Pankhurst (1979)). The observation of Pankhurst (1979) that the more siliceous Glen Sanda Granodiorite has generally lower REE concentrations than the Loch Sunart Granodiorite is borne out.

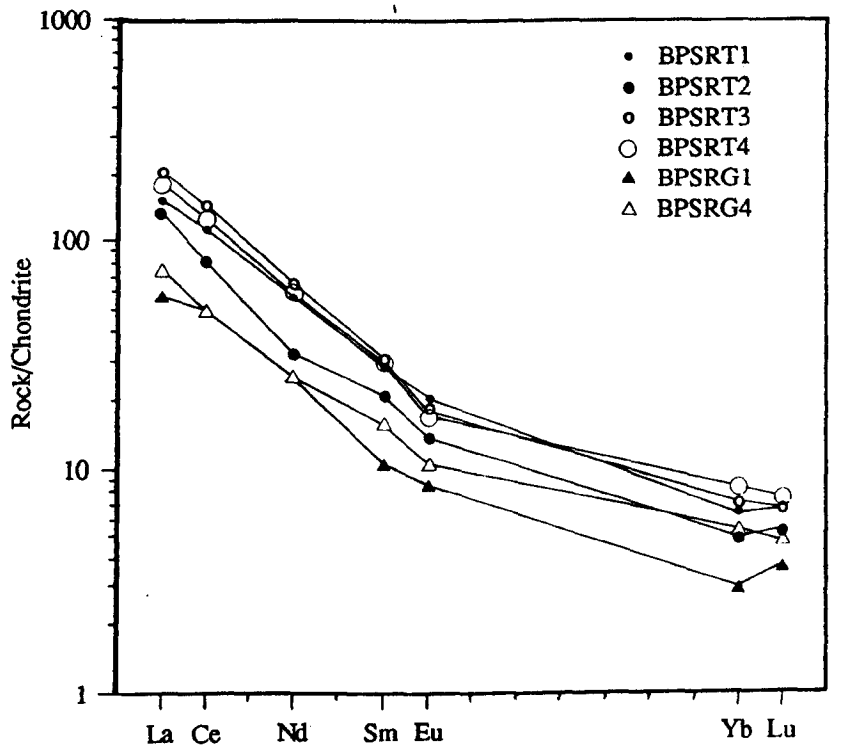

Fig. 7.13. Chondrite-normalised plot of REE concentrations in the subset of samples. The chondritic values used are those recommended by Nakamura (1974).

7.4.2) The abundances of mineral phases in the subset of samples.

A note on the modal analysis of accessory phases by point counting.

Modal analysis of minerals present in accessory quantities by point counting of thin sections should be treated with caution; Gromet & Silver (1983) determined the modal quantities of all phases in a single granodiorite by counting 18,000 points over 10 thin sections and still found that the errors for accessory phases, based on counting statistics, were unacceptably high. The basis of modal analysis by point counting is that it is performed across a two-dimensional surface and most thin sections of coarse grained rocks can be considered to be a good approximation to this ideal. However, very small mineral grains (often present as inclusions) may be overestimated by point-counting because the 'area' being counted is actually a three-dimensional volume. It has also been noted (*eg.* Gromet & Silver, 1983; Sawka, 1988 and Mittlefehldt & Miller, 1983) that because accessory phases are commonly small, errors due to misidentification are more likely.

The mineral abundance data.

For the purpose of this study the abundances of major phases (and titanite in the Loch Sunart Granodiorite) were obtained by point counting and those of zircon and apatite were calculated by the methods advocated by Sawka & Chappell (1988); apatite from the CIPW norm and zircon on the basis of 0.1% zircon per 700 ppm whole rock Zr. These methods overestimate apatite and zircon abundances as they do not account for P and Zr contained in other phases, although for comparisons between similar and related rocks they are deemed adequate. Sawka & Chappell (1988) calculated the abundance of titanite by assuming that all the whole rock Ta is to be found in that phase and that the concentration of Ta in titanite from a given rock is constant, they used an analogous method, using Th, to calculate allanite abundances. These methods have not been employed due to the ubiquitous zoning present in these phases, a problem acknowledged by Sawka & Chappell (1988). Titanite was included when performing point counting, due to the lack of a suitable alternative method for calculating titanite abundances. The errors, estimated from counting statistics, in the measured abundances of titanite are still high, $\geq 50\%$ (1σ).

Table 7.2. Mineral abundance data; major phases and titanite by point counting (≥1000 points per thin section), apatite and zircon by calculation, all expressed as volume %. Also shown are the other minerals present (represented by √), in all cases abundances are low, estimated to be less than 0.1%. The text gives an explanation of the methods used and discusses the reliability of the information.

	Loch Sunart Granodiorite: Non-Porphyritic		Porphyritic		Glen Sanda Granodiorite	
Sample	BPSRT1	BPSRT2	BPSRT3	BPSRT4	BPSRG1	BPSRG4
Point Counting Data:						
Plagioclase	54	48	54	51	49	48
Alkali-Feldspar	12	18	12	15	21	23
Quartz	15	21	16	18	23	22
Hornblende	5.2	9.0	9.2	7.5	-	-
Biotite	7.5	5.6	7.1	5.9	5.5	5.6
Titanite	0.8	0.3	0.8	0.6	-	√
Opaques and Other Accessories.	1.5	1.9	1.1	2.0	1.5	1.2
Calculated Abundances:						
Zircon	0.037	0.025	0.031	0.0328	0.017	0.021
Apatite	0.85	0.40	0.78	0.64	0.19	0.24
Other Minerals Present:						
Allanite	-	-	-	-	√	√
Monazite	-	-	-	-	√	√
Magnetite/ Ilmenite	√	√	√	√	√	√

For the reasons outlined above the mineral abundance data presented in Table 7.2 should only be used as a *guide* to the abundances of the accessory phases, the absolute values given are virtually meaningless. The lack of a rapid, and above all, reliable method for obtaining information on the abundance of phases present in accessory quantities is a serious hindrance to quantitative studies.

7.5) THE CHEMISTRY OF MAJOR MINERAL PHASES FROM THE SUBSET OF SAMPLES.

The chemistry of major mineral phases from the subset of samples was determined by electron microprobe. Full details of the methods and results are given in Appendices 2F and 8 respectively.

7.5.1) Plagioclase feldspar.

Optically it can be seen that the plagioclase feldspars in all the samples are continuously zoned from centre to edge, multiple discontinuous zoning is only rarely found. Microprobe analysis confirmed the presence of continuous zoning, and show that it is towards more albitic edge compositions (see Fig. 7.14). Overall the plagioclase analyses are very restricted in their compositional range.

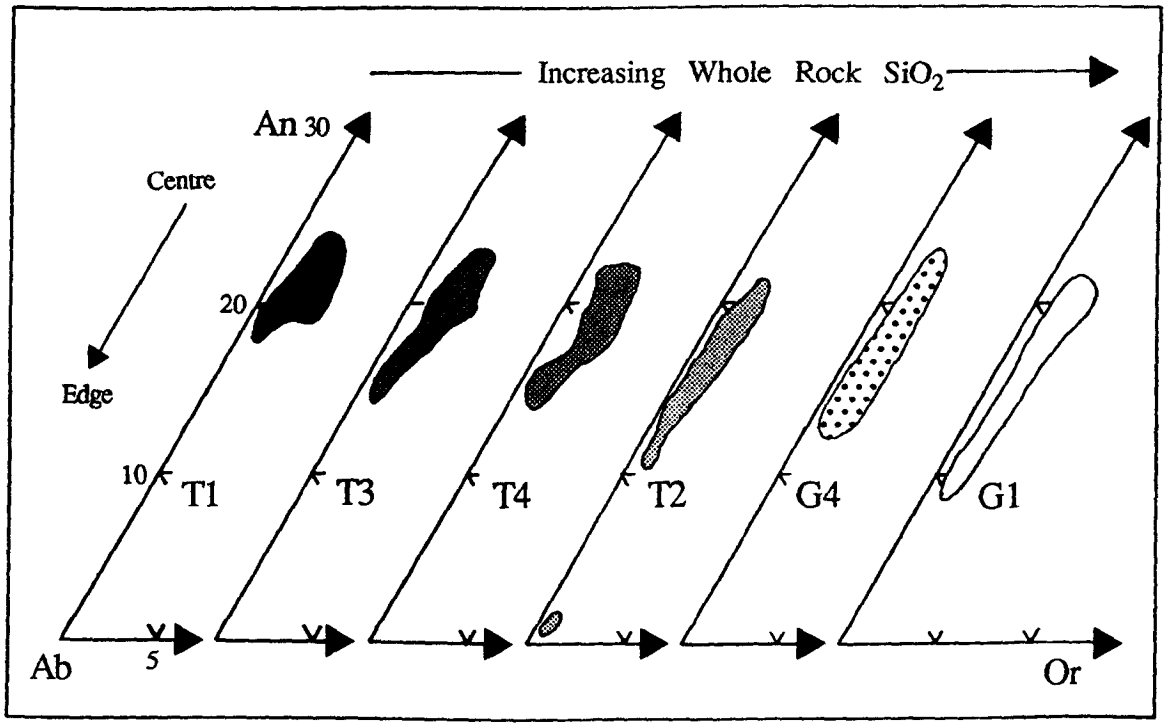

Fig. 7.14. Plot of plagioclase compositions from the Strontian Complex projected onto part of the ternary feldspar system.

In the Loch Sunart Granodiorite there is also a change in composition between the samples; T1, the sample with the lowest SiO_2 content (60 wt% SiO_2), has plagioclase feldspars which are generally less albitic than those of T2 (69 wt% SiO_2). The compositional contrast between the centre and edge compositions is greater in T2 (about Ab_6) than in T1 (about Ab_{12}). A few grains have distinct, strongly albitic ($Or_{0-1}Ab_{93-99}An_{1-7}$) areas around their edges which are discontinuous, in terms of composition, with the interior of the grain. Plagioclases from G1 and G4 of the Glen Sanda Granodiorite are indistinguishable from one another and have compositions similar to those from the Loch Sunart Granodiorite. The plagioclase feldspar from each of the Loch Sunart Granodiorite samples have similar compositional ranges.

Ba was not included in the original analysis programme, however later some plagioclase feldspars from each of the samples were re-analysed with Ba included, it was found that they did not contain detectable quantities of Ba so the original analyses were retained.

7.5.2) Alkali-feldspar.

The alkali-feldspars are generally microperthitic, but some areas are apparently free of intergrowth, although they are probably cryptoperthitic. In most cases the alkali-feldspars do not contain detectable Ca, although, unlike the plagioclases, Ba was found in significant quantities. The preference that Ba has for the alkali-feldspar over plagioclase is the pattern commonly observed (Heier, 1962). The analyses are presented on a diagram (Fig. 7.15) with albite, orthoclase and celsian (Cn) end members.

The alkali-feldspars often contain vein-like areas (up to 15μm across) or irregular patches of Ba-rich alkali-feldspar (~Cn_{10}), in grains that otherwise contain no more than Cn_4 (see Plate 7.1). Such areas are present in all samples, not just T1 from which analyses are reported. In all cases they have an epitaxial relationship to their host alkali-feldspar, they often seen to cross-cut microperthite structures and do not continue into adjacent phases. These areas with high Ba concentration are a relatively minor constituent of the total alkali-feldspar. The distribution of Ba in relation to the visible microperthite structures has not been investigated.

Leaving aside the Ba-rich areas, the alkali-feldspars from all the samples have a restricted range of composition in terms of orthoclase, albite and celsian end members. Most grains have centre compositions which are more enriched in the albite and celsian components than the edge compositions. The actual texture of the internal compositional variations (zonation) is not apparent optically. The four samples from the Loch Sunart Granodiorite show small but distinct differences of composition in terms of both alkali and Ba content. Alkali-feldspar analyses from T1 are more albitic and have a higher Ba contents than those from the more evolved T2. T3 and T4 have Ba concentrations intermediate between T1 and T2 and show a greater spread in terms of albite and orthoclase end members. The alkali-feldspar analyses from the Glen Sanda Granodiorite samples are virtually identical in terms of albite and orthoclase end members, although Ba concentration is slightly higher in G1.

Plate 7.1. ZCI of an alkali-feldspar in a thin section of BPSRT1 (Loch Sunart Granodiorite). The high bright vein-like areas have higher concentrations of Ba than the darker grey host. Further explanation is given in the text.
15 kV, 20 nA, (6,7), scale bar 100 μm.

Plate 7.2. ZCI of amphibole grain in a thin section of BPSRT1 (Loch Sunart Granodiorite). The black is quartz, the light grey area is hornblende and the generally middle grey area between the two is actinolite, note that the compositional boundary between the hornblende and the actinolite is discontinuous but does not represent a boundary between distinct crystals.
15 kV, 20 nA, (6,7), scale bar 10 μm.

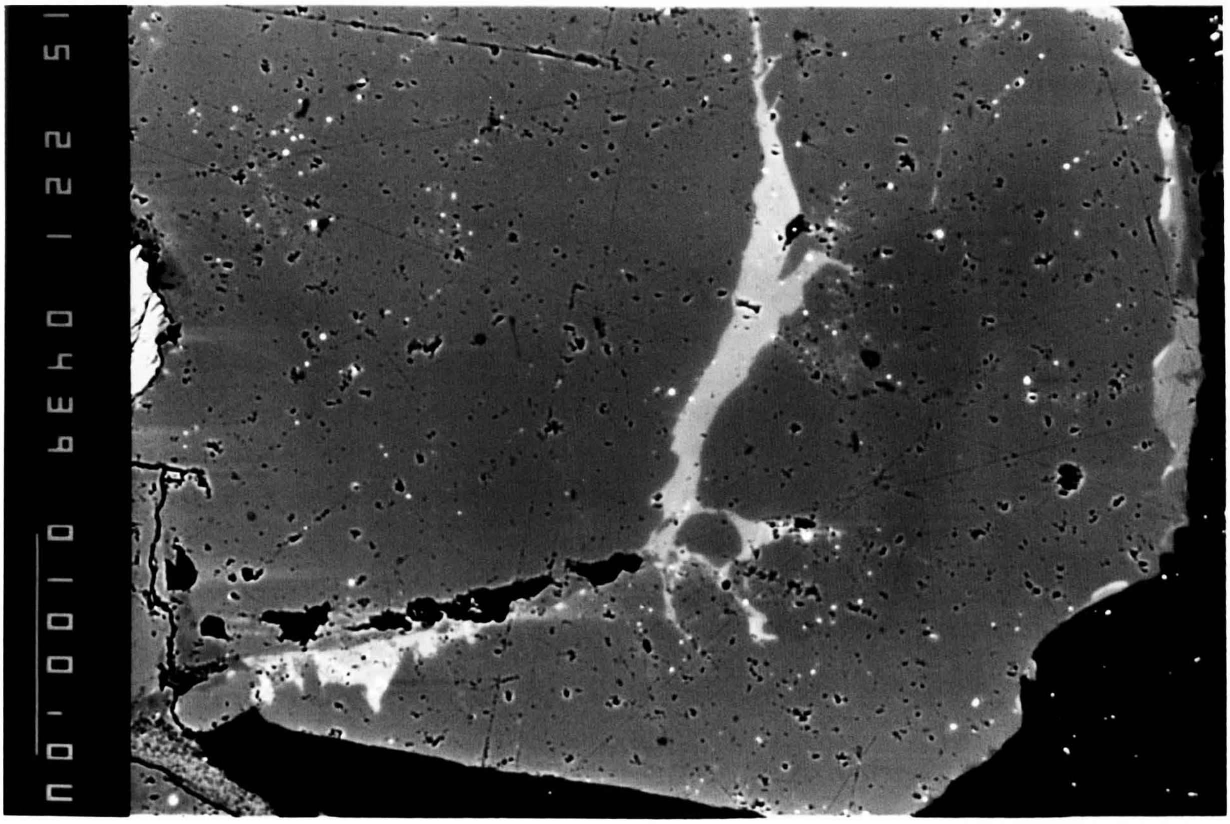

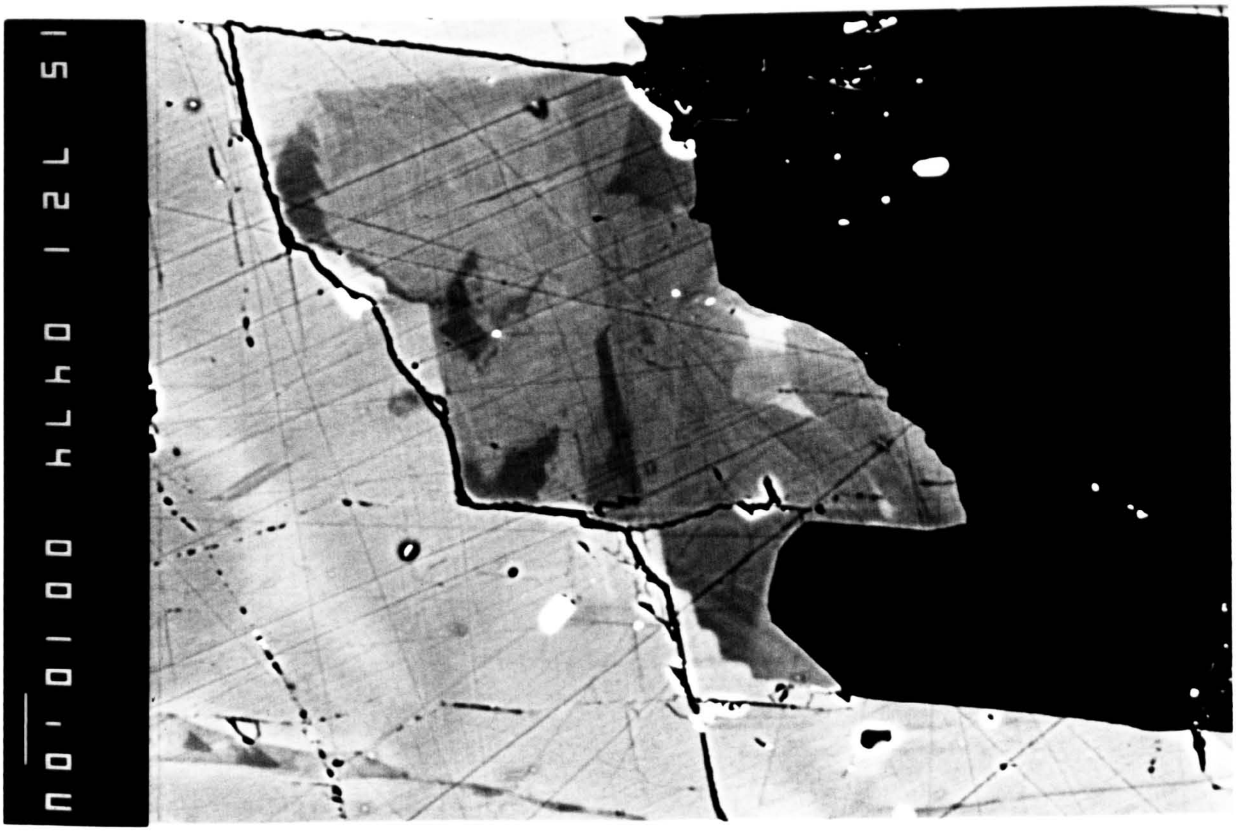

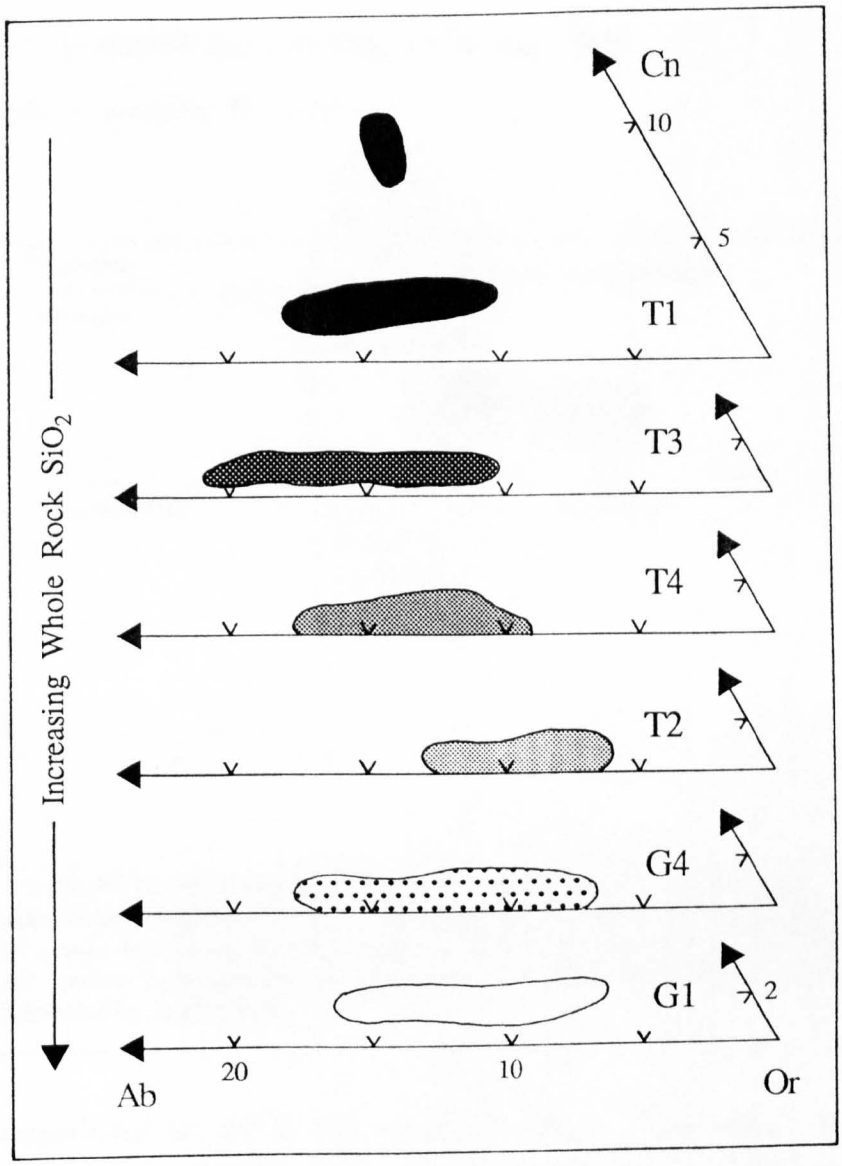

Fig. 7.15. Plot of alkali-feldspar compositions from the Strontian Complex projected onto part of a ternary system with orthoclase, albite and celsian (Cn) end members.

7.5.3) Amphibole.

All the mineral names used are those recommended by the International Mineralogical Association report on the nomenclature of amphiboles compiled by Leake (1978). As described earlier, hornblende is only occasionally present in the Glen Sanda Granodiorite and was not found in either G1 or G4. The microprobe results for amphiboles from the Loch Sunart Granodiorite are presented graphically in Figure 7.16.

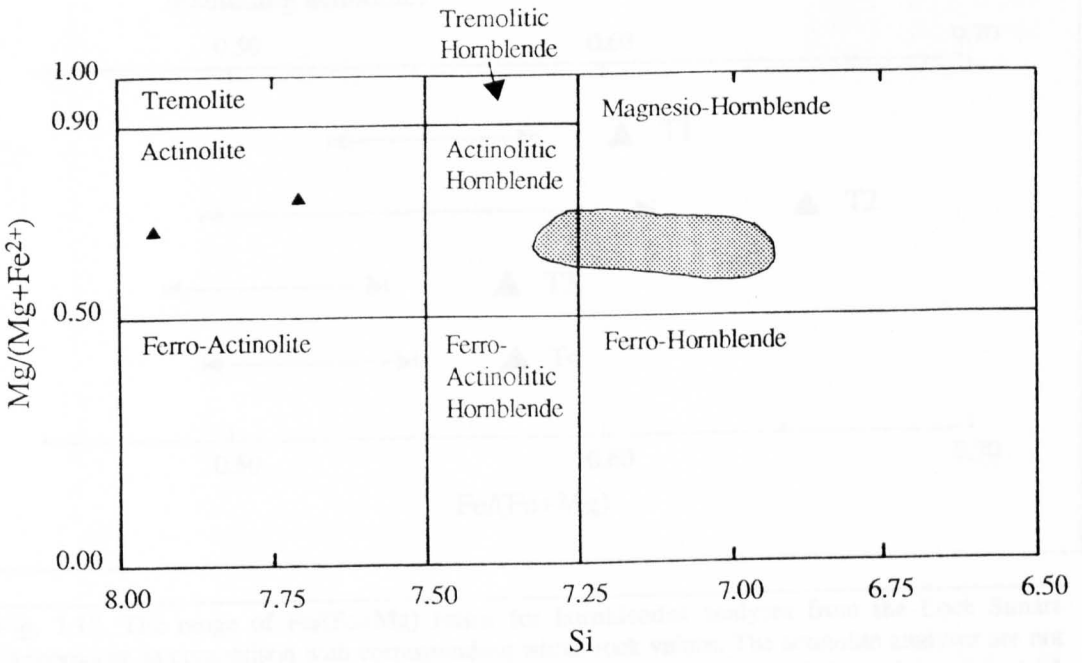

Fig. 7.16. Amphibole compositions from the Loch Sunart Granodiorite plotted on the calcic amphibole classification diagram of Leake (1978); number of Si cations plotted against the cationic $Mg/(Mg+Fe^{2+})$ ratio. Amphibole mineral formula were calculated on the basis of 23 oxygens. The number of Fe^{2+} cations in the total Fe was estimated from the electron microprobe analyses by the method recommended by Leake (1978).

All the amphiboles are calcic and most fall into a group which straddles the magnesio-hornblende/actinolitic hornblende boundary, although all the grains studied have areas, usually the rims, with actinolite compositions. There is no continuum of composition between the hornblendes and the actinolites. Plate 7.2 shows an amphibole grain which is predominantly hornblende but has an actinolitic edge, the boundary between the two is sharp. It is important to note that actinolite is over represented in terms of number of analyses, the maximum amount present in any one crystal is usually only a few percent. Apart from having substantially different Mg/(Mg+Fe) ratios and much lower concentrations of Al, the actinolites have lower concentrations of Ti and greater concentrations of Mg, Si and Ca than the hornblendes.

The compositional variation of the hornblendes is limited, although there are increases, towards the rims, in Al, Fe, Ti, Na and K, and decreases in Si and Mg. The range of the Fe/(Fe+Mg) ratios (excluding the actinolite analyses) for the four samples is shown diagrammatically in Figure 7.17, also shown are the whole rock Fe/(Fe+Mg) ratios. The Fe/(Fe+Mg) ratios of the crystal edges (the highest values) vary in sympathy with the whole rocks values.

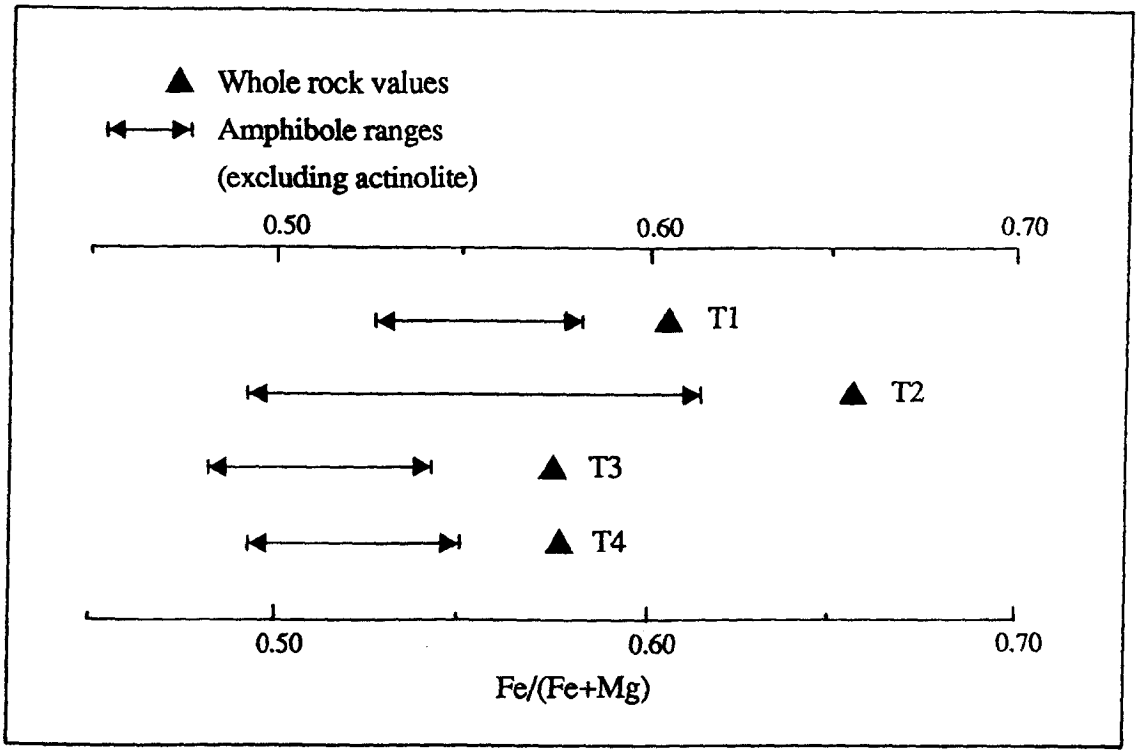

Fig. 7.17. The range of Fe/(Fe+Mg) ratios for hornblendes analyses from the Loch Sunart Granodiorite in comparison with corresponding whole rock values. The actinolite analyses are not shown. To enable comparison, the weight percent oxide values of the amphibole analyses were used for the calculation of the ratios, with the FeO being recalculated to Fe_2O_3.

7.5.4) Biotite.

The biotites from the Loch Sunart Granodiorite are on the whole fresh and unaltered, although some grains show limited replacement by chlorite; in contrast those of the Glen Sanda Granodiorite are extensively replaced by chlorite. Many areas, which are apparently biotite (being pleochroic from yellow to red-brown), give mixed biotite/chlorite microprobe analyses. The biotites of G1 and G4 had sufficient un-chloritised areas to allow analysis.

Overall, the biotites from both parts of the Complex show a very restricted compositional range; within individual samples inter-grain variations are limited and no *systematic* intra-grain variations are discernible, however there are small, but distinct, differences in the composition of biotites *between* samples.

The biotites from the Glen Sanda Granodiorite have generally higher concentrations of Al, and to a lesser extent Ti and Mn, in the octahedral site than those of the Loch Sunart Granodiorite. This is reflected in the lower overall Mg and Fe content of biotites from the Glen Sanda Granodiorite when compared with those from the Loch Sunart Granodiorite (Fig. 7.18), Mg and Fe are the main constituents of the octahedral site. Within both the Loch Sunart Granodiorite and the Glen Sanda Granodiorite biotites the concentration of these elements varies only slightly.

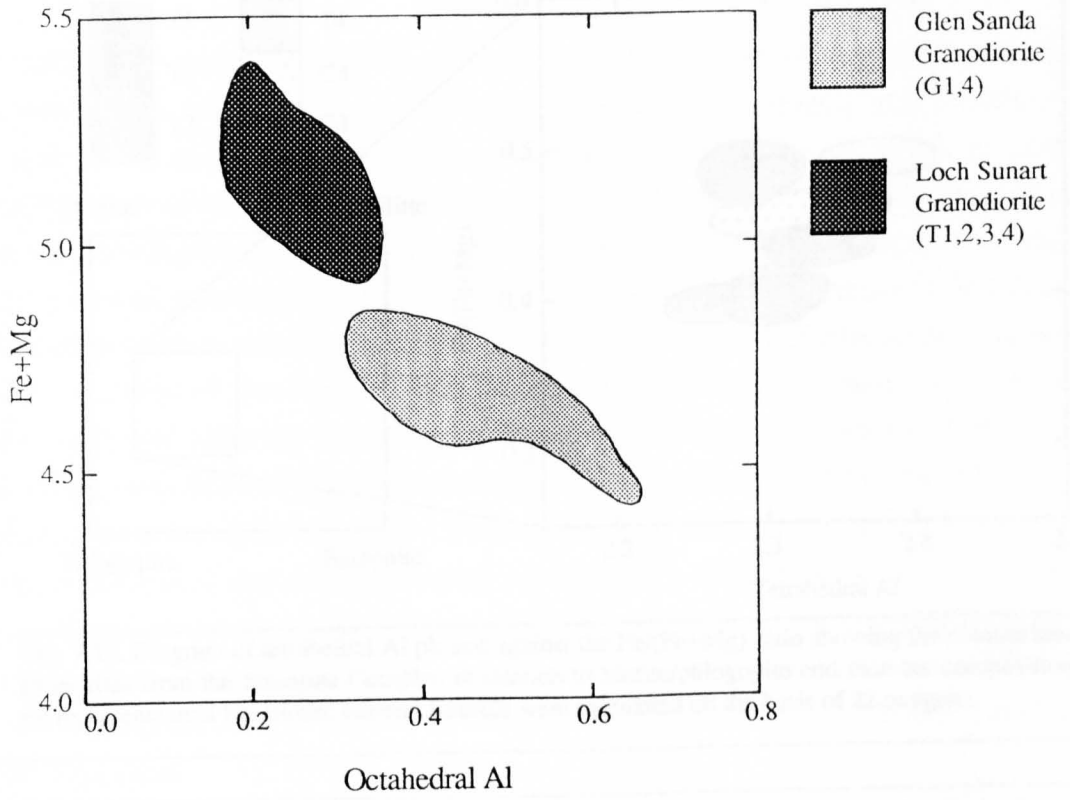

Fig. 7.18. Diagram showing the comparison between the octahedral Al and total Fe+Mg contents of biotites from the Loch Sunart Granodiorite and the Glen Sanda Granodiorite. Biotite mineral formula were calculated on the basis of 22 oxygens.

Within individual samples the biotite Fe/(Fe+Mg) ratios show a limited range, although there are notable differences between samples (Fig. 7.19). The ratios show no apparent relation to the trend of whole rock evolution, but, like the amphibole edge compositions, they do vary in sympathy with the whole rock Fe/(Fe+Mg) values (Fig. 7.20). This confirms the earlier assertion that the scatter in the whole rock Fe/(Fe+Mg) is not due to analytical uncertainty.

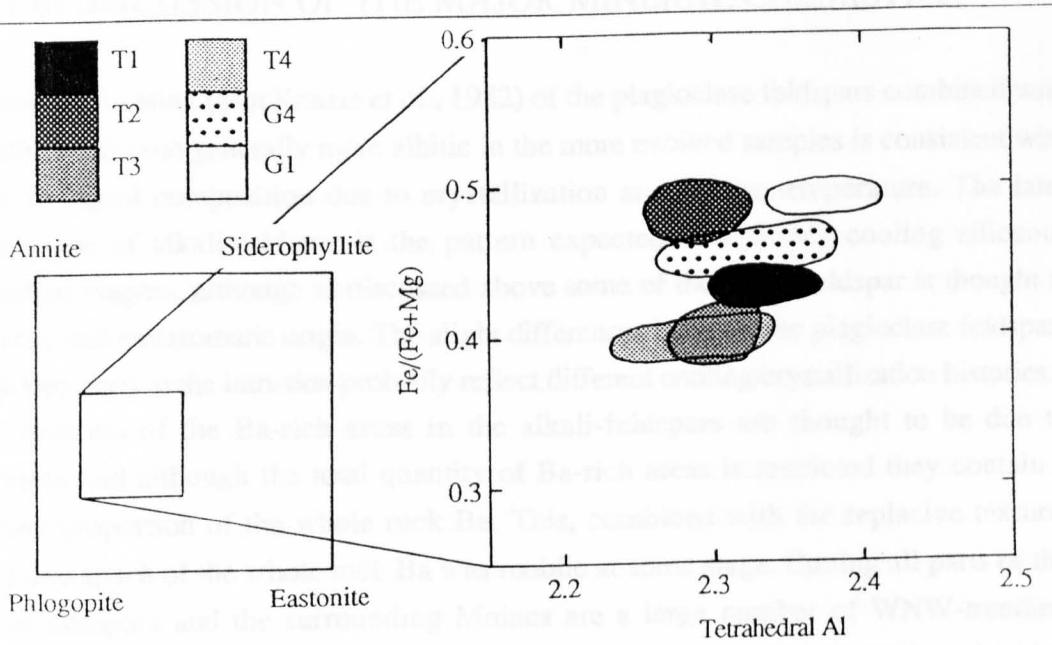

Fig. 7.19. Diagram of tetrahedral Al plotted against the Fe/(Fe+Mg) ratio showing the compositions of biotites from the Strontian Complex in relation to biotite/phlogopite end member compositions. Fe represents total Fe. Biotite mineral formula were calculated on the basis of 22 oxygens.

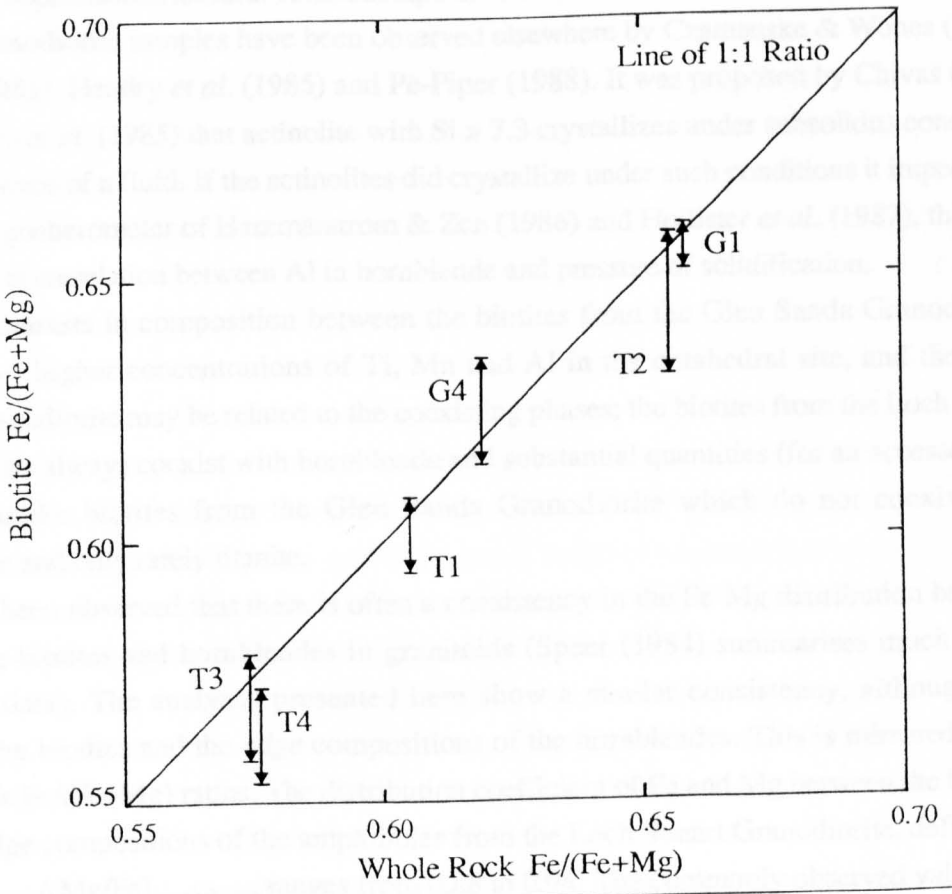

Fig. 7.20. The range of Fe/(Fe+Mg) ratios for biotite analyses from the Strontian Complex plotted against corresponding whole rock ratios. To enable comparison, the weight percent oxide values of the biotite analyses were used for the calculation of the ratios, with the FeO being recalculated to Fe_2O_3.

7.6) DISCUSSION OF THE MAJOR MINERAL CHEMISTRY.

The normal zoning (MacKenzie *et al.*, 1982) of the plagioclase feldspars combined with fact that they become generally more albitic in the more evolved samples is consistent with changes in liquid composition due to crystallization and falling temperature. The later crystallization of alkali-feldspar is the pattern expected in a slowly cooling siliceous calc-alkaline magma, although as discussed above some of the alkali-feldspar is thought to have a later still metasomatic origin. The slight differences between the plagioclase feldspars from the two parts to the intrusion probably reflect different cooling/crystallization histories.

The textures of the Ba-rich areas in the alkali-feldspars are thought to be due to replacement and although the total quantity of Ba-rich areas is restricted they contain a significant proportion of the whole rock Ba. This, combined with the replacive texture, suggests that much of the whole rock Ba was mobile at some stage. Cutting all parts of the Strontian Complex and the surrounding Moines are a large number of WNW-trending Permo-Carboniferous dykes of basic composition, over half of which show alteration that can be related to later baryte, calcite, galena and sphalerite vein mineralization (Gallagher, 1964). Whether the Ba-rich areas within the feldspars are related to this later mineralization event is not clear.

The compositional/textural relationships of the actinolite and hornblende in the Loch Sunart Granodiorite samples have been observed elsewhere by Czamanske & Wones (1973), Chivas (1981), Hendry *et al.* (1985) and Pe-Piper (1988). It was proposed by Chivas (1981) and Hendry *et al.* (1985) that actinolite with Si > 7.3 crystallizes under subsolidus conditions in the presence of a fluid. If the actinolites did crystallize under such conditions it impedes the use of the geobarometer of Hammarstrom & Zen (1986) and Hollister *et al.* (1987), this uses an empirical correlation between Al in hornblende and pressure of solidification.

The contrasts in composition between the biotites from the Glen Sanda Granodiorite, which have higher concentrations of Ti, Mn and Al in the octahedral site, and the Loch Sunart Granodiorite may be related to the coexisting phases; the biotites from the Loch Sunart Granodiorite always coexist with hornblende and substantial quantities (for an accessory) of titanite, unlike biotites from the Glen Sanda Granodiorite which do not coexist with hornblende and only rarely titanite.

It has been observed that there is often a consistency in the Fe-Mg distribution between coexisting biotites and hornblendes in granitoids (Speer (1984) summarises much of the available data). The analyses presented here show a similar consistency, although it is between the biotites and the *edge* compositions of the hornblendes. This is mirrored in the whole rock Fe/(Fe+Mg) ratios. The distribution coefficient of Fe and Mg between the biotites and the edge compositions of the amphiboles from the Loch Sunart Granodiorite, defined as $(Mg/Fe)_{biotite}/(Mg/Fe)_{amphibole}$, ranges from 0.88 to 0.94. The commonly observed values for this parameter range between 1.1 and 0.66 (Speer, 1984). The consistency of the Fe-Mg distribution between the whole rocks, the biotites, and the hornblende edges (in the Loch Sunart Granodiorite), either reflects equilibrium growth or post crystallization equilibration.

7.7) SUMMARY.

1) Both the Loch Sunart Granodiorite and the Glen Sanda Granodiorite have calc-alkaline chemistries.

2) For most whole rock compositional parameters there is no overlap or gap between the Loch Sunart Granodiorite and the Glen Sanda Granodiorite, except in the case of total Fe where there is a 'compositional gap'. When elemental ratios and some trace elements are considered further differences become apparent.

2) The Loch Sunart Granodiorite is not normally zoned, since the most evolved parts are often to be found adjacent to the margins, *or* reversely zoned, because there are significant deviations from a simple concentric distribution pattern. Due to this departure from concentricity it is difficult to envisage the likely three-dimensional distribution pattern.

3) The existence of steep compositional gradients suggests that the Loch Sunart Granodiorite may consist of various smaller pulses intruded more or less contemporaneously, since all the rocks appear to be closely related by fractionation processes.

4) The REE distribution patterns are LREE enriched, have no Eu anomaly and are essentially parallel. The REE abundances are highly variable, beyond that expected from analytical uncertainties, but with a *general* trend to lower concentrations in the more evolved rocks.

5) Overall the range of composition shown by the major phases from the Loch Sunart Granodiorite and the Glen Sanda Granodiorite is restricted, and there are few systematic differences in the mineral chemistry of the two parts.

6) Plagioclase feldspars from the Glen Sanda Granodiorite have similar compositions and compositional ranges to those of the Loch Sunart Granodiorite. The plagioclases from all samples are normally zoned, with more albitic compositions at the crystal edges. Between the samples of the Loch Sunart Granodiorite there is a slight progression towards more albitic compositions in the more evolved samples.

7) Like the plagioclases the alkali-feldspars have similar compositions in the samples from both the Loch Sunart Granodiorite and the Glen Sanda Granodiorite. The alkali-feldspars in all samples are generally zoned towards edge compositions which are lower in albite and celsian components. Between samples from the Loch Sunart Granodiorite there is a progression with increasing whole rock evolution towards lower overall Ba content in the alkali-feldspars. All samples have grains with distinct vein-like Ba-rich areas.

8) Amphibole is only found in the Loch Sunart Granodiorite samples, most are hornblendes, but have distinct actinolitic rims, there is no continuum of composition with the host hornblende. The hornblende themselves show enrichments in Al, Fe, and Ti and depletions in Si and Mg towards the crystal edges. The Fe/(Fe+Mg) ratios of the hornblende crystal edges (excluding the actinolites) reflect the whole rock Fe/(Fe+Mg) values, other than this the composition of amphiboles from the four samples is similar.

9) The biotites from the Glen Sanda Granodiorite have marginally higher contents of Al, Ti and Mn in the octahedral site than those of the Loch Sunart Granodiorite. Within individual samples the biotites have a very restricted range of composition although there are slight but distinct differences between samples, notably in terms of Fe/(Fe+Mg) ratios and to lesser extent tetrahedral Al. The biotite Fe/(Fe+Mg) ratios vary in sympathy with the Fe/(Fe+Mg) values of their host rock.

Chapter 8
The accessory minerals of the Strontian Complex.

8.1) INTRODUCTION.

This chapter has three principal aims: 1) to interpret and discuss the implications of compositional zoning within zircons, titanites and apatites from the Strontian Complex; 2) to evaluate the extent to which bulk-melt composition (*ie.* the composition of the medium of growth) influences titanite composition given that the kinetics of titanite growth determine the type of compositional zoning; and 3) to estimate the distribution of the REE between the accessory phases within a single sample each from the Loch Sunart Granodiorite and the Glen Sanda Granodiorite.

8.2) ZIRCON - ZONING TEXTURES AND MINERAL CHEMISTRY.

The study of zircon chemistry was restricted to two samples from the subset of samples, BPSRT1 from the Loch Sunart Granodiorite and BPSRG1 from the Glen Sanda Granodiorite. Some of the results discussed here were presented in Chapter 3 where they were used to illustrate the compositional variations responsible for the various zoning structures. This section is concerned with: 1) the zoning textures and compositional variations of cogenetic zircon, *ie.* the rims of zircons and zircons without core structures (core structures are assumed to represent refractory inherited material); 2) the internal zoning textures of core structures; and 3) the compositional variations of core structures from the Glen Sanda Granodiorite (the Loch Sunart Granodiorite zircons do not contain sufficient core material for a representative study). All the Z-contrast images shown in this section are of separated zircons mounted in epoxy. Full details of electron microprobe analyses are given in Appendix 3.

8.2.1) Compositional variations of cogenetic zircon.

The zircons grains from the two samples, BPSRG1 (Glen Sanda Granodiorite) and BPSRT1 (Loch Sunart Granodiorite), are quite distinct, those from the Glen Sanda Granodiorite have large subhedral or anhedral core structures whilst those from the Loch Sunart Granodiorite have very few core structures (these are described in more detail in Section 8.2.2). With the exception of the obvious textural differences in terms of core structures, the zoning of the cogenetic zircon of both samples is dominantly of the multiple crystal face-parallel type, although there is also usually sector zoning in the form of non-equivalence between sectors of the patterns of multiple zoning, see Plate 8.1 - BPSRT1 and Plates 8.2 and 8.3 - BPSRG1. In the zircons from both samples the pyramidal sectors have more zones with relative enrichments in Y, the HREE, Th and U, whilst the prism sectors have higher concentrations of Hf.

Whilst the patterns of zoning and *relative* distribution of elements in the two zircon samples are similar, there are significant compositional differences; typical analyses showing the range of concentrations of the detected elements in the two zircon samples are given in

Table 8.1. The zircons of BPSRG1 have generally higher concentrations of Y, the HREE, Th and U, and this manifests itself in two forms: 1) these elements were detected in more of the BPSRG1 analyses when compared with the BPSRT1 analyses, *ie.* these elements were below detection limits in fewer of the analyses obtained from BPSRG1 zircons; and 2) even in the zones from BPSRT1 zircons with relatively high concentrations of these elements the absolute concentrations are still less than comparable zones in BPSRG1 zircons. Both of these points can be illustrated by the following example. Fifty seven electron microprobe analyses were obtained from BPSRT1 zircons and of these only 34 detected the presence of U, the average of the *detected* concentration of UO_2 being 0.10 wt%; this contrasts with the 21 analyses obtained from BPSRG1 zircons which consistently detected U in all 21 analyses and in addition the average UO_2 concentration of those analyses was higher, 0.16 wt%.

Table 8.1. Comparison of the maximum detected concentrations (wt% oxide) of various trace elements in zircons from BPSRT1 (Loch Sunart Granodiorite) and BPSRG1 (Glen Sanda Granodiorite).

Element	BPSRT1	BPSRG1
Y_2O_3	0.179	0.459
Dy_2O_3	0.049	0.072
Er_2O_3	0.045	0.073
Yb_2O_3	0.099	0.160
ThO_2	0.292	0.244
UO_2	0.245	0.480

Apart from the obvious multiple crystal face-parallel zoning there are no systematic variations in the concentrations of Y, the HREE, Hf, Th and U between the centres and the edges of BPSRT1 zircons, however between the centres and edges of BPSRG1 zircons there are general decreases in Y, the HREE, Th and U, and marked increases in Hf concentration, typically from ~1.2 wt% to ~2.2 wt%.

8.2.2) Zircon core structures in the Loch Sunart Granodiorite.

Plate 8.1 shows a selection of six zircon grains from the Loch Sunart Granodiorite, the first four (Plates 8.1(a), (b), (c) and (d)) contain no visible evidence of inheritance, the last two (Plates 8.1(e) and f) both apparently contain inheritance in the form of anhedral cores. A survey of some 100 zircon grains of varying sizes and morphologies revealed that less than 1 grain in 10 contains a core structure similar to those shown in Plates 8.1(e) and (f). The amount of inherited zircon was visually estimated as being less than 5% of the total amount of zircon.

It should be noted that the zircon grain-mount preparation procedure is designed to maximise the exposed area of any inherited core material that may be present. This is achieved by selecting grains of similar size and placing them in the mount in such a way that cutting and polishing them will result in the centres of as many grains as possible being

Plate 8.1. ZCI of zircons from the Loch Sunart Granodiorite of the Strontian Complex. All the grains show marked crystal face-parallel zoning. The first four grains ((a), (b), (c) and (d)) contain no visible evidence, however grains (e) and (f) both contain small rounded cores. The significance of these cores structures are discussed in the text.

(a) 15 kV, 20 nA, (7,7), scale bar 100 μm.

(b) 15 kV, 20 nA, (7,7), scale bar 100 μm.

(c) 15 kV, 20 nA, (7,7), scale bar 100 μm.

(d) 15 kV, 20 nA, (7,7), scale bar 10 μm.

(e) 15 kV, 20 nA, (7,7), scale bar 100 μm.

(f) 15 kV, 20 nA, (7,7), scale bar 100 μm.

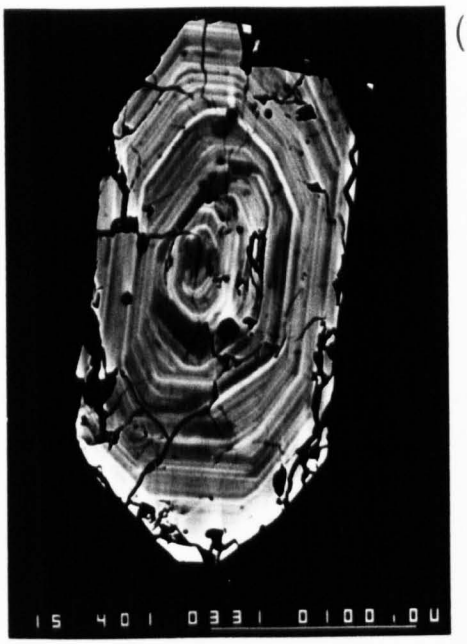
(a)

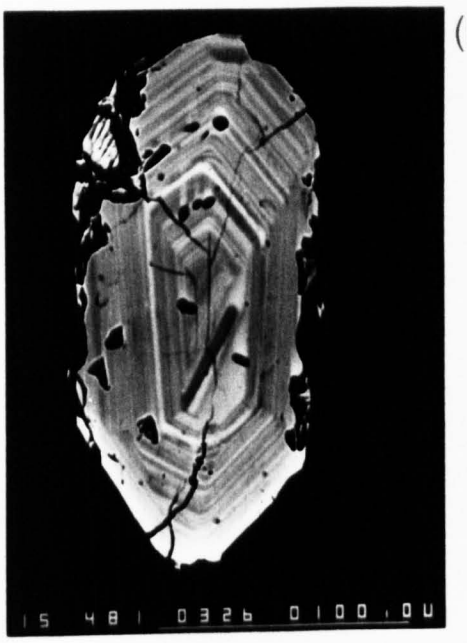
(b)

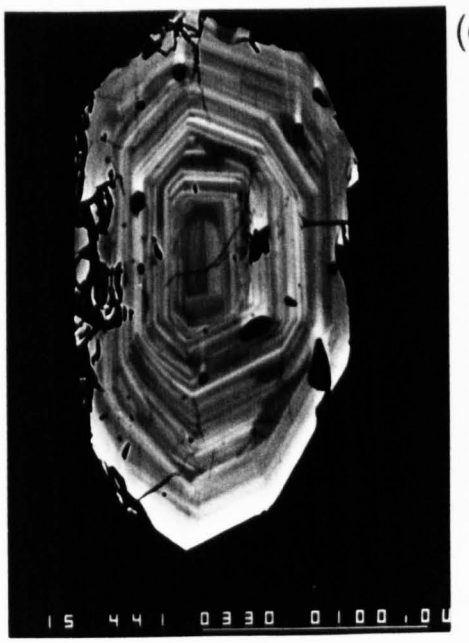
(c)

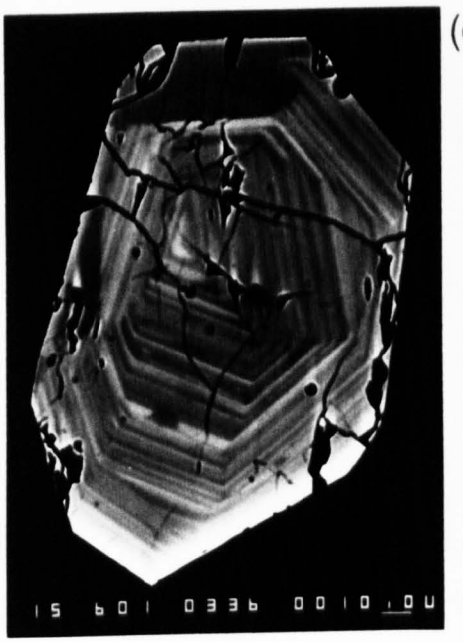
(d)

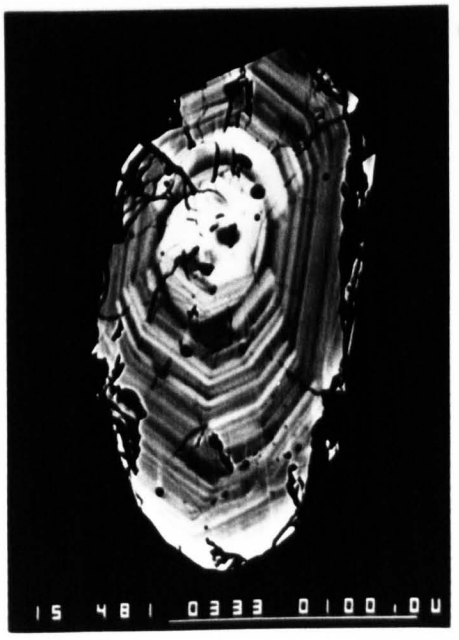
(e)


(f)

exposed, *ie.* there is a bias introduced and the visual estimates of the amount of inheritance obtained from a grain population mounted in such a way are actually overestimates.

8.2.3) Zircon core structures in the Glen Sanda Granodiorite.

Textural observations on the zircon core structures of the Glen Sanda Granodiorite.

Plates 8.2 and 8.3 show a selection of 12 zircon grains from the Glen Sanda Granodiorite, all the grains contain subhedral and anhedral core structures. A survey of around 100 grains of varying sizes and morphologies revealed that > 95% of the grains contain subhedral and anhedral core structures. The amount of inherited zircon present within the rock is estimated as being > 50% of the total amount of zircon.

The large amount of core material present within the Glen Sanda Granodiorite zircon population means that it is possible to study in some detail their internal textures and their composition. The ZCI textural studies have observed that the core structures present within the Glen Sanda Granodiorite display a wide variety of compositional zoning types, these, for the purposes of description only, have been arbitrarily divided into six groups.

1) Cores with only very faint internal compositional zoning (Plate 8.2(a)), these are largely devoid of the fine-scale multiple crystal face-parallel zoning that is so prevalent in the rims of many of the granitoid zircons described in Chapter 3.

2) Cores with multiple crystal face-parallel zoning that is markedly different from similar zoning in the rims in terms of η and spacing of discontinuous interfaces (Plate 8.2(b), (c) and (d)).

3) Cores with compositional sector zoning (Plate 8.2(e)).

4) Cores which contain a large number of inclusions (Plate 8.2(f) and Plate 8.3(a)). Semi-quantitative electron microprobe analysis of these inclusions show them to include quartz, feldspar, biotite and most commonly apatite, some of the inclusions would appear to be SiO_2-rich glass, although this could be an artifact of a mixed analysis of quartz and feldspar.

5) Cores with complex internal patterns of non-planar interfaces. Some of these interfaces truncate other types of zoning, notably crystal face-parallel zoning (Plate 8.3(b)).

6) Cores which appear to have complex multi-stage histories. For example the grain in Plate 8.3(c) has two core structures and the grains in Plates 8.3(d), 8.3(e) and 8.3(f) appear to have been fractured and subsequently filled by new zircon growth.

It should be stressed that the variety of grains present is much greater than the descriptions given above would suggest and the arbitrary division into six groups is not intended to imply that there are six distinct populations of inherited zircon within the Glen Sanda Granodiorite.

Plate 8.2. ZCI of zircons from the Loch Sunart Granodiorite of the Strontian Complex, also see Plate 8.3. All the grains contain large core structures which have a variety of compositional zoning types, these are described in some detail in the text.

(a) 15 kV, 20 nA, (7,7), scale bar 100 μm.
(b) 15 kV, 20 nA, (7,7), scale bar 100 μm.
(c) 15 kV, 20 nA, (7,7), scale bar 100 μm.
(d) 15 kV, 20 nA, (7,7), scale bar 100 μm.
(e) 15 kV, 20 nA, (7,7), scale bar 100 μm.
(f) 15 kV, 20 nA, (7,7), scale bar 100 μm.

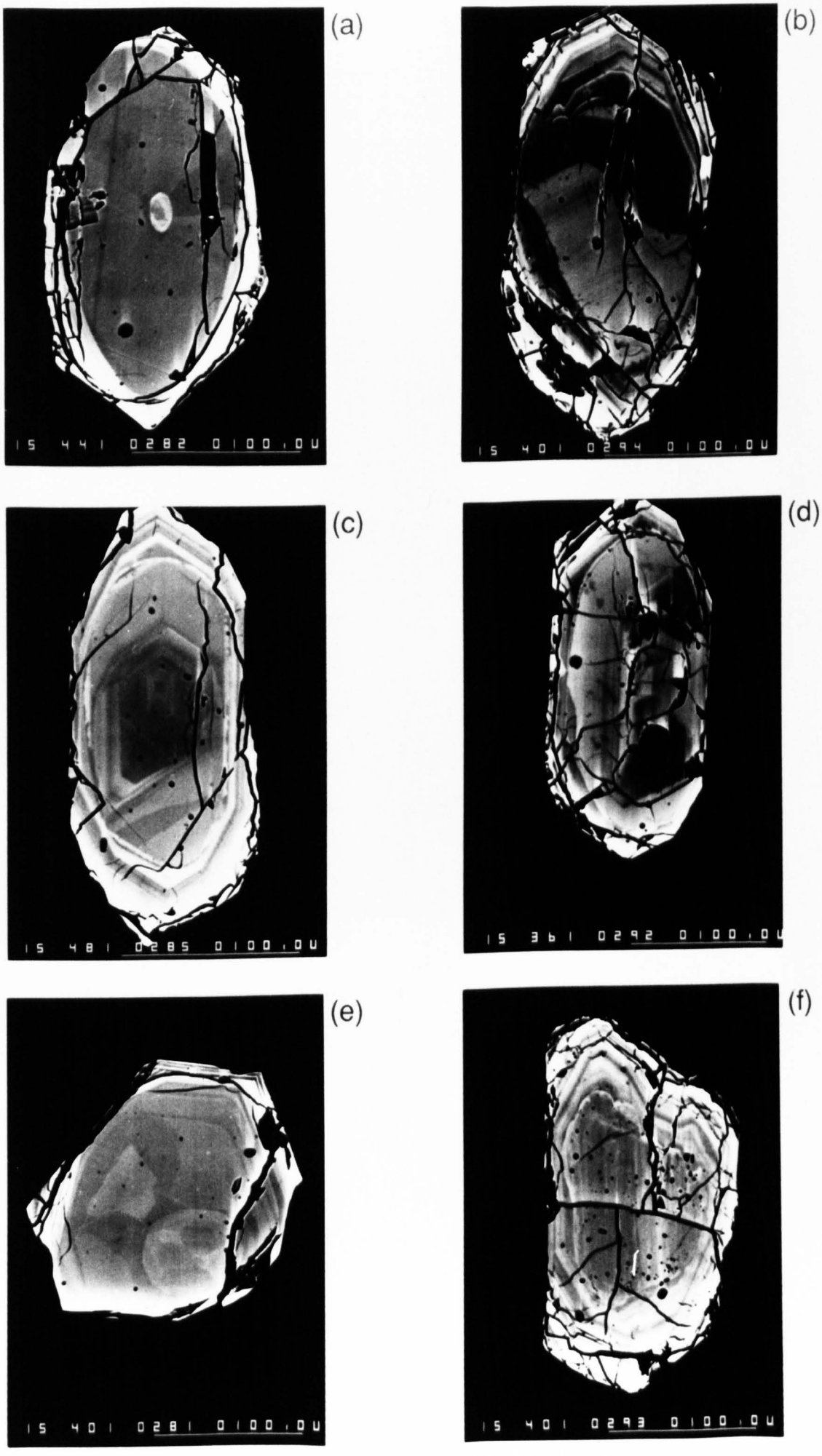
(a)
(b)
(c)
(d)
(e)
(f)

Plate 8.3. ZCI of zircons from the Loch Sunart Granodiorite of the Strontian Complex, also see Plate 8.2. All the grains contain large core structures which have a variety of compositional zoning types, these are described in some detail in the text.

(a) 15 kV, 20 nA, (7,7), scale bar 100 μm.
(b) 15 kV, 20 nA, (7,7), scale bar 100 μm.
(c) 15 kV, 20 nA, (7,7), scale bar 10 μm.
(d) 15 kV, 20 nA, (7,7), scale bar 100 μm.
(e) 15 kV, 20 nA, (7,7), scale bar 100 μm.
(f) 15 kV, 20 nA, (7,7), scale bar 100 μm.


(a)
15 401 0297 0100.00


(b)
15 401 0291 0100.00


(c)
15 601 0307 0010.00

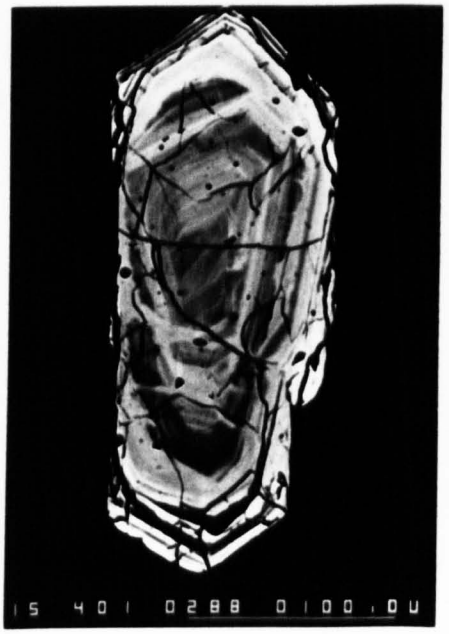
(d)
15 401 0288 0100.00


(e)
15 441 0283 0100.00


(f)
15 361 0289 0100.00

Compositional observations on the zircon core structures of the Glen Sanda Granodiorite.

Given that the inherited cores of the Glen Sanda Granodiorite zircons have a wide variety of types and styles of zoning it might be expected that the cores would show a similar diversity in composition. To test this some 40 electron microprobe analyses from texturally diverse cores were obtained. On average 1-2 analyses were carried on each core with areas of both high and low values of η being targeted. Table 8.1 documents the range of elemental concentrations observed in the cores, for comparison the maximum detected concentrations for the rims are also given. Full listings of the analyses are given in Appendix 3.

Table 8.2. The minimum and maximum detected concentrations (wt% oxide) of various trace elements from the cores of BPSRG1 (Glen Sanda Granodiorite) zircons. For comparison purposes the maximum concentrations of the same elements in the rims are also given.

	BPSRG1 - Cores:		BPSRG1 - Rims:
Element	Minimum Detected Concentration	Maximum Detected Concentration (n = 39)	Maximum Detected Concentration (n = 21)
Y_2O_3	-	1.001	0.459
Al_2O_3	-	0.047	0.077
FeO	-	0.341	0.050
MnO	-	0.093	-
MgO	-	0.023	-
CaO	-	0.440	0.108
P_2O_5	-	0.146	-
Ce_2O_3	-	0.112	-
Nd_2O_3	-	0.065	-
Dy_2O_3	-	0.076	0.072
Er_2O_3	-	0.149	0.073
Yb_2O_3	-	0.209	0.160
ThO_2	-	1.721	0.244
UO_2	-	0.970	0.480

The results can be summarised as follows.

1) The cores of zircons from the Glen Sanda Granodiorite show a greater range and diversity of composition than the rims. Within individual cores the range of compositional variation is restricted, for example Hf usually varies by less than 0.2 wt%, whereas the core population, when taken as a whole, shows a much the greater range of Hf concentration, ~1.1 wt%.

2) Between cores elements such as Y, Er, Yb, U and Th can vary in concentration by greater than an order of magnitude from below detection limits (~0.03wt% for many of these elements) to concentrations as high as 1.00 wt% Y_2O_3, 0.073 wt% Er_2O_3, 0.160 wt% Yb_2O_3, 0.244 wt% ThO_2 and 0.480 wt% UO_2.

3) A greater number and range of elements have been detected within the cores than has been found in the rims, for example elements such Al, Ca, Fe, and Mg which were generally not detected in the analysis of rims have been detected within some of the cores.

4) Although HREE such as Er and Yb were frequently detected within the rims of zircons from the Glen Sanda Granodiorite, the other 'lighter' REE were not detected, however, in some of the cores from the Glen Sanda Granodiorite other REE such as Dy and Ce were detected, particularly in those analyses which contained relatively large concentrations of the HREE.

8.2.4) Discussion.

Compositional variations of cogenetic zircon.

The zircons of BPSRG1 (Glen Sanda Granodiorite) have generally higher concentrations of Y, the HREE, Th and U and than those of BPSRT1 (Loch Sunart Granodiorite), despite the fact that the whole rock concentrations of Y and the HREE are lower in BPSRG1 (see Figure 7.13 and Table 7.2). This suggests three possibilities, which are not mutually exclusive.

1) The zircons of BPSRT1 crystallized after many of the other REE-rich phases in that rock, such that the zircons crystallized from a melt much depleted in REE. Gromet & Silver (1983), Sawka *et al.* (1984) and Sawka (1988) have all claimed to have observed cases where the crystallization order of accessory mineral phases can influence both the absolute REE concentrations and the REE distribution patterns of different minerals. The significance of accessory mineral crystallization order is further explored in Section 8.4.4.

2) During crystallization of BPSRG1 the zircon/melt partition coefficients for the elements of interest were higher than the zircon/liquid partition coefficients of BPSRT1. Little is known specifically about what influences REE partitioning behaviour in zircon/liquid systems, although in other systems (*eg.* titanite/liquid, Green & Pearson, 1986a) it is usually changes in melt composition and more specifically melt structure.

3) Crystal growth kinetics were important in controlling the effective partition coefficients that operated in the zircon/liquid system, resulting in substantial deviations from the equilibrium conditions (*ie.* the processes described in Chapter 5).

The order of crystallization of the accessory phases in the two samples is difficult to assess purely on petrographic considerations. However, since both samples contain inherited zircon, it must have been a liquidus phase within both magmas during initial crystallization. From this it is inferred that zircon occupied the same place in the crystallization order of the two samples. Thus different orders of crystallization are not considered to be important in determining the differences in the chemistry of the two zircon populations.

In general it has been observed that increasing the SiO_2 content of a magma results in increased accessory mineral/liquid REE partition coefficients (Mahood & Hildreth (1983) from partition studies on accessory minerals from the Bishop Tuff; and Green and Pearson (1986a) on titanite/liquid REE partitioning studies), this is thought to be due to greater polymerisation of the melt (Mahood & Hildreth, 1983). Given that BPSRG1 has a higher SiO_2 content (~73 wt%) than BPSRT1 (~60 wt%), and thus was probably more polymerised, it is inferred that it also must have had higher zircon/liquid REE partition

coefficients and this is consistent with the observed compositional differences between the two zircon populations.

Greater melt polymerisation would also be expected to reduce elemental diffusivities (Henderson *et al.*, 1985), and since this is considered to be the dominant control on kinetic disequilibrium in granitoid accessory minerals (see Chapter 5) greater melt polymerisation would allow the effective REE partition coefficients to deviate more from the equilibrium values than the effective partition coefficients of a less highly polymerised melt. Thus solely by considering melt polymerisation (and ignoring the likely effects of polymerisation state on equilibrium partition coefficients) it would be expected that zircons grown in a polymerised melt, under conditions where diffusion is the rate controlling step, would have effective partition coefficients which were lower than zircons grown in a less polymerised melt. If melt polymerisation does have this effect, in the case of the two zircon samples considered here it would appear to be less important than the expected changes in the partition coefficients brought about by changes in melt composition.

The progressive changes in composition towards the edges of the Glen Sanda Granodiorite zircons are thought mainly to reflect progressive changes in bulk melt composition caused by progressive magma crystallization.

Core structures in the Glen Sanda Granodiorite zircons.

The diversity of composition and types of zoning textures shown by the zircon cores from the Glen Sanda Granodiorite and the apparent multi-stage histories of some of them is considered to be consistent with the cores being refractory inherited material, but in addition it is also taken to indicate that the zircon population of the Glen Sanda Granodiorite has mixed inheritance in the sense of Miller *et al.* (1988). The preservation of this textural and compositional diversity indicates that with respect to many elements the zircon cores did not chemically equilibrate with each other or their surroundings during the magmatic event. The state of Sm-Nd isotopic equilibrium between the zircon cores and their host rocks is described in Chapter 9.

It should be stated that there is no existing independent evidence to substantiate the claim that the Glen Sanda Granodiorite has mixed inheritance, it can only be proved unambiguously by isotopic analysis. However, increasingly it is being realised that potential granitoid source regions, *ie.* a significant volume of the continental crust, are heterogeneous in terms of rock type, chemistry, age and isotopic composition on scales that are relevant to magma generation (Miller *et al.*, 1988) and thus it is likely that if the crust is heterogeneous and a granitoid melt is produced from such a crust that any inherited zircon present will consist of grains with a variety of ages, *ie.* have mixed inheritance. It is important to note that U-Pb isotopic analysis of zircons containing mixed inheritance will give an upper age intercept that does not necessarily have any absolute geological significance.

Zircons which have a variety of ages will have originally crystallized in a number of different environments, been subject to a variety of processes and will thus have different chemistries and internal compositional zoning textures (this will likely include visual evidence

chemistries and internal compositional zoning textures (this will likely include visual evidence of multi-stage histories). Whether mixed inheritance is evident within the scale of a single hand specimen will depend on the extent of convective mixing during magma segregation, ascent and emplacement or the extent of involvement of detrital sedimentary rocks in the melting event (Miller *et al.*, 1988). It is worth noting that mixed zircon inheritance has been identified in granitoids that are thought to have been derived from melting of both dominantly sedimentary protoliths (*eg.* Harrison *et al.*, 1987) and dominantly igneous protoliths (*eg.* Williams *et al.*, 1988). In both of these occurrences the evidence for mixed zircon inheritance came from data obtained using *in situ* 'SHRIMP' ion microprobe dating. If, as Miller *et al.* (1988) claim, the continental crust is heterogeneous in terms of rock type and age on scales that are relevant to magma generation, then occurrences of mixed inheritance in granitoids should be commonplace and occurrences of inheritance with a single age should be restricted.

If we assume that the Glen Sanda Granodiorite does contain mixed inheritance then convective mixing must have occurred during magma segregation, ascent and emplacement, *or* a substantial amount of detrital sedimentary material was involved in initial melting or partially assimilated during ascent and emplacement. Clearly these possibilities are not mutually exclusive, although determining which process is dominant would require the use of additional, independent evidence about the nature and types of source involved. However, existing isotope data (εNd values, $^{87}Sr/^{86}Sr$ initial ratios and the O and S stable isotope ratios - summarised in Table 6.4) indicate that there was a large crustal input in the genesis of the Glen Sanda Granodiorite (Halliday, 1984).

8.3) TITANITE - ZONING TEXTURES AND MINERAL CHEMISTRY.

The chemistry of titanites from five of the subset of samples was studied, the sixth rock, BP/SR/G1, did not contain titanite (see Table 7.2).

8.3.1) Compositional zoning of titanite.

All the titanites within these rocks are compositionally sector zoned in the manner described in Chapter 4, Plates 8.4, 8.5, 8.6, 8.7 and 8.8 show examples of typical titanite grains from each of the five samples from which titanites were analysed. None of the titanite grains from any of the four samples contain core structures. Some of the titanite grains (most notably those of BPSRT4) have very prominent crystal face-parallel zoning towards their edges, these areas are devoid of structures that are related to compositional sector zoning.

8.3.2) Titanite compositional variations.

A total of between 25-30 electron microprobe analyses were obtained from 3-4 grains from each of the five samples. Complete details of the analyses are given in Appendix 4. The visual patterns of compositional sector zoning and range of grey-levels within each grain

Plate 8.4. ZCI of typical compositionally sector zoned titanite crystal from BPSRT1 of the Loch Sunart Granodiorite. This particular crystal is very large ~ 2.5mm long. The very bright area to the right of the grain is an opaque oxide phase.
15 kV, 20 nA, (6,7), scale bar 1000 μm.

Plate 8.5. ZCI of typical compositionally sector zoned titanite crystal from BPSRT2 of the Loch Sunart Granodiorite. This grain also has very marked crystal face-parallel zoning. The dark, almost black, crystal partially embedded in the lower part of the grain is an apatite.
15 kV, 20 nA, (6,7), scale bar 100 μm.

no'0001 hi20 08h 5l

no'0010 2be0 l0E 5l

Plate 8.6. ZCI of typical compositionally sector zoned titanite crystal from BPSRT3 of the Loch Sunart Granodiorite. The small black areas are apatite inclusions.
15 kV, 20 nA, (6,7), scale bar 100 μm.

Plate 8.7. ZCI of typical compositionally sector zoned titanite crystal from BPSRT4 of the Loch Sunart Granodiorite. This grain in common with other titanites in this rock has a rim that is devoid of compositional sector zoning.
15 kV, 20 nA, (6,7), scale bar 100 μm.

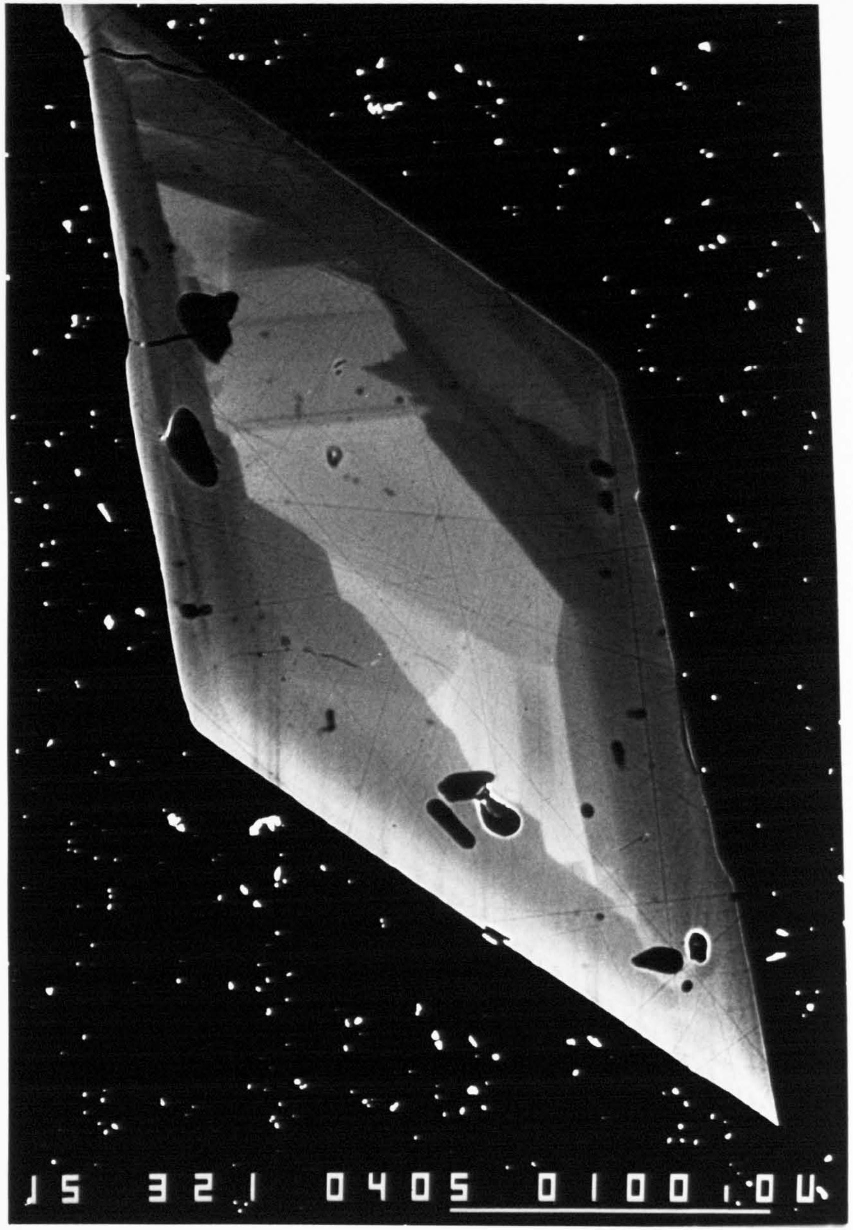
15 321 0405 0100.0U

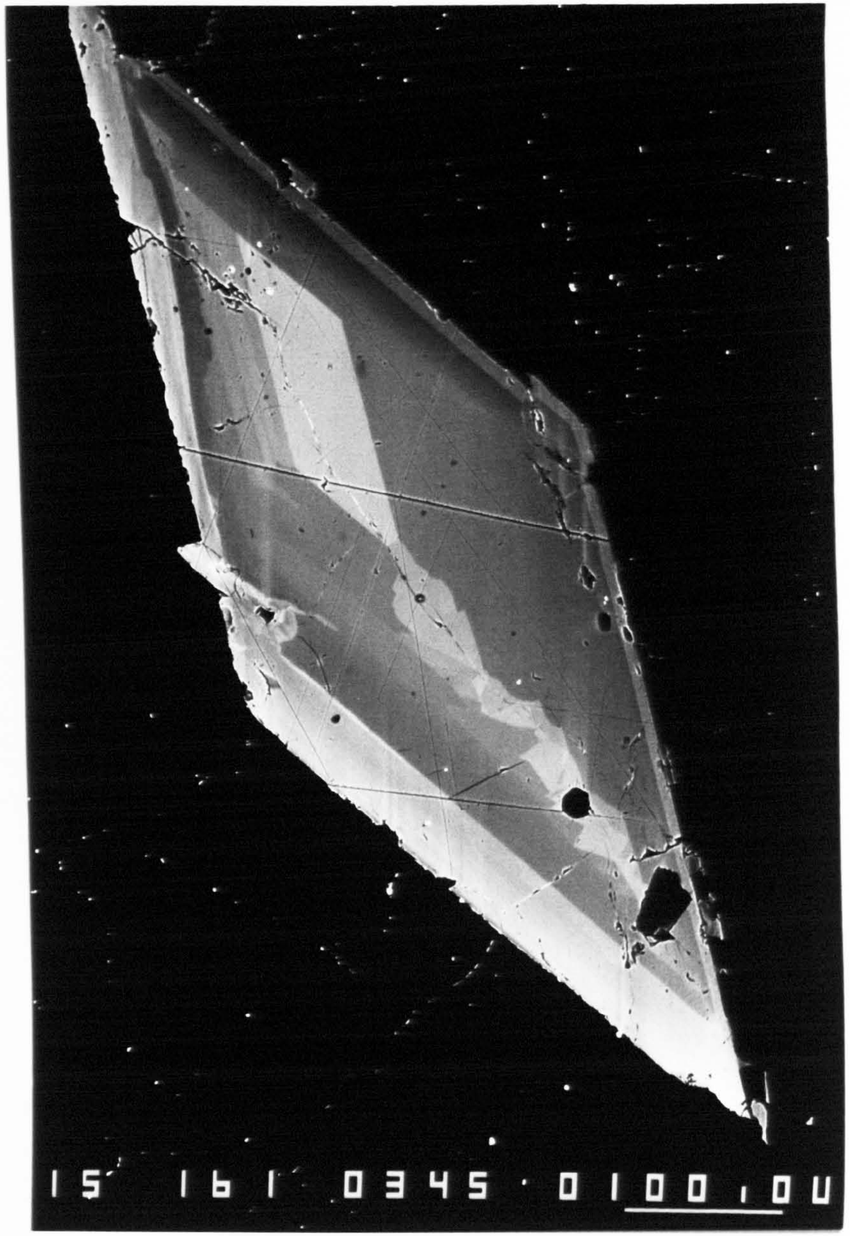
15 161 0345 0100.0U

Plate 8.8. ZCI of typical compositionally sector zoned titanite crystal from BPSRG4 of the Loch Sunart Granodiorite. This grain has a projection on the left hand side which may be a limited manifestation of skeletal growth, this is not a twinning related structure. The dark areas are apatite inclusions.
15 kV, 20 nA, (6,7), scale bar 100 μm.

Plate 8.9. ZCI of large apatite crystal from BPSRT4. This contains a small anhedral core structure within a euhedral crystal. The rim is virtually unzoned. The significance of core structures in apatites is discussed in the text and in particular Section .8.5.2.
15 kV, 20 nA, (6,7), scale bar 100 μm.

no 0010 LHO 1.92 SI

no 0010 8040 104 SI

sectors present were analysed and in addition analyses were obtained from areas of both high and low η. The range of composition within single grains is relatively large, for example total REE content typically ranges from ~0.75 to 4.5 wt%, although this is for the most part a function of the presence of compositional sector zoning. Due to both the presence of compositional sector zoning and the visual complexity of that zoning it is difficult to say if there are any significant centre to edge changes in composition within any of the titanites analysed, although if present such changes are clearly considerably less that the total within grain variation due to compositional sector zoning.

Since compositional sector zoning is mainly responsible for the observed range of titanite compositions within all five of the samples it is necessary when comparing the chemistry of titanites from different samples to look at the total range of composition displayed by each sample and the ratios of elements which have similar chemical characteristics. This latter statement is based on the assumption that elements with similar chemistries will be affected by the kinetic processes of crystal growth to a similar degree. An example of such a group of elements is the REE which although they show large variations in total concentration between sectors their relative distribution patterns have similar shapes, there being a strong coherence in the behaviour of the REE as a group (Fig. 8.1).

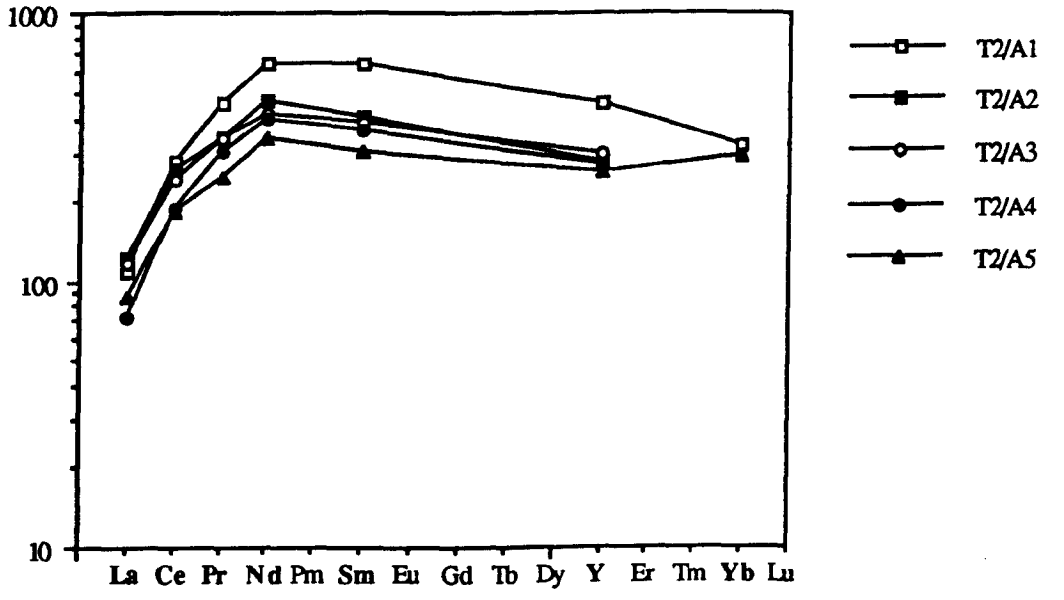

Fig. 8.1. The rock-normalised REE distribution patterns for five electron microprobe analyses of a single compositionally sector zoned titanite crystal from BPSRT2, the analyses were obtained from three different sectors. Note the similarity in the pattern shapes. The analysis numbers correspond to those given in the appendices. The error bars shown are for analysis number T2/A5.

The titanite grains from each of the samples show remarkably similar ranges of composition to one another; the REE, Fe and Mn are both found in similar concentrations in titanites from each of the samples (Figs. 8.2 and 8.3), although the titanites from BPSRT2 (the most evolved sample from the Loch Sunart Granodiorite) have slightly greater maximum concentrations of the REE, Fe and Mn. The titanites from BPSRG4 (Glen Sanda Granodiorite) have distinctly higher concentrations of Mn, Na and Al (Fig. 8.3). Between the Loch Sunart Granodiorite samples Na and Mn show no systematic variations. It is important to note that the ranges of composition displayed by all the titanites analysed is almost entirely due to presence of compositional sector zoning.

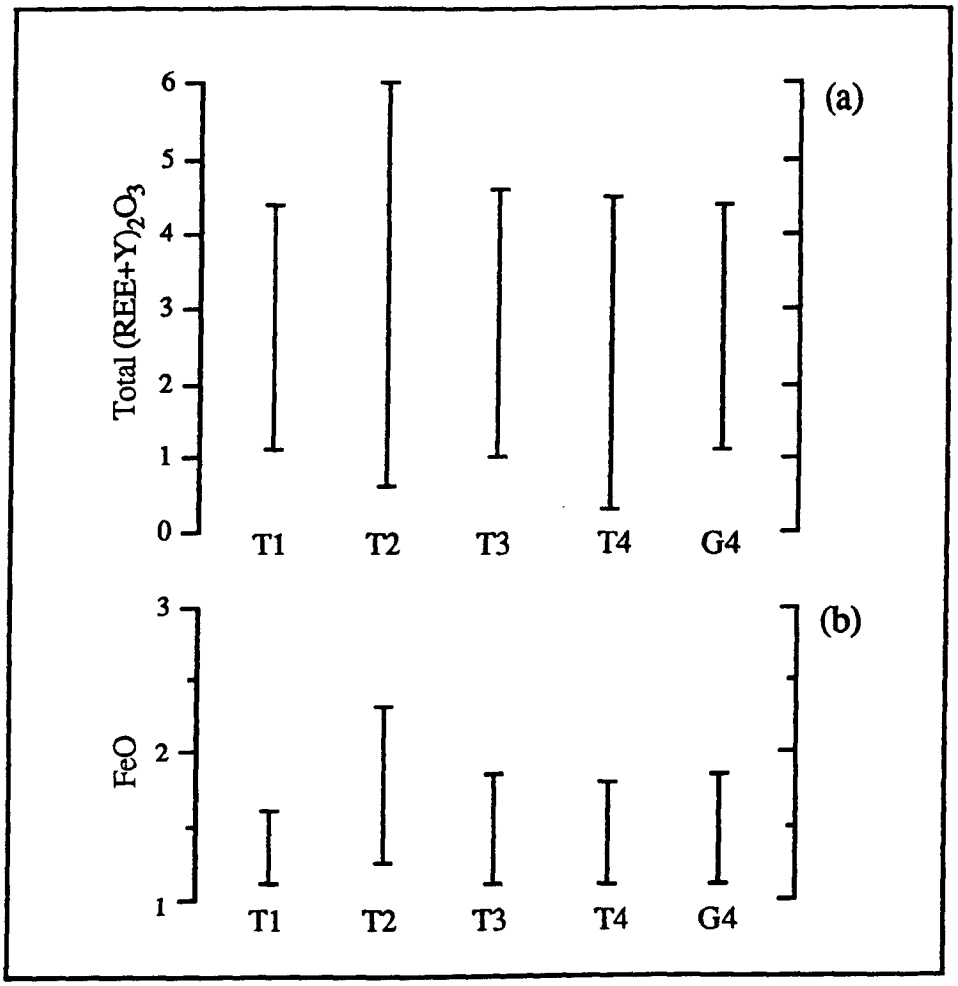

Fig. 8.2. The range of total $(REE+Y)_2O_3$ (a) and FeO (b) concentration displayed by compositionally sector zoned titanites from each of the five samples, BPSRG1 did not contain titanite. Note that the titanites of BPSRT2 have slightly higher maximum concentrations of the REE and Fe.

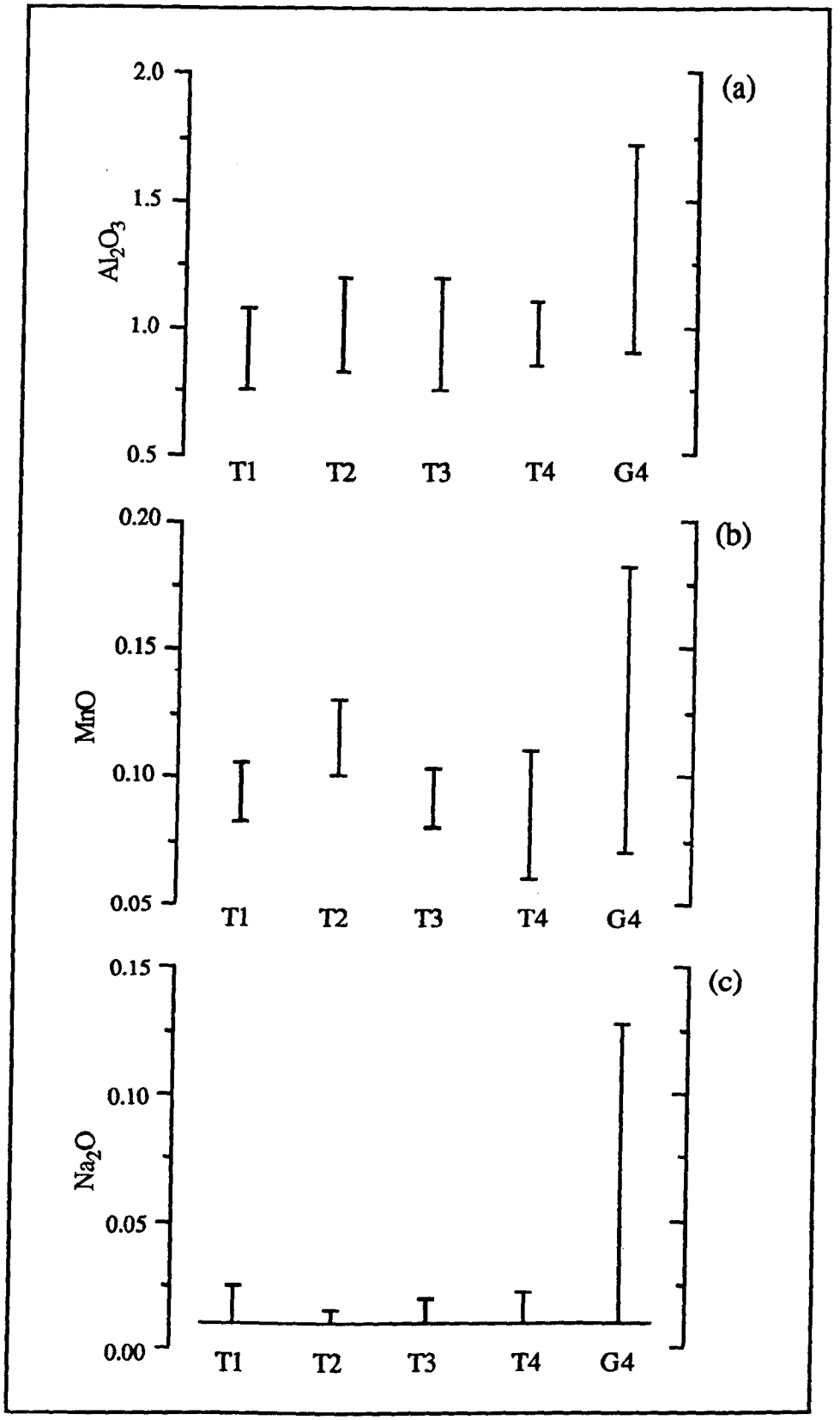

Fig. 8.3. The range of Al_2O_3 (a), MnO (b) and Na_2O (c) concentrations displayed by compositionally sector zoned titanites from each of the five samples. Note that titanites BPSRG4 have higher maximum concentrations of Al, Mn and Na, also those of BPSRT2 also have a higher maximum concentration of Mn than the titanites of the other Loch Sunart Granodiorite. The continuous line in (c) is the approximate lowest limit of detection of Na.

8.3.3) Discussion.

Titanite zoning structures.

The presence of compositional sector zoning (a primary magmatic texture - see Section 5.4) is taken to indicate that kinetically induced disequilibrium in trace element partitioning occurred during the growth of all titanites from these samples. Studies of these and other samples from both the Loch Sunart Granodiorite and the Glen Sanda Granodiorite show that compositional sector zoning of titanites is not just a locally developed feature caused by an unusual growth regime, but probably represents a ubiquitous feature developed in response to the kinetic processes that *normally* accompany titanite nucleation and growth in magmas of this general composition.

The change from compositional sector zoning to purely crystal face-parallel zoning that has been observed in some grains (Plate 8.7) means that there has been a distinct change in the growth regime such that the processes that cause compositional sector zoning (in Section 5.4.2 this was interpreted to be interface kinetics) no longer operate. This could be brought about by a change in the relative rates of crystal growth and elemental diffusion caused either by slower absolute crystal growth rate or more rapid elemental diffusion. The sharp change in the two growth regimes, compositional sector zoning and then crystal face-parallel zoning, could imply one of two things: 1) the growth conditions within the magma underwent a relatively rapid change; or 2) there a sharp cut-off in the conditions necessary for the development of compositional sector zoning in titanite, *ie.* there is some threshold set of conditions that needs to be met before compositional sector zoning can be developed at all, either side of this threshold compositional sector zoning is either developed or it is not.

Compositional variations.

The fact that the ranges of composition displayed by titanites from each of the five rocks is almost entirely due to the presence of compositional sector zoning implies that the kinetic processes of titanite growth and element partitioning largely determine the actual chemistry of the grains and that the equilibrium partition coefficients for the system titanite/melt have only a subordinate effect in determining the composition of titanites. Thus it would appear that in the case of the Loch Sunart Granodiorite and the Glen Sanda Granodiorite that bulk-magma composition had a negligible effect on the absolute chemistry of titanite and the kinetic factors allowed the effective partition coefficients to deviate significantly from equilibrium.

As a final comment in this section: it is worth noting that a simple centre/edge or grain traverse analysis strategy applied to the titanite grains shown here (or indeed most of the accessory phases encountered during the course of this research) would arrive at potentially misleading conclusions if it were assumed that the texture of the zoning reflected continuous centre to edge variations of composition. In general the actual distribution of compositional variation within a given grain coupled with the assumption that the texture of the zoning reflected continuous centre to edge variations of composition would give the impression that

the centres of the grains were relatively enriched in REE in comparison with the edges.

8.4) THE DISTRIBUTION OF THE REE AMONGST THE ACCESSORY PHASES.

If accessory phases are zoned (as is often the case) it is impossible, just using a few selected electron microprobe analyses, to quantify absolutely the contribution that each phase makes to the whole rock REE-budget. It may be possible using bulk analysis of mineral separates to obtain representative average compositions for each of the minerals, although this can lead to selective analysis of a particular size fraction or selective analysis of parts of grains or analysis of inclusions of other phases. However, the very fact that the accessory phases *are* commonly zoned means that to quantify the contribution that each phase makes to controlling the REE (even if this is possible in absolute terms) may be of limited practical use. Thus for the purposes of this section it is assumed that the REE in calc-alkaline granitoid rocks are dominantly controlled by the accessory phases (Gromet & Silver, 1983 and Sawka, 1988) and further demonstration of this is not attempted.

The implications of the fact that the REE are dominantly controlled by accessory phases and the fact that the different minerals often have very different rock normalised REE distribution patterns are considered in this section. This theme is further expanded in Chapter 9 which examines the Sm-Nd isotopic composition of the accessory phases from the Strontian Complex. In all cases the mineral REE concentrations have been normalised to whole rock concentrations, which facilitates investigation of how the relative distribution of the REE in each mineral differs from the whole rock distribution. This is directly analogous to using the REE concentrations of chondrites to study how the relative distribution of the REE in whole rock samples differs from that of a chondritic Bulk Earth. Normalising mineral REE concentrations to chondritic values is of little use in a petrogenetic sense since the shape of mineral/chondrite REE distribution patterns is dependent not only on the relative partitioning of the different REE but also the relative concentrations of the REE in the medium of growth at the time of crystallization.

For two of the samples, BPSRT1 (Loch Sunart Granodiorite) and BPSRG1 (Glen Sanda Granodiorite), zircons, titanites and apatites were analysed and their REE concentrations were normalised to whole rock REE concentrations. The chondrite normalised REE distribution patterns of the whole rock samples BPSRT1 and BPSRG1 are similar to one another, *ie.* they are approximately parallel, both are LREE enriched and neither has a pronounced Eu anomaly. The absolute concentration of the REE in BPSRG1 is much lower than in BPSRT1 (Table 7.2). The similarity of the chondrite normalised patterns of the two rocks is confirmed by the close similarity of their respective Sm/Nd ratios as measured by isotope dilution during Sm-Nd isotope analysis, see Chapter 9 and in particular Table 9.1.

8.4.1) Zircon.

The fact that of the REE only Er and Yb were detected by electron microprobe means that it is not possible to produce representative mineral/rock REE distribution patterns for the two zircon samples, however since the other REE must be below detection limits the detection of Er and Yb only is consistent with the zircons having HREE enriched mineral/rock distribution patterns. The Sm/Nd ratios obtained from the BPSRG1 zircons by isotope dilution during the course of Sm-Nd isotope analysis (see Table 9.1) confirms that the zircons from both rocks have an affinity for the HREE. The low concentration of the REE in zircons from both samples combined with the fact that zircon, relative to the other accessory phases, is present in very small modal quantities means that zircon does not contain a significant quantity of the total REE content of the whole rock.

8.4.2) Apatite.

The apatites within both the BPSRT1 and BPSRG1 samples are generally small, less than 100 μm, and are usually not zoned on Z-contrast images. The exception to this latter statement are a few larger grains (see Plate 8.9) that occasionally contain subhedral core structures, the significance of these core structures in apatites is discussed in the Section 8.5. Texturally the apatites are generally euhedral and occur as numerous small inclusions in mafic phases (biotite and hornblende), felsic phases (plagioclase and alkali-feldspar) and accessory phases (zircon, titanite).

Ten apparently unzoned apatites from both samples were analysed with the aim of determining their REE distribution patterns, typical rock normalised patterns for apatites from BPSRT1 and BPSRG1 are shown in Figure. 8.4, full details of the analyses are given in Appendix 5.

The following points should be noted.

1) Only La, Ce and Nd were detected in the apatites of BPSRT1, all the other REE were below the limit of detection. Thus even without a complete REE distribution pattern it is apparent that the apatites of BPSRT1 must be LREE enriched relative to whole rock and therefore to chondrite (the chondrite normalised distribution pattern for these apatites is not shown). The Sm/Nd ratio obtained by isotope dilution during Sm-Nd isotope analysis (see Table 9.1) of apatites from BPSRT1 is less than the Bulk Earth value (*ie.* they are LREE enriched) and this is consistent with the electron microprobe data.

2) The REE distribution patterns for apatites from BPSRG1 are HREE enriched relative to both whole rock and to chondrite (the chondrite normalised distribution pattern is not shown). Again this is confirmed by the Sm/Nd ratios obtained during isotopic analysis (see Table 9.1), which indicated that the apatites of BPSRG1 have ratios that are greater than chondritic Bulk Earth, *ie.* HREE enriched.

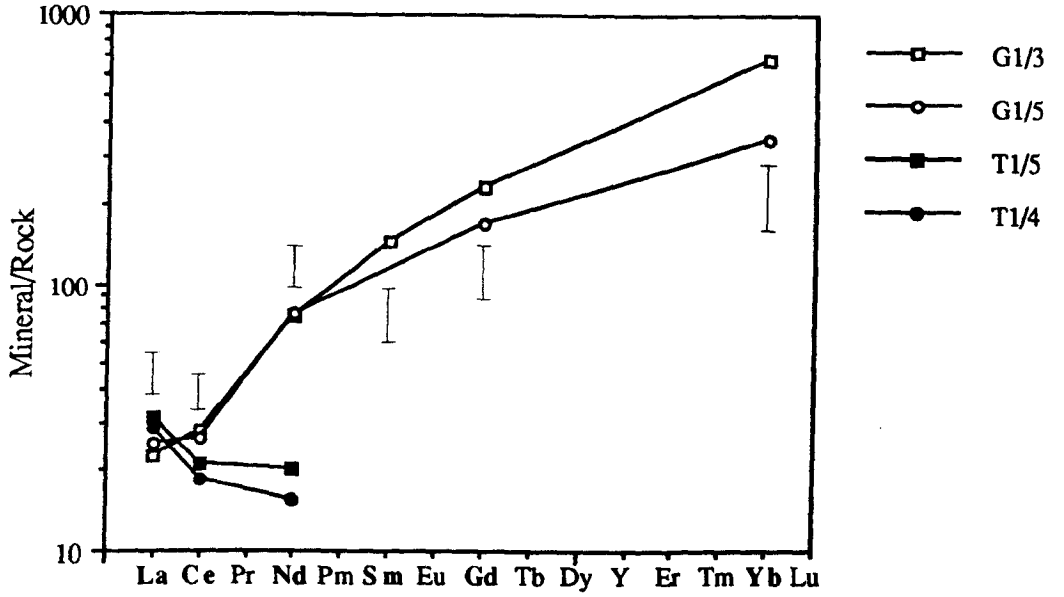

Fig. 8.4. Typical rock-normalised REE distribution patterns for four electron microprobe analyses of two apatites from BPSRG1 (open symbols) and two apatites from BPSRT1 (closed symbols). Even though their respective host rocks have very similar chondrite-normalised distribution patterns the rock-normalised patterns for the apatites from the two rocks are very different. The analysis numbers correspond to those given in the appendices. The error bars shown are for analysis number G1/5.

8.4.3) Titanite.

Titanite is not present in the sample from the Glen Sanda Granodiorite, BPSRG1 (Table 7.2). Even although the titanites from BPSRT1 are strongly zoned with respect to the REE they still contain much higher absolute concentrations of the REE than either zircon or apatite, this pattern is consistent with the findings of Gromet & Silver (1983) and Sawka (1988) for zircon-, apatite- and titanite-bearing granitoid rocks of the Sierra Nevada Batholith.

Rock normalised distribution patterns for titanites from BPSRT1 are shown in Figure 8.5, the patterns are mainly flat with slight depletions in the LREE (La and Ce in particular). The fact that the REE distribution pattern is mainly flat means that the distribution of the MREE in titanite is similar to that of the whole rock. Such patterns are in accord with the Sm/Nd ratios obtained during isotopic analysis, the whole rock Sm/Nd ratio for BPSRT1 is very similar to that obtained from the titanite grain separate from the same rock (see Table 9.1).

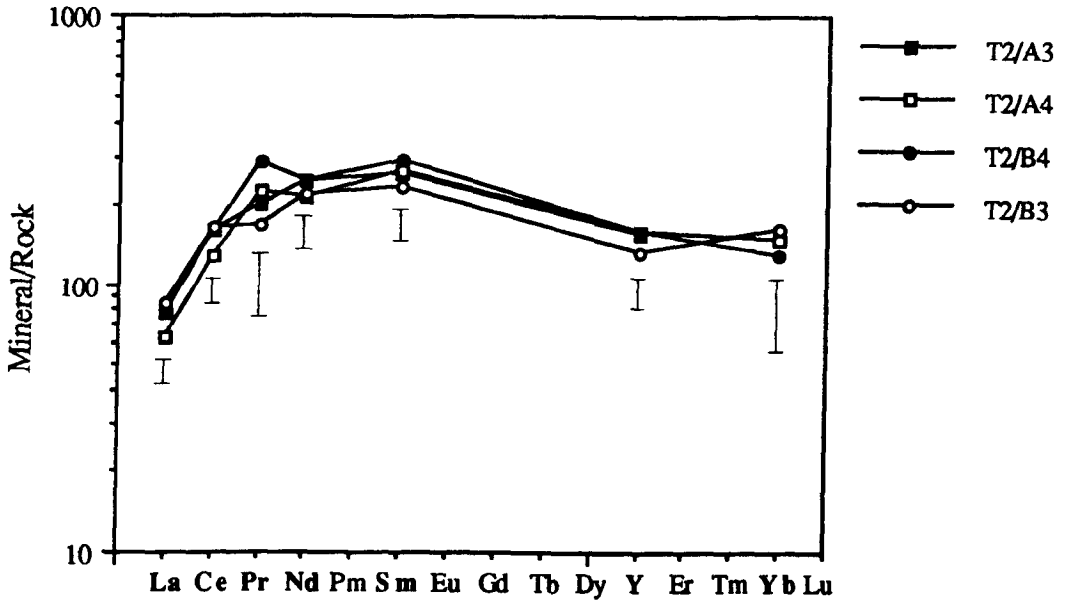

Fig. 8.5. Typical rock-normalised REE distribution patterns for four electron microprobe analyses of titanites from BPSRT1. Note that the patterns are generally flat, although there are notable depletions in the LREE, in particular La, Ce and to a lesser extent Pr. The analysis numbers correspond to those given in the appendices. The error bars shown are for analysis number T2/A4.

8.4.4) Discussion.

The individual accessory phases from BPSRT1 and BPSRG1 have very different whole rock normalised REE distribution patterns from one another and this, in part, is due to the different accessory-phase/melt systems having different *relative* partition coefficients for the REE (see Watson (1980) for zircon, Watson and Green (1981) for apatite and Green and Pearson (1986a) for titanite). A necessary corollary of this is that by crystallizing a particular accessory phase it is possible to change the relative concentrations of the REE of the remaining melt (Gromet & Silver, 1983). Thus the order of crystallization of REE-rich accessory phases from a given melt can have as a great a control over the REE distribution pattern of a mineral as the relative mineral/melt distribution coefficients (Sawka, 1988). The fact that the rock normalised REE distribution patterns for the apatites from BPSRT1 and BPSRG1 are very different from one another, even though their respective host rocks have very similar chondrite normalised REE distribution patterns, is thought to be due to the apatites from the two rocks having occupied different places in the order of crystallization of the two samples.

The generally flat rock-normalised REE distribution patterns of the titanites from BPSRT1 is consistent with them being the main phase that controls the REE abundances. In the BPSRG1 sample both accessory phases (zircon and apatite) have HREE enriched patterns (relative to whole rock) and this requires that the LREE must be largely contained within some other phase. Since BPSRG1 also contains accessory allanite and monazite (Table 7.2)

and both of these phases have markedly higher partition coefficients for the LREE than the HREE (allanite - Brooks *et al.* (1981), monazite - Mittlefehldt & Miller, (1983)) it is likely that the LREE of BPSRG1 are contained mainly within these two phases.

8.5) EVIDENCE FOR REFRACTORY BEHAVIOUR WITHIN TITANITE AND APATITE FROM THE STRONTIAN COMPLEX.

This section uses the data and interpretations outlined above critically to assess the likelihood of there having been refractory apatite and titanite in the magmas of the Strontian Complex. Published experimentally determined zircon and apatite saturation data will be used along with the textural evidence already presented to assess the possible state of saturation with respect to P (and therefore apatite) of the Strontian magmas. Assessment of titanite stability, for which there is no similar experimental solubility data, relies almost totally on the interpretation of the internal zoning structures given in Section 8.3.1.

8.5.1) Accessory phase stability in felsic melts.

Watson & Harrison (1983) determined that the main controls on zircon solubility are the temperature and composition of the melt, they expressed their model of zircon solubility with the following equation:

$$\ln D_{Zr}^{\text{zircon/melt}} = \{-3.80 - [0.85\,(M - 1)]\} + 12900/T \qquad \text{(Eqn. 8.1)}$$

where $D_{Zr}^{\text{zircon/melt}}$ is the concentration ratio (wt%) of Zr in the stoichiometric zircon to that in the melt, T is the temperature in °K, and M is a cation ratio - (Na + K + 2Ca)/(Al·Si).

There have been several experimental studies of the influence of P saturation on apatite stability in silicate melts during partial melting and crystallization (eg. Ryerson & Hess, 1980; Harrison & Watson, 1984). Harrison & Watson (1984) found that the primary controls on P solubility are the temperature and SiO_2 concentration of the melt, they expressed this in the following equation:

$$\ln D_P^{\text{apatite/melt}} = [(8400 + ((SiO_2 - 0.5)\,2.64 \times 10^4))/T] - [3.1 + (12.4\,(SiO_2 - 0.5))] \qquad \text{(Eqn. 8.2)}$$

where $D_P^{\text{apatite/melt}}$ is the concentration ratio (wt%) of P in a stoichiometric fluor-apatite to that in the melt, SiO_2 is the weight fraction of silica in the melt, and T is the temperature (°K).

Unlike apatite and zircon, there has been no directly comparable work on the solubility of titanite in silicate melts of felsic composition. There has, however, been work on the general solubility of TiO_2 by Green & Pearson (1986b) and Ryerson & Watson (1987) which suggests that TiO_2 saturation occurs in felsic melts at about the 1% level. In addition Wones (1989) stressed the role of high oxygen fugacity in the stabilisation of titanite and magnetite

in granitic rocks. The common early crystallization of titanite in felsic melts is indicated by its common occurrence as a phenocryst phase in crystal-poor dacites and rhyolites (Ewart, 1979).

Much of the experimental work on element solubility has shown that elements such as Zr, P and Ti have a greater stability in peralkaline melts than in peraluminous melts. Gwinn & Hess (1989) called this the "peralkaline effect" and concluded that it was due to the highly charged cations being stabilised by excess alkalis (over alumina) in the peralkaline melts. The limited solubility of Zr, P and Ti in peraluminous melts raises the possibility of accessory phases that are stabilised by saturation of these elements being residual during partial melting and thus having the potential to be entrained in the melt (Watson & Harrison, 1984).

The zircon and apatite solubility equations can be used to predict the concentration of Zr and P that a given magma is able to dissolve at a given temperature, or by independently estimating temperature it is possible to determine whether a given magma was over or undersaturated with respect to Zr or P. Apparent oversaturation of a given element in a rock could be due to several processes: 1) the presence of a refractory mineral which contains a significant proportion of that phase; 2) the rock composition not representing a previous liquid composition, *ie.* there has been some crystal/liquid fractionation; and 3) *complete* assimilation of country rock or magma mixing causing crystallization of a phase due to the resultant liquid being oversaturated with respect a particular component.

8.5.2) Were any of the accessory phases of the Strontian Complex partially refractory?

Refractory accessory phases in the Loch Sunart Granodiorite.

Textural evidence, Section 8.2.2, indicates that the amount of inherited zircon within the Loch Sunart Granodiorite is limited (< 5%), this suggests that this part of the Complex may have been just oversaturated with respect to Zr. Thus the temperatures obtained using the zircon saturation equation (Eqn. 8.1) should be representative of the peak melting temperatures (Harrison *et al.*, 1987) of the Loch Sunart Granodiorite magma.

Zr saturation temperatures were calculated for the 59 whole rock samples of the Loch Sunart Granodiorite used in Chapter 7. The temperatures have a restricted range from 734 to 796°C with the arithmetic mean being 768°C. Approximately 90% of the temperature determinations are within ±20°C of this average, the claimed analytical uncertainty for the technique is ±30°C (Harrison *et al.*, 1987). The remarkable coherence of these results (despite the fact that Zr abundances vary by between 109 and 238ppm) strongly suggests that the values reflect the prevailing temperature during separation of the magma from its source. If the observed compositional range of the whole rocks represented the products of fractional crystallization then it would be expected that determination of temperatures from the bulk rock chemistries would yield variable and geologically unrealistic temperatures. Sawka (1988) also used the Zr saturation equation of Watson & Harrison (1983) to calculate Zr saturation temperatures and observed that the more evolved samples gave *higher* temperatures

than the less evolved, this was thought to be an artifact of crystal/liquid fractionation processes.

Equation 8.2 was then used to determine the theoretical P saturation levels in the Loch Sunart Granodiorite, it is assumed that the arithmetic mean Zr saturation temperature of 768°C represents the temperature attained during melting. The theoretical concentrations obtained are some 75% less than the actual concentrations as measured by XRF (Appendix 6), this apparently indicates that P was oversaturated in the original magma. This can be stated in another way; the P saturation temperatures calculated from the *measured* P concentrations range from about 940-1025°C, these are approximately 200°C higher than the equivalent Zr saturation temperatures for the same rocks. It is possible that this apparent excess P is due to the presence of refractory apatite or due to magma mixing or country rock assimilation, however, the presence of anhedral and subhedral cores (see Plate 8.9) in some of the apatite crystals suggests that at least part of the oversaturation could be due to the presence of refractory apatite.

As described earlier the compositional zoning of the titanites from the Loch Sunart Granodiorite is dominated by sector zoning, no anhedral or subhedral core structures were observed and this is taken to indicate that refractory titanite did not exist in the Loch Sunart Granodiorite.

Refractory accessory phases in the Glen Sanda Granodiorite.

The amount of inherited zircon in the Glen Sanda Granodiorite, estimated from the textural observations presented earlier, is considered to be in the order of ~ 50% of the total amount zircon. Using this figure the whole rock concentrations of Zr in the rock were corrected for the presence of inherited zircon and the revised figure of Zr concentration used to calculate the Zr saturation temperatures. The calculated temperatures for 34 rocks from the Glen Sanda Granodiorite have a restricted range, from 697 to 736°C, with the arithmetic mean being 716°C. As with the analogous temperatures calculated for the Loch Sunart Granodiorite, the restricted temperature range is thought to indicate that the rock compositions are representative of original liquid compositions and that the values themselves therefore represent the temperatures prevailing during separation of the magma from its source. As before, the temperatures are used in the determination of the theoretical levels of P saturation for the Glen Sanda Granodiorite magma. The calculated P saturation concentrations obtained are in the order 75% less than the measured concentrations, the temperature that would be required to saturate a magma of the composition of the Glen Sanda Granodiorite with respect to the measured P concentrations would be approximately 900-950°C, which is considered to be unrealistically high. The presence of subhedral and anhedral cores in some of the apatite crystals (Plate 8.9) means that it is possible that the oversaturation could be due to the presence of refractory apatite, although it could also be due magma mixing or assimilation as outlined above.

Titanite is only occasionally present in samples from the Glen Sanda Granodiorite. The titanites that have been studied (*eg.* Plates 8.4 and 8.5) do not have anhedral cores and thus it

is considered that they were not partially refractory.

8.6) GENERAL DISCUSSION.

The marked zoning that is present within the accessory phases of the Strontian Complex, and in particular titanite, implies that the kinetic influences that control partitioning of trace elements into accessory phases are of widespread importance and not merely a locally developed phenomenon. The presence of this primary magmatic zoning means that it is possible to determine the importance or otherwise of subsolidus processes that may have affected the minerals since crystallization. In the case of the Strontian Complex the limited subsolidus alteration and recrystallization processes that produced the thin actinolitic rims on the hornblendes of the Loch Sunart Granodiorite and resulted in the partial redistribution of K (to form the phenocrysts of the Loch Sunart Granodiorite porphyritic facies) and Ba (to form the replacive Ba-rich vein-like areas in alkali-feldspar), seems to have had no effect on titanite (the main REE containing phase) or zircon. The fact that the apatites from both parts to the complex are generally unzoned may indicate that they were re-equilibrated in a subsolidus environment or that they never became zoned during initial magmatic growth.

The very restricted range of Zr saturation temperatures (Watson & Harrison, 1983) obtained from both the Loch Sunart Granodiorite and the Glen Sanda Granodiorite rocks implies that the rocks represent original liquid compositions and thus the compositional variations were produced by differential partial melting rather than *in situ* fractional crystallization (separation of crystals and melt) at the current level of exposure. Substantial fractional crystallization involving the accessory phases, which have very different rock normalised REE distribution patterns, would have produced a sequence of rocks with very variable chondrite normalised REE distribution patterns, such patterns were not observed during the course of this work (Section 7.4.1) or by Pankhurst (1979). In addition both of these observations are consistent with the pattern of spatial distribution of composition observed in the Loch Sunart Granodiorite (see Section 7.2.2) being due to several smaller already differentiated pulses intruded more or less contemporaneously.

Even though the chemistry of the major minerals shows a restricted range their composition would still appear to be linked closely to whole rock chemistry: the plagioclase feldspars show a slight progression towards more evolved compositions in the more evolved rocks; the Fe/(Fe+Mg) ratios of both the biotites and the hornblendes (in the case of the Loch Sunart Granodiorite samples) show a correlation with whole rock Fe/(Fe+Mg) ratios. However, this does not appear to be reflected in the observed compositions of titanites from the same rocks, the titanites from each of the samples show a similar compositional range and this range is largely due to the fact that the titanites are compositionally sector zoned. In the case of the Loch Sunart Granodiorite and the Glen Sanda Granodiorite it would appear that due to the kinetic factors of titanite growth that bulk-magma composition had a negligible effect on the absolute chemistry of titanite.

8.7) SUMMARY.

1) The zircons from the the Loch Sunart Granodiorite and the Glen Sanda Granodiorite are distinctly different from one another in two important respects. Firstly, most zircons grains from BPSRG1 (Glen Sanda Granodiorite) contain large core structures, which are interpreted as representing inherited refractory material, whilst the zircons from BPSRT1 (Loch Sunart Granodiorite) only occasionally contain small core structures. Both of these observations are consistent with the published U-Pb zircon data. Secondly, the cogenetic zircon (the rim material) from BPSRG1 contains generally higher concentrations of Y, the HREE, Th and U than the cogenetic zircon from BPSRT1. It is thought that the melt from which the BPSRG1 zircons grew was more polymerised and that this caused the zircon/melt partition coefficients for Y, the HREE, Th and U to be higher. It would appear that, unlike titanite growth, the growth kinetics of zircon in the Strontian Complex magmas did not strongly influence absolute chemistry.

2) Texturally and compositionally the core structures of the zircons from BPSRG1 are very diverse; there are cores which are virtually unzoned, those with compositional sector zoning, those with crystal face-parallel zoning and those which apparently have had multi-stage histories. This diversity of zoning type and composition is thought to be consistent with the interpretation that the cores represent refractory material incorporated from the magma source or sources, but in addition it is also taken to indicate that the inherited zircon population of the Glen Sanda Granodiorite has mixed inheritance. The fact that the continental crust is often heterogeneous in terms of both rock type and age means that examples of mixed zircon inheritance in granites with a substantial crustal input are probably very common. The preservation of the textural and compositional features within the core population indicates that the cores did not chemically equilibrate with their surroundings within the duration of the magmatic event.

3) All the titanites within the subset of samples from the Strontian Complex are compositionally sector zoned, this implies that compositional sector zoning is not due to an unusual set of growth conditions but is probably a response to the *normal* set of growth conditions that accompany titanite nucleation and growth in magmas of this general composition in a plutonic environment. Titanites from each of the five samples show a very similar range of composition to one another and this range is largely a function of the fact that they are compositionally sector zoned, the influence of the medium of growth on their composition would thus appear to be negligible, *ie.* the kinetics of titanite growth largely determine the range of composition that each grain displays. This contrasts with the progressive whole rock correlated changes in major mineral composition that were described in Chapter 7.

4) Some of the titanite grains have outer rims that do not display compositional sector zoning (although the rest of the grain is compositionally sector zoned) but show marked crystal face-parallel zoning structures. This change from compositional sector zoning to purely crystal face-parallel zoning implies that there has been a distinct change in the growth

regime such that the processes that cause compositional sector zoning no longer operate. This change may be due to a distinct event or it may indicate that there is a sharp cut-off in the conditions necessary for the development of compositional sector zoning in titanite, either side of which compositional sector zoning is either developed or it is not.

5) The preservation of the primary magmatic zoning textures of both titanites and zircons suggests that the subsolidus alteration process or processes that affected the hornblendes to produce the actinolitic rims, resulted in the porphyritic facies of the Loch Sunart Granodiorite and gave rise to the Ba-rich areas of the alkali-feldspars did not affect the titanites or the zircons.

6) Only HREE were ever detected in the zircons from BPSRT1 and BPSRG1 and although it is not possible to produce complete REE distribution patterns the fact that only HREE were detected is consistent with the zircons from both samples having HREE enriched rock normalised distribution patterns. In the apatites from BPSRT1 only the LREE were detected and this is consistent with them having LREE enriched rock normalised distribution patterns. This contrasts with the apatites from BPSRG1 which have HREE enriched rock normalised distribution patterns, almost complete REE distribution patterns were obtainable from the apatites of this rock. Titanite is not present in the BPSRG1 sample, however titanites from the BPSRT1 sample give rock-normalised distribution patterns for the REE that are generally flat, although there are notable relative depletions in the LREE, particularly La and Ce. The LREE of sample BPSRG1 must be contained within the allanite and monazite known to be present.

7) Given that the two whole rocks samples (BPSRT1 and BPSRG1) have very similar chondrite-normalised distribution patterns the fact that the rock normalised distribution patterns for their respective accessory phase are variable is due to two factors; firstly, different mineral phases have different relative mineral/melt partition coefficients for the REE; and secondly, the order of crystallization of the containing phases. This latter point is exemplified by the fact that the apatites from the two samples have very different rock normalised REE distribution patterns even though they probably had very similar relative partition coefficients for the REE. The fact the different accessory phases from both the Loch Sunart Granodiorite and the Glen Sanda Granodiorite have different rock normalised REE distribution patterns is consistent with the fact that substantial fractional crystallization involving the accessory phases did not occur since this would have resulted in rocks with very variable chondrite-normalised distribution patterns, such patterns have not been observed.

8) The range of Zr saturation temperatures calculated for the Loch Sunart Granodiorite using the experimentally determined Zr solubility equation of Watson & Harrison (1983) is very restricted, within the claimed error of the technique. This coherence suggests that the values reflect the prevailing temperature during separation of the magma from its source. If the observed compositional range of the whole rocks represented the products of fractional crystallization then it would be expected that determination of temperatures from the bulk rock chemistries would yield variable and geologically unrealistic temperatures.

9) Halliday *et al.* (1979) showed that there was substantial inheritance in the zircons of the Glen Sanda Granodiorite and this is supported by the textural observations of this work. The observation by Rogers & Dunning (1990, in press) that a small quantity of inherited zircon exists within the Loch Sunart Granodiorite is also consistent with the observations of this work. From the existence of anhedral cores in some apatite crystals and from P saturation considerations it is considered possible that there is refractory apatite in both the Loch Sunart Granodiorite and the Glen Sanda Granodiorite. Textural observations do not indicate the presence of any anhedral cores in titanite and from this the presence of refractory titanite is considered unlikely.

Chapter 9
Sm-Nd isotopic studies of REE-rich accessory minerals from the Strontian Complex.

9.1) INTRODUCTION.

The case for and against refractory behaviour in the accessory phases of the Strontian Complex was outlined in Chapter 8, but can be summarised as follows: 1) substantial inheritance *does* exist in zircons from the Glen Sanda Granodiorite (Halliday *et al.* (1979), the textural observations of this work support this (see Section 8.2.3); 2) a small amount of inherited zircon exists within the Loch Sunart Granodiorite (Rogers & Dunning, 1990, in press), this small quantity is consistent with the textural observations of this work (see Section 8.2.2); 3) from P saturation considerations and the existence of anhedral cores in some apatite crystals it is considered possible that there is refractory apatite in both parts to the complex; and 4) from textural considerations we would not expect to find refractory titanite in either part. This chapter documents the Sm-Nd isotopic composition of the accessory phases from the Strontian Complex to assess the state of isotopic equilibrium in the light of the predictions on possible refractory behaviour.

9.2) Sm-Nd ISOTOPIC DISEQUILIBRIUM.

It has already been demonstrated that the accessory phases of both parts of the Strontian Complex contain most of the REE of the whole rock and that the different minerals have different REE distribution patterns (Section 8.4). Given that different minerals will have different Sm/Nd ratios, through time they will evolve to have different $^{143}Nd/^{144}Nd$ ratios (Fig. 9.1), the whole rock $^{143}Nd/^{144}Nd$ ratio being a weighted average of the different mineral ratios. This situation will prevail in any rock where there are different phases with different Sm/Nd ratios.

A given partial melt will only have the isotopic signature of its source (the weighted average of the mineral values) if complete equilibration between the melt and the various minerals in the source takes place; if equilibrium is not achieved then the $^{143}Nd/^{144}Nd$ ratio of the extracted melt may not be representative of the source value. O'Nions & Pankhurst (1974) discussed isotopic disequilibrium melting with respect to Rb-Sr isotope systematics, however the principles are the same for other radiogenic isotope systems, including Sm-Nd. They stated that if isotopic equilibration was not achieved between the source and the melt then varying degrees of partial melting would produce melts of varying isotopic signatures. For example, Beswick & Carmichael (1978) suggested that the contribution of apatite during melting of mantle sources may be of critical importance in determining the isotopic ratios of Nd and Pb in mafic magmas.

Disequilibrium melting could also be identified if isotopically unequilibrated residual source material (restite, Chappell, *et al.* (1987)) were to be entrained in the melt, although it would obviously be difficult to distinguish, purely on the basis of isotopic data, restite from other refractory minerals incorporated into the magma during ascent or emplacement.

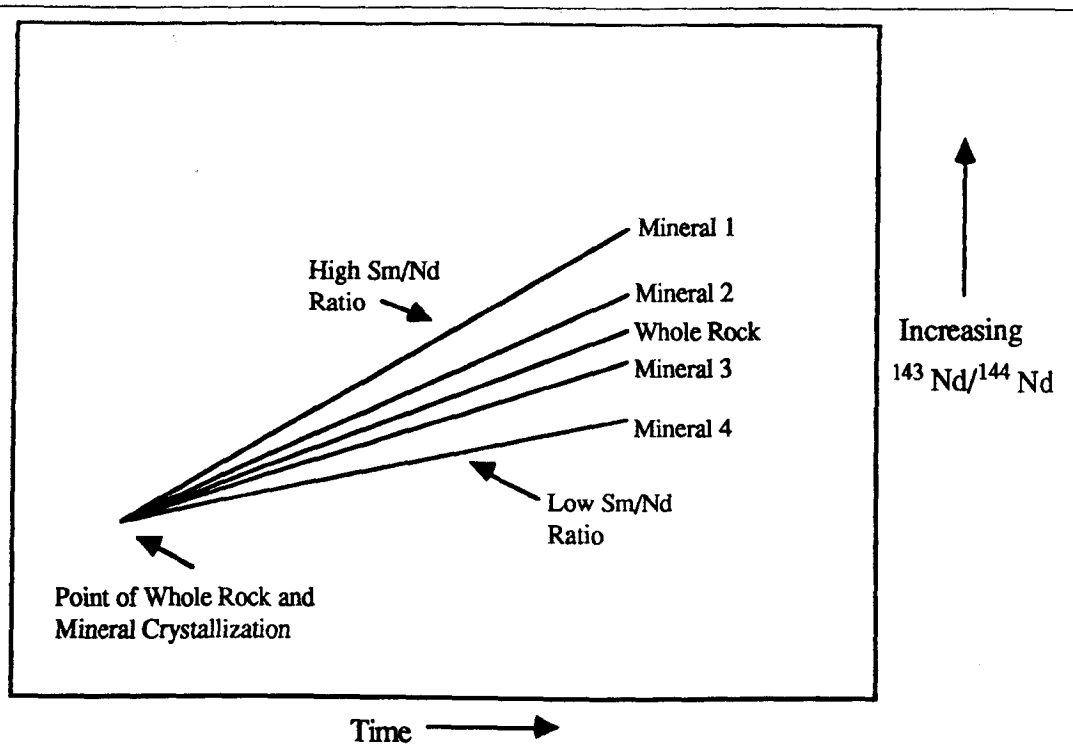

Fig. 9.1. Diagram showing the effect of the Sm/Nd ratio of different minerals on their $^{143}Nd/^{144}Nd$ ratios with the passage of time. Also represented (schematically) is the fact that the whole rock Sm/Nd and $^{143}Nd/^{144}Nd$ ratios are weighted averages of the minerals ratios.

It should be noted that isotopic disequilibrium within a rock could also arise due to mixing between isotopically distinct magmas that had partially crystallized prior to mixing. For example, Geist *et al.* (1988) described Sm-Nd isotopic disequilibrium between plagioclase megacrysts and their host andesite in the Edgecumbe Volcanic Field, SE Alaska; the plagioclase population was interpreted as representing a mixture, one from a mafic magma that had partially crystallized prior to partially assimilating a contaminant (siliceous crust), another from the refractory contaminant and a third in equilibrium with the matrix of the resultant rock.

9.3) Sm-Nd ISOTOPE VALUES IN STRONTIAN ACCESSORY MINERALS.

To test whether the accessory phases from the Strontian Complex are in isotopic equilibrium with respect to Sm-Nd isotope systematics isotope analyses of the following accessory minerals were determined (the method of mineral separations is given in Appendix 2A).

1) BPSRT1 (Loch Sunart Granodiorite) - apatite and titanite.

2) BPSRG1 (Glen Sanda Granodiorite) - apatite and zircon.

3) BPSRA1 (from 'Appinite PG' of Holden (1987)) - apatite and titanite.

All the minerals used for isotopic analysis were hand picked, the selected grains had a

Table 9.1. Whole rock and accessory mineral Sm-Nd isotopic data. WR - Whole Rock; Ap - Apatite; Ti - Titanite; Zr - Zircon. The Last number of the sample denotes duplicate dissolutions.

Sample	Sm (ppm)	Nd (ppm)	Sm/Nd	$^{147}Sm/^{144}Nd$	$^{143}Nd/^{144}Nd$	$^{143}Nd/^{144}Nd$ (425 Ma)	εNd	T_{CHUR}	Comments
Loch Sunart Granodiorite - BPSRT1									
T1 WR	7.42	38.84	0.1910	0.1156	0.512389±58	0.512067	- 0.5	0.47	-
T1 Ap	30.73	209.54	0.1467	0.0886	0.512299±58	0.512052	- 0.8	-	-
T1 Ti	540.39	2907.57	0.1859	0.1124	0.512367±39	0.512054	- 0.7	-	>250 μm,<500 μm
Glen Sanda Granodiorite - BPSRG1									
G1 WR	2.51	13.05	0.1923	0.1164	0.512148±35	0.511824	- 5.2	0.93	-
G1 Ap1	355.32	816.42	0.4352	0.2631	0.512475±52	0.511743	- 6.8	-	-
G1 Ap2	382.04	887.62	0.4304	0.2602	0.512519±28	0.511795	- 5.8	-	-
G1 Zr1	56.82	140.77	0.4036	0.2440	0.512283±55	0.511604	- 9.5	-	Mixed shape population
G1 Zr4	78.57	198.55	0.3957	0.2392	0.512267±51	0.511601	- 9.6	-	Mixed shape population
Appinite PG of Holden (1987) - BPSRA1									
A1 WR	18.65	98.19	0.1899	0.1148	0.512355±29	0.512035	- 1.1	0.58	-
A1 Ap	186.51	1113.60	0.1675	0.1012	0.512363±50	0.512081	- 0.2	-	-
A1 Ti1	1301.49	6746.06	0.1929	0.1166	0.512296±68	0.511971	- 2.3	-	>125 μm,<250 μm
A1 Ti2	927.57	4357.42	0.2129	0.1287	0.512340±42	0.511982	- 2.1	-	>250 μm,<500 μm

variety of morphologies, were crack free and had as few inclusions as possible; altered, cracked and cloudy grains were rejected. The methods used to determine the Nd isotopic composition and the Sm and Nd concentrations of the mineral separates and whole rocks are given in Appendix 2G, this appendix also gives details of the parameters used in calculation of εNd values and T_{CHUR} ages. The full results are given in Table 9.1.

Summary of the Sm-Nd isotope results.

The analytical uncertainties in the measured $^{143}Nd/^{144}Nd$ ratios give εNd values which are considered to be better than ±1.1 units (2σ), this was estimated from the uncertainty on the measured $^{143}Nd/^{144}Nd$ ratio of A1 Ti1 (this analysis has the greatest uncertainty of $^{143}Nd/^{144}Nd$ ratio). Most of the results have lower analytical uncertainties than this, down to ±0.5 εNd units.

1) The whole rock εNd_{425} values for BPSRT1, BPSRG1 and BPSRA1 agree, within analytical uncertainty, with the previously published values for the respective facies of the pluton (see Table 6.4 in Chapter 6).

2) The apatite and titanite εNd_{425} values for BPSRT1 are in equilibrium with each other and are similar to the whole rock value, *ie.* the values agree within analytical uncertainty.

3) The two apatite εNd_{425} values for BPSRG1 are in equilibrium with each other and are similar to the whole rock value.

4) The two BPSRG1 zircon εNd_{425} values (- 9.5) are not in equilibrium with the apatites or the whole rock, the values being some 3 εNd units more negative. This difference is beyond that expected from analytical uncertainty.

5) The apatite and titanite εNd_{425} values for BPSRA1 appear to be in equilibrium with each other and their host rock.

9.4) DISCUSSION OF THE RESULTS.

9.4.1) Sm-Nd isotopes in accessory phases other than zircon.

With the exception of the zircon separate from BPSRG1 (Glen Sanda Granodiorite), the whole rocks and their respective accessory minerals appear to be in isotopic equilibrium with respect to Sm-Nd isotopes. There are three possible explanations for this: 1) they crystallized in equilibrium from an isotopically homogeneous melt, *ie.* devoid of refractory minerals; 2) any refractory minerals present were equilibrated before or during the melting/crystallization event; and 3) any disequilibrium is masked by the analytical uncertainty of the technique. On this last point it should be noted that the long half life of ^{147}Sm (106Ga) and the limited fractionation (in comparison with the analogous Rb-Sr isotope system) of Sm relative to Nd between phases mean that it is entirely possible that analytical uncertainty could mask slight disequilibrium within these phases. However, at the present scale of study the degree of disequilibrium (if any) is insignificant.

Very little is known about the behaviour of Sm-Nd isotopic systems in REE-rich accessory phases during high grade metamorphism or melting. Watson *et al.* (1985) carried out experiments on the diffusion of Sm, Sr and Pb in apatites at elevated temperatures (900-1250°C) and established Arrhenius relationships for the diffusive behaviour of Sm, Sr and Pb which enabled extrapolation to lower temperatures. They concluded that at temperatures below ~760°C Sm-Nd isotopic source information may be retained in refractory apatites during melting events with durations shorter than 10^6 years. If there is a refractory apatite component within any of the three Strontian samples then clearly the conditions and duration of heating and melting were such that it was able to equilibrate or that it is of such a small proportion as to have no significant effect on the measured values.

There is no textural evidence (*ie.* subhedral and anhedral cores) of refractory behaviour in the titanites from either the Loch Sunart Granodiorite or Appinite PG (of Holden (1987)), this is consistent with the fact that the Sm-Nd isotopes of the titanite separates are in equilibrium with the host rock and apatite values.

The effect of metamorphism on the Sm-Nd isotope systematics of apatite and titanite from a ~3.6Ga tonalitic augen gneiss from northern Michigan were described by Futa (1981), the results indicated that they were reset with respect to their Sm-Nd isotope systematics during a metamorphism at 1.75Ga. This would suggest that during prolonged heating that the Nd (and presumably the other REE) within apatite and titanite is sufficiently mobile that equilibration of Nd isotopes is possible. The Sm-Nd systematics of other phases in the same rock, allanite, biotite, quartz and plagioclase, were also reset during the 1.75Ga metamorphic event. Futa (1981) also explored the Sm-Nd systematics of zircon from the same rock, this is discussed below.

9.4.2) Sm-Nd isotopes in zircons from the Glen Sanda Granodiorite.

In the case of the zircons from the Glen Sanda Granodiorite their εNd_{425} values are clearly not in equilibrium with the other phases analysed or with the whole rock. This disequilibrium could have two possible explanations: 1) zircon has experienced some post-crystallization disturbance of its Sm-Nd isotope systematics which did not affect the other REE-rich phases; or 2) the zircons from the Glen Sanda Granodiorite (which are known to contain substantial inheritance (Halliday *et al.*, 1979)) did not *completely* equilibrate with respect to Sm-Nd isotopes within the duration of the magmatic event and thus retained some record of their Sm-Nd isotopic history. The fact that the zircons from the Glen Sanda Granodiorite are known from U-Pb analysis to contain inheritance means that a model whereby two isotopically distinct partially crystallized magmas subsequently mixed cannot be the sole explanation of the observed disequilibrium.

Isotopic disturbance of zircons within the Glen Sanda Granodiorite is considered unlikely as there is no independent evidence of a post-crystallization (425Ma) event affecting the Strontian Complex and as described earlier the zircons selected for analysis were all of high integrity. Futa (1981) observed that two zircon fractions from the ~3.6Ga tonalitic augen

gneiss described above did not retain the $^{143}Nd/^{144}Nd$ ratios required to plot on either the 3.6Ga isochron line (the age of the rock) or the 1.75Ga isochron line (the age of metamorphism), instead the $^{143}Nd/^{144}Nd$ ratios of the zircons plot on a much younger isochron line, defined by the $^{143}Nd/^{144}Nd$ and $^{147}Sm/^{144}Nd$ ratios of the zircons and the $^{143}Nd/^{144}Nd$ ratio of the whole rock at ~3.6Ga. Futa (1981) observed that the zircon 'ages' do not correspond to any known geological event, but pointed out that they are similar to U-Pb lower intercept ages for U-rich zircons from the same augen gneiss obtained by Peterman *et al.* (1980). Futa (1981) speculated that the extensive radiation damage suffered by the zircons may make movement of Sm and Nd more likely under milder geological conditions. The possibility of mixed Sm-Nd zircon systematics was not considered by Futa (1981).

There has been no experimental work on diffusion of REE in zircons and this is a major drawback to discussing the behaviour of Sm-Nd isotopes in zircons during heating and incorporation into a magma, however some basic comments and observations can be made. Unlike the U-Pb isotopic system in zircons (and other minerals) which can be reset purely by outward diffusion of radiogenic Pb, the equilibration of Nd isotopes requires both outward *and* inward diffusion of Nd (and by inference the other REE), outward diffusion of Nd will not alter the $^{143}Nd/^{144}Nd$ ratio of the zircon, the ratio can only be altered by equilibration with another source of Nd with a different $^{143}Nd/^{144}Nd$ ratio. Previously (Chapters 3, 5 and 8) it was noted that the inherited cores of zircons often retain what is considered to be their primary zoning textures and in addition it was observed that the REE compositions of the refractory zircons cores are highly variable and it was argued that this was consistent with the cores having a variety of ultimate sources. The compositional discontinuities within cores, which at least in part are caused by variations in REE content, are often sharp, it would be expected that if there had been significant chemical diffusion of the REE (inward or outward) that sharp compositional discontinuities would be at least partially destroyed by the processes of diffusion. Recently, on the basis of experimental work, Baker (1989) has demonstrated that chemical diffusion of Sr (in response to a chemical potential gradient) may be much slower than self-diffusion of Sr; *ie.* diffusion that occurs in the absence of a chemical potential gradient and usually modelled as a "random walk" phenomenon. Although this has only been experimentally demonstrated for Sr, Baker (1989) states that such behaviour is consistent with current multicomponent diffusion theory. This, coupled with the fact diffusive transport of elements in a chemical potential gradient is rate-limited by chemical diffusivities and isotopic equilibration of an element is rate-limited by self-diffusivities (Baker, 1989) means that isotopic equilibration may not be accompanied chemical equilibration. Thus the fact that the zircon cores are not in *chemical* equilibrium with their rims or each other does not necessarily imply that they are also in *isotopic* disequilibrium. Equally, however, the existence of chemical equilibration would imply that isotopic equilibration had occurred. Thus despite the observations of Baker (1989) the preservation of chemical disequilibrium in the inherited zircon population of the Glen Sanda Granodiorite does not rule out the possibility of there being Sm-Nd isotopic disequilibrium in zircons.

For the purposes of further discussion it is assumed that the zircon εNd_{425} values of the Glen Sanda Granodiorite zircons do represent, at least in part, a record of the pre-melting Sm-Nd history of the inherited zircon population. The εNd_{425} values of the BPSRG1 zircon separate must represent a combination of the Nd isotopic composition of the cores, which *may* have been partially equilibrated, and that of the rims. The rims are assumed to be in isotopic equilibrium with the other Sm-Nd containing phases and will thus have a εNd_{425} value of ~ - 6. Given that the whole grain εNd_{425} value of the zircons is -9.5 then the cores will have more negative εNd_{425} values than the whole grain value, how much more will depend on the relative concentration of Sm and Nd in the cores and rims and the proportion of core and rim material. If the earlier assertion (Section 8.2.4) that the inherited zircon population of the Glen Sanda Granodiorite has mixed inheritance is correct then the actual εNd_{425} value of the core material will represent an average, this should be borne in mind when considering the following discussion.

9.5) Sm-Nd ISOTOPIC DISEQUILIBRIUM IN ZIRCONS.

From both published analyses (*eg.* Nagasawa, 1970; Gromet & Silver, 1983; Mahood & Hildreth, 1983) and experimentally-determined partitioning information (Watson, 1980) we would expect zircons, in general, to have higher Sm/Nd ratios than both typical sialic continental crust and many other REE-rich accessory phases. Such zircons will evolve in a given time interval to higher εNd values than either the other phases or the whole rock, the principles of this were illustrated in Figure 9.1. The Nd isotopic signature of any granitic partial *melt* extracted from this sialic crust will of course depend on the extent of equilibration, but for the purposes of this discussion it is assumed that most of the REE are controlled by a single phase which has a Sm/Nd ratio similar to the whole rock value (*eg.* Mineral 3 of Fig. 9.1). Zircon is assumed on the basis of published studies (*eg.* Gromet & Silver, 1983 and Sawka, 1988) to contain a very small proportion of the total whole rock REE content and thus does not significantly contribute to the whole rock Nd isotopic signature. If the REE are controlled dominantly by a single phase then a partial melt extracted from such a source will result in a melt with a Nd isotopic signature which is not vastly different from that of the source. In view of the textural evidence presented earlier any zircon entrained in this melt may remain undissolved and unequilibrated and hence may retain its own Nd isotopic composition. Subsequent Sm-Nd isotopic analysis will show the zircon $^{143}Nd/^{144}Nd$ ratios to be *higher* than the resultant host rock ratio if, as stated above, the bulk of the REE are not found in the zircon.

The fact that the zircon separates from BPSRG1 have *lower* εNd value than their host rock despite having higher Sm/Nd ratios suggests two possibilities which are not mutually exclusive.

1) The chemistries of the zircon *cores* in this rock are unusual (different from the expected norm) by virtue of having Sm/Nd values lower than that of their host rock, *ie.* the sialic continental crust. This can only be tested by selected analysis of the core material.

2) That there was another, more primitive source for some of the Nd present within the Glen Sanda Granodiorite; that is there was mixing of an older source, characterised by strongly negative εNd_{425} values, with a younger more isotopically primitive source with much higher εNd_{425} values.

Two models based on the possibility of mixing of isotopically distinct sources will be discussed. Both are general models intended to illustrate the broad possibilities involved with inherited Sm-Nd systematics and both assume that the undissolved zircon does not equilibrate with the environment in which it is found. The first model assumes that the zircons crystallized in sialic continental crust shortly after it was stabilised from a mantle source (arbitrarily chosen to be ~2.6Ga), *ie.* the zircons had initial $^{143}Nd/^{144}Nd$ ratios that were close to contemporaneous mantle values at the time of crystallisation. The second assumes that the zircons crystallized from a magma, produced by the melting of sialic material that had been resident in the crust for a long period of time, such that the $^{143}Nd/^{144}Nd$ initial ratios of the zircons were much lower than the contemporaneous mantle values.

Model 1 (Fig. 9.2).

This model assumes that the sialic continental crust and the zircons remained isotopically undisturbed from the time of crust separation (and zircon crystallization) from the mantle until

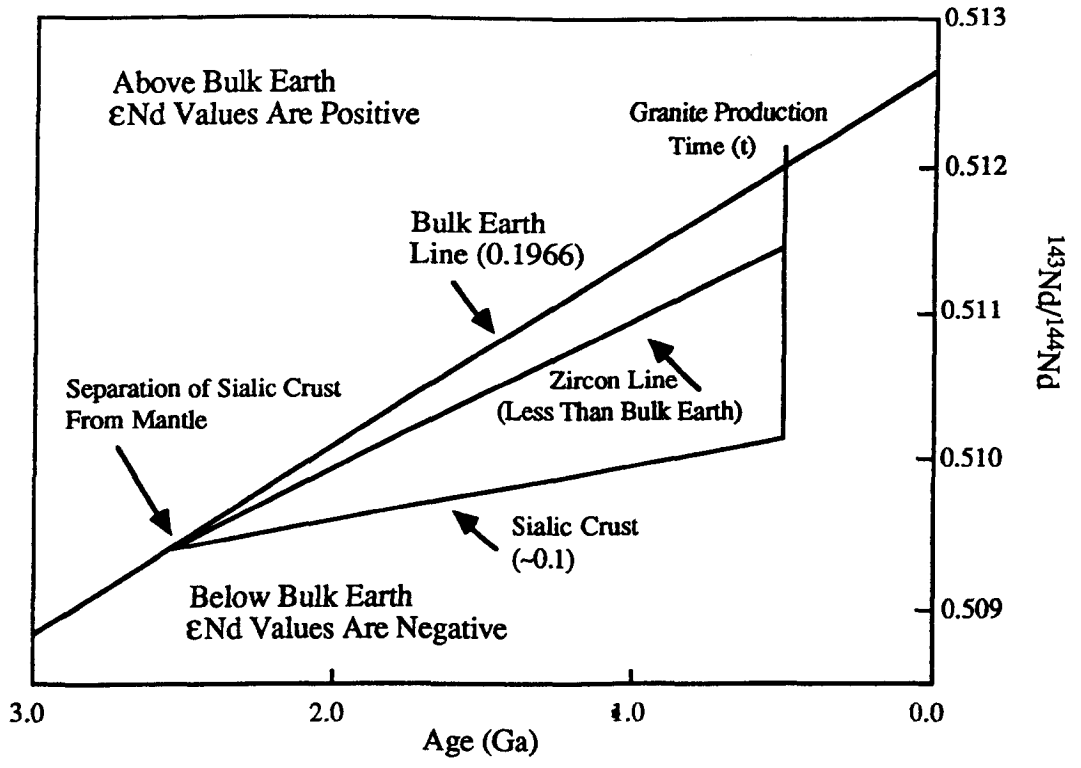

Fig. 9.2. **Model 1.** This assumes that the zircons crystallized from a source which had not long been stabilised from the mantle and thus for the zircons to evolve to negative εNd they must have $^{147}Sm/^{144}Nd$ ratios which are less than bulk earth, which is 0.1966. The values in brackets are the $^{147}Sm/^{144}Nd$ ratios. See text for further explanation.

the time of melting (t) to produce the granite. The isotopic evolution of these old zircons will depend on the their Sm/Nd ratios; if the zircons are to evolve to have negative ε_tNd values then their average $^{147}Sm/^{144}Nd$ ratio *must* be less than the Bulk Earth value (0.1966) assuming that the mantle source did not have a low εNd value at the time of crust separation. Subsequent mixing of the sialic source with a younger source with higher $^{143}Nd/^{144}Nd$ values could produce the desired relationship between the whole rock and zircon $^{143}Nd/^{144}Nd$ values. The principles of the mixing process are outlined in Figure 9.3. The resultant whole rock $^{143}Nd/^{144}Nd$ value (point **3**) is the result of mixing of a primitive Nd isotopic source (**2**) with an old sialic source (**1**). The actual value of the mixture will depend on the proportions of the two sources and their respective Nd concentrations. The $^{143}Nd/^{144}Nd$ value of the zircon rims will have be the same as the mixed rock (*ie.* point **3**). The whole zircon grain $^{143}Nd/^{144}Nd$ value (point **5**, core + rim) will also be a mixture, between the inherited zircon value (**4**) and the mixed whole rock value (**3**). It should be clear that the relative $^{143}Nd/^{144}Nd$ values of a whole zircon grain analysis (**5**) and its host rock (**3**) will depend on the proportions of both mixing processes mixing and the absolute concentrations of Nd, they need not always have the relationship shown in Figure 9.3.

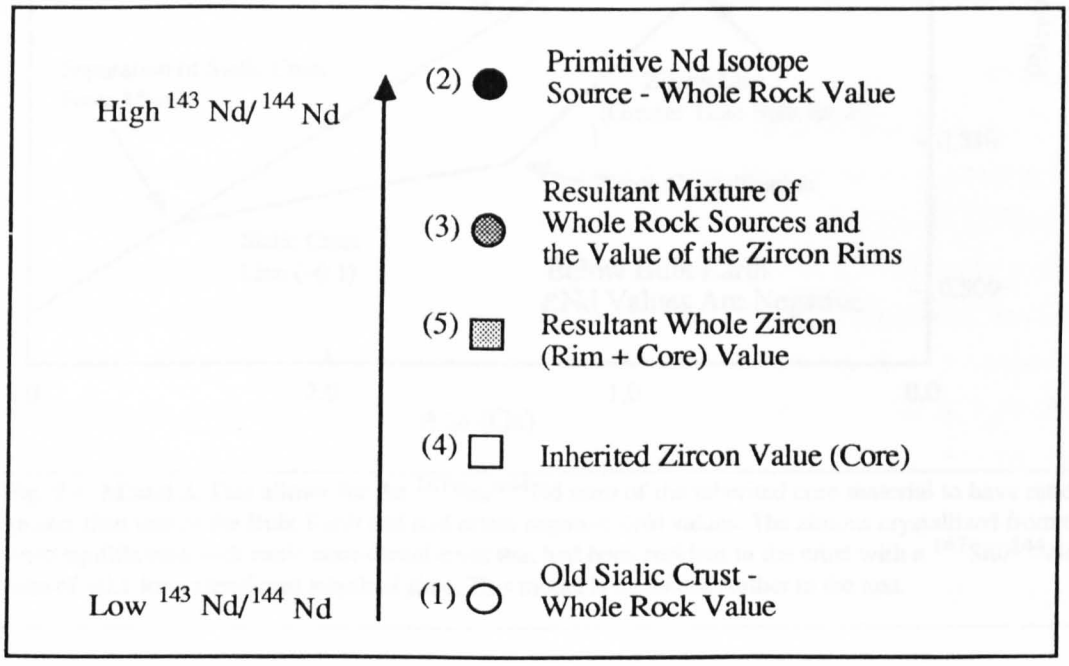

Fig. 9.3. Schematic diagram showing how the $^{143}Nd/^{144}Nd$ ratio of a whole zircon grain (5) (core + rim) can be derived by mixing of an inherited zircon ratio (4) and the ratio of the rim (2). The rim ratio is also the product of mixing of two isotopically distinct sources, (1) and (2). This mixing model is further explained in the text.

Model 2 (Fig. 9.4).

If the $^{147}Sm/^{144}Nd$ ratios of the zircon cores in the Glen Sanda Granodiorite are to be typical of zircons and therefore greater than Bulk Earth (0.1966) then constraints may be placed upon their history on an Nd isotope evolution diagram (Fig. 9.4). Assuming that the observed Nd isotopic relationships between whole rock and zircon in the Glen Sanda

Granodiorite are the result of mixing processes at 425Ma similar to those outlined above (Model 1 and Fig. 9.3) , then the fact that the cores of the Glen Sanda Granodiorite zircons had lower $^{143}Nd/^{144}Nd$ ratios at 425Ma than contemporaneous Bulk Earth implies that the evolutionary paths for zircons and Bulk Earth must have diverged at some time in the past. Clearly, in this case, the zircons cannot have crystallized from a magma shortly after extraction from a chondrite or more depleted mantle. Instead they must have grown during melting of pre-existing crust at some time subsequent to its extraction from the mantle. This pre-existing crust with its attendant low $^{147}Sm/^{144}Nd$ ratio would have had time to evolve to $^{143}Nd/^{144}Nd$ ratios lower than Bulk Earth by the time of zircon crystallization.

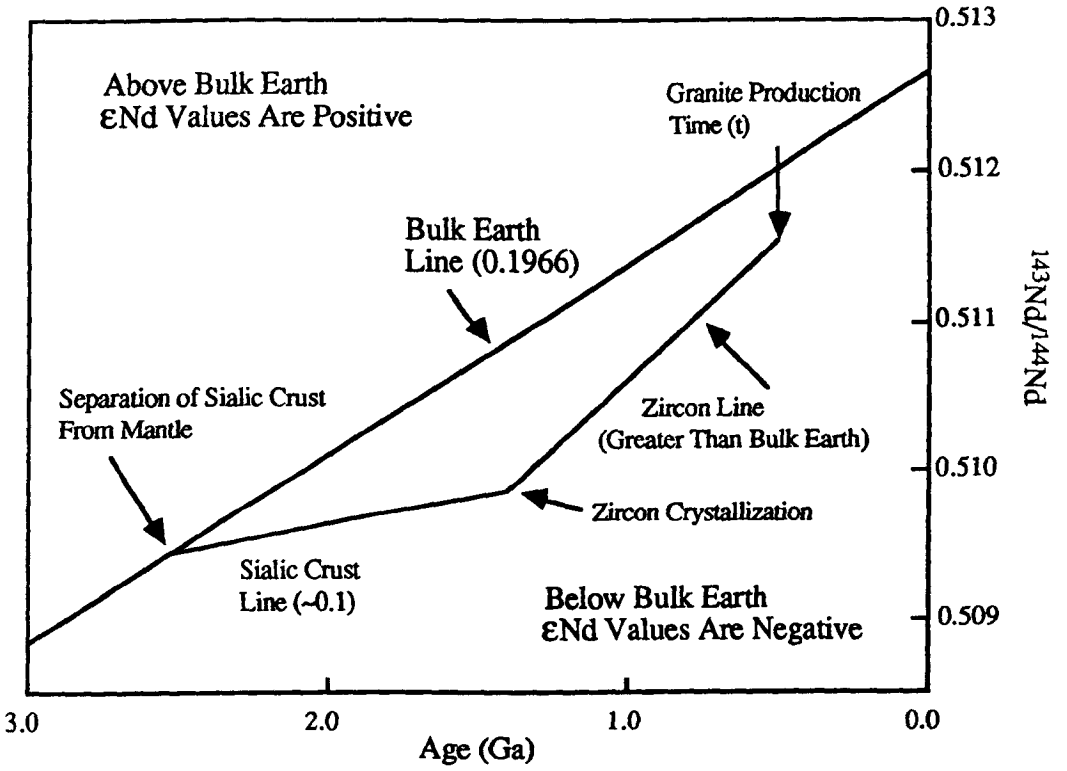

Fig. 9.4. **Model 2.** This allows for the $^{147}Sm/^{144}Nd$ ratio of the inherited core material to have ratio greater than that of the Bulk Earth and still retain negative εNd values. The zircons crystallized from or were equilibrated with sialic continental crust that had been resident in the crust with a $^{147}Sm/^{144}Nd$ ratio of ~0.1 for a significant length of time. This model is explained further in the text.

It should be noted that zircon cores with $^{147}Sm/^{144}Nd$ ratios less than Bulk Earth (Model 1) could still have been involved in a model similar to Model 2 where they are produced during a crustal melting episode, but it is not *necessary* to invoke such a model, whereas with cores which have $^{147}Sm/^{144}Nd$ ratios greater than Bulk Earth such a model is necessary. Inherited zircons with negative εNd_t values at the time of incorporation into the final magma which are not in equilibrium with their host rock and which have $^{147}Sm/^{144}Nd$ ratios greater than Bulk Earth *must* have been involved in a model similar in general concept to Model 2.

If the inherited zircon population of the Glen Sanda Granodiorite is a collection of grains with different sources and ages then the Nd isotopic composition of the bulk zircon population will be the result of numerous combinations of variations on the two general models outlined above. However, on the basis of the likely Sm/Nd ratios to be expected in zircons it is thought that the majority of the inherited zircons of the Glen Sanda Granodiorite originally crystallized or were equilibrated with crust that had $^{143}Nd/^{144}Nd$ ratios that were significantly lower than contemporaneous mantle values.

9.6) QUANTITATIVE MODELLING OF Sm-Nd ISOTOPIC DISEQUILIBRIUM IN ZIRCONS FROM THE GLEN SANDA GRANODIORITE.

Quantitatively modelling is hindered in two respects: 1) the measured εNd_{425} and $^{147}Sm/^{144}Nd$ values are both averages of the inherited core and the rim, the actual core value is not known; and 2) the core value is also an average of all the cores, these may have widely varying ages and compositions. The average εNd_{425} value of the cores in the Glen Sanda Granodiorite must be more negative than -9.5, how much more is dependent on the proportion of core to rim and their respective Sm and Nd concentrations.

Bearing in mind the difficulties in quantitatively modelling Sm-Nd disequilibrium the following discussion illustrates a possible quantitative model based on Model 2, see Fig. 9.5. Its purpose is to illustrate the potential of such a model rather than to account directly for the measured Nd isotopic composition of the inherited zircons in the Glen Sanda Granodiorite. Initially the model considers that zircon crystallization took place at 1.5Ga, the approximate upper intercept age of the U-Pb zircon discordia for the Glen Sanda Granodiorite determined by Halliday *et al.* (1979), this age does not correlate to the timing of any known local geological event probably because the inherited zircon population consists of a number of ages (see Section 8.2.4). The effect on the model of using ages of known local geological events is also considered.

1) At 2.92Ga Lewisian sialic continental crust separated from the mantle, this crust had an initial $^{143}Nd/^{144}Nd$ ratio of 0.508959 and a typical $^{147}Sm/^{144}Nd$ ratio of 0.10 (age and ratios from Hamilton *et al.*, 1979).

2) At 1.5Ga there was a reworking event which resulted in either zircon crystallization or isotopic equilibration, the zircons took on the prevailing $^{143}Nd/^{144}Nd$ ratio that the 2.92Ga crust had evolved to by 1.5Ga . The zircons are assumed, for the sake of the model, to have had a $^{147}Sm/^{144}Nd$ ratio of 0.24, similar to the value of the bulk zircon fraction analysed.

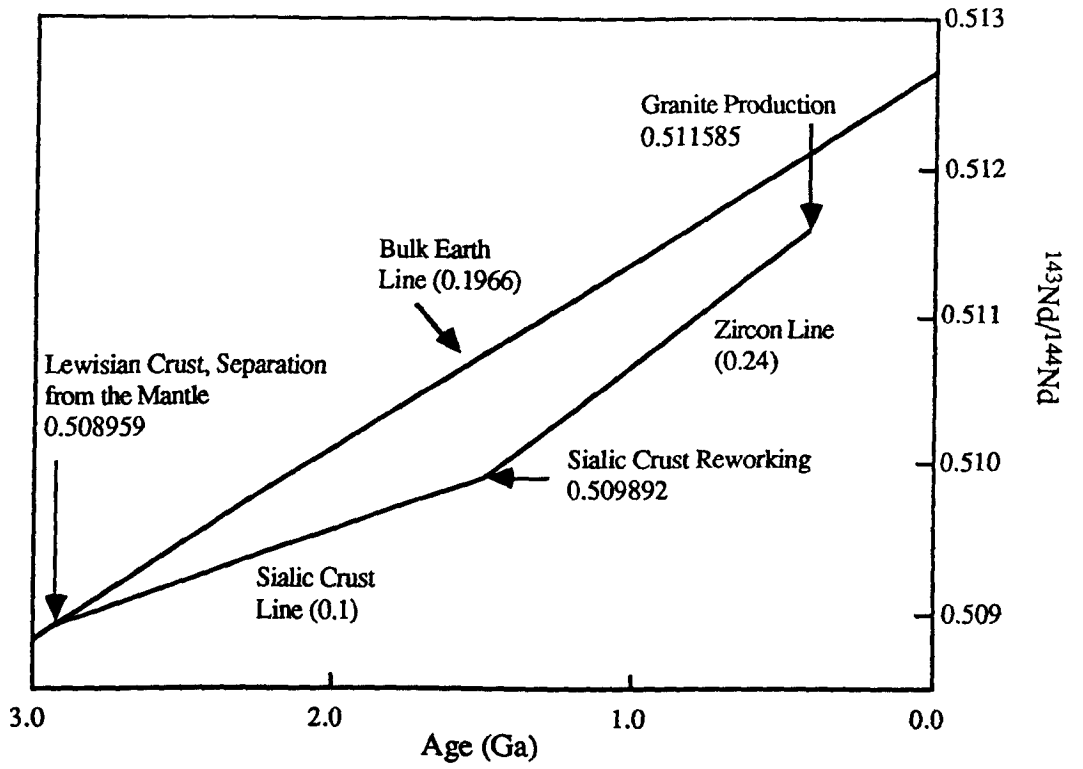

Fig. 9.5. A quantitative model of the Sm-Nd evolution of inherited zircons from the Glen Sanda Granodiorite, involving crystallization of zircon (with $^{147}Sm/^{144}Nd$ ratios greater than bulk earth) due to a reworking of sialic crust with a long crustal residence time. Values in brackets are $^{147}Sm/^{144}Nd$ ratios. Full details of the model are given in the text.

3) Between 1.5Ga and 425Ma (the time of granite production) these zircons evolved to have $^{143}Nd/^{144}Nd$ ratios of 0.511585, this equates to a εNd_{425} value of -9.9.

4) If an age of ~1.75 Ga (the approximate age of the Laxfordian event which affected the Lewisian) is used as the timing of the sialic crust reworking the inherited zircons would give a εNd_{425} value of -5.4. If, on the other hand, we use a reworking age of ~1.0Ga (a Grenvillian age) the resulting εNd_{425} value for the inherited zircons would be -18.7.

9.7) SUMMARY AND CONCLUSIONS.

The presence of inherited zircon in the Glen Sanda Granodiorite, which is inferred from both textural evidence presented earlier and from the previous U-Pb isotopic work (Halliday *et al.*, 1979), is also manifest in the Sm-Nd isotope systematics. It is believed that this is the first such description of Sm-Nd disequilibrium in zircons from young (non-Archaean) plutonic rocks. The differences in the $^{143}Nd/^{144}Nd$ ratios of the zircons and whole rock at the time of crystallization of the Glen Sanda Granodiorite suggest that the zircons were not totally reset with respect to their Sm-Nd isotopic systematics within the duration of the melting and crystallization event. In addition to the isotopic results both the preservation of internal compositional discontinuities and the highly variable REE concentrations of the zircon cores

implies that the diffusion and exchange of the REE, and by inference Sm and Nd, with the Glen Sanda Granodiorite melt was not an efficient process and did not *completely* equilibrate the melt with respect to their REE content. However, the findings of Baker (1989) outlined above (Section 9.4.2) mean that it is not possible to infer from the textural and compositional evidence that there is also Nd-isotopic disequilibrium.

The zircons from the Glen Sanda Granodiorite have εNd_{425} values which are more negative than that of their host rock. This could be due to two possibilities.

1) The inherited zircon cores crystallized with initial $^{143}Nd/^{144}Nd$ ratios close to the values of contemporaneous mantle and therefore must have $^{147}Sm/^{144}Nd$ ratios very much lower than the Bulk Earth value (0.1966) (Model 1).

2) The inherited zircons crystallized from, or were equilibrated with, material that had a $^{143}Nd/^{144}Nd$ ratio that was significantly lower than Bulk Earth values of the time. Such zircons could have $^{147}Sm/^{144}Nd$ ratios higher than Bulk Earth and still retain negative εNd values (Model 2), how long they could retain negative values would depend on their initial $^{143}Nd/^{144}Nd$ ratios and their $^{147}Sm/^{144}Nd$ ratios.

From both published determinations of typical zircon Sm/Nd ratios and the bulk (core plus rim) Sm/Nd ratio of the Glen Sanda Granodiorite zircon separates it is thought that majority of the inherited zircon cores in the Glen Sanda Granodiorite originally crystallized with $^{143}Nd/^{144}Nd$ ratios significantly less than contemporaneous mantle values at the time of crystallization.

If the inherited zircon component of granitoids *commonly* retain their Sm-Nd isotopic composition during prolonged crustal melting events then they could potentially yield useful qualitative information about the Sm-Nd isotopic environment in which they originally grew. Quantifying possible models is hindered by lack of detailed knowledge of the actual $^{143}Nd/^{144}Nd$ and Sm/Nd ratios of the inherited material, the measured ratios being averages of the core and rim material, and the strong likelihood that the inherited cores themselves have a wide variety of ages, sources and Sm/Nd ratios.

Apatite and titanite, the other phases for which Sm-Nd isotopes were determined, were both in equilibrium with their respective host rocks. Of these, only apatite shows any evidence (through apparent P oversaturation and textural studies) of refractory behaviour. The fact that the apatite is in equilibrium with its host rocks suggests that either apatite was not refractory (and consequently an alternative explanation is required for the apparent P oversaturation and textural observations), or it equilibrated as a refractory phase during the melting/crystallization event. Equilibration of apatite with respect to Sm-Nd isotopes would be expected from the findings of Watson *et al.* (1985) on the diffusion behaviour of Sm in apatites at elevated temperatures.

Chapter 10
Summary, suggestions for future work and concluding remarks.

10.1) SUMMARY.

10.1.1) Zoning in zircon and titanite.

Textural studies of the accessory minerals, facilitated by exploiting the backscattered electron (BSE) technique, have demonstrated that accessory zircon and titanite from calc-alkaline granitoids and related rocks are virtually ubiquitously zoned, the zoning textures identified ranging from multiple crystal face-parallel zoning, subhedral and anhedral core structures to compositional sector zoning. Until recently studies of compositional zoning in minerals relied heavily on centre/edge (so called 'core/rim') or grain-traverse strategies of electron microprobe analysis, however the complexity of the zoning structures commonly identified during the course of this research must call into doubt interpretations of mineral chemistry based on such strategies. Increasingly, new techniques (*eg.* laser-interferometry and Nomarski interference imaging) are being developed and established techniques (*eg.* cathodoluminescence) more fully exploited such that the internal compositional zoning of minerals can be visualised and this in turn means that interpretations of mineral chemistry become less dependent on *a priori* assumptions about the texture of the zoning. It should be the duty of all mineralogists and petrologists to investigate the *texture* of the internal compositional variations of a mineral before attempting to interpret its chemistry. Not to look at the texture is directly analogous to taking whole rock samples from an area in which the field relationships are not known, *ie.* unless the "blunderbuss" analytical strategy is adopted then there is a high probability of misinterpretation.

The zoning textures of zircon and titanite that were observed indicate that the chemistry of these minerals in granitoid rocks is strongly influenced by the kinetic factors of crystal growth, namely within-magma elemental diffusion rates, crystal growth rates and interface kinetics, and that there was commonly chemical disequilibrium between the growing mineral and its environment. The presence of zoning in these two accessory mineral phases is largely a reflection of fundamental magma properties and the processes linked to crystal growth rather than unusual growth conditions. These textures indicate that even in plutonic granitoid environments, disequilibrium induced by the kinetics of crystal growth commonly occurs and that the disequilibrium recorded in the zoned grains is preserved after crystallization of the grain and during the subsequent subsolidus temperature interval.

10.1.2) The Strontian Complex.

Whole rock chemistry.

On the basis of whole rock chemistry and previously published petrographic and structural observations (*ie.* Sabine, 1963; Munro, 1965; Hutton, 1988a and 1988b) it was decided to clarify the relationships between the mapped rock units of the Strontian Complex by renaming them; the two outer rock units (the 'tonalitic granodiorite' and the 'porphyritic granodiorite' of past usage), have been named the Loch Sunart Granodiorite (with outer

non-porphyritic facies and inner porphyritic facies) and the clearly later 'biotite granite' has been renamed the Glen Sanda Granodiorite. The Loch Sunart Granodiorite (~60-70 wt% SiO_2) and the Glen Sanda Granodiorite (~70-73 wt% SiO_2) show no extensive overlap in composition while only in terms of total Fe content is there a 'compositional gap'. The two facies of the Loch Sunart Granodiorite are, with the exception of their K_2O content, chemically indistinguishable and this is consistent with the spatial distribution of composition across the Loch Sunart Granodiorite which does not show a concentric pattern or a pattern related to the mapped position of the internal boundary of the porphyritic facies.

The geographical pattern of compositional variation suggests that the Loch Sunart Granodiorite was emplaced as a number of small essentially contemporaneous pulses and that the differentiation process that produced the compositional variations displayed by the whole rock chemistry took place prior to emplacement. The decoupled distribution of K_2O relative to other whole rock chemical parameters is thought to indicate that K was partially mobile in a late fluid phase and thus the alkali-feldspar phenocrysts of the porphyritic facies of the Loch Sunart Granodiorite are late and replacive. The central position of the porphyritic facies (away from the intrusion margins) and the shape of the intrusion (inwardly dipping contacts) suggests that this late fluid was concentrated towards the roof, although this is difficult to prove since the roof has been removed by subsequent erosion.

Major mineral chemistry.

The mineral chemistry of six samples was studied, these samples cover the entire range of whole rock composition present within the Complex. The normal zoning (in the sense of MacKenzie *et al.*, 1982) of the plagioclase feldspars of both the Loch Sunart Granodiorite and the Glen Sanda Granodiorite combined with fact that they become generally more albitic in the more evolved samples suggests that the crystallization of plagioclase was dependent on bulk-magma composition and temperature. The Ba-rich areas present in all alkali-feldspars are thought to have a replacive origin and although the total quantity of these Ba-rich areas is restricted they must contain a significant proportion of the whole rock Ba. This, combined with the replacive texture, suggests that Ba, in addition to K, was also partially mobile although there no evidence of a correlation between the distribution of Ba and that of K.

The actinolitic rims found on many of the hornblendes of the Loch Sunart Granodiorite are thought to be due to crystallization or alteration (substantial addition and loss of components) under subsolidus conditions in the presence of a fluid. The amount of actinolite is very limited and the dominant amphibole (> 95%) is hornblende. The biotites from the Glen Sanda Granodiorite have higher concentrations of Ti, Mn and Al in the octahedral site than those of the Loch Sunart Granodiorite, this is probably related to the coexisting mineral phases; the biotites from the Loch Sunart Granodiorite always coexist with hornblende and substantial quantities (for an accessory) of titanite, unlike biotites from the Glen Sanda Granodiorite which do not coexist with hornblende and only rarely titanite. The biotites and the *edge* compositions of the hornblendes show a consistency in their Fe-Mg distribution which is mirrored in the whole rock Fe/(Fe+Mg). The consistency of the Fe-Mg distribution

between the whole rocks, the biotites, and the hornblende edges (in the Loch Sunart Granodiorite), either reflects equilibrium growth or post-crystallization equilibration.

Observation on the accessory minerals.

The zircons from the Loch Sunart Granodiorite and the Glen Sanda Granodiorite differ in two important respects.

1) The zircons from the Loch Sunart Granodiorite (sample BPSRT1) only occasionally contain core structures (interpreted to represent inherited material), this is in marked contrast to the zircons of the Glen Sanda Granodiorite (sample BPSRG1) most of which (~95%) contain large core structures. The core structures of the Glen Sanda Granodiorite are very diverse in terms of their types of internal zoning and their composition. This diversity indicates that the inherited zircon cores did not equilibrate with the magma and it is also thought to be consistent with the zircon inheritance being mixed in the sense of Miller *et al.* (1988), *ie.* having a variety of ultimate sources and ages. This mixed inheritance, if it exists, is consistent with the existing published radiogenic and stable isotope data that indicate that there was substantial crustal input into the Glen Sanda Granodiorite magma(s).

2) The cogenetic zircon material of the Loch Sunart Granodiorite (*ie.* the grains without the cores and the rims of grains with cores) generally has much lower concentrations of Y, the HREE, Th and U than the cogenetic zircon material of the Glen Sanda Granodiorite, this is despite the fact that the Glen Sanda Granodiorite has lower overall concentration of Y and the REE. This is primarily thought to be due to higher zircon/liquid partition coefficients in the Glen Sanda Granodiorite melt.

The titanites from both Loch Sunart Granodiorite and the BPSRG1 Glen Sanda Granodiorite have compositional sector zoning which is a ubiquitously-developed feature in these rocks. This implies that the kinetic processes responsible for compositional sector zoning in titanite normally accompany nucleation and growth and that compositional sector zoning does not represent a response to an unusual set of growth conditions developed only locally within the magma. The compositional range displayed by the titanites from five rocks from the Strontian Complex (four from the Loch Sunart Granodiorite and one from the Glen Sanda Granodiorite) is dominantly a function of the fact that they have compositional sector zoning. Titanites from each of the five samples samples show a very similar range of composition to one another and thus the influence of the medium of growth on their composition would thus appear to be negligible and that the kinetics of titanite growth largely determine the internal compositional range.

The fact that only the HREE were ever detected in the zircons from BPSRT1 and BPSRG1 is consistent with the zircons from both samples having HREE enriched rock normalised distribution patterns. The apatites from BPSRT1 have LREE patterns (only the LREE were ever detected), this contrasts with the apatites from BPSRG1 which have HREE enriched patterns (almost complete patterns were obtainable for the apatites from BPSRG1). Titanite is not present in the BPSRG1 sample, however titanites from the BPSRT1 sample give rock normalised distribution patterns for the REE that are generally flat, although there

are notable relative depletions in the LREE, particularly La and Ce. The generally flat patterns shown by the titanites is a consequence of the fact they contain most of the whole rock budget of the REE. Since both the zircons and titanites of BPSRG1 are HREE-enriched relative to whole rock it is thought that the LREE are contained within allanite and monazite both of which are known to be present within the Glen Sanda Granodiorite but of low modal abundance.

Even though the whole rock samples BPSRT1 and BPSRG1 have very similar chondrite-normalised REE distribution patterns the rock-normalised REE distribution patterns for their accessory phases are very variable within a single rock and between rocks. This variability has three prime causes: 1) the different accessory minerals have different relative mineral/melt partition coefficients for the REE; 2) the accessory mineral assemblage present; and 3) the crystallization order of the accessory mineral assemblage. The importance of the last two points is best illustrated by the fact that the apatites from the two samples have very different rock-normalised REE distributions, this is thought to be due to the accessory mineral assemblages that are present in each of the rocks (BPSRT1: titanite, apatite and zircon; BPSRG1 apatite, zircon, allanite and monazite) and the crystallization order of that assemblage.

10.1.3) Sm-Nd isotopic disequilibrium in zircons.

Sm-Nd isotopic analysis of accessory phases from three rocks of the Strontian Complex show that the apatite and titanite separates from each rock are in isotopic equilibrium with each other and their respective host rocks. However, two zircon separates from the Glen Sanda Granodiorite were not in Sm-Nd isotopic equilibrium with their host rock, this is thought to be due to the presence of an inherited component to their Sm-Nd isotopic systematics. Thus the diffusion of the REE within zircons at crustal melting temperatures must have been sufficiently slow to prevent complete Sm-Nd isotopic equilibration within the time-scale of the Strontian magmatic event, *ie.* initial melting through to final crystallization. The strongly negative εNd_{425} values of the zircons, given that they have $^{147}Sm/^{144}Nd$ which are greater than Bulk Earth, is taken to indicate that the inherited component of the zircons crystallized from, or was equilibrated with, material that had been resident in the crust for a considerable period of time. In addition, the fact that the zircons have εNd_{425} values which are more negative than their host rock indicates that the host rock was produced by mixing of at least two isotopically distinct sources.

10.2) SUGGESTIONS FOR FUTURE WORK.

10.2.1) Accessory mineral zoning.

Limited studies of other accessory phases, notably apatite and allanite, have shown that these phases are also commonly zoned and thus worthy of study. As many of the zoning textures in zircon and titanite described here were not visible using conventional transmitted or reflected light optical techniques it is likely that other minerals (included here are major phases) previously thought to be unzoned may be similarly zoned.

Many of the zircon and titanite zoning textures identified during the course of this research apparently represent chemical disequilibrium and such textures appear to be the norm (and are by no means exceptional). This casts doubt on the validity of the use of experimentally-determined equilibrium partition coefficients for elements that concentrate into these phases. The work presented here suggests that the determination of effective partition coefficients from the study of 'real' systems may potentially be of more use, partition coefficients determined on minerals found in crystal-poor volcanic rocks may yield more reliable information about effective partition coefficients than studies of plutonic rocks.

In addition to looking at other minerals, it may be instructive to look at the zoning textures of accessory minerals found in other environments, of particular interest would be rocks of peralkaline composition. On the basis of experimental work (*eg.* Henderson *et al.*, 1985) it is known that the diffusion of elements in silicate melts is strongly dependent on the melt structure and that in turn melt structure is a function of melt composition. Several studies (*eg.* Watson and Harrison, 1983, and Gwinn & Hess, 1989) have noted that the solubility of highly charged cations (*eg.* Ti^{4+}, Fe^{3+} and Zr^{4+}) is dependent on the excess concentration of alkalis needed to charge balance aluminium, excess alkalies resulting in increased solubilities for highly charged cations; Gwinn & Hess (1989) termed this the "peralkaline effect". Baker (1990) experimentally demonstrated that chemical diffusivities of most elements in silicate magmas (except the alkalis) is dependent on the alkali/aluminium ratio of the magma such that at a ratio of unity (metaluminous) there is a diffusivity minimum and in strongly peraluminous and peralkaline melts diffusivities are generally higher. Baker (1990) also stated that these findings are in accord with those of Riebling (1966) who demonstrated that for melts of 75 mol% SiO_2 in the Na_2O-Al_2O_3-SiO_2 system the viscosity coefficient goes through a maximum where the alkali/alumina ratio is equal to one. Other studies have suggested that within silicate melts the REE may complex with F (Ponader & Brown, 1989). All these features suggest that the behaviour of highly charged elements within peralkaline and F-rich melts may contrast strongly with the behaviour of highly charged elements within calc-alkaline magmas. Given that the rate of processes such as diffusion may be very different in peralkaline and F-rich magmas compared with peraluminous and metaluminous systems it is possible that the zoning textures of accessory phases grown in such magmas may be very different from those found in calc-alkaline rocks.

Studying the zoning textures of minerals thought to have crystallized from, or have been altered by, late stage melts and fluids may allow us to understand better the mobility of elements in such systems. The identification of vein-like (replacive) Ba-rich areas in alkali-feldspars from the Strontian Complex (see Section 7.5.2) is a simple but effective example of how careful textural studies of minerals, in conjunction with quantitative electron microprobe analysis, can reveal the mobility of elements in magmatic and hydrothermal systems.

10.2.2) Sm-Nd isotopes in REE-rich accessory phases.

The occurrence of Sm-Nd isotopic disequilibrium in zircons recorded in the Glen Sanda Granodiorite of the Strontian Complex is unique in the literature. It is important to test whether this occurs in other granitoid zircon populations with known U-Pb isotope inheritance. Abrasion of zircon grains with Sm-Nd isotopic disequilibrium caused by inheritance would concentrate the core material and allow more representative $^{143}Nd/^{144}Nd$ and $^{147}Sm/^{144}Nd$ ratios for the cores to be obtained and this in turn would help further to constrain potential models of the $^{143}Nd/^{144}Nd$-time evolution of the inherited zircons. An alternative, although less complete alternative, would be to use an ion microprobe to obtain elemental Sm/Nd ratios (Reed, 1986) by selective analysis of zircon cores. From Sm/Nd elemental ratios it is possible to calculate, using the known relative abundances of Sm and Nd isotopes, $^{147}Sm/^{144}Nd$ ratios. Knowledge of $^{147}Sm/^{144}Nd$ ratios would help constrain, to some extent, models of the Nd isotopic evolution of the inherited zircons. The ion microprobe is not able to measure $^{143}Nd/^{144}Nd$ ratios with sufficient precision.

If inherited zircon populations do commonly contain a variety of ages then, unless selective Sm-Nd isotopic analysis of individual cores is possible (which at present is not the case), it will be difficult to quantify further the models outlined in Chapter 9. However, even the semi-quantitative information that can be derived from the occurrence of Sm-Nd isotopic disequilibrium in zircons may be of considerable value in determining the nature of source regions and processes that occurred during granitoid magma production.

Clearly the next problem that needs addressing is the behaviour during heating of the Sm-Nd isotopic systematics of other mineral phases, this may be best addressed through the study of REE-rich phases in well characterised high-grade metamorphic terrains. For example, Vance & O'Nions (1990) on the basis of chemical and isotopic studies of zoned garnets stated "it is possible that large ($\geq$ 10 mm) garnets may remain closed systems for Nd and Sm diffusion right up to granulite facies temperatures". Laboratory based experimental studies may be of limited use because of the long duration experimental runs that would be necessary to produce meaningful results.

10.3) CONCLUDING REMARKS.

The results presented here emphatically confirm the assertion of E.B. Watson and T.M. Harrison who, in their 1984 review paper, "Accessory minerals and the geochemical evolution of crustal magmatic systems: a summary and prospectus of experimental approaches", stated the following:

"Our current belief is that complete trace element and isotopic equilibrium between crustal melts and residual accessory minerals will rarely be attained...it is specifically those increases in preserved *disequilibrium* (their italics) that may contain the most information about rock histories - information that can be extracted only if the fundamental accessory-phase parameters have been well characterized".

Bibliography.

AFTALION, M. & VAN BREEMEN, O, 1980. U-Pb Zircon, Monazite and Rb-Sr Whole Rock Systematics of Granitic Gneiss and Psammitic to Semi-Pelitic Host Gneiss From Glenfinnan, Northwestern Scotland. *Contributions to Mineralogy and Petrology*, **72**, 87-98.

ALBARÈDE, F. & BOTTINGA, Y., 1972. Kinetic disequilibrium in trace element partitioning between phenocryst and host lava. *Geochimica et Cosmochimica Acta*, **36**, 141-156.

ÅMLI, R. & GRIFFIN, W.L., 1975. Microprobe Analysis of REE Minerals Using Empirical Correction Factors. *American Mineralogist*, **60**, 599-606.

ANONYMOUS, 1959. *Summary of Progress of the Geological Survey of Great Britain and the Museum of Practical Geology for the Year 1958*. HMSO, London.

ASHWORTH, J.R. & TYLER, I.M., 1973. The distribution of metamorphic temperatures around the Strontian Granodiorite. *Geological Magazine*, **120**, 281-290.

BACON, C.R., 1989. Crystallization of accessory phases in magmas by local saturation adjacent to phenocrysts. *Geochimica et Cosmochimica Acta*, **53**, 1055-1066.

BAKER. D.R., 1989. Tracer versus trace element diffusion: Diffusional decoupling of Sr concentration from Sr isotopic composition. *Geochimica et Cosmochimica Acta*, **53**, 3015-3023.

BAKER. D.R., 1990. Chemical interdiffusion of dacite and rhyolite: anhydrous measurements at 1 atm and 10 kbar, application of transition state theory, and diffusion in zoned magma chambers. *Contributions to Mineralogy and Petrology*, **104**, 407-423.

BARBEY, P., BERTRAND, J.-M., ANGOUA, S. & DAUTEL, D., 1989. Petrology and U/Pb geochronology of the Telohat migmatites, Aleksod, Central Hoggar, Algeria. *Contributions to Mineralogy and Petrology*, **101**, 207-219.

BERNAU, R. & FRANZ, G., 1987. Crystal chemistry and genesis of Nb-, V-, and Al-rich metamorphic titanites from Egypt and Greece. *The Canadian Mineralogist*, **25**, 695-705.

BESWICK, A.E. & CARMICHAEL, I.S.E., 1978. Constraints on Mantle Source Compositions Imposed by Phosphorous and the Rare-Earth Elements. *Contributions to Mineralogy and Petrology*, **67**, 317-330.

BLACK, L.P., WILLIAMS, I.S. & COMPSTON, W., 1986. Four zircon ages from one rock: the history of a 3930Ma-old granulite from Mount Sones, Enderby Land, Antartica. *Contributions to Mineralogy and Petrology*, **94**, 427-437.

BROOK, M., BREWER, M.S. & POWELL, D., 1976. Grenville age for rocks in the Moine of north-western Scotland. *Nature*, **260**, 515-517.

BROOKS, C.K., HENDERSON, P. & RØNSBO, J.G., 1981. Rare-earth partition between allanite and glass in the obsidian of Sandy Braes, Northern Ireland. *Mineralogical Magazine*, **44**, 157-160.

BROWN, P.E., 1983. Caledonian and Earlier Magmatism. In: CRAIG, G.Y. (Ed.), *Geology of Scotland*. Scottish Academic Press, Edinburgh, 167-204.

CAHN, J.W., HILLIG, W.B. & SEARS, G.W., 1964. The molecular mechanism of crystallization. *Acta Metallurgica*, **12**, 291-296.

CARUBA, R., BAUMER, A., MANO, J. & TURCO, G., 1975. Étude comparitive des

propriétés respectives de zircons hydroxylés synthétiques et de zircons métamictes naturels; hypothèse de genèse des malacons. Pétrologie, **1**, 57-70.

CHAPPELL, B.W. & WHITE, A.J.R., 1976. Plutonic rocks of the Lachlan mobile zone. *25th International Geological Congress Excursion Guide 13c.*

CHAPPELL, B.W., WHITE, A.J.R. & WYBORN, D., 1987. The Importance of Residual Source Material (Restite) in Granite Petrogenesis. *Journal of Petrology*, **28**, 1111-1138.

CHASE, A.B. & OSMER, J.A., 1966. Growth and Preferential Doping of Zircon and Thorite. *Journal of the Electrochemical Society*, **113**, 198-199.

CHIVAS, A.R., 1981. Geochemical Evidence for Magmatic Fluids in Porphyry Copper Mineralization. Part I. Mafic Silicates from the Koloula Igneous Complex. *Contributions to Mineralogy and Petrology*, **78**, 389-403.

CLARK, A.M., 1974. A tantalum-rich variety of sphene. *Mineralogical Magazine*, **39**, 55-61.

COMPSTON, W. & KRÖNER, A., 1988. Multiple zircon growth within early Archaean tonalitic gneiss from the Ancient Gneiss Complex, Swaziland. *Earth and Planetary Science Letters*, **87**, 13-28.

COPELAND, P., PARRISH, R.R. & HARRISON, T.M., 1988. Identification of inherited radiogenic Pb in monazite and its implications for U-Pb systematics. *Nature*, **333**, 760-763.

CZAMANSKE, G.K. & WONES, D.R., 1973. Oxidation During Magmatic Differentiation Finnmarka Complex, Oslo Area, Norway: Part 2, The Mafic Silicates. *Journal of Petrology*, **14**, 349-380.

DEER, W.A., HOWIE, R.A. & ZUSSMAN, J., 1982. *Rock-Forming Minerals: Volume 1A - Second Edition. Orthosilicates.* Longman, London.

DONALDSON, C.H., 1979. An Experimental Investigation of the Delay in Nucleation of Olivine in Mafic Magmas. *Contributions to Mineralogy and Petrology*, **69**, 21-32.

DONALDSON, C.H., 1985. A comment on crystal shapes resulting from dissolution in magmas. *Mineralogical Magazine*, **49**, 129-132.

DOWNES, M.J., 1974. Sector and oscillatory zoning in calcic augites from M. Etna, Sicily. *Contributions to Mineralogy and Petrology*, **47**, 187-196.

DOWTY, E., 1976. Crystal structure and crystal growth: II. Sector zoning in minerals. *American Mineralogist*, **61**, 460-469.

DOWTY, E., 1980. Crystal growth and nucleation theory and the numerical simulation of igneous crystallization. In: HARGRAVES, R.B. (Ed.), *Physics of Magmatic Processes.* Princeton University Press, Princeton, 419-485.

DRAKE, M.J. & WEILL, D.F., 1972. New rare earth element standards for microprobe analysis. *Chemical Geology*, **10**, 179-181.

DUNCUMB, P. & REED, S.J.B., 1968. In: HEINRICH, F.J. (Ed.), *Quantitative Electron Microprobe Analysis.* National Bureau of Standards Special Publication, **298**.

EWART, A., 1979. A review of the mineralogy and chemistry of the Tertiary-Recent dacitic, latitic, rhyolitic and related salic volcanic rocks. In: BARKER, F. (Ed.), *Trondhjemites,*

Dacites and Related Rocks. Developments in Petrology, 6, Elsevier, Amsterdam, 13-122.

EXLEY, R.A., 1980. Microprobe studies of REE-rich accessory minerals: implications for Skye granite petrogenesis and REE mobility in hydrothermal systems. *Earth and Planetary Science Letters*, **48**, 97-110.

FIELDING, P.E., 1970. The distribution of uranium, rare earths, and color centers in a crystal of natural zircon. *American Mineralogist*, **55**, 428-440.

FRANZ, G. & SPEAR, F.S., 1985. Aluminous titanite (sphene) from the Eclogite Zone, south-central Tauern Window, Austria. *Chemical Geology*, **50**, 33-46.

FUTA, K., 1981. Sm-Nd systematics of a tonalitic augen gneiss and its constituent minerals from northern Michigan. *Geochimica et Cosmochimica Acta*, **45**, 1245-1249.

GALLAGHER, M.J., 1964. Rock Alteration in Some Mineralized Basic Dykes in Britain. *Transactions of the Institution of Mining and Metallurgy*, **73**, 826-840.

GAMBLE, R.P. & TAYLOR, L.A., 1980. Crystal/liquid partitioning in augite: effects of cooling rate. *Earth and Planetary Science Letters*, **47**, 21-33

GEE, D.G., GUEZOU, J.C., ROBERTS, D. & WOLFF, F.C., 1985. The central-southern part of the Scandinavian Caledonides. In: GEE, D.G. & STURT, B.A. (Eds.), *The Caledonide Orogen - Scandinavia and Related Areas*. Wiley, Chichester, 109-133.

GEIST, D.J., MYERS, J.D. & FROST, C.D., 1988. Megacryst-bulk rock isotopic disequilibrium as an indicator of contamination processes: The Edgecumbe Volcanic Field, SE Alaska. *Contributions to Mineralogy and Petrology*, **99**, 105-112.

GOLDSTEIN, J.I., NEWBURY, D.E., ECHLIN, P., JOY, D.C., FIORI, C. & LIFSHIN, E., 1981. *Scanning Electron Microscopy and X-Ray Microanalysis*. Plenum Press, New York.

GOVINDARAJU, K., 1984. Compilation of working values and sample descriptions for 170 international reference samples of mainly silicate rocks and minerals. *Geostandards Newsletter*, **8**, Special Issue.

GREEN, T.H. & PEARSON, N.J., 1986a. Rare-earth element partitioning between sphene and coexisting silicate liquid at high pressure and temperature. *Chemical Geology*, **55**, 105-119.

GREEN, T.H. & PEARSON, N.J., 1986b. Ti-rich accessory phase saturation in hydrous mafic-felsic compositions at high P,T. *Chemical Geology*, **54**, 185-201.

GREEN, T.H. & WATSON, E.B., 1982. Crystallization of Apatite in Natural Magmas Under High Pressure, Hydrous Conditions, with Particular Reference to `Orogenic` Rock Series. *Contributions to Mineralogy and Petrology*, **79**, 96-105.

GROMET, L.P. & SILVER, L.T., 1983. Rare earth element distributions among minerals in a granodiorite and their petrogenetic implications. *Geochimica et Cosmochimica Acta*, **47**, 925-939.

GULSON, B.L. & KROGH, T.E., 1973. Old lead components in the young Bergell Massif, south-east Swiss Alps. *Contributions to Mineralogy and Petrology*, **40**, 239-252.

GWINN, R. & HESS, P.C., 1989. Iron and titanium solution properties in peraluminous and

peralkaline rhyolitic liquids. *Contributions to Mineralogy and Petrology*, **101**, 326-338.

HALL, A., 1987. *Igneous Petrology*. Longman Scientific and Technical, Harlow, England.

HALL, M.G. & LLOYD, G.E., 1983. The SEM examination of geological samples with a semiconductor backscattered-electron detector: reply. *American Mineralogist*, **68**, 843-844.

HALLIDAY, A.N. 1984. Coupled Sm-Nd and U-Pb systematics in late Caledonian granites and the basement under northern Britain. *Nature*, **307**, 229-233.

HALLIDAY, A.N., AFTALION, M., VAN BREEMEN, O. & JOCELYN, J., 1979. Petrogenetic significance of Rb-Sr and U-Pb isotopic systems in the 400 Ma old British Isles granitoids and their hosts. In: HARRIS, A.L., HOLLAND, C.H. & LEAKE, B.E. (Eds.), *The Caledonides of the British Isles - reviewed*. Geological Society of London Special Publication. Scottish Academic Press, Edinburgh, 653-661.

HALLIDAY, A.N., FALLICK, A.E., HUTCHESON, J. & HILDRETH, W., 1984. A Nd, Sr and O isotopic investigation into the causes of chemical and isotopic zonation in the Bishop Tuff, California. *Earth and Planetary Science Letters*, **68**, 379-391.

HAMILTON, P.J., O'NIONS, R.K. & PANKHURST, R.J., 1980. Isotopic evidence for the provenance of some Caledonian granites. *Nature*, **287**, 279-284.

HAMILTON, P.J., EVENSON, N.M., O'NIONS, R.K. & TARNEY, J., 1979. Sm-Nd systematics of Lewisian gneisses: implications for the origin of granulites. *Nature*, **277**, 25-28.

HAMMARSTROM, J.M. & ZEN, E-AN, 1986. Aluminium in hornblende: an empirical igneous geobarometer. *American Mineralogist*, **71**, 1297-1313.

HARMON, R.S., 1984. Stable isotope geochemistry of Caledonian granitoids from the British Isles and east Greenland. *Physics of Earth and Planetary Interiors*, **35**, 105-120.

HARMON, R.S. & HALLIDAY, A.N., 1980. Oxygen and strontium isotope relationships in the British late Caledonian granites. *Nature*, **283**, 21-25.

HARRISON, T.M., ALEINIKOFF, J.N. & COMPSTON, W., 1987. Observations and controls on the occurrence of inherited zircon in Concord-type granitoids, New Hampshire. *Geochimica et Cosmochimica Acta*, **51**, 2549-2558.

HARRISON, T.M. & WATSON, E.B., 1984. The behaviour of apatite during crustal anatexis: Equilibrium and kinetic considerations. *Geochimica et Cosmochimica*, **48**, 1467-1477.

HARRISON, T.M. & WATSON, E.B., 1983. Kinetics of Zircon Dissolution and Zirconium Diffusion In Granitic Melts of Variable Water Content. *Contributions to Mineralogy and Petrology*, **84**, 66-72.

HARVEY, P.K., TAYLOR, D.M., HENDRY, R.D. & BANCROFT, F., 1973. An accurate fusion method for the analysis of rocks and chemically related materials by X-ray fluorescence spectrometry. X-Ray *Spectrometry*, **2**, 33-44.

HEIER, K.S., 1962. Trace elements in feldspars - a review. *Norsk Geologisk Tidsskrift*, **42**, 415-454.

HEINRICH, K.F.J., 1966. In: CASTAING, R., DESCHAMPS, P. & PHILIBERT, J. (Eds.), *X-Ray Optics and Microanalysis, 4th International Congress on X-Ray Optics and*

Microanalysis. Hermann, Paris.

HEINRICH, K.F.J., 1969. National Bureau of Standards Technical Note 521.

HENDERSON, P., NOLAN, J., CUNNINGHAM, G.C. & LOWRY, R.K., 1985. Structural controls and mechanisms of diffusion in natural silicate melts. *Contributions to Mineralogy and Petrology*, **89**, 263-272.

HENDRY, D.A.F., CHIVAS, A.R., LONG, J.V.P. & REED, S.J.B., 1985. Chemical differences between minerals from mineralizing and barren intrusions from some North American porphyry copper deposits. *Contributions to Mineralogy and Petrology*, **89**, 317-329.

HOFFMAN, J.F. & LONG, J.V.P., 1984. Unusual sector zoning in Lewisian zircons. *Mineralogical Magazine*, **48**, 513-517.

HOLDEN, P., 1987. *Source and equilibration studies of xenoliths from the Caledonian Granites of Scotland*. Unpublished Ph.D. Thesis, University of St. Andrews.

HOLDEN, P., HALLIDAY, A.N. & STEPHENS, W.E., 1987. Neodymium and strontium isotope content of microdiorite enclaves points to mantle input to granitoid production. *Nature*, **330**, 53-56.

HOLDER, M.T., 1979. An emplacement mechanism for post-tectonic granites and its implications for their geochemical features. In: ATHERTON, M.P. & TARNEY, J. (Eds.), *Origin of Granite Batholiths: Geochemical Evidence*. Shiva Publishing Ltd, Nantwich, England, 116-128.

HOLLISTER, L.S., 1970. Origin, mechanism, and consequences of compositional sector zoning in staurolite. *American Mineralogist*, **55**, 742-766.

HOLLISTER, L.S., GRISSOM, G.C., PETERS, E.K., STOWELL, H.H. & SISSON, V.B., 1987. Confirmation of the empirical correlation of Al in hornblende with pressure of solidification of calc-alkaline plutons. *American Mineralogist*, **72**, 231-239.

HOLMES, A., 1921. *Petrographic Methods and Calculations*. Murby and Company, London.

HOSOYA, S. & KITAMURA, M., 1978. *In-situ* observation of recovery process from rounded to faceted morphology in $NaClO_3$. *Mineralogical Journal (Japan)*, **9**, 137-146.

HUTTON, D.H.W., 1988a. Granite emplacement mechanisms and tectonic controls: inferences from deformation studies. *Transactions of the Royal Society of Edinburgh: Earth Sciences*, **79**, 245-255.

HUTTON, D.H.W., 1988b. Igneous emplacement in a shear-zone termination: The biotite granite at Strontian, Scotland. *Geological Society of America Bulletin*, **100**, 1392-1399.

INSTITUTE OF GEOLOGICAL SCIENCES (now the British Geological Survey). Scotland Solid Sheets 44, 52 and 53. 1:50,000 Map Series.

IRVINE, T.N. & BARAGAR, W.R.A., 1971. A Guide to the Chemical Classification of the Common Volcanic Rocks. *Canadian Journal of Earth Sciences*, **8**, 523-548.

JOHNSON, M.R.W., 1983. Torridonian-Moine. In: CRAIG, G.Y. (Ed.). *Geology of Scotland*. Scottish Academic Press, Edinburgh, 49-75.

JOHNSTONE, G.S., SMITH, D.I. & HARRIS, A.L., 1969. The Moinian assemblage of Scotland. In: KAY, M. (Ed.). North Atlantic-geology and continental drift: a symposium.

Memoir of the American Association of Petroleum Geologists, **12**, 229-234.

KIRKPATRICK, R.J., 1975. Crystal growth from a melt: A review. *American Mineralogist*, **60**, 798-814.

KIRKPATRICK, R.J., 1981. Kinetics of crystallization of igneous rocks. In: LASAGA, A.C. & KIRKPATRICK, R.J. (Eds.), *Reviews in Mineralogy, Volume 8, Kinetcs of Geochemical Processes*, Mineralogical Society of America, 321-398.

KITAMURA, M & SUNAGAWA, I, 1977. The effective distribution of solute and the anisotropy of a crystal. *International Conference on Crystal Growth, Collected Abstracts*, **5**, 91.

KOUCHI, A., HOSOYA, S., KITAMURA, M., TAKEI, H. & SUNAGAWA, I., 1983a. The Effects of Crystallographic Orientation, Interface Type and Growth Kinetics on Ni Distribution Between Olivine and Its Melt. *Physics and Chemistry of Minerals*, **9**, 167-172.

KOUCHI, A., SUGAWARA, Y., KASHIMA, K. & SUNAGAWA, I., 1983b. Laboratory Growth of Sector Zoned Clinopyroxenes in the System $CaMgSi_2O_6$-$CaTiAl_2O_6$. *Contributions to Mineralogy and Petrology*, **83**, 177-184.

KROGH, T.E., 1982a. Improved accuracy of U-Pb zircon dating by the creation of more concordant fractions using a high gradient magnetic separation technique. *Geochimica et Cosmochimica Acta*, **46**, 631-635.

KROGH, T.E., 1982b. Improved accuracy of U-Pb zircon ages by the creation of more concordant systems using an air abrasion technique. *Geochimica et Cosmochimica Acta*, **46**, 637-649.

KROGH, T.E., 1986. Single zircon analysis and the provenance of Meguma and Spruce Brook sediments in eastern Canada. *Terra Cognita*, **6**, 152.

LEAKE, B.E., 1978. Nomenclature of amphiboles. *Mineralogical Magazine*, **42**, 533-63.

LARSEN, L.M., 1981. Sector Zoned Aegirine From the Ilimaussaq Alkaline Intrusion, South Greenland. *Contributions to Mineralogy and Petrology*, **76**, 285-291.

LAOUAR, R., 1987. *A sulphur isotope study of the Caledonian granites of Britain and Ireland.* Unpublished M.Sc. Thesis, University of Glasgow.

LIPOVA, I.M. & MAYEVA, M.M., 1971. The relation of Zr/Hf ratio in zircon to crystal morphology. *Geochemistry International*, **8**, 785-791. (Translated from Geokhimiya, No. 10 (1971), 1261-1267).

LLOYD, G.E., 1987. Atomic number and crystallographic contrast images with the SEM: a review of backscattered electron techniques. *Mineralogical Magazine*, **51**, 3-19.

LOFGREN, G., 1973. Experimental crystallization of synthetic plagioclase at prescribed cooling rates (abstract). *EOS Transactions American Geophysical Union*, **54**, 482.

LOFGREN, G., 1980. Experimental studies on the dynamic crystallization of silicate melts. In: HARGRAVES, R.B. (Ed.), *Physics of Magmatic Processes*. Princeton University Press, Princeton, 487-551.

LONG, P.E., 1978. Experimental determination of partition coefficients for Rb, Sr and Ba between alkali feldspar and silicate liquid. *Geochimica et Cosmochimica Acta*, **42**,

833-846.

MACKIE, W., 1926. The Heavier Accessory Minerals in the Granites of Scotland. *Transactions of the Edinburgh Geolological Society*, **12**, 22-40.

MAHOOD, G. & HILDRETH, W., 1983. Large partition coefficients for trace elements in high-silica rhyolites. *Geochimica et Cosmochimica Acta*, **47**, 11-30.

MACGREGOR, A.G. & KENNEDY, W.Q., 1932. The Morvern-Strontian 'Granite'. *Summary of Progress of the Geological Survey for 1931 - Part II*, 105-119.

MACKENZIE, W.S., DONALDSON, C.H. & GUILFORD, C., 1982. *Atlas of igneous rocks and their textures*. Longman, London.

MARSTON, R.J., 1970. The Foyers granitic complex, Inverness-shire, Scotland. *Quarterly Journal of the Geological Society of London*, **126**, 331-368.

MERCY, E.L.P., 1963. The geochemistry of some Caledonian granitic and metasedimentary rocks. In: JOHNSON, M.R.W. & STEWART, F.H. (Eds.), *The British Caledonides*. Oliver & Boyd, Edinburgh and London, 189-215.

MILLER, C.F., WATSON, E.B. & HARRISON, T.M., 1988. Perspectives on the source, segregation and transport of granitoid magmas. *Transactions of the Royal Society of Edinburgh: Earth Sciences*, **79**, 135-156.

MILLER, J.A. & BROWN, P.E., 1965. Potassium-Argon Age Studies in Scotland. *Geological Magazine*, **102**, 106-134.

MITTLEFEHLDT, D.W. & MILLER, C.F., 1983. Geochemistry of the Sweetwater Wash Pluton, California: Implications for "anomalous" trace element behaviour during differentiation of felsic magmas. *Geochimica et Cosmochimica Acta*, **47**, 109-124.

MUNRO, M., 1965. Some structural features of the Caledonian granitic complex at Strontian, Argyllshire. *Scottish Journal of Geology*, **1**, 152-175.

MUNRO, M., 1973. Structures in the south-eastern portion of the Strontian granitic complex, Argyllshire. *Scottish Journal of Geology*, **9**, 99-108.

MURATA, K., 1973. *Scanning Electron Microscopy/1973.*. IIT Research Institute, Chicago.

NAGASAWA, H., 1970. Rare earth concentrations in zircons and apatites and their host dacites and granites. *Earth and Planetary Science Letters*, **9**, 359-364.

NAKAMURA, N., 1974. Determination of REE, Ba, Fe, Mg, Na and K in carbonaceous and ordinary chondrites. *Geochimica et Cosmochimica Acta*, **38**, 757-775.

NAKAMURA, Y., 1973. Origin of Sector-Zoning of Igneous Clinopyroxenes. *American Mineralogist*, **58**, 986-990.

NASLUND, H.R., 1984. Supersaturation and crystal growth in the roof-zone of the Skaergaard magma chamber. *Contributions to Mineralogy and Petrology*, **86**, 89-93.

NORRISH, K. & HUTTON, J.T., 1969. An accurate X-ray spectrographic method for the analysis of a wide range of geological samples. *Geochimica et Cosmochimica Acta*, **33**, 431-453.

OATLEY, C.W., 1972. *The Scanning Electron Microscope*. Cambridge University Press.

OHNENSTETTER, D.R., REMOND, G., CLAUDE, J.M. CARUBA, R. & CESBRON, F., 1989. Hour-glass structure in zircons from Corsican ophiolitic albitite. *GAC Program With*

Abstracts, **14**, A73.

O'NIONS, R.K. & PANKHURST, R.J., 1974. Petrogenetic Significance of Isotope and Trace Element Variations in Volcanic Rocks From the Mid-Atlantic. *Journal of Petrology*, **15**, 603-634.

PANKHUSRT, R.J., 1979. Isotope and trace element evidence for the origin and evolution of Caledonian granites in the Scottish Highlands. In: ATHERTON, M.P. & TARNEY, J. (Eds.), *Origin of Granite Batholiths: Geochemical Evidence*. Shiva Publishing Ltd, Nantwich, England, 18-33.

PATERSON, B.A., STEPHENS, W.E. & HERD, D.A., 1989. Zoning in granitoid accessory minerals as revealed by backscattered electron imagery. *Mineralogical Magazine*, **53**, 55-61.

PETERMAN, Z.E., ZARTMAN, R.E. & SIMS, P.K., 1980. Tonalitic gneiss of early Archean age from northern Michigan. *Geological Society of America Special Publication*, **182**, 125.

PE-PIPER, G., 1988. Calcic amphiboles of mafic rocks of the Jeffers Brook plutonic complex, Nova Scotia, Canada. *American Mineralogist*, **73**, 993-1006.

PHILIBERT, J., 1963. In: PATTEE, H.H., COSSLETT, V.E. & ENGSTRÖM, A. (Eds.), *Proceedings of the 3rd International Symposium on X-ray Optics and X-ray Microanalysis*. Stanford University.

PIDGEON, R.T. & AFTALION, M., 1978. Cogenetic and inherited zircon U-Pb systems in granites: Palaeozoic granites of Scotland and England. In: BOWES, D.R. & LEAKE, B.E. (Eds.), *Crustal evolution in northwestern Britain and adjacent regions*. Geological Journal Special Issue No. 10. Seal House Press, Liverpool, 183-248.

POLDERVAART, A., 1956. Zircons in rocks. 2. Igneous rocks. *American Journal of Science*, **254**, 521-554.

PONADER, C.W. & BROWN, G.E., 1989. Rare earth elements in silicate glass/melt systems: II. Interactions of La, Gd and Yb with halogens. *Geochimica et Cosmochimica Acta*, **53**, 2905-2914.

PUPIN, J.-P., BONIN, B, TESSIER, M. & TURCO, G., 1978. Rôle de l'eau sur les caractères morphologiques et la cristallisation du zircon dans les granitoïdes. *Bulletin de la Société Géologique de France*, **20**, 721-725.

PURDY, J.W. & JÄGER, E., 1976. K-Ar ages on rock-forming minerals from the central Alps. *Memoir of the Institute of Geology and Mineralogy, University of Padova*, **30**, 1-31.

RATHBONE, P.A. & HARRIS, A.L., 1979. Basement-cover relationships at Lewisian inliers in the Moine rocks. In: HARRIS, A.L., HOLLAND, C.H. & LEAKE, B.E. (Eds.), *The Caledonides of the British Isles - reviewed.* Geological Society of London Special Publication. Scottish Academic Press, Edinburgh, 101-107.

REED, S.J.B., 1965. Characteristic fluorescence corrections in electron-probe microanalysis. *British Journal of Applied Physics*, **16**, 913.

REED, S.J.B., 1986. Ion microprobe determination of rare earth elements in accessory

minerals. *Mineralogical Magazine*, **50**, 3-15.

RIBBE, P.H., 1984. Titanite (Sphene). In: RIBBE, P.H. (Ed.), *Reviews in Mineralogy,Volume 5, Second Edition: Orthosilicates*. Mineralogical Society of America, 137-154.

RICHARD, P., SHIMIZU, N. & ALLÈGRE, C.J., 1976. $^{143}Nd/^{146}Nd$, a natural tracer: an application to oceanic basalts. *Earth and Planetary Science Letters*, **31**, 269-278.

RIEBLING, E.F., 1966. Structure of sodium aluminosilicate melts containing at least 50 mole % SiO_2 at 1500°C. *Journal of Chemical Physics*, **44**, 2857-2865.

ROBERTS, A.M. & HARRIS, A.L., 1983. The Loch Quoich Line - a limit of early Palaeozoic crustal reworking in the Moine of the Northern Highlands of Scotland. *Journal of the Geological Society*, **140**, 833-892.

ROBERTS, D. & WOLFF, F.C., 1981. Tectonostratigraphic development of the Trondheim region Caledonides, Central Norway. *Journal of Structural Geology*, **3**, 487-494.

ROBERTSON, D.C., 1988. *The Geological Evolution of the Krâkmo Area West Central Norway*. Unpublished B.Sc. Thesis, University of St. Andrews.

ROBINSON, K., GIBBS, G.V. & RIBBE, P.H., 1971. The structure of zircon: a comparison with garnet. *American Mineralogist*, **56**, 782-790.

ROBINSON, B.W. & NICKEL, E.H., 1983. The SEM examination of geological samples with a semiconductor backscattered-electron detector: discussion. *American Mineralogist*, **68**, 840-842.

ROBINSON, V.N.E., 1975. Back-scattered electron imaging. In: JOHARI, O. & CORRIN, I. (Eds.), *Scanning Electron Microscopy/1975.*, IITRI, Chicago.

ROBSON, D.A., 1987. The Persistence of Zircons in the Clastics of the Sedimentary Succession of Northern Britain: An SEM Study. In: Marshall, J.R. (Ed.), *Clastic Particles: Scanning Electron Microscopy and Shape Analysis of Sedimentary and Volcanic Clasts*. Van Nostrand Reinhold Company, New York, 51-64.

ROEDER, P.L., 1985. Electron-microprobe analysis of minerals for rare-earth elements: use of calculated peak-overlap corrections. *Canadian Mineralogist*, **23**, 263-271.

ROGERS, G. & DUNNING, G.R., 1990. Geochronology of appinitic and related granitic magmatism in the W Highlands of Scotland: constraints on the timing of transcurrent fault movement. *Journal of the Geological Society of London*, (in press).

ROMANS, P.A., BROWN, L.L. & WHITE, J.C., 1975. An Electron Microprobe Study of Yttrium, Rare Earth, and Phosphorous Distribution in Zoned and Ordinary Zircon. *American Mineralogist*, **60**, 475-480.

RYERSON, F.J. & HESS, P.C., 1980. The role of P_2O_5 in silicate melts. *Geochimica et Cosmochimica Acta*, **44**, 611-624.

RYERSON, F.J. & WATSON, E.B., 1987. Rutile saturation in magmas: implications for Ti-Nb-Ta depletion in island-arc basalts. *Earth and Planetary Science Letters*, **86**, 225-239.

SABINE, P.A., 1963. The Strontian granite complex, Argyllshire. *Bulletin of the Geolological Survey of Great Britain*, **20**, 6-42.

SAWKA, W.N., 1988. REE and trace element variations in accessory minerals and hornblende from the strongly zoned McMurry Meadows Pluton California. *Transactions of the Royal Society of Edinburgh: Earth Sciences*, **79**, 157-168.

SAWKA, W.N. & CHAPPELL, B.W., 1988. Fractionation of uranium, thorium and rare earth elements in a granodiorite: implications for heat production distributions in the Sierra Nevada batholith, California, U.S.A. *Geochimica et Cosmochimica Acta*, **52**, 1131-1143.

SAWKA, W.N., CHAPPELL, B.W. & NORRISH, K., 1984. Light-rare-earth-element zoning in sphene and allanite during granitoid fractionation. *Geology*, **12**, 131-134.

SCHÄRER, U. & ALLÈGRE, C.J., 1982. Investigation of the Archaean crust by single-grain dating of detrital zircon in a graywacke of the Slave Province, Canada. *Canadian Journal of Earth Sciences*, **94**, 438-451.

SCOTT, V.D. & LOVE, G., 1983. *Quantitative Electron-Probe Microanalysis*. Ellis Horwood Limited, Chichester.

SILVER, L.T. & DEUTSCH, S., 1963. Uranium-lead isotopic variations in zircons: A case study. *Journal of Geology*, **71**, 721-758.

SMITH, A.L., 1970. Sphene, perovskite and coexisting Fe-Ti oxide minerals. *American Mineralogist*, **55**, 264-269.

SPEER, J.A., 1982. Zircon. In: RIBBE, P.H. (Ed.), *Reviews in Mineralogy, Volume 5, Second Edition: Orthosilicates*. Mineralogical Society of America, 67-112.

SPEER, J.A., 1984. Micas in Igneous Rocks. In: BAILEY, S.W. (Ed.), *Reviews in Mineralogy, Volume 13: Micas*. Mineralogical Society of America, 299-356

STEIGER, R.H. & JÄGER, E., 1977. Subcommission on Geochronology: convention on the use of decay constants in geo- and cosmochronology. *Earth and Planetary Science Letters*, **36**, 359-362.

STEPHENS, W.E., 1988. Granitoid plutonism in the Caledonian orogen of Europe. In: HARRIS, A.L. & FETTES. D.J. (Eds.), *The Caledonian-Appalachian Orogen*. Geological Society of London Special Publication. Blackwell, Oxford, 389-403.

STRECKEISEN, A.L., 1976. To each plutonic rock its proper name. *Earth Science Reviews*, **12**, 1-33.

TURNER, D.L. & FORBES, R.B., 1976. K-Ar studies in two deep basement drill holes: a new geologic estimate of argon blocking for biotite. *EOS Transactions American Geophysical Union*, **57**, 353.

TYLER, I.M. & ASHWORTH, J.R., 1982. Sillimanite-Potash Feldspar Assemblages in Graphitic Pelites, Strontian Area, Scotland. *Contributions to Mineralogy and Petrology*, **81**, 18-29.

VAN BREEMEN, O. AFTALION, M., PANKHURST, R.J. & RICHARDSON, S.W., 1979. Age of the Glen Dessary Syenite, Inverness-shire: diachronous Palaeozoic metamorphism Across the Great Glen. *Scottish Journal of Geology*, **15**, 49-62.

VANCE, D. & O'NIONS, R.K., 1990. Isotopic chronometry of zoned garnets: growth kinetics and metamorphic histories. *Earth and Planetary Science Letters*, **97**, 227-240.

VERNE, J., 1864. *A Journey to the Centre of the Earth.* Minster Classics, London (© 1967 Lancer Books, Inc.).

WATSON, E. B., 1979. Zircon Saturation in Felsic Liquids: Experimental Results and Applications to Trace Element Geochemistry. *Contributions to Mineralogy and Petrology*, **70**, 407-419.

WATSON, E.B., 1980. Some experimentally determined zircon/liquid partition coefficients for the rare earth elements. *Geochimica et Cosmochimica Acta*, **44**, 895-897.

WATSON, E.B., 1985. Henry's law behaviour in simple systems and in magmas: Criteria for discerning concentration-dependant partition cosfficients in nature. *Geochimica et Cosmochimica Acta*, **49**, 917-923.

WATSON, E.B. & GREEN, T.H., 1981. Apatite/liquid partition coefficients for the rare earth elements and strontium. *Earth and Planetary Science Letters*, **56**, 405-421.

WATSON, E.B. & HARRISON, T.M., 1983. Zircon saturation revisited: temperature and composition effects in a variety of magma types. *Earth and Planetary Science Letters*, **64**, 295-304.

WATSON, E.B. & HARRISON, T.M., 1984. Accessory minerals and the geochemical evolution of crustal magmatic systems: a summary and prospectus of experimental approaches. *Physics of the Earth and Planetary Interiors*, **35**, 19-30.

WATSON, E.B., HARRISON, T.M. & RYERSON, F.J., 1985. Diffusion of Sm, Sr, and Pb in fluorapatite. *Geochimica et Cosmochimica Acta*, **49**, 1813-1823.

WILLIAMS, I.S., CHEN, Y., CHAPPELL, B.W. & COMPSTON, W., 1988. Dating sources of Bega Batholith granites by ion microprobe. *Geological Society of Australia Abstracts*, **21**, 424.

WILLIAMS, I.S. & CLAESSON, S., 1987. Isotopic evidence for the Precambrian provenance and Caledonian metamorphism of the high grade paragneisses from the Seve Nappes, Scandanavian Caledonides. II. Ion microprobe zircon U-Th-Pb. *Contributions to Mineralogy and Petrology*, **97**, 205-217.

WINCHESTER, J.A., 1974. The zonal pattern of regional metamorphism in the Scottish Caledonides. *Journal of the Geological Society*, **130**, 509-524.

WONES, D.R., 1989. Significance of the assemblage titanite + magnetite + quartz in granitic rocks. *American Mineralogist*, **74**, 744-749.

YELISEYEVA, O.P., 1977. Content and distribution of uranium, thorium, yttrium and the rare earth elements in accessory minerals in granitoids. *Geochemistry International*, **14** (No. 5), 37-49. (Translated from *Geokhimiya*, No. 9 (1977), 1338-1351).

ZHANG, Y, WALKER, D. & LESHER, C.E., 1989. Diffusive crystal dissolution. *Contributions to Mineralogy and Petrology*, **102**, 492-513.

Appendices.

Appendix 1) Sample localities.

Appendix 1A) The Caledonian Strontian Complex, NW Highlands, Scotland.

LSG NPF - Loch Sunart Granodiorite, Non-Porphyritic Facies.
LSG PF - Loch Sunart Granodiorite, Porphyritic Facies.
GSG - Glen Sanda Granodiorite.
A - Appinite
All samples, except those with BPSR stem, were collected by W.E. Stephens.

Sample	Grid Reference	Rock Unit/Type	Sample	Grid Reference	Rock Unit/Type
Str NO53	NM 864 531	LSG PF	83SR62	NM 855 641	LSG NPF
Str NO54	NM 833 656	LSG NPF	83SR63	NM 863 632	LSG NPF
Str NO55	NM 788 613	LSG PF	83SR64	NM 847 626	LSG NPF
Str NO56	NM 809 613	LSG PF	83SR65	NM 837 617	LSG PF
Str NO57	NM 784 610	LSG NPF	83SR66	NM 822 619	LSG PF
83SR18	NM 819 643	LSG NPF	83SR67	NM 824 634	LSG PF
83SR19	NM 815 652	LSG NPF	83SR68	NM 794 576	LSG PF
83SR20	NM 807 646	LSG NPF	83SR69	NM 813 588	LSG PF
83SR20A	NM 774 599	LSG NPF	83SR70	NM 819 575	LSG PF
83SR22	NM 796 638	LSG NPF	83SR72	NM 805 573	LSG PF
83SR23	NM 793 632	LSG NPF	83SR73	NM 795 555	LSG PF
83SR24	NM 787 626	LSG NPF	84SR2	NM 749 493	LSG PF
83SR25	NM 863 604	LSG NPF	84SR4	NM 766 490	GSG
83SR26	NM 885 541	LSG PF	84SR5	NM 775 480	GSG
83SR27	NM 745 508	LSG NPF	84SR6	NM 760 471	GSG
83SR28	NM 753 536	LSG NPF	84SR7	NM 751 466	LSG PF
83SR29	NM 756 534	LSG PF	84SR8	NM 742 470	LSG NPF
83SR30	NM 760 548	LSG NPF	84SR9	NM 743 483	LSG NPF
83SR31	NM 763 547	LSG PF	84SR10	NM 744 499	LSG NPF
83SR33	NM 780 554	LSG PF	84SR11	NM 753 413	GSG
83SR34	NM 776 565	LSG PF	84SR12	NM 748 413	GSG
83SR35	NM 771 577	LSG NPF	84SR13	NM 740 408	GSG
83SR36	NM 785 596	LSG PF	84SR14	NM 766 418	GSG
83SR38	NM 804 557	GSG	84SR15	NM 769 431	GSG
83SR39	NM 829 542	LSG NPF	84SR16	NM 782 429	GSG
83SR40	NM 841 532	LSG PF	84SR17	NM 790 435	GSG
83SR41	NM 870 524	LSG PF	84SR18	NM 799 443	GSG
83SR42	NM 762 506	LSG PF	84SR19	NM 798 453	GSG
83SR43	NM 775 500	GSG	84SR20	NM 808 458	GSG
83SR44	NM 785 506	GSG	84SR21	NM 815 463	GSG
83SR45	NM 786 517	GSG	84SR22	NM 826 470	GSG
83SR46	NM 788 525	GSG	84SR26	NM 860 594	LSG NPF
83SR47	NM 798 539	GSG	84SR27	NM 847 580	LSG NPF
83SR48	NM 789 545	GSG	84SR29	NM 832 587	LSG PF
83SR49	NM 783 537	LSG PF	84SR30	NM 844 593	LSG NPF
83SR50	NM 774 532	LSG PF	84SR31	NM 848 600	LSG NPF
83SR51	NM 833 503	GSG	84SR32	NM 836 658	LSG NPF
83SR52	NM 817 501	GSG	BPSRT1	NM 842 610	LSG NPF
83SR53	NM 810 491	GSG	BPSRT2	NM 860 608	LSG NPF
83SR54	NM 815 481	GSG	BPSRT3	NM 801 610	LSG PF
83SR55	NM 835 478	GSG	BPSRT4	NM 780 560	LSG PF
83SR56	NM 841 493	GSG	BPSRG1	NM 810 551	GSG
83SR57	NM 856 513	GSG	BPSRG2	NM 805 523	GSG
83SR58	NM 844 521	LSG PF	BPSRG3	NM 795 523	GSG
83SR59	NM 814 636	LSG PF	BPSRG4	NM 786 482	GSG
83SR60	NM 829 627	LSG PF	BPSRG5	NM 778 463	GSG
83SR61	NM 845 636	LSG NPF	BPSRA1	NM 795 603	A

Localities and sources of additional analyses used in the contouring of composition in the Loch Sunart Granodiorite:

Sample	Grid Reference	Rock Unit/Type	Source
S23/281	NM 853 651	LSG NPF	Mercy (1963)
S24/282	NM 849 646	LSG NPF	"
S25/283	NM 841 641	LSG NPF	"
S14/231	NM 794 633	LSG NPF	"
S15/232	NM 791 637	LSG NPF	"
S3/220	NM 777 609	LSG NPF	"
S2/219	NM 779 610	LSG NPF	"
S1/218	NM 783 611	LSG NPF	"
S6/223	NM 776 609	LSG NPF	"
S41864*	NM 761 505	LSG PF	Sabine (1963)
S205G	NM 846 610	LSG NPF	Holden (1987)
S208G	NM 786 612	LSG PF	"
S213G	NM 781 595	LSG PF	"
S340G	NM 806 603	LSG PF	"
S343G	NM 818 603	LSG PF	"
S347G	NM 796 602	LSG PF	"
S351G	NM 743 507	LSG NPF	"
S352G	NM 802 609	LSG PF	"

* Lab. No. 1734. First reported in *Summary of Progress of the Geological Survey for 1958* (published 1959).

Appendix 1B) Other sample localities.

Sample	Locality	Grid Reference	RockUnit/Type
RAT 11/1	Ratagain, NW Highlands, Scotland.	NG 8913 1733	Diorite.
RAT 13/1	Ratagain, NW Highlands, Scotland.	NG 8872 1741	Diorite.
AB 40	Kameruka, South East Australia.	-	Kameruka Granodiorite, part of the Bega Batholith of the Lachlan Fold Belt.
DR 55A	Kråkmo area, West Central Norway	6284 5705	Granodioritic augen gneiss (Robertson, 1988) Precambrian body part of Caledonian Tannas Nappe (Gee et al., 1985).

Ratagain samples collected by W.E. Stephens.
The Kameruka Granodiorite sample AB 40 was loaned by I.S. Williams of the Australian National University.
DR 55A was collected by D.C. Robertson.

Appendix 2) Methods.

Appendix 2A) Accessory mineral separation and preparation.

Accessory minerals were separated from three samples (BPSRA1, BPSRT1 and BPSRG1) using the facilities at the SURRC, East Kilbride. Approximately 20kg of each sample was crushed to less than 2mm using manual methods (a sledgehammer!), a Sturtevant jaw crusher with steel jaws and a disc grinder. Mineral separation was achieved by using a Wifley water table, a Frantz magnetic separator and heavy liquids. All the minerals used for ZCI studies and Sm-Nd isotopic analysis were either selected from the separates by hand picking or further purified by picking. The zircons mounted in epoxy were selected by size and morphological criteria so that subsequent grinding and polishing would cut all the grains as near their centres as possible. Several grain mounts were required to cover the range of sizes and shapes encountered.

Appendix 2B) Whole rock sample preparation for XRF, INAA and isotopic analysis.

Samples of 2-3kg were prepared by removing all surface weathering using a grinding wheel. The samples were then crushed using a Lake and Elliot hydraulic splitter with stainless steel jaws, a Sturtevant jaw crusher with steel jaws and a tungsten carbide Tema swing mill. The latter reduces the sample to less than 200 mesh.

Appendix 2C) Whole rock XRF analysis.

Major elements were determined using fused glass beads prepared from 0.5g of rock powder, 2.5g of Spectroflux 105 and ammonium nitrate as an oxidant. X-ray analysis was performed on a Philips PW 1212 using a Rh tube for primary excitation. Calibration was done with reference to a monitor (H12, supplied by K. Norrish) and 25 international rock standards. Matrix corrections were applied on an iterative basis by on-line computer. This is essentially the method of Norrish and Hutton (1969).

Trace elements were determined using pressed powder discs prepared with Moviol as a binder. Primary excitation was by Rh tube and analysed by either LiF 200 or LiF 220 crystals. The apparent fluorescence values are calculated for the better international standards by inverting the normal matrix correction procedure. The apparent fluorescence values are then regressed against their intensities (already corrected for line overlap or blank values) and the coefficients of the line used in analysis. All intensities are calculated in terms of a monitor used in the first sample position to help correct for machine drift.

Appendix 2D) Contour maps of composition: the 'Surface II Graphics System'.

Surface II is a computer programme used for the creation of contour maps of spatially distributed data. It has undergone several updates and modifications since it first became available in 1975, the version used here was last updated in September 1985. It contours a grid matrix of Z values estimated from irregularly spaced X,Y and Z sample data points For all the contour maps the same method was used; the 50 by 50 grid matrix of Z values was calculated from a distance weighted average of the nearest four data points, the scaled inverse distance squared being used as the weighting function, the contours were smoothed by interpolating to a finer grid using a bicubic spline interpolation. The contoured maps were subsequently traced onto a suitable base map of the Strontian Complex.

Appendix 2E) Whole rock INAA .

Samples of 0.1 g, including standards, were individually packed in Al foil; each packet was irradiated along with Fe wire flux monitors (Goodfellow Metals FE005152, 99.5 % purity) in a flux of 3.6×10^{12} $n.cm^{-2}s^{-1}$ for 6 hours. After 3-4 days the powders were separated from their flux monitors and transferred to ampules to ensure constant geometry during the counting process. Gamma emitters with energies below 150 KeV were counted with a LEPD Ge(Li) detector and gamma emitters with energies above 150 KeV were counted with an 80cm coaxial Ge(Li) detector. Counting was performed on two occasions; the first, 4-5 days after irradiation, the second, 11-12 days. Both detectors were controlled using an EGG-ORTEC Data Acquisition and Analysis System. Results were calculated by comparing the induced activities with those induced in the standard (BCR-1), measurements on the Fe wire flux monitors were used to correct for variations in the flux experienced by the samples. The REE concentrations of BCR-1 used in the calculation process are those recommended by Govindaraju (1984). A St. Andrews University, Department of Geology, internal standard (80/NSY - a nepheline syenite) was run as an unknown, the REE concentrations obtained closely agreed with previously determined values.

Appendix 2F) Major mineral electron microprobe analysis.

The microprobe analysis of the major phases were made on a JEOL 733 Superprobe equipped with WDS operating at 15kV and 20nA. A focussed beam was used for amphiboles, but it was defocussed for biotites (10μm diameter), plagioclase feldspars (10μm diameter) alkali-feldspars (50μm diameter) and for narrow Ba-rich areas in the alkali-feldspars (10μm diameter). Count times were 10s on peak and 5s on two background positions. The following standards were used; wollastonite (Si,Ca), corundum (Al), rutile (Ti), ferrite (Fe), manganese, periclase (Mg), jadeite (Na), orthoclase (K), barite (Ba). Apparent concentrations were corrected using the ZAF methods outlined in Section 2.3.1.

Appendix 2G) Sm-Nd isotopic analysis.

Weighed samples, both powdered rock and mineral separates, were dissolved in concentrated HF and 16M HNO_3 in sealed PFA teflon (Savillex) beakers. The zircon separates underwent the same dissolution procedure except that the HF/HNO_3 dissolution was performed in PTFE teflon bombs in an oven at 220°C for 5 days. After drying down the residue was redissolved in 16M HNO_3 and re-dried prior dissolution in 6M HCl. Sm and Nd concentrations were determined by isotope dilution, an aliquot of the sample was spiked with a ^{152}Sm spike and a ^{145}Nd spike, the amount of spike used was adjusted depending on the approximate concentration of Sm and Nd expected in the sample. Chemical separations of the bulk REE fraction were performed using standard cation exchange columns with techniques similar to Richard *et al.* (1976). Sm and Nd were isolated using PTFE teflon columns with techniques similar to Halliday *et al.* (1984). All analyses were performed on a fully automated V. G. Isomass 54E mass spectrometer. The separated Sm and Nd were run as metal species on triple filament assemblies, the sample being loaded in dilute H_3PO_4 on one of the Ta side filaments, the centre filament being Re. All isotopic data were corrected for machine discrimination using $^{146}Nd/^{144}Nd$ = 0.7219. The Johnson and Mathey Nd standard gave a $^{143}Nd/^{144}Nd$ value of 0.511839±17 (2σ) during the course of this study. Analytical blanks for Sm and Nd were <0.2ng. Sample εNd and T_{CHUR} (for whole rock determinations only) values were calculated using present day bulk earth parameters; $^{143}Nd/^{144}Nd$ = 0.512638, $^{147}Sm/^{144}Nd$ = 0.1966. Decay constant (λ) for $^{147}Sm = 6.54 \times 10^{-12}\ a^{-1}$.

Appendix 3: Electron microprobe analyses: zircons.

For analyses cross referenced with a plate number the first part of the analysis coding denotes the plate number (*eg.* 3.1); the second part denotes the analysis number, for analyses not cross referenced with a plate number a letter is used to denote different grains, this is then followed by the analysis number. All the concentrations are expressed as wt% oxide, Fe is calculated as FeO. n.d. - not detected. The structural formulae of the zircon analyses have been calculated to 16 oxygens.

Zircon Analyses: Strontian - BPSRT1.

	3.1/1	3.1/2	3.1/3	3.1/4	3.1/5	3.1/6	3.1/7	3.1/8
SiO_2	32.155	31.883	31.969	32.144	32.186	32.082	32.016	31.945
ZrO_2	65.518	66.018	66.212	66.365	65.857	65.717	65.841	66.383
HfO_2	1.553	1.511	1.451	1.445	1.429	1.474	1.460	1.524
Y_2O_3	n.d.	0.179	n.d.	0.053	0.112	0.021	0.043	n.d.
Al_2O_3	n.d.	n.d.	n.d.	n.d.	n.d.	n.d.	n.d.	n.d.
FeO	n.d.	n.d.	n.d.	n.d.	n.d.	n.d.	n.d.	n.d.
MnO	n.d.	n.d.	n.d.	n.d.	n.d.	n.d.	n.d.	n.d.
MgO	n.d.	n.d.	n.d.	n.d.	0.009	n.d.	n.d.	n.d.
CaO	n.d.	n.d.	n.d.	n.d.	n.d.	n.d.	n.d.	n.d.
P_2O_5	n.d.	n.d.	n.d.	n.d.	n.d.	n.d.	n.d.	n.d.
La_2O_3	n.d.	n.d.	n.d.	n.d.	n.d.	n.d.	n.d.	n.d.
Ce_2O_3	n.d.	n.d.	n.d.	n.d.	n.d.	n.d.	n.d.	n.d.
Pr_2O_3	n.d.	n.d.	n.d.	n.d.	n.d.	n.d.	n.d.	n.d.
Nd_2O_3	n.d.	n.d.	n.d.	n.d.	n.d.	n.d.	n.d.	n.d.
Sm_2O_3	n.d.	n.d.	n.d.	n.d.	n.d.	n.d.	n.d.	n.d.
Dy_2O_3	n.d.	n.d.	n.d.	n.d.	n.d.	n.d.	n.d.	n.d.
Er_2O_3	n.d.	0.041	n.d.	n.d.	0.032	0.039	0.028	n.d.
Yb_2O_3	0.027	0.099	n.d.	0.025	0.037	n.d.	0.028	0.023
ThO_2	n.d.	0.122	n.d.	0.038	0.038	n.d.	n.d.	0.059
UO_2	n.d.	0.197	n.d.	0.056	0.105	n.d.	n.d.	0.057
TOTAL	99.226	100.050	99.632	100.176	99.796	99.333	99.416	99.991
Si	3.98007	3.93944	3.94955	3.95477	3.96845	3.96921	3.96244	3.94081
Zr	3.95484	3.97789	3.98906	3.98173	3.95986	3.96495	3.97388	3.99358
Hf	0.05490	0.05331	0.05118	0.05074	0.05032	0.05205	0.05158	0.05367
Y	-	0.01179	-	0.00352	0.00734	0.00140	0.00288	-
Al	-	-	-	-	-	-	-	-
Fe2+	-	-	-	-	-	-	-	-
Mn	-	-	-	-	-	-	-	-
Mg	-	-	-	-	0.00172	-	-	-
Ca	-	-	-	-	-	-	-	-
P	-	-	-	-	-	-	-	-
La	-	-	-	-	-	-	-	-
Ce	-	-	-	-	-	-	-	-
Pr	-	-	-	-	-	-	-	-
Nd	-	-	-	-	-	-	-	-
Sm	-	-	-	-	-	-	-	-
Dy	-	-	-	-	-	-	-	-
Er	-	0.00162	-	-	0.00125	0.00153	-	-
Yb	0.00104	0.00374	-	0.00094	0.00140	-	0.00106	0.00089
Th	-	0.00344	-	0.00106	0.00108	-	0.00051	0.00165
U	-	0.00696	-	0.00197	0.00373	-	-	0.00202
TOTAL	7.99085	7.98640	7.98979	7.99473	7.99343	7.98774	7.99236	7.99262

Zircon Analyses: Strontian - BPSRT1.

	3.1/9	3.2/1	3.2/2	3.2/3	3.2/4	3.2/5	3.2/6	3.2/7
SiO_2	31.907	32.332	32.072	32.402	32.450	32.161	32.139	32.330
ZrO_2	65.971	66.184	65.260	65.942	66.350	65.832	66.032	66.276
HfO_2	1.420	1.583	1.575	1.554	1.704	1.485	1.614	1.559
Y_2O_3	0.077	n.d.	0.062	0.030	n.d.	0.060	n.d.	0.080
Al_2O_3	n.d.	n.d.	n.d.	n.d.	n.d.	n.d.	n.d.	n.d.
FeO	n.d.	n.d.	n.d.	0.036	n.d.	0.010	0.013	n.d.
MnO	n.d.	n.d.	n.d.	n.d.	n.d.	n.d.	n.d.	n.d.
MgO	n.d.	0.012	n.d.	n.d.	n.d.	n.d.	n.d.	n.d.
CaO	n.d.	n.d.	n.d.	n.d.	n.d.	n.d.	n.d.	n.d.
P_2O_5	n.d.	n.d.	n.d.	n.d.	n.d.	n.d.	n.d.	n.d.
La_2O_3	n.d.	n.d.	n.d.	n.d.	n.d.	n.d.	n.d.	n.d.
Ce_2O_3	n.d.	n.d.	n.d.	n.d.	n.d.	n.d.	n.d.	n.d.
Pr_2O_3	n.d.	n.d.	n.d.	n.d.	n.d.	n.d.	n.d.	n.d.
Nd_2O_3	n.d.	n.d.	n.d.	n.d.	n.d.	n.d.	n.d.	n.d.
Sm_2O_3	n.d.	n.d.	n.d.	n.d.	n.d.	n.d.	n.d.	n.d.
Dy_2O_3	n.d.	n.d.	n.d.	n.d.	n.d.	n.d.	n.d.	n.d.
Er_2O_3	0.020	n.d.	0.032	n.d.	n.d.	0.045	n.d.	n.d.
Yb_2O_3	0.032	0.028	0.043	n.d.	n.d.	0.017	n.d.	n.d.
ThO_2	0.046	n.d.	0.087	0.025	0.021	0.112	n.d.	0.110
UO_2	0.093	n.d.	0.148	0.034	0.055	0.145	0.035	0.135
TOTAL	99.566	100.139	99.279	100.023	100.580	99.867	99.833	100.490
Si	3.94965	3.97061	3.97714	3.98154	3.97073	3.96749	3.96301	3.96383
Zr	3.98242	3.96369	3.94646	3.95150	3.95928	3.96046	3.97070	3.96260
Hf	0.05017	0.05551	0.05576	0.05451	0.05954	0.05232	0.05682	0.05458
Y	0.00510	-	0.00409	0.00201	0.00073	0.00393	-	0.00522
Al	-	-	-	-	-	-	-	-
Fe2+	-	-	-	0.00372	-	0.00112	0.00136	-
Mn	-	-	-	-	-	-	-	-
Mg	-	0.00228	-	-	-	-	-	-
Ca	-	-	-	-	-	-	-	-
P	-	-	-	-	-	-	-	-
La	-	-	-	-	-	-	-	-
Ce	-	-	-	-	-	-	-	-
Pr	-	-	-	-	-	-	-	-
Nd	-	-	-	-	-	-	-	-
Sm	-	-	-	-	-	-	-	-
Dy	-	-	-	-	-	-	-	-
Er	0.00078	-	0.00125	-	-	0.00176	-	-
Yb	0.00123	0.00108	0.00166	-	-	0.00067	-	-
Th	0.00130	-	0.00246	0.00070	0.00060	0.00315	-	0.00308
U	0.00330	-	0.00525	0.00122	0.00193	0.00512	0.00123	0.00476
TOTAL	7.99395	7.99317	7.99407	7.99520	7.99281	7.99602	7.99312	7.99407

Zircon Analyses: Strontian - BPSRT1.

	3.2/8	3.2/9	3.2/10	3.2/11	3.2/12	3.2/13	3.2/14	3.2/15
SiO_2	32.458	31.939	32.077	32.161	32.279	32.360	32.278	32.255
ZrO_2	66.371	65.834	65.034	66.087	66.567	66.291	66.538	66.922
HfO_2	1.617	1.405	1.497	1.686	1.461	1.669	1.589	1.714
Y_2O_3	n.d.	0.092	0.039	0.080	0.053	n.d.	0.031	n.d.
Al_2O_3	n.d.	n.d.	n.d.	n.d.	n.d.	n.d.	n.d.	n.d.
FeO	n.d.	n.d.	n.d.	n.d.	n.d.	0.057	0.067	n.d.
MnO	n.d.	n.d.	n.d.	n.d.	n.d.	n.d.	n.d.	n.d.
MgO	n.d.	n.d.	n.d.	n.d.	n.d.	n.d.	n.d.	n.d.
CaO	n.d.	n.d.	n.d.	n.d.	n.d.	n.d.	n.d.	n.d.
P_2O_5	n.d.	n.d.	n.d.	0.042	n.d.	n.d.	n.d.	n.d.
La_2O_3	n.d.	n.d.	n.d.	n.d.	n.d.	n.d.	n.d.	n.d.
Ce_2O_3	n.d.	n.d.	n.d.	n.d.	n.d.	n.d.	n.d.	n.d.
Pr_2O_3	n.d.	n.d.	n.d.	n.d.	0.033	0.066	n.d.	n.d.
Nd_2O_3	n.d.	n.d.	n.d.	n.d.	n.d.	n.d.	0.045	n.d.
Sm_2O_3	n.d.	n.d.	n.d.	n.d.	n.d.	n.d.	n.d.	n.d.
Dy_2O_3	n.d.	n.d.	n.d.	n.d.	n.d.	n.d.	0.049	n.d.
Er_2O_3	0.044	n.d.	n.d.	0.035	n.d.	n.d.	n.d.	n.d.
Yb_2O_3	n.d.	0.067	n.d.	0.016	0.025	n.d.	0.035	0.028
ThO_2	0.043	0.292	0.067	0.100	0.051	n.d.	0.072	n.d.
UO_2	0.065	0.245	0.105	0.181	0.043	0.029	0.132	0.031
TOTAL	100.598	99.874	98.801	100.388	100.510	100.472	100.836	100.950
Si	3.97036	3.95014	3.98789	3.95330	3.95577	3.96279	3.95046	3.94064
Zr	3.95918	3.97056	3.94276	3.96160	3.97818	3.95879	3.97121	3.98702
Hf	0.05649	0.04960	0.05313	0.05917	0.05111	0.05837	0.05552	0.05979
Y	-	0.00609	0.00259	0.00527	0.00346	0.00219	0.00202	-
Al	-	-	-	-	-	-	-	-
Fe2+	-	-	-	-	-	0.00585	0.00694	-
Mn	-	-	-	-	-	-	-	-
Mg	-	-	-	-	-	-	-	-
Ca	-	-	-	-	-	-	-	-
P	-	-	-	0.00439	-	-	-	-
La	-	-	-	-	-	-	-	-
Ce	-	-	-	-	-	-	-	-
Pr	-	-	-	-	0.00149	0.00297	-	-
Nd	-	-	-	-	-	-	0.00202	-
Sm	-	-	-	-	-	-	-	-
Dy	-	-	-	-	-	-	0.00193	-
Er	0.00169	-	-	0.00138	-	-	-	-
Yb	-	0.00256	-	0.00062	0.00095	-	0.00133	0.00105
Th	0.00120	0.00822	0.00192	0.00280	0.00142	-	0.00200	-
U	0.00230	0.00868	0.00374	0.00638	0.00153	0.00103	0.00463	0.00110
TOTAL	7.99122	7.99585	7.99230	7.99491	7.99391	8.01872	7.99806	7.89960

Zircon Analyses: Strontian - BPSRT1.

	3.2/16	3.2/17	3.16/1	3.16/2	3.16/3	3.16/4	3.16/5	3.16/6
SiO_2	32.104	32.278	31.883	32.395	31.845	32.029	32.075	32.275
ZrO_2	66.809	67.399	66.453	65.564	65.639	66.013	66.068	65.731
HfO_2	1.688	1.617	1.571	1.496	1.569	1.411	1.520	1.553
Y_2O_3	n.d.	n.d.	n.d.	0.032	n.d.	0.104	n.d.	0.028
Al_2O_3	n.d.	n.d.	n.d.	n.d.	n.d.	n.d.	n.d.	n.d.
FeO	n.d.	n.d.	n.d.	n.d.	n.d.	n.d.	n.d.	n.d.
MnO	n.d.	n.d.	n.d.	n.d.	n.d.	n.d.	n.d.	n.d.
MgO	n.d.	n.d.	n.d.	0.009	n.d.	n.d.	n.d.	n.d.
CaO	n.d.	n.d.	n.d.	n.d.	n.d.	n.d.	n.d.	n.d.
P_2O_5	n.d.	n.d.	n.d.	n.d.	n.d.	n.d.	n.d.	n.d.
La_2O_3	n.d.	n.d.	n.d.	n.d.	n.d.	n.d.	n.d.	n.d.
Ce_2O_3	n.d.	0.038	n.d.	n.d.	n.d.	n.d.	n.d.	n.d.
Pr_2O_3	n.d.	n.d.	n.d.	n.d.	n.d.	n.d.	n.d.	n.d.
Nd_2O_3	n.d.	n.d.	n.d.	n.d.	n.d.	n.d.	n.d.	n.d.
Sm_2O_3	n.d.	n.d.	n.d.	n.d.	n.d.	n.d.	n.d.	n.d.
Dy_2O_3	n.d.	0.030	n.d.	n.d.	n.d.	n.d.	n.d.	n.d.
Er_2O_3	n.d.	n.d.	n.d.	n.d.	n.d.	n.d.	n.d.	n.d.
Yb_2O_3	n.d.	n.d.	n.d.	n.d.	n.d.	n.d.	n.d.	n.d.
ThO_2	n.d.	n.d.	0.025	n.d.	n.d.	n.d.	n.d.	n.d.
UO_2	0.040	0.033	n.d.	0.042	n.d.	0.085	n.d.	0.054
TOTAL	100.641	100.895	99.932	99.538	99.077	99.704	99.717	99.641
Si	3.93495	3.92919	3.93435	3.97483	3.95553	3.95570	3.95808	3.97934
Zr	3.99334	4.00095	3.99899	3.95416	3.97594	3.97583	3.97585	3.95210
Hf	0.05909	0.05618	0.05534	0.05322	0.05565	0.04976	0.05357	0.05466
Y	-	-	-	0.00214	-	0.00684	-	0.00187
Al	-	-	-	-	-	-	-	-
Fe2+	-	-	-	-	-	-	-	-
Mn	-	-	-	-	-	-	-	-
Mg	-	-	-	0.00171	-	-	-	-
Ca	-	-	-	-	-	-	-	-
P	-	-	-	-	-	-	-	-
La	-	-	-	-	-	-	-	-
Ce	-	0.00171	-	-	-	-	-	-
Pr	-	-	-	-	-	-	-	-
Nd	-	-	-	-	-	-	-	-
Sm	-	-	-	-	-	-	-	-
Dy	-	0.00118	-	-	-	-	-	-
Er	-	-	-	-	-	-	-	-
Yb	-	-	-	-	-	-	-	-
Th	-	-	0.00070	-	-	-	-	-
U	0.00141	0.00114	-	0.00152	-	0.00301	-	0.00193
TOTAL	7.98879	7.99035	7.98938	7.98669	7.98798	7.99330	7.98923	7.98990

Zircon Analyses: Strontian - BPSRT1.

	3.16/7	3.16/8	3.16/9	3.16/10	3.16/11	3.18/1	3.18/2	3.18/3
SiO_2	31.560	32.020	32.029	32.251	32.257	31.787	32.287	32.238
ZrO_2	66.007	65.207	66.077	66.743	66.950	65.794	65.740	65.534
HfO_2	1.602	1.574	1.510	1.543	1.416	1.422	1.404	1.547
Y_2O_3	n.d.	n.d.	0.056	0.053	0.074	0.020	0.081	n.d.
Al_2O_3	n.d.	n.d.	n.d.	n.d.	n.d.	n.d.	n.d.	n.d.
FeO	n.d.	n.d.	n.d.	n.d.	n.d.	n.d.	n.d.	n.d.
MnO	n.d.	n.d.	n.d.	n.d.	n.d.	n.d.	n.d.	n.d.
MgO	n.d.	n.d.	n.d.	n.d.	n.d.	n.d.	n.d.	n.d.
CaO	n.d.	n.d.	n.d.	n.d.	n.d.	n.d.	n.d.	n.d.
P_2O_5	n.d.	n.d.	n.d.	n.d.	n.d.	n.d.	n.d.	n.d.
La_2O_3	n.d.	n.d.	n.d.	n.d.	n.d.	n.d.	n.d.	n.d.
Ce_2O_3	n.d.	n.d.	n.d.	n.d.	n.d.	n.d.	n.d.	n.d.
Pr_2O_3	n.d.	n.d.	n.d.	n.d.	n.d.	n.d.	n.d.	n.d.
Nd_2O_3	n.d.	n.d.	n.d.	n.d.	n.d.	n.d.	n.d.	n.d.
Sm_2O_3	n.d.	n.d.	n.d.	n.d.	n.d.	n.d.	n.d.	n.d.
Dy_2O_3	n.d.	n.d.	n.d.	n.d.	n.d.	n.d.	n.d.	n.d.
Er_2O_3	n.d.	n.d.	n.d.	n.d.	0.022	n.d.	0.024	n.d.
Yb_2O_3	n.d.	n.d.	0.030	n.d.	0.047	0.029	0.037	n.d.
ThO_2	0.025	n.d.	0.051	n.d.	0.041	n.d.	0.067	0.021
UO_2	0.049	n.d.	0.088	0.052	0.045	0.061	0.083	0.035
TOTAL	99.243	99.301	99.785	100.633	100.853	99.113	99.632	99.375
Si	3.94810	3.94894	3.95236	3.94699	3.94271	3.94936	3.95930	3.96749
Zr	3.98110	3.98389	3.97634	3.98329	3.99063	3.98638	3.97534	3.96457
Hf	0.05722	0.05632	0.05321	0.05391	0.04943	0.05043	0.05011	0.05520
Y	-	-	0.00369	0.00345	0.00481	0.00136	0.00541	-
Al	-	-	-	-	-	-	-	-
Fe2+	-	-	-	-	-	-	-	-
Mn	-	-	-	-	-	-	-	-
Mg	-	-	-	-	-	-	-	-
Ca	-	-	-	-	-	-	-	-
P	-	-	-	-	-	-	-	-
La	-	-	-	-	-	-	-	-
Ce	-	-	-	-	-	-	-	-
Pr	-	-	-	-	-	-	-	-
Nd	-	-	-	-	-	-	-	-
Sm	-	-	-	-	-	-	-	-
Dy	-	-	-	-	-	-	-	-
Er	-	-	-	-	0.00087	-	0.00095	-
Yb	-	-	0.00114	-	0.00176	0.00112	0.00142	-
Th	0.00071	-	0.00145	-	0.00114	-	0.00191	0.00059
U	0.00177	-	0.00313	0.00185	0.00157	0.00220	0.00297	0.00128
TOTAL	7.98890	7.98915	7.98763	7.98949	7.99292	7.99085	7.99741	7.98913

Zircon Analyses: Strontian - BPSRT1.

	3.18/4	3.18/5	3.18/6	3.18/7	3.18/8	3.18/9	3.18/10	3.18/11
SiO_2	32.028	32.316	32.328	32.521	32.101	31.997	32.039	32.086
ZrO_2	66.512	66.119	66.594	66.887	66.060	66.364	66.726	67.086
HfO_2	1.525	1.485	1.355	1.534	1.508	1.492	1.409	1.644
Y_2O_3	0.148	0.169	0.111	0.024	0.039	0.059	0.040	0.019
Al_2O_3	n.d.	n.d.	n.d.	n.d.	n.d.	n.d.	n.d.	n.d.
FeO	n.d.	n.d.	n.d.	n.d.	n.d.	n.d.	n.d.	n.d.
MnO	n.d.	n.d.	n.d.	n.d.	n.d.	n.d.	n.d.	n.d.
MgO	n.d.	n.d.	n.d.	n.d.	n.d.	n.d.	n.d.	n.d.
CaO	n.d.	n.d.	n.d.	n.d.	n.d.	n.d.	n.d.	n.d.
P_2O_5	n.d.	n.d.	n.d.	n.d.	n.d.	n.d.	n.d.	n.d.
La_2O_3	n.d.	n.d.	n.d.	n.d.	n.d.	n.d.	n.d.	n.d.
Ce_2O_3	n.d.	n.d.	n.d.	n.d.	n.d.	n.d.	n.d.	n.d.
Pr_2O_3	n.d.	n.d.	n.d.	n.d.	n.d.	n.d.	n.d.	n.d.
Nd_2O_3	n.d.	n.d.	n.d.	n.d.	n.d.	n.d.	n.d.	n.d.
Sm_2O_3	n.d.	n.d.	n.d.	n.d.	n.d.	n.d.	n.d.	n.d.
Dy_2O_3	n.d.	n.d.	n.d.	n.d.	n.d.	n.d.	n.d.	n.d.
Er_2O_3	0.033	0.038	0.036	n.d.	n.d.	0.025	n.d.	n.d.
Yb_2O_3	0.053	0.060	0.035	n.d.	n.d.	0.034	n.d.	n.d.
ThO_2	0.041	0.085	0.023	n.d.	0.055	0.123	0.041	n.d.
UO_2	0.138	0.156	0.068	0.060	0.077	0.144	0.070	n.d.
TOTAL	100.478	100.428	100.550	100.588	99.840	100.238	100.325	100.835
Si	3.93623	3.96543	3.95934	3.94505	3.95867	3.94143	3.93731	3.92838
Zr	3.98631	3.95662	3.97736	3.98644	3.97267	3.98649	3.99883	4.00542
Hf	0.05351	0.05202	0.04737	0.05312	0.05311	0.05247	0.04944	0.05745
Y	0.00970	0.01107	0.00728	0.00157	0.00260	0.00392	0.00262	0.00129
Al	-	-	-	-	-	-	-	-
Fe2+	-	-	-	-	-	-	-	-
Mn	-	-	-	-	-	-	-	-
Mg	-	-	-	-	-	-	-	-
Ca	-	-	-	-	-	-	-	-
P	-	-	-	-	-	-	-	-
La	-	-	-	-	-	-	-	-
Ce	-	-	-	-	-	-	-	-
Pr	-	-	-	-	-	-	-	-
Nd	-	-	-	-	-	-	-	-
Sm	-	-	-	-	-	-	-	-
Dy	-	-	-	-	-	-	-	-
Er	0.00128	0.00147	0.00142	-	-	0.00098	-	0.00146
Yb	0.00200	0.00227	0.00132	-	-	0.00128	-	0.00011
Th	0.00115	0.00237	0.00066	-	0.00156	0.00345	0.00114	0.00051
U	0.00485	0.00547	0.00238	0.00208	0.00271	0.00508	0.00246	0.00058
TOTAL	7.99503	7.99672	7.99713	7.98826	7.99132	7.99165	7.99180	7.99125

Zircon Analyses: Strontian - BPSRT1.

	3.18/12	3.18/13	3.18/14	3.18/15	3.18/16	3.18/17	3.18/18	3.18/19
SiO_2	32.011	31.945	31.812	32.489	32.687	32.407	32.210	31.917
ZrO_2	66.747	66.337	66.038	66.236	66.381	66.557	66.123	65.864
HfO_2	1.552	1.615	1.519	1.723	1.727	1.793	1.503	1.729
Y_2O_3	0.039	n.d.	0.041	0.033	n.d.	0.020	n.d.	n.d.
Al_2O_3	n.d.	n.d.	n.d.	n.d.	n.d.	n.d.	n.d.	n.d.
FeO	n.d.	n.d.	n.d.	n.d.	n.d.	n.d.	n.d.	n.d.
MnO	n.d.	n.d.	n.d.	n.d.	n.d.	n.d.	n.d.	n.d.
MgO	n.d.	n.d.	n.d.	n.d.	n.d.	n.d.	n.d.	n.d.
CaO	n.d.	n.d.	n.d.	n.d.	n.d.	n.d.	n.d.	n.d.
P_2O_5	n.d.	n.d.	n.d.	n.d.	n.d.	n.d.	n.d.	n.d.
La_2O_3	n.d.	n.d.	n.d.	n.d.	n.d.	n.d.	n.d.	n.d.
Ce_2O_3	n.d.	n.d.	n.d.	n.d.	n.d.	n.d.	n.d.	n.d.
Pr_2O_3	n.d.	n.d.	n.d.	n.d.	n.d.	n.d.	n.d.	n.d.
Nd_2O_3	n.d.	n.d.	n.d.	n.d.	n.d.	n.d.	n.d.	n.d.
Sm_2O_3	n.d.	n.d.	n.d.	n.d.	n.d.	n.d.	n.d.	n.d.
Dy_2O_3	n.d.	n.d.	n.d.	n.d.	n.d.	n.d.	n.d.	n.d.
Er_2O_3	n.d.	n.d.	n.d.	n.d.	n.d.	n.d.	n.d.	n.d.
Yb_2O_3	0.024	n.d.	n.d.	0.029	n.d.	n.d.	0.062	n.d.
ThO_2	n.d.	n.d.	n.d.	n.d.	n.d.	n.d.	n.d.	n.d.
UO_2	n.d.	n.d.	0.063	n.d.	n.d.	n.d.	n.d.	n.d.
TOTAL	100.395	99.919	100.453	100.537	100.824	100.757	99.898	99.510
Si	3.93593	3.94200	3.94275	3.97618	3.98368	3.96087	3.96587	3.95013
Zr	4.00217	3.99205	3.99140	3.95317	3.94524	3.96702	3.97018	3.97517
Hf	0.05448	0.05689	0.05375	0.06019	0.06008	0.06256	0.05285	0.06109
Y	0.00259	-	0.00271	0.00220	-	0.00133	-	-
Al	-	-	-	-	-	-	-	-
Fe2+	-	-	-	-	-	-	-	-
Mn	-	-	-	-	-	-	-	-
Mg	-	-	-	-	-	-	-	-
Ca	-	-	-	-	-	-	-	-
P	-	-	-	-	-	-	-	-
La	-	-	-	-	-	-	-	-
Ce	-	-	-	-	-	-	-	-
Pr	-	-	-	-	-	-	-	-
Nd	-	-	-	-	-	-	-	-
Sm	-	-	-	-	-	-	-	-
Dy	-	-	-	-	-	-	-	-
Er	-	-	-	-	-	-	-	-
Yb	0.00093	-	-	0.00109	-	-	0.00235	-
Th	-	-	-	-	-	-	-	-
U	-	-	0.00224	-	-	-	-	-
TOTAL	7.99687	7.99173	7.99344	7.99158	7.99002	7.99178	7.99125	7.98639

Zircon Analyses: Strontian - BPSRT1.

	3.18/20
SiO_2	32.253
ZrO_2	65.176
HfO_2	1.716
Y_2O_3	n.d.
Al_2O_3	n.d.
FeO	n.d.
MnO	n.d.
MgO	n.d.
CaO	n.d.
P_2O_5	n.d.
La_2O_3	n.d.
Ce_2O_3	n.d.
Pr_2O_3	n.d.
Nd_2O_3	n.d.
Sm_2O_3	n.d.
Dy_2O_3	n.d.
Er_2O_3	n.d.
Yb_2O_3	n.d.
ThO_2	n.d.
UO_2	n.d.
TOTAL	99.145
Si	3.99451
Zr	3.93639
Hf	0.06067
Y	-
Al	-
Fe2+	-
Mn	-
Mg	-
Ca	-
P	-
La	-
Ce	-
Pr	-
Nd	-
Sm	-
Dy	-
Er	-
Yb	-
Th	-
U	-
TOTAL	7.99157

Zircon Analyses: Strontian - BPSRG1 - Rims.

	3.3/1	3.3/2	3.3/3	3.4/4	3.3/5	3.3/6	3.3/7	3.3/8
SiO_2	32.033	31.833	31.946	31.851	32.687	31.882	31.747	31.743
ZrO_2	66.613	64.897	66.600	66.723	66.260	66.776	66.397	66.197
HfO_2	1.298	1.349	1.407	1.531	1.568	1.481	1.609	1.519
Y_2O_3	0.031	0.120	0.086	0.047	0.061	0.066	0.028	0.069
Al_2O_3	n.d.	n.d.	n.d.	n.d.	n.d.	n.d.	n.d.	n.d.
FeO	n.d.	n.d.	n.d.	n.d.	n.d.	n.d.	n.d.	n.d.
MnO	n.d.	n.d.	n.d.	n.d.	n.d.	n.d.	n.d.	n.d.
MgO	n.d.	n.d.	n.d.	n.d.	n.d.	n.d.	n.d.	n.d.
CaO	n.d.	n.d.	n.d.	n.d.	n.d.	n.d.	n.d.	n.d.
P_2O_5	n.d.	n.d.	n.d.	n.d.	n.d.	n.d.	n.d.	n.d.
La_2O_3	n.d.	n.d.	n.d.	n.d.	n.d.	n.d.	n.d.	n.d.
Ce_2O_3	n.d.	n.d.	n.d.	n.d.	n.d.	n.d.	n.d.	n.d.
Pr_2O_3	n.d.	n.d.	n.d.	n.d.	n.d.	n.d.	n.d.	n.d.
Nd_2O_3	n.d.	n.d.	n.d.	n.d.	n.d.	n.d.	n.d.	n.d.
Sm_2O_3	n.d.	n.d.	n.d.	n.d.	n.d.	n.d.	n.d.	n.d.
Dy_2O_3	n.d.	n.d.	n.d.	n.d.	n.d.	n.d.	n.d.	0.055
Er_2O_3	0.036	0.045	n.d.	n.d.	n.d.	0.038	n.d.	0.023
Yb_2O_3	0.023	0.054	0.048	0.029	n.d.	0.030	0.033	0.046
ThO_2	n.d.	0.139	0.076	0.057	0.103	0.218	0.050	0.244
UO_2	0.039	0.188	0.108	0.080	0.110	0.218	0.111	0.261
TOTAL	99.973	98.685	100.270	100.318	100.789	100.709	99.975	100.157
Si	3.94263	3.97396	3.93126	3.92255	3.94217	3.90466	3.92487	3.92453
Zr	3.99819	3.95081	3.99678	4.00720	3.98522	4.01801	4.00304	3.99113
Hf	0.04562	0.04810	0.04944	0.05385	0.05400	0.05177	0.05680	0.05362
Y	0.00205	0.00799	0.00563	0.00312	0.00395	0.00436	0.00188	0.00457
Al	-	-	-	-	-	-	-	-
Fe2+	-	-	-	-	-	-	-	-
Mn	-	-	-	-	-	-	-	-
Mg	-	-	-	-	-	-	-	-
Ca	-	-	-	-	-	-	-	-
P	-	-	-	-	-	-	-	-
La	-	-	-	-	-	-	-	-
Ce	-	-	-	-	-	-	-	-
Pr	-	-	-	-	-	-	-	-
Nd	-	-	-	-	-	-	-	-
Sm	-	-	-	-	-	-	-	-
Dy	-	-	-	-	-	-	-	0.00222
Er	0.00140	0.00178	-	-	-	0.00147	-	0.00092
Yb	0.00087	0.00208	0.00182	0.00109	-	0.00114	0.00127	0.00175
Th	-	0.00396	0.00214	0.00162	0.00283	0.00609	0.00141	0.00687
U	0.00138	0.00672	0.00381	0.00284	0.00380	0.00766	0.00392	0.00924
TOTAL	7.99214	7.99540	7.99088	7.99227	7.99197	7.99516	7.99319	7.99485

Zircon Analyses: Strontian - BPSRG1 - Rims.

	3.3/9	3.3/10	3.3/11	3.3/12	A1	A2	A3	A4
SiO_2	32.066	32.140	32.246	32.496	31.877	32.140	32.019	31.686
ZrO_2	66.743	66.032	65.551	66.121	65.746	65.737	65.968	65.646
HfO_2	1.923	2.245	2.166	2.219	1.781	1.739	1.811	1.617
Y_2O_3	n.d.	n.d.	n.d.	n.d.	0.030	0.033	0.083	0.459
Al_2O_3	n.d.	n.d.	n.d.	n.d.	n.d.	n.d.	n.d.	n.d.
FeO	n.d.	n.d.	n.d.	n.d.	n.d.	n.d.	n.d.	n.d.
MnO	n.d.	n.d.	n.d.	n.d.	n.d.	n.d.	n.d.	n.d.
MgO	n.d.	n.d.	n.d.	n.d.	n.d.	n.d.	n.d.	n.d.
CaO	n.d.	n.d.	n.d.	n.d.	n.d.	n.d.	n.d.	n.d.
P_2O_5	n.d.	n.d.	n.d.	n.d.	n.d.	n.d.	n.d.	n.d.
La_2O_3	n.d.	n.d.	n.d.	n.d.	n.d.	n.d.	n.d.	n.d.
Ce_2O_3	n.d.	n.d.	n.d.	n.d.	n.d.	n.d.	n.d.	n.d.
Pr_2O_3	n.d.	n.d.	n.d.	n.d.	n.d.	n.d.	n.d.	n.d.
Nd_2O_3	n.d.	n.d.	n.d.	n.d.	n.d.	n.d.	n.d.	n.d.
Sm_2O_3	n.d.	n.d.	n.d.	n.d.	n.d.	n.d.	n.d.	n.d.
Dy_2O_3	n.d.	n.d.	n.d.	n.d.	n.d.	0.055	0.045	0.072
Er_2O_3	n.d.	n.d.	n.d.	n.d.	n.d.	0.035	0.035	0.073
Yb_2O_3	n.d.	n.d.	n.d.	n.d.	0.034	0.052	0.056	0.160
ThO_2	0.039	n.d.	0.036	n.d.	n.d.	n.d.	n.d.	0.091
UO_2	0.122	0.053	0.136	0.060	0.101	0.271	0.221	0.480
TOTAL	100.893	100.470	100.135	100.896	99.539	100.062	100.238	100.278
Si	3.92859	3.92106	3.91155	3.91243	3.95000	3.96441	3.94845	3.91798
Zr	3.98772	3.98800	3.99591	3.99958	3.97290	3.95419	3.96707	3.95845
Hf	0.06726	0.07818	0.07502	0.07627	0.06303	0.06125	0.06377	0.05710
Y	-	-	-	-	0.00201	0.00221	0.00549	0.03025
Al	-	-	-	-	-	-	-	-
Fe2+	-	-	-	-	-	-	-	-
Mn	-	-	-	-	-	-	-	-
Mg	-	-	-	-	-	-	-	-
Ca	-	-	-	-	-	-	-	-
P	-	-	-	-	-	-	-	-
La	-	-	-	-	-	-	-	-
Ce	-	-	-	-	-	-	-	-
Pr	-	-	-	-	-	-	-	-
Nd	-	-	-	-	-	-	-	-
Sm	-	-	-	-	-	-	-	-
Dy	-	-	-	-	-	0.00220	0.00181	0.00289
Er	-	-	-	-	-	0.00135	0.00137	0.00287
Yb	-	-	-	-	0.00131	0.00198	0.00213	0.00603
Th	0.00110	-	0.00099	-	-	-	-	0.00258
U	0.00430	0.00187	0.00475	0.00209	0.00361	0.00959	0.00782	0.01699
TOTAL	7.98897	7.98911	7.98822	7.99037	7.99286	7.99718	7.99791	7.99514

Zircon Analyses: Strontian - BPSRG1 - Rims.

	B1	B2	B3	B4	B5
SiO_2	32.026	32.228	31.738	32.286	32.242
ZrO_2	66.030	66.832	65.387	65.958	66.026
HfO_2	1.978	1.833	1.583	1.736	2.487
Y_2O_3	0.023	0.031	0.078	n.d.	0.254
Al_2O_3	0.007	0.010	0.005	n.d.	0.077
FeO	n.d.	n.d.	n.d.	n.d.	0.050
MnO	n.d.	n.d.	n.d.	n.d.	n.d.
MgO	n.d.	n.d.	n.d.	n.d.	n.d.
CaO	n.d.	n.d.	n.d.	n.d.	0.108
P_2O_5	n.d.	n.d.	n.d.	n.d.	n.d.
La_2O_3	n.d.	n.d.	n.d.	n.d.	n.d.
Ce_2O_3	n.d.	n.d.	n.d.	n.d.	n.d.
Pr_2O_3	n.d.	n.d.	n.d.	n.d.	n.d.
Nd_2O_3	n.d.	n.d.	n.d.	n.d.	n.d.
Sm_2O_3	n.d.	n.d.	n.d.	n.d.	n.d.
Dy_2O_3	n.d.	n.d.	n.d.	n.d.	n.d.
Er_2O_3	n.d.	n.d.	n.d.	n.d.	n.d.
Yb_2O_3	n.d.	n.d.	0.038	n.d.	0.070
ThO_2	n.d.	n.d.	0.046	n.d.	0.053
UO_2	0.111	0.100	0.119	0.139	0.328
TOTAL	100.168	100.993	98.989	100.119	99.695
Si	3.94533	3.93650	3.95307	3.96671	3.93055
Zr	3.96683	3.98094	3.97154	3.95182	3.92525
Hf	0.06955	0.06393	0.05630	0.06089	0.08654
Y	0.00152	0.00201	0.00522	-	0.01649
Al	-	-	-	-	0.01112
Fe2+	-	-	-	-	0.00516
Mn	-	-	-	-	-
Mg	-	-	-	-	-
Ca	-	-	-	-	0.01419
P	-	-	-	-	-
La	-	-	-	-	-
Ce	-	-	-	-	-
Pr	-	-	-	-	-
Nd	-	-	-	-	-
Sm	-	-	-	-	-
Dy	-	-	-	-	-
Er	-	-	-	-	-
Yb	-	-	0.00145	-	0.00261
Th	-	-	0.00131	-	0.00147
U	0.00393	0.00352	0.00425	0.00490	0.01144
TOTAL	7.98716	7.98690	7.99314	7.98432	8.00482

Zircon Analyses: Strontian - BPSRG1 - Cores.

	A1	A2	A3	B1	B2	C1	C2	C3
SiO_2	31.844	32.208	32.675	32.500	32.639	32.100	32.486	32.428
ZrO_2	66.582	65.875	66.539	65.378	65.513	65.184	66.094	65.206
HfO_2	1.346	1.898	1.888	2.021	1.704	1.826	1.934	1.730
Y_2O_3	0.041	0.101	0.028	n.d.	n.d.	n.d.	0.035	n.d.
Al_2O_3	n.d.	n.d.	n.d.	n.d.	n.d.	n.d.	n.d.	n.d.
FeO	n.d.	n.d.	n.d.	n.d.	n.d.	n.d.	n.d.	n.d.
MnO	n.d.	n.d.	n.d.	n.d.	n.d.	n.d.	n.d.	n.d.
MgO	n.d.	n.d.	n.d.	n.d.	n.d.	n.d.	n.d.	n.d.
CaO	n.d.	n.d.	n.d.	n.d.	n.d.	n.d.	n.d.	n.d.
P_2O_5	n.d.	n.d.	n.d.	n.d.	n.d.	n.d.	n.d.	n.d.
La_2O_3	n.d.	n.d.	n.d.	n.d.	n.d.	n.d.	n.d.	n.d.
Ce_2O_3	n.d.	n.d.	n.d.	n.d.	n.d.	n.d.	n.d.	n.d.
Pr_2O_3	n.d.	n.d.	n.d.	n.d.	n.d.	n.d.	n.d.	n.d.
Nd_2O_3	n.d.	n.d.	n.d.	n.d.	n.d.	n.d.	n.d.	n.d.
Sm_2O_3	n.d.	n.d.	n.d.	n.d.	n.d.	n.d.	n.d.	n.d.
Dy_2O_3	n.d.	n.d.	n.d.	n.d.	n.d.	n.d.	n.d.	n.d.
Er_2O_3	n.d.	n.d.	n.d.	n.d.	n.d.	n.d.	n.d.	n.d.
Yb_2O_3	n.d.	0.058	n.d.	n.d.	n.d.	n.d.	n.d.	n.d.
ThO_2	n.d.	0.057	n.d.	n.d.	n.d.	n.d.	n.d.	n.d.
UO_2	n.d.	0.139	0.041	0.111	n.d.	0.039	0.038	n.d.
TOTAL	99.772	100.336	101.171	100.010	99.856	99.149	99.588	99.364
Si	3.95979	3.97532	3.97382	3.99382	4.03653	3.98223	3.99035	3.98776
Zr	3.97693	3.93398	3.94632	3.91793	3.89079	3.94341	3.92973	3.94112
Hf	0.04780	0.06588	0.06557	0.07090	0.06016	0.06467	0.06889	0.06169
Y	0.00276	0.00655	0.00186	-	-	-	0.00233	-
Al	-	-	-	-	-	-	-	-
Fe2+	-	-	-	-	-	-	-	-
Mn	-	-	-	-	-	-	-	-
Mg	-	-	-	-	-	-	-	-
Ca	-	-	-	-	-	-	-	-
P	-	-	-	-	-	-	-	-
La	-	-	-	-	-	-	-	-
Ce	-	-	-	-	-	-	-	-
Pr	-	-	-	-	-	-	-	-
Nd	-	-	-	-	-	-	-	-
Sm	-	-	-	-	-	-	-	-
Dy	-	-	-	-	-	-	-	-
Er	-	-	-	-	-	-	-	-
Yb	-	0.00216	-	-	-	-	-	-
Th	-	0.00159	-	-	-	-	-	-
U	-	0.00483	0.00144	0.00390	-	0.00140	0.00135	-
TOTAL	7.98728	7.99031	7.98901	7.98655	7.98748	7.99171	7.99265	7.99057

Zircon Analyses: Strontian - BPSRG1 - Cores.

	D1	D2	D3	E1	E2	F1	F2	G1
SiO_2	32.110	32.155	31.796	31.480	31.395	30.977	31.504	31.959
ZrO_2	65.969	65.864	64.583	64.511	64.502	63.190	64.193	67.080
HfO_2	1.908	1.433	1.198	1.866	1.680	1.538	1.917	1.295
Y_2O_3	n.d.	n.d.	0.512	0.051	0.051	0.127	0.033	0.038
Al_2O_3	n.d.	n.d.	0.039	n.d.	n.d.	n.d.	n.d.	n.d.
FeO	n.d.	n.d.	0.077	n.d.	n.d.	n.d.	n.d.	n.d.
MnO	n.d.	n.d.	n.d.	n.d.	n.d.	n.d.	n.d.	n.d.
MgO	n.d.	n.d.	n.d.	n.d.	n.d.	n.d.	n.d.	n.d.
CaO	n.d.	n.d.	0.071	n.d.	n.d.	n.d.	n.d.	n.d.
P_2O_5	n.d.	n.d.	n.d.	n.d.	n.d.	n.d.	n.d.	n.d.
La_2O_3	n.d.	n.d.	n.d.	n.d.	n.d.	n.d.	n.d.	n.d.
Ce_2O_3	n.d.	n.d.	0.046	n.d.	n.d.	n.d.	n.d.	n.d.
Pr_2O_3	n.d.	n.d.	n.d.	n.d.	n.d.	n.d.	n.d.	n.d.
Nd_2O_3	n.d.	n.d.	n.d.	n.d.	n.d.	n.d.	n.d.	n.d.
Sm_2O_3	n.d.	n.d.	n.d.	n.d.	n.d.	n.d.	n.d.	n.d.
Dy_2O_3	n.d.	n.d.	0.023	n.d.	0.036	n.d.	n.d.	n.d.
Er_2O_3	n.d.	n.d.	0.070	n.d.	0.030	n.d.	n.d.	n.d.
Yb_2O_3	n.d.	n.d.	0.119	n.d.	0.037	0.046	0.043	n.d.
ThO_2	n.d.	n.d.	0.291	n.d.	n.d.	n.d.	n.d.	n.d.
UO_2	n.d.	n.d.	0.427	0.097	0.095	n.d.	0.182	n.d.
TOTAL	99.987	99.452	99.229	99.005	99.826	99.878	99.872	100.372
Si	3.95579	3.97114	3.95971	3.95952	3.95592	3.97337	3.97011	3.92652
Zr	3.96322	3.96676	3.92212	3.95694	3.96356	3.95259	3.94494	4.01907
Hf	0.06713	0.05051	0.04260	0.06700	0.06044	0.05631	0.06897	0.04542
Y	-	-	0.03396	0.00346	0.00342	0.00873	0.00226	0.00253
Al	-	-	0.00585	-	-	-	-	-
Fe2+	-	-	0.00808	-	-	-	-	-
Mn	-	-	-	-	-	-	-	-
Mg	-	-	-	-	-	-	-	-
Ca	-	-	0.00952	-	-	-	-	-
P	-	-	-	-	-	-	-	-
La	-	-	-	-	-	-	-	-
Ce	-	-	0.00212	-	-	-	-	-
Pr	-	-	-	-	-	-	-	-
Nd	-	-	-	-	-	-	-	-
Sm	-	-	-	-	-	-	-	-
Dy	-	-	-	-	0.00149	-	-	-
Er	-	-	0.00274	-	0.00121	-	-	-
Yb	-	-	0.00452	-	0.00144	0.00181	0.00167	-
Th	-	-	0.00825	-	-	-	-	-
U	-	-	0.01521	0.00351	0.00345	-	0.00658	-
TOTAL	7.98614	7.98841	8.01468	7.99043	7.99093	7.99281	7.99453	7.99354

Zircon Analyses: Strontian - BPSRG1 - Cores.

	G2	H1	I1	I2	J1	J2	J3	K1
SiO_2	32.214	31.574	32.236	31.798	31.654	31.876	31.996	32.061
ZrO_2	66.806	66.515	66.512	66.663	66.027	65.745	66.349	65.849
HfO_2	1.305	1.427	1.336	1.507	1.144	1.120	2.151	1.632
Y_2O_3	0.124	0.530	0.226	0.070	0.194	0.878	n.d.	0.050
Al_2O_3	n.d.	n.d.	n.d.	n.d.	n.d.	n.d.	n.d.	n.d.
FeO	n.d.	n.d.	n.d.	n.d.	n.d.	n.d.	n.d.	n.d.
MnO	n.d.	n.d.	n.d.	n.d.	n.d.	n.d.	n.d.	n.d.
MgO	n.d.	n.d.	n.d.	n.d.	n.d.	n.d.	n.d.	n.d.
CaO	n.d.	n.d.	n.d.	n.d.	n.d.	n.d.	n.d.	n.d.
P_2O_5	n.d.	n.d.	n.d.	n.d.	n.d.	n.d.	n.d.	n.d.
La_2O_3	n.d.	n.d.	n.d.	n.d.	n.d.	n.d.	n.d.	n.d.
Ce_2O_3	n.d.	n.d.	n.d.	n.d.	n.d.	n.d.	n.d.	n.d.
Pr_2O_3	n.d.	n.d.	n.d.	n.d.	n.d.	n.d.	n.d.	n.d.
Nd_2O_3	n.d.	n.d.	n.d.	n.d.	n.d.	n.d.	n.d.	n.d.
Sm_2O_3	n.d.	n.d.	n.d.	n.d.	n.d.	n.d.	n.d.	n.d.
Dy_2O_3	n.d.	0.076	n.d.	n.d.	n.d.	n.d.	n.d.	n.d.
Er_2O_3	n.d.	0.094	0.039	n.d.	n.d.	0.117	n.d.	n.d.
Yb_2O_3	0.055	0.150	0.059	0.043	0.067	0.190	0.045	n.d.
ThO_2	n.d.	0.205	0.064	n.d.	n.d.	0.045	n.d.	n.d.
UO_2	n.d.	0.175	0.030	n.d.	0.045	0.047	0.164	n.d.
TOTAL	100.504	100.246	100.502	100.081	99.131	100.018	100.705	99.592
Si	3.91702	3.92305	3.92000	3.92167	3.93513	3.93310	3.93219	3.96400
Zr	4.02067	3.96740	4.00353	4.00940	4.00285	3.95596	3.97638	3.97033
Hf	0.04529	0.04983	0.04639	0.05305	0.04062	0.03945	0.07547	0.05760
Y	0.00804	0.03454	0.01466	0.00462	0.01285	0.05765	-	0.00330
Al	-	-	-	-	-	-	-	-
Fe2+	-	-	-	-	-	-	-	-
Mn	-	-	-	-	-	-	-	-
Mg	-	-	-	-	-	-	-	-
Ca	-	-	-	-	-	-	-	-
P	-	-	-	-	-	-	-	-
La	-	-	-	-	-	-	-	-
Ce	-	-	-	-	-	-	-	-
Pr	-	-	-	-	-	-	-	-
Nd	-	-	-	-	-	-	-	-
Sm	-	-	-	-	-	-	-	-
Dy	-	0.00302	-	-	-	-	-	-
Er	-	0.00362	0.00151	-	-	0.00453	-	-
Yb	0.00206	0.00560	0.00218	0.00163	0.00257	0.00715	0.00169	-
Th	-	0.00571	0.00179	-	-	0.00126	-	-
U	-	0.00614	0.00104	-	0.00161	0.00166	0.00578	-
TOTAL	7.99308	7.99891	7.99110	7.99037	7.99563	8.00076	7.99151	7.99523

Zircon Analyses: Strontian - BPSRG1 - Cores.

	L1	M1	N1	O1	P1	Q1	R1	S1
SiO_2	32.674	32.439	32.545	32.665	32.491	32.135	32.038	32.481
ZrO_2	64.585	65.390	64.649	64.466	64.130	64.632	65.890	62.789
HfO_2	1.764	1.788	1.623	1.845	1.214	2.205	1.767	1.169
Y_2O_3	0.153	0.061	0.163	0.046	0.676	0.056	n.d.	1.001
Al_2O_3	n.d.	n.d.	n.d.	n.d.	n.d.	n.d.	n.d.	0.037
FeO	n.d.	n.d.	n.d.	n.d.	0.020	n.d.	n.d.	0.034
MnO	n.d.	n.d.	n.d.	n.d.	n.d.	n.d.	n.d.	0.013
MgO	n.d.	n.d.	n.d.	n.d.	n.d.	n.d.	n.d.	n.d.
CaO	n.d.	n.d.	n.d.	n.d.	0.045	n.d.	n.d.	0.324
P_2O_5	n.d.	n.d.	n.d.	n.d.	0.146	n.d.	n.d.	0.090
La_2O_3	n.d.	n.d.	n.d.	n.d.	n.d.	n.d.	n.d.	n.d.
Ce_2O_3	n.d.	n.d.	n.d.	n.d.	0.058	n.d.	n.d.	0.112
Pr_2O_3	n.d.	n.d.	n.d.	n.d.	n.d.	n.d.	n.d.	n.d.
Nd_2O_3	n.d.	n.d.	n.d.	n.d.	n.d.	n.d.	n.d.	n.d.
Sm_2O_3	n.d.	n.d.	n.d.	n.d.	n.d.	n.d.	n.d.	n.d.
Dy_2O_3	n.d.	n.d.	n.d.	n.d.	0.103	n.d.	n.d.	0.055
Er_2O_3	n.d.	n.d.	n.d.	n.d.	0.096	0.058	n.d.	0.149
Yb_2O_3	0.045	0.048	0.060	n.d.	0.119	0.065	n.d.	0.209
ThO_2	0.054	n.d.	n.d.	n.d.	0.371	n.d.	n.d.	0.702
UO_2	0.127	0.099	0.091	n.d.	0.310	0.160	n.d.	0.606
TOTAL	99.402	99.825	99.131	99.022	99.779	99.311	99.695	99.771
Si	4.00024	3.99170	3.96343	4.00562	4.00486	4.01337	3.99025	3.98780
Zr	3.91615	3.92483	3.93260	3.91519	3.85141	3.87539	3.94127	3.81693
Hf	0.06361	0.06481	0.06011	0.06664	0.04554	0.07863	0.06284	0.04227
Y	0.01028	0.00412	0.01129	0.00309	-	-	-	0.06750
Al	-	-	-	-	-	-	-	0.00566
Fe2+	-	-	-	-	0.00228	-	-	0.00360
Mn	-	-	-	-	-	-	-	0.00147
Mg	-	-	-	-	-	-	-	-
Ca	-	-	-	-	0.00637	-	-	0.04400
P	-	-	-	-	0.01632	-	-	0.00967
La	-	-	-	-	-	-	-	-
Ce	-	-	-	-	0.00282	-	-	0.00520
Pr	-	-	-	-	-	-	-	-
Nd	-	-	-	-	-	-	-	-
Sm	-	-	-	-	-	-	-	-
Dy	-	-	-	-	0.00438	-	-	0.00226
Er	-	-	-	-	0.00397	0.00230	-	0.00595
Yb	0.00174	0.00187	0.00239	-	0.00479	0.00250	-	0.00808
Th	0.00157	-	-	-	0.01110	-	-	0.02024
U	0.00459	0.00361	0.00339	-	0.01165	0.00574	-	0.02198
TOTAL	7.99818	7.99094	7.98321	7.99054	8.01273	7.98165	7.99436	8.04261

Zircon Analyses: Strontian - BPSRG1 - Cores.

	T1	U1	V1	W1	X1	Y1	Z1
SiO_2	32.326	31.275	32.153	32.631	32.816	31.856	32.242
ZrO_2	64.783	62.054	64.291	65.136	65.765	66.100	65.182
HfO_2	1.957	1.402	1.847	1.221	1.206	1.405	1.926
Y_2O_3	0.048	0.533	0.031	n.d.	n.d.	n.d.	n.d.
Al_2O_3	n.d.	0.047	n.d.	n.d.	n.d.	n.d.	n.d.
FeO	n.d.	0.341	n.d.	n.d.	n.d.	n.d.	n.d.
MnO	n.d.	0.093	n.d.	n.d.	n.d.	n.d.	n.d.
MgO	n.d.	0.023	n.d.	n.d.	n.d.	n.d.	n.d.
CaO	n.d.	0.440	n.d.	n.d.	n.d.	n.d.	n.d.
P_2O_5	n.d.	0.079	n.d.	n.d.	n.d.	n.d.	n.d.
La_2O_3	n.d.	n.d.	n.d.	n.d.	n.d.	n.d.	n.d.
Ce_2O_3	n.d.	0.058	n.d.	n.d.	n.d.	n.d.	n.d.
Pr_2O_3	n.d.	n.d.	n.d.	n.d.	n.d.	n.d.	n.d.
Nd_2O_3	n.d.	0.065	n.d.	n.d.	n.d.	n.d.	n.d.
Sm_2O_3	n.d.	n.d.	n.d.	n.d.	n.d.	n.d.	n.d.
Dy_2O_3	n.d.	0.057	n.d.	n.d.	n.d.	n.d.	n.d.
Er_2O_3	n.d.	0.072	n.d.	n.d.	n.d.	n.d.	n.d.
Yb_2O_3	n.d.	0.113	n.d.	n.d.	n.d.	n.d.	n.d.
ThO_2	n.d.	1.721	0.054	n.d.	n.d.	n.d.	n.d.
UO_2	0.058	0.970	0.094	n.d.	n.d.	n.d.	0.041
TOTAL	99.172	99.336	99.470	98.988	99.787	99.361	99.391
Si	4.03394	3.97142	4.00891	3.99478	3.98645	3.96222	3.98746
Zr	3.88155	3.78075	3.90909	3.95000	3.95733	3.97899	3.93187
Hf	0.06972	0.05084	0.06575	0.04403	0.04315	0.04989	0.06909
Y	0.00324	0.03601	0.00209	-	-	-	-
Al	-	0.00714	-	-	-	-	-
Fe2+	-	0.03625	-	-	-	-	-
Mn	-	0.01001	-	-	-	-	-
Mg	-	0.00440	-	-	-	-	-
Ca	-	0.05994	-	-	-	-	-
P	-	0.00854	-	-	-	-	-
La	-	-	-	-	-	-	-
Ce	-	0.00270	-	-	-	-	-
Pr	-	-	-	-	-	-	-
Nd	-	0.00300	-	-	-	-	-
Sm	-	-	-	-	-	-	-
Dy	-	0.00233	-	-	-	-	-
Er	-	0.00288	-	-	-	-	-
Yb	-	0.00437	-	-	-	-	-
Th	-	0.04973	0.00153	-	-	-	0.00042
U	0.00208	0.03525	0.00337	-	-	-	0.00149
TOTAL	7.99053	8.00556	7.99074	7.98881	7.98693	7.99110	7.98991

Zircon Analyses: Ratagain - RAT 13/1.

	3.15/1	3.15/2	3.15/3	3.15/4	3.15/5	3.15/6	3.15/7	3.15/8
SiO_2	31.874	32.104	31.737	31.843	31.874	31.871	31.943	31.821
ZrO_2	66.300	65.902	65.838	66.276	65.954	66.569	66.808	66.314
HfO_2	1.308	1.201	1.519	1.433	1.452	1.241	1.510	1.210
Y_2O_3	n.d.	n.d.	n.d.	n.d.	n.d.	n.d.	0.034	n.d.
Al_2O_3	n.d.	n.d.	n.d.	n.d.	n.d.	n.d.	n.d.	n.d.
FeO	n.d.	0.019	0.014	n.d.	n.d.	n.d.	n.d.	n.d.
MnO	n.d.	n.d.	n.d.	n.d.	n.d.	n.d.	n.d.	n.d.
MgO	n.d.	n.d.	n.d.	n.d.	n.d.	n.d.	n.d.	n.d.
CaO	n.d.	n.d.	n.d.	n.d.	n.d.	n.d.	n.d.	n.d.
P_2O_5	n.d.	n.d.	n.d.	n.d.	n.d.	n.d.	n.d.	n.d.
La_2O_3	n.d.	n.d.	n.d.	n.d.	n.d.	n.d.	n.d.	n.d.
Ce_2O_3	n.d.	n.d.	n.d.	n.d.	n.d.	n.d.	n.d.	n.d.
Pr_2O_3	n.d.	n.d.	n.d.	n.d.	n.d.	n.d.	n.d.	n.d.
Nd_2O_3	n.d.	n.d.	n.d.	n.d.	n.d.	n.d.	n.d.	n.d.
Sm_2O_3	n.d.	n.d.	n.d.	n.d.	n.d.	n.d.	n.d.	n.d.
Dy_2O_3	n.d.	n.d.	n.d.	n.d.	n.d.	n.d.	n.d.	n.d.
Er_2O_3	n.d.	n.d.	n.d.	n.d.	n.d.	n.d.	n.d.	n.d.
Yb_2O_3	n.d.	n.d.	n.d.	n.d.	n.d.	n.d.	n.d.	n.d.
ThO_2	0.035	0.035	n.d.	n.d.	n.d.	n.d.	0.050	n.d.
UO_2	0.046	n.d.	n.d.	n.d.	0.050	n.d.	n.d.	n.d.
TOTAL	99.576	99.261	99.108	99.552	99.330	99.681	100.345	99.345
Si	3.92646	3.93839	3.92909	3.94081	3.95055	3.93532	3.92764	3.94090
Zr	4.01580	4.00750	4.00777	3.99990	3.98637	4.00848	4.00597	4.00508
Hf	0.04675	0.04342	0.05457	0.05065	0.05137	0.04377	0.05300	0.04278
Y	-	-	-	-	-	-	0.00225	-
Al	-	-	-	-	-	-	-	-
Fe^{2+}	-	0.00210	0.00149	-	-	-	-	-
Mn	-	-	-	-	-	-	-	-
Mg	-	-	-	-	-	-	-	-
Ca	-	-	-	-	-	-	-	-
P	-	-	-	-	-	-	-	-
La	-	-	-	-	-	-	-	-
Ce	-	-	-	-	-	-	-	-
Pr	-	-	-	-	-	-	-	-
Nd	-	-	-	-	-	-	-	-
Sm	-	-	-	-	-	-	-	-
Dy	-	-	-	-	-	-	-	-
Er	-	-	-	-	-	-	-	-
Yb	-	-	-	-	-	-	-	-
Th	0.00100	0.00102	-	-	-	-	0.00141	-
U	0.00165	-	-	-	0.00179	-	-	-
TOTAL	7.99425	7.99253	7.99292	7.99136	7.98829	7.98757	7.99027	7.98876

Zircon Analyses: Ratagain - RAT 13/1.

	3.15/9	3.15/10
SiO_2	31.840	32.517
ZrO_2	65.718	65.953
HfO_2	1.470	1.278
Y_2O_3	n.d.	n.d.
Al_2O_3	n.d.	n.d.
FeO	n.d.	n.d.
MnO	n.d.	n.d.
MgO	n.d.	n.d.
CaO	n.d.	n.d.
P_2O_5	n.d.	n.d.
La_2O_3	n.d.	n.d.
Ce_2O_3	n.d.	n.d.
Pr_2O_3	n.d.	n.d.
Nd_2O_3	n.d.	n.d.
Sm_2O_3	n.d.	n.d.
Dy_2O_3	n.d.	n.d.
Er_2O_3	n.d.	n.d.
Yb_2O_3	n.d.	n.d.
ThO_2	n.d.	n.d.
UO_2	n.d.	n.d.
TOTAL	99.028	99.748
Si	3.99591	3.96309
Zr	3.98182	3.98487
Hf	0.05215	0.04662
Y	-	-
Al	-	-
Fe^{2+}	-	-
Mn	-	-
Mg	-	-
Ca	-	-
P	-	-
La	-	-
Ce	-	-
Pr	-	-
Nd	-	-
Sm	-	-
Dy	-	-
Er	-	-
Yb	-	-
Th	-	-
U	-	-
TOTAL	7.98988	7.99458

Appendix 4: Electron microprobe analyses: titanites.

For analyses cross referenced with a plate number the first part of the analysis coding denotes the plate number (*eg.* 3.1); the second part denotes the analysis number, for analyses not cross referenced with a plate number the rock number is given and a letter is used to denote different grains, this is then followed by the analysis number. All the concentrations are expressed as wt% oxide, Fe is calculated as FeO. n.d. - not detected. The structural formulae of the titanite analyses have been calculated on the basis of 20 oxygens.

Titanite Analyses: Strontian - BPSRA1

	4.1/1	4.1/2	4.1/3	4.1/4	4.1/5	4.1/6	4.1/7	4.1/8
SiO_2	30.21	30.29	29.88	30.07	30.07	29.75	29.75	29.86
TiO_2	36.86	36.58	35.91	35.80	36.44	35.76	36.48	36.73
Al_2O_3	1.03	1.10	1.28	1.38	1.21	1.08	1.08	0.98
FeO	0.94	1.13	1.26	1.21	1.06	1.23	1.17	1.07
MnO	0.06	0.06	0.05	0.07	0.06	0.06	0.07	0.06
MgO	n.d.	n.d.	n.d.	n.d.	n.d.	n.d.	n.d.	n.d.
CaO	27.56	27.51	26.55	26.53	26.97	25.73	26.46	26.82
La_2O_3	0.18	0.15	0.42	0.40	0.27	0.57	0.57	0.41
Ce_2O_3	0.62	0.64	1.48	1.35	1.03	1.81	1.89	1.43
Pr_2O_3	n.d.	n.d.	0.14	0.20	0.12	0.24	0.21	0.22
Nd_2O_3	0.41	0.41	0.83	0.85	0.65	1.22	1.12	0.90
Sm_2O_3	0.13	0.11	0.17	0.24	0.12	0.12	0.20	0.12
Yb_2O_3	n.d.	n.d.	n.d.	n.d.	n.d.	n.d.	n.d.	n.d.
Y_2O_3	0.23	0.25	0.34	0.30	0.09	0.23	0.21	0.24
TOTAL	98.23	98.23	98.31	98.40	98.09	98.80	99.21	98.84
Si	4.0560	4.0676	4.0512	4.0684	4.0582	4.0699	4.0198	4.0281
Ti	3.7218	3.6943	3.6616	3.6427	3.6986	3.6792	3.7071	3.7264
Al	0.1630	0.1741	0.2045	0.2201	0.1925	0.1741	0.1720	0.1558
Fe2+	0.1055	0.1269	0.1428	0.1369	0.1196	0.1407	0.1322	0.1207
Mn	0.0068	0.0068	0.0057	0.0080	0.0068	0.0069	0.0080	0.0068
Mg	-	-	-	-	-	-	-	-
Ca	3.9648	3.9584	3.8571	3.8461	3.9001	3.7717	3.8309	3.8767
La	0.0089	0.0074	0.0210	0.0199	0.0134	0.0287	0.0284	0.0204
Ce	0.0304	0.0314	0.0734	0.0668	0.0508	0.0906	0.0934	0.0706
Pr	-	-	0.0069	0.0098	0.0059	0.0119	0.0103	0.0108
Nd	0.0198	0.0198	0.0405	0.0414	0.0316	0.0601	0.0545	0.0437
Sm	0.0060	0.0050	0.0079	0.0111	0.0055	0.0056	0.0093	0.0055
Yb	-	-	-	-	-	-	-	-
Y	0.0164	0.0178	0.0245	0.0216	0.0064	0.0167	0.0151	0.0172
TOTAL	12.0998	12.1101	12.0976	12.0933	12.0899	12.0567	12.0814	12.0832

Titanite Analyses: Strontian - BPSRA1

	4.1/9	4.1/10	4.1/11	4.1/12	4.1/13	4.1/14	4.1/15	4.1/16
SiO_2	30.00	30.11	29.70	29.75	29.87	30.04	30.06	29.63
TiO_2	37.00	37.21	36.31	36.43	36.88	37.68	37.28	36.16
Al_2O_3	0.86	0.79	1.08	1.10	0.99	0.82	0.87	1.21
FeO	0.86	0.88	1.24	1.18	1.06	0.79	0.78	1.35
MnO	0.05	0.04	0.06	0.05	0.07	0.05	0.05	0.06
MgO	n.d.	n.d.	n.d.	n.d.	n.d.	n.d.	n.d.	n.d.
CaO	26.71	27.10	26.53	26.38	26.68	27.00	27.36	26.71
La_2O_3	0.32	0.22	0.59	0.55	0.45	0.32	0.30	0.45
Ce_2O_3	1.18	1.03	1.83	1.86	1.51	1.09	0.89	1.68
Pr_2O_3	0.19	0.15	0.23	0.23	0.15	0.16	n.d.	0.18
Nd_2O_3	0.64	0.52	1.28	1.08	0.97	0.61	0.55	1.01
Sm_2O_3	0.07	0.06	0.19	0.17	0.17	0.06	0.07	0.20
Yb_2O_3	n.d.	n.d.	n.d.	n.d.	n.d.	n.d.	n.d.	n.d.
Y_2O_3	0.13	n.d.	0.22	0.20	0.13	0.11	0.17	0.18
TOTAL	98.01	98.11	99.26	98.98	98.93	98.73	98.38	98.82
Si	4.0548	4.0559	4.0172	4.0251	4.0263	4.0281	4.0384	4.0134
Ti	3.7610	3.7695	3.6936	3.7069	3.7387	3.7998	3.7667	3.6836
Al	0.1370	0.1254	0.1722	0.1754	0.1573	0.1296	0.1377	0.1932
Fe2+	0.0972	0.0991	0.1402	0.1335	0.1194	0.0885	0.0876	0.1529
Mn	0.0057	0.0045	0.0068	0.0057	0.0079	0.0056	0.0056	0.0068
Mg	-	-	-	-	-	-	-	-
Ca	3.8683	3.9114	3.8450	3.8244	3.8535	3.8793	3.9385	3.8766
La	0.0159	0.0109	0.0294	0.0274	0.0223	0.0158	0.0148	0.0224
Ce	0.0583	0.0507	0.0906	0.0921	0.0745	0.0535	0.0437	0.0833
Pr	0.0093	0.0073	0.0113	0.0113	0.0073	0.0078	-	0.0088
Nd	0.0311	0.0252	0.0623	0.0526	0.0471	0.0294	0.0266	0.0493
Sm	0.0032	0.0027	0.0088	0.0079	0.0078	0.0027	0.0032	0.0093
Yb	-	-	-	-	-	-	-	-
Y	0.0093	-	0.0158	0.0144	0.0093	0.0078	0.0121	0.0129
TOTAL	12.0518	12.0632	12.0938	12.0772	12.0720	12.0485	12.0756	12.1131

Titanite Analyses: Strontian - BPSRA1

	4.1/17	4.1/18	4.1/19	4.1/20	4.1/21	4.1/22	4.1/23	4.1/24
SiO_2	29.69	29.97	30.20	30.21	29.81	30.06	29.92	29.96
TiO_2	36.45	36.93	37.42	37.57	35.87	36.32	35.54	35.92
Al_2O_3	1.22	1.15	1.04	1.07	1.19	1.12	1.34	1.31
FeO	1.11	1.15	0.87	0.88	1.12	0.95	1.25	1.12
MnO	0.06	0.07	0.05	0.06	0.06	0.05	0.06	0.04
MgO	n.d.	n.d.	n.d.	n.d.	n.d.	n.d.	n.d.	n.d.
CaO	27.06	27.33	27.86	27.98	26.38	26.76	26.23	26.60
La_2O_3	0.38	0.30	0.15	0.14	0.44	0.32	0.39	0.26
Ce_2O_3	1.47	1.25	0.76	0.61	1.53	1.24	1.43	1.11
Pr_2O_3	0.16	0.21	0.17	n.d.	0.15	0.13	0.18	0.12
Nd_2O_3	0.91	0.77	0.41	0.40	0.94	0.80	0.86	0.74
Sm_2O_3	0.10	0.11	0.03	0.09	0.17	0.12	0.13	0.14
Yb_2O_3	n.d.	n.d.	n.d.	n.d.	n.d.	n.d.	n.d.	n.d.
Y_2O_3	0.21	0.23	n.d.	0.09	0.24	0.28	0.28	0.30
TOTAL	98.82	99.47	98.96	99.10	97.90	98.15	97.61	97.62
Si	4.0080	4.0106	4.0273	4.0189	4.0589	4.0652	4.0784	4.0687
Ti	3.7005	3.7167	3.7528	3.7589	3.6731	3.6940	3.6433	3.6686
Al	0.1941	0.1814	0.1635	0.1678	0.1910	0.1785	0.2153	0.2097
Fe2+	0.1253	0.1287	0.0970	0.0979	0.1275	0.1074	0.1425	0.1272
Mn	0.0068	0.0079	0.0056	0.0067	0.0069	0.0057	0.0069	0.0046
Mg	-	-	-	-	-	-	-	-
Ca	3.9141	3.9189	3.9809	3.9884	3.8487	3.8777	3.8310	3.8707
La	0.0189	0.0148	0.0073	0.0068	0.0220	0.0159	0.0196	0.0130
Ce	0.0726	0.0612	0.0371	0.0297	0.0762	0.0613	0.0713	0.0551
Pr	0.0078	0.0102	0.0082	-	0.0074	0.0064	0.0089	0.0059
Nd	0.0442	0.0371	0.0197	0.0191	0.0461	0.0389	0.0422	0.0362
Sm	0.0046	0.0050	0.0013	0.0041	0.0079	0.0055	0.0061	0.0065
Yb	-	-	-	-	-	-	-	-
Y	0.0150	0.0163	-	0.0063	0.0173	0.0201	0.0203	0.0216
TOTAL	12.1182	12.1094	12.1011	12.1051	12.0837	12.0772	12.0862	12.0884

Titanite Analyses: Strontian - BPSRA1

	4.1/25	4.1/26
SiO_2	30.01	29.98
TiO_2	35.47	36.39
Al_2O_3	1.36	1.27
FeO	1.29	1.05
MnO	0.04	0.05
MgO	n.d.	n.d.
CaO	26.45	26.85
La_2O_3	0.41	0.28
Ce_2O_3	1.45	1.13
Pr_2O_3	0.22	0.09
Nd_2O_3	0.88	0.68
Sm_2O_3	0.15	0.13
Yb_2O_3	n.d.	n.d.
Y_2O_3	0.25	0.31
TOTAL	97.98	98.21
Si	4.0794	4.0475
Ti	3.6262	3.6948
Al	0.2179	0.2021
Fe2+	0.1466	0.1185
Mn	0.0046	0.0057
Mg	-	-
Ca	3.8526	3.8841
La	0.0205	0.0139
Ce	0.0721	0.0558
Pr	0.0108	0.0044
Nd	0.0431	0.0330
Sm	0.0070	0.0060
Yb	-	-
Y	0.0180	0.0222
TOTAL	12.0994	12.0887

Titanite Analyses: Strontian - BPSRA1

	4.1/A	4.1/B	4.1/C	4.1/D	4.1/E	4.1/F
Na_2O	0.018	0.021	n.d.	n.d.	n.d.	n.d.
MgO	0.017	0.011	0.010	0.011	0.029	0.016
Al_2O_3	1.091	0.936	1.253	1.166	1.349	1.275
SiO_2	28.710	29.004	28.935	29.052	29.067	28.952
K_2O	n.d.	n.d.	n.d.	n.d.	n.d.	n.d.
CaO	25.478	26.527	25.995	26.872	26.519	26.845
TiO_2	37.128	37.212	36.868	37.988	37.216	37.633
V_2O_5	n.d.	n.d.	n.d.	n.d.	n.d.	n.d.
MnO	0.061	0.054	0.059	0.062	0.065	0.067
FeO	1.284	1.102	1.361	1.176	1.388	1.185
Y_2O_3	0.234	0.226	0.241	0.244	0.253	0.238
Nb_2O_5	0.341	0.395	0.324	0.294	0.223	0.168
La_2O_3	0.562	0.467	0.468	0.372	0.370	0.329
Ce_2O_3	2.017	1.566	1.726	1.258	1.543	1.136
Pr_2O_3	0.256	0.192	0.238	0.160	0.182	0.148
Nd_2O_3	1.160	0.902	0.964	0.776	0.907	0.667
Sm_2O_3	0.177	0.116	0.155	0.077	0.150	0.140
Gd_2O_3	0.073	n.d.	0.066	n.d.	0.071	n.d.
Dy_2O_3	n.d.	0.088	0.050	0.054	0.058	0.089
Yb_2O_3	n.d.	n.d.	n.d.	n.d.	0.022	0.023
Ta_2O_5	n.d.	n.d.	n.d.	n.d.	n.d.	n.d.
ThO_2	0.070	0.094	0.070	0.050	0.044	0.045
UO_2	n.d.	n.d.	n.d.	0.051	0.035	0.039
TOTAL	98.852	99.065	98.855	99.775	99.547	99.162
Na	0.00494	0.00546	0.00010	-	-	-
Mg	0.00363	0.00219	0.00220	0.00231	0.00588	0.00321
Al	0.17530	0.14797	0.20073	0.18431	0.21416	0.20244
Si	3.91260	3.88919	3.93038	3.89245	3.91398	3.89875
K	-	-	-	-	-	-
Ca	3.72046	3.81128	3.78362	3.85779	3.82624	3.87349
Ti	3.80529	3.85340	3.76636	3.82773	3.76878	3.81124
V	-	-	-	-	-	-
Mn	0.00705	0.00616	0.00689	0.00709	0.00745	0.00764
Fe	0.14644	0.12368	0.15471	0.13178	0.15637	0.13346
Y	0.01697	0.01613	0.01742	0.01744	0.01815	0.01711
Nb	0.02104	0.02400	0.01991	0.01782	0.01359	0.01023
La	0.02826	0.02312	0.02344	0.01838	0.01840	0.01636
Ce	0.10063	0.07689	0.08584	0.06174	0.07607	0.05601
Pr	0.01273	0.00940	0.01179	0.00785	0.00897	0.00730
Nd	0.05699	0.04360	0.04721	0.03750	0.04402	0.03238
Sm	0.00834	0.00537	0.00728	0.00356	0.00697	0.00652
Gd	0.00331	-	0.00298	-	0.00318	-
Dy	0.00058	0.00381	0.00222	0.00234	0.00252	0.00386
Yb	-	-	-	-	0.00093	0.00095
Ta	-	-	-	-	-	-
Th	0.00219	0.00286	0.00217	0.00153	0.00136	0.00139
U	-	-	-	0.00198	0.00135	0.00151
TOTAL	12.03636	12.05136	12.06853	12.07936	12.09327	12.09256

Titanite Analyses: Strontian - BPSRT1

	T1/A1	T1/A2	T1/A3	T1/A4	T1/A5	T1/A6	T1/A7	T1/A8
Na_2O	0.013	0.022	0.020	0.025	0.013	n.d.	n.d.	n.d.
MgO	0.012	0.013	0.007	0.016	0.009	0.014	0.009	0.008
Al_2O_3	0.936	0.983	1.004	0.952	0.914	1.075	0.978	0.969
SiO_2	28.492	28.373	28.477	28.160	28.360	28.443	28.500	28.677
K_2O	n.d.	n.d.	n.d.	n.d.	n.d.	n.d.	n.d.	n.d.
CaO	25.825	25.675	25.542	25.538	25.906	26.486	26.579	26.568
TiO_2	37.138	36.692	36.726	36.688	36.801	36.834	37.209	37.480
V_2O_5	n.d.	n.d.	n.d.	n.d.	n.d.	n.d.	n.d.	n.d.
MnO	0.097	0.093	0.086	0.088	0.091	0.103	0.095	0.098
FeO	1.196	1.509	1.590	1.540	1.483	1.442	1.420	1.341
Y_2O_3	0.186	0.305	0.364	0.321	0.285	0.166	0.126	0.120
Nb_2O_5	0.396	0.501	0.337	0.330	0.364	0.195	0.189	0.155
La_2O_3	0.519	0.487	0.482	0.340	0.379	0.383	0.353	0.347
Ce_2O_3	1.733	1.829	1.793	1.496	1.530	1.146	1.088	0.913
Pr_2O_3	0.188	0.180	0.309	0.171	0.154	0.170	0.091	0.065
Nd_2O_3	0.649	0.916	1.036	0.900	0.815	0.498	0.481	0.317
Sm_2O_3	0.070	0.156	0.198	0.170	0.128	0.074	n.d.	n.d.
Gd_2O_3	0.050	0.048	0.075	0.108	0.074	n.d.	n.d.	n.d.
Dy_2O_3	n.d.	0.061	0.122	0.076	0.066	n.d.	n.d.	n.d.
Yb_2O_3	n.d.	0.026	0.021	0.032	0.025	0.025	0.038	0.027
Ta_2O_5	n.d.	n.d.	n.d.	n.d.	n.d.	n.d.	n.d.	n.d.
ThO_2	0.062	0.070	0.074	0.045	0.062	n.d.	0.049	n.d.
UO_2	n.d.	n.d.	n.d.	n.d.	n.d.	n.d.	n.d.	n.d.
TOTAL	97.775	98.109	98.548	97.150	97.528	97.235	97.316	97.183
Na	0.00353	0.00602	0.00542	0.01231	0.00352	-	-	-
Mg	0.00263	0.00274	0.00145	0.00340	0.00190	0.00286	0.00189	0.00173
Al	0.15145	0.15934	0.16221	0.15533	0.14838	0.17407	0.15809	0.15608
Si	3.90859	3.89770	3.90268	3.89591	3.90469	3.90540	3.90471	3.91826
K	-	-	-	-	-	-	-	-
Ca	3.79608	3.77931	3.75079	3.78586	3.82177	3.89671	3.90188	3.88961
Ti	3.83149	3.79079	3.78523	3.81728	3.81053	3.80359	3.83393	3.85137
V	-	-	-	-	-	-	-	-
Mn	0.01130	0.01090	0.01007	0.01038	0.01069	0.01203	0.01103	0.01143
Fe	0.13723	0.17339	0.18229	0.17820	0.17081	0.16558	0.16272	0.15323
Y	0.01359	0.02229	0.02661	0.02366	0.02091	0.01218	0.00919	0.00877
Nb	0.02459	0.03114	0.02088	0.02067	0.02268	0.01210	0.01173	0.00958
La	0.02627	0.02471	0.02438	0.01735	0.01927	0.01940	0.01788	0.01748
Ce	0.08705	0.09201	0.08999	0.07578	0.07714	0.05762	0.05458	0.04568
Pr	0.00942	0.00903	0.01544	0.00865	0.00774	0.00851	0.00458	0.00325
Nd	0.03212	0.04539	0.05119	0.04490	0.04046	0.02464	0.02374	0.01563
Sm	0.00331	0.00739	0.00936	0.00814	0.00611	0.00351	-	-
Gd	0.00227	0.00220	0.00340	0.00496	0.00340	-	-	-
Dy	-	0.00273	0.00539	0.00341	0.00295	-	-	-
Yb	-	0.00111	0.00088	0.00135	0.00108	0.00105	0.00160	0.00112
Ta	-	-	-	-	-	-	-	-
Th	0.00194	0.00219	0.00233	0.00142	0.00195	-	0.00154	-
U	-	-	-	-	-	-	-	-
TOTAL	12.05672	12.09765	12.06494	12.07785	12.08043	12.11111	12.10564	12.08833

Titanite Analyses: Strontian - BPSRT1

	T1/A9	T1/A10	T1/A11	T1/A12	T1/B1	T1/B2	T1/B3	T1/B4
Na_2O	n.d.	n.d.	0.009	n.d.	n.d.	0.019	0.013	0.012
MgO	0.011	0.010	0.008	0.018	0.007	0.013	0.007	0.009
Al_2O_3	0.911	0.815	0.958	1.094	0.897	0.985	0.902	1.003
SiO_2	28.375	28.599	28.802	28.611	28.314	28.286	28.316	28.254
K_2O	n.d.	n.d.	n.d.	n.d.	n.d.	n.d.	n.d.	n.d.
CaO	26.560	26.895	26.958	26.047	25.960	25.287	25.658	25.298
TiO_2	37.169	37.887	37.881	37.473	37.128	36.248	36.370	36.110
V_2O_5	n.d.	n.d.	n.d.	n.d.	n.d.	n.d.	n.d.	n.d.
MnO	0.106	0.094	0.091	0.088	0.093	0.093	0.090	0.089
FeO	1.253	1.121	1.073	1.600	1.241	1.466	1.501	1.563
Y_2O_3	0.223	0.053	0.040	0.173	0.184	0.331	0.362	0.351
Nb_2O_5	0.223	0.128	0.104	0.153	0.286	0.429	0.376	0.535
La_2O_3	0.402	0.211	0.237	0.345	0.492	0.445	0.364	0.455
Ce_2O_3	1.254	0.553	0.538	1.195	1.546	1.712	1.449	1.798
Pr_2O_3	0.123	0.062	0.067	0.114	0.169	0.236	0.240	0.215
Nd_2O_3	0.598	0.213	0.175	0.551	0.632	0.943	0.904	1.028
Sm_2O_3	0.101	n.d.	n.d.	0.086	0.054	0.173	0.180	0.177
Gd_2O_3	n.d.	n.d.	n.d.	n.d.	n.d.	0.080	0.072	0.070
Dy_2O_3	0.072	0.073	n.d.	0.043	n.d.	0.082	0.071	0.071
Yb_2O_3	n.d.	n.d.	n.d.	n.d.	n.d.	n.d.	0.024	n.d.
Ta_2O_5	n.d.	n.d.	n.d.	n.d.	n.d.	n.d.	n.d.	n.d.
ThO_2	n.d.	n.d.	n.d.	n.d.	0.053	0.064	0.058	0.087
UO_2	n.d.	n.d.	n.d.	n.d.	n.d.	n.d.	n.d.	n.d.
TOTAL	97.473	96.871	97.108	97.7165	97.149	97.217	97.337	97.417
Na	-	-	0.00245	-	-	0.00529	0.00359	0.00327
Mg	0.00229	0.00215	0.00164	0.00378	0.00160	0.00283	0.00150	0.00202
Al	0.14798	0.13120	0.15376	0.17793	0.14582	0.16121	0.14740	0.16398
Si	3.90808	3.90484	3.91842	3.94505	3.90102	3.92384	3.92211	3.91639
K	-	-	-	-	-	-	-	-
Ca	3.84579	3.93478	3.92981	3.84830	3.83242	3.75867	3.80806	3.75737
Ti	3.85003	3.89048	3.87587	3.78221	3.84711	3.78168	3.78864	3.76433
V	-	-	-	-	-	-	-	-
Mn	0.01245	0.01088	0.01056	0.01030	0.01088	0.01102	0.01063	0.01053
Fe	0.14432	0.12809	0.12212	0.18453	0.14299	0.17013	0.17398	0.18121
Y	0.01637	0.00385	0.00293	0.01275	0.01354	0.02446	0.02669	0.02592
Nb	0.01389	0.00795	0.00640	0.00958	0.01782	0.02692	0.02359	0.03354
La	0.02042	0.01067	0.01189	0.01756	0.02501	0.02280	0.01861	0.02328
Ce	0.06323	0.02765	0.02682	0.06032	0.07799	0.08695	0.07352	0.09127
Pr	0.00618	0.00310	0.00336	0.00576	0.00851	0.01196	0.01213	0.01090
Nd	0.02970	0.01048	0.00860	0.02740	0.03139	0.04714	0.04512	0.05136
Sm	0.00481	-	-	0.00408	0.00258	0.00830	0.00863	0.00846
Gd	-	-	-	-	-	0.00370	0.00333	0.00324
Dy	0.00322	0.00324	-	0.00194	-	0.00366	0.00319	0.00320
Yb	-	-	-	-	-	-	0.00102	-
Ta	-	-	-	-	-	-	-	-
Th	-	-	-	-	0.00166	0.00203	0.00185	0.00275
U	-	-	-	-	-	-	-	-
TOTAL	12.07272	12.08147	12.08453	12.09964	12.06713	12.05996	12.07813	12.06325

Titanite Analyses: Strontian - BPSRT1

	T1/B5	T1/B6	T1/B7	T1/B8	T1/B9	T1/B10	T1/B11	T1/B12
Na_2O	0.015	0.015	n.d.	n.d.	n.d.	n.d.	n.d.	n.d.
MgO	0.010	0.015	0.008	0.008	0.014	0.007	0.006	0.005
Al_2O_3	0.854	0.749	1.093	1.024	1.048	1.015	0.909	0.978
SiO_2	28.432	28.483	28.540	28.505	28.249	28.312	28.268	28.561
K_2O	n.d.	n.d.	n.d.	n.d.	n.d.	n.d.	n.d.	n.d.
CaO	25.600	26.346	26.363	26.438	25.840	26.127	26.068	26.767
TiO_2	37.061	37.630	36.741	37.130	36.047	36.475	37.107	37.510
V_2O_5	n.d.	n.d.	n.d.	n.d.	n.d.	0.068	n.d.	0.086
MnO	0.088	0.084	0.104	0.094	0.090	0.100	0.095	0.097
FeO	1.291	1.258	1.528	1.396	1.688	1.560	1.216	1.126
Y_2O_3	0.156	0.151	0.245	0.151	0.236	0.150	0.217	0.081
Nb_2O_5	0.341	0.281	0.208	0.202	0.234	0.206	0.212	0.153
La_2O_3	0.519	0.465	0.328	0.369	0.355	0.346	0.324	0.277
Ce_2O_3	1.469	1.312	1.170	1.117	1.246	1.147	1.216	0.712
Pr_2O_3	0.149	0.108	0.142	0.154	0.171	0.121	0.147	n.d.
Nd_2O_3	0.585	0.489	0.677	0.474	0.654	0.517	0.578	0.249
Sm_2O_3	0.045	n.d.	0.100	0.049	0.096	0.059	0.082	0.049
Gd_2O_3	n.d.	0.047	0.052	0.053	0.068	n.d.	n.d.	0.046
Dy_2O_3	n.d.	n.d.	0.049	n.d.	0.051	0.046	0.046	n.d.
Yb_2O_3	n.d.	n.d.	0.022	n.d.	n.d.	n.d.	n.d.	n.d.
Ta_2O_5	n.d.	n.d.	n.d.	n.d.	n.d.	n.d.	n.d.	n.d.
ThO_2	0.073	0.087	0.009	0.029	0.051	n.d.	n.d.	n.d.
UO_2	n.d.	n.d.	n.d.	n.d.	n.d.	n.d.	n.d.	n.d.
TOTAL	96.825	97.631	97.534	97.308	96.203	96.373	96.594	96.808
Na	0.00412	0.00408	-	-	-	-	-	-
Mg	0.00216	0.00305	0.00171	0.00167	0.00294	0.00152	0.00135	0.00108
Al	0.13899	0.12088	0.17662	0.16543	0.17200	0.16572	0.14804	0.15790
Si	3.92434	3.89688	3.91163	3.90633	3.93068	3.92067	3.90518	3.90845
K	-	-	-	-	-	-	-	-
Ca	3.78613	3.86230	3.87170	3.88224	3.85253	3.87675	3.85874	3.92480
Ti	3.84710	3.87183	3.78717	3.82680	3.77207	3.79874	3.85524	3.86039
V	-	-	-	-	-	0.00624	-	0.00781
M	0.01033	0.00975	0.01208	0.01099	0.01066	0.01183	0.01117	0.01125
Fe	0.14903	0.14399	0.17516	0.15999	0.19642	0.18072	0.14053	0.12887
Y	0.01146	0.01100	0.01790	0.01103	0.01751	0.01106	0.01598	0.00592
Nb	0.02127	0.01740	0.01293	0.01256	0.01472	0.01291	0.01324	0.00946
La	0.02646	0.02348	0.01658	0.01869	0.01824	0.01767	0.01654	0.01399
Ce	0.07427	0.06574	0.05875	0.05606	0.06350	0.05817	0.06151	0.03569
Pr	0.00753	0.00539	0.00711	0.00772	0.00868	0.00611	0.00743	-
Nd	0.02910	0.02413	0.03347	0.02344	0.03282	0.02583	0.02879	0.01231
Sm	0.00215	-	0.00475	0.00233	0.00462	0.00283	0.00392	0.00233
Gd	-	0.00216	0.00238	0.00241	0.00315	-	-	0.00211
Dy	-	-	0.00216	-	0.00231	0.00207	0.00206	-
Yb	-	-	0.00095	-	-	-	-	-
Ta	-	-	-	-	-	-	-	-
Th	0.00230	0.00273	-	-	0.00164	-	-	-
U	-	-	-	-	-	-	-	-
TOTAL	12.04463	12.07127	12.10605	12.09677	12.10853	12.10377	12.07583	12.08724

Titanite Analyses: Strontian - BPSRT1

	T1/B13	T1/B14	T1/B15
Na_2O	n.d.	n.d.	0.008
MgO	0.011	0.010	0.009
Al_2O_3	0.985	0.993	0.828
SiO_2	28.580	28.601	28.467
K_2O	n.d.	n.d.	n.d.
CaO	26.674	26.484	26.415
TiO_2	37.034	37.089	37.553
V_2O_5	n.d.	n.d.	n.d.
MnO	0.096	0.103	0.085
FeO	1.318	1.409	1.120
Y_2O_3	0.139	0.159	0.162
Nb_2O_5	0.195	0.167	0.213
La_2O_3	0.327	0.359	0.409
Ce_2O_3	0.946	0.940	1.113
Pr_2O_3	0.138	0.064	0.099
Nd_2O_3	0.324	0.392	0.468
Sm_2O_3	n.d.	0.070	0.101
Gd_2O_3	n.d.	n.d.	n.d.
Dy_2O_3	n.d.	0.059	0.045
Yb_2O_3	0.032	n.d.	0.028
Ta_2O_5	n.d.	n.d.	0.008
ThO_2	n.d.	0.048	n.d.
UO_2	n.d.	n.d.	n.d.
TOTAL	96.932	97.071	97.282
Na	-	-	0.00215
Mg	0.00231	0.00220	0.00202
Al	0.15945	0.16053	0.13375
Si	3.92143	3.92100	3.90024
K	-	-	-
Ca	3.92161	3.89037	3.87797
Ti	3.82152	3.82387	3.86946
V	-	-	-
Mn	0.01119	0.01198	0.00987
Fe	0.15133	0.16157	0.12842
Y	0.01017	0.01163	0.01181
Nb	0.01212	0.01037	0.01325
La	0.01657	0.01816	0.02069
Ce	0.04752	0.04721	0.05584
Pr	0.00694	0.00323	0.00497
Nd	0.01605	0.01938	0.02314
Sm	-	0.00335	0.00477
Gd	-	-	-
Dy	-	0.00260	0.00200
Yb	0.00135	-	0.00119
Ta	-	-	0.00030
Th	-	0.00151	-
U	-	-	-
TOTAL	12.10535	12.09697	12.07138

Titanite Analyses: Strontian - BPSRT2

	T2/A1	T2/A2	T2/A3	T2/A4	T2/A5	T2/A6	T2/A7	T2/A8
Na_2O	0.012	0.015	n.d.	n.d.	n.d.	n.d.	n.d.	n.d.
MgO	0.005	0.014	0.009	0.016	0.006	0.012	0.012	0.007
Al_2O_3	0.991	1.123	0.981	1.118	0.998	1.087	0.996	1.146
SiO_2	28.174	28.722	28.856	28.923	28.813	28.933	29.178	29.345
K_2O	n.d.	n.d.	n.d.	n.d.	n.d.	n.d.	n.d.	n.d.
CaO	24.849	25.741	26.294	26.240	26.209	26.769	26.641	26.910
TiO_2	35.774	37.200	37.267	36.060	36.222	37.125	37.628	36.837
V_2O_5	n.d.	n.d.	n.d.	n.d.	n.d.	n.d.	0.047	0.049
MnO	0.118	0.114	0.113	0.123	0.109	0.103	0.103	0.107
FeO	1.877	1.609	1.827	1.946	1.740	1.856	1.692	1.847
Y_2O_3	0.580	0.351	0.374	0.345	0.324	0.241	0.141	0.207
Nb_2O_5	0.299	0.326	0.259	0.177	0.189	0.130	0.137	0.159
La_2O_3	0.558	0.621	0.599	0.368	0.440	0.411	0.396	0.388
Ce_2O_3	2.297	2.112	1.948	1.517	1.500	1.331	1.005	1.168
Pr_2O_3	0.343	0.257	0.258	0.231	0.185	0.166	0.131	0.148
Nd_2O_3	1.539	1.126	0.989	0.945	0.818	0.632	0.363	0.563
Sm_2O_3	0.315	0.204	0.194	0.180	0.150	0.059	0.055	0.077
Gd_2O_3	0.169	0.109	0.059	0.103	0.086	0.049	n.d.	0.044
Dy_2O_3	0.140	0.085	0.087	0.111	0.070	0.090	n.d.	0.052
Yb_2O_3	0.039	n.d.	n.d.	n.d.	0.036	0.023	n.d.	n.d.
Ta_2O_5	n.d.	n.d.	n.d.	n.d.	n.d.	n.d.	n.d.	n.d.
ThO_2	0.043	0.039	n.d.	n.d.	n.d.	n.d.	n.d.	n.d.
UO_2	n.d.	n.d.	n.d.	n.d.	n.d.	n.d.	n.d.	n.d.
TOTAL	97.932	99.879	100.328	98.505	97.971	99.081	98.581	98.169
Na	0.00338	0.00414	-	-	-	-	-	-
Mg	0.00111	0.00298	0.00196	0.00327	0.00132	0.00243	0.00251	0.00152
Al	0.16201	0.17930	0.15588	0.18018	0.16138	0.17342	0.15854	0.18212
Si	3.90582	3.88860	3.88896	3.95271	3.95174	3.91339	3.93697	3.95408
K	-	-	-	-	-	-	-	-
Ca	3.69119	3.73424	3.79705	3.84247	3.85165	3.87966	3.85168	3.88518
Ti	3.72975	3.78766	3.77725	3.70612	3.73614	3.77642	3.81828	3.73296
V	-	-	-	-	-	-	0.00420	0.00437
Mn	0.01396	0.01317	0.01300	0.01429	0.01270	0.01189	0.01178	0.01226
Fe	0.21768	0.18228	0.20593	0.22245	0.19968	0.20999	0.19099	0.20823
Y	0.04280	0.02533	0.02686	0.02508	0.02368	0.01734	0.01018	0.01484
Nb	0.01879	0.01996	0.01580	0.01098	0.01175	0.00799	0.00838	0.00973
La	0.02855	0.03105	0.02981	0.01854	0.02229	0.02051	0.01974	0.01930
Ce	0.11658	0.10472	0.09613	0.07593	0.07532	0.06592	0.04968	0.05764
Pr	0.01735	0.01268	0.01267	0.01151	0.00926	0.00820	0.00645	0.00727
Nd	0.07693	0.05497	0.04807	0.04655	0.04045	0.03081	0.01767	0.02734
Sm	0.01507	0.00955	0.00903	0.00850	0.00713	0.00276	0.00260	0.00358
Gd	0.00777	0.00491	0.00265	0.00467	0.00392	0.00223	-	0.00199
Dy	0.00626	0.00373	0.00377	0.00490	0.00312	0.00392	-	0.00228
Yb	0.00167	-	-	-	0.00150	0.00095	-	-
Ta	-	-	-	-	-	-	-	-
Th	0.00136	0.00121	-	-	-	-	-	-
U	-	-	-	-	-	-	-	-
TOTAL	12.07504	12.09638	12.09953	12.13228	12.11806	12.13157	12.09278	12.12994

Titanite Analyses: Strontian - BPSRT2

	T2/A9	T2/A10	T2/A11	T2/A12	T2/B1	T2/B2	T2/B3	T2/B4
Na_2O	n.d.	0.016	n.d.	n.d.	n.d.	n.d.	0.010	n.d.
MgO	0.006	0.013	0.013	0.015	0.012	0.010	0.006	0.010
Al_2O_3	1.193	1.138	1.213	1.177	1.144	0.963	0.912	1.161
SiO_2	29.305	28.616	28.750	28.803	28.603	28.391	28.652	28.787
K_2O	n.d.	n.d.	n.d.	n.d.	n.d.	n.d.	n.d.	n.d.
CaO	28.046	25.395	25.532	25.783	25.406	25.575	26.141	26.014
TiO_2	37.641	35.398	35.172	35.663	36.140	36.188	36.813	35.882
V_2O_5	0.084	n.d.	n.d.	n.d.	n.d.	n.d.	n.d.	n.d.
MnO	0.108	0.129	0.123	0.128	0.111	0.108	0.111	0.115
FeO	1.359	2.037	2.340	2.208	1.533	1.549	1.438	2.012
Y_2O_3	0.085	0.472	0.469	0.378	0.305	0.362	0.248	0.259
Nb_2O_5	0.161	0.234	0.135	0.160	0.265	0.320	0.338	0.110
La_2O_3	0.082	0.453	0.352	0.413	0.711	0.472	0.432	0.372
Ce_2O_3	0.266	1.755	1.566	1.397	2.076	1.605	1.459	1.383
Pr_2O_3	0.017	0.279	0.234	0.180	0.222	0.216	0.145	0.207
Nd_2O_3	0.104	1.223	1.123	0.914	1.137	0.908	0.631	0.764
Sm_2O_3	n.d.	0.283	0.244	0.156	0.174	0.180	0.112	0.149
Gd_2O_3	n.d.	0.151	0.125	0.077	0.063	0.079	0.078	0.098
Dy_2O_3	n.d.	0.126	0.080	0.084	0.092	0.087	0.070	0.052
Yb_2O_3	n.d.	n.d.	n.d.	n.d.	n.d.	n.d.	n.d.	n.d.
Ta_2O_5	0.035	0.029	0.054	0.069	0.030	0.007	0.048	0.053
ThO_2	n.d.	n.d.	n.d.	n.d.	0.064	0.060	n.d.	n.d.
UO_2	0.037	n.d.	n.d.	n.d.	n.d.	n.d.	n.d.	n.d.
TOTAL	98.601	97.930	97.691	97.707	98.221	97.156	97.754	97.479
Na	-	0.00439	-	-	-	-	0.00273	-
Mg	0.00121	0.00280	0.00284	0.00324	0.00260	0.00218	0.00134	0.00221
Al	0.18844	0.18543	0.19752	0.19104	0.18558	0.15723	0.14738	0.18846
Si	3.92422	3.95396	3.97115	3.96499	3.93446	3.93127	3.92721	3.96206
K	-	-	-	-	-	-	-	-
Ca	4.02416	3.75982	3.77888	3.80300	3.74464	3.79450	3.83920	3.83644
Ti	3.79074	3.67829	3.65366	3.69207	3.73867	3.76841	3.79471	3.71411
V	0.00743	-	-	-	-	-	-	-
Mn	0.01235	0.01512	0.01447	0.01496	0.01299	0.01266	0.01293	0.01340
Fe	0.15229	0.23545	0.27040	0.25421	0.17639	0.17944	0.16490	0.23159
Y	0.00610	0.03474	0.03453	0.02774	0.02238	0.02671	0.01814	0.01899
Nb	0.00974	0.01464	0.00847	0.00997	0.01650	0.02004	0.02098	0.00685
La	0.00407	0.02310	0.01795	0.02099	0.03611	0.02411	0.02188	0.01889
Ce	0.01306	0.08877	0.07919	0.07044	0.10459	0.08139	0.07324	0.06971
Pr	0.00084	0.01406	0.01180	0.00902	0.01117	0.01094	0.00726	0.01041
Nd	0.00504	0.06092	0.05591	0.04537	0.05640	0.04531	0.03120	0.03790
Sm	-	0.01348	0.01163	0.00742	0.00826	0.00862	0.00529	0.00706
Gd	-	0.00695	0.00574	0.00351	0.00290	0.00365	0.00358	0.00447
Dy	-	0.00564	0.00360	0.00376	0.00409	0.00389	0.00310	0.00231
Yb	-	-	-	-	-	-	-	-
Ta	-	0.00110	-	-	-	-	-	-
Th	-	-	-	-	0.00202	0.00191	-	-
U	0.00143	-	-	-	-	-	-	-
TOTAL	12.14686	12.11204	12.13267	12.12984	12.07137	12.07963	12.08279	12.12943

Titanite Analyses: Strontian - BPSRT2

	T2/B5	T2/B6	T2/B7	T2/C1	T2/C2	T2/C3	T2/C4	T2/C5
Na_2O	n.d.	n.d.	n.d.	n.d.	n.d.	0.007	n.d.	n.d.
MgO	0.014	0.020	0.008	0.012	0.014	0.007	0.011	0.012
Al_2O_3	1.026	1.195	2.533	1.118	0.900	0.842	1.088	1.127
SiO_2	28.844	28.655	30.648	28.792	28.619	28.436	28.891	28.979
K_2O	n.d.	0.028	0.277	n.d.	n.d.	n.d.	n.d.	n.d.
CaO	26.550	25.853	25.670	26.221	26.378	26.332	26.531	26.773
TiO_2	36.753	35.711	34.353	36.951	37.173	37.047	36.865	36.814
V_2O_5	n.d.	n.d.	n.d.	n.d.	n.d.	n.d.	n.d.	n.d.
MnO	0.108	0.101	0.119	0.100	0.092	0.103	0.109	0.101
FeO	1.552	1.887	1.418	1.409	1.255	1.333	1.744	1.723
Y_2O_3	0.150	0.316	0.036	0.237	0.156	0.214	0.229	0.263
Nb_2O_5	0.159	0.098	0.155	0.337	0.259	0.322	0.129	0.152
La_2O_3	0.323	0.354	0.204	0.570	0.598	0.509	0.336	0.365
Ce_2O_3	1.113	1.427	0.462	1.882	1.629	1.374	1.190	1.264
Pr_2O_3	0.063	0.181	0.014	0.171	0.173	0.158	0.183	0.200
Nd_2O_3	0.444	0.871	0.160	0.845	0.528	0.599	0.606	0.685
Sm_2O_3	0.051	0.150	n.d.	0.124	0.055	0.102	0.071	0.140
Gd_2O_3	n.d.	0.086	n.d.	0.077	n.d.	0.048	n.d.	0.045
Dy_2O_3	n.d.	0.051	n.d.	n.d.	0.048	0.040	n.d.	0.071
Yb_2O_3	0.022	n.d.	n.d.	0.026	n.d.	n.d.	0.026	n.d.
Ta_2O_5	n.d.	n.d.	n.d.	n.d.	n.d.	n.d.	n.d.	n.d.
ThO_2	n.d.	n.d.	0.046	0.077	0.062	0.074	0.007	0.021
UO_2	n.d.	n.d.	0.052	n.d.	n.d.	n.d.	n.d.	n.d.
TOTAL	97.333	97.071	96.453	99.043	98.089	97.639	98.204	98.857
Na	-	-	-	-	-	0.00199	-	-
Mg	0.00287	0.00430	0.00171	0.00257	0.00297	0.00145	0.00233	0.00246
Al	0.16560	0.19482	0.40524	0.17911	0.14510	0.13626	0.17454	0.18012
Si	3.94643	3.96114	4.15801	3.91100	3.91008	3.90310	3.93145	3.92773
K	-	0.00507	0.04794	-	-	-	-	-
Ca	3.89229	3.82936	3.73162	3.81658	3.86160	3.87288	3.86844	3.88818
Ti	3.78179	3.71257	3.50508	3.77492	3.81964	3.82432	3.77281	3.75253
V	-	-	-	-	-	-	-	-
Mn	0.01262	0.01187	0.01377	0.01151	0.01067	0.01201	0.01259	0.01169
Fe	0.17767	0.21822	0.16093	0.16011	0.14348	0.15303	0.19848	0.19540
Y	0.01095	0.02326	0.00265	0.01713	0.01134	0.01568	0.01659	0.01898
Nb	0.00989	0.00617	0.00953	0.02070	0.01601	0.02003	0.00797	0.00933
La	0.01634	0.01806	0.01021	0.02856	0.03017	0.02576	0.01686	0.01827
Ce	0.05579	0.07225	0.02294	0.09360	0.08152	0.06907	0.05930	0.06274
Pr	0.00318	0.00915	0.00073	0.00849	0.00862	0.00790	0.00907	0.00991
Nd	0.02189	0.04341	0.00785	0.04139	0.02603	0.02963	0.02975	0.03346
Sm	0.00244	0.00715	-	0.00584	0.00263	0.00482	0.00333	0.00656
Gd	-	0.00396	-	0.00349	-	0.00222	-	0.00205
Dy	-	0.00227	-	-	0.00212	0.00178	-	0.00310
Yb	0.00093	-	-	0.00109	-	-	0.00110	-
Ta	-	-	-	-	-	-	-	-
Th	-	-	0.00144	0.00239	0.00195	0.00232	-	-
U	-	-	0.00203	-	-	-	-	-
TOTAL	12.10922	12.12793	12.09823	12.08567	12.08223	12.08872	12.11642	12.13273

Titanite Analyses: Strontian - BPSRT2

	T2/C6	T2/C7	T2/C8
Na_2O	n.d.	n.d.	n.d.
MgO	0.009	0.008	0.006
Al_2O_3	1.118	1.142	1.060
SiO_2	28.895	28.743	28.636
K_2O	n.d.	n.d.	0.013
CaO	26.789	26.359	26.971
TiO_2	36.649	36.465	36.907
V_2O_5	n.d.	n.d.	
MnO	0.106	0.108	0.105
FeO	1.689	1.750	1.299
Y_2O_3	0.216	0.275	0.125
Nb_2O_5	0.096	0.141	0.184
La_2O_3	0.363	0.362	0.169
Ce_2O_3	1.148	1.249	0.529
Pr_2O_3	0.129	0.127	0.032
Nd_2O_3	0.551	0.644	0.227
Sm_2O_3	0.098	0.144	n.d.
Gd_2O_3	n.d.	0.064	n.d.
Dy_2O_3	n.d.	0.046	n.d.
Yb_2O_3	n.d.	n.d.	n.d.
Ta_2O_5	n.d.	n.d.	n.d.
ThO_2	0.043	n.d.	0.048
UO_2	n.d.	n.d.	n.d.
TOTAL	98.031	97.730	96.5226
Na	-	-	-
Mg	0.00197	0.00173	0.00137
Al	0.17972	0.18439	0.17152
Si	3.93736	3.93642	3.92820
K	-	-	0.00231
Ca	3.91140	3.86798	3.96438
Ti	3.75573	3.75580	3.80758
V	-	-	0.00591
Mn	0.01232	0.01254	0.01230
Fe	0.19257	0.20053	0.14906
Y	0.01566	0.02010	0.00914
Nb	0.00597	0.00878	0.01144
La	0.01826	0.01833	0.00855
Ce	0.05727	0.06265	0.02659
Pr	0.00641	0.00634	0.00162
Nd	0.02707	0.03180	0.01125
Sm	0.00464	0.00683	-
Gd	-	0.00291	-
Dy	-	0.00204	-
Yb	-	-	-
Ta	-	-	-
Th	0.00134	-	0.00150
U	-	-	-
TOTAL	12.13469	12.12306	12.11962

Titanite Analyses: Strontian - BPSRT3

	T3/A1	T3/A2	T3/A3	T3/A4	T3/A5	T3/A6	T3/A7	T3/A8
Na_2O	n.d.	0.010	0.018	0.012	n.d.	n.d.	n.d.	n.d.
MgO	0.019	0.009	0.017	0.015	0.013	0.019	0.009	0.013
Al_2O_3	0.989	0.787	0.946	0.913	0.998	1.051	1.033	1.154
SiO_2	28.587	28.761	28.440	28.501	28.704	28.757	28.779	28.576
K_2O	n.d.	n.d.	n.d.	n.d.	n.d.	n.d.	n.d.	n.d.
CaO	25.876	26.814	26.064	26.021	26.346	26.712	27.167	26.372
TiO_2	36.886	37.885	36.902	36.995	36.966	36.740	37.628	36.390
V_2O_5	n.d.	n.d.	n.d.	n.d.	n.d.	n.d.	0.091	0.076
MnO	0.091	0.095	0.079	0.099	0.099	0.091	0.088	0.096
FeO	1.282	1.174	1.465	1.439	1.577	1.678	1.410	1.688
Y_2O_3	0.173	0.068	0.213	0.142	0.100	0.099	0.032	0.162
Nb_2O_5	0.322	0.350	0.420	0.376	0.247	0.168	0.092	0.144
La_2O_3	0.658	0.443	0.595	0.625	0.508	0.399	0.316	0.427
Ce_2O_3	1.866	1.032	1.890	1.772	1.421	1.208	0.703	1.414
Pr_2O_3	0.205	0.068	0.183	0.146	0.148	0.067	0.049	0.119
Nd_2O_3	0.672	0.257	0.738	0.598	0.527	0.378	0.188	0.523
Sm_2O_3	0.047	n.d.	0.061	0.060	0.071	0.052	n.d.	0.044
Gd_2O_3	n.d.	0.048	n.d.	n.d.	n.d.	n.d.	n.d.	n.d.
Dy_2O_3	n.d.	n.d.	0.081	0.044	n.d.	0.046	n.d.	n.d.
Yb_2O_3	n.d.	n.d.	n.d.	n.d.	n.d.	n.d.	n.d.	n.d.
Ta_2O_5	n.d.	n.d.	n.d.	n.d.	n.d.	n.d.	n.d.	n.d.
ThO_2	0.067	0.144	0.136	0.134	0.077	0.057	0.075	0.056
UO_2	n.d.	n.d.	n.d.	n.d.	n.d.	n.d.	n.d.	n.d.
TOTAL	97.860	98.060	98.370	98.024	97.928	97.601	97.744	97.346
Na	-	0.00263	0.00496	0.00340	-	-	-	-
Mg	0.00388	0.00196	0.00359	0.00318	0.00283	0.00393	0.00196	0.00278
Al	0.16005	0.12597	0.15282	0.14752	0.16082	0.16947	0.16524	0.18695
Si	3.92113	3.90464	3.89414	3.90559	3.92195	3.93148	3.90445	3.92593
K	-	-	-	-	-	-	-	-
Ca	3.80311	3.90067	3.82407	3.82061	3.85725	3.91303	3.94943	3.88215
Ti	3.80502	3.86813	3.80011	3.81257	3.79851	3.77748	3.83934	3.75995
V	-	-	-	-	-	-	0.00822	0.00697
Mn	0.01060	0.01092	0.00924	0.01158	0.01155	0.01059	0.01011	0.01124
Fe	0.14706	0.13335	0.16782	0.16493	0.18023	0.19189	0.16005	0.19401
Y	0.01265	0.00497	0.01555	0.01038	0.00733	0.00724	0.00237	0.01186
Nb	0.02000	0.02148	0.02601	0.02331	0.01526	0.01043	0.00567	0.00897
La	0.03331	0.02218	0.03008	0.03160	0.02564	0.02015	0.01583	0.02163
Ce	0.09371	0.05130	0.09477	0.08892	0.07112	0.06048	0.03496	0.07115
Pr	0.01027	0.00338	0.00917	0.00730	0.00736	0.00334	0.00242	0.00599
Nd	0.03321	0.01258	0.03644	0.02955	0.02598	0.01862	0.00922	0.02593
Sm	0.00225	-	0.00292	0.00286	0.00338	0.00247	-	0.00210
Gd	-	0.00218	-	-	-	-	-	-
Dy	-	-	0.00360	0.00195	-	0.00205	-	-
Yb	-	-	-	-	-	-	-	-
Ta	-	-	-	-	-	-	-	-
Th	0.00211	0.00445	0.00424	0.00419	0.00241	0.00177	0.00232	0.00175
U	-	-	-	-	-	-	-	-
TOTAL	12.04673	12.07636	12.08526	12.07629	12.09833	12.12983	12.11724	12.12405

Titanite Analyses: Strontian - BPSRT3

	T3/A9	T3/B1	T3/B2	T3/B4	T3/B5	T3/B6	T3/B7	T3/B8
Na_2O	n.d.	0.008	0.010	n.d.	n.d.	n.d.	n.d.	n.d.
MgO	0.014	0.010	0.009	0.010	0.011	0.009	0.007	0.007
Al_2O_3	1.013	0.899	0.770	0.792	1.105	0.985	1.074	0.991
SiO_2	28.825	28.260	28.599	28.797	28.753	28.983	28.978	28.901
K_2O	n.d.	n.d.	n.d.	n.d.	n.d.	n.d.	n.d.	n.d.
CaO	27.041	26.234	26.878	26.893	26.844	27.349	27.036	27.238
TiO_2	37.509	37.303	37.906	38.066	37.111	37.763	37.199	38.061
V_2O_5	n.d.	n.d.	n.d.	0.129	n.d.	n.d.	0.075	n.d.
MnO	0.092	0.097	0.093	0.098	0.098	0.083	0.094	0.086
FeO	1.416	1.109	1.135	1.116	1.521	1.288	1.441	1.062
Y_2O_3	0.085	0.055	0.075	0.065	0.093	0.085	0.099	0.106
Nb_2O_5	0.112	0.281	0.392	0.288	0.173	0.120	0.176	0.091
La_2O_3	0.330	0.616	0.482	0.494	0.416	0.285	0.338	0.272
Ce_2O_3	0.784	1.458	1.098	0.923	1.105	0.686	0.924	0.669
Pr_2O_3	0.051	0.081	0.081	0.090	0.110	0.050	0.114	0.058
Nd_2O_3	0.207	0.375	0.334	0.267	0.351	0.136	0.289	0.259
Sm_2O_3	n.d.	n.d.	0.050	n.d.	0.074	n.d.	n.d.	n.d.
Gd_2O_3	n.d.	n.d.	n.d.	n.d.	n.d.	n.d.	n.d.	n.d.
Dy_2O_3	0.039	n.d.	n.d.	n.d.	n.d.	n.d.	n.d.	n.d.
Yb_2O_3	n.d.	n.d.	n.d.	n.d.	n.d.	n.d.	n.d.	n.d.
Ta_2O_5	n.d.	n.d.	n.d.	n.d.	n.d.	n.d.	n.d.	n.d.
ThO_2	0.076	0.078	0.151	0.144	0.063	0.078	0.069	0.087
UO_2	n.d.	n.d.	n.d.	n.d.	n.d.	n.d.	n.d.	n.d.
TOTAL	97.700	97.007	98.200	98.279	97.885	98.0279	97.969	98.092
Na	-	0.00237	0.00276	-	-	-	-	-
Mg	0.00289	0.00205	0.00190	0.00213	0.00223	0.00181	0.00151	0.00151
Al	0.16231	0.14604	0.12337	0.12640	0.17745	0.15711	0.17186	0.15792
Si	3.91651	3.89062	3.88423	3.89706	3.91541	3.91786	3.93055	3.90483
K	-	-	-	-	-	-	-	-
Ca	3.93678	3.86989	3.91160	3.89967	3.91677	3.96129	3.92942	3.94325
Ti	3.83284	3.86225	3.87184	3.87425	3.80056	3.83899	3.79464	3.86739
V	-	-	-	0.01159	-	-	-	-
Mn	0.01066	0.01133	0.01080	0.01128	0.01130	0.00952	0.01085	0.00987
Fe	0.16090	0.12775	0.12895	0.12638	0.17324	0.14569	0.16350	0.12005
Y	0.00615	0.00403	0.00542	0.00468	0.00678	0.00611	0.00719	0.00765
Nb	0.00692	0.01753	0.02410	0.01764	0.01070	0.00733	0.01083	0.00557
La	0.01653	0.03131	0.02417	0.02468	0.02091	0.01421	0.01692	0.01355
Ce	0.03902	0.07352	0.05462	0.04576	0.05511	0.03397	0.04592	0.03312
Pr	0.00255	0.00409	0.00402	0.00447	0.00548	0.00248	0.00563	0.00286
Nd	0.01017	0.01863	0.01634	0.01303	0.01724	0.00663	0.01413	0.01265
Sm	-	-	0.00234	-	0.00348	-	-	-
Gd	-	-	-	-	-	-	-	-
Dy	0.00170	-	-	-	-	-	-	-
Yb	-	-	-	-	-	-	-	-
Ta	-	-	-	-	-	-	-	-
Th	0.00235	0.00246	0.00467	0.00445	0.00198	0.00239	0.00214	0.00269
U	-	-	-	-	-	-	-	-
TOTAL	12.11391	12.07195	12.07984	12.06863	12.12138	12.11317	12.11448	12.09503

Titanite Analyses: Strontian - BPSRT3

	T3/C1	T3/C2	T3/C3	T3/C4	T3/C5	T3/C6	T3/C7	T3/C8
Na_2O	n.d.	n.d.	n.d.	n.d.	n.d.	n.d.	n.d.	n.d.
MgO	0.017	0.013	0.014	0.012	0.014	0.010	0.018	0.015
Al_2O_3	1.037	0.974	0.804	0.814	1.212	1.053	1.038	1.095
SiO_2	28.289	28.588	28.482	28.514	28.294	28.649	28.476	28.605
K_2O	n.d.	n.d.	n.d.	n.d.	n.d.	n.d.	n.d.	n.d.
CaO	25.168	26.230	26.424	26.535	25.605	26.606	26.007	26.289
TiO_2	36.076	37.046	37.389	37.738	35.822	37.088	36.463	36.504
V_2O_5	n.d.	n.d.	n.d.	n.d.	n.d.	n.d.	n.d.	n.d.
MnO	0.096	0.096	0.097	0.096	0.094	0.096	0.085	0.085
FeO	1.669	1.390	1.207	1.173	1.866	1.501	1.617	1.624
Y_2O_3	0.319	0.131	0.060	0.088	0.263	0.073	0.185	0.114
Nb_2O_5	0.530	0.241	0.344	0.347	0.180	0.141	0.244	0.201
La_2O_3	0.553	0.483	0.546	0.465	0.363	0.380	0.402	0.385
Ce_2O_3	2.070	1.372	1.228	1.043	1.449	0.937	1.375	1.151
Pr_2O_3	0.282	0.130	0.115	0.084	0.198	0.105	0.139	0.092
Nd_2O_3	1.005	0.497	0.337	0.260	0.788	0.257	0.662	0.443
Sm_2O_3	0.148	n.d.	n.d.	0.056	0.161	n.d.	0.092	0.046
Gd_2O_3	n.d.	n.d.	n.d.	n.d.	0.060	n.d.	n.d.	n.d.
Dy_2O_3	0.073	0.046	n.d.	n.d.	0.062	n.d.	n.d.	0.045
Yb_2O_3	0.021	n.d.	n.d.	0.024	0.033	n.d.	n.d.	n.d.
Ta_2O_5	n.d.	n.d.	n.d.	n.d.	n.d.	n.d.	n.d.	n.d.
ThO_2	0.119	0.084	0.134	0.144	0.079	0.081	0.062	0.048
UO_2	n.d.	n.d.	n.d.	n.d.	n.d.	n.d.	n.d.	n.d.
TOTAL	97.647	97.447	97.271	97.465	97.589	97.057	97.017	96.814
Na	-	-	-	-	-	-	-	-
Mg	0.00365	0.00275	0.00286	0.00256	0.00308	0.00214	0.00376	0.00326
Al	0.16930	0.15752	0.13004	0.13111	0.19860	0.17002	0.16882	0.17780
Si	3.91694	3.91857	3.90631	3.89543	3.93280	3.92355	3.92856	3.93763
K	-	-	-	-	-	-	-	-
Ca	3.73409	3.85248	3.88324	3.88429	3.81343	3.90427	3.84460	3.87763
Ti	3.75673	3.81886	3.85656	3.87725	3.74465	3.81993	3.78326	3.77909
V	-	-	-	-	-	-	-	-
Mn	0.01133	0.01118	0.01131	0.01114	0.01111	0.01119	0.01003	0.01001
Fe	0.19330	0.15935	0.13849	0.13405	0.21694	0.17200	0.18661	0.18700
Y	0.02354	0.00961	0.00442	0.00646	0.01947	0.00534	0.01360	0.00837
Nb	0.03319	0.01493	0.02138	0.02148	0.01133	0.00876	0.01525	0.01255
La	0.02826	0.02445	0.02764	0.02347	0.01864	0.01924	0.02050	0.01955
Ce	0.10493	0.06886	0.06167	0.05218	0.07374	0.04702	0.06947	0.05802
Pr	0.01424	0.00649	0.00577	0.00422	0.01004	0.00528	0.00700	0.00461
Nd	0.05017	0.02455	0.01666	0.01281	0.03947	0.01269	0.03293	0.02197
Sm	0.00710	-	-	0.00267	0.00772	-	0.00441	0.00221
Gd	-	-	-	-	0.00278	-	-	-
Dy	0.00325	0.00204	-	-	0.00277	-	-	0.00202
Yb	0.00091	-	-	0.00103	0.00139	-	-	-
Ta	-	-	-	-	-	-	-	-
Th	0.00375	0.00262	0.00419	0.00450	0.00251	0.00254	0.00194	0.00151
U	-	-	-	-	-	-	-	-
TOTAL	12.06412	12.08362	12.07549	12.06936	12.11374	12.11025	12.09929	12.10942

Titanite Analyses: Strontian - BPSRT3

	T3/C9	T3/C10	T3/C11	T3/C12
Na_2O	n.d.	n.d.	n.d.	n.d.
MgO	0.018	0.009	0.009	0.006
Al_2O_3	1.037	0.967	0.986	0.974
SiO_2	28.495	28.581	28.645	28.623
K_2O	n.d.	n.d.	n.d.	n.d.
CaO	26.576	26.774	26.833	27.047
TiO_2	36.851	37.413	37.488	37.491
V_2O_5	n.d.	n.d.	0.096	0.085
MnO	0.103	0.100	0.091	0.082
FeO	1.519	1.349	1.254	1.315
Y_2O_3	0.072	0.093	0.088	0.042
Nb_2O_5	0.162	0.124	0.096	0.084
La_2O_3	0.383	0.301	0.284	0.206
Ce_2O_3	0.999	0.625	0.614	0.443
Pr_2O_3	0.089	0.055	0.082	n.d.
Nd_2O_3	0.308	0.170	0.186	0.193
Sm_2O_3	n.d.	0.044	0.047	n.d.
Gd_2O_3	n.d.	0.000	0.012	n.d.
Dy_2O_3	n.d.	n.d.	n.d.	n.d.
Yb_2O_3	n.d.	n.d.	n.d.	n.d.
Ta_2O_5	n.d.	n.d.	n.d.	n.d.
ThO_2	0.067	0.070	0.070	n.d.
UO_2	n.d.	n.d.	n.d.	n.d.
TOTAL	96.838	96.807	96.950	96.715
Na	-	-	-	-
Mg	0.00368	0.00185	0.00183	0.00132
Al	0.16809	0.15616	0.15894	0.15703
Si	3.91724	3.91229	3.91338	3.91239
K	-	-	-	-
Ca	3.91463	3.92704	3.92804	3.96133
Ti	3.80988	3.85149	3.85166	3.85399
V	-	-	0.00867	0.00772
Mn	0.01202	0.01169	0.01053	0.00955
Fe	0.17463	0.15445	0.14334	0.15042
Y	0.00527	0.00680	0.00643	0.00308
Nb	0.01012	0.00772	0.00593	0.00520
La	0.01946	0.01521	0.01432	0.01042
Ce	0.05027	0.03132	0.03072	0.02219
Pr	0.00449	0.00274	0.00412	-
Nd	0.01526	0.00840	0.00916	0.00950
Sm	-	0.00207	0.00224	-
Gd	-	0.00003	0.00058	-
Dy	-	-	-	-
Yb	-	-	-	-
Ta	-	-	-	-
Th	0.00209	0.00219	0.00218	-
U	-	-	-	-
TOTAL	12.11653	12.10101	12.09653	12.10968

Titanite Analyses: Strontian - BPSRT4

	T4/A1	T4/A2	T4/A3	T4/A4	T4/A5	T4/A6	T4/A9	T4/A10
Na_2O	0.021	0.012	0.016	n.d.	0.011	n.d.	n.d.	n.d.
MgO	0.016	0.018	0.015	0.014	0.014	0.015	0.010	0.009
Al_2O_3	1.019	1.019	0.902	1.093	0.988	1.163	0.969	1.030
SiO_2	28.685	28.771	28.690	28.563	28.613	28.717	28.822	28.799
K_2O	n.d.	n.d.	n.d.	n.d.	n.d.	n.d.	n.d.	n.d.
CaO	25.519	25.885	25.873	25.966	25.930	26.253	26.498	26.489
TiO_2	35.671	36.152	36.717	35.907	36.413	36.237	36.271	36.899
V_2O_5	0.061	0.026	0.020	0.033	0.029	0.028	0.048	0.134
MnO	0.094	0.087	0.093	0.096	0.087	0.098	0.107	0.096
FeO	1.640	1.351	1.443	1.793	1.511	1.677	1.711	1.372
Y_2O_3	0.352	0.192	0.178	0.246	0.187	0.173	0.068	0.182
Nb_2O_5	0.407	0.348	0.369	0.206	0.279	0.152	0.333	0.173
La_2O_3	0.482	0.562	0.613	0.405	0.433	0.382	0.624	0.260
Ce_2O_3	2.005	1.913	1.749	1.482	1.463	1.325	1.296	0.750
Pr_2O_3	0.263	0.197	0.138	0.185	0.180	0.195	0.113	0.066
Nd_2O_3	1.103	0.801	0.643	0.858	0.739	0.628	0.282	0.296
Sm_2O_3	0.163	0.118	0.053	0.133	0.101	0.046	0.047	0.080
Gd_2O_3	0.078	n.d.	n.d.	0.045	0.073	0.050	n.d.	n.d.
Dy_2O_3	0.118	0.050	n.d.	0.047	n.d.	0.044	n.d.	0.042
Yb_2O_3	n.d.	n.d.	n.d.	n.d.	n.d.	n.d.	n.d.	n.d.
Ta_2O_5	n.d.	n.d.	n.d.	n.d.	n.d.	n.d.	n.d.	n.d.
ThO_2	0.092	0.096	0.125	0.063	0.060	0.079	0.153	0.071
UO_2	n.d.	n.d.	n.d.	n.d.	n.d.	n.d.	0.053	n.d.
TOTAL	97.892	97.699	97.864	97.183	97.200	97.321	97.460	96.851
Na	0.00583	0.00336	0.00439	-	0.00318	-	-	-
Mg	0.00335	0.00369	0.00323	0.00300	0.00295	0.00315	0.00218	0.00198
Al	0.16594	0.16533	0.14609	0.17816	0.16059	0.18853	0.15685	0.16642
Si	3.95933	3.95813	3.93888	3.94640	3.94344	3.94693	3.95407	3.94468
K	-	-	-	-	-	-	-	-
Ca	3.77413	3.81567	3.80609	3.84408	3.82921	3.86623	3.89525	3.88774
Ti	3.70279	3.74034	3.79113	3.73109	3.77417	3.74560	3.74232	3.80107
V	-	-	-	-	-	-	-	0.01190
Mn	0.01109	0.01020	0.01092	0.01127	0.01019	0.01140	0.01249	0.01124
Fe	0.18938	0.15548	0.16578	0.20728	0.17422	0.19279	0.19632	0.15722
Y	0.02587	0.01407	0.01301	0.01813	0.01378	0.01270	0.00501	0.01331
Nb	0.02542	0.02168	0.02291	0.01291	0.01738	0.00948	0.02065	0.01073
La	0.02455	0.02856	0.03108	0.02066	0.02202	0.01939	0.03159	0.01317
Ce	0.10135	0.09639	0.08795	0.07496	0.07384	0.06668	0.06513	0.03765
Pr	0.01326	0.00991	0.00694	0.00932	0.00903	0.00978	0.00565	0.00332
Nd	0.05487	0.03974	0.03184	0.04275	0.03674	0.03112	0.01395	0.01461
Sm	0.00779	0.00560	0.00252	0.00635	0.00480	0.00218	0.00225	0.00380
Gd	0.00358	-	-	0.00209	0.00334	0.00228	-	-
Dy	0.00528	0.00224	-	0.00213	-	0.00196	0.00008	0.00188
Yb	-	-	-	-	-	-	-	-
Ta	-	-	-	-	-	-	-	-
Th	0.00289	0.00302	0.00393	0.00198	0.00191	0.00247	0.00480	0.00223
U	-	-	-	-	-	-	0.00208	-
TOTAL	12.08627	12.08037	12.07027	12.11895	12.08714	12.11784	12.11886	12.08964

Titanite Analyses: Strontian - BPSRT4

	T4/A11	T4/A12	T4/A13	T4/B1	T4/B2	T4/B3	T4/B4	T4/B5
Na_2O	n.d.	n.d.	n.d.	0.008	n.d.	0.018	0.011	n.d.
MgO	0.011	0.013	0.011	0.012	0.011	0.018	0.012	0.010
Al_2O_3	1.010	1.045	1.099	0.952	0.952	0.865	0.884	1.019
SiO_2	28.839	28.755	28.465	28.813	28.811	28.687	28.701	28.885
K_2O	n.d.	n.d.	n.d.	n.d.	n.d.	n.d.	n.d.	n.d.
CaO	26.845	26.516	25.890	26.401	26.149	26.076	25.874	26.843
TiO_2	37.097	36.490	36.001	37.362	37.369	37.238	36.871	37.238
V_2O_5	n.d.	n.d.	n.d.	n.d.	n.d.	n.d.	n.d.	n.d.
MnO	0.098	0.100	0.095	0.091	0.100	0.089	0.090	0.098
FeO	1.327	1.517	1.619	1.178	1.252	1.357	1.353	1.439
Y_2O_3	0.150	0.097	0.204	0.060	0.077	0.157	0.139	0.059
Nb_2O_5	0.143	0.185	0.202	0.291	0.296	0.385	0.422	0.151
La_2O_3	0.346	0.375	0.355	0.565	0.652	0.611	0.623	0.368
Ce_2O_3	0.633	1.063	1.277	1.307	1.624	1.660	1.713	0.828
Pr_2O_3	0.044	0.088	0.153	0.094	0.120	0.151	0.172	0.064
Nd_2O_3	0.266	0.356	0.624	0.331	0.434	0.534	0.594	0.250
Sm_2O_3	n.d.	0.045	0.100	n.d.	0.039	n.d.	0.048	n.d.
Gd_2O_3	n.d.	n.d.	n.d.	n.d.	n.d.	n.d.	n.d.	n.d.
Dy_2O_3	0.039	n.d.	0.040	0.047	n.d.	n.d.	n.d.	n.d.
Yb_2O_3	n.d.	n.d.	n.d.	n.d.	n.d.	n.d.	n.d.	n.d.
Ta_2O_5	n.d.	n.d.	n.d.	n.d.	n.d.	n.d.	n.d.	n.d.
ThO_2	0.080	0.058	0.072	0.081	0.074	0.134	0.118	0.063
UO_2	n.d.	n.d.	n.d.	n.d.	n.d.	n.d.	n.d.	n.d.
TOTAL	97.070	96.821	96.308	97.690	98.058	98.115	97.755	97.461
Na	-	-	-	0.00222	-	0.00484	0.00308	-
Mg	0.00238	0.00266	0.00246	0.00254	0.00229	0.00382	0.00247	0.00213
Al	0.16274	0.16941	0.17989	0.15312	0.15304	0.13928	0.14302	0.16361
Si	3.94057	3.95226	3.95052	3.92937	3.92667	3.91792	3.93576	3.93350
K	-	-	-	-	-	-	-	-
Ca	3.93036	3.90525	3.85008	3.85786	3.81864	3.81599	3.80180	3.91686
Ti	3.81208	3.77197	3.75758	3.83194	3.83028	3.82480	3.80251	3.81377
V	-	-	-	-	-	-	-	-
Mn	0.01138	0.01171	0.01119	0.01060	0.01155	0.01029	0.01052	0.01136
Fe	0.15165	0.17448	0.18793	0.13440	0.14275	0.15508	0.15522	0.16398
Y	0.01092	0.00715	0.01512	0.00438	0.00565	0.01142	0.01017	0.00431
Nb	0.00885	0.01151	0.01269	0.01797	0.01826	0.02377	0.02616	0.00930
La	0.01744	0.01905	0.01819	0.02845	0.03280	0.03081	0.03152	0.01851
Ce	0.03170	0.05349	0.06491	0.06527	0.08105	0.08302	0.08600	0.04128
Pr	0.00221	0.00441	0.00775	0.00470	0.00598	0.00752	0.00860	0.00318
Nd	0.01313	0.01764	0.03122	0.01631	0.02132	0.02629	0.02936	0.01229
Sm	-	0.00216	0.00478	-	0.00186	-	0.00230	-
Gd	-	-	-	-	-	-	-	-
Dy	0.00172	-	0.00178	0.00209	-	-	-	-
Yb	-	-	-	-	-	-	-	-
Ta	-	-	-	-	-	-	-	-
Th	0.00250	0.00181	0.00227	0.00252	0.00232	0.00417	0.00368	0.00196
U	-	-	-	-	-	-	-	-
TOTAL	12.10734	12.1149	12.10378	12.06882	12.06056	12.06517	12.05843	12.10517

Titanite Analyses: Strontian - BPSRT4

	T4/B6	T4/B7	T4/B8	T4/B9	T4/B10	T4/B11	T4/B12	T4/B13
Na_2O	n.d.	n.d.	n.d.	n.d.	n.d.	n.d.	n.d.	n.d.
MgO	0.013	0.014	0.009	0.012	0.014	0.018	0.006	0.009
Al_2O_3	1.012	1.007	1.000	1.024	1.021	0.977	0.968	1.013
SiO_2	29.010	28.960	29.098	29.011	29.112	29.123	29.044	29.021
K_2O	n.d.	n.d.	n.d.	0.005	n.d.	n.d.	n.d.	n.d.
CaO	26.938	26.866	26.998	26.897	26.966	27.086	26.683	26.810
TiO_2	37.507	37.537	37.352	37.533	37.348	37.778	37.372	37.071
V_2O_5	n.d.	n.d.	n.d.	n.d.	0.123	n.d.	n.d.	n.d.
MnO	0.097	0.091	0.100	0.097	0.094	0.090	0.101	0.092
FeO	1.470	1.466	1.374	1.248	1.364	1.289	1.366	1.402
Y_2O_3	0.083	0.071	0.050	0.114	0.052	0.062	0.116	0.226
Nb_2O_5	0.132	0.129	0.135	0.131	0.146	0.127	0.175	0.179
La_2O_3	0.367	0.316	0.322	0.373	0.316	0.251	0.416	0.255
Ce_2O_3	0.834	0.770	0.798	0.830	0.718	0.597	0.822	0.670
Pr_2O_3	0.105	n.d.	0.055	0.050	0.068	n.d.	0.057	0.045
Nd_2O_3	0.199	0.225	0.210	0.273	0.212	0.152	0.248	0.246
Sm_2O_3	n.d.	n.d.	n.d.	0.042	n.d.	n.d.	n.d.	n.d.
Gd_2O_3	0.016	0.015	0.020	0.002	0.025	n.d.	n.d.	n.d.
Dy_2O_3	n.d.	n.d.	n.d.	n.d.	n.d.	n.d.	n.d.	0.059
Yb_2O_3	n.d.	n.d.	n.d.	n.d.	n.d.	n.d.	n.d.	n.d.
Ta_2O_5	n.d.	n.d.	n.d.	n.d.	n.d.	n.d.	n.d.	n.d.
ThO_2	0.068	0.075	0.069	0.061	0.041	0.103	0.059	0.046
UO_2	n.d.	n.d.	n.d.	n.d.	n.d.	n.d.	n.d.	n.d.
TOTAL	97.976	97.676	97.658	97.798	97.725	97.766	97.572	97.305
Na	-	-	-	-	-	-	-	-
Mg	0.00276	0.00299	0.00184	0.00250	0.00301	0.00362	0.00133	0.00199
Al	0.16164	0.16125	0.16010	0.16383	0.16323	0.15589	0.15532	0.16285
Si	3.93061	3.93065	3.94927	3.93442	3.94565	3.93867	3.94931	3.95405
K	-	-	-	0.00086	-	-	-	-
Ca	3.91081	3.90711	3.92627	3.90854	3.91609	3.92511	3.88784	3.91392
Ti	3.82184	3.83155	3.81263	3.82812	3.80684	3.84242	3.82184	3.79849
V	-	-	-	-	0.01102	-	-	-
Mn	0.01119	0.01049	0.01154	0.01120	0.01088	0.01035	0.01170	0.01064
Fe	0.16664	0.16644	0.15606	0.14158	0.15461	0.14582	0.15542	0.15979
Y	0.00598	0.00515	0.00367	0.00822	0.00379	0.00449	0.00843	0.01643
Nb	0.00808	0.00792	0.00832	0.00806	0.00897	0.00781	0.01076	0.01104
La	0.01834	0.01581	0.01614	0.01869	0.01579	0.01256	0.02086	0.01281
Ce	0.04140	0.03830	0.03965	0.04121	0.03563	0.02956	0.04093	0.03344
Pr	0.00521	-	0.00275	0.00251	0.00340	-	0.00283	0.00226
Nd	0.00973	0.01104	0.01031	0.01336	0.01037	0.00741	0.01217	0.01212
Sm	-	-	-	0.00200	-	-	-	-
Gd	-	0.00071	0.00091	0.00013	0.00115	-	-	-
Dy	-	-	-	-	-	-	-	0.00259
Yb	-	-	-	-	-	-	-	-
Ta	-	-	-	-	-	-	-	-
Th	0.00211	0.00233	0.00215	0.00191	0.00127	0.00319	0.00184	0.00145
U	-	-	-	-	-	-	-	-
TOTAL	12.10479	12.10085	12.10507	12.09275	12.09821	12.09446	12.08889	12.10293

Titanite Analyses: Strontian - BPSRT4

	T4/B14	T4/C1	T4/C2	T4/C3	T4/C4	T4/C5	T4/C6	T4/C7
Na_2O	n.d.	0.022	0.016	n.d.	n.d.	n.d.	n.d.	n.d.
MgO	0.027	0.009	0.018	0.013	0.007	0.014	0.010	0.013
Al_2O_3	1.089	0.969	0.948	0.876	0.779	1.033	1.010	0.996
SiO_2	29.060	28.610	28.767	28.848	28.860	29.096	28.914	28.930
K_2O	0.104	n.d.	n.d.	n.d.	n.d.	n.d.	n.d.	n.d.
CaO	26.957	25.220	25.725	26.029	26.435	26.727	26.565	26.787
TiO_2	37.041	35.702	36.755	37.102	37.573	36.961	36.804	37.079
V_2O_5	0.097	n.d.	n.d.	n.d.	n.d.	n.d.	0.086	0.070
MnO	0.062	0.084	0.088	0.091	0.082	0.098	0.092	0.111
FeO	1.502	1.496	1.311	1.355	1.147	1.423	1.424	1.334
Y_2O_3	0.014	0.235	0.157	0.117	0.068	0.051	0.068	0.174
Nb_2O_5	0.006	0.372	0.321	0.332	0.263	0.104	0.142	0.168
La_2O_3	0.131	0.534	0.557	0.575	0.523	0.311	0.314	0.245
Ce_2O_3	0.175	1.793	1.714	1.494	1.045	0.751	0.721	0.609
Pr_2O_3	n.d.	0.185	0.204	0.144	0.087	0.063	0.050	0.062
Nd_2O_3	0.031	0.783	0.637	0.418	0.275	0.228	0.167	0.203
Sm_2O_3	n.d.	0.074	0.046	n.d.	0.041	n.d.	n.d.	0.061
Gd_2O_3	n.d.	0.052	n.d.	n.d.	n.d.	n.d.	n.d.	0.051
Dy_2O_3	n.d.	n.d.	n.d.	0.059	n.d.	n.d.	n.d.	n.d.
Yb_2O_3	n.d.	n.d.	n.d.	n.d.	n.d.	n.d.	n.d.	n.d.
Ta_2O_5	n.d.	n.d.	n.d.	n.d.	n.d.	n.d.	n.d.	n.d.
ThO_2	n.d.	0.112	0.072	0.097	0.152	0.082	0.058	n.d.
UO_2	n.d.	n.d.	n.d.	n.d.	n.d.	n.d.	n.d.	n.d.
TOTAL	96.412	96.446	97.498	97.962	97.453	97.044	96.498	97.029
Na	-	0.00614	0.00428	-	-	-	-	-
Mg	0.00557	0.00199	0.00380	0.00271	0.00160	0.00303	0.00218	0.00266
Al	0.17531	0.15895	0.15340	0.14124	0.12541	0.16625	0.16336	0.16036
Si	3.96754	3.97943	3.94871	3.94356	3.93814	3.97026	3.96533	3.94914
K	0.01813	-	-	-	-	-	-	-
Ca	3.94356	3.75872	3.78352	3.81271	3.86513	3.90780	3.90369	3.91799
Ti	3.80328	3.73457	3.79427	3.81444	3.85581	3.79304	3.79593	3.80650
V	0.00875	-	-	-	-	-	0.00782	0.00631
Mn	0.00727	0.00993	0.01024	0.01056	0.00951	0.01136	0.01071	0.01293
Fe	0.17156	0.17411	0.15060	0.15500	0.13095	0.16243	0.16340	0.15230
Y	0.00103	0.01742	0.01150	0.00856	0.00498	0.00370	0.00502	0.01265
Nb	0.00041	0.02340	0.01993	0.02056	0.01625	0.00646	0.00884	0.01038
La	0.00662	0.02739	0.02822	0.02900	0.02632	0.01568	0.01588	0.01234
Ce	0.00877	0.09133	0.08614	0.07477	0.05221	0.03754	0.03624	0.03045
Pr	-	0.00942	0.01021	0.00720	0.00434	0.00317	0.00251	0.00308
Nd	0.00157	0.03927	0.03151	0.02061	0.01356	0.01124	0.00829	0.00998
Sm	-	0.00358	0.00221	-	0.00193	-	-	0.00289
Gd	-	0.00243	-	-	-	-	-	0.00232
Dy	-	-	-	-	-	-	-	-
Yb	-	-	-	-	-	-	-	-
Ta	-	-	-	-	-	-	-	-
Th	-	0.00355	0.00225	0.00302	0.00474	0.00254	0.00182	-
U	-	-	-	-	-	-	-	-
TOTAL	12.12679	12.05586	12.05157	12.05624	12.05783	12.10107	12.09605	12.09896

Titanite Analyses: Strontian - BPSRT4

	T4/C8
Na_2O	n.d.
MgO	0.010
Al_2O_3	1.058
SiO_2	29.001
K_2O	0.030
CaO	26.584
TiO_2	36.988
V_2O_5	n.d.
MnO	0.086
FeO	1.303
Y_2O_3	0.209
Nb_2O_5	0.172
La_2O_3	0.258
Ce_2O_3	0.663
Pr_2O_3	0.120
Nd_2O_3	0.273
Sm_2O_3	0.053
Gd_2O_3	n.d.
Dy_2O_3	0.056
Yb_2O_3	0.027
Ta_2O_5	n.d.
ThO_2	0.054
UO_2	n.d.
TOTAL	97.069
Na	-
Mg	0.00217
Al	0.17032
Si	3.95990
K	0.00526
Ca	3.88941
Ti	3.79825
V	-
Mn	0.01005
Fe	0.14882
Y	0.01522
Nb	0.01062
La	0.01299
Ce	0.03315
Pr	0.00601
Nd	0.01347
Sm	0.00253
Gd	-
Dy	0.00248
Yb	0.00114
Ta	-
Th	0.00169
U	-
TOTAL	12.09223

Titanite Analyses: Strontian - BPSRG4

	G4/A1	G4/A2	G4/A3	G4/A4	G4/A5	G4/A6	G4/A7	G4/A8
Na_2O	0.010	n.d.	n.d.	n.d.	0.008	n.d.	n.d.	n.d.
MgO	0.006	0.013	0.005	0.006	0.011	0.006	0.010	0.004
Al_2O_3	1.053	1.176	1.093	0.889	1.092	1.038	1.017	1.153
SiO_2	28.132	28.557	28.707	28.901	28.701	28.753	28.726	28.659
K_2O	n.d.	n.d.	n.d.	n.d.	n.d.	n.d.	n.d.	n.d.
CaO	25.811	26.322	26.631	27.092	26.454	26.573	26.036	26.379
TiO_2	36.627	37.235	37.397	38.062	37.476	37.199	37.265	36.673
V_2O_5	n.d.	n.d.	n.d.	n.d.	n.d.	0.080	n.d.	n.d.
MnO	0.095	0.117	0.112	0.105	0.097	0.107	0.106	0.114
FeO	1.119	1.245	1.203	1.143	1.215	1.472	1.394	1.539
Y_2O_3	0.318	0.243	0.196	0.249	0.241	0.274	0.345	0.470
Nb_2O_5	0.195	0.219	0.279	0.223	0.205	0.221	0.363	0.534
La_2O_3	0.356	0.371	0.384	0.212	0.391	0.269	0.344	0.318
Ce_2O_3	1.427	1.416	1.295	0.821	1.385	1.036	1.247	1.158
Pr_2O_3	0.175	0.168	0.166	0.118	0.175	0.116	0.185	0.171
Nd_2O_3	0.878	0.724	0.600	0.423	0.821	0.490	0.701	0.854
Sm_2O_3	0.161	0.112	0.109	0.105	0.091	0.089	0.123	0.211
Gd_2O_3	0.087	0.076	n.d.	0.061	0.064	n.d.	0.087	0.143
Dy_2O_3	0.103	0.042	0.060	n.d.	0.051	0.065	0.040	0.124
Yb_2O_3	n.d.	n.d.	n.d.	n.d.	n.d.	n.d.	n.d.	n.d.
Ta_2O_5	n.d.	n.d.	n.d.	n.d.	n.d.	n.d.	n.d.	n.d.
ThO_2	0.047	n.d.	0.045	n.d.	n.d.	n.d.	n.d.	0.054
UO_2	n.d.	n.d.	n.d.	n.d.	n.d.	n.d.	n.d.	n.d.
TOTAL	96.656	98.158	98.390	98.517	98.520	97.912	98.1476	98.658
Na	0.00274	-	-	-	0.00213	-	-	-
Mg	0.00130	0.00270	0.00101	0.00122	0.00236	0.00136	0.00207	0.00085
Al	0.17230	0.18913	0.17501	0.14156	0.17498	0.16669	0.16340	0.18518
Si	3.90224	3.89316	3.89847	3.90053	3.89855	3.91492	3.91496	3.90331
K	-	-	-	-	-	-	-	-
Ca	3.83635	3.84503	3.87518	3.91791	3.85031	3.87684	3.80203	3.84974
Ti	3.82089	3.81754	3.81941	3.86335	3.82832	3.80909	3.81952	3.75640
V	-	-	-	-	-	0.00722	-	-
Mn	0.01119	0.01360	0.01298	0.01209	0.01125	0.01235	0.01224	0.01318
Fe	0.12990	0.14195	0.13663	0.12906	0.13805	0.16770	0.15889	0.17535
Y	0.02347	0.01765	0.01422	0.01794	0.01742	0.01989	0.02506	0.03409
Nb	0.01223	0.01349	0.01717	0.01363	0.01260	0.01364	0.02237	0.03288
La	0.01823	0.01867	0.01925	0.01059	0.01959	0.01352	0.01732	0.01601
Ce	0.07250	0.07071	0.06440	0.04058	0.06890	0.05168	0.06222	0.05777
Pr	0.00885	0.00836	0.00825	0.00583	0.00869	0.00575	0.00920	0.00849
Nd	0.04392	0.03557	0.02938	0.02061	0.04018	0.02407	0.03446	0.04195
Sm	0.00773	0.00530	0.00510	0.00488	0.00430	0.00420	0.00579	0.00990
Gd	0.00402	0.00347	-	0.00277	0.00288	-	0.00394	0.00648
Dy	0.00463	0.00185	0.00263	-	0.00224	0.00288	0.00179	0.00545
Yb	-	-	-	-	-	-	0.00121	0.00114
Ta	-	-	-	-	-	-	-	-
Th	0.00149	-	0.00139	-	-	-	-	0.00169
U	-	-	-	-	-	-	-	-
TOTAL	12.07702	12.08517	12.08807	12.08785	12.08411	12.09784	12.06303	12.01034

Titanite Analyses: Strontian - BPSRG4

	G4/A9	G4/A10	G4/B1	G4/B2	G4/B3	G4/B5	G4/B6	G4/B9
Na_2O	n.d.	0.017	0.010	n.d.	n.d.	0.068	0.075	0.068
MgO	0.008	0.007	0.004	0.007	0.005	n.d.	n.d.	n.d.
Al_2O_3	1.139	1.227	1.202	1.019	1.247	1.770	1.694	1.289
SiO_2	29.005	28.978	28.662	28.562	28.566	28.857	29.126	28.861
K_2O	n.d.	n.d.	n.d.	n.d.	n.d.	n.d.	n.d.	0.028
CaO	27.151	27.256	26.312	25.701	26.758	25.955	26.828	26.417
TiO_2	37.265	37.146	36.835	36.727	36.785	35.452	35.985	36.498
V_2O_5	n.d.	n.d.	n.d.	n.d.	n.d.	0.070	n.d.	n.d.
MnO	0.112	0.120	0.160	0.101	0.132	0.180	0.172	0.120
FeO	1.643	1.657	1.325	1.499	1.477	1.860	1.586	1.512
Y_2O_3	0.215	0.298	0.774	0.362	0.373	0.362	0.180	0.083
Nb_2O_5	0.122	0.147	0.504	0.289	0.190	0.352	0.252	0.143
La_2O_3	0.165	0.143	0.078	0.414	0.142	0.048	0.050	0.098
Ce_2O_3	0.747	0.649	0.535	1.590	0.612	0.307	0.233	0.551
Pr_2O_3	0.109	0.099	0.136	0.256	0.084	0.095	0.071	0.061
Nd_2O_3	0.377	0.453	0.570	0.875	0.476	0.436	0.247	0.368
Sm_2O_3	0.075	0.099	0.142	0.137	0.087	0.129	0.060	0.121
Gd_2O_3	0.052	0.052	0.145	0.093	0.076	0.188	0.048	0.047
Dy_2O_3	n.d.	0.059	0.142	0.092	0.060	0.171	0.098	0.087
Yb_2O_3	n.d.	0.025	0.057	0.047	n.d.	0.105	0.035	0.027
Ta_2O_5	n.d.	n.d.	n.d.	n.d.	n.d.	n.d.	n.d.	n.d.
ThO_2	n.d.	n.d.	n.d.	0.054	n.d.	n.d.	n.d.	n.d.
UO_2	n.d.	n.d.	n.d.	n.d.	n.d.	n.d.	n.d.	n.d.
TOTAL	98.306	98.534	98.657	97.907	97.191	96.471	96.833	96.479
Na	-	0.00466	0.00277	-	-	0.01829	0.01999	0.01817
Mg	0.00163	0.00159	0.00081	0.00149	0.00118	-	-	-
Al	0.18166	0.19535	0.19360	0.16490	0.20129	0.28706	0.27251	0.20859
Si	3.92214	3.91315	3.91292	3.92069	3.90931	3.96968	3.97229	3.96147
K	-	-	-	-	-	-	-	0.00504
Ca	3.93395	3.94374	3.84898	3.78023	3.92372	3.82580	3.92056	3.88525
Ti	3.78962	3.77237	3.78190	3.79148	3.78590	3.66771	3.69099	3.76763
V	-	0.00632	-	-	-	0.00639	-	-
Mn	0.01288	0.01377	0.01854	0.01184	0.01533	0.02099	0.01990	0.01405
Fe	0.18584	0.18713	0.15132	0.17213	0.16904	0.21400	0.18093	0.17362
Y	0.01547	0.02146	0.05626	0.02645	0.02719	0.02655	0.01306	0.00612
Nb	0.00748	0.00902	0.03115	0.01799	0.01179	0.02194	0.01554	0.00887
La	0.00823	0.00712	0.00393	0.02096	0.00718	0.00246	0.00253	0.00498
Ce	0.03701	0.03210	0.02674	0.07991	0.03068	0.01546	0.01164	0.02771
Pr	0.00540	0.00490	0.00678	0.01283	0.00420	0.00476	0.00354	0.00307
Nd	0.01840	0.02206	0.02804	0.04329	0.02350	0.02162	0.01216	0.01820
Sm	0.00350	0.00460	0.00670	0.00649	0.00410	0.00613	0.00285	0.00573
Gd	0.00237	0.00236	0.00657	0.00425	0.00348	0.00858	0.00218	0.00217
Dy	-	0.00258	0.00628	0.00406	0.00265	0.00757	0.00431	0.00385
Yb	-	0.00105	0.00237	0.00197	-	0.00441	0.00146	0.00113
Ta	0.00066	0.00016	0.00055	0.00047	0.00090	0.00146	0.00122	0.00007
Th	-	-	-	0.00170	-	-	-	-
U	-	-	-	-	-	-	-	-
TOTAL	12.13285	12.14628	12.08848	12.07186	12.12724	12.13476	12.15273	12.12147

Titanite Analyses: Strontian - BPSRG4

	G4/B10	G4/C1	G4/C2	G4/C3	G4/C4	G4/C5	G4/C6	G4/C7
Na_2O	0.058	0.089	0.115	0.096	0.083	0.101	0.067	0.127
MgO	n.d.	n.d.	0.014	n.d.	n.d.	n.d.	n.d.	n.d.
Al_2O_3	1.197	1.155	0.961	1.018	0.970	1.195	1.209	1.627
SiO_2	29.063	29.319	29.332	29.208	28.568	28.712	28.567	28.190
K_2O	n.d.	n.d.	n.d.	n.d.	n.d.	n.d.	n.d.	n.d.
CaO	26.782	27.387	26.831	26.726	26.508	26.929	26.617	24.846
TiO_2	36.861	37.507	37.964	37.490	37.435	37.428	36.921	34.984
V_2O_5	n.d.	n.d.	n.d.	n.d.	n.d.	n.d.	n.d.	n.d.
MnO	0.134	0.112	0.111	0.106	0.111	0.129	0.133	0.185
FeO	1.678	1.510	1.358	1.464	1.307	1.310	1.326	1.670
Y_2O_3	0.085	0.116	0.220	0.217	0.247	0.397	0.173	1.576
Nb_2O_5	0.172	0.120	0.215	0.325	0.325	0.162	0.202	0.540
La_2O_3	0.119	0.205	0.312	0.401	0.320	0.095	0.110	0.060
Ce_2O_3	0.650	0.849	1.190	1.412	1.035	0.623	0.501	0.553
Pr_2O_3	0.067	0.113	0.140	0.196	0.140	0.083	0.082	0.153
Nd_2O_3	0.382	0.470	0.713	0.752	0.578	0.460	0.381	0.834
Sm_2O_3	0.113	0.035	0.134	0.133	0.095	0.131	0.111	0.324
Gd_2O_3	0.057	0.057	n.d.	0.047	n.d.	0.103	0.075	0.346
Dy_2O_3	0.054	0.040	0.079	0.078	0.044	0.055	0.074	0.360
Yb_2O_3	0.025	n.d.	n.d.	n.d.	n.d.	0.039	0.028	0.132
Ta_2O_5	n.d.	n.d.	n.d.	n.d.	n.d.	n.d.	n.d.	n.d.
ThO_2	n.d.	n.d.	n.d.	n.d.	n.d.	n.d.	n.d.	n.d.
UO_2	n.d.	n.d.	n.d.	n.d.	n.d.	n.d.	n.d.	n.d.
TOTAL	97.584	99.155	99.843	99.805	97.980	97.994	96.642	96.737
Na	0.01529	0.02319	0.02990	0.02512	0.02193	0.02662	0.01800	0.03451
Mg	0.00117	0.00093	0.00281	-	-	-	-	-
Al	0.19193	0.18274	0.15159	0.16128	0.15585	0.19128	0.19559	0.26710
Si	3.95185	3.93219	3.92351	3.92220	3.89366	3.89651	3.91919	3.92389
K	-	-	-	-	-	-	-	-
Ca	3.90212	3.93564	3.84555	3.84547	3.87121	3.91585	3.91285	3.70579
Ti	3.76946	3.78314	3.81910	3.78613	3.83715	3.82002	3.80942	3.66230
V	0.00187	0.00062	0.00355	0.00217	0.00190	0.00002	0.00218	0.00227
Mn	0.01553	0.01273	0.01262	0.01213	0.01289	0.01488	0.01547	0.02187
Fe	0.19083	0.16946	0.15197	0.16450	0.14903	0.14868	0.15219	0.19444
Y	0.00620	0.00829	0.01571	0.01550	0.01798	0.02867	0.01264	0.11677
Nb	0.01059	0.00733	0.01305	0.01977	0.02005	0.00994	0.01254	0.03401
La	0.00598	0.01014	0.01539	0.01988	0.01611	0.00477	0.00559	0.00311
Ce	0.03237	0.04173	0.05831	0.06943	0.05167	0.03099	0.02519	0.02820
Pr	0.00332	0.00552	0.00682	0.00962	0.00695	0.00412	0.00413	0.00780
Nd	0.01874	0.02273	0.03438	0.03642	0.02839	0.02249	0.01884	0.04184
Sm	0.00531	0.00162	0.00620	0.00618	0.00448	0.00615	0.00529	0.01558
Gd	0.00257	0.00253	-	0.00212	-	0.00466	0.00343	0.01596
Dy	0.00238	0.00173	0.00343	0.00337	0.00196	0.00242	0.00328	0.01618
Yb	0.00103	-	-	-	-	0.00163	0.00118	0.00560
Ta	-	-	-	-	-	-	-	-
Th	-	-	-	-	0.00169	-	-	-
U	-	-	-	-	-	-	-	-
TOTAL	12.13074	12.14467	12.09833	12.10574	12.09943	12.13235	12.11974	12.10873

Titanite Analyses: Ratagain - RAT 11/1

	4.2/1	4.2/2	4.2/3	4.2/4	4.2/5	4.2/6	4.2/7	4.2/8
SiO_2	29.40	29.51	29.39	29.70	29.43	29.58	29.91	29.66
TiO_2	34.73	35.38	34.93	34.96	35.24	34.62	36.04	34.89
Al_2O_3	1.04	1.07	1.09	1.17	1.15	1.25	1.04	1.12
FeO	1.86	1.60	1.84	2.03	1.91	2.06	1.67	1.93
MnO	0.08	0.08	0.07	0.08	0.09	0.08	0.08	0.09
MgO	n.d.	n.d.	n.d.	n.d.	n.d.	n.d.	n.d.	n.d.
CaO	25.13	25.46	25.26	26.23	26.41	26.19	27.09	26.19
La_2O_3	0.60	0.60	0.61	0.46	0.46	0.45	1.00	0.51
Ce_2O_3	2.25	2.13	2.16	1.63	1.42	1.66	0.39	1.68
Pr_2O_3	0.34	0.23	0.35	0.28	0.17	0.21	0.09	0.22
Nd_2O_3	1.45	1.27	1.43	1.01	0.89	1.06	0.47	0.97
Sm_2O_3	0.26	0.22	0.25	0.17	0.14	0.21	0.08	0.13
Yb_2O_3	n.d.	n.d.	n.d.	n.d.	n.d.	n.d.	n.d.	n.d.
Y_2O_3	0.37	0.34	0.36	0.21	0.20	0.22	0.09	0.23
TOTAL	97.51	97.89	97.75	97.93	97.51	97.64	97.95	97.62
Si	4.0721	4.0559	4.0589	4.0676	4.0394	4.0673	4.0544	4.0732
Ti	3.6177	3.6571	3.6280	3.6009	3.6377	3.5800	3.6740	3.6035
Al	0.1698	0.1733	0.1774	0.1889	0.1860	0.2026	0.1662	0.1813
Fe2+	0.2154	0.1839	0.2125	0.2325	0.2192	0.2368	0.1893	0.2216
Mn	0.0093	0.0093	0.0081	0.0092	0.0104	0.0093	0.0091	0.0104
Mg	-	-	-	-	-	-	-	-
Ca	3.7296	3.7495	3.7380	3.8493	3.8841	3.8586	3.9347	3.8538
La	0.0306	0.0304	0.0310	0.0232	0.0232	0.0228	0.0499	0.0258
Ce	0.1140	0.1071	0.1092	0.0817	0.0713	0.0835	0.0193	0.0844
Pr	0.0171	0.0115	0.0176	0.0139	0.0085	0.0105	0.0044	0.0110
Nd	0.0723	0.0629	0.0711	0.0498	0.0440	0.0525	0.0229	0.0480
Sm	0.0124	0.0104	0.0119	0.0080	0.0066	0.0099	0.0037	0.0061
Yb	-	-	-	-	-	-	-	-
Y	0.0272	0.0248	0.0265	0.0153	0.0146	0.0160	0.0064	0.0168
TOTAL	12.0882	12.0766	12.0902	12.1408	12.1456	12.1525	12.1349	12.1364

Appendix 5: Electron microprobe analyses: apatites.

The first part of the analysis coding (*eg.* T1) denotes the rock: the second part the analysis number. All the concentrations are expressed as wt% oxide, Fe is calculated as FeO. n.d. - not detected. The structural formulae of the apatite analyses have been on the basis of 26 (O, F).

Apatite Analyses: Strontian - BPSRT1.

	T1/1	T1/2	T1/3	T1/4	T1/5	T1/6	T1/7	T1/8
F	3.940	3.128	3.243	3.028	3.596	3.347	3.455	3.246
Na_2O	0.101	0.038	0.099	0.084	0.081	0.076	0.058	0.180
MgO	0.017	n.d.	0.017	0.011	n.d.	0.020	n.d.	0.010
Al_2O_3	n.d.	n.d.	n.d.	n.d.	n.d.	n.d.	n.d.	n.d.
SiO_2	0.134	0.259	0.134	0.236	0.264	0.236	0.104	0.311
P_2O_5	41.343	41.073	41.292	41.206	40.867	40.784	41.876	41.359
S	0.055	0.044	0.055	0.052	0.063	0.048	0.046	0.144
K2O	n.d.	0.051	n.d.	n.d.	n.d.	0.024	n.d.	n.d.
CaO	54.448	55.338	54.455	55.343	54.526	54.959	54.543	54.614
FeO	0.185	0.128	0.185	0.135	0.193	0.309	0.074	0.192
SrO	0.116	0.098	0.115	0.106	0.107	0.115	0.110	0.094
BaO	n.d.	n.d.	n.d.	n.d.	n.d.	n.d.	n.d.	n.d.
La_2O_3	0.053	0.187	0.045	0.166	0.182	0.195	0.053	0.121
Ce_2O_3	0.054	0.201	0.054	0.207	0.237	0.229	0.066	0.130
Pr_2O_3	n.d.	n.d.	n.d.	n.d.	n.d.	n.d.	n.d.	n.d.
Nd_2O_3	0.039	0.056	0.040	0.065	0.086	n.d.	n.d.	n.d.
Sm_2O_3	n.d.	n.d.	n.d.	n.d.	n.d.	n.d.	n.d.	n.d.
Gd_2O_3	n.d.	n.d.	n.d.	n.d.	n.d.	n.d.	n.d.	n.d.
Dy_2O_3	0.049	n.d.	0.048	n.d.	n.d.	n.d.	n.d.	n.d.
Er_2O_3	n.d.	n.d.	n.d.	n.d.	n.d.	n.d.	n.d.	n.d.
Yb_2O_3	n.d.	n.d.	n.d.	n.d.	n.d.	n.d.	n.d.	n.d.
ThO_2	n.d.	n.d.	n.d.	n.d.	n.d.	n.d.	n.d.	n.d.
UO_2	n.d.	n.d.	n.d.	n.d.	n.d.	n.d.	n.d.	n.d.
TOTAL	100.621	100.719	99.870	100.793	100.341	100.499	100.501	100.600
F	2.03483	1.63530	1.69966	1.58298	1.87592	1.75131	1.79110	1.72474
Na	0.03213	0.01246	0.03180	0.02717	0.02616	0.02444	0.01843	0.05882
Mg	0.00425	-	0.00429	0.00278	-	0.00507	-	0.00267
Al	-	-	-	-	-	-	-	-
Si	0.02196	0.04294	0.02223	0.03900	0.04362	0.03912	0.01704	0.05239
P	5.71576	5.74798	5.79282	5.76604	5.70667	5.71176	5.81149	5.74034
S	0.00683	0.00552	0.00693	0.00651	0.00786	0.00595	0.00565	0.01816
K	-	0.01075	-	-	-	0.00521	-	-
Ca	9.52701	9.80108	9.66852	9.80111	9.63629	9.74127	9.57984	9.65117
Fe^{2+}	0.02532	0.01769	0.02570	0.01868	0.02670	0.04284	0.01014	0.02703
Sr	0.01098	0.00947	0.01113	0.01022	0.01031	0.01105	0.01045	0.00924
Ba	-	-	-	-	-	-	-	-
La	0.00324	0.01141	0.00278	0.01011	0.01107	0.01193	0.00320	0.00753
Ce	0.00324	0.01219	0.00329	0.01257	0.01431	0.01390	0.00396	0.00799
Pr	-	-	-	-	0.00078	-	-	-
Nd	0.00233	0.00338	0.00238	0.00388	0.00516	-	-	-
Sm	-	-	-	-	-	-	-	-
Gd	-	-	-	-	-	-	-	-
Dy	0.00258	-	0.00259	-	-	-	-	-
Er	-	-	-	-	-	-	-	-
Yb	-	-	-	-	-	-	-	-
Th	-	-	-	-	-	-	-	-
U	-	-	-	-	-	-	-	-
TOTAL	17.33914	17.31837	17.28302	17.29368	17.37394	17.37693	17.25716	17.31637

Apatite Analyses: Strontian - BPSRT1 and BPSRG1.

	T1/9	T1/10	G1/1	G1/2	G1/3	G1/4	G1/5	G1/6
F	2.814	3.552	4.093	4.518	2.894	2.680	2.634	2.692
Na_2O	0.159	0.085	0.198	0.181	0.271	0.220	0.216	0.191
MgO	0.281	0.016	0.026	n.d.	n.d.	n.d.	0.058	n.d.
Al_2O_3	0.087	n.d.	n.d.	n.d.	n.d.	n.d.	n.d.	n.d.
SiO_2	1.025	0.108	0.124	0.131	0.290	0.230	0.238	0.146
P_2O_5	41.467	41.869	41.496	41.757	41.140	42.403	42.499	42.738
S	0.077	0.057	0.058	0.036	0.050	0.041	0.025	0.010
K2O	n.d.	n.d.	0.054	n.d.	n.d.	n.d.	n.d.	n.d.
CaO	52.580	54.789	53.737	54.210	53.348	54.664	54.183	54.016
FeO	0.359	0.053	0.302	0.221	0.435	0.130	0.134	0.151
SrO	0.115	0.113	0.024	n.d.	0.050	0.053	0.030	0.059
BaO	n.d.	n.d.	n.d.	n.d.	n.d.	n.d.	n.d.	n.d.
La_2O_3	0.191	0.088	0.035	0.055	0.050	0.047	0.039	0.056
Ce_2O_3	0.340	0.097	0.119	0.105	0.142	0.076	0.132	0.132
Pr_2O_3	n.d.	n.d.	n.d.	n.d.	n.d.	n.d.	n.d.	n.d.
Nd_2O_3	0.106	n.d.	0.144	0.107	0.141	0.076	0.122	0.145
Sm_2O_3	n.d.	n.d.	n.d.	n.d.	0.036	n.d.	n.d.	n.d.
Gd_2O_3	n.d.	n.d.	n.d.	n.d.	0.066	0.053	0.033	0.048
Dy_2O_3	n.d.	n.d.	0.082	0.068	0.061	0.066	n.d.	0.038
Er_2O_3	n.d.	n.d.	n.d.	0.031	0.041	0.036	0.023	0.035
Yb_2O_3	n.d.	n.d.	n.d.	0.021	0.050	n.d.	n.d.	0.026
ThO_2	n.d.	n.d.	n.d.	n.d.	n.d.	n.d.	n.d.	n.d.
UO_2	n.d.	n.d.	n.d.	n.d.	n.d.	n.d.	n.d.	n.d.
TOTAL	99.723	100.973	100.601	101.600	99.065	99.775	100.366	100.483
F	1.49646	1.83323	2.10973	2.29638	1.53484	1.39575	1.37529	1.40310
Na	0.05193	0.02717	0.06259	0.05658	0.08811	0.07024	0.06914	0.06103
Mg	0.07061	0.00401	0.00636	-	-	-	0.01427	-
Al	0.01724	-	-	-	-	-	-	-
Si	0.17240	0.01767	0.02035	0.02118	0.04863	0.03787	0.03929	0.02406
P	5.76102	5.78430	5.72531	5.68142	5.84086	5.91179	5.94029	5.96317
S	0.00980	0.00705	0.00716	0.00434	0.00629	0.00506	0.00309	0.00123
K	-	0.00012	0.01139	-	-	-	-	-
Ca	9.47349	9.57966	9.38355	9.33487	9.58579	9.64542	9.58494	9.53856
Fe^{2+}	0.05054	0.00726	0.04118	0.02977	0.06100	0.01790	0.01850	0.02081
Sr	0.01125	0.01072	0.00230	-	0.00486	0.00506	0.00287	0.00563
Ba	-	-	-	-	-	-	-	-
La	0.01184	0.00530	0.00214	0.00330	0.00309	0.00285	0.00237	0.00340
Ce	0.02094	0.00584	0.00711	0.00620	0.00871	0.00458	0.00797	0.00796
Pr	-	-	-	-	-	-	-	-
Nd	0.00643	-	0.00847	0.00620	0.00852	0.00451	0.00725	0.00861
Sm	-	-	-	-	0.00208	-	-	-
Gd	-	-	-	-	0.00366	0.00289	0.00180	0.00262
Dy	-	-	0.00433	0.00354	0.00329	0.00350	-	0.00201
Er	-	-	-	0.00158	0.00216	0.00186	0.00119	0.00181
Yb	-	-	-	0.00104	0.00255	-	-	0.00130
Th	-	-	-	-	-	-	-	-
U	-	-	-	-	-	-	-	-
TOTAL	17.15165	17.29409	17.39938	17.46094	17.20456	17.10936	17.06834	17.04547

Apatite Analyses: Strontian - BPSRG1.

	G1/7	G1/8	G1/9	G1/10
F	2.721	2.917	2.835	2.792
Na_2O	0.227	0.196	0.197	0.233
MgO	n.d.	n.d.	n.d.	n.d.
Al_2O_3	n.d.	n.d.	n.d.	n.d.
SiO_2	0.194	0.180	0.167	0.156
P_2O_5	42.780	41.883	41.992	42.387
S	0.030	0.023	0.022	0.029
K2O	n.d.	n.d.	0.020	0.102
CaO	53.758	53.922	54.022	53.446
FeO	0.085	0.188	0.167	0.046
SrO	0.037	0.052	0.042	0.035
BaO	n.d.	n.d.	n.d.	n.d.
La_2O_3	0.047	0.038	n.d.	0.044
Ce_2O_3	0.138	0.085	0.116	0.170
Pr_2O_3	n.d.	n.d.	n.d.	0.043
Nd_2O_3	0.102	0.118	0.094	0.137
Sm_2O_3	n.d.	n.d.	n.d.	n.d.
Gd_2O_3	0.034	0.091	0.080	n.d.
Dy_2O_3	0.093	0.119	0.063	0.065
Er_2O_3	0.029	n.d.	0.035	n.d.
Yb_2O_3	0.030	0.058	0.039	0.029
ThO_2	n.d.	n.d.	n.d.	n.d.
UO_2	n.d.	n.d.	n.d.	n.d.
TOTAL	100.305	99.870	99.891	99.714
F	1.41816	1.53067	1.48765	1.46416
Na	0.07253	0.06305	0.06337	0.07491
Mg	-	-	-	-
Al	-	-	-	-
Si	0.03197	0.02986	0.02770	0.02586
P	5.96881	5.88345	5.89881	5.95052
S	0.00371	0.00286	0.00274	0.00360
K	-	-	0.00423	0.02157
Ca	9.49264	9.58646	9.60430	9.49587
Fe^{2+}	0.01171	0.02608	0.02317	0.00637
Sr	0.00353	0.00500	0.00404	0.00336
Ba	-	-	-	-
La	0.00285	0.00232	-	0.00269
Ce	0.00832	0.00516	0.00704	0.01032
Pr	-	-	-	0.00259
Nd	0.00605	0.00705	0.00562	0.00818
Sm	-	-	-	-
Gd	0.00185	0.00500	0.00440	-
Dy	0.00493	0.00636	0.00336	0.00347
Er	0.00150	-	0.00182	-
Yb	0.00150	0.00293	0.00197	0.00146
Th	-	-	-	-
U	-	-	-	-
TOTAL	17.03013	17.15638	17.14035	17.07505

Appendix 6) XRF Analyses: whole rocks - Strontian.

Appendix 6A) Analytical precision.

The precision estimates are based on six replicates on six separate beads or pressed powder pellets (trace elements and MnO) of a granodiorite and the standard deviation values are derived in the manner of Harvey *et al.* (1973). Precision estimates expressed as wt% for major element oxides and as ppm for trace elements.

Element	Standard Deviation	Element	Standard Deviation
SiO_2	0.177	Sr	1.8
TiO_2	0.006	Rb	1.4
Al_2O_3	0.042	Th	4.2
Fe_2O_3	0.114	Pb	0.8
MnO	0.0003	Zn	0.7
MgO	0.035	Cu	0.8
CaO	0.010	Ni	1.2
Na_2O	0.099	Cr	1.4
K_2O	0.013	V	0.9
P_2O_5	0.011	Ba	8.0
Nb	2.0	Hf	0.41
Zr	6.9	Ce	2.0
Y	1.5	La	1.3

Appendix 6B) The electron microprobe analyses.

The analysis codings are cross referenced with sample localities given in Appendix 1. Oxide concentrations are given in wt%, trace elements in ppm. Fe is expressed as Fe_2O_3.

Sample	Str N053	Str N054	Str N055	Str N056	Str N057	83SR18	83SR19	83SR20
SiO_2	62.42	62.05	64.68	62.61	63.20	68.63	67.84	63.67
TiO_2	0.85	0.87	0.74	0.86	0.89	0.52	0.67	0.70
Al_2O_3	16.61	16.30	15.73	16.69	16.81	15.75	16.25	16.29
Fe_2O_3	4.52	4.59	3.93	4.37	4.46	2.90	3.45	4.06
MnO	0.08	0.08	0.07	0.07	0.07	0.04	0.05	0.06
MgO	2.97	2.99	2.56	2.96	2.85	1.58	2.09	2.44
CaO	4.19	4.78	3.63	4.12	4.19	2.75	3.34	3.91
Na_2O	4.67	4.13	4.39	5.09	4.67	5.14	4.79	4.46
K_2O	3.15	2.82	3.42	3.05	2.58	2.43	1.74	2.54
P_2O_5	0.31	0.31	0.27	0.35	0.30	0.18	0.22	0.26
Loss	0.20	1.00	1.00	0.40	0.20	0.60	0.20	0.40
TOTAL	100.31	100.20	100.70	100.88	100.52	100.73	100.83	99.06
Nb	13	13	10	12	12	6	8	14
Zr	190	238	153	202	188	135	145	177
Y	19	21	15	18	19	7	8	14
Sr	1174	1019	1054	1228	1221	902	949	1005
Rb	61	81	64	52	50	53	63	46
Th	9	20	18	6	7	10	13	8
Pb	16	15	17	18	7	10	12	17
Zn	72	68	60	64	66	10	2	15
Cu	20	11	13	16	7	49	58	56
Ni	48	55	47	51	49	32	36	43
Cr	64	94	61	68	64	36	45	59
V	92	95	80	90	84	52	55	72
Ba	1429	909	1068	1164	1049	665	365	999
Hf	5	9	8	9	10	6	6	5
Ce	107	78	74	94	90	57	68	79
La	66	42	59	57	38	43	56	41

Sample	83SR20A	83SR22	83SR23	83SR24	83SR25	83SR26	83SR27	83SR28
SiO_2	69.88	64.13	65.33	66.46	65.71	61.34	63.03	63.77
TiO_2	0.46	0.71	0.63	0.50	0.58	0.86	0.80	0.80
Al_2O_3	14.43	16.51	16.46	15.30	16.54	16.59	16.52	15.44
Fe_2O_3	3.09	4.13	3.65	3.22	3.77	4.45	4.46	4.45
MnO	0.05	0.06	0.06	0.05	0.06	0.07	0.08	0.07
MgO	2.24	2.32	2.33	2.38	2.96	2.68	2.99	3.03
CaO	3.08	4.05	3.58	2.96	3.52	3.00	4.16	4.13
Na_2O	3.41	4.43	5.02	4.50	4.05	5.90	3.80	4.38
K_2O	2.79	2.48	2.66	3.04	1.95	2.76	2.94	3.21
P_2O_5	0.30	0.26	0.23	0.20	0.25	0.38	0.29	0.29
Loss	0.40	n.d.	0.60	0.40	0.80	1.60	0.20	n.d.
TOTAL	100.35	99.36	100.82	99.23	100.40	99.89	99.56	99.81
Nb	11	13	14	9	12	15	21	13
Zr	195	178	195	141	159	215	225	198
Y	12	18	13	9	11	17	26	15
Sr	701	1026	974	870	782	658	985	880
Rb	41	62	59	65	82	44	63	83
Th	0	8	1	15	2	11	8	9
Pb	19	16	9	22	11	8	6	19
Zn	32	100	90	7	0	19	7	12
Cu	46	69	64	45	62	84	63	57
Ni	29	57	53	33	42	49	47	60
Cr	34	92	80	36	74	74	83	107
V	58	79	74	50	59	91	86	88
Ba	928	927	927	836	765	1090	1140	745
Hf	8	7	7	5	5	6	7	8
Ce	73	89	79	38	40	110	100	81
La	47	47	35	29	24	60	46	31

Sample	83SR29	83SR30	83SR31	83SR33	83SR34	83SR35	83SR36	83SR38
SiO_2	63.99	63.22	62.63	62.15	63.80	65.00	63.20	71.10
TiO_2	0.67	0.79	0.84	0.86	0.96	0.90	0.98	0.22
Al_2O_3	16.08	16.67	15.98	16.57	15.90	15.91	16.10	15.16
Fe_2O_3	3.92	4.41	4.52	4.54	4.24	3.97	4.49	1.73
MnO	0.06	0.07	0.07	0.07	0.09	0.08	0.08	0.03
MgO	2.53	2.63	2.87	2.83	2.93	2.82	3.15	0.90
CaO	3.61	4.22	3.82	4.13	3.94	3.71	3.90	1.79
Na_2O	4.93	4.88	4.51	4.13	3.05	3.11	3.21	4.22
K_2O	3.29	2.65	3.10	3.14	3.18	2.99	3.10	3.65
P_2O_5	0.30	0.29	0.39	0.36	0.31	0.29	0.32	0.20
Loss	0.20	0.60	1.00	1.40	1.00	0.40	0.60	0.40
TOTAL	99.85	100.73	100.00	100.48	99.69	99.45	99.42	99.58
Nb	11	11	14	15	15	10	12	6
Zr	193	193	194	195	199	166	192	125
Y	14	15	16	20	23	13	11	9
Sr	1059	1156	1016	1124	1109	1096	1133	538
Rb	56	41	58	53	56	56	59	115
Th	8	12	16	8	6	9	8	6
Pb	20	18	16	14	19	23	14	32
Zn	9	13	3	13	63	48	66	14
Cu	57	67	65	66	12	0	18	39
Ni	48	50	54	53	53	44	56	14
Cr	63	64	70	78	75	62	75	4
V	76	79	74	110	85	66	92	30
Ba	960	1126	895	1036	1011	981	1001	806
Hf	8	7	7	7	7	6	4	5
Ce	93	102	115	153	113	90	94	42
La	52	49	62	64	58	39	50	23

Sample	83SR39	83SR40	83SR41	83SR42	83SR43	83SR44	83SR45	83SR46
SiO_2	64.89	66.34	67.26	63.67	73.30	69.98	71.41	70.67
TiO_2	0.58	0.52	0.51	0.72	0.18	0.25	0.22	0.20
Al_2O_3	15.84	16.22	15.63	15.99	14.90	15.72	15.57	16.10
Fe_2O_3	3.58	3.32	3.36	4.32	1.48	1.95	1.74	1.58
MnO	0.06	0.06	0.06	0.07	0.03	0.03	0.03	0.03
MgO	2.12	2.13	2.36	2.78	0.63	0.98	0.65	0.65
CaO	2.98	2.62	2.66	3.63	1.20	1.83	1.45	1.55
Na_2O	4.32	4.40	3.98	4.86	3.01	5.07	3.92	4.14
K_2O	3.54	3.55	3.60	3.08	4.41	3.47	3.87	4.68
P_2O_5	0.27	0.29	0.27	0.31	0.06	0.12	0.08	0.10
Loss	1.40	0.20	0.80	0.80	0.20	n.d.	0.80	0.20
TOTAL	99.80	99.89	100.71	100.47	99.57	99.61	99.91	100.14
Nb	12	10	10	13	1	3	4	6
Zr	109	172	154	177	103	146	124	115
Y	11	13	11	16	2	5	4	7
Sr	798	895	796	962	487	630	510	537
Rb	55	75	61	65	114	99	113	149
Th	14	25	20	11	6	18	17	18
Pb	20	24	24	22	40	26	25	44
Zn	9	5	1	6	11	4	10	7
Cu	44	49	48	63	28	41	38	36
Ni	36	32	34	47	11	13	10	10
Cr	41	33	40	57	0	0	0	0
V	58	55	55	75	21	31	23	24
Ba	895	919	802	775	813	974	767	1296
Hf	7	4	7	6	5	8	5	6
Ce	87	94	77	99	71	42	50	65
La	48	45	43	45	33	18	27	31

Sample	83SR47	83SR48	83SR49	83SR50	83SR51	83SR52	83SR53	83SR54
SiO_2	71.30	72.06	61.42	68.78	71.65	69.75	70.53	72.08
TiO_2	0.22	0.23	0.77	0.42	0.21	0.30	0.27	0.21
Al_2O_3	15.34	15.30	17.01	15.99	15.17	16.02	15.52	15.38
Fe_2O_3	1.73	1.75	4.49	2.68	1.63	2.10	1.95	1.61
MnO	0.03	0.03	0.07	0.04	0.03	0.03	0.04	0.04
MgO	0.48	0.73	3.14	1.58	0.96	1.01	0.97	0.65
CaO	1.75	1.64	4.08	2.56	1.58	1.98	1.79	1.22
Na_2O	4.08	4.11	4.11	4.24	4.22	3.90	4.13	4.00
K_2O	3.60	3.74	3.05	3.27	4.12	3.37	3.40	3.99
P_2O_5	0.09	0.07	0.35	0.16	0.14	0.16	0.13	0.14
Loss	1.00	0.80	1.20	0.60	0.40	0.20	0.60	1.40
TOTAL	99.81	100.65	99.99	100.55	100.31	99.04	99.51	100.89
Nb	6	6	13	8	7	5	6	7
Zr	134	129	193	173	118	154	137	155
Y	6	7	18	11	5	7	9	9
Sr	549	538	1161	726	531	655	555	415
Rb	109	122	59	85	132	104	116	136
Th	8	12	8	10	6	5	11	14
Pb	27	29	20	20	28	23	28	26
Zn	6	12	13	23	17	5	11	10
Cu	42	35	61	45	40	46	41	39
Ni	13	13	51	19	12	12	12	8
Cr	1	0	61	25	0	2	4	0
V	23	25	83	39	27	31	29	28
Ba	847	892	1061	1034	1036	1059	814	760
Hf	5	7	7	7	5	7	5	7
Ce	59	55	114	84	46	33	43	58
La	26	19	55	30	9	28	20	30

Sample	83SR55	83SR56	83SR57	83SR58	83SR59	83SR60	83SR61	83SR62
SiO_2	70.61	71.54	71.29	67.68	62.31	62.15	62.16	62.69
TiO_2	0.30	0.20	0.25	0.39	0.73	0.77	0.80	0.74
Al_2O_3	16.42	15.92	15.68	15.60	15.90	16.08	16.86	16.45
Fe_2O_3	2.09	1.57	1.83	2.92	4.24	4.42	4.38	4.14
MnO	0.03	0.03	0.03	0.05	0.07	0.07	0.07	0.06
MgO	0.90	0.58	0.78	2.06	3.43	3.64	3.05	2.34
CaO	2.06	1.33	1.88	2.85	3.64	3.88	4.34	3.89
Na_2O	4.63	4.88	4.22	4.22	4.78	4.49	4.83	5.44
K_2O	3.34	3.78	3.57	2.46	3.30	3.07	2.48	2.20
P_2O_5	0.14	0.10	0.11	0.21	0.34	0.34	0.29	0.26
Loss	0.20	0.60	0.20	1.60	1.60	1.40	0.40	1.00
TOTAL	100.96	100.72	100.02	100.26	100.61	100.60	99.93	99.47
Nb	6	6	6	8	12	12	15	12
Zr	194	133	133	160	192	192	217	188
Y	8	8	7	12	14	13	16	14
Sr	679	479	574	825	1038	1167	1137	1076
Rb	125	130	105	72	62	45	45	45
Th	7	10	8	11	17	10	8	5
Pb	30	27	23	21	23	20	14	16
Zn	7	10	6	6	18	9	4	61
Cu	51	38	46	48	63	63	56	6
Ni	12	10	11	25	51	58	46	37
Cr	4	1	2	30	61	79	68	60
V	29	26	28	57	74	88	81	75
Ba	1170	933	817	821	940	1049	911	888
Hf	9	6	6	6	7	6	6	8
Ce	52	55	46	68	107	93	86	67
La	31	17	26	25	55	44	39	36

Sample	83SR63	83SR64	83SR65	83SR66	83SR67	83SR68	83SR69	83SR70
SiO_2	63.92	63.62	62.34	62.05	62.48	62.12	61.61	66.09
TiO_2	0.73	0.70	0.80	0.83	0.80	0.77	0.80	0.52
Al_2O_3	16.52	16.80	16.11	16.30	16.56	16.47	16.69	15.28
Fe_2O_3	3.98	4.18	4.46	4.63	4.53	4.40	5.57	3.33
MnO	0.06	0.07	0.07	0.07	0.07	0.07	0.07	0.05
MgO	2.29	3.08	2.66	2.79	3.13	3.24	3.50	2.44
CaO	4.03	4.07	3.64	4.41	4.12	3.98	3.80	3.01
Na_2O	5.87	5.14	5.95	4.24	4.44	4.61	4.36	4.49
K_2O	2.55	2.24	2.86	3.25	3.05	2.93	2.89	3.70
P_2O_5	0.22	0.28	0.35	0.40	0.35	0.35	0.35	0.24
Loss	0.20	0.40	0.60	1.60	0.40	0.40	0.60	0.80
TOTAL	100.61	100.86	100.13	100.86	100.22	99.62	100.53	100.20
Nb	14	11	9	13	17	11	10	9
Zr	179	170	184	201	218	190	202	162
Y	16	13	12	15	16	13	11	12
Sr	1009	1141	1138	1069	1132	1177	1205	868
Rb	47	46	44	58	58	51	52	65
Th	3	0	3	11	12	18	10	17
Pb	11	12	16	13	17	17	22	25
Zn	58	1	57	10	14	14	16	7
Cu	8	59	7	64	64	59	59	45
Ni	36	45	48	55	54	55	51	36
Cr	50	65	67	83	75	71	72	39
V	71	83	76	85	81	85	78	64
Ba	812	1014	1056	1099	984	899	928	984
Hf	7	8	7	9	7	9	6	6
Ce	78	97	87	95	110	97	121	84
La	42	35	52	53	55	34	53	38

Sample	83SR72	83SR73	84SR2	84SR4	84SR5	84SR6	84SR7	84SR8
SiO_2	60.34	61.26	61.23	70.56	68.90	70.87	61.18	60.79
TiO_2	0.76	0.74	0.83	0.32	0.38	0.37	0.85	0.96
Al_2O_3	16.30	16.57	16.38	15.24	15.67	14.54	16.19	17.01
Fe_2O_3	4.34	4.50	4.48	1.83	2.15	1.99	4.57	4.75
MnO	0.07	0.07	0.05	0.02	0.01	0.01	0.04	0.04
MgO	3.28	3.37	2.58	0.73	0.27	1.08	2.76	2.98
CaO	3.62	3.91	4.02	1.66	1.85	1.46	3.98	4.70
Na_2O	4.66	4.74	5.64	5.05	5.22	4.52	5.32	5.93
K_2O	3.37	3.06	2.99	3.76	3.34	4.21	3.11	1.83
P_2O_5	0.33	0.35	0.33	0.08	0.16	0.17	0.36	0.32
Loss	1.40	0.40	0.60	0.40	0.40	0.60	1.00	0.60
TOTAL	98.79	99.28	99.42	99.84	98.58	100.01	99.66	100.14
Nb	12	9	10	2	2	4	8	13
Zr	202	218	217	146	167	137	204	232
Y	15	14	18	13	12	12	17	19
Sr	1171	1202	1170	542	712	602	1185	1109
Rb	58	54	57	107	99	95	59	56
Th	5	8	11	5	9	13	5	10
Pb	25	19	21	29	28	28	16	16
Zn	16	11	56	36	46	26	58	60
Cu	64	60	24	21	23	17	20	28
Ni	47	49	52	12	14	19	48	50
Cr	68	63	46	0	0	0	45	47
V	77	84	83	26	24	34	88	88
Ba	1289	1109	1012	903	1092	846	1110	467
Hf	7	7	8	9	10	8	7	10
Ce	116	112	97	42	62	46	111	86
La	52	49	60	28	32	29	61	48

Sample	84SR9	84SR10	84SR11	84SR12	84SR13	84SR14	84SR15	84SR16
SiO_2	63.22	62.54	71.08	69.32	70.29	71.20	73.23	71.45
TiO_2	0.79	0.87	0.29	0.39	0.31	0.32	0.27	0.31
Al_2O_3	16.03	16.01	15.01	15.54	14.77	14.45	14.63	14.91
Fe_2O_3	4.07	4.45	1.59	2.02	1.73	1.81	1.47	1.71
MnO	0.03	0.05	0.01	0.01	0.02	0.01	0.01	0.02
MgO	2.28	3.00	0.43	0.62	1.03	0.81	0.54	0.41
CaO	3.63	3.97	1.62	2.04	1.51	1.54	0.99	1.12
Na_2O	5.09	4.93	4.63	5.57	4.88	4.99	4.86	4.88
K_2O	2.73	2.97	3.87	3.43	3.62	3.83	4.20	3.94
P_2O_5	0.26	0.27	0.10	0.11	0.18	0.11	0.10	0.09
Loss	0.60	0.60	0.80	0.60	0.60	0.60	0.40	0.60
TOTAL	99.00	99.95	99.60	99.87	99.12	99.82	100.85	99.60
Nb	9	14	2	2	2	7	7	6
Zr	199	230	119	166	135	146	135	153
Y	17	20	6	10	10	13	14	11
Sr	1029	961	478	641	535	405	362	432
Rb	59	64	123	102	112	150	176	140
Th	7	4	10	4	4	22	19	21
Pb	15	17	33	25	26	30	31	33
Zn	54	62	32	47	37	44	40	41
Cu	24	21	19	19	11	18	17	19
Ni	38	46	11	13	10	11	10	11
Cr	16	33	0	0	0	0	0	0
V	76	81	19	30	4	21	16	21
Ba	1030	1174	757	1079	813	503	541	598
Hf	9	9	7	9	8	8	8	8
Ce	79	81	35	50	67	58	43	71
La	44	44	21	29	37	30	31	40

Sample	84SR17	84SR18	84SR19	84SR20	84SR21	84SR22	84SR26	84SR27
SiO_2	71.79	73.44	71.85	71.84	71.10	70.53	61.08	60.21
TiO_2	0.30	0.24	0.22	0.30	0.29	0.32	0.89	0.94
Al_2O_3	15.04	14.26	14.56	14.07	15.22	15.09	16.95	16.57
Fe_2O_3	1.68	1.50	1.39	1.79	1.70	1.75	4.54	4.75
MnO	0.01	0.01	n.d.	0.02	0.01	0.01	0.05	0.04
MgO	0.49	0.39	0.56	0.66	0.63	0.90	2.81	3.16
CaO	1.07	0.87	0.83	0.79	1.36	1.44	4.57	4.21
Na_2O	4.88	4.72	4.51	4.78	5.10	4.97	5.19	5.66
K_2O	4.21	4.04	4.43	4.22	3.93	3.79	1.83	2.67
P_2O_5	0.12	0.09	0.06	0.13	0.11	0.13	0.43	0.38
Loss	0.60	0.80	0.80	0.60	0.80	0.80	0.40	1.20
TOTAL	100.35	100.52	99.36	99.35	100.43	99.93	99.00	100.10
Nb	6	5	6	9	4	3	14	9
Zr	148	132	120	138	167	171	207	209
Y	11	9	11	13	11	10	26	16
Sr	428	379	334	362	443	486	1143	1234
Rb	161	144	168	165	139	125	62	53
Th	16	13	10	16	15	8	1	3
Pb	28	25	27	31	26	26	12	18
Zn	43	36	28	45	37	40	68	65
Cu	16	15	14	15	16	11	13	21
Ni	8	7	8	12	10	7	38	49
Cr	0	0	0	0	0	0	124	57
V	16	18	14	20	21	21	87	85
Ba	666	665	721	602	819	1003	630	1143
Hf	8	7	6	8	9	9	9	8
Ce	57	59	51	61	56	56	105	94
La	29	38	31	30	38	34	49	45

Sample	84SR29	84SR30	84SR31	84SR32	BPSRT1	BPSRT2	BPSRT3	BPSRT4
SiO_2	59.13	60.62	60.30	62.83	60.34	69.07	62.25	64.37
TiO_2	0.94	0.93	0.90	0.76	0.95	0.48	0.89	0.74
Al_2O_3	16.61	16.68	16.63	16.16	17.10	15.32	16.03	15.59
Fe_2O_3	4.88	4.70	4.86	3.95	4.93	2.66	4.44	3.92
MnO	0.05	0.05	0.06	0.04	0.08	0.05	0.07	0.07
MgO	3.20	2.49	3.07	2.78	3.22	1.40	3.30	2.88
CaO	4.40	4.07	4.18	4.09	4.80	1.97	3.76	3.43
K_2O	5.66	5.49	5.41	5.44	5.43	4.41	4.37	4.17
K2O	2.61	2.75	2.43	2.54	2.26	3.95	3.56	3.78
P_2O_5	0.37	0.31	0.39	0.20	0.36	0.17	0.33	0.27
Loss	1.20	1.40	1.00	1.00	0.80	0.80	0.60	0.60
TOTAL	99.36	99.79	99.53	100.05	100.59	100.50	99.90	100.08
Nb	8	8	6	4	10	9	14	15
Zr	224	212	208	178	260	174	214	196
Y	15	16	16	15	18	10	18	20
Sr	1268	1175	1234	1060	1263	655	1107	931
Rb	48	53	55	75	43	100	67	74
Th	4	5	5	8	10	14	18	30
Pb	14	18	18	18	13	24	18	18
Zn	64	61	66	55	71	48	60	42
Cu	20	15	11	18	8	20	19	18
Ni	52	44	46	40	50	15	49	43
Cr	65	53	66	64	71	19	61	58
V	86	84	97	77	107	50	92	68
Ba	1040	1153	1038	923	1150	981	1111	964
Hf	6	7	8	7	7	5	6	6
Ce	110	90	101	71	75	54	90	86
La	57	48	51	30	37	33	57	45

Sample	BPSRG1	BPSRG2	BPSRG3	BPSRG4	BPSRG5
SiO_2	72.93	71.69	71.71	71.14	72.74
TiO_2	0.18	0.27	0.28	0.30	0.19
Al_2O_3	14.75	14.97	15.49	15.47	15.16
Fe_2O_3	1.25	1.67	1.64	1.76	1.15
MnO	0.03	0.04	0.02	0.04	0.02
MgO	0.65	0.70	1.08	1.08	0.80
CaO	1.20	1.23	1.29	1.79	1.05
Na_2O	4.58	5.09	4.21	4.22	3.93
K_2O	4.14	3.21	4.11	4.04	4.92
P_2O_5	0.08	0.10	0.11	0.10	0.08
Loss	0.60	1.00	0.80	0.20	0.40
TOTAL	100.55	100.15	100.93	100.34	100.64
Nb	5	9	5	6	7
Zr	117	148	144	144	117
Y	11	13	7	17	10
Sr	458	461	538	543	436
Rb	130	127	128	133	168
Th	13	14	13	22	17
Pb	32	33	27	32	35
Zn	16	38	30	34	21
Cu	13	17	15	16	17
Ni	9	10	7	10	9
Cr	3	9	9	9	2
V	18	25	23	25	12
Ba	753	792	913	964	1112
Hf	4	5	5	4	4
Ce	30	41	51	45	27
La	14	23	33	22	21

Appendix 7) Whole Rock INAA: The Subset of Samples - Strontian.

Figures are in ppm. Figures in brackets are the 1σ errors.

Sample	BPSRT1	BPSRT2	BPSRT3	BPSRT4	BPSRG1	BPSRG4
La	49.7 (6%)	43.9 (6%)	66.6 (6%)	59.1 (6%)	19.0 (9%)	24.7 (8%)
Ce	97.3 (7%)	70.1 (7%)	122.6 (6%)	109.3 (6%)	42.7 (8%)	43.7 (7%)
Nd	36.4 (9%)	20.5 (11%)	41.6 (9%)	36.7 (9%)	16.0 (13%)	16.1 (13%)
Sm	5.82 (2%)	4.30 (2%)	6.21 (2%)	5.89 (2%)	2.14 (3%)	3.15 (2%)
Eu	1.58 (11%)	1.06 (13%)	1.39 (12%)	1.38 (11%)	0.66 (16%)	0.81 (13%)
Yb	1.42 (10%)	1.08 (11%)	1.53 (9%)	1.80 (9%)	0.65 (18%)	1.18 (11%)
Lu	0.22 (6%)	0.18 (6%)	0.23 (5%)	0.25 (5%)	0.13 (8%)	0.16 (6%)

Appendix 8) Electron microprobe analyses: major phases - Strontian.

Appendix 8A) Detection limits and analytical precision.

Detection limits.

The detection limits (wt%) were calculated (using Equation 2.4) from the number of counts obtained from peak and background positions from the relevant element standards using the beam conditions and count times outlined in Appendix 2F. As discussed in Section 2.3.1 the calculated values should only be used as a approximate guide to the expected detection limits.

Element Oxide	Detection Limit (wt%)
SiO2	0.015
TiO2	0.019
Al2O3	0.090
FeO	0.031
MnO	0.030
MgO	0.010
CaO	0.014
BaO	0.060
Na2O	0.027
K2O	0.023

Analytical precision.

Values of analytical precision (± wt%) were calculated from the combined analytical uncertainties of the standards and unknowns using Equations 2.5 and 2.6. The table below gives analytical precision values for typical alkali-feldspar, biotite, amphibole and plagioclase microprobe analyses.

Element Oxide	Alkali-Feldspar	Biotite	Amphibole	Plagioclase Feldspar
SiO2	65.66 (±0.30)	37.50 (±0.21)	49.24 (±0.24)	60.61 (±0.27)
TiO2	-	3.33 (±0.11)	1.15 (±0.07)	-
Al2O3	20.48 (±0.14)	15.29 (±0.11)	6.36 (±0.08)	24.92 (±0.15)
FeO	-	17.98 (±0.30)	14.72 (±0.27)	-
MnO	-	0.23 (±0.06)	0.41 (±0.07)	-
MgO	-	13.28 (±0.12)	14.29 (±0.12)	-
CaO	-	-	11.98 (±0.19)	5.20 (±0.12)
BaO	1.49 (±0.11)	-	-	-
Na2O	1.26 (±0.07)	0.06 (±0.05)	1.23 (±0.07)	8.54 (±0.17)
K2O	14.30 (±0.29)	9.87 (±0.22)	0.64 (±0.05)	0.33 (±0.04)

Appendix 8B) The electron microprobe analyses.

The first part of the analysis coding (*eg.* T3) denotes the rock: the second part the analysis number, in the case of alkali-feldspar and plagioclase feldspar a letter denotes individual grains. All the concentrations are expressed as wt% oxide, Fe is calculated as FeO. n.d. - not detected. Alkali-feldspar and plagioclase feldspar structural formula have been calculated to 32 oxygens, amphibole and biotite analyses to 23 oxygens.

Alkali Feldspar Analyses: Strontian - BPSRT1.

	T1/A1	T1/A2	T1/A3	T1/A4	T1/B1	T1/B2	T1/B3	T1/B4
SiO_2	60.72	63.30	61.27	64.41	63.47	63.94	63.34	63.49
TiO_2	n.d.	n.d.	n.d.	n.d.	n.d.	n.d.	n.d.	n.d.
Al_2O_3	19.96	18.92	20.26	18.14	18.57	18.20	18.39	18.42
FeO	n.d.	0.04	n.d.	n.d.	0.06	n.d.	0.09	0.13
MnO	n.d.	n.d.	n.d.	n.d.	n.d.	n.d.	n.d.	n.d.
MgO	n.d.	n.d.	n.d.	n.d.	n.d.	n.d.	n.d.	n.d.
CaO	n.d.	n.d.	n.d.	n.d.	n.d.	n.d.	n.d.	n.d.
BaO	5.36	1.35	5.25	0.29	1.47	1.22	1.23	1.19
Na_2O	0.97	1.36	1.04	0.46	1.30	1.24	1.25	1.55
K_2O	13.31	14.46	12.96	15.47	14.08	14.31	14.88	14.14
TOTAL	100.32	99.43	100.78	98.77	98.95	98.91	99.18	98.92
Si	11.5473	11.8367	11.5536	12.0304	11.9055	11.9743	11.8958	11.9130
Ti	-	-	-	-	-	-	-	-
Al	4.4750	4.1709	4.5040	3.9944	4.1066	4.0182	4.0718	4.0747
Fe^{2+}	-	-	-	-	-	-	-	-
Mn	-	-	-	-	-	-	-	-
Mg	-	-	-	-	-	-	-	-
Ca	-	-	-	-	-	-	-	-
Ba	0.3994	0.0989	0.3879	0.0212	0.1080	0.0895	0.0905	0.0875
Na	0.3577	0.4931	0.3802	0.1666	0.4728	0.4503	0.4552	0.5639
K	3.2293	3.4496	3.1178	3.6864	3.3695	3.4190	3.5653	3.3849
TOTAL	20.0087	20.0492	19.9435	19.8989	19.9624	19.9513	20.0786	20.0240

Alkali Feldspar Analyses: Strontian - BPSRT1.

	T1/B5	T1/B6	T1/B7	T1/B8	T1/B9	T1/B10	T1/C1	T1/C2
SiO_2	63.33	64.23	62.06	63.10	63.64	63.86	63.55	62.91
TiO_2	n.d.	n.d.	n.d.	n.d.	n.d.	n.d.	n.d.	n.d.
Al_2O_3	18.68	18.52	19.46	19.08	18.48	18.66	18.51	18.41
FeO	0.07	0.13	n.d.	0.07	0.10	0.08	0.11	0.15
MnO	n.d.	n.d.	n.d.	n.d.	n.d.	n.d.	n.d.	n.d.
MgO	n.d.	n.d.	n.d.	n.d.	n.d.	n.d.	n.d.	n.d.
CaO	n.d.	n.d.	n.d.	n.d.	n.d.	n.d.	n.d.	n.d.
BaO	1.16	1.15	4.25	1.54	1.49	1.42	1.45	1.39
Na_2O	1.47	1.19	1.08	1.35	1.11	1.27	1.14	1.31
K_2O	14.52	14.46	13.72	13.95	14.49	14.27	14.86	14.38
TOTAL	99.23	99.68	100.57	99.09	99.31	99.56	99.62	98.55
Si	11.8626	11.9471	11.6821	11.8254	11.9188	11.9080	11.8934	11.8864
Ti	-	-	-	-	-	-	-	-
Al	4.1251	4.0612	4.3186	4.2155	4.0803	4.1021	4.0840	4.1008
Fe^{2+}	-	-	-	-	-	-	-	-
Mn	-	-	-	-	-	-	-	-
Mg	-	-	-	-	-	-	-	-
Ca	-	-	-	-	-	-	-	-
Ba	0.0851	0.0838	0.3135	0.1131	0.1093	0.1038	0.1063	0.1029
Na	0.5339	0.4292	0.3942	0.4906	0.4031	0.4592	0.4137	0.4799
K	3.4699	3.4314	3.2949	3.3353	3.4622	3.3948	3.5481	3.4663
TOTAL	20.0767	19.9526	20.0032	19.9798	19.9737	19.9679	20.0455	20.0363

Alkali Feldspar Analyses: Strontian - BPSRT1 and BPSRT2.

	T1/C3	T1/C4	T1/C5	T1/C6	T2/A1	T2/A2	T2/A3	T2/B1
SiO_2	63.35	63.52	63.54	63.99	64.89	64.58	64.77	63.71
TiO_2	n.d.	n.d.	n.d.	n.d.	n.d.	n.d.	n.d.	n.d.
Al_2O_3	18.72	18.73	18.41	18.49	18.66	18.20	18.26	18.32
FeO	0.09	0.34	0.13	0.10	0.11	0.05	n.d.	0.05
MnO	n.d.	n.d.	n.d.	n.d.	n.d.	n.d.	n.d.	n.d.
MgO	n.d.	n.d.	n.d.	n.d.	n.d.	n.d.	n.d.	n.d.
CaO	n.d.	n.d.	n.d.	n.d.	n.d.	n.d.	n.d.	n.d.
BaO	1.42	1.53	1.56	1.20	0.21	0.18	0.23	0.20
Na_2O	1.24	1.06	1.01	1.82	0.87	0.96	1.00	1.02
K_2O	14.51	14.88	14.92	13.80	15.99	15.77	15.51	15.76
TOTAL	99.53	100.06	99.57	99.40	100.73	99.74	99.77	99.11
Si	11.8772	11.8673	11.9084	11.9249	11.9404	11.9866	11.9955	11.9267
Ti	-	-	-	-	-	-	-	-
Al	4.1247	4.1254	4.0677	4.0622	4.0480	3.9825	3.9869	4.0432
Fe^{2+}	-	-	-	-	-	-	-	-
Mn	-	-	-	-	-	-	-	-
Mg	-	-	-	-	-	-	-	-
Ca	-	-	-	-	-	-	-	-
Ba	0.1040	0.1120	0.1146	0.0876	0.0151	0.0131	0.0167	0.0147
Na	0.4494	0.3840	0.3670	0.6576	0.3104	0.3455	0.3591	0.3702
K	3.4598	3.5467	3.5674	3.2810	3.7538	3.7343	3.6647	3.7640
TOTAL	20.0150	20.0354	20.0250	20.0133	20.0677	20.0620	20.0229	20.1188

Alkali Feldspar Analyses: Strontian - BPSRT2.

	T2/B2	T2/B3	T2/B4	T2/C1	T2/D1	T2/D2	T2/E1	T2/E2
SiO_2	64.68	64.33	64.04	64.48	64.36	63.86	64.35	64.60
TiO_2	n.d.	n.d.	n.d.	n.d.	n.d.	n.d.	n.d.	n.d.
Al_2O_3	18.33	18.30	18.19	18.28	18.44	18.10	18.29	18.28
FeO	0.06	0.11	0.06	0.16	0.14	0.14	0.07	0.07
MnO	n.d.	n.d.	n.d.	n.d.	n.d.	n.d.	n.d.	n.d.
MgO	n.d.	n.d.	n.d.	n.d.	n.d.	n.d.	n.d.	n.d.
CaO	n.d.	n.d.	n.d.	n.d.	n.d.	n.d.	n.d.	n.d.
BaO	0.13	0.24	0.13	0.20	0.22	0.23	0.18	0.21
Na_2O	1.21	0.88	0.94	0.86	0.82	0.67	0.95	1.06
K_2O	15.25	15.71	15.73	15.80	15.94	16.14	15.63	15.39
TOTAL	99.66	99.57	99.09	99.78	99.92	99.14	100.24	99.61
Si	11.9829	11.9691	11.9671	11.9770	11.9477	11.9670	11.9717	11.9870
Ti	-	-	-	-	-	-	-	-
Al	4.0035	4.0141	4.0073	4.0030	4.0357	3.9987	4.0115	3.9989
Fe^{2+}	-	-	-	-	-	-	-	-
Mn	-	-	-	-	-	-	-	-
Mg	-	-	-	-	-	-	-	-
CaO	-	-	-	-	-	-	-	-
Ba	0.0094	0.0175	0.0095	0.0146	0.0160	0.0169	0.0131	0.0153
Na	0.4347	0.3175	0.3406	0.3097	0.2952	0.2434	0.3427	0.3814
K	3.6045	3.7291	3.7501	3.7442	3.7752	3.8587	3.7098	3.6433
TOTAL	20.0349	20.0472	20.0746	20.0485	20.0697	20.0847	20.0488	20.0259

Alkali Feldspar Analyses: Strontian - BPSRT2.

	T2/F1	T2/F2	T2/F3	T2/F4	T2/F5	T2/F6	T2/G1	T2/G2
SiO2	64.47	64.56	64.71	64.72	64.60	64.40	64.57	64.82
TiO2	n.d.	n.d.	n.d.	n.d.	n.d.	n.d.	n.d.	n.d.
Al2O3	18.59	18.33	18.38	18.47	18.41	18.35	18.42	18.34
FeO	n.d.	0.13	n.d.	0.08	0.09	0.09	0.11	0.08
MnO	n.d.	n.d.	n.d.	n.d.	n.d.	n.d.	n.d.	n.d.
MgO	n.d.	n.d.	n.d.	n.d.	n.d.	n.d.	n.d.	n.d.
CaO	n.d.	n.d.	n.d.	n.d.	n.d.	n.d.	n.d.	n.d.
BaO	0.93	0.40	0.13	0.09	0.29	0.27	0.12	0.19
Na2O	0.81	1.39	1.19	0.87	1.01	0.96	1.19	1.18
K2O	16.03	15.10	15.25	15.63	15.43	15.56	15.19	15.38
TOTAL	99.83	99.91	99.66	99.86	99.83	99.63	99.60	99.99
Si	11.9120	11.9645	11.9795	11.9747	11.9705	11.9666	11.9710	11.9828
Ti	-	-	-	-	-	-	-	-
Al	4.0494	4.0048	4.0114	4.0288	4.0218	4.0198	4.0260	3.9970
Fe2+	-	-	-	-	-	-	-	-
Mn	-	-	-	-	-	-	-	-
Mg	-	-	-	-	-	-	-	-
Ca	-	-	-	-	-	-	-	-
Ba	0.0673	0.0290	0.0094	0.0065	0.0211	0.0197	0.0087	0.0138
Na	0.2902	0.4995	0.4271	0.3121	0.3629	0.3459	0.4278	0.4230
K	3.7787	3.5702	3.6018	3.6895	3.6478	3.6887	3.5928	3.6273
TOTAL	20.0977	20.0679	20.0293	20.0117	20.0240	20.0407	20.0263	20.0438

Alkali Feldspar Analyses: Strontian - BPSRT3.

	T3/A1	T3/A2	T3/A3	T3/A4	T3/A5	T3/A6	T3/A7	T3/A8
SiO2	63.86	63.82	64.46	63.94	64.24	64.22	64.18	64.24
TiO2	n.d.	n.d.	n.d.	n.d.	n.d.	n.d.	n.d.	n.d.
Al2O3	18.61	18.61	18.76	18.60	18.88	18.71	18.70	18.43
FeO	0.07	0.15	0.05	0.12	0.12	0.12	0.04	0.03
MnO	n.d.	n.d.	n.d.	n.d.	n.d.	n.d.	n.d.	n.d.
MgO	n.d.	n.d.	n.d.	n.d.	n.d.	n.d.	n.d.	n.d.
CaO	n.d.	n.d.	n.d.	n.d.	n.d.	n.d.	n.d.	n.d.
BaO	0.62	0.77	0.79	0.86	0.89	0.78	0.66	0.53
Na2O	1.71	1.71	1.86	1.73	2.05	1.44	1.12	1.34
K2O	14.31	14.31	14.10	14.20	13.85	14.43	15.27	14.80
TOTAL	99.11	99.22	99.97	99.33	99.91	99.58	99.93	99.34
Si	11.9045	11.8986	11.9093	11.9066	11.8799	11.9179	11.9049	11.9503
Ti	-	-	-	-	-	-	-	-
Al	4.0899	4.0905	4.0862	4.0833	4.1162	4.0935	4.0894	4.0419
Fe2+	-	-	-	-	-	-	-	-
Mn	-	-	-	-	-	-	-	-
Mg	-	-	-	-	-	-	-	-
Ca	-	-	-	-	-	-	-	-
Ba	0.0453	0.0562	0.0572	0.0627	0.0645	0.0567	0.0480	0.0386
Na	0.6181	0.6182	0.6663	0.6246	0.7351	0.5182	0.4028	0.4833
K	3.4033	3.4038	3.3235	3.3735	3.2677	3.4165	3.6136	3.5125
TOTAL	20.0612	20.0672	20.0425	20.0508	20.0634	20.0027	20.0587	20.0267

Alkali Feldspar Analyses: Strontian - BPSRT3.

	T3/A9	T3/B1	T3/B2	T3/B3	T3/B4	T3/B5	T3/C1	T3/C2
SiO2	63.88	64.61	64.71	64.63	64.23	64.34	64.46	64.97
TiO2	n.d.	n.d.	n.d.	n.d.	n.d.	n.d.	n.d.	n.d.
Al2O3	18.46	18.63	18.57	18.56	18.62	18.65	18.69	18.49
FeO	0.12	0.06	0.07	0.16	n.d.	n.d.	0.05	0.13
MnO	n.d.	n.d.	n.d.	n.d.	n.d.	n.d.	n.d.	n.d.
MgO	n.d.	n.d.	n.d.	n.d.	n.d.	n.d.	n.d.	n.d.
CaO	n.d.	n.d.	n.d.	n.d.	n.d.	n.d.	n.d.	n.d.
BaO	0.48	0.54	0.42	0.63	0.67	0.52	0.51	0.34
Na2O	1.41	1.98	1.87	1.81	1.15	1.49	1.24	1.49
K2O	14.75	14.00	14.30	14.21	15.29	14.95	15.25	14.82
TOTAL	99.10	99.82	99.94	100.00	99.96	99.95	100.21	100.24
Si	11.9284	11.9353	11.9447	11.9445	11.9139	11.9117	11.9163	11.9713
Ti	-	-	-	-	-	-	-	-
Al	4.0639	4.0573	4.0411	4.0439	4.0718	4.0706	4.0733	4.0165
Fe2+	-	-	-	-	-	-	-	-
Mn	-	-	-	-	-	-	-	-
Mg	-	-	-	-	-	-	-	-
Ca	-	-	-	-	-	-	-	-
Ba	0.0351	0.0391	0.0304	0.0456	0.0487	0.0377	0.0369	0.0245
Na	0.5105	0.7092	0.6693	0.6486	0.4136	0.5349	0.4445	0.5323
K	3.5139	3.2995	3.3676	3.3505	3.6183	3.5311	3.5967	3.4838
TOTAL	20.0518	20.0404	20.0532	20.0331	20.0662	20.0860	20.0677	20.0285

Alkali Feldspar Analyses: Strontian - BPSRT3 and BPSRT4.

	T3/C3	T3/C4	T3/C5	T3/C6	T4/A1	T4/A2	T4/A3	T4/A4
SiO2	63.93	63.85	63.88	64.64	64.25	64.08	64.17	63.88
TiO2	n.d.	n.d.	n.d.	n.d.	n.d.	n.d.	n.d.	n.d.
Al2O3	18.56	18.58	18.63	18.71	18.40	18.73	18.38	18.66
FeO	0.09	0.08	0.05	0.11	n.d.	0.09	0.10	0.10
MnO	n.d.	n.d.	n.d.	n.d.	n.d.	n.d.	n.d.	n.d.
MgO	n.d.	n.d.	n.d.	n.d.	n.d.	n.d.	n.d.	n.d.
CaO	n.d.	n.d.	n.d.	n.d.	n.d.	n.d.	n.d.	n.d.
BaO	0.54	0.50	1.12	0.44	0.30	0.44	0.51	0.71
Na2O	1.37	1.59	0.82	2.24	1.50	1.84	1.40	1.48
K2O	14.52	14.53	15.77	13.56	14.63	14.32	15.08	14.64
TOTAL	99.01	99.13	100.27	99.70	99.08	99.50	99.64	99.47
Si	11.9298	11.9093	11.8847	11.9317	11.9575	11.8961	11.9372	11.8978
Ti	-	-	-	-	-	-	-	-
Al	4.0831	4.0856	4.0863	4.0716	4.0371	4.0993	4.0309	4.0973
Fe2+	-	-	-	-	-	-	-	-
Mn	-	-	-	-	-	-	-	-
Mg	-	-	-	-	-	-	-	-
Ca	-	-	-	-	-	-	-	-
Ba	0.0395	0.0365	0.0816	0.0318	0.0219	0.0320	0.0372	0.0518
Na	0.4957	0.5750	0.2958	0.8017	0.5413	0.6623	0.5050	0.5345
K	3.4568	3.4576	3.7432	3.1933	3.4737	3.3916	3.5789	3.4788
TOTAL	20.0049	20.0641	20.0916	20.0301	20.0315	20.0813	20.0893	20.0602

Alkali Feldspar Analyses: Strontian - BPSRT4.

	T4/A5	T4/A6	T4/A7	T4/A8	T4/B1	T4/B2	T4/B3	T4/C1
SiO2	64.08	63.77	63.77	63.62	64.19	63.75	63.50	64.57
TiO2	n.d.	n.d.	n.d.	n.d.	n.d.	n.d.	n.d.	n.d.
Al2O3	18.35	18.42	18.43	18.90	18.23	18.43	18.18	18.38
FeO	0.15	0.11	0.07	0.14	0.08	0.06	n.d.	0.06
MnO	n.d.	n.d.	n.d.	n.d.	n.d.	n.d.	n.d.	n.d.
MgO	n.d.	n.d.	n.d.	n.d.	n.d.	n.d.	n.d.	n.d.
CaO	n.d.	n.d.	n.d.	n.d.	n.d.	n.d.	n.d.	n.d.
BaO	0.58	0.88	0.63	1.15	0.32	0.35	0.20	0.39
Na2O	1.42	1.20	1.30	1.91	1.13	1.36	1.39	0.86
K2O	14.76	14.96	14.90	13.93	15.32	14.94	15.06	15.47
TOTAL	99.24	99.34	99.10	99.64	99.27	98.89	98.33	99.73
Si	11.9476	11.9221	11.9236	11.8466	11.9694	11.9244	11.9402	11.9783
Ti	-	-	-	-	-	-	-	-
Al	4.0335	4.0599	4.0626	4.1490	4.0075	4.0642	4.0301	4.0198
Fe^{2+}	-	-	-	-	-	-	-	-
Mn	-	-	-	-	-	-	-	-
Mg	-	-	-	-	-	-	-	-
Ca	-	-	-	-	-	-	-	-
Ba	0.0424	0.0645	0.0462	0.0839	0.0234	0.0257	0.0147	0.0283
Na	0.5133	0.4350	0.4713	0.6896	0.4086	0.4932	0.5068	0.3093
K	3.5110	3.5682	3.5543	3.3093	3.6446	3.5652	3.6128	3.6613
TOTAL	20.0478	20.0496	20.0579	20.0784	20.0534	20.0727	20.1046	19.9971

Alkali Feldspar Analyses: Strontian - BPSRT4.

	T4/C2	T4/C3	T4/C4	T4/C5	T4/C6	T4/C7	T4/C8	T4/C9
SiO2	64.08	64.57	64.67	64.67	64.51	64.81	64.83	64.99
TiO2	n.d.	n.d.	n.d.	n.d.	n.d.	n.d.	n.d.	n.d.
Al2O3	18.18	18.36	18.45	18.53	18.47	18.48	18.42	18.51
FeO	0.08	0.10	n.d.	0.05	0.11	0.06	0.05	0.14
MnO	n.d.	n.d.	n.d.	n.d.	n.d.	n.d.	n.d.	n.d.
MgO	n.d.	n.d.	n.d.	n.d.	n.d.	n.d.	n.d.	n.d.
CaO	n.d.	n.d.	n.d.	n.d.	n.d.	n.d.	n.d.	n.d.
BaO	0.29	0.26	0.22	0.29	0.33	0.29	0.30	0.23
Na2O	0.88	1.22	1.37	1.55	1.18	1.91	1.70	1.79
K2O	15.72	15.35	15.00	14.76	15.04	14.30	14.56	14.15
TOTAL	99.23	99.86	99.71	99.85	99.64	99.85	99.86	99.81
Si	11.9703	11.9654	11.9656	11.9524	11.9636	11.9612	11.9718	11.9822
Ti	-	-	-	-	-	-	-	-
Al	4.0037	4.0110	4.0245	4.0375	4.0382	4.0209	4.0101	4.0233
Fe^{2+}	-	-	-	-	-	-	-	-
Mn	-	-	-	-	-	-	-	-
Mg	-	-	-	-	-	-	-	-
Ca	-	-	-	-	-	-	-	-
Ba	0.0212	0.0189	0.0159	0.0210	0.0240	0.0210	0.0217	0.0166
Na	0.3187	0.4384	0.4915	0.5555	0.4243	0.6835	0.6087	0.6399
K	3.7464	3.6290	3.5408	3.4803	3.5585	3.3671	3.4303	3.3283
TOTAL	20.0604	20.0627	20.0383	20.0467	20.0086	20.0536	20.0426	19.9903

Alkali Feldspar Analyses: Strontian - BPSRG1.

	G1/A1	G1/A2	G1/A3	G1/A4	G1/A5	G1/A6	G1/A7	G1/A8
SiO2	64.25	63.68	64.36	64.11	64.15	63.56	63.19	64.19
TiO2	n.d.	n.d.	n.d.	n.d.	n.d.	n.d.	n.d.	n.d.
Al2O3	18.55	18.57	18.59	18.35	18.76	18.59	18.54	18.41
FeO	n.d.	n.d.	0.09	0.07	n.d.	0.06	n.d.	n.d.
MnO	n.d.	n.d.	n.d.	n.d.	n.d.	n.d.	n.d.	n.d.
MgO	n.d.	n.d.	n.d.	n.d.	n.d.	n.d.	n.d.	n.d.
CaO	n.d.	n.d.	n.d.	n.d.	n.d.	n.d.	n.d.	n.d.
BaO	0.62	1.11	0.95	0.66	1.12	1.24	1.23	0.15
Na2O	1.01	1.22	1.15	0.98	1.19	0.80	1.46	1.10
K2O	15.63	14.93	15.29	15.62	15.29	15.70	14.53	15.32
TOTAL	100.06	99.51	100.43	99.79	100.51	99.95	98.95	99.17
Si	11.9191	11.8930	11.9161	11.9384	11.8782	11.8755	11.8714	11.9539
Ti	-	-	-	-	-	-	-	-
Al	4.0570	4.0887	4.0577	4.0285	4.0952	4.0948	4.1063	4.0419
Fe^{2+}	-	-	-	-	-	-	-	-
Mn	-	-	-	-	-	-	-	-
Mg	-	-	-	-	-	-	-	-
Ca	-	-	-	-	-	-	-	-
Ba	0.0451	0.0812	0.0689	0.0482	0.0813	0.0908	0.0905	0.0109
Na	0.3633	0.4418	0.4128	0.3538	0.4272	0.2898	0.5318	0.3972
K	3.6992	3.5574	3.6117	3.7109	3.6120	3.7424	3.4826	3.6398
TOTAL	20.0837	20.0622	20.0673	20.0798	20.0938	20.0932	20.0827	20.0437

Alkali Feldspar Analyses: Strontian - BPSRG1.

	G1/B1	G1/B2	G1/B3	G1/C1	G1/C2	G1/C3	G1/D1	G1/D2
SiO2	64.34	64.40	64.20	64.41	64.03	63.98	63.79	63.17
TiO2	n.d.	n.d.	n.d.	n.d.	n.d.	n.d.	n.d.	n.d.
Al2O3	18.10	18.16	18.07	18.19	18.32	18.33	18.24	18.58
FeO	0.06	n.d.	0.09	0.08	0.05	0.05	n.d.	0.06
MnO	n.d.	n.d.	n.d.	n.d.	n.d.	n.d.	n.d.	n.d.
MgO	n.d.	n.d.	n.d.	n.d.	n.d.	n.d.	n.d.	n.d.
CaO	n.d.	n.d.	n.d.	n.d.	n.d.	n.d.	n.d.	n.d.
BaO	0.16	0.11	0.14	n.d.	0.12	0.35	0.67	1.30
Na2O	1.12	1.14	0.71	0.93	0.87	0.74	1.27	0.61
K2O	15.39	15.40	15.84	15.40	15.70	15.98	15.13	15.64
TOTAL	99.17	99.21	99.05	99.94	99.09	99.43	99.10	99.36
Si	11.9944	11.9893	11.9998	12.0033	11.9569	11.9433	11.9387	11.8717
Ti	-	-	-	-	-	-	-	-
Al	3.9780	3.9858	3.9819	3.9964	4.0332	4.0340	4.0245	4.1166
Fe^{2+}	-	-	-	-	-	-	-	-
Mn	-	-	-	-	-	-	-	-
Mg	-	-	-	-	-	-	-	-
Ca	-	-	-	-	-	-	-	-
Ba	0.0117	0.0080	0.0103	-	0.0088	0.0256	0.0491	0.0957
Na	0.4048	0.4115	0.2573	0.3360	0.3150	0.2678	0.4609	0.2223
K	3.6603	3.6577	3.7773	3.6614	3.7404	3.8057	3.6126	3.7499
TOTAL	20.0492	20.0524	20.0265	19.9972	20.0542	20.0765	20.0858	20.0561

Alkali Feldspar Analyses: Strontian - BPSRG1 and BPSRG4.

	G1/D3	G1/D4	G1/D5	G1/D6	G4/A1	G4/A2	G4/A3	G4/A4
SiO_2	63.17	64.36	63.90	63.59	64.67	64.76	64.98	65.07
TiO_2	n.d.	n.d.	n.d.	n.d.	n.d.	n.d.	n.d.	n.d.
Al_2O_3	18.58	18.37	18.59	18.57	18.52	18.52	18.40	18.45
FeO	n.d.	n.d.	0.07	n.d.	0.07	0.06	0.10	0.12
MnO	n.d.	n.d.	n.d.	n.d.	n.d.	n.d.	n.d.	n.d.
MgO	n.d.	n.d.	n.d.	n.d.	n.d.	n.d.	n.d.	n.d.
CaO	n.d.	n.d.	n.d.	n.d.	n.d.	n.d.	n.d.	n.d.
BaO	0.87	0.72	0.97	0.94	0.10	0.30	0.19	0.17
Na_2O	1.33	1.30	1.67	1.05	1.11	1.32	1.26	1.82
K_2O	14.67	14.77	14.23	15.09	15.67	15.10	15.26	14.25
TOTAL	99.62	99.52	99.43	99.26	100.14	100.06	100.19	99.88
Si	11.8779	11.9622	11.9056	11.8977	11.9481	11.9580	11.9828	11.9884
Ti	-	-	-	-	-	-	-	-
Al	4.1187	4.0252	4.0834	4.0961	4.0339	4.0316	4.0002	4.0074
Fe^{2+}	-	-	-	-	-	-	-	-
Mn	-	-	-	-	-	-	-	-
Mg	-	-	-	-	-	-	-	-
Ca	-	-	-	-	-	-	-	-
Ba	0.0641	0.0524	0.0708	0.0689	0.0072	0.0217	0.0137	0.0123
Na	0.4849	0.4685	0.6033	0.3809	0.3976	0.4726	0.4505	0.6502
K	3.5192	3.5023	3.3825	3.6020	3.6936	3.5572	3.5902	3.3495
TOTAL	20.0648	20.0106	20.0456	20.0457	20.0805	20.0411	20.0374	20.0077

Alkali Feldspar Analyses: Strontian - BPSRG4.

	G4/A5	G4/A6	G4/A7	G4/A8	G4/A9	G4/A10	G4/B1	G4/B2
SiO_2	64.86	64.53	64.64	64.81	64.88	64.61	64.32	65.08
TiO_2	n.d.	n.d.	n.d.	n.d.	n.d.	n.d.	n.d.	n.d.
Al_2O_3	18.34	18.45	18.52	18.62	18.80	18.39	18.48	18.49
FeO	0.10	0.06	0.08	0.06	0.10	0.05	0.10	n.d.
MnO	n.d.	n.d.	n.d.	n.d.	n.d.	n.d.	n.d.	n.d.
MgO	n.d.	n.d.	n.d.	n.d.	n.d.	n.d.	n.d.	n.d.
CaO	n.d.	n.d.	n.d.	n.d.	n.d.	n.d.	n.d.	n.d.
BaO	0.35	0.22	0.34	0.31	0.25	0.55	0.68	0.23
Na_2O	1.73	0.85	0.88	1.09	1.14	1.83	1.15	1.63
K_2O	14.39	15.78	15.55	15.38	15.26	14.15	15.16	14.76
TOTAL	99.77	99.89	100.01	100.27	100.43	99.58	99.89	100.19
Si	11.9871	11.9595	11.9609	11.9509	11.9358	11.9678	11.9407	11.9726
Ti	-	-	-	-	-	-	-	-
Al	3.9960	4.0312	4.0401	4.0479	4.0774	4.0159	4.0446	4.0102
Fe^{2+}	-	-	-	-	-	-	-	-
Mn	-	-	-	-	-	-	-	-
Mg	-	-	-	-	-	-	-	-
Ca	-	-	-	-	-	-	-	-
Ba	0.0253	0.0160	0.0247	0.0224	0.0180	0.0399	0.0495	0.0166
Na	0.6199	0.3054	0.3157	0.3897	0.4066	0.6573	0.4140	0.5814
K	3.3930	3.7311	3.6709	3.6182	3.5816	3.3439	3.5906	3.4643
TOTAL	20.0214	20.0432	20.0123	20.0291	20.0196	20.0248	20.0393	20.0451

Alkali Feldspar Analyses: Strontian - BPSRG4.

	G4/C1	G4/C2	G4/C3	G4/C4	G4/C5	G4/C6	G4/C7	G4/C8
SiO_2	64.44	65.24	64.87	64.66	64.68	64.95	64.73	64.46
TiO_2	n.d.	n.d.	n.d.	n.d.	n.d.	n.d.	n.d.	n.d.
Al_2O_2	18.29	18.36	18.41	18.36	18.45	18.46	18.43	18.67
FeO	0.04	0.08	0.06	0.12	0.06	0.09	0.11	0.07
MnO	n.d.	n.d.	n.d.	n.d.	n.d.	n.d.	n.d.	n.d.
MgO	n.d.	n.d.	n.d.	n.d.	n.d.	n.d.	n.d.	n.d.
CaO	n.d.	n.d.	n.d.	n.d.	n.d.	n.d.	n.d.	n.d.
BaO	0.15	0.21	n.d.	0.16	0.25	0.49	0.42	0.77
Na_2O	0.83	0.79	1.20	0.78	1.29	1.37	1.02	1.27
K_2O	16.13	16.23	15.66	16.36	15.13	15.05	15.54	15.23
TOTAL	99.88	100.91	100.20	100.44	99.86	100.41	100.67	100.47
Si	11.9626	11.9879	11.9680	11.9573	11.9648	11.9679	11.9650	11.9106
Ti	-	-	-	-	-	-	-	-
Al	4.0029	3.9773	4.0042	4.0027	4.0237	4.0101	4.0163	4.0670
Fe^{2+}	-	-	-	-	-	-	-	-
Mn	-	-	-	-	-	-	-	-
Mg	-	-	-	-	-	-	-	-
Ca	-	-	-	-	-	-	-	-
Ba	0.0109	0.0151	-	0.0116	0.0181	0.0354	0.0304	0.0557
Na	0.2988	0.2815	0.4293	0.2797	0.4627	0.4895	0.3656	0.4550
K	3.8202	3.8048	3.6860	3.8598	3.5707	3.5380	3.6647	3.5902
TOTAL	20.0954	20.0666	20.0875	20.1111	20.0400	20.0408	20.0420	20.0786

Amphibole Analyses: Strontian - BPSRT1.

	T1/1	T1/2	T1/3	T1/4	T1/5	T1/6	T1/7	T1/8
SiO_2	48.04	47.62	48.14	47.56	48.02	47.00	54.32	46.20
TiO_2	1.02	0.97	1.02	1.17	0.95	1.18	0.10	1.08
Al_2O_3	6.11	5.85	5.78	6.33	6.00	7.06	0.70	7.42
FeO	14.07	13.95	14.17	14.48	14.14	14.86	12.85	15.30
MnO	0.35	0.28	0.36	0.35	0.43	0.28	0.48	0.29
MgO	14.06	13.95	13.70	13.35	13.50	12.85	15.00	12.19
CaO	11.71	11.71	11.82	11.76	11.84	11.83	12.48	11.55
Na_2O	1.25	1.21	1.14	1.33	1.22	1.30	0.34	1.44
K_2O	0.58	0.58	0.57	0.59	0.57	0.74	0.07	0.71
TOTAL	97.24	96.12	96.74	96.92	96.67	97.10	96.34	96.21
Si	7.1026	7.1200	7.1552	7.0736	7.1430	6.9975	7.9434	6.9642
Ti	0.1134	0.1091	0.1140	0.1309	0.1063	0.1321	0.0110	0.1224
Al	1.0650	1.0312	1.0128	1.1099	1.0522	1.2392	0.1207	1.3186
Fe^{2+}	1.7397	1.7444	1.7614	1.8011	1.7591	1.8503	1.5715	1.9289
Mn	0.0438	0.0355	0.0453	0.0441	0.0542	0.0353	0.0595	0.0370
Mg	3.0980	3.1085	3.0347	2.9591	2.9928	2.8512	3.2690	2.7385
Ca	1.8551	1.8760	1.8825	1.8741	1.8871	1.8872	1.9555	1.8656
Na	0.3583	0.3508	0.3285	0.3835	0.3519	0.3753	0.0964	0.4209
K	0.1094	0.1106	0.1081	0.1120	0.1082	0.1406	0.0131	0.1365
TOTAL	15.4854	15.4860	5.4427	15.4883	15.4547	15.5087	15.0400	15.5327

Amphibole Analyses: Strontian - BPSRT1 and BPSRT2.

	T1/9	T1/10	T2/1	T2/2	T2/3	T2/4	T2/5	T2/6
SiO_2	46.38	47.38	48.86	48.04	47.47	47.70	46.69	48.60
TiO_2	1.01	0.87	1.18	1.31	1.30	0.78	1.16	0.68
Al_2O_3	7.49	6.80	6.11	6.56	6.61	6.26	7.05	5.65
FeO	15.12	14.75	12.48	12.55	13.17	14.80	16.71	13.93
MnO	0.42	0.33	0.42	0.49	0.34	0.51	0.67	0.46
MgO	12.53	12.95	14.31	14.10	14.11	12.70	11.67	12.74
CaO	12.02	11.92	11.61	11.52	11.53	11.31	11.20	11.52
Na_2O	1.33	1.20	1.32	1.60	1.74	1.56	1.55	1.14
K_2O	0.79	0.69	0.53	0.58	0.61	0.53	0.63	0.46
TOTAL	97.12	96.94	96.82	96.75	96.88	96.15	97.33	95.18
Si	6.9326	7.0586	7.1817	7.0901	7.0283	7.1543	6.9990	7.3067
Ti	0.1135	0.0975	0.1304	0.1454	0.1448	0.0880	0.1308	0.0769
Al	1.3199	1.1943	1.0588	1.1414	1.1538	1.1069	1.2459	1.0014
Fe^{2+}	1.8901	1.8378	1.5341	1.5491	1.6308	1.8564	2.0949	1.7515
Mn	0.0532	0.0416	0.0523	0.0613	0.0426	0.0648	0.0851	0.0586
Mg	2.7913	2.8752	3.1347	3.1013	3.1134	2.8388	2.6071	2.8545
Ca	1.9252	1.9028	1.8285	1.8218	1.8292	1.8176	1.7990	1.8558
Na	0.3855	0.3466	0.3762	0.4579	0.4995	0.4537	0.4505	0.3323
K	0.1507	0.1311	0.0994	0.1092	0.1152	0.1014	0.1205	0.0882
TOTAL	15.5619	15.4856	15.3962	15.4774	15.5575	15.4819	15.5328	15.3260

Amphibole Analyses: Strontian - BPSRT2 and BPSRT3.

	T2/7	T2/8	T2/9	T2/10	T3/1	T3/2	T3/3	T3/4
SiO_2	47.94	49.18	47.33	47.03	48.52	47.31	49.18	47.33
TiO_2	1.00	0.69	0.85	0.71	0.72	1.17	1.02	0.98
Al_2O_3	6.23	4.96	6.84	6.34	5.89	6.52	5.58	6.57
FeO	14.96	14.58	15.29	16.08	13.29	14.19	12.34	14.30
MnO	0.64	0.51	0.49	0.57	0.32	0.29	0.36	0.36
MgO	12.71	13.94	12.54	12.06	14.10	13.68	14.68	13.49
CaO	11.47	11.35	11.20	11.34	11.96	11.32	11.45	11.40
Na_2O	1.46	1.21	1.61	1.59	1.37	1.54	1.35	1.43
K_2O	0.55	0.39	0.63	0.63	0.57	0.65	0.53	0.68
TOTAL	96.96	96.81	96.78	96.35	96.74	96.67	96.49	96.54
Si	7.1389	7.2905	7.0739	7.1006	7.1791	7.0453	7.2425	7.0616
Ti	0.1120	0.0769	0.0955	0.0806	0.0801	0.1310	0.1130	0.1100
Al	1.0937	0.8668	1.2052	1.1285	1.0274	1.1447	0.9688	1.1556
Fe^{2+}	1.8631	1.8076	1.9112	2.0304	1.6446	1.7673	1.5198	1.7843
Mn	0.0807	0.0640	0.0620	0.0729	0.0401	0.0366	0.0449	0.0455
Mg	2.8207	3.0797	2.7932	2.7136	3.1092	3.0361	3.2219	2.9996
Ca	1.8302	1.8028	1.7936	1.8345	1.8962	1.8063	1.8068	1.8225
Na	0.4216	0.3478	0.4666	0.4655	0.3930	0.4447	0.3855	0.4137
K	0.1045	0.0738	0.1201	0.1214	0.1076	0.1235	0.0996	0.1294
TOTAL	15.4653	15.4100	15.5213	15.5480	15.4774	15.5354	15.4027	15.5222

Amphibole Analyses: Strontian - BPSRT3 and BPSRT4.

	T3/5	T3/6	T3/7	T3/8	T3/9	T3/10	T4/1	T4/2
SiO_2	53.31	47.97	46.68	47.44	48.97	47.88	48.88	48.17
TiO_2	0.06	1.04	1.48	1.07	1.02	1.22	1.04	1.13
Al_2O_3	2.49	5.87	6.85	6.57	5.97	6.39	6.13	6.38
FeO	11.15	13.27	13.81	13.95	13.14	13.37	13.74	13.83
MnO	0.33	0.41	0.32	0.32	0.48	0.29	0.45	0.38
MgO	16.55	14.05	13.60	13.54	14.03	13.68	14.08	13.72
CaO	12.27	11.53	11.37	11.51	11.64	11.43	11.85	11.61
Na_2O	0.50	1.42	1.82	1.58	1.55	1.59	1.17	1.33
K_2O	0.11	0.58	0.68	0.65	0.55	0.58	0.57	0.66
TOTAL	96.77	96.14	96.61	96.63	97.35	96.43	97.97	97.25
Si	7.7074	7.1472	6.9640	7.0621	7.1894	7.1108	7.1509	7.1107
Ti	0.0065	0.1165	0.1661	0.1198	0.1126	0.1363	0.1144	0.1255
Al	0.4244	1.0311	1.2048	1.1530	1.0333	1.1188	1.0573	1.1103
Fe^{2+}	1.3482	1.6535	1.7230	1.7368	1.6134	1.6606	1.6811	1.7074
Mn	0.0404	0.0517	0.0404	0.0404	0.0597	0.0365	0.0558	0.0475
Mg	3.5660	3.1198	3.0238	3.0039	3.0697	3.0278	3.0698	3.0184
Ca	1.9008	1.8407	1.8175	1.8359	1.8311	1.8189	1.8576	1.8364
Na	0.1402	0.4102	0.5265	0.4560	0.4412	0.4579	0.3319	0.3807
K	0.0203	0.1102	0.1294	0.1234	0.1030	0.1099	0.1064	0.1243
TOTAL	15.1541	15.4810	15.5955	15.5314	15.4535	15.4774	15.4252	15.4611

Amphibole Analyses: Strontian - BPSRT4.

	T4/3	T4/4	T4/5	T4/6	T4/7	T4/8	T4/9	T4/10
SiO_2	47.28	48.98	47.89	48.01	49.60	48.08	48.90	48.15
TiO_2	1.02	0.92	0.88	0.91	1.05	1.06	1.25	1.07
Al_2O_3	6.95	5.74	6.50	6.50	5.29	6.59	5.90	6.50
FeO	14.41	13.05	13.79	14.05	12.97	13.94	13.33	13.47
MnO	0.48	0.35	0.43	0.42	0.42	0.41	0.36	0.43
MgO	13.15	14.31	13.44	13.62	14.50	13.57	14.12	13.54
CaO	11.60	11.41	11.49	11.62	11.80	11.64	11.65	11.59
Na_2O	1.54	1.29	1.32	1.40	1.16	1.34	1.40	1.39
K_2O	0.71	0.54	0.68	0.68	0.49	0.66	0.61	0.62
TOTAL	97.18	96.59	96.45	97.21	97.31	97.33	97.55	96.76
Si	7.0241	7.2282	7.1269	7.0998	7.2650	7.0965	7.1710	7.1276
Ti	0.1140	0.1021	0.0985	0.1012	0.1157	0.1177	0.1379	0.1191
Al	1.2173	0.9987	1.1404	1.1332	0.9135	1.1467	1.0200	1.1344
Fe^{2+}	1.7904	1.6106	1.7163	1.7377	1.5888	1.7207	1.6348	1.6676
Mn	0.0604	0.0438	0.0542	0.0526	0.0521	0.0513	0.0447	0.0539
Mg	2.9115	3.1473	2.9808	3.0017	3.1652	2.9850	3.0859	2.9871
Ca	1.8466	1.8042	1.8322	1.8413	1.8519	1.8409	1.8306	1.8383
Na	0.4436	0.3691	0.3809	0.4014	0.3294	0.3835	0.3981	0.3990
K	0.1346	0.1017	0.1291	0.1283	0.0916	0.1243	0.1141	0.1171
TOTAL	15.5424	15.4057	15.4594	15.4972	15.3731	15.4664	15.4372	15.4441

Biotite Analyses: Strontian - BPSRT1.

	T1/1	T1/2	T1/3	T1/4	T1/5	T1/6	T1/7	T1/8
SiO_2	37.99	37.60	37.42	37.31	37.06	37.51	37.20	37.36
TiO_2	3.26	3.34	3.42	3.09	2.53	2.74	3.01	2.78
Al_2O_3	15.03	14.93	14.32	14.78	14.82	14.92	14.67	14.81
FeO	17.49	17.40	17.05	17.50	17.55	17.48	16.70	17.45
MnO	0.26	0.20	0.19	0.24	0.26	0.20	0.30	0.21
MgO	12.55	12.70	12.63	12.87	12.92	12.75	12.68	12.72
CaO	0.03	0.06	n.d.	n.d.	n.d.	n.d.	0.12	n.d.
Na_2O	0.06	0.14	0.10	0.11	0.11	0.10	0.11	0.13
K_2O	9.26	9.39	9.41	9.70	9.26	9.84	9.52	9.51
TOTAL	95.99	95.85	94.59	95.60	94.58	95.61	94.38	95.00
Si	5.6852	5.6478	5.6912	5.6329	5.6502	5.6642	5.6717	5.6679
Ti	0.3669	0.3773	0.3912	0.3509	0.2901	0.3112	0.3451	0.3172
Al	2.6517	2.6439	2.5676	2.6307	2.6638	2.6561	2.6369	2.6489
Fe^{2+}	2.1890	2.1858	2.1687	2.2096	2.2377	2.2076	2.1294	2.2141
Mn	0.0330	0.0254	0.0245	0.0307	0.0336	0.0256	0.0387	0.0270
Mg	2.7990	2.8430	2.8628	2.8958	2.9356	2.8694	2.8812	2.8760
Ca	0.0048	0.0097	-	-	-	-	0.0196	-
Na	0.0174	0.0408	0.0295	0.0322	0.0325	0.0293	0.0325	0.0382
K	1.7679	1.7994	1.8259	1.8684	1.8012	1.8957	1.8518	1.8407
TOTAL	15.5148	15.5731	15.5614	15.6512	15.6447	15.6590	15.6069	15.6299

Biotite Analyses: Strontian - BPSRT1 and BPSRT2.

	T1/9	T1/10	T2/1	T2/2	T2/3	T2/4	T2/5	T2/6
SiO_2	37.47	37.46	36.76	37.32	36.96	37.20	37.34	37.36
TiO_2	3.28	3.10	3.33	3.22	2.63	2.73	2.72	2.48
Al_2O_3	14.65	14.89	14.17	14.41	14.00	14.17	13.95	14.57
FeO	16.73	17.01	19.37	19.12	19.36	18.62	19.94	18.81
MnO	0.21	0.21	0.42	0.31	0.40	0.33	0.42	0.43
MgO	12.43	12.58	11.37	11.43	11.21	11.56	12.04	11.77
CaO	0.05	0.04	n.d.	0.05	n.d.	n.d.	0.06	0.05
Na_2O	0.11	0.09	0.10	0.08	0.08	0.13	0.17	0.11
K_2O	9.58	9.69	9.46	9.45	9.53	9.24	9.35	9.41
TOTAL	94.56	95.13	94.98	95.39	94.17	93.98	95.99	94.99
Si	5.6951	5.6688	5.6467	5.6854	5.7251	5.7365	5.6807	5.7072
Ti	0.3749	0.3528	0.3847	0.3689	0.3064	0.3166	0.3112	0.2849
Al	2.6251	2.6565	2.5661	2.5880	2.5566	2.5761	2.5020	2.6240
Fe^{2+}	2.1266	2.1528	2.4884	2.4360	2.5080	2.4014	2.5370	2.4031
Mn	0.0270	0.0269	0.0546	0.0400	0.0525	0.0431	0.0541	0.0556
Mg	2.8156	2.8372	2.6029	2.5950	2.5879	2.6567	2.7298	2.6796
Ca	0.0081	0.0065	-	0.0082	-	-	0.0098	0.0082
Na	0.0324	0.0264	0.0298	0.0236	0.0240	0.0389	0.0501	0.0326
K	1.8576	1.8708	1.8539	1.8367	1.8833	1.8179	1.8148	1.8339
TOTAL	15.5625	15.5987	15.6273	15.5818	15.6439	15.5872	15.6896	15.6292

Biotite Analyses: Strontian - BPSRT2 and BPSRT3.

	T2/7	T2/8	T2/9	T2/10	T3/1	T3/2	T3/3	T3/4
SiO2	37.71	37.39	37.13	36.87	37.57	37.76	37.58	37.39
TiO2	2.37	1.78	2.52	2.70	3.08	3.17	2.74	2.77
Al2O3	14.51	14.99	14.54	14.37	14.21	14.12	14.25	13.96
FeO	18.82	18.52	18.97	19.17	16.12	16.31	16.05	16.43
MnO	0.41	0.47	0.37	0.41	0.18	0.23	0.27	0.25
MgO	12.14	12.01	11.80	11.45	13.90	13.75	14.15	13.97
CaO	n.d.	n.d.	n.d.	n.d.	n.d.	n.d.	n.d.	n.d.
Na2O	0.07	0.09	0.09	0.08	0.07	0.12	0.09	0.06
K2O	9.65	9.37	9.40	9.52	9.53	9.67	9.29	9.33
TOTAL	95.68	94.62	94.82	94.57	94.66	95.13	94.42	94.16
Si	5.7197	5.7197	5.6880	5.6800	5.6847	5.6949	5.6926	5.6959
Ti	0.2703	0.2048	0.2903	0.3128	0.3505	0.3596	0.3121	0.3174
Al	2.5946	2.7034	2.6260	2.6099	2.5348	2.5106	2.5448	2.5072
Fe2+	2.3873	2.3694	2.4304	2.4698	2.0399	2.0572	2.0333	2.0933
Mn	0.0527	0.0609	0.0480	0.0535	0.0231	0.0294	0.0346	0.0323
Mg	2.7442	2.7380	2.6940	2.6288	3.1344	3.0906	3.1944	3.1717
Ca	-	-	-	-	-	-	-	-
Na	0.0206	0.0267	0.0267	0.0239	0.0205	0.0351	0.0264	0.0177
K	1.8673	1.8287	1.8372	1.8711	1.8397	1.8607	1.7954	1.8133
TOTAL	15.6567	15.6515	15.6406	15.6498	15.6275	15.6381	15.6337	15.6487

Biotite Analyses: Strontian - BPSRT3 and BPSRT4.

	T3/5	T3/6	T3/7	T3/8	T3/9	T3/10	T4/1	T4/2
SiO2	37.43	37.72	37.76	37.92	37.83	37.96	37.51	38.35
TiO2	3.19	2.86	2.99	2.60	2.93	2.93	2.44	2.65
Al2O3	14.03	14.42	14.25	14.25	14.21	14.35	13.87	14.17
FeO	16.70	16.18	16.90	16.71	16.55	16.50	16.22	16.24
MnO	0.22	0.23	0.19	0.22	0.30	0.16	0.28	0.22
MgO	13.51	13.81	13.74	13.82	13.95	13.88	14.49	14.07
CaO	0.07	n.d.	n.d.	n.d.	n.d.	n.d.	n.d.	0.04
Na2O	0.12	0.06	0.09	0.05	n.d.	0.13	n.d.	0.11
K2O	9.69	9.56	9.63	9.59	9.37	9.45	9.15	9.23
TOTAL	94.96	94.84	95.55	95.16	95.14	95.36	93.96	95.14
Si	5.6740	5.6953	5.6813	5.7189	5.6981	5.7013	5.7128	5.7583
Ti	0.3637	0.3248	0.3383	0.2949	0.3319	0.3310	0.2795	0.2992
Al	2.5073	2.5668	2.5277	2.5337	2.5234	2.5409	2.4904	2.5083
Fe2+	2.1172	2.0431	2.1266	2.1076	2.0848	2.0726	2.0660	2.0393
Mn	0.0282	0.0294	0.0242	0.0281	0.0383	0.0204	0.0361	0.0280
Mg	3.0522	3.1076	3.0810	3.1062	3.1315	3.1069	3.2889	3.1485
Ca	0.0114	-	-	-	-	-	-	0.0064
Na	0.0353	0.0176	0.0263	0.0146	-	0.0379	-	0.0320
K	1.8740	1.8415	1.8485	1.8452	1.8006	1.8108	1.7779	1.7681
TOTAL	15.6633	15.6261	15.6539	15.6493	15.6086	15.6216	15.6515	15.5883

Biotite Analyses: Strontian - BPSRT4.

	T4/3	T4/4	T4/5	T4/6	T4/7	T4/8	T4/9	T4/10
SiO2	38.08	37.83	38.11	38.12	38.30	37.56	37.72	38.36
TiO2	2.81	2.70	2.86	2.47	2.77	3.02	2.91	3.02
Al2O3	14.15	14.16	14.19	14.47	14.11	14.21	14.19	14.48
FeO	15.97	16.77	16.58	16.38	16.41	16.79	16.77	16.58
MnO	0.25	0.23	0.25	0.25	0.30	0.26	0.25	0.30
MgO	13.76	14.33	13.97	14.32	14.10	13.85	13.87	13.76
CaO	0.04	n.d.	n.d.	n.d.	0.01	n.d.	0.05	n.d.
Na2O	0.06	0.07	0.05	0.07	0.05	0.08	0.05	0.06
K2O	9.76	9.20	9.62	9.74	9.69	9.57	9.47	9.68
TOTAL	94.93	95.35	95.69	95.86	95.78	95.41	95.34	96.29
Si	5.7455	5.6897	5.7153	5.7020	5.7339	5.6645	5.6853	5.7126
Ti	0.3189	0.3054	0.3226	0.2779	0.3119	0.3425	0.3299	0.3382
Al	2.5170	2.5108	2.5088	2.5517	2.4904	2.5265	2.5215	2.5422
Fe2+	2.0152	22.1094	2.0795	2.0491	2.0546	2.1177	2.1139	2.0650
Mn	0.0320	0.0293	0.0318	0.0317	0.0380	0.0332	0.0319	0.0378
Mg	3.0941	3.2120	3.1223	3.1923	3.1459	3.1129	3.1156	3.0539
Ca	0.0065	-	-	-	0.0016	-	0.0081	-
Na	0.0176	0.0204	0.0145	0.0203	0.0145	0.0234	0.0146	0.0173
K	1.8787	1.7653	1.8406	1.8587	1.8508	1.8413	1.8210	1.8391
TOTAL	15.6253	15.6424	15.6353	15.6838	15.6417	15.6621	15.6419	15.6063

Biotite Analyses: Strontian - BPSRG1.

	G1/1	G1/2	G1/3	G1/4	G1/5	G1/6	G1/7	G1/8
SiO2	37.15	37.19	37.13	36.72	37.47	36.94	37.07	37.15
TiO2	3.36	3.06	3.20	3.25	3.30	2.93	2.99	3.03
Al2O3	17.03	16.81	16.38	16.44	16.43	16.42	16.58	16.74
FeO	17.21	17.82	18.19	17.80	17.55	17.52	17.83	17.91
MnO	0.32	0.46	0.52	0.46	0.45	0.26	0.39	0.49
MgO	10.19	10.15	10.44	10.33	10.32	10.28	10.42	10.51
CaO	n.d.	n.d.	n.d.	0.03	n.d.	n.d.	n.d.	0.04
Na2O	0.09	0.08	0.09	0.08	0.09	0.08	0.07	0.07
K2O	10.07	10.09	10.09	9.99	9.87	9.84	10.03	10.17
TOTAL	95.42	95.66	96.10	95.10	95.48	94.27	95.43	96.18
Si	5.6044	5.6177	5.6036	5.5885	5.6547	5.6486	5.6169	5.5935
Ti	0.3812	0.3476	0.3632	0.3720	0.3745	0.3370	0.3407	0.3431
Al	3.0288	2.9936	2.9143	2.9497	2.9231	2.9601	2.9617	2.9715
Fe2+	2.1713	2.2512	2.2959	2.2656	2.2150	2.2406	2.2594	2.2553
Mn	0.0409	0.0589	0.0665	0.0593	0.0575	0.0337	0.0501	0.0625
Mg	2.2910	2.2850	2.3481	2.3430	2.3211	2.3427	2.3530	2.3584
Ca	-	-	-	0.0049	-	-	-	0.0065
Na	0.0263	0.0234	0.0263	0.0236	0.0263	0.0237	0.0206	0.0204
K	1.9381	1.9445	1.9427	1.9397	1.9003	1.9197	1.9389	1.9536
TOTAL	15.4822	15.5218	15.5606	15.5463	15.4726	15.5060	15.5413	15.5647

Biotite Analyses: Strontian - BPSRG1 and BPSRG4.

	G1/9	G1/10	G4/1	G4/2	G4/3	G4/4	G4/5	G4/6
SiO_2	37.31	37.28	37.96	38.24	37.48	37.91	37.90	37.20
TiO_2	3.02	3.16	3.48	3.37	3.83	3.59	3.60	3.38
Al_2O_3	16.51	16.32	15.15	15.68	15.27	14.97	15.49	15.11
FeO	18.33	18.44	17.07	16.64	17.61	17.21	17.08	16.65
MnO	0.30	0.46	0.50	0.48	0.38	0.57	0.43	0.43
MgO	10.64	10.73	11.92	11.58	11.45	11.84	11.47	11.56
CaO	n.d.	n.d.	0.04	n.d.	n.d.	n.d.	n.d.	n.d.
Na_2O	0.14	0.06	0.06	0.07	0.07	0.09	n.d.	0.06
K_2O	10.04	10.12	9.75	9.82	10.05	9.80	9.75	9.84
TOTAL	96.33	96.57	95.93	95.88	96.14	95.98	95.72	94.23
Si	5.6090	5.5988	5.6915	5.7156	5.6354	5.6909	5.6888	5.6811
Ti	0.3414	0.3569	0.3924	0.3788	0.4331	0.4053	0.4064	0.3882
Al	2.9261	2.8895	2.6780	2.7630	2.7068	2.6493	2.7411	2.7205
Fe^{2+}	2.3046	2.3161	2.1405	2.0800	2.2144	2.1607	2.1441	2.1266
Mn	0.0382	0.0585	0.0635	0.0608	0.0484	0.0725	0.0547	0.0556
Mg	2.3839	2.4016	2.6635	2.5795	2.5658	2.6489	2.5658	2.6310
Ca	-	-	0.0064	-	-	-	-	-
Na	0.0408	0.0175	0.0174	0.0203	0.0204	0.0262	-	0.0178
K	1.9256	1.9390	1.8650	1.8726	1.9279	1.8769	1.8671	1.9172
TOTAL	15.5697	15.5778	15.5183	15.4705	15.5522	15.5306	15.4679	15.5380

Biotite Analyses: Strontian - BPSRG4.

	G4/7	G4/8	G4/9	G4/10
SiO_2	38.83	37.34	37.38	37.13
TiO_2	3.70	4.12	3.33	3.85
Al_2O_3	15.57	15.59	15.04	15.37
FeO	16.76	16.58	17.30	17.50
MnO	0.56	0.43	0.42	0.38
MgO	11.39	11.31	11.07	11.20
CaO	0.05	0.04	n.d.	0.04
Na_2O	0.10	0.04	n.d.	0.09
K_2O	9.17	9.93	9.60	9.65
TOTAL	96.13	95.38	94.14	95.21
Si	5.7633	5.6286	5.7183	5.6271
Ti	0.4130	0.4671	0.3831	0.4388
Al	2.7244	2.7705	2.7125	2.7461
Fe^{2+}	2.0804	2.0902	2.2134	2.2180
Mn	0.0704	0.0549	0.0544	0.0488
Mg	2.5195	2.5408	2.5238	2.5296
Ca	0.0080	0.0065	-	0.0065
Na	0.0288	0.0117	-	0.0264
K	1.7364	1.9097	1.8736	1.8658
TOTAL	15.3441	15.4798	15.4791	15.5072

Plagioclase Analyses: Strontian - BPSRT1.

	T1/A1	T1/A2	T1/A3	T1/A4	T1/A5	T1/A6	T1/A7	T1/A8
SiO_2	62.59	62.38	61.64	62.33	61.92	62.07	61.66	62.22
TiO_2	n.d.	n.d.	n.d.	n.d.	n.d.	n.d.	n.d.	n.d.
Al_2O_3	23.05	23.03	23.79	23.22	23.39	23.38	23.24	22.54
FeO	0.08	0.11	0.15	0.15	0.15	0.16	0.11	0.17
MnO	n.d.	n.d.	n.d.	n.d.	n.d.	n.d.	n.d.	n.d.
MgO	n.d.	n.d.	n.d.	n.d.	n.d.	n.d.	n.d.	n.d.
CaO	4.29	4.07	5.19	4.50	4.62	4.36	4.33	4.04
Na_2O	9.27	9.43	8.82	8.88	8.68	8.94	8.75	8.86
K_2O	0.29	0.25	0.40	0.50	0.50	0.56	0.60	0.64
TOTAL	99.57	99.27	99.99	99.58	99.26	99.47	98.69	98.47
Si	11.1409	11.1368	10.9678	11.1057	11.0687	11.0768	11.0840	11.2002
Ti	-	-	-	-	-	-	-	-
Al	4.8370	4.8472	4.9904	4.8775	4.9293	4.9189	4.9251	4.7834
Fe^{2+}	0.0119	0.0164	0.0223	0.0224	0.0224	0.0239	0.0165	0.0256
Mn	-	-	-	-	-	-	-	-
Mg	-	-	-	-	-	-	-	-
Ca	0.8182	0.7786	0.9895	0.8591	0.8849	0.8337	0.8340	0.7792
Na	3.1994	3.2643	3.0429	3.0678	3.0085	3.0934	3.0498	3.0924
K	0.0659	0.0569	0.0908	0.1137	0.1140	0.1275	0.1376	0.1470
TOTAL	20.0732	20.1003	20.1038	20.0462	20.0279	20.0742	20.0471	20.0278

Plagioclase Analyses: Strontian - BPSRT1.

	T1/A9	T1/A10	T1/B1	T1/B2	T1/B3	T1/B4	T1/B5	T1/B6
SiO_2	61.68	62.34	63.03	63.01	63.03	61.97	62.04	62.53
TiO_2	n.d.	n.d.	n.d.	n.d.	n.d.	n.d.	n.d.	n.d.
Al_2O_3	23.20	23.10	23.05	23.23	23.12	23.16	23.61	22.62
FeO	0.18	0.07	n.d.	0.14	0.13	0.15	n.d.	0.12
MnO	n.d.	n.d.	n.d.	n.d.	n.d.	n.d.	n.d.	n.d.
MgO	n.d.	n.d.	n.d.	n.d.	n.d.	n.d.	n.d.	n.d.
CaO	4.54	4.34	4.02	4.25	4.19	4.63	4.89	4.14
Na_2O	8.91	9.21	9.49	9.30	9.24	8.12	8.90	8.86
K_2O	0.50	0.25	0.23	0.40	0.43	0.48	0.37	0.60
TOTAL	99.01	99.31	99.82	100.33	100.14	98.51	99.81	98.87
Si	11.0662	11.1243	11.1758	11.1373	11.1572	11.1306	11.0333	11.2055
Ti	-	-	-	-	-	-	-	-
Al	4.9072	4.8596	4.8182	4.8407	4.8249	4.9042	4.9501	4.7788
Fe^{2+}	0.0270	0.0104	-	0.0207	0.0192	0.0225	-	0.0180
Mn	-	-	-	-	-	-	-	-
Mg	-	-	-	-	-	-	-	-
Ca	0.8728	0.8298	0.7637	0.8049	0.7947	0.8911	0.9318	0.7949
Na	3.0996	3.1866	3.2626	3.1873	3.1714	2.8279	3.0689	3.0785
K	0.1144	0.0569	0.0520	0.0902	0.0971	0.1100	0.0839	0.1372
TOTAL	20.0872	20.0677	20.0724	20.0811	20.0646	19.8862	20.0681	20.0129

Plagioclase Analyses: Strontian - BPSRT1.

	T1/B7	T1/B8	T1/B9	T1/B10	T1/B11	T1/B12	T1/C1	T1/C2
SiO_2	62.50	62.29	62.02	62.00	61.72	63.01	62.91	63.08
TiO_2	n.d.	n.d.	n.d.	n.d.	n.d.	n.d.	n.d.	n.d.
Al_2O_3	23.45	23.94	23.88	23.31	23.40	22.90	23.07	23.08
FeO	0.16	0.15	0.12	0.13	n.d.	0.22	0.09	n.d.
MnO	n.d.	n.d.	n.d.	n.d.	n.d.	n.d.	n.d.	n.d.
MgO	n.d.	n.d.	n.d.	n.d.	n.d.	n.d.	n.d.	n.d.
CaO	4.55	5.21	4.90	4.79	4.62	3.85	4.20	4.21
Na_2O	8.81	8.88	8.92	8.45	8.89	9.50	9.08	9.31
K_2O	0.60	0.32	0.48	0.45	0.37	0.20	0.18	0.14
TOTAL	100.07	100.79	100.32	99.13	99.00	99.68	99.53	99.82
Si	11.0864	10.9861	10.9907	11.0874	11.0569	11.1916	11.1772	11.1769
Ti	-	-	-	-	-	-	-	-
Al	4.9039	4.9778	4.9890	4.9144	4.9421	4.7952	4.8322	4.8212
Fe^{2+}	0.0237	0.0221	0.0178	0.0194	-	0.0327	0.0134	-
Mn	-	-	-	-	-	-	-	-
Mg	-	-	-	-	-	-	-	-
Ca	0.8648	0.9846	0.9304	0.9178	0.8868	0.7327	0.7996	0.7993
Na	3.0301	3.0367	3.0650	2.9300	3.0880	3.2717	3.1280	3.1985
K	0.1358	0.0720	0.1085	0.1027	0.0846	0.0453	0.0408	0.0316
TOTAL	20.0446	20.0794	20.1015	19.9717	20.0583	20.0693	19.9911	20.0276

Plagioclase Analyses: Strontian - BPSRT1.

	T1/C3	T1/C4	T1/C5	T1/C6	T1/C7	T1/C8	T1/C9	T1/C10
SiO_2	62.08	62.80	61.92	61.46	62.46	62.69	62.32	62.90
TiO_2	n.d.	n.d.	n.d.	n.d.	n.d.	n.d.	n.d.	n.d.
Al_2O_3	23.81	22.96	23.60	23.93	23.45	23.49	23.44	23.47
FeO	0.10	0.08	n.d.	0.12	0.18	0.12	0.11	n.d.
MnO	n.d.	n.d.	n.d.	n.d.	n.d.	n.d.	n.d.	n.d.
MgO	n.d.	n.d.	n.d.	n.d.	n.d.	n.d.	n.d.	n.d.
CaO	5.05	4.10	4.82	5.03	4.60	4.37	4.84	4.29
Na_2O	8.98	8.93	8.72	9.00	9.07	9.37	9.03	9.25
K_2O	0.36	0.49	0.49	0.39	0.50	0.32	0.29	0.17
TOTAL	100.38	99.36	99.55	99.93	100.26	100.36	100.03	100.08
Si	10.9940	11.1873	11.0383	10.9444	11.0683	11.0839	11.0602	11.1219
Ti	-	-	-	-	-	-	-	-
Al	4.9711	4.8220	4.9599	5.0237	4.8990	4.8963	4.9043	4.8925
Fe^{2+}	0.0148	0.0119	-	0.0179	0.0267	0.0177	0.0163	-
Mn	-	-	-	-	-	-	-	-
Mg	-	-	-	-	-	-	-	-
Ca	0.9583	0.7826	0.9207	0.9598	0.8734	0.8279	0.9204	0.8128
Na	3.0835	3.0845	3.0141	3.1075	3.1164	3.2122	3.1073	3.1713
K	0.0813	0.1114	0.1114	0.0886	0.1130	0.0722	0.0657	0.0383
TOTAL	20.1029	19.9996	20.0445	20.1418	20.0969	20.1102	20.0742	20.0367

Plagioclase Analyses: Strontian - BPSRT1 and BPSRT2.

	T1/C11	T1/C12	T2/A1	T2/A2	T2/A3	T2/B1	T2/B2	T2/B3
SiO_2	62.76	62.68	63.93	62.73	63.49	64.15	62.86	63.91
TiO_2	n.d.	n.d.	n.d.	n.d.	n.d.	n.d.	n.d.	n.d.
Al_2O_3	23.26	23.16	22.31	22.52	21.85	21.72	22.80	21.83
FeO	0.16	0.13	0.06	0.12	0.06	0.11	0.09	0.06
MnO	n.d.	n.d.	n.d.	n.d.	n.d.	n.d.	n.d.	n.d.
MgO	n.d.	n.d.	n.d.	n.d.	n.d.	n.d.	n.d.	n.d.
CaO	4.35	4.19	3.25	3.56	3.03	2.62	4.00	3.07
Na_2O	9.20	9.33	10.56	1n.d.	10.12	10.47	9.61	9.20
K_2O	0.40	0.40	0.20	0.27	0.20	0.18	0.14	0.26
TOTAL	100.13	99.89	100.31	99.20	98.75	99.25	99.50	98.33
Si	11.1189	11.1298	11.2894	11.2102	11.3594	11.4124	11.1871	11.4349
Ti	-	-	-	-	-	-	-	-
Al	4.8582	4.8483	4.6447	4.7445	4.6088	4.5554	4.7837	4.6047
Fe^{2+}	0.0237	0.0193	0.0089	0.0179	0.0090	0.0164	0.0134	0.0090
Mn	-	-	-	-	-	-	-	-
Mg	-	-	-	-	-	-	-	-
Ca	0.8258	0.7972	0.6150	0.6817	0.5809	0.4994	0.7628	0.5886
Na	3.1603	3.2122	3.6157	3.4650	3.5107	3.6116	3.3162	3.1917
K	0.0904	0.0906	0.0451	0.0616	0.0457	0.0409	0.0318	0.0593
TOTAL	20.0774	20.0975	20.2187	20.1809	20.1144	20.1361	20.0950	19.8882

Plagioclase Analyses: Strontian - BPSRT2.

	T2/B4	T2/C1	T2/C2	T2/C3	T2/C4	T2/D1	T2/D2	T2/E1
SiO_2	67.78	63.66	63.03	62.60	64.55	62.99	62.74	64.40
TiO_2	n.d.	n.d.	n.d.	n.d.	n.d.	n.d.	n.d.	n.d.
Al_2O_3	19.33	22.06	22.46	22.69	22.13	22.94	23.07	22.23
FeO	0.07	0.13	0.10	0.15	0.17	0.07	0.11	n.d.
MnO	n.d.	n.d.	n.d.	n.d.	n.d.	n.d.	n.d.	n.d.
MgO	n.d.	n.d.	n.d.	n.d.	n.d.	n.d.	n.d.	n.d.
CaO	0.20	3.27	3.60	3.98	3.18	4.13	4.50	3.26
Na_2O	12.19	10.14	9.93	9.59	10.61	9.75	9.65	10.20
K_2O	0.09	0.17	0.14	0.25	0.15	0.20	0.19	0.17
TOTAL	99.66	99.43	99.26	99.26	100.79	100.08	100.26	100.26
Si	11.9245	11.3247	11.2406	11.1803	11.3391	11.1604	11.1126	11.3479
Ti	-	-	-	-	-	-	-	-
Al	4.0092	4.6265	4.7221	4.7775	4.5830	4.7917	4.8173	4.6180
Fe^{2+}	0.0103	0.0193	0.0149	0.0224	0.0250	0.0104	0.0163	-
Mn	-	-	-	-	-	-	-	-
Mg	-	-	-	-	-	-	-	-
Ca	0.0377	0.6233	0.6879	0.7617	0.5986	0.7841	0.8540	0.6155
Na	4.1582	3.4976	3.4337	3.3210	3.6138	3.3495	3.3141	3.4850
K	0.0202	0.0386	0.0319	0.0570	0.0336	0.0452	0.0429	0.0382
TOTAL	20.1601	20.1301	20.1311	20.1199	20.1931	20.1412	20.1573	20.1047

Plagioclase Analyses: Strontian - BPSRT2.

	T2/E2	T2/E3	T2/E4	T2/E5	T2/E6	T2/E7	T2/E8	T2/F1
SiO_2	63.52	63.95	62.10	62.47	63.47	62.20	63.34	65.46
TiO_2	n.d.	n.d.	n.d.	n.d.	n.d.	n.d.	n.d.	n.d.
Al_2O_3	22.82	22.57	23.52	23.05	22.46	23.10	22.12	21.35
FeO	0.05	0.07	0.11	0.11	0.09	0.07	0.13	n.d.
MnO	n.d.	n.d.	n.d.	n.d.	n.d.	n.d.	n.d.	n.d.
MgO	n.d.	n.d.	n.d.	n.d.	n.d.	n.d.	n.d.	n.d.
CaO	4.03	3.67	4.54	4.41	3.87	4.73	3.42	2.05
Na_2O	9.86	9.88	9.41	9.42	9.97	9.60	10.09	11.03
K_2O	0.22	0.31	0.35	0.37	0.22	0.30	0.29	0.12
TOTAL	100.50	100.45	100.03	99.83	100.08	100.00	99.39	100.01
Si	11.2020	11.2700	11.0342	11.1127	11.2407	11.0655	11.2895	11.5322
Ti	-	-	-	-	-	-	-	-
Al	4.7445	4.6892	4.9269	4.8340	4.6895	4.8448	4.6480	4.4342
Fe^{2+}	0.0074	0.0103	0.0163	0.0164	0.0133	0.0104	0.0194	-
Mn	-	-	-	-	-	-	-	-
Mg	-	-	-	-	-	-	-	-
Ca	0.7615	0.6930	0.8644	0.8406	0.7344	0.9016	0.6532	0.3870
Na	3.3715	3.3760	3.2419	3.2491	3.4236	3.3114	3.4870	3.7677
K	0.0495	0.0697	0.0793	0.0840	0.0497	0.0681	0.0659	0.0270
TOTAL	20.1363	20.1083	20.1630	20.1368	20.1512	20.2019	20.1630	20.1481

Plagioclase Analyses: Strontian - BPSRT2.

	T2/F2	T2/G1	T2/G2	T2/G3	T2/G4	T2/G5	T2/G6	T2/H1
SiO_2	64.00	64.35	67.00	63.57	63.84	64.25	63.45	63.95
TiO_2	n.d.	n.d.	n.d.	n.d.	n.d.	n.d.	n.d.	n.d.
Al_2O_3	22.00	22.22	19.78	22.08	22.13	21.62	22.07	22.11
FeO	0.06	0.06	n.d.	n.d.	0.06	0.03	0.08	0.10
MnO	n.d.	n.d.	n.d.	n.d.	n.d.	n.d.	n.d.	n.d.
MgO	n.d.	n.d.	n.d.	n.d.	n.d.	n.d.	n.d.	n.d.
CaO	3.29	3.06	0.45	3.23	3.20	2.95	3.07	3.00
Na_2O	10.26	10.58	12.07	10.31	10.20	10.71	10.46	10.13
K_2O	0.28	0.15	0.05	0.19	0.21	0.13	0.24	0.15
TOTAL	99.89	100.42	99.35	99.38	99.64	99.69	99.37	99.44
Si	11.3396	11.3345	11.8326	11.3162	11.3294	11.3979	11.3065	11.3554
Ti	-	-	-	-	-	-	-	-
Al	4.5955	4.6141	4.1183	4.6338	4.6300	4.5216	4.6364	4.6285
Fe^{2+}	0.0089	0.0088	-	-	0.0089	0.0045	0.0119	0.0149
Mn	-	-	-	-	-	-	-	-
Mg	-	-	-	-	-	-	-	-
Ca	0.6246	0.5775	0.0852	0.6161	0.6085	0.5607	0.5862	0.5708
Na	3.5248	3.6133	4.1331	3.5586	3.5098	3.6839	3.6140	3.4877
K	0.0633	0.0337	0.0113	0.0432	0.0475	0.0294	0.0546	0.0340
TOTAL	20.1567	20.1820	20.1805	20.1678	20.1342	20.1980	20.2096	20.0912

Plagioclase Analyses: Strontian - BPSRT2 and BPSRT3.

	T2/H2	T2/H3	T2/H4	T3/A1	T3/A2	T3/B1	T3/B2	T3/B3
SiO_2	63.16	62.98	65.13	63.96	62.84	64.83	62.41	63.08
TiO_2	n.d.	n.d.	n.d.	n.d.	n.d.	n.d.	n.d.	n.d.
Al_2O_3	22.66	23.11	21.27	22.19	22.56	21.91	22.90	22.95
FeO	0.17	0.10	0.14	0.17	0.13	n.d.	0.11	n.d.
MnO	n.d.	n.d.	n.d.	n.d.	n.d.	n.d.	n.d.	n.d.
MgO	n.d.	n.d.	n.d.	n.d.	n.d.	n.d.	n.d.	n.d.
CaO	4.01	4.15	2.28	3.19	3.98	2.58	4.21	4.25
Na_2O	9.84	9.75	10.56	10.06	9.43	10.41	9.23	9.38
K_2O	0.34	0.39	0.19	0.18	0.30	0.14	0.22	0.32
TOTAL	100.18	100.48	99.57	99.75	99.24	99.87	99.08	99.98
Si	11.1919	11.1310	11.5279	11.3336	11.2163	11.4394	11.1566	11.1772
Ti	-	-	-	-	-	-	-	-
Al	4.7338	4.8152	4.4384	4.6356	4.7472	4.5578	4.8262	4.7941
Fe^{2+}	0.0252	0.0148	0.0207	0.0252	0.0194	-	0.0164	-
Mn	-	-	-	-	-	-	-	-
Mg	-	-	-	-	-	-	-	-
Ca	0.7614	0.7859	0.4324	0.6057	0.7612	0.4878	0.8064	0.8069
Na	3.3808	3.3412	3.6241	3.4564	3.2636	3.5616	3.1992	3.2226
K	0.0769	0.0879	0.0429	0.0407	0.0683	0.0315	0.0502	0.0723
TOTAL	20.1700	20.1760	20.0864	20.0972	20.0760	20.0782	20.0550	20.0732

Plagioclase Analyses: Strontian - BPSRT3.

	T3/C1	T3/C2	T3/C3	T3/C4	T3/C5	T3/C6	T3/C7	T3/C8
SiO_2	63.46	62.79	62.35	62.71	62.00	62.83	62.48	61.77
TiO_2	n.d.	n.d.	n.d.	n.d.	n.d.	n.d.	n.d.	n.d.
Al_2O_3	22.70	22.96	23.34	23.08	23.43	23.11	23.08	23.13
FeO	n.d.	0.18	0.15	0.25	0.21	0.17	0.16	0.10
MnO	n.d.	n.d.	n.d.	n.d.	n.d.	n.d.	n.d.	n.d.
MgO	n.d.	n.d.	n.d.	n.d.	n.d.	n.d.	n.d.	n.d.
CaO	3.91	4.18	4.50	3.95	4.94	4.55	4.62	4.82
Na_2O	9.58	9.29	9.27	8.69	8.93	9.24	9.03	9.01
K_2O	0.28	0.43	0.55	0.58	0.49	0.46	0.49	0.49
TOTAL	99.93	99.83	100.16	99.26	100.00	100.36	99.86	99.32
Si	11.2369	11.1569	11.0685	11.1813	11.0300	11.1206	11.1121	11.0588
Ti	-	-	-	-	-	-	-	-
Al	4.7387	4.8097	4.8847	4.8515	4.9141	4.8222	4.8393	4.8820
Fe^{2+}	-	0.0267	0.0223	0.0373	0.0312	0.0252	0.0238	0.0150
Mn	-	-	-	-	-	-	-	-
Mg	-	-	-	-	-	-	-	-
Ca	0.7419	0.7958	0.8560	0.7547	0.9417	0.8629	0.8804	0.9246
Na	3.2891	3.2006	3.1908	3.0043	3.0804	3.1710	3.1139	3.1277
K	0.0633	0.0975	0.1246	0.1319	0.1112	0.1039	0.1112	0.1119
TOTAL	20.0699	20.0873	20.1468	19.9610	20.1087	20.1058	20.0808	20.1200

Plagioclase Analyses: Strontian - BPSRT3.

	T3/C9	T3/C10	T3/D1	T3/D2	T3/D3	T3/D4	T3/D5	T3/D6
SiO_2	62.20	62.44	63.01	62.54	62.22	61.88	62.45	63.02
TiO_2	n.d.	n.d.	n.d.	n.d.	n.d.	n.d.	n.d.	n.d.
Al_2O_3	23.19	23.15	22.34	22.84	23.05	23.17	23.04	22.50
FeO	0.19	0.15	0.18	0.14	0.11	0.16	0.14	0.22
MnO	n.d.	n.d.	n.d.	n.d.	n.d.	n.d.	n.d.	n.d.
MgO	n.d.	n.d.	n.d.	n.d.	n.d.	n.d.	n.d.	n.d.
CaO	4.36	4.33	3.66	4.36	4.55	4.61	4.17	3.73
Na_2O	9.21	9.09	9.75	9.25	9.06	8.84	9.12	9.50
K_2O	0.46	0.55	0.30	0.27	0.35	0.32	0.29	0.41
TOTAL	99.61	99.71	99.24	99.40	99.34	98.98	99.21	99.38
Si	11.0909	11.1161	11.2492	11.1555	11.1122	11.0883	11.1483	11.2359
Ti	-	-	-	-	-	-	-	-
Al	4.8749	4.8588	4.7020	4.8030	4.8532	4.8947	4.8489	4.7293
Fe^{2+}	0.0283	0.0223	0.0269	0.0209	0.0164	0.0240	0.0209	0.0328
Mn	-	-	-	-	-	-	-	-
Mg	-	-	-	-	-	-	-	-
Ca	0.8330	0.8260	0.7001	0.8333	0.8707	0.8851	0.7976	0.7126
Na	3.1842	3.1378	3.3751	3.1992	3.1374	3.0714	3.1567	3.2841
K	0.1046	0.1249	0.0683	0.0614	0.0797	0.0732	0.0666	0.0933
TOTAL	20.1161	20.0859	20.1215	20.0733	20.0697	20.0366	20.0386	20.0881

Plagioclase Analyses: Strontian - BPSRT3.

	T3/E1	T3/E2	T3/E3	T3/E4	T3/E5	T3/E6	T3/E7	T3/E8
SiO_2	63.44	63.73	62.27	62.35	62.27	62.54	61.84	62.12
TiO_2	n.d.	n.d.	n.d.	n.d.	n.d.	n.d.	n.d.	n.d.
Al_2O_3	22.33	22.38	22.92	22.83	22.12	22.72	22.95	22.87
FeO	0.21	0.18	0.12	0.15	0.23	0.25	0.16	n.d.
MnO	n.d.	n.d.	n.d.	n.d.	n.d.	n.d.	n.d.	n.d.
MgO	n.d.	n.d.	n.d.	n.d.	n.d.	n.d.	n.d.	n.d.
CaO	3.41	3.57	4.10	4.16	4.18	4.08	4.46	4.29
Na_2O	9.72	9.71	9.23	9.14	9.34	9.24	8.99	9.34
K_2O	0.29	0.19	0.47	0.44	0.47	0.41	0.38	0.37
TOTAL	99.40	99.76	99.11	99.07	98.61	99.24	98.78	98.99
Si	11.2904	11.2954	11.1437	11.1590	11.2146	11.1767	11.1089	11.1319
Ti	-	-	-	-	-	-	-	-
Al	4.6851	4.6763	4.8356	4.8171	4.6965	4.7869	4.8604	4.8316
Fe^{2+}	0.0313	0.0267	0.0180	0.0225	0.0346	0.0374	0.0240	-
Mn	-	-	-	-	-	-	-	-
Mg	-	-	-	-	-	-	-	-
Ca	0.6503	0.6780	0.7862	0.7978	0.8066	0.7813	0.8585	0.8237
Na	3.3541	3.3369	3.2027	3.1718	3.2615	3.2018	3.1313	3.2453
K	0.0658	0.0430	0.1073	0.1005	0.1080	0.0935	0.0871	0.0846
TOTAL	20.0770	20.0563	20.0935	20.0686	20.1219	20.0775	20.0702	20.1172

Plagioclase Analyses: Strontian - BPSRT3 and BPSRT4.

	T3/E9	T3/E10	T3/E11	T4/A1	T4/A2	T4/B1	T4/B2	T4/B3
SiO_2	63.24	62.73	63.32	62.18	62.35	63.71	63.14	62.00
TiO_2	n.d.	n.d.	n.d.	n.d.	n.d.	n.d.	n.d.	n.d.
Al_2O_3	22.89	22.51	22.39	22.76	22.76	22.48	21.98	22.96
FeO	0.18	0.10	n.d.	0.17	0.17	0.13	0.17	0.15
MnO	n.d.	n.d.	n.d.	n.d.	n.d.	n.d.	n.d.	n.d.
MgO	n.d.	n.d.	n.d.	n.d.	n.d.	n.d.	n.d.	n.d.
CaO	3.98	3.72	3.46	4.31	4.12	3.44	3.44	4.39
Na_2O	9.35	9.45	9.88	9.25	9.28	9.73	9.62	8.83
K_2O	0.42	0.28	0.20	0.33	0.48	0.29	0.32	0.47
TOTAL	100.06	98.79	99.25	99.00	99.16	99.78	98.67	98.80
Si	11.1987	11.2346	11.2790	11.1442	11.1583	11.2895	11.3187	11.1278
Ti	-	-	-	-	-	-	-	-
Al	4.7787	4.7528	4.7019	4.8090	4.8020	4.6962	4.6452	4.8582
Fe^{2+}	0.0267	0.0150	-	0.0255	0.0254	0.0193	0.0255	0.0225
Mn	-	-	-	-	-	-	-	-
Mg	-	-	-	-	-	-	-	-
Ca	0.7552	0.7139	0.6604	0.8277	0.7900	0.6532	0.6608	0.8443
Na	3.2104	3.2816	3.4123	3.2144	3.2202	3.3431	3.3438	3.0729
K	0.0949	0.0640	0.0455	0.0755	0.1096	0.0656	0.0732	0.1076
TOTAL	20.0645	20.0618	20.0990	20.0963	20.1056	20.0667	20.0671	20.0333

Plagioclase Analyses: Strontian - BPSRT4.

	T4/B4	T4/B5	T4/C1	T4/C2	T4/C3	T4/C4	T4/C5	T4/C6
SiO_2	62.95	61.78	64.38	63.35	62.41	62.72	63.25	62.75
TiO_2	n.d.	n.d.	n.d.	n.d.	n.d.	n.d.	n.d.	n.d.
Al_2O_3	22.51	22.75	22.06	22.68	22.74	22.60	22.39	22.83
FeO	0.14	0.17	0.16	0.14	0.26	0.18	0.20	0.13
MnO	n.d.	n.d.	n.d.	n.d.	n.d.	n.d.	n.d.	n.d.
MgO	n.d.	n.d.	n.d.	n.d.	n.d.	n.d.	n.d.	n.d.
CaO	3.93	4.40	3.41	4.07	4.30	4.12	3.71	4.08
Na_2O	9.23	8.82	10.09	9.64	9.05	9.59	9.63	9.08
K_2O	0.57	0.49	0.17	0.36	0.50	0.28	0.57	0.57
TOTAL	99.33	98.41	100.27	100.24	99.26	99.49	99.75	99.44
Si	11.2319	11.1371	11.3539	11.2086	11.1602	11.1846	11.2484	11.1854
Ti	-	-	-	-	-	-	-	-
Al	4.7350	4.8350	4.5866	4.7308	4.7940	4.7513	4.6943	4.7977
Fe^{2+}	0.0209	0.0256	0.0236	0.0207	0.0389	0.0268	0.0297	0.0194
Mn	-	-	-	-	-	-	-	-
Mg	-	-	-	-	-	-	-	-
Ca	0.7514	0.8499	0.6444	0.7716	0.8239	0.7872	0.7070	0.7793
Na	3.1932	3.0829	3.4503	3.3071	3.1378	3.3159	3.3207	3.1383
K	0.1298	0.1127	0.0382	0.0813	0.1141	0.0637	0.1293	0.1296
TOTAL	20.0621	20.0432	20.0970	20.1202	20.0688	20.1296	20.1294	20.0497

Plagioclase Analyses: Strontian - BPSRT4.

	T4/C7	T4/C8	T4/C9	T4/C10	T4/C11	T4/D1	T4/D2	T4/D3
SiO_2	62.38	62.77	62.50	62.36	62.21	63.86	63.65	63.45
TiO_2	n.d.	n.d.	n.d.	n.d.	n.d.	n.d.	n.d.	n.d.
Al_2O_3	23.15	22.99	23.17	23.17	23.59	22.03	21.86	22.19
FeO	0.16	0.19	0.18	0.14	0.19	n.d.	0.08	0.11
MnO	n.d.	n.d.	n.d.	n.d.	n.d.	n.d.	n.d.	n.d.
MgO	n.d.	n.d.	n.d.	n.d.	n.d.	n.d.	n.d.	n.d.
CaO	4.36	4.45	4.63	4.78	4.82	3.24	3.08	3.41
Na_2O	9.20	9.15	8.97	9.33	9.19	10.25	9.89	9.97
K_2O	0.41	0.47	0.47	0.41	0.46	0.19	0.32	0.36
TOTAL	99.66	100.02	99.92	100.19	100.46	99.57	98.88	99.49
Si	11.1092	11.1410	11.1061	11.0715	11.0190	11.3398	11.3714	11.2937
Ti	-	-	-	-	-	-	-	-
Al	4.8605	4.8106	4.8539	4.8497	4.9260	4.6119	4.6042	4.6564
Fe^{2+}	0.0238	0.0282	0.0268	0.0208	0.0281	-	0.0120	0.0164
Mn	-	-	-	-	-	-	-	-
Mg	-	-	-	-	-	-	-	-
Ca	0.8320	0.8463	0.8816	0.9093	0.9148	0.6165	0.5896	0.6504
Na	3.1768	3.1489	3.0906	3.2118	3.1562	3.5291	3.4259	3.4409
K	0.0932	0.1064	0.1066	0.0929	0.1039	0.0430	0.0729	0.0818
TOTAL	20.0955	20.0814	20.0655	20.1560	20.1481	20.1403	20.0760	20.1394

Plagioclase Analyses: Strontian - BPSRT4 and BPSRG1.

	T4/D4	T4/D5	T4/D6	G1/A1	G1/A2	G1/A3	G1/A4	G1/A5
SiO_2	61.74	64.48	62.27	64.95	64.49	64.40	64.74	65.55
TiO_2	n.d.	n.d.	n.d.	n.d.	n.d.	n.d.	n.d.	n.d.
Al_2O_3	23.14	21.14	22.62	21.86	21.78	22.34	22.10	21.10
FeO	0.07	0.17	0.14	0.17	0.06	0.10	n.d.	0.07
MnO	n.d.	n.d.	n.d.	n.d.	n.d.	n.d.	n.d.	n.d.
MgO	n.d.	n.d.	n.d.	n.d.	n.d.	n.d.	n.d.	n.d.
CaO	4.66	4.48	4.16	2.72	2.87	3.07	2.87	1.96
Na_2O	9.16	9.14	9.25	10.29	10.24	10.15	10.39	10.74
K_2O	0.18	0.36	0.37	0.23	0.27	0.23	0.22	0.20
TOTAL	98.95	99.77	98.81	100.22	99.71	100.29	100.32	99.62
Si	11.0715	11.4920	11.1746	11.4453	11.4223	11.3491	11.3923	11.5856
Ti	-	-	-	-	-	-	-	-
Al	4.8920	4.4214	4.7856	4.5414	4.5479	4.6414	4.5848	4.3966
Fe^{2+}	0.0105	0.0252	0.0210	-	-	-	-	-
Mn	-	-	-	-	-	-	-	-
Mg	-	-	-	-	-	-	-	-
Ca	0.8954	0.8516	0.7999	0.5136	0.5447	0.5797	0.5411	0.3712
Na	3.1849	3.1440	3.2185	3.5158	3.5167	3.4682	3.5450	3.6806
K	0.0412	0.0815	0.0847	0.0517	0.0610	0.0517	0.0494	0.0451
TOTAL	20.0956	19.9629	20.0843	20.0678	20.0926	20.0902	20.1126	20.0790

Plagioclase Analyses: Strontian - BPSRG1.

	G1/A6	G1/B1	G1/B2	G1/B3	G1/B4	G1/B5	G1/C1	G1/C2
SiO_2	65.22	63.85	63.80	64.02	64.07	63.07	64.64	62.17
TiO_2	n.d.	n.d.	n.d.	n.d.	n.d.	n.d.	n.d.	n.d.
Al_2O_3	21.43	21.92	21.91	22.37	22.31	23.02	21.98	23.44
FeO	0.08	n.d.	n.d.	n.d.	0.11	0.09	0.06	0.08
MnO	n.d.	n.d.	n.d.	n.d.	n.d.	n.d.	n.d.	n.d.
MgO	n.d.	n.d.	n.d.	n.d.	n.d.	n.d.	n.d.	n.d.
CaO	2.33	3.04	3.13	3.10	3.27	4.13	2.94	4.55
Na_2O	10.56	10.11	9.52	9.85	9.73	9.19	10.89	9.16
K_2O	0.22	0.22	0.31	0.31	0.26	0.24	0.20	0.27
TOTAL	99.84	99.14	98.67	99.65	99.75	99.74	100.71	99.67
Si	11.5172	11.3724	11.3975	11.3393	11.3464	11.1915	11.3662	11.0697
Ti	-	-	-	-	-	-	-	-
Al	4.4614	4.6028	4.6145	4.6711	4.6579	4.8157	4.5565	4.9204
Fe^{2+}	-	-	-	-	-	-	-	-
Mn	-	-	-	-	-	-	-	-
Mg	-	-	-	-	-	-	-	-
Ca	0.4409	0.5802	0.5991	0.5883	0.6205	0.7853	0.5539	0.8681
Na	3.6157	3.4915	3.2976	3.3828	3.3410	3.1619	3.7129	3.1624
K	0.0496	0.0500	0.0707	0.0701	0.0587	0.0543	0.0449	0.0613
TOTAL	20.0848	20.0969	19.9793	20.0516	20.0246	20.0087	20.2344	20.0819

Plagioclase Analyses: Strontian - BPSRG1.

	G1/C3	G1/C4	G1/C5	G1/C6	G1/C7	G1/D1	G1/D2	G1/D3
SiO_2	62.46	62.87	61.95	64.71	64.63	65.18	64.74	63.72
TiO_2	n.d.	n.d.	n.d.	n.d.	n.d.	n.d.	n.d.	n.d.
Al_2O_3	22.91	23.00	23.71	22.20	22.24	21.95	21.97	22.45
FeO	0.06	n.d.	n.d.	0.09	n.d.	0.11	n.d.	n.d.
MnO	n.d.	n.d.	n.d.	n.d.	n.d.	n.d.	n.d.	n.d.
MgO	n.d.	n.d.	n.d.	n.d.	n.d.	n.d.	n.d.	n.d.
CaO	4.16	4.16	4.18	2.83	2.96	2.57	2.97	3.36
Na_2O	9.20	9.18	8.79	10.17	10.32	10.47	9.94	9.30
K_2O	0.27	0.23	0.61	0.23	0.20	0.21	0.24	0.18
TOTAL	99.06	99.44	99.24	100.23	100.35	100.49	99.86	99.01
Si	11.1671	11.1820	11.0614	11.3953	11.3702	11.4467	11.4266	11.3361
Ti	-	-	-	-	-	-	-	-
Al	4.8289	4.8227	4.9910	4.6089	4.6127	4.5445	4.5715	4.7086
Fe^{2+}	-	-	-	-	-	-	-	-
Mn	-	-	-	-	-	-	-	-
Mg	-	-	-	-	-	-	-	-
Ca	0.7969	0.7928	0.7997	0.5340	0.5580	0.4836	0.5617	0.6405
Na	3.1893	3.1658	3.0431	3.4725	3.5203	3.5652	3.4017	3.2080
K	0.0616	0.0522	0.1390	0.0517	0.0449	0.0471	0.0540	0.0409
TOTAL	20.0439	20.0156	20.0342	20.0623	20.1061	20.0871	20.0155	19.9341

Plagioclase Analyses: Strontian - BPSRG1 and BPSRG4.

	G1/D4	G1/D5	G4/A1	G4/A2	G4/A3	G4/A4	G4/A5	G4/A6
SiO_2	63.76	64.67	64.19	64.54	63.79	63.85	63.99	64.18
TiO_2	n.d.	n.d.	n.d.	n.d.	n.d.	n.d.	n.d.	n.d.
Al_2O_3	22.55	22.22	21.87	21.84	22.48	22.47	22.73	21.80
FeO	n.d.	0.08	0.10	0.06	0.05	0.11	0.13	0.06
MnO	n.d.	n.d.	n.d.	n.d.	n.d.	n.d.	n.d.	n.d.
MgO	n.d.	n.d.	n.d.	n.d.	n.d.	n.d.	n.d.	n.d.
CaO	3.55	2.84	3.03	3.02	3.78	3.75	3.83	3.15
Na_2O	9.90	10.33	10.25	10.12	9.75	9.66	9.85	10.18
K_2O	0.25	0.31	0.24	0.27	0.26	0.44	0.29	0.19
TOTAL	100.01	100.45	99.68	99.85	100.11	100.28	100.82	99.56
Si	11.2751	11.3775	11.3868	11.4154	11.2777	11.2822	11.2501	11.3923
Ti	-	-	-	-	-	-	-	-
Al	4.7012	4.6087	4.5737	4.5541	4.6854	4.6808	4.7112	4.5620
Fe^{2+}	-	-	-	-	-	-	-	-
Mn	-	-	-	-	-	-	-	-
Mg	-	-	-	-	-	-	-	-
Ca	0.6727	0.5354	0.5759	0.5724	0.7161	0.7100	0.7215	0.5991
Na	3.3945	3.5238	3.5255	3.4706	3.3422	3.3096	3.3578	3.5037
K	0.0564	0.0696	0.0543	0.0609	0.0586	0.0992	0.0650	0.0430
TOTAL	20.0998	20.1149	20.1163	20.0734	20.0801	20.0818	20.1057	20.1001

Plagioclase Analyses: Strontian - BPSRG4.

	G4/A7	G4/B1	G4/B2	G4/B3	G4/B4	G4/C1	G4/C2	G4/C3
SiO_2	63.99	63.68	62.84	62.42	64.99	64.69	64.71	63.68
TiO_2	n.d.	n.d.	n.d.	n.d.	n.d.	n.d.	n.d.	n.d.
Al_2O_3	21.65	22.67	23.29	23.40	22.30	22.13	22.45	22.64
FeO	0.10	n.d.	0.05	0.07	0.13	n.d.	0.08	0.16
MnO	n.d.	n.d.	n.d.	n.d.	n.d.	n.d.	n.d.	n.d.
MgO	n.d.	n.d.	n.d.	n.d.	n.d.	n.d.	n.d.	n.d.
CaO	3.11	3.83	4.43	4.71	3.17	2.97	3.09	4.14
Na_2O	10.05	9.59	9.23	8.78	9.95	10.13	10.14	9.48
K_2O	0.24	0.29	0.31	0.28	0.23	0.12	0.12	0.26
TOTAL	99.14	100.06	100.15	99.66	100.77	100.04	100.59	100.36
Si	11.4080	11.2561	11.1247	11.0995	11.3890	11.4146	11.3565	11.2466
Ti	-	-	-	-	-	-	-	-
Al	4.5503	4.7242	4.8608	4.9055	4.6071	4.5823	4.6449	4.7139
Fe^{2+}	-	-	-	-	-	-	-	-
Mn	-	-	-	-	-	-	-	-
Mg	-	-	-	-	-	-	-	-
Ca	0.5941	0.7254	0.8403	0.8974	0.5952	0.5589	0.5811	0.7835
Na	3.4740	3.2868	3.1682	3.0272	3.3809	3.4498	3.4505	3.2463
K	0.0546	0.0654	0.0700	0.0635	0.0514	0.0269	0.0269	0.0586
TOTAL	20.0811	20.0579	20.0641	19.9931	20.0236	20.0326	20.0597	20.0489

Plagioclase Analyses: Strontian - BPSRG4.

	G4/C4	G4/C5	G4/C6	G4/C7	G4/D1	G4/D2	G4/D3	G4/D4
SiO_2	62.27	63.85	64.68	65.12	63.39	63.24	63.61	64.77
TiO_2	n.d.	n.d.	n.d.	n.d.	n.d.	n.d.	n.d.	n.d.
Al_2O_3	23.05	22.43	22.10	22.04	22.98	23.18	22.91	21.92
FeO	0.05	0.10	0.09	0.06	0.06	0.07	0.12	n.d.
MnO	n.d.	n.d.	n.d.	n.d.	n.d.	n.d.	n.d.	n.d.
MgO	n.d.	n.d.	n.d.	n.d.	n.d.	n.d.	n.d.	n.d.
CaO	4.13	3.82	3.13	2.64	3.97	4.12	4.03	3.04
Na_2O	9.30	9.62	9.93	9.72	9.30	9.33	9.25	10.07
K_2O	0.23	0.41	0.25	0.14	0.18	0.18	0.23	0.24
TOTAL	99.03	100.23	100.18	99.72	99.88	100.12	100.15	100.04
Si	11.1389	11.2855	11.3985	11.4776	11.2193	11.1777	11.2356	11.4210
Ti	-	-	-	-	-	-	-	-
Al	4.8610	4.6739	4.5915	4.5797	4.7949	4.8302	4.7707	4.5568
Fe^{2+}	-	-	-	-	-	-	-	-
Mn	-	-	-	-	-	-	-	-
Mg	-	-	-	-	-	-	-	-
Ca	0.7916	0.7235	0.5910	0.4986	0.7529	0.7803	0.7627	0.5744
Na	3.2256	3.2969	3.3931	3.3218	3.1915	3.1975	3.1680	3.4429
K	0.0525	0.0925	0.0562	0.0315	0.0406	0.0406	0.0518	0.0540
TOTAL	20.0696	20.0722	20.0304	19.9092	19.9993	20.0262	19.9889	20.0491

Plagioclase Analyses: Strontian - BPSRG4.

	G4/E1	G4/E2	G4/E3
SiO_2	65.18	64.51	64.45
TiO_2	n.d.	n.d.	n.d.
Al_2O_3	22.27	22.26	21.80
FeO	0.07	0.10	n.d.
MnO	n.d.	n.d.	n.d.
MgO	n.d.	n.d.	n.d.
CaO	3.01	3.32	3.10
Na_2O	10.02	9.97	9.97
K_2O	0.41	0.36	0.23
TOTAL	100.96	100.52	99.55
Si	11.4011	11.3526	11.4207
Ti	-	-	-
Al	4.5924	4.6183	4.5542
Fe^{2+}	-	-	-
Mn	-	-	-
Mg	-	-	-
Ca	0.5642	0.6260	0.5886
Na	3.3984	3.4020	3.4255
K	0.0915	0.0808	0.0520
TOTAL	20.0476	20.0797	20.0410